frontiers | Research Topics

The roles of immune cell homeostasis in cancer research and therapeutic response

Edited by
Zhijie Xu, Jianhua Zhou, Abhimanyu Thakur, Kui Zhang and Zhi-Yao He

Published in
Frontiers in Pharmacology

ISSN 1664-8714
ISBN 978-2-8325-2919-5
DOI 10.3389/978-2-8325-2919-5

About Frontiers

Frontiers is more than just an open access publisher of scholarly articles: it is a pioneering approach to the world of academia, radically improving the way scholarly research is managed. The grand vision of Frontiers is a world where all people have an equal opportunity to seek, share and generate knowledge. Frontiers provides immediate and permanent online open access to all its publications, but this alone is not enough to realize our grand goals.

Frontiers journal series

The Frontiers journal series is a multi-tier and interdisciplinary set of open-access, online journals, promising a paradigm shift from the current review, selection and dissemination processes in academic publishing. All Frontiers journals are driven by researchers for researchers; therefore, they constitute a service to the scholarly community. At the same time, the *Frontiers journal series* operates on a revolutionary invention, the tiered publishing system, initially addressing specific communities of scholars, and gradually climbing up to broader public understanding, thus serving the interests of the lay society, too.

Dedication to quality

Each Frontiers article is a landmark of the highest quality, thanks to genuinely collaborative interactions between authors and review editors, who include some of the world's best academicians. Research must be certified by peers before entering a stream of knowledge that may eventually reach the public - and shape society; therefore, Frontiers only applies the most rigorous and unbiased reviews. Frontiers revolutionizes research publishing by freely delivering the most outstanding research, evaluated with no bias from both the academic and social point of view. By applying the most advanced information technologies, Frontiers is catapulting scholarly publishing into a new generation.

What are Frontiers Research Topics?

Frontiers Research Topics are very popular trademarks of the *Frontiers journals series*: they are collections of at least ten articles, all centered on a particular subject. With their unique mix of varied contributions from Original Research to Review Articles, Frontiers Research Topics unify the most influential researchers, the latest key findings and historical advances in a hot research area.

Find out more on how to host your own Frontiers Research Topic or contribute to one as an author by contacting the Frontiers editorial office: frontiersin.org/about/contact

The roles of immune cell homeostasis in cancer research and therapeutic response

Topic editors

Zhijie Xu — Central South University, China
Jianhua Zhou — Central South University, China
Abhimanyu Thakur — The University of Chicago, United States
Kui Zhang — The University of Chicago, United States
Zhi-Yao He — Sichuan University, China

Citation

Xu, Z., Zhou, J., Thakur, A., Zhang, K., He, Z.-Y., eds. (2023). *The roles of immune cell homeostasis in cancer research and therapeutic response*. Lausanne: Frontiers Media SA. doi: 10.3389/978-2-8325-2919-5

Table of contents

frontiers | Frontiers in Pharmacology

TYPE Editorial
PUBLISHED 21 June 2023
DOI 10.3389/fphar.2023.1227996

OPEN ACCESS

EDITED AND REVIEWED BY
Olivier Feron,
Université catholique de Louvain,
Belgium

*CORRESPONDENCE
Kui Zhang,
zhangk87@gmail.com,
kuizhang@uchicago.edu
Abhimanyu Thakur,
abithakur1211@gmail.com

RECEIVED 24 May 2023
ACCEPTED 13 June 2023
PUBLISHED 21 June 2023

CITATION
Zhang K, Thakur A, Xu Z and He Z-Y (2023), Editorial: The roles of immune cell homeostasis in cancer research and therapeutic response.
Front. Pharmacol. 14:1227996.
doi: 10.3389/fphar.2023.1227996

Editorial: The roles of immune cell homeostasis in cancer research and therapeutic response

Kui Zhang[1]*, Abhimanyu Thakur[2]*, Zhijie Xu[3] and Zhi-Yao He[4]

[1]State Key Laboratory of Resource Insects, Medical Research Institute, Southwest University, Chongqing, China, [2]The Pritzker School of Molecular Engineering, Ben May Department for Cancer Research, University of Chicago, Chicago, IL, United States, [3]Department of Pathology, Xiangya Hospital, Central South University, Changsha, Hunan, China, [4]Department of Pharmacy, West China Hospital, Sichuan University, Chengdu, Sichuan, China

KEYWORDS

tumor microenvironment (TME), immune cell homeostasis, cancer pathogenesis, therapeutic response, tumor-immune cell interaction, cancer-associated molecules, immune cell-based therapeutic targets

Editorial on the Research Topic
The roles of immune cell homeostasis in cancer research and therapeutic response

Immune cells within the tumor microenvironment (TME) significantly contribute to the composition and dynamics of the TME, thereby influencing cancer pathogenesis and therapeutic response. The dynamic balance of interactions among immune cells and between immune cells and tumor cells has been identified as a promising therapeutic strategy for treating various cancers. Several therapies have been demonstrated to alleviate such immune disorders and restore immune cell homeostasis. Therefore, it is urgently necessary to deeply explore the significant implications of immune cell homeostasis in cancers, and to unravel the underlying molecular mechanisms and biological functions of this interplay, with the goal of improving treatment efficacy.

This Research Topic aims to explore the Frontier research in the context of immune cell homeostasis in the TME, with a spotlight on 1) immune cell-based strategies for cancer research and treatment; 2) the interaction between cancer cells and immune cells; 3) the molecular mechanisms of tumor-infiltrating immune cell regulation; 4) underlying roles of cancer-associated molecules in immune cell infiltration; 5) clinical or bioinformatics analyses to explore immune cell-based therapeutic targets.

Huang et al. focused their research on the integration of artificial intelligence with immunosignals for the precision treatment of liver diseases associated with Hepatitis B Virus (HBV). They identified CLST and aCD4, two immunosignals integral to the virus's pathogenesis, as key players in the inflammation, fibrosis, and hepatocellular carcinoma triggered by HBV. Using gene set variation analysis, they developed immunogenomic signatures that streamlined the creation of robust diagnostic and prognostic models. The clinical application of CLST and aCD4 as indicators could significantly improve the precision management of hepatocellular carcinoma. This study provides an in-depth understanding of the gene characteristics tied to the immune microenvironment in HBV infection and offers subtle insights for the clinical management of HBV-related hepatocellular carcinoma, thereby establishing a strong foundation for precision medicine. Liu et al. successfully integrated machine learning to build classifiers related to aberrant alternative splicing (AS) events. These classifiers are

designed to predict prognosis and the response to immunotherapy in patients with hepatocellular carcinoma. They found that AS can be instrumental in classifying HCC subtypes, as it alters the activity of tumor-related pathways through differential splicing effects. This, in turn, impacts the TME and plays a role in immune reprogramming. The authors have outlined the clinical and molecular characteristics, offering a fresh approach for personalized treatment of HCC patients.

Glioma is one of the most common types of primary brain tumor. Li et al. reveal that the transcription factor ZBTB42 is highly expressed in glioma, it could be regarded as a promising prognostic factor for glioma. Moreover, ZBTB42 appears to be linked to immune cell infiltration, potentially playing a role in the immune-suppressive TME. Notably, the study also found a correlation between ZBTB42 and stem cell markers, indicating a positive association with glioma stemness. Therefore, the research identifies ZBTB42 as a prognostic biomarker for glioma, with its function tied to both the suppressive TME and the stemness of glioma. Fang et al. found that URB2 is also significantly overexpressed in glioma, and has a potential oncogenic role, as evidenced by the substantial impairment of cell viability upon its knockdown. Its expression level can independently predict overall survival. Interestingly, a strong link between URB2 and immune responses has been discovered, with the URB2 phenotype possibly contributing to immune suppression in GBM. This study indicated URB2 may serve as a crucial tool for prognosis prediction and immunotherapy guidance in glioma treatment. Luo et al. conducted a bioinformatic analysis of IL-15, a cytokine with diverse roles in immune regulation and tumorigenesis, as a potential prognostic biomarker across various cancers and its link to exercise's anti-cancer effects. They discovered that IL-15 is generally downregulated in most cancers, with its high expression predicting better survival outcomes. Amplification emerged as the most common mutation type in IL-15's genome. Additionally, IL-15 expression correlated with the infiltration levels of different immune cells and positively associated with ferroptosis/cuproptosis-related genes (ACSL4 and LIPT1) across various cancers. This study underscores IL-15's potential as a prognostic biomarker for patient outcomes, immune responses, and ferroptosis/cuproptosis in pan-cancer, shedding light on exercise's anti-cancer effects.

Li et al. found that tissues resistant to TPF chemotherapy, a regimen comprising Docetaxel, Cisplatin, and Fluorouracil, in HPSCC patients exhibited upregulated T cell activation and downregulated glycolysis. They identified SEC61G as a key gene negatively correlated with $CD8^+$ T cells and involved in glycolysis. Their findings suggest that while enhanced glycolysis may promote immune escape, it may also increase TPF chemotherapy response. Targeting the E2F1/SEC61G pathway could potentially boost MHC-I expression, offering a new therapeutic avenue.

Zeng et al. analyzed the link between TGF-β signaling pathway-related genes (TSRGs), clinical prognosis, the TME, and immunotherapy in gastric cancer. This study discerned two unique TGF-β subgroups in gastric cancer, with one subgroup showing an immunosuppressive environment and reduced survival. A new TGF-β-related prognostic model was developed, indicating that patients with lower risk scores have improved prognosis and are more responsive to immunotherapy. These insights emphasize the role of TSRGs in shaping the tumor immune microenvironment and tailoring immunotherapy for gastric cancer patients. Interestingly, TGF-β has also been explored as a potential prognostic biomarker for glioma. Chen et al. have identified a crucial connection between serine and glycine metabolism-related genes (SGMGs) and both the prognosis and immune microenvironment of glioma. They've constructed a unique SGMG signature that holds promise in predicting patient prognosis and immune responses. This research implies that SGMGs could potentially steer the choice of immunotherapy in treating glioma. Qi et al. analyzed the genomic and transcriptomic profiles of 34 anoikis-related genes (ARGs), which are crucial for maintaining immune cell balance. The researchers found significant differences in ARG expression between soft-tissue sarcoma and normal tissues, suggesting a potential disruption of immune homeostasis in cancer. Their anoikis scoring system, which effectively predicted immune cell infiltration and immunotherapy response, could serve as a tool for assessing immune status and guiding personalized immunotherapy in cancer treatment. Meng et al. identified two molecular subtypes in uveal melanoma (UM) based on matrix-remodeling associated genes (MAGs), which showed significant differences in clinical outcomes. They developed a risk score system involving six MAGs that effectively predicted prognosis and immune activity. Their findings suggest that this MAGs-based system could enhance prognosis assessment and guide clinical decision-making in UM, highlighting the role of immune cell homeostasis in cancer therapy response.

Clearly, these research findings will serve as a critical source of information to benefit all stakeholders involved in understanding the impact of immune cell homeostasis in cancer and their potential therapeutic responses.

Author contributions

KZ served as a guest associate editor for this research topic and was responsible for writing the manuscript. ZX acted as a guest editor of the research topic and undertook the editing of the text. Lastly, AT and Z-YH contributed as guest associate editors of the research topic, focusing on revising the text. All authors listed have made a substantial, direct, and intellectual contribution to the work and approved it for publication.

Acknowledgments

Expressing profound gratitude, we acknowledge all the authors, reviewers and editor whose invaluable contributions have enriched this Research Topic.

Conflict of interest

The authors declare that the research was conducted in the absence of any commercial or financial relationships that could be construed as a potential conflict of interest.

Publisher's note

frontiers | Frontiers in Pharmacology

TYPE Original Research
PUBLISHED 03 October 2022
DOI 10.3389/fphar.2022.1019988

OPEN ACCESS

EDITED BY
Zhijie Xu,
Central South University, China

REVIEWED BY
Zhengyi Zhu,
Nanjing Drum Tower Hospital, China
Jun Wang,
Sun Yat-sen University Cancer Center (SYSUCC), China

*CORRESPONDENCE
Jian Wang,
wangjian197906@126.com
Tao Wang,
13061931996@163.com
Bo Zhai,
zhaiboshi@sina.com
Lei Pan,
10264@renji.com

†These authors have contributed equally to this work

SPECIALTY SECTION
This article was submitted to Pharmacology of Anti-Cancer Drugs, a section of the journal Frontiers in Pharmacology

RECEIVED 15 August 2022
ACCEPTED 13 September 2022
PUBLISHED 03 October 2022

CITATION
Liu W, Zhao S, Xu W, Xiang J, Li C, Li J, Ding H, Zhang H, Zhang Y, Huang H, Wang J, Wang T, Zhai B and Pan L (2022), Integrating machine learning to construct aberrant alternative splicing event related classifiers to predict prognosis and immunotherapy response in patients with hepatocellular carcinoma. *Front. Pharmacol.* 13:1019988. doi: 10.3389/fphar.2022.1019988

Integrating machine learning to construct aberrant alternative splicing event related classifiers to predict prognosis and immunotherapy response in patients with hepatocellular carcinoma

Wangrui Liu[1†], Shuai Zhao[2†], Wenhao Xu[3†], Jianfeng Xiang[1†], Chuanyu Li[4†], Jun Li[5,6], Han Ding[2], Hailiang Zhang[3], Yichi Zhang[2], Haineng Huang[4], Jian Wang[2]*, Tao Wang[1]*, Bo Zhai[1,7]* and Lei Pan[1]*

[1]Department of Interventional Oncology, Renji Hospital, Shanghai Jiao Tong University School of Medicine, Shanghai, China, [2]Department of Transplantation, Xinhua Hospital Affiliated to Shanghai Jiao Tong University School of Medicine, Shanghai, China, [3]Department of Urology, Fudan University Shanghai Cancer Center, Shanghai, China, [4]Affiliated Hospital of Youjiang Medical University for Nationalities, Baise, China, [5]Department of Hepatobiliary Surgery, Tenth People's Hospital of Tongji University, Shanghai, China, [6]Department of Hepatic Surgery, Eastern Hepatobiliary Surgery Hospital, Naval Medical University, Shanghai, China, [7]State Key Laboratory of Oncogenes and Related Genes, Shanghai Cancer Institute, Reni Hospital, School of Medicine, Shanghai Jiao Tong University, Shanghai, China

Introduction: In hepatocellular carcinoma (HCC), alternative splicing (AS) is related to tumor invasion and progression.

Methods: We used HCC data from a public database to identify AS subtypes by unsupervised clustering. Through feature analysis of different splicing subtypes and acquisition of the differential alternative splicing events (DASEs) combined with enrichment analysis, the differences in several subtypes were explored, cell function studies have also demonstrated that it plays an important role in HCC.

Results: Finally, in keeping with the differences between these subtypes, DASEs identified survival-related AS times, and were used to construct risk proportional regression models. AS was found to be useful for the classification of HCC subtypes, which changed the activity of tumor-related pathways through differential splicing effects, affected the tumor microenvironment, and participated in immune reprogramming.

Conclusion: In this study, we described the clinical and molecular characteristics providing a new approach for the personalized treatment of HCC patients.

KEYWORDS

hepatocellular carcinoma, tumor microenvironment, immune checkpoint molecules, alternative splicing event, machine learning

Introduction

Hepatocellular carcinoma (HCC) has become the second leading cause of cancer-related deaths worldwide, with more than 800,000 deaths each year (Sung et al., 2021). Surgical resection, liver transplantation, tumor ablation, and interventional techniques are all potential treatment methods (Bishay et al., 2016; Guro et al., 2016; Sun et al., 2019; Yoon and Lee, 2019). However, improvements in the prognosis of liver cancer remain challenging. The therapeutic effects of first-line HCC drugs such as sorafenib are poor (Galun et al., 2017; Saffo and Taddei, 2019), and no prognostic classification and markers have been identified to provide guidance for personalized treatment (Liu et al., 2020a; Zhao et al., 2021a; Zhao et al., 2021b). Therefore, a new treatment strategy is required to predict the prognosis of liver cancer.

Aberrant alternative splicing (AS) is the result of splicing regulatory sequence mutations or ectopic RNA binding protein regulation. It plays an indispensable role in cancer and many other diseases (Gamundi et al., 2008; Fu and Ares, 2014; Shiraishi et al., 2018). Although integrated multiomics analyses have been reported in HCC subtypes, splicing characteristics and splicing regulatory networks are rarely systematically discussed. We previously studied the regulatory mechanism of AS-related genes and their effect on the prognosis of some malignant tumors (Liu et al., 2020b). On this basis in the current study, we conducted a comprehensive analysis of HCC subtype classification and splicing characteristics and their relationship with clinical characteristics, gene mutations, pathway changes, and immune heterogeneity.

Materials and methods

Patients and tissue samples from online databases and real-world cohorts

All splicing data for liver cancer were downloaded from the cancer genome atlas (TCGA) SpliceSeq database including AS data, expression data, phenotype data, and survival data (Supplementary Table S1).

We also downloaded the human genome sequence from the TCGA database (Barrett et al., 2013), the human gtf file from the Ensembl database (Yates et al., 2020), and the Gene Set Variation Analysis (GSVA) gene set (Hänzelmann et al., 2013) and immune cell-related gene set.The variable splicing score was calculated by the network tool Maximum Entropy (Kim et al., 2018).

Sample clustering and survival differences

We used the R package Rtsne (v0.15), which based on the t-distributed stochastic neighbor embedding (t-SNE) method, to cluster the samples according to their PSI values (Chen et al., 2021). Because the clinical feature grouping is displayed in t-SNE, the sample division was not obvious. Therefore, the R package ConsensusClusterPlus (v1.50.0) was used to perform unsupervised clustering of the samples (Zheng et al., 2020). The Kaplan–Meier algorithm was used to obtain the PSI-based AS subtype, and t-SNE was undertaken for verification and presentation of the results, followed by analysis by the R packages survival (v3. 2–7) and survminer (v0.4.8) to determine the survival of the samples and construct Kaplan–Meier curves (Rizvi et al., 2019; Wang et al., 2020).

To further detect the differences in the distribution of age, sex, grade, pathologic T stage, alcohol, hepatitis B, and hepatitis C groups in the AS subtypes, Fisher test was applied (Di Francesco et al., 2019).

Identification and presentation of subtype differences in AS events, and analysis of the differential alternative splicing events

DASEs of cancer samples and normal samples were called according to the PSI value of AS. DASEs met two conditions: 1) Wilcoxon rank-sum test between groups reached a significant level (after Bonferroni correction adjustment $p < 0.05$); and 2) Chi-squared test based on the median PSI reaching a significant level ($p < 0.05$). After DASEs were obtained, those whose average PSI of cancer samples were greater than the average PSI of normal samples were regarded as upregulated, and those whose PSI were less were regarded as downregulated. Next, DASEs between samples of different subtypes and normal samples were collected in the same way, and the number of different AS types in the relevant subtypes was counted, with the results included in a histogram. After obtaining the DASEs between subtypes, the overlap similarity of the upregulated and downregulated DASEs between subtypes was calculated as follows: Overlapping similarity = intersection of two sets/ minimum value of the two sets. According to the obtained DASEs, analysis of variance was used to screen differential AS events between the two subtypes, with a threshold of $p < 0.05$, and then the intersection was taken for subsequent analyses.

Analysis of splicing characteristics of DASEs in alternative splicing subtypes, corresponding gene expression display and GSVA difference analysis

In a further analysis of the AS score, GC content, and AS fragment length of DASEs, Python 3.8.8 (Spyder (Anaconda3)) was

first used to obtain the reference sequence of each chromosome from the reference genome (Paillusseau et al., 2020), and the splice site positions provided by TCGA SpliceSeq database were combined to obtain all DASEs with alternate acceptor site (AA), alternate donor site (AD), exon skip (ES), retained intron (RI) sequence, and 5′ or 3′ splice site sequence splicing types. To calculate the AS score, the first 3′ position sequence of AA, the second 3′ position sequence of AA, the first 5′ position sequence of AD, and the second 5′ position sequence of AD were extracted according to the requirements of MaxEntScan. The ' site sequence, the 5′ and 3′ site sequence of ES, and the 5′ and 3′ site sequence of RI were analyzed online to obtain the score of the corresponding site, which was shown in a box plot. The GC content was the percentage of G and C bases in the entire AS sequence. Alternative splicing length = log10 (exon/intron length). Finally, a box plot was drawn to show the GC content and AS length. We identified genes corresponding to DASEs from the AS information, and then drew a heat map to show the expression of the corresponding gene [log2 (fpkm-uq+1)].

All gene sets were downloaded from the MSigDB database (Guo and Wan, 2014), and the R package GSVA (v1.34.0) was used to calculate the enrichment scores of each sample for different gene sets according to the expression data, and the cumulative distribution curve of GSVA scores was drawn according to the different subtypes. Then the R package limma (v3.42.2) was used to obtain the enriched differential gene sets (DESs) in different subtype samples and normal samples (Ritchie et al., 2015), and the threshold to |logFC|> 0.5 and adj.P.Val<0.05 was called. A bar graph was drawn to plot the upregulated and downregulated adjustments in different subtypes of DESs.

Analysis of the correlation between differential gene sets, AS events, and AS factors

The correlation between the differential gene sets within the subtypes and the AS events was further calculated. First, the AS event was selected according to a PSI interquartile range of greater than 0.05 as the threshold in the samples, and then the screening results were used to calculate the Spearman's correlation coefficient (coef) for the differential gene set. Alternative splicing-related pathways (SPs) in the MSigDB database were searched using "splice", "splicing", and "spliceosome" as keywords, and protein-coding genes in related pathways were used as splicing factors (SFs). After that, Spearman's correlation coefficients of AS events and SPs and SFs were further calculated, and then the largest |coef. of SP| and |coef. of SF| corresponding to each AS event was selected to construct a scatter plot. Because coef. of SP and coef. of SF had the greatest number of AS events greater than 0.5 at the same time, the relevant AS events were selected for further PSI display, as well as the strongly correlated SP enrichment score of each subtype and the strongly correlated SF differential expression [edgeR (v3.28.1)] (Robinson et al., 2010). The R package estimate (v1.0.13) was used to calculate the StromalScore, ImmuneScore, ESTIMATEScore, and TumorPurity of all samples in TCGA-LIHC data, and the immune cell-related gene set was used to calculate the enrichment scores of 28 immune infiltrating cells, combined with immune checkpoints.

Combining mRNA expression profiles to predict differences in AS typing immunotherapy and drug sensitivity

To predict whether an immunosuppressive agent has a therapeutic effect on different AS subtypes, SubMap was used to map different AS subtype samples to samples with inhibitor processing information (Ay et al., 2011), as well as to calculate the similarity between the samples and then predict the possible effects of variant splicing subtypes on treatment with two inhibitors.

The R package pRRophetic (v 0.5) was then to predict the sample's response to 138 drugs (Geeleher et al., 2014), generating predicted IC_{50} values, and then the differences in the IC_{50} value of the samples of different AS subtypes was further counted using Kruskal's algorithm to detect the significant differences. Next adj.$p < 0.05$ was used to screen for significantly different drugs, and the IC_{50} values of bosutinib, dasatinib, midostaurin, elesclomol, pazopanib, bortezomib, sorafenib, docetaxel, and gefitinib were plotted in box plots.

Construction of a prognostic model of AS

Cancer samples were collected according to the PSI value of differential AS in the previous step combined with OS data, and batch Cox one-way regression analysis was performed on differential AS. After regression analysis, $p < 0.05$ was used as a threshold to screen significantly related AS events for subsequent analyses.

Lasso regression was further performed on the single-factor Cox regression results and a risk scoring model was built. This process mainly relied on the R package glmnet (v4.0–2). In the glmnet function (Engebretsen and Bohlin, 2019), Y is Surv (time, event), and family is Cox. To build a more accurate regression model, we first used cross-validation for lambda screening, then selected the model corresponding to lamdba.min, and further extracted the expression matrix of related genes in the model, and then calculated the risk score of each sample according to the following formula:

$$\mathrm{RScore_i} = \sum_{j=1}^{n} \mathrm{PSI_{ji}} \times \beta_j$$

Where PSI represents the PSI value of the corresponding AS, β represents the regression coef. of the corresponding gene in the

lasso regression result, and RScore represents the PSI value of the significantly related AS event in each sample multiplied by the corresponding AS event. The coef was then calculated, where i is the sample and j is the AS event. On the basis of the risk score of the sample, the high and low risk groups were divided by the median as the node and combined with the overall survival (OS) and disease-free interval (DFI) data to generate a Kaplan–Meier curve, with a p-value of <0.05 indicating that the difference between the high and low risk groups was significant.

Validation in human HCC tissues

Paired tumoral and adjacent normal samples were from patients diagnosed with HCC and accepted surgery at the Department of Transplantation, Xinhua Hospital affiliated to Shanghai Jiao Tong University School of Medicine (Shanghai, China) after the written informed consent. All these samples were kept and processed as previously described. RT-PCR was implemented using transcripts specific primers by 2 × Green PCR Mix (Vazyme, Nanjing, China). Splicing specific transcripts were distinguished using agarose gel electrophoresis and grayscale-measured using software ImageJ (Rawak Software Inc., Stuttgart, Germany). PSI of each lane was calculated by the greyscale of the longer transcript divided by the sum greyscale of the longer and the shorter transcripts.

Results

Splicing clustering and clinical features of HCC subtypes

HCC AS data (percentage of samples with PSI value = 100%) was downloaded from TCGA SpliceSeq database, and 11,179 AS events were obtained, corresponding to 4423 genes, which included 568 AAs, 469 ADs, 968 alternate promoters (APs), 6346 alternate terminators (ATs), 1992 ESs, 29 mutually exclusive exons (MEs), and 807 retained introns (RIs). At the same time, relevant HCC expression data and clinical data were downloaded from the UCSC Xena database, and 370 cancer samples and 50 normal samples were obtained after integration.

According to the t-SNE method, the PSI values of all samples were displayed in clusters, and a scatter plot revealed that the cancer samples could be clearly distinguished from the normal samples (Figure 1A). Next, unsupervised clustering of cancer samples was performed to obtain five subtype samples (Figure 1B). The t-SNE method was used to demonstrate that cluster 1 and cluster 2 samples were relatively similar in the five subtype samples, and cluster 3 and cluster 5 samples were similar. Therefore, cluster 1 and cluster 2 were merged into cluster 1, and cluster 3 and cluster 5 were merged into cluster 3, and finally three subtypes (cluster 1, cluster 3, cluster 4) were obtained. The scatter plot shows that the three subtypes were more distinct from each other (Figure 1C).Then, we analyzed the correlation between cluster samples and clinical traits such as age, sex, grade, pathological stage, type, alcohol consumption, and hepatitis B/C infection, and found that AS also affects various clinical characteristics of HCC (Figure 1D).

Analysis of differences in survival between subtypes, clinical characteristics, and distribution of typical types

The survival analysis of the three subtypes was further based on OS, and a Kaplan–Meier curve was generated. The results showed that the survival difference of the three subtypes was significant, and the survival curve of cluster 4 samples dropped faster (Figure 1E).

The distribution differences of age, sex, grade, pathological T stage, alcohol consumption, hepatitis B, and hepatitis C groupings in AS subtypes were further examined (Figures 1F–M). The results showed that there were significant differences in the distribution of age, grade, pathological T stage, and hepatitis B groupings among the subtypes. For age, cluster 1 was more than 65 years old and had significantly more samples than cluster 4 (Figure 1F). For grade, the number of G1–2 samples in cluster 1 was significantly higher than that in cluster 3 and cluster 4 (Figure 1J). For pathological T stage, the number of T3–4 samples in cluster 4 was significantly higher than in cluster 1 (Figure 1K). For stage, the number of stage III–IV samples in cluster 4 was significantly higher than that in cluster 1 and cluster 3 (Figure 1H). For hepatitis B, there were significantly more hepatitis B patients in cluster 3 than cluster 1 (Figure 1L). These data indicate that AS exhibits different patterns according to the histological type of HCC and is closely related to clinical characteristics and patient survival, and thus is suitable as a subtype classification.

Overall differences in AS events and identification of subtype differences in AS events

On the basis of the PSI value of AS, the DASEs of cancer samples and normal samples were retrieved. After threshold screening, 1,777 DASEs were obtained, of which 977 were upregulated and 800 were downregulated, corresponding to 1,005 genes (Supplementary Table S2). According to the type of AS, DASEs had the most AT events, followed by ES, RI, and AP, and the corresponding genes also had the most AT events. The UpSet chart showed that 17 genes had AT and ES at the same time, and 11 genes had AP and ES at the same time (Figures 2A–C, Supplementary Table S3).

Next, the DASEs between the three subtypes and the normal samples were obtained. Cluster 1-normal had 1,681 DASEs, including 948 that were upregulated and 733 that were downregulated; cluster 3-normal had 2,545 DASEs, including

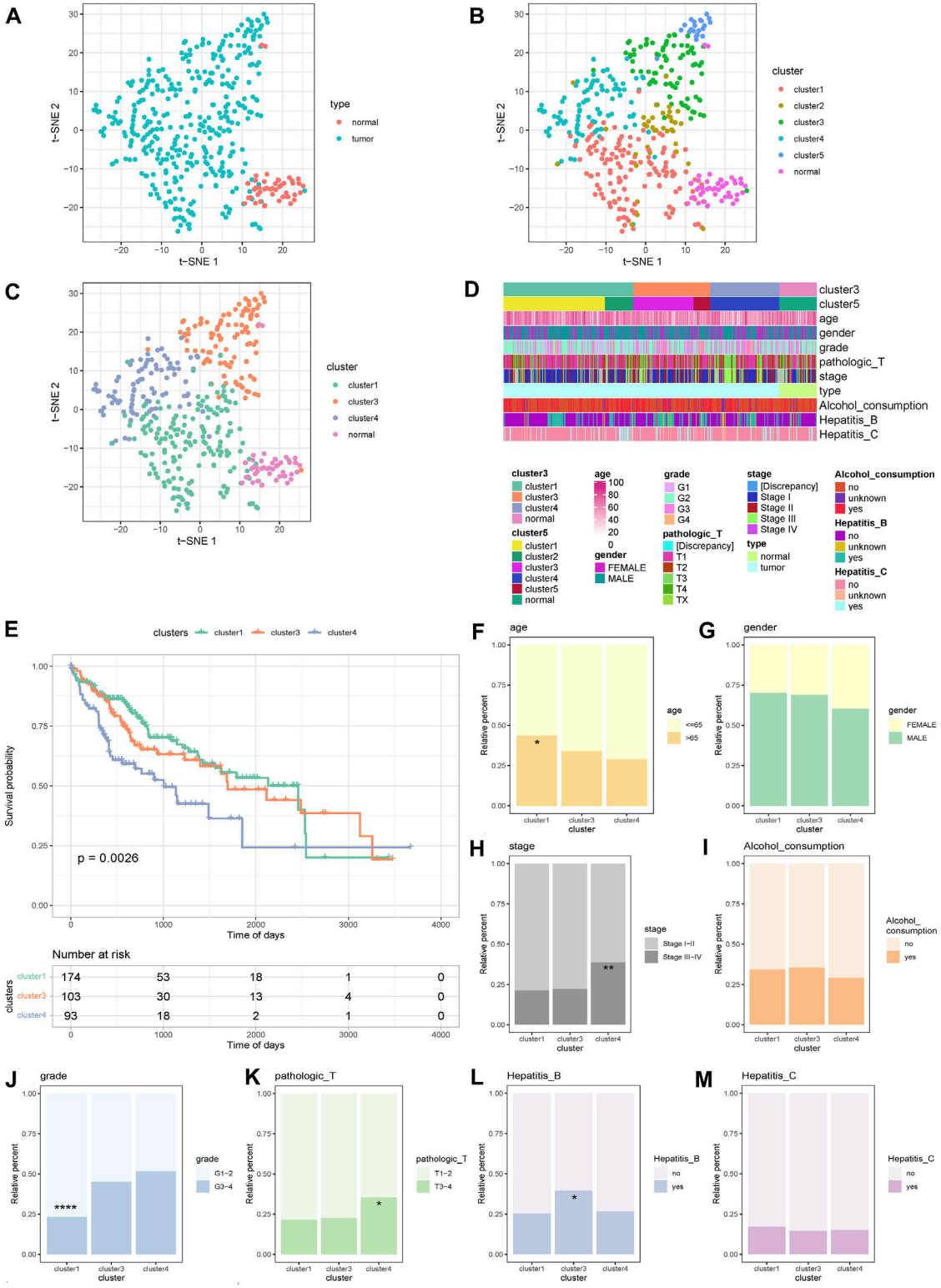

FIGURE 1
Sample cluster display and survival differences and clinical analysis. **(A)** Cluster scatter plot display of cancer samples and normal samples. **(B)** Unsupervised clustering scatter plot display of cancer samples in 5 categories. **(C)** Scatter plot display of 5 categories of samples merged into 3 categories.**(D)** Clustering Heat map display of samples and clinical traits. **(E)** KM curves of 3 alternative splicing subtypes. **(F–M)** Display of clinical features and distribution of typical types. ****$p < 0.0001$; ***$p < 0.001$; **$p < 0.01$; *$p < 0.05$.

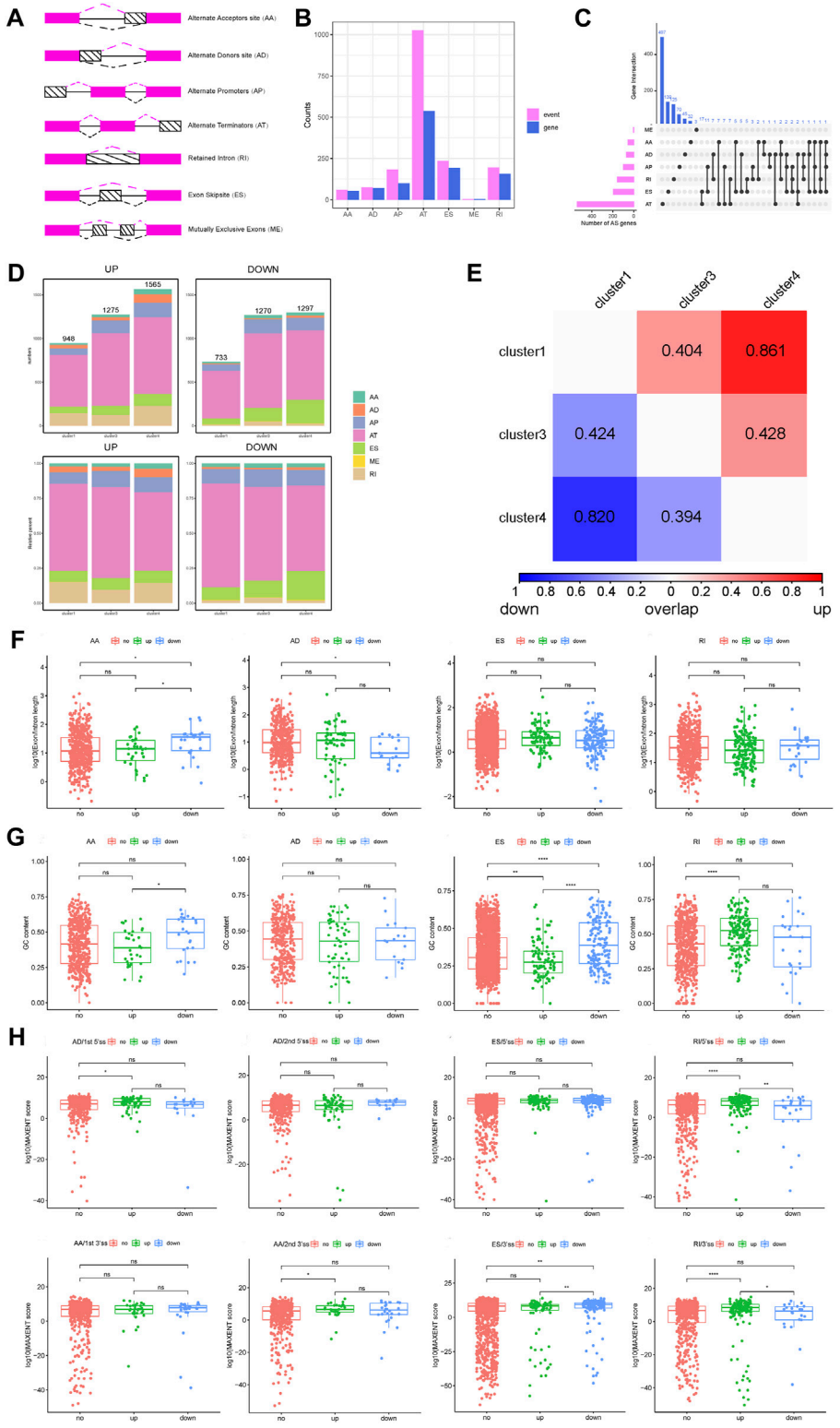

FIGURE 2
Analysis of DASEs and DASEs between subtypes and alternative splicing fragment length and score of the overall DASEs. **(A)** Schematic diagram of alternative splicing types. **(B)** Statistics of the number of splicing types of DASEs and corresponding gene splicing types. **(C)** UpSet diagram of the different alternative splicing types of DASEs corresponding genes. **(D)**Statistics of alternative splicing types of DASEs of each subtype. **(E)**Overlap similarity of DASEs up and down between subtypes. **(F)**Alternative splicing fragment length of overall DASEs. **(G)** GC content of overall DASEs. **(H)** Alternative splicing score for overall DASEs.

1,275 that were upregulated and 1,270 that were downregulated; and cluster 4-normal had 2,862 DASEs, including 1,565 that were upregulated and 1,297 that were downgraded. (Figure 2D, Supplementary Table S4). After obtaining the DASEs between the subtypes, the overlap similarity of the upregulated and downregulated DASEs was calculated between the subtypes. The heat map in Figure 3E shows that in cluster 1 and cluster 4, regardless of the upregulation or downregulation of DASEs, the overlap similarity was relatively high, at greater than 0.8 in both (Figure 2E).

Analysis of splicing characteristics of DASEs in AS subtypes

The AS score, GC content, and AS fragment length of the overall DASEs were further analyzed. For the length of AS fragments, the AS length of downregulated AAs was significantly higher than that of upregulated AAs and unchanged AAs, while the AS length of downregulated ADs was significantly lower than that of unchanged ADs, ESs, and RIs. There were no significant differences among the three groups (Figure 2F).

For GC content, the GC content of downregulated AAs was significantly higher than that of upregulated AAs, and the GC content of downregulated ESs was significantly higher than that of upregulated ESs and unchanged ESs. The GC content of upregulated RIs was significantly higher than that of upregulated RIs (Figure 2G).

For the AS score, the score of the first 5′ site of upregulated ADs was significantly higher than the score of the first 5′ site of unchanged ADs (Figure 2I), and the score of the second 3′ site of upregulated AAs was significantly higher than the score of the second 3′ locus of unchanged AAs (Figure 2H). Conversely, the score of the 3′ locus of downregulated ESs was significantly higher than that of the other two groups (Figure 2H). Furthermore, the score of the 5′ locus of upregulated RIs was significantly higher than the score of 5′ sites with downregulated RIs and 5′ sites with no change in RIs, and the score of 3’ sites with upregulated RIs was also significantly higher than the other two groups (Figure 2H).

Correlation analysis of DASE-corresponding genes in AS subtypes

Next, we analyzed the total DASEs corresponding to 1,005 genes, and drew heat maps based on the expression of related genes. The heat map showed that the overall gene expression of cluster 3 samples was high, while the overall gene expression of cluster 4 samples was low (Figure 3A).

A total of 32,284 gene sets was downloaded from the MSigDB database. The enrichment score of each sample for all gene sets

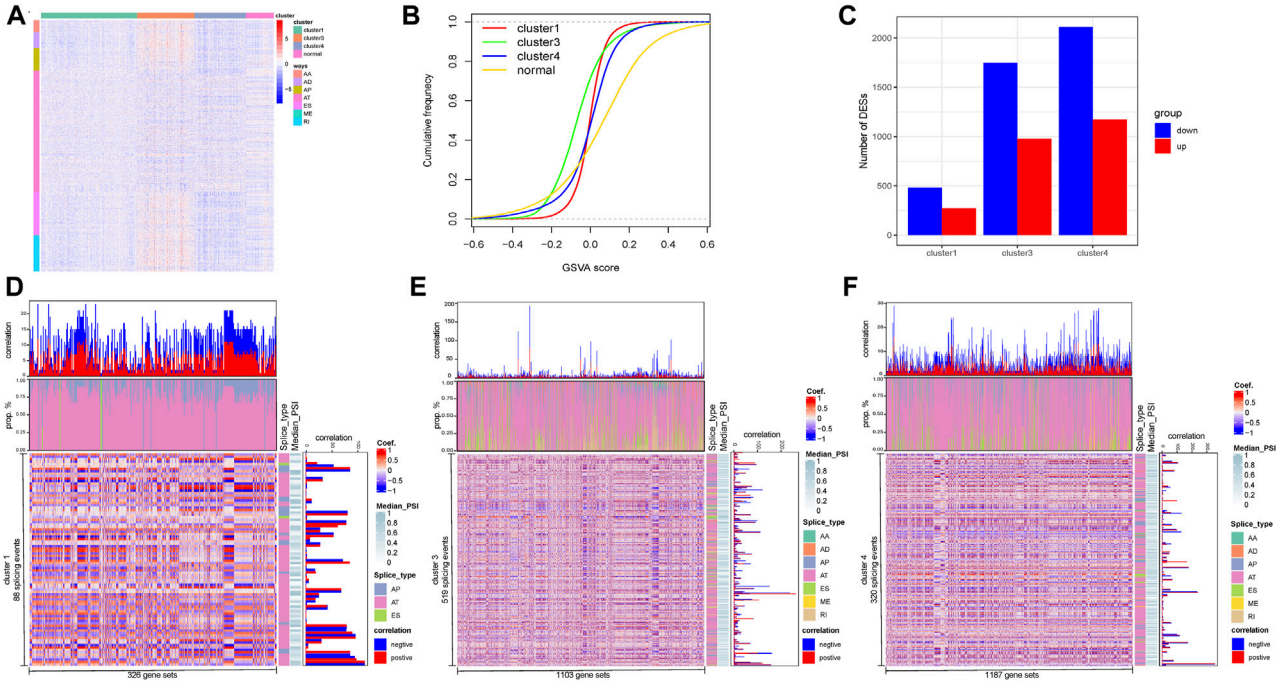

FIGURE 3
Analysis of DASEs Corresponding Genes and Alternative Splicing Events and GSVA Analysis. **(A)** Heat map of DASEs corresponding gene expression. **(B)** Statistics of the number of differential enrichment pathways of each subtype compared with normal samples. **(C)** We exploited a Nomogram to evaluate the prognosis of HCC with prediction model of POLD1 expression and pTNM stage. **(D–F)** Display of strong correlation between differential gene sets and alternative splicing events.

was obtained and the cumulative distribution curve of GSVA scores according to different subtypes was generated. The score curve showed that compared with normal samples, the GSVA score distribution of samples of other subtypes was relatively. The score distribution of cluster 1 samples among subtypes was the most concentrated, while cluster 3 samples had more scores of less than 0, and cluster 4 had more scores of greater than 0 (Figure 3B). After obtaining the DESs of different subtype samples and normal samples, for all subtypes, there were more downregulated enrichment pathways than upregulated enrichment pathways, and cluster 4 samples and normal samples had the most different pathways (Figure 3C, Supplementary Tables S5, S6).

Correlations between differential gene sets within subtypes and AS events were further calculated. According to the interquartile range of the sample PSI, 3,662 AS events were screened, and strong correlations were screened from each subtype according to a Spearman's correlation coefficient greater than 0.6. Eighty-eight splicing events and 326 gene sets in cluster 1 samples had a strong correlation, 519 splicing events in cluster 3 samples and 1,103 gene sets had a strong correlation, and 320 splicing events and 1,187 gene sets in cluster 4 samples were strongly correlated (Figures 3D–F). The above research showed that cluster 4, which had the most splicing events, gene sets, and differential pathways, was closely related to worst overall survival. These results partly describe the differences between the internal and external environments of HCC subtypes and normal tissue cells and the corresponding different splicing regulatory mechanisms.

Correlation analysis of AS pathways, AS events, and AS factors

Twenty-four SPs and 370 SFs were identified from the MSigDB database. In further calculations of the Spearman's correlation coefficients of AS events and SPs and SFs, a scatter plot showed that the coef. of SP and coef. of SF at the same time were greater than 0.5 AS events, including 138 AS events in each subtype. A heat map of the median of related events showed that the PSI value of cluster 3 samples was higher than that of the other subtypes, and the enrichment score of SPs of cluster 3 samples was higher. For SFs, in the cluster 4 samples, some SFs were significantly downregulated (Figures 4A,B; Supplementary Table S7). A Venn diagram of SPs and differential pathways showed that there was one pathway in common, namely GOMF_PRE_MRNA_5_SPLICE_SITE_BINDING (Figure 4C). Therefore, these subtype-specific changes in HCC, including pathway activation and SF expression, may be related to its severe abnormal splicing (Supplementary Table S8). To characterize the splicing-based mechanisms that may contribute to the relative malignancy of HCC, we performed analyses according to the up- and down-regulation of DASE-related gene formation in subtypes. We selected PABPN1, CCDC12, ISY1 and PQBP1 for analysis based on the effect of SFs on survival in HCC. The ΔPSI values were determined for 25 each tumor-normal pair, and eight out of nine AS events showed a significant positive correlation ($p < 0.01$).

The longer spliced isoforms of these SFs were significantly overexpressed in all HCC subtypes and validated by RT-PCR in HCC tissues (Figures 4D,E). These may suggest that longer transcripts of PABPN1, CCDC12 and ISY1 are important for maintaining cancer cell survival ($p < 0.01$). The difference in PSI of PQBP1 was not significant ($p = 0.081$), but the trend was consistent with the other three SFs. Therefore, the upregulation of PSI in HCC may be responsible for the upregulation of SFs such as PABPN1, CCDC12, ISY1 and PQBP1. Overall, the heterogeneity and homogeneity of splicing changes in HCC-related pathways may suggest a distinct role for alternative splicing in tumorigenesis and maintenance of cancer cell survival. Irregular splicing may regulate isoform switching of genes in cancer biological pathways and mRNA expression to promote HCC infiltration and invasion.

Immune-related and clinically relevant analysis of AS subtypes

We further explored the immune status of AS subtypes. A heat map showed that the StromalScore, ImmuneScore, and ESTIMATEScore of the cluster 3 samples were slightly lower than the other two subtypes. From median data, the tumor purity of cancer samples was significantly higher than that of normal samples, and the immune-related scores were significantly lower than normal samples. There was no significant difference in the expression of immune checkpoints and the enrichment scores of related pathways in each subtype. For most immune cells, the immune cell score of normal samples was significantly higher than that of cancer samples. In addition, cluster 4 samples had a higher activated CD4 T cell enrichment score and a lower activated CD8 T cell enrichment score. For G3–4 and hepatitis B patients, the related differences were also obvious (Figure 5A).

Kaplan-Meier analysis was further performed within the group for grade grouping and hepatitis B grouping. This showed that for the G3–4 samples, the Kaplan–Meier curves between the internal AS subtypes were significantly different, and for the samples with hepatitis B, the Kaplan–Meier curves between the internal AS subtypes were significantly different (Figures 5B–E). The above results suggest that the anti-tumor immune response produced by SF can be offset by the tumor micro environment (TME), and aggressive cancer cells with a large number of intracellular mutations and tumor-associated antigens survive immune reprogramming. Therefore, blocking these immunosuppressive molecular pathways should be combined with immunotherapy against neoantigens to regulate the immune response of HCC patients.

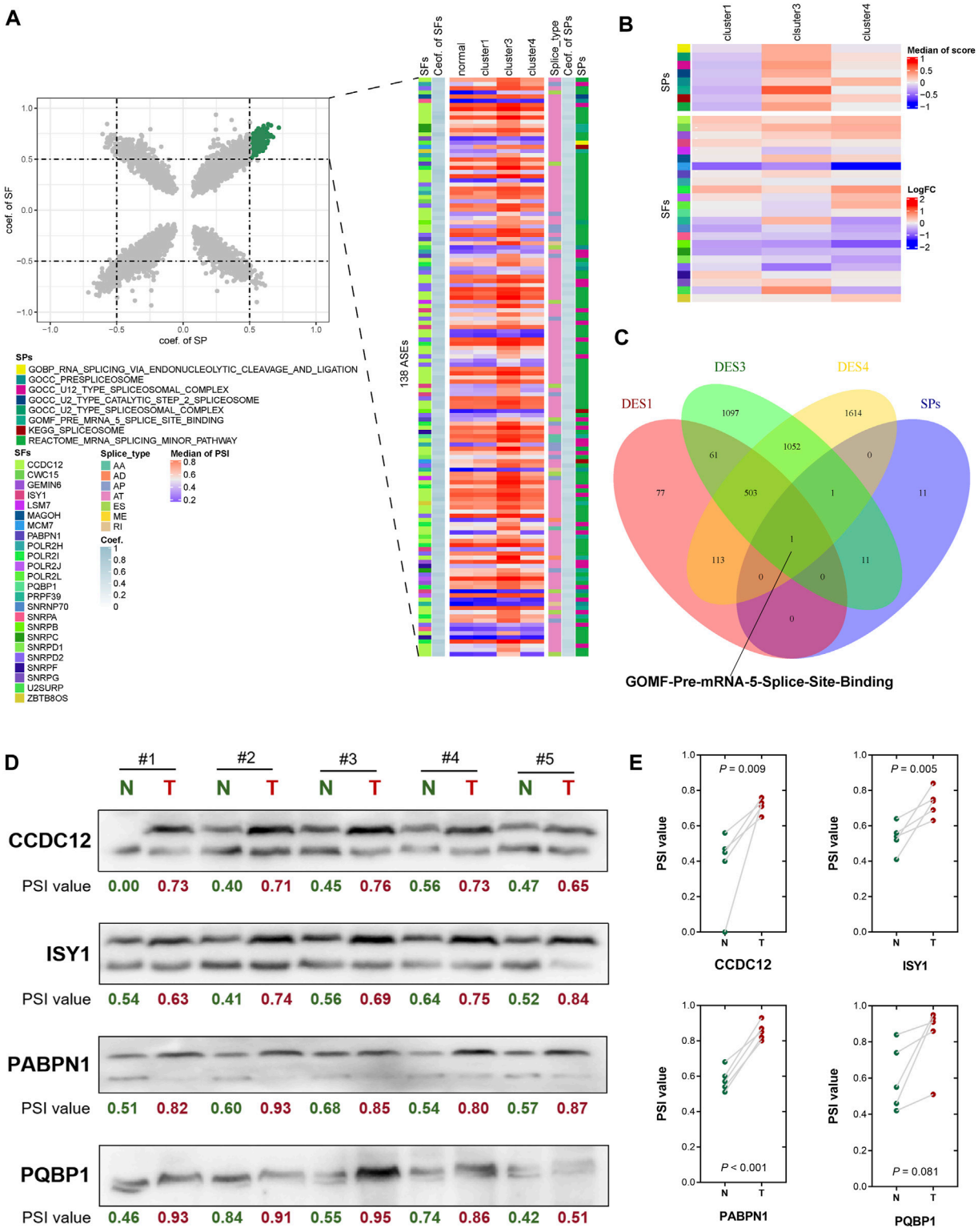

FIGURE 4
Correlation analysis of alternative splicing pathways, alternative splicing events and alternative splicing factors. **(A)** Scatter plot showing the association between alternative splicing events and SPs and SFs. **(B)** Heat map showing the association between alternative splicing events and SPs and SFs. **(C)** Venn diagram shows the common pathways of SPs and differential pathways. **(D)** Differentially expressed splicing transcripts of CCDC12, ISY1, PABPN1 and PQBP1 were validated in human HCC tissues by RT-PCR and consequent agarose gel electrophoresis. PSI of each lane was calculated by the greyscale of the longer transcript divide the sum greyscale of the longer and the shorter transcripts. **(E)** Significance of difference between HCC tumor and adjacent normal tissues for splicing of CCDC12, ISY1, PABPN1 and PQBP1 were evaluated separately by two-tailed paired *t*-test.

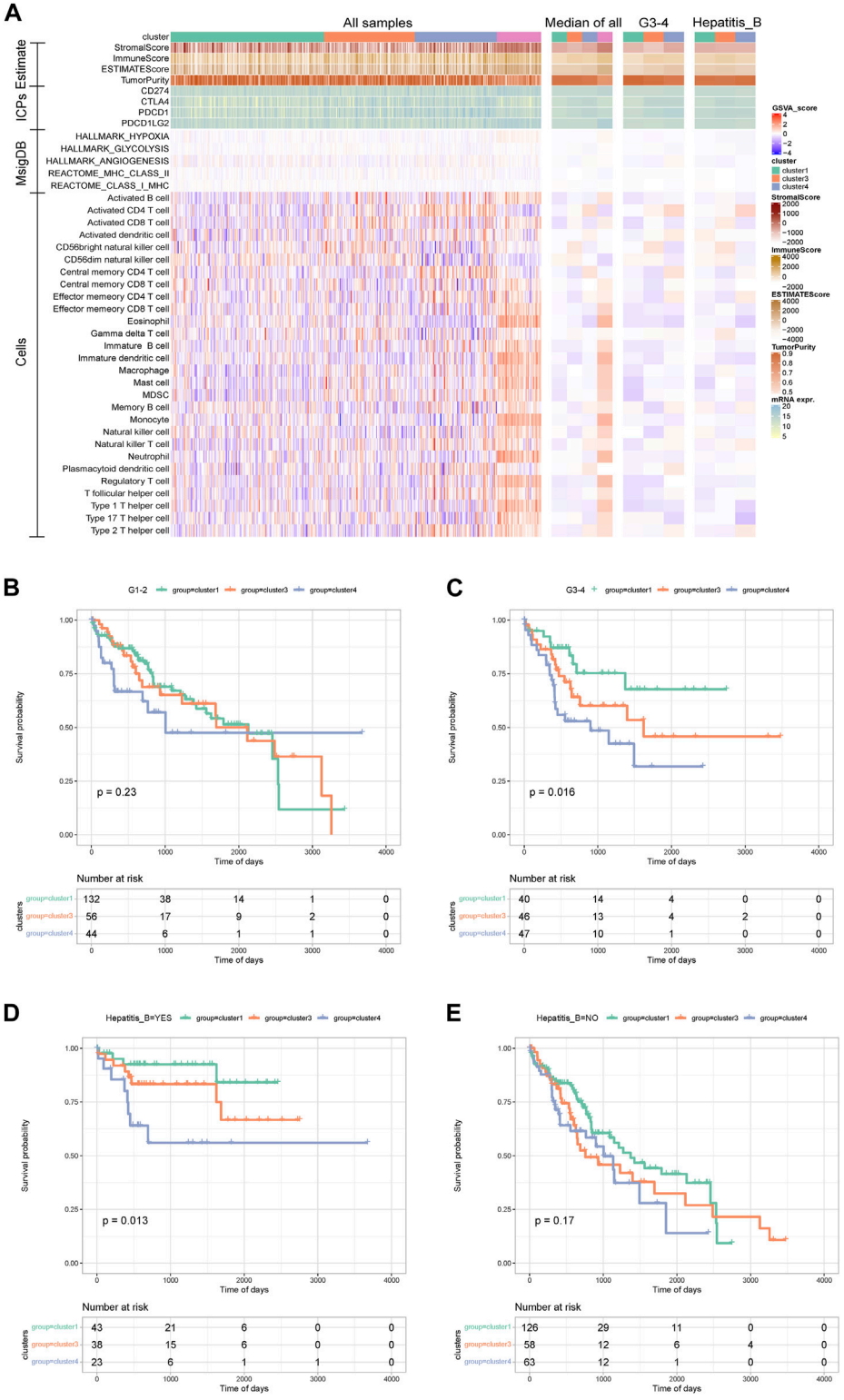

FIGURE 5
Analysis between alternative splicing subtypes and immunity and clinical survival. **(A)**The heat map shows the immune status of alternative splicing subtypes. **(B–E)** KM curve between grade group and Hepatitis_B group.

Combining mRNA expression profiles to predict differences in AS for immunotherapy and drug sensitivity

Using SubMap to predict the possible therapeutic effects of related immunosuppressive agents on different AS subtypes, the results showed that the similarity between cluster 4 samples and CTLA4 response samples reached a significant level, suggesting that CTLA4 inhibitors may have a better effect on cluster 4 samples. (Supplementary Figure S1).

We further predicted the samples' responses to 138 drugs to obtain predicted IC50 values. The results showed that there were significant differences in the degree of response of 111 drugs among the different subtypes (Supplementary Table S9). The IC50 values of bosutinib, dasatinib, midostaurin, elesclomol, pazopanib, bortezomib, sorafenib, docetaxel, and gefitinib were plotted in box plots. For bosutinib, dasatinib, midostaurin, elesclomol, pazopanib, and bortezomib, the efficacy of cluster 1 and cluster 4 was relatively good and the efficacy of cluster 3 was relatively poor, while cluster 3 mainly

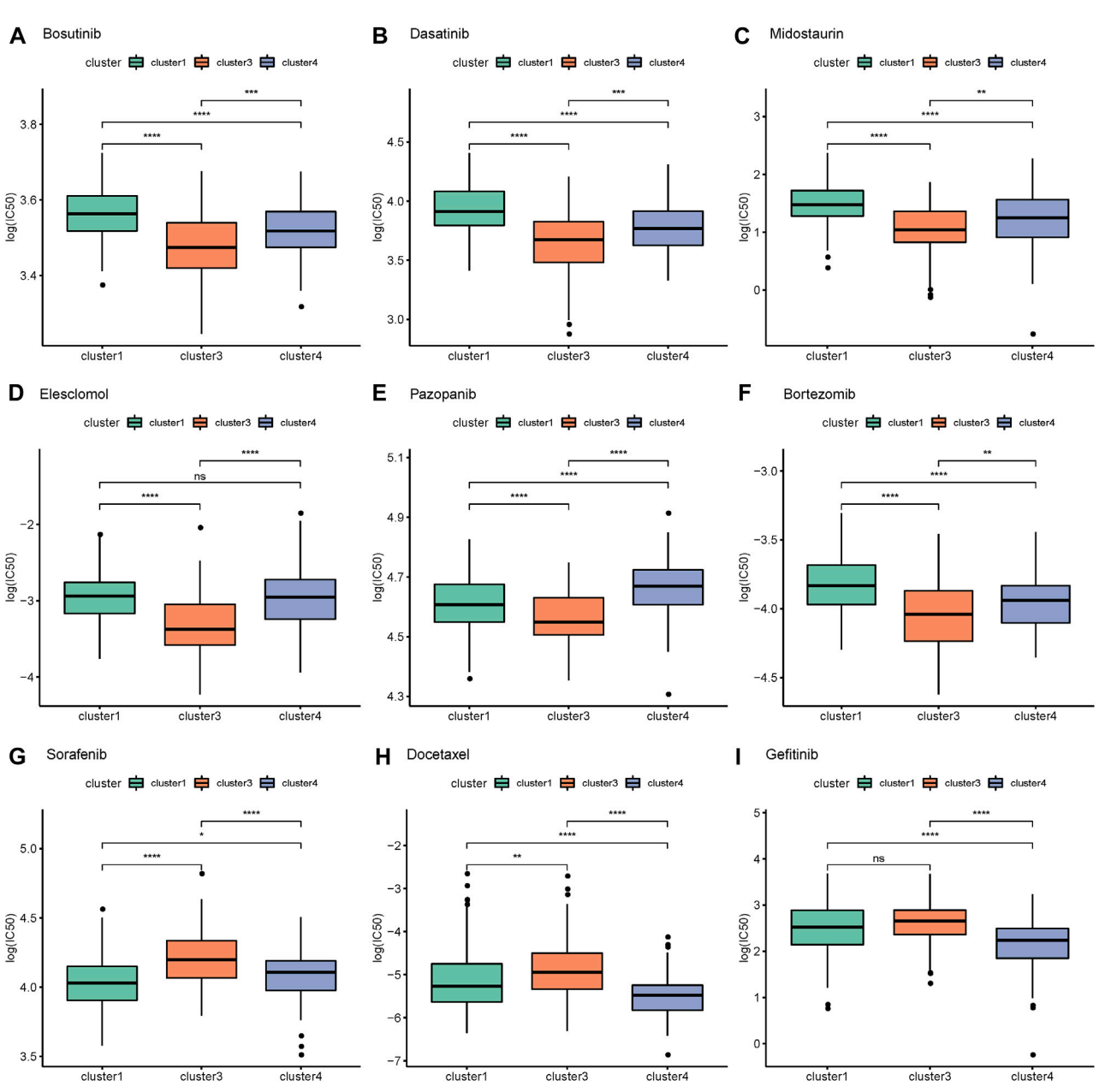

FIGURE 6
Response of alternative splicing subtypes to drugs. **(A)** Bosutinib **(B)** Dasatinib **(C)** Midostaurin **(D)** Elesclomol **(E)** Pazopanib **(F)** Bortezomib **(G)** Sorafenib **(H)** Docetaxel **(I)** Gefitinib.

responded well to sorafenib, docetaxel, and gefitinib (Figures 6A–I) 0Screening of AS events and construction of a prognostic model of AS.

According to the obtained PSI values of DASEs, the differential AS events between subtypes were screened. There were 1,109 DASEs between cluster 1 and cluster 3, 1,154 DASEs between cluster 3 and cluster 4, and 1,177 DASEs between cluster 1 and cluster 4. Intersection of the three clusters resulted in a total of 455 DASEs for subsequent analysis (Figure 7A). Using cancer samples, on the basis of PSI values of the shared DASEs obtained in the previous step combined with the OS data, batch Cox one-way regression analysis was performed on differential AS, and 111 survival-related DASEs were obtained (Figure 7B).

Lasso regression was then performed on 111 survival-related DASEs, and 20 AS events were obtained to construct a risk model. Regression coefficients and PSI values were analyzed to obtain the following risk scores: PSI39967 * (−5.5748) + PSI64018 * (−2.0928) + PSI46796 * (−0.5633) + PSI83140 * (−0.3544) + PSI44266 * (0.3162) + PSI85919 * (−0.3101) + PSI50488 * (−0.2602) + PSI19307 * (−0.1502) + PSI17008 * (−0.0950) + PSI19309 * (1.0474) E−13) + PSI50489 * 0.0014 + PSI85920 * 0.0023 + PSI85601 * 0.0223 + PSI58889 * 0.5534 + PSI1730 * 0.6888 + PSI24866 * 1.0308 + PSI61665 * 1.0423 + PSI 82016 * 1.6102 + PSI18599 * 40.6609 + PSI24760 * 51.4456 (Figures 7C–E).

Further validation of the prognostic model of AS

According to the risk score of the samples, the high and low risk groups were divided by the median as the node, and a Kaplan–Meier curve was drawn on the basis of the OS data and DFI data. The results showed that the difference between

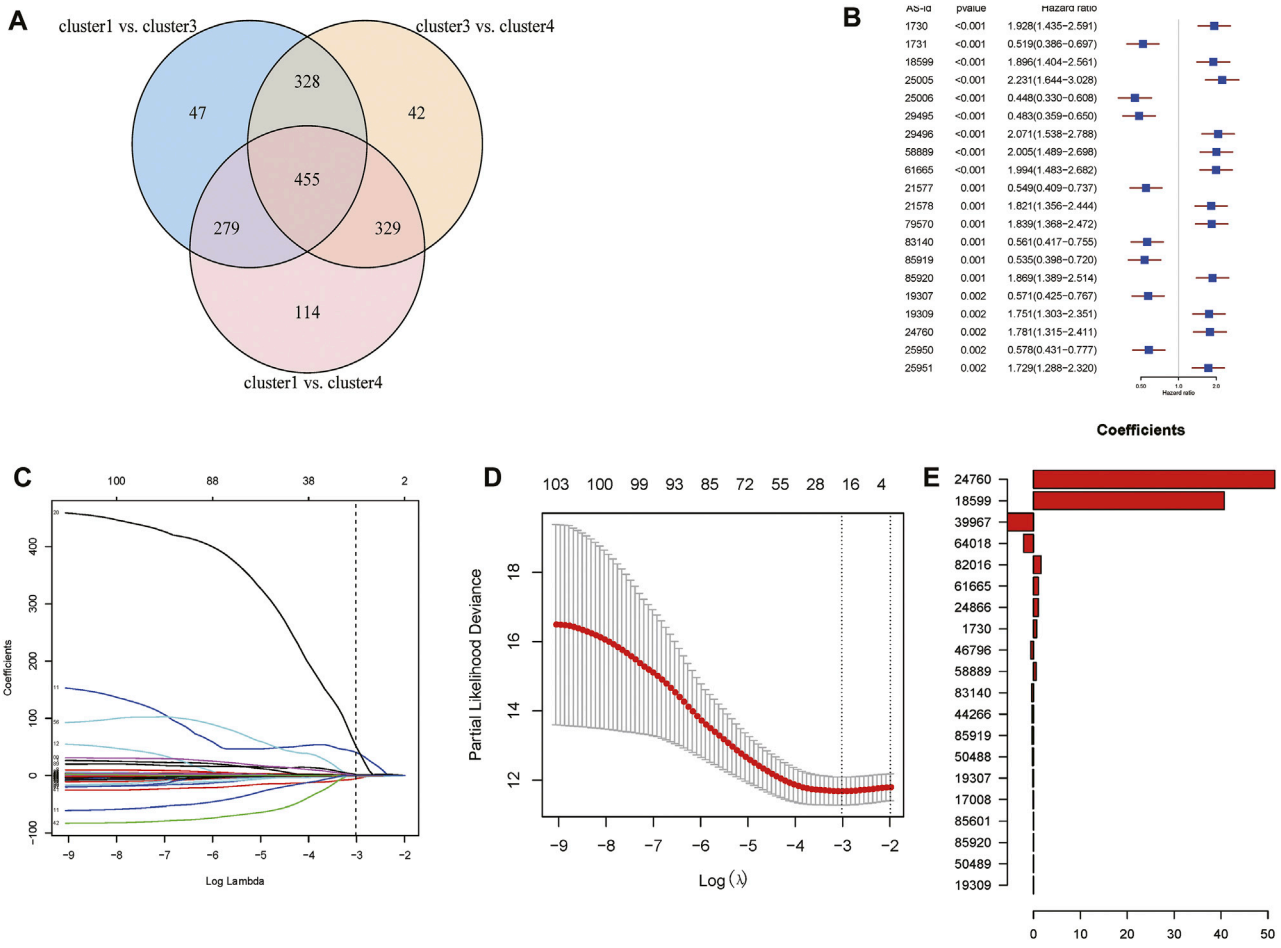

FIGURE 7
Analysis of Differential Alternative Splicing Events between Subtypes. **(A)**Venn diagram of alternative splicing events for differences between subtypes. **(B)** Top 20 single factor cox regression results. **(C)** Display the corresponding changes of lambda and variable coefficients. **(D)** Obtain lambda.min through cross-validation. **(E)** Display the regression coefficients corresponding to the variables after screening.

the high and low risk groups was significant (OS, $p < 0.0001$; DFI, $p = 0.0083$; Figures 8A–F). The sample risk score was used as the model prediction result, combined with the survival data to calculate the AUC value of the model, and then an ROC curve was drawn. The AUC values of 1-, 3-, and 5-year OS were all greater than 0.7, indicating that the model has good performance (Figure 8G). A Sankey diagram was constructed to show the relationship between risk score grouping, AS subtypes, and stage and grade groupings. As shown in Figure 8H, most of the cluster 1 samples belonged to the low-risk group, most of the cluster 1 samples were G1 and stage I samples, and most of the cluster 4 samples belonged to the high-risk group, consistent with the results of the Kaplan-Meier analysis.

Discussion/conclusion

HCC is the most common primary liver cancer. Liver cancer is the sixth most common cancer and the second leading cause of cancer-related deaths worldwide. In the past few decades, the incidence of liver cancer and liver cancer-related deaths has increased in many parts of the world, including China (Siegel et al., 2021). Sorafenib remains the only targeted drug for the treatment of advanced liver cancer. As a chemotherapy-resistant tumor, HCC has an unsatisfactory response to radiotherapy and chemotherapy. In addition, patients with advanced liver cancer usually have obvious underlying liver disease, and thus the prognosis of patients is often poor and the mechanism is not understood.

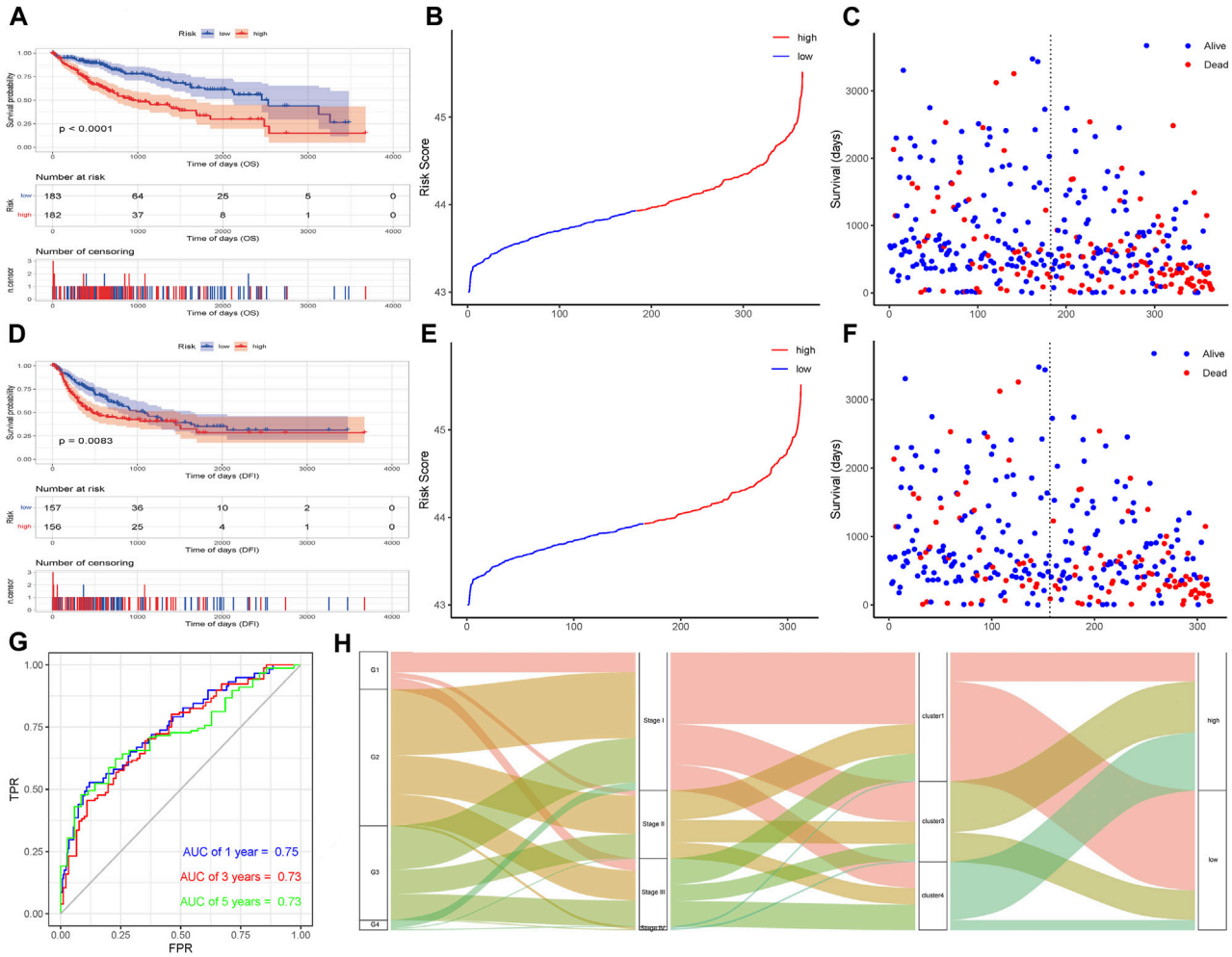

FIGURE 8
Effectiveness verification of a risk model based on PSI events. **(A)**Build model KM curve verification based on OS-based lasso regression. **(B)** Curve graph of risk scores of all samples based on OS. **(C)** Scatter plot of survival time of all samples based on OS. **(D)** Build model KM based on lasso regression of DFI Curve verification. **(E)** Curve graph of risk scores of all samples based on DFI. **(F)** Scatter plot of survival time of all samples based on DFI. **(G)** Time-based ROC curve. **(H)** Sankey diagram of clinical traits, risk grouping and alternative splicing subtype.

Alternative splicing can be regulated by many different mechanisms, such as histone modification and DNA methylation, which are usually associated with specific SFs or transcriptional elongation (Li et al., 2018; Sessa et al., 2019). The latest research identified a significant correlation between intragenic DNA methylation and exon usage in solid tumors (Sun et al., 2020). There are also reports that mitochondria are involved in the regulation of transcriptional activity, which has a great influence on splicing regulation (Guantes et al., 2015). Alternative splicing is the main mechanism to increase the transcriptional diversity of eukaryotes (Pan et al., 2008; Wang et al., 2008). Dozens of abnormal splice variants are associated with human diseases (Schrock et al., 2016; Urbanski et al., 2018; Di et al., 2019). Studies have shown that these AS events play wide-ranging roles in the process of carcinogenesis, participating in cell proliferation, apoptosis, epithelial–mesenchymal transition, hypoxia, angiogenesis, and immune escape (Chen et al., 2018; Du et al., 2022). These previous studies have shown that in addition to classic cis-/trans-acting regulation, there are many other mechanisms of AS regulation (Yae et al., 2012; Picard, 2022; Zhang et al., 2022). Here, we use GSVA to conduct a comprehensive pathway analysis of 32,284 gene sets in MSigDB. We demonstrated that splicing regulation is also affected by many pathways, including negative/positive regulation of mRNA splicing by spliceosomes, pre-mRNA 5′-splice site binding, and the mRNA splicing minor pathway, among others. These pathways may constitute the basic environment for irregular splicing in HCC subtypes and affect the TME. We also observed changes in the mRNA expression of several SFs in different HCC subtypes. To determine how these changes are related to pathway activation and AS regulation, more research is required.

Future research aims to determine the molecular drivers of the transition from cluster 1 to cluster 4 subtypes. These changes may be triggered by changes in the genome or by epigenetic or transcriptional regulators that have been shown to drive splicing factor changes in other tumor types. Understanding these mechanisms will allow us to determine the development of AS-based HCC treatments. AS research is moving in the direction of making full use of the potential of AS in precision medicine.

In this analysis, we identified AS subtypes through unsupervised clustering, analyzed the characteristics of different spliced subtypes, obtained DASEs, and combined the findings with GSVA enrichment analysis to explore the differences in the subtypes. Finally, on the basis of the DASEs of different subtypes, the survival-related AS time was identified, and the PSI value was used to construct a risk proportional regression model to guide prognosis. We systematically described clinical, splicing, transcriptomic, genomic, and immunological characteristics, and identified the underlying regulatory mechanisms of AS in HCC subtypes (Supplementary Figure S2).

Our research shows that the splicing regulation of SFs may play a role in the transformation and survival of HCC cancer cells. We studied AS comprehensively and systematically and used TCGA data to explore possible non-classical regulatory mechanisms in HCC. The data sample size of our research was sufficient, and the results of the verification data are good and have strong statistical significance, covering a wide range of fields. Our findings may provide the foundation for more in-depth research in the future, such as studies of the splicing regulation mechanism, cancer biomarker design, targeted drug screening, and other clinical applications.

Data availability statement

The original contributions presented in the study are included in the article/Supplementary Material, further inquiries can be directed to the corresponding author.

Ethics statement

The study was approved by the ethics committee of the Xinhua Hospital affiliated to Shanghai Jiao Tong University School of Medicine (Shanghai, China). Written informed consent was obtained from all participants.

Author contributions

WL and SZ carried out the molecular genetic studies, participated in the sequence alignment and drafted the manuscript. LP, JW, and TW carried out the immunoassays. CL, HD, BZ, and JL participated in the sequence alignment. LP, JX, and TW participated in the design of the study and performed the statistical analyses. HH, SZ, WX, JX, and HZ conceived the study, participated in the study design and coordination and helped to draft the manuscript. All authors contributed to the article and approved the submitted version.

Funding

This study was supported by grants from the National Natural Science Foundation of China (No. 82103520, 81772531), National Key Research and Development Program (2020YFC0122305), the General Program from the National Natural Science Foundation of China (82070619), the Medical Engineering Cross Fund of Shanghai Jiaotong University (No. YG2021QN50), Program of Shanghai Academic/Technology Research Leader (19XD1425000), Program of Shanghai for Medical Guide (18411968900), Program of Shanghai for Clinical Skill Training and Clinical Practice Innovations (SHDC2020CR4027).

Acknowledgments

We thank H. Nikki March, from Liwen Bianji (Edanz) (www.liwenbianji.cn), for editing the English text of a draft of this manuscript.

Conflict of interest

The authors declare that the research was conducted in the absence of any commercial or financial relationships that could be construed as a potential conflict of interest.

Publisher's note

All claims expressed in this article are solely those of the authors and do not necessarily represent those of their affiliated organizations, or those of the publisher, the editors and the reviewers. Any product that may be evaluated in this article, or claim that may be made by its manufacturer, is not guaranteed or endorsed by the publisher.

Supplementary material

The Supplementary Material for this article can be found online at: https://www.frontiersin.org/articles/10.3389/fphar.2022.1019988/full#supplementary-material

SUPPLEMENTARY FIGURE S1
Significant degree of similarity between alternative splicing subtypes and various responses.

SUPPLEMENTARY FIGURE S2
Flowchart of this study.

References

Ay, F., Kellis, M., and Kahveci, T. (2011). SubMAP: Aligning metabolic pathways with subnetwork mappings. *J. Comput. Biol.* 18, 219–235. doi:10.1089/cmb.2010.0280

Barrett, T., Wilhite, S. E., Ledoux, P., Evangelista, C., Kim, I. F., Tomashevsky, M., et al. (2013). NCBI geo: Archive for functional genomics data sets--update. *Nucleic Acids Res.* 41, D991–D995. doi:10.1093/nar/gks1193

Bishay, V. L., Biederman, D. M., Ward, T. J., van der Bom, I. M., Patel, R. S., Kim, E., et al. (2016). Transradial approach for hepatic radioembolization: Initial results and technique. *AJR. Am. J. Roentgenol.* 207, 1112–1121. doi:10.2214/ajr.15.15615

Chen, C., Zhao, S., Karnad, A., and Freeman, J. W. (2018). The biology and role of CD44 in cancer progression: Therapeutic implications. *J. Hematol. Oncol.* 11, 64. doi:10.1186/s13045-018-0605-5

Chen, L., Zhang, K., Sun, J., Tang, J., and Zhou, J. (2021). Development and validation of an autophagy-stroma-based microenvironment gene signature for risk stratification in colorectal cancer. *Onco. Targets. Ther.* 14, 3503–3515. doi:10.2147/ott.S312003

Di, C., Syafrizayanti, Q., Zhang, Y., Chen, Y., Wang, X., Zhang, Q., et al. (2019). Function, clinical application, and strategies of Pre-mRNA splicing in cancer. *Cell Death Differ.* 26, 1181–1194. doi:10.1038/s41418-018-0231-3

Di Francesco, F., De Marco, G., Sommella, A., and Lanza, A. (2019). Splinting vs not splinting four implants supporting a maxillary overdenture: A systematic review. *Int. J. Prosthodont.* 32, 509–518. doi:10.11607/ijp.6333

Du, Y., Dennis, B., Ramirez, V., Li, C., Wang, J., and Meireles, C. L. (2022). Experiences and disease self-management in individuals living with chronic kidney disease: Qualitative analysis of the national kidney foundation's online community. *BMC Nephrol.* 2 (2), 88–101. doi:10.1186/s12882-022-02717-7

Engebretsen, S., and Bohlin, J. (2019). *Statistical predictions with glmnet. Clin. Epigenetics* 11, 123. doi:10.1186/s13148-019-0730-1

Fu, X. D., and Ares, M., Jr. (2014). Context-dependent control of alternative splicing by RNA-binding proteins. *Nat. Rev. Genet.* 15, 689–701. doi:10.1038/nrg3778

Galun, D., Srdic-Rajic, T., Bogdanovic, A., Loncar, Z., and Zuvela, M. (2017). *Targeted therapy and personalized medicine in hepatocellular carcinoma: Drug resistance, mechanisms, and treatment strategies. J. Hepatocell. Carcinoma* 4, 93–103. doi:10.2147/jhc.S106529

Gamundi, M. J., Hernan, I., Muntanyola, M., Maseras, M., López-Romero, P., Alvarez, R., et al. (2008). Transcriptional expression of cis-acting and trans-acting splicing mutations cause autosomal dominant retinitis pigmentosa. *Hum. Mutat.* 29, 869–878. doi:10.1002/humu.20747

Geeleher, P., Cox, N., and Huang, R. S. (2014). pRRophetic: an R package for prediction of clinical chemotherapeutic response from tumor gene expression levels. *PLoS One* 9, e107468. doi:10.1371/journal.pone.0107468

Guantes, R., Rastrojo, A., Neves, R., Lima, A., Aguado, B., and Iborra, F. J. (2015). *Global variability in gene expression and alternative splicing is modulated by mitochondrial content. Genome Res.* 25, 633–644. doi:10.1101/gr.178426.114

Guo, N. L., and Wan, Y. W. (2014). Network-based identification of biomarkers coexpressed with multiple pathways. *Cancer Inf.* 13, 37–47. doi:10.4137/cin.S14054

Guro, H., Cho, J. Y., Han, H. S., Yoon, Y. S., Choi, Y., and Periyasamy, M. (2016). *Current status of laparoscopic liver resection for hepatocellular carcinoma. Clin. Mol. Hepatol.* 22, 212–218. doi:10.3350/cmh.2016.0026

Hänzelmann, S., Castelo, R., and Guinney, J. (2013). Gsva: Gene set variation analysis for microarray and RNA-seq data. *BMC Bioinforma.* 14, 7. doi:10.1186/1471-2105-14-7

Kim, H. J., Bae, M., and Jin, D. (2018). On a robust MaxEnt process regression model with sample-selection. *Entropy (Basel)* 20, E262. doi:10.3390/e20040262

Li, S., Zhang, J., Huang, S., and He, X. (2018). Genome-wide analysis reveals that exon methylation facilitates its selective usage in the human transcriptome. *Brief. Bioinform.* 19, 754–764. doi:10.1093/bib/bbx019

Liu, W. R., Li, C. Y., Xu, W. H., Liu, X. J., Tang, H. D., and Huang, H. N. (2020). Genome-wide analyses of the prognosis-related mRNA alternative splicing landscape and novel splicing factors based on large-scale low grade glioma cohort. *Aging (Albany NY)* 12, 13684–13700. doi:10.18632/aging.103491

Liu, W., Xu, W., Chen, Y., Gu, L., Sun, X., Qu, Y., et al. (2020). Elevated double-strand break repair protein RAD50 predicts poor prognosis in Hepatitis B virus-related hepatocellular carcinoma: A study based on Chinese high-risk cohorts. *J. Cancer* 11, 5941–5952. doi:10.7150/jca.46703

Paillusseau, C., Gandar, F., Schilliger, L., and Chetboul, V. (2020). Two-dimensional echocardiographic measurements in the ball Python (Python regius). *J. Zoo. Wildl. Med.* 50, 976–982. doi:10.1638/2019-0032

Pan, Q., Shai, O., Lee, L. J., Frey, B. J., and Blencowe, B. J. (2008). *Deep surveying of alternative splicing complexity in the human transcriptome by high-throughput sequencing. Nat. Genet.* 40, 1413–1415. doi:10.1038/ng.259

Picard, M. (2022). Why do we care more about disease than health? *Phenomics* 2, 145–155. doi:10.1007/s43657-021-00037-8

Ritchie, M. E., Phipson, B., Wu, D., Hu, Y., Law, C. W., Shi, W., et al. (2015). Limma powers differential expression analyses for RNA-sequencing and microarray studies. *Nucleic Acids Res.* 43, e47. doi:10.1093/nar/gkv007

Rizvi, A. A., Karaesmen, E., Morgan, M., Preus, L., Wang, J., Sovic, M., et al. (2019). gwasurvivr: an R package for genome-wide survival analysis. *Bioinformatics* 35, 1968–1970. doi:10.1093/bioinformatics/bty920

Robinson, M. D., McCarthy, D. J., and Smyth, G. K. (2010). edgeR: a Bioconductor package for differential expression analysis of digital gene expression data. *Bioinformatics* 26, 139–140. doi:10.1093/bioinformatics/btp616

Saffo, S., and Taddei, T. H. (2019). Systemic management for advanced hepatocellular carcinoma: A review of the molecular pathways of carcinogenesis, current and emerging therapies, and novel treatment strategies. *Dig. Dis. Sci.* 64, 1016–1029. doi:10.1007/s10620-019-05582-x

Schrock, A. B., Frampton, G. M., Suh, J., Chalmers, Z. R., Rosenzweig, M., Erlich, R. L., et al. (2016). Characterization of 298 patients with lung cancer harboring MET exon 14 skipping alterations. *J. Thorac. Oncol.* 11, 1493–1502. doi:10.1016/j.jtho.2016.06.004

Sessa, A., Fagnocchi, L., Mastrototaro, G., Massimino, L., Zaghi, M., Indrigo, M., et al. (2019). SETD5 regulates chromatin methylation state and preserves global transcriptional fidelity during brain development and neuronal wiring. *Neuron* 104, 271–289. e213. doi:10.1016/j.neuron.2019.07.013

Shiraishi, Y., Kataoka, K., Chiba, K., Okada, A., Kogure, Y., Tanaka, H., et al. (2018). A comprehensive characterization of cis-acting splicing-associated variants in human cancer. *Genome Res.* 28, 1111–1125. doi:10.1101/gr.231951.117

Siegel, R. L., Miller, K. D., Fuchs, H. E., and Jemal, A. (2021). Cancer Statistics, 2021. *Ca. Cancer J. Clin.* 71, 7–33. doi:10.3322/caac.21654

Sun, J. Y., Yin, T., Zhang, X. Y., and Lu, X. J. (2019). *Therapeutic advances for patients with intermediate hepatocellular carcinoma*. *J. Cell. Physiol.* 234, 12116–12121. doi:10.1002/jcp.28019

Sun, X., Tian, Y., Wang, J., Sun, Z., and Zhu, Y. (2020). Genome-wide analysis reveals the association between alternative splicing and DNA methylation across human solid tumors. *BMC Med. Genomics* 13, 4. doi:10.1186/s12920-019-0654-9

Sung, H., Ferlay, J., Siegel, R. L., Laversanne, M., Soerjomataram, I., Jemal, A., et al. (2021). Global cancer Statistics 2020: GLOBOCAN estimates of incidence and mortality worldwide for 36 cancers in 185 countries. *Ca. Cancer J. Clin.* 71, 209–249. doi:10.3322/caac.21660

Urbanski, L. M., Leclair, N., and Anczuków, O. (2018). Alternative-splicing defects in cancer: Splicing regulators and their downstream targets, guiding the way to novel cancer therapeutics. *Wiley Interdiscip. Rev. RNA* 9, e1476. doi:10.1002/wrna.1476

Wang, E. T., Sandberg, R., Luo, S., Khrebtukova, I., Zhang, L., Mayr, C., et al. (2008). Alternative isoform regulation in human tissue transcriptomes. *Nature* 456, 470–476. doi:10.1038/nature07509

Wang, S., Su, W., Zhong, C., Yang, T., Chen, W., Chen, G., et al. (2020). An eight-CircRNA assessment model for predicting biochemical recurrence in prostate cancer. *Front. Cell Dev. Biol.* 8, 599494. doi:10.3389/fcell.2020.599494

Yae, T., Tsuchihashi, K., Ishimoto, T., Motohara, T., Yoshikawa, M., Yoshida, G. J., et al. (2012). Alternative splicing of CD44 mRNA by ESRP1 enhances lung colonization of metastatic cancer cell. *Nat. Commun.* 3, 883. doi:10.1038/ncomms1892

Yates, A. D., Achuthan, P., Akanni, W., Allen, J., Allen, J., Alvarez-Jarreta, J., et al. (2020). Ensembl 2020. *Nucleic Acids Res.* 48, D682–d688. doi:10.1093/nar/gkz966

Yoon, Y. I., and Lee, S. G. (2019). Living donor liver transplantation for hepatocellular carcinoma: An asian perspective. *Dig. Dis. Sci.* 64, 993–1000. doi:10.1007/s10620-019-05551-4

Zhang, L., Su, W., Liu, S., Huang, C., Ghalandari, B., Divsalar, A., et al. (2022). Recent progresses in electrochemical DNA biosensors for MicroRNA detection. *Phenomics* 2, 18–32. doi:10.1007/s43657-021-00032-z

Zhao, S., Wei, C., Tang, H., Ding, H., Han, B., Chen, S., et al. (2021). Elevated DNA polymerase delta 1 expression correlates with tumor progression and immunosuppressive tumor microenvironment in hepatocellular carcinoma. *Front. Oncol.* 11, 736363. doi:10.3389/fonc.2021.736363

Zhao, S., Zhang, Y., Lu, X., Ding, H., Han, B., Song, X., et al. (2021). CDC20 regulates the cell proliferation and radiosensitivity of P53 mutant HCC cells through the Bcl-2/Bax pathway. *Int. J. Biol. Sci.* 17, 3608–3621. doi:10.7150/ijbs.64003

Zheng, J., Zhang, T., Guo, W., Zhou, C., Cui, X., Gao, L., et al. (2020). Integrative analysis of multi-omics identified the prognostic biomarkers in acute myelogenous leukemia. *Front. Oncol.* 10, 591937. doi:10.3389/fonc.2020.591937

frontiers | Frontiers in Pharmacology

TYPE Mini Review
PUBLISHED 12 October 2022
DOI 10.3389/fphar.2022.1034129

OPEN ACCESS

EDITED BY
Zhijie Xu,
Central South University, China

REVIEWED BY
Yaming Shan,
Jilin University, China
Nan Song,
Capital Medical University, China

*CORRESPONDENCE
Xin Wu,
wuxindoctor@qq.com
Xuelei Ma,
drmaxuelei@gmail.com

†These authors share first authorship

SPECIALTY SECTION
This article was submitted to Pharmacology of Anti-Cancer Drugs, a section of the journal Frontiers in Pharmacology

RECEIVED 01 September 2022
ACCEPTED 20 September 2022
PUBLISHED 12 October 2022

CITATION
Zheng A, Zhang L, Yang J, Yin X, Zhang T, Wu X and Ma X (2022), Physical activity prevents tumor metastasis through modulation of immune function. *Front. Pharmacol.* 13:1034129. doi: 10.3389/fphar.2022.1034129

Physical activity prevents tumor metastasis through modulation of immune function

Aiping Zheng[1,2†], Lei Zhang[3†], Jiaqing Yang[4], Xiaomeng Yin[1], Tao Zhang[1], Xin Wu[2,5*] and Xuelei Ma[1*]

[1]Division of Biotherapy, Cancer Center, West China Hospital, Cancer Center, Sichuan University, Chengdu, China, [2]Head and Neck Oncology Ward, Cancer Center, West China Hospital, Cancer Center, Sichuan University, Chengdu, China, [3]Department of Obstetrics & Gynecology, Chengdu First People's Hospital & Chengdu Integrated TCM & Western Medicine Hospital, Chengdu, China, [4]West China School of Medicine, West China Hospital, Sichuan University, Chengdu, China, [5]Head and Neck Oncology Ward, Division of Radiotherapy Oncology, Cancer Center, West China Hospital, Chengdu, China

Metastasis is responsible for 90% of deaths in cancer patients. Most patients diagnosed with metastatic cancer will die within 5 years. PA is good for health and has become an emerging adjuvant therapy for cancer survivors. Regular moderate exercise substantially lowers the incidence and recurrence of several cancers, alleviates cancer-related adverse events, enhances the efficacy of anti-cancer treatments, and improves the quality of life of cancer patients. Revealing the mechanisms of PA inhibiting tumor metastasis could upgrade our understanding of cancer biology and help researchers explore new therapeutic strategies to improve survival in cancer patients. However, it remains poorly understood how physical activity prevents metastasis by modulating tumor behavior. The immune system is involved in each step of tumor metastasis. From invasion to colonization, immune cells interact with tumor cells to secret cytokines and proteases to remodel the tumor microenvironment. Substantial studies demonstrated the ability of physical activity to induce antitumor effects of immune cells. This provides the possibility that physical activity can modulate immune cells behavior to attenuate tumor metastasis. The purpose of this review is to discuss and summarize the critical link between immune function and exercise in metastasis prevention.

KEYWORDS

physical activity, tumor metastasis, microenvironment, immune function, immune cells

1 Introduction

Cancer metastasis is an important cause of death in cancer patients, with up to 90% of solid tumor patients dying from metastasis (Steeg, 2016). Most patients diagnosed with metastatic cancer will die within 5 years. The majority of current treatments concentrate on resection or elimination of primary tumor. Moreover, some clinical treatment

strategies such as surgery have been demonstrated to aggravate cancer metastasis (Ma et al., 2019). Finding a safe and effective therapy for metastasis remains urgent.

Physical activity (PA) is good for improving physical and mental health. Nowadays, PA has become an important adjuvant therapy for cancer patients and has a remarkable influence on reinforcing conventional cancer therapies (Schmitz et al., 2019). Compared to other cancer treatments, PA has almost no toxic side effects, shows significant safety, and reduces treatment-related adverse events. According to the World Health Organization (WHO), cancer survivors should undertake at least 150–300 min of moderate intensity physical activity, or 75 min of vigorous intensity physical activity per week (Bull et al., 2020). Recently, PA has been shown to reduce the incidence of various cancers and improve the survival of cancer patients. A previous prospective cohort study reported that PA was negatively correlated with the incidence of post-menopausal breast cancer (Bellocco et al., 2016). Besides breast cancer, compelling evidence revealed that PA reduced the risk of additional cancer types, including colon, kidney, endometrial, bladder, esophageal and stomach cancers (Rock et al., 2020). Some prospective observational studies found that PA after cancer diagnosis may decrease cancer mortality, especially in colon (Meyerhardt et al., 2006), breast (Rock et al., 2020) and endometrial (Friedenreich et al., 2020) cancers. In addition, PA has been shown to improve the fatigue and quality of life (QoL) of cancer survivors, relieving anxiety and depression (Schmidt et al., 2015). However, whether PA has beneficial effects on metastasis is more attractive. Revealing the mechanisms of PA inhibiting tumor metastasis could upgrade our understanding of cancer biology and help researchers explore new therapeutic strategies to improve survival in cancer patients. In order to explore the potential mechanism linking PA with metastasis, some preclinical studies established various exercising animal models, especially running and swimming.

The immune system can effectively prevent the occurrence, development and metastasis of primary tumors through immune surveillance. Immune cells can recognize tumor-specific antigens and destroy cancer cells. Recently, some studies suggested that the modulation of the immune system through PA can significantly affect the exercise-dependent prevention of tumor metastasis (Lucia and Ramírez, 2016; Febbraio, 2017). Therefore, the aim of this review was to discuss and summarize recent findings that highlight the critical link between immune function and exercise in metastasis prevention.

2 Tumor metastasis and Physical activity

Tumor metastasis is a tangled and complicated process that can be categorized into five stages: invasion, intravasation, circulation, extravasation, and colonization. The cells were isolated from the primary tumor and acquired an invasive mesenchymal phenotype. In turn, invasive tumor cells infiltrate the blood vessels, a process closely related to vascular permeability and the interaction between tumor cells and endothelial cells. Once in circulation, invasive tumor cells are called circulating tumor cells (CTCs), and they confront challenges such as shear stress, oxidative stress, and immune surveillance. A few surviving CTCs invade blood vessels and colonize distant tissues, forming metastases. Emerging evidence suggests that physical exercise inhibits not only the invasion of tumor cells, but also the survival and distant colonization of circulating tumor cells. A schematic illustration of the association of exercise and metastasis is shown in Figure 1.

2.1 Physical activity and invasion

PA has been confirmed to attenuate the invasion of tumor cells *via* inhibiting epithelial-mesenchymal transition (EMT). A study showed that voluntary exercise led to an intratumor increase in E-cadherin levels and an intratumor decrease in the nuclear levels of *β*-catenin in ApcMin/+ mice (Ju et al., 2008). As is known to all, decreased expression of E-cadherin and increased expression of vimentin are the main characteristics of EMT. PA regulates multiple pathways to attenuate EMT. Moderate swimming could suppress EMT induced by TGF-β in transplanted hepatocellular carcinoma cells *via* promoting dopamine receptor 2 (DR2) activity (Zhang et al., 2016a). High-performance sports and resistance training can induce skeletal muscle to release myokine irisin. Irisin could inhibit EMT and invasion of tumor cells *via* the PI3K/Akt/Snail pathway has been demonstrated (Shao et al., 2017). Another study reported that irisin could be relevant to the activation of AMPK (Tang et al., 2016). Irisin downregulated the mTOR pathway and inhibited EMT of human pancreatic cancer cells *via* activating the AMPK (Liu et al., 2018). Moreover, irisin reversed the IL-6 induced EMT and downregulated the expression of MMP-2 by suppressing the STAT3/Snail signaling pathway (Kong et al., 2017).

2.2 Physical activity and intravasation

Physical exercise could influence intra-tumor angiogenesis by altering vascular epithelial growth factor (VEGF) in serum and tumor tissue. In prostate cancer, exercise induced the upregulation of HIF-1α and VEGF *via* activating MEK/MAPK and PI3K/mTOR signaling pathway, which is associated with a shift to tumor vascular normalization and inhibition of tumor metastasis (Jones et al., 2012). Data from ultrasonographic and thermographic also indicated higher vascularization of mammary tumors in exercised rats (Faustino-Rocha et al., 2017). The hypoxia and high permeability of the intratumoral vasculature also promote the intravasation of tumor cells.

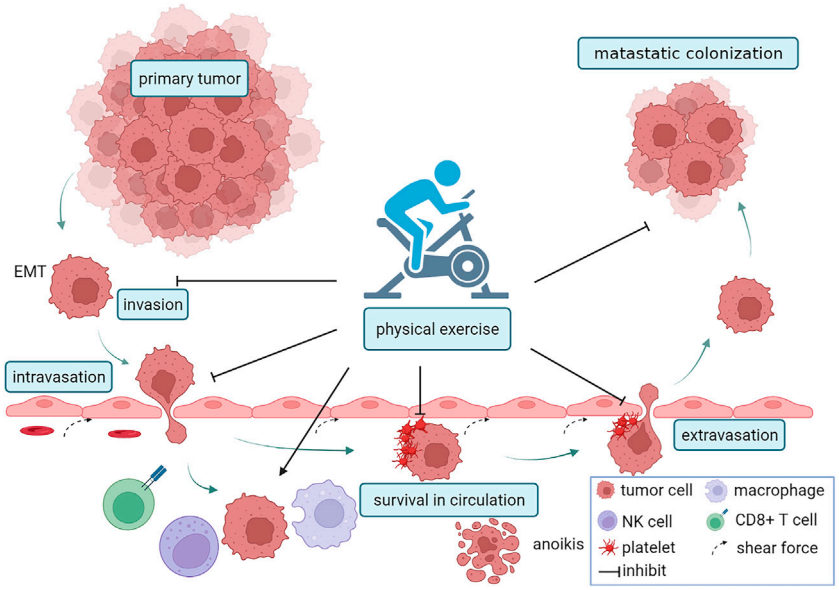

FIGURE 1
PA and the metastatic cascade. Firstly, PA reduced the invasion of tumor cells by inhibiting EMT. Next, PA reduced vascular permeability, inhibitd the interaction between endothelial cells and tumor cells, and suppressed intravasation. Exercise can also inhibit the survival of circulating tumor cells (CTCs) by increasing vascular shear force, recruiting macrophages, NK cells, and CD8+T cells, regulating metabolism and inducing anoikis. Exercise inhibitd platelet-tumor cells aggregates and the capacity of tumor cells to adhere to endothelial cells, which suppress extravasation. The figure was created with BioRender.com.

Physical exercise enhances tumor perfusion, diminishes hypoxia and transforms an aggressive tumor phenotype with abnormal leaky tumor vasculature to a weakly invasive tumor phenotype with normalized and mature vasculature (McCullough et al., 2014). Previous studies have demonstrated that physical exercise increases microvessel density and vessel maturity (Jones et al., 2012). In Ewing sarcoma, exercise modulated S1PR1 and S1PR2 expression, remodelling vasculature to reduce vessel hyperpermeability.

2.3 Physical activity and survival of circulating tumor cells

CTCs exposed to the circulation need to face various physical and biological stressors such as shear force, immune system surveillance, anoikis, and so on. Only a small portion (0.1%) of CTCs survive, and they have a relatively short half-life of about 1.0–2.4 h in circulation. Many studies have shown that exercise reduced CTCs in cancer patients. For instance, using a microfluidic antibody-mediated capture device to quantify CTCs inside venous blood of stage I-III colon cancer patients, researchers found that exercise led to a significant decrease in CTCs (Brown et al., 2018a). Exercise leads to an obvious increase in vascular shear force. During moderate-intensity exercise, the hemodynamic shear force can increase to 60 dyn/cm^2 in human arteries and 5.2–6.2 dyn/cm^2 in human veins (Tanaka et al., 2006). A previous study investigated the impact of hemodynamic shear force on the CTCs survival. The result revealed that high shear stress of 60 dyn/cm^2 at intensive exercise killed more than 90% of CTCs within the first 4 h of circulation, contrasted with low shear stress of 15 dyn/cm^2 at the resting state only killed 48% of CTCs (Regmi et al., 2017). Anoikis resistance played an important role in maintaining the survival of CTCs within circulation. HIF-1α protected CTCs from anoikis cell death by keeping an EMT state of CTCs (Majidpoor and Mortezaee, 2021). In untrained humans, acute exercise induced a transient increase of HIF-1α levels, while regular endurance exercise steadily reduced HIF-1α (Lundby et al., 2006; Wu et al., 2020a). Hippo signaling pathway has also been reported to be correlated with anoikis resistance. In metastatic breast cancer, up-regulated expression of zinc finger protein 367 (ZNF367) inhibited Hippo signaling pathway, giving rise to anoikis resistance and increased CTCs in circulation (Wu et al., 2020b). Exercise-conditioned sera could activate the Hippo signaling pathway and increase the inactivation of YAP (Baldelli et al., 2021). Exercise-induced epinephrine and norepinephrine also activated the tumor suppressor Hippo signaling pathway and promoted the phosphorylation of YAP. The phosphorylation then contributed to the sequestration of YAP in cytoplasm, which deterring the induction of tumor cell proliferation and survival by target genes (Dethlefsen et al., 2017). The effects of exercise on immune surveillance will be described in detail later.

2.4 Physical activity and extravasation

Surviving CTCs must arrest in the circulation and then start extravasation. In a previous study, long-term exercise led to a consistent lower retention of tumor cells in the pulmonary capillary bed compared with sedentary mice (MacNeil and Hoffman-Goetz, 1993a). Similarly, another study detected the radioactivity of ^{51}Cr labelled CIRAS 1 tumor cells in lungs, liver, spleen and kidney. Researchers found that exercising mice showed a lower retention of radioactivity in secondary organs after tumor cells were injected into a tail vein (Hoffmann-Goetz et al., 1994).

2.5 Physical activity and colonization

Exercise may change the microenvironment of the major sites of metastases to inhibit the process of colonization. Recently, a study reported that exercise suppressed ovarian cancer colonization in the peritoneal cavity (Morrisson et al., 2021). The secretion of CCL2 and IL-15 had a significant increase in the peritoneal fluid of exercised mice. CCL2 can recruit macrophages and enhance their cytotoxicity. IL-15 can increase the reactivity of NK cells and CD8$^+$Tcells in the peritoneal environment. Exercise also decreased the level of CCL22, VEGF, and CCL12 in peritoneal fluid. These cytokines lead to an immunosuppressive microenvironment by recruiting MDSC and Treg cells. Lung is a common metastasis site in malignant tumors, and it is also dramatically modulated by exercise. A further mechanism exploration found that exercise elevated antitumor cytotoxicity of alveolar macrophages by increasing the levels of tumor necrosis factor or reactive nitrogen intermediates (Davis et al., 1998). In order to successfully colonize the bone, tumor cells must escape the dormancy and keep proliferation. Tumor–osteoblast interactions have been proved to promote the dormancy of tumor cells. Physical exercise activated Cx43 hemichannels, and mechanically stimulated osteocytes to secrete Wnt and OPN (Fan et al., 2020), enhancing osteoblast activity and promoting the dormancy. Simultaneously, exercise increased the release of ATP from osteocytes (Genetos et al., 2007). The ATP-rich tumor microenvironment has been reported to suppress the proliferation of various tumor cells.

3 Tumor metastasis and immune function

The immune system can be divided into natural and adaptive immunity, and these two immune responses work synergistically to protect the organism (Wang et al., 2020). Natural immunity, also called innate immunity, is a semi-specific and extensive form of immunity. Natural immunity includes multiple immune cells and soluble factors and plays important roles in battling against pathogens. For example, neutrophils, macrophages, dendritic cells (DCs), natural killer (NK) cells, complement proteins and antimicrobial peptides (Janeway and Medzhitov, 2002). Adaptive immunity, also called acquired immunity or specific immunity, is a type of immune response that is generated by contact with a specific pathogen that can be recognized and initiated against the specific pathogen (Bonilla and Oettgen, 2010). Adaptive immunity consists mainly of T and B lymphocytes. T cells mediate cellular immune responses, while B cells are closely associated with the humoral immune response.

In the process of tumor metastasis, most cytotoxic innate and adaptive immune cells can synergistically control tumor behavior. A large number of cytotoxic immune cells such as NK and CD8$^+$ T cells infiltrated around the primary tumor to eliminate many immunogenic cancer cells (Pagès et al., 2010). Natural killer (NK) cells can mediate tumor cells apoptosis *via* releasing granzyme B- and perforin. Cytotoxic CD8$^+$ T cells kill tumor cells by secreting TNF-α and IFN-γ, while CD4$^+$ T cells produce multiple cytokines to boost anti-tumor immune responses (Swann and Smyth, 2007; Ostrand-Rosenberg, 2008). The high levels of NK cells and cytotoxic T cells infiltration around the tumor are associated with better prognosis in cancer survivors (Nelson, 2008). CTCs are particularly sensitive to circulating immune cells. Circulating immune cells can directly and indirectly affect the viability of CTCs to control cancer metastasis (Dianat-Moghadam et al., 2021). The recruitment of cytotoxic M1 macrophages and N1 neutrophils, NK cells and mature DCs can all contribute to the elimination of CTCs.

However, some immunosuppressive cells such as myeloid-derived suppressor cells (MDSC) and regulatory T cells (Tregs), can secrete multiple cytokines and proteases to reshape the tumor microenvironment and promote immune escape, thereby promoting tumor metastasis (Smith and Kang, 2013). As tumors progress, cancer cells can secret multiple cytokines such as IL-4 and IL-13 to induce polarization of M2 macrophages and N2 neutrophils, which contributes to angiogenesis, extracellular matrix (ECM) remodeling and immune evasion. In addition, immature DCs also play important roles in facilitating tumor metastasis (Gonzalez et al., 2018).

4 Physical activity-dependent modulation of immune cells

PA has a positive effect on the human immune system, especially the innate immune system. During PA, cytotoxic immune cells are mobilized into the circulation through stress-induced shear stress and adrenergic signaling (Idorn and Hojman, 2016). This mobilization is not to induce the body to produce a new generation of immune cells, but to recruit the existing storage of immune cells (Walsh et al., 2011). According to numerous studies, chronic and acute physical exercise show significant responses in terms of immune cells redistribution, activity and function in cancer

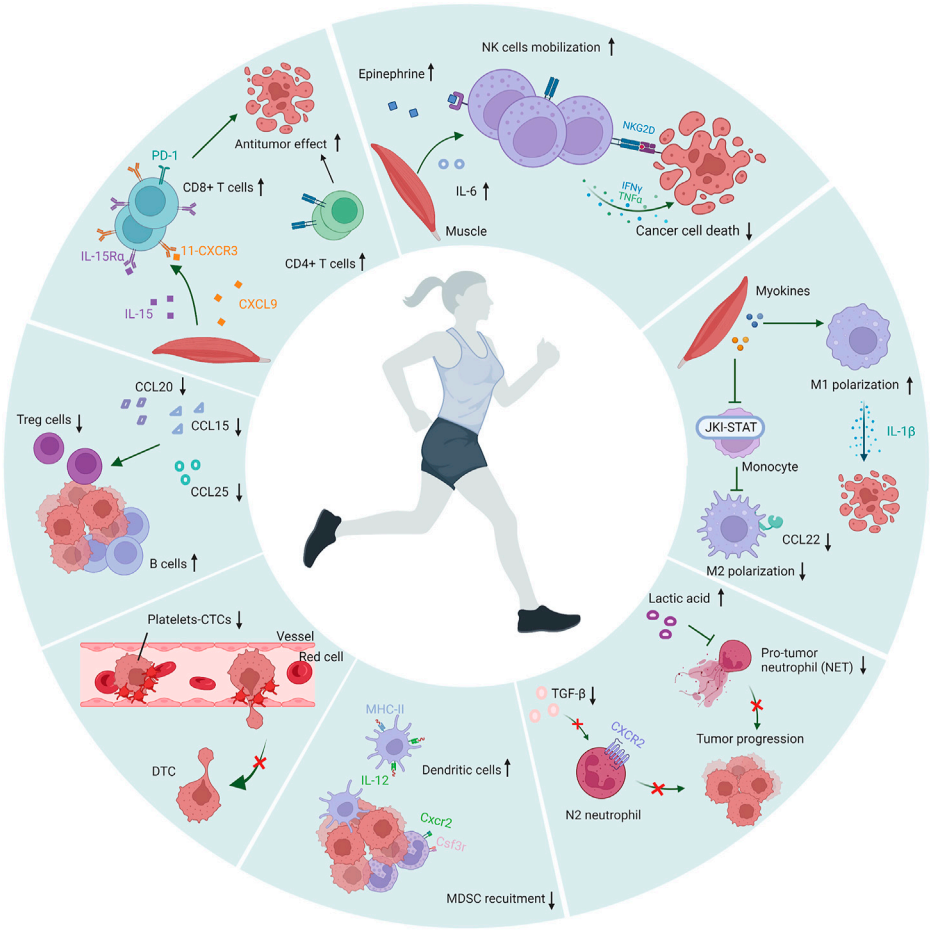

FIGURE 2
Modulation of immune cells during exercise. During physical activity, the numbers and antitumor effects of NK cells, dendritic cells, T cells and B cells were increased, the polarization of M2 macrophages and N2 neutrophils are inhibited, and the recruitment of MDSC and Treg was suppressed. Moreover, PA inhibited the formation of platelet-CTCs aggregates and reduced the adhesion of platelets to endothelial cells. The figure was created with BioRender.com.

patients. The intensity and duration of exercise also affects the redistribution of immune cells to the circulation (Robson et al., 1999; Freidenreich and Volek, 2012; Bigley and Simpson, 2015). In some tumor-bearing animal models, exercise led to an increase in the number and function of effector cells and a decrease in immunosuppressive cells (Thompson et al., 2010; Hagar et al., 2019). Here we discuss the effect of exercise on multiple immune cells in the process of metastasis. A schematic illustration of the association of exercise and immune cells is shown in Figure 2.

4.1 Physical activity and natural immune cells

As the first-line defenders against pathogens, natural immune cells are hot topics to exercise immunology.

4.1.1 Natural killer cells

Among natural immune cells, NK cells are the most responsive to exercise, showing exercise-dependent acute mobilization. The number of NK cells can be increased to more than six-fold during a brief stair climb, without immediate functional decrease after rest (Millard et al., 2013). This rapid mobilization of NK cells is mainly related to the exercise intensity-dependent changes in catecholamine concentrations (Kappel et al., 1991). NK cells have the most abundant β-adrenergic receptors in all immune cells (Landmann, 1992). Systemic administration of epinephrine mimics the exercise-induced increase in circulating NK cell infiltration, while nonselective and selective β1-and β2-blockers can block this mobilization effect from exercise (Murray et al., 1992). During acute PA, muscle-derived cytokines such as IL-15, IL-7, and IL-6 are also involved in NK cells activation (Benatti and

Pedersen, 2015). However, after long-term exercise, the number of circulating NK cells was reduced, which may due to tissue migration or re-marginalization (Timmons and Cieslak, 2008). PA not only increases the number of circulating NK cells, but also enhances their antitumor activity. A previous study has demonstrated that exercise enhanced splenic NK cells activity in tumor-bearing mice (MacNeil and Hoffman-Goetz, 1993b). Another study has found that mice randomly assigned to the voluntary wheel had an obvious increase in NK cells infiltration in various tumor models (melanoma, Lewis lung cancer and liver cancer), leading to reductions in tumor incidence, growth and metastases. Exercise recruits NK cells *via* β-adrenergic signaling and induces muscle-derived IL-6 to redistribute and activate NK cells. Moreover, the expression levels of NK cell-related activating receptor ligands (NKG2D, MULT1, H60a, and Clr-b) also had an increase in the tumors of running mice, revealing that exercise worked on the mobilization of NK cells and the formation of NK cell activated tumor microenvironment (Pedersen et al., 2016).

4.1.2 Macrophages

Macrophages also play a pivotal role in controlling tumor metastasis. M1 macrophages have the capacity to diminish a large number of CTCs, while M2 macrophages are related to the promotion of tumor metastasis. Exercise can enhance antitumor macrophage cytotoxicity and suppress the polarization of macrophages to the M2 (Davis et al., 1998; Goh et al., 2012). Short-term moderate-exercise training led to an increase in macrophages antitumor cytotoxicity and decreased the lung tumor metastases of injected B16 melanoma cells (Murphy et al., 2004). Another recent study using a triple-negative breast cancer mouse model reported that exercise reduced M2 macrophage polarization by inhibiting the JAK-STAT signaling pathway, thus decreasing lung cancer metastasis (Kim et al., 2020). M2 macrophages secreted chemokine CCL22, which attracted CCR4-expressing Tregs in circulation toward the CCL22 gradient, thus facilitating the recruitment of Tregs. Exercise contributed to a significant decrease in CCL22 mRNA expression in M2 macrophages and resulted in a reduction in Treg recruitment, which delayed invasive breast cancer progression and metastasis in polyoma middle T oncoprotein (PyMT) transgenic mouse (Goh et al., 2013). Similarly, in an ApcMin/+ mouse model, the mRNA expression of M2 related macrophage markers such as CD206, CCL22 and Arg consistently decreased in exercise mice (McClellan et al., 2014).

4.1.3 Neutrophils

Some recent studies revealed that neutrophils promoted the metastasis potential of cancer cells. In circulation, neutrophils induced the aggregation of tumor cells to improve the survival rate of CTCs (Szczerba et al., 2019). Neutrophil extracellular traps (NETs) released by neutrophils was also demonstrated to enhance the tumor metastasis. Some studies have shown that exercise can inhibit NETs formation (Shi et al., 2020). The accumulation of exercise-induced lactic acid decreases the release of NETs in serum (Shi et al., 2019). A recent study reported that exercise mitigated liver ischemia-reperfusion injury derived inflammatory responses and metastasis *via* inhibiting neutrophil recruitment and diminishing NETs release in the mouse model of colorectal adenocarcinoma (Yazdani et al., 2021). Nevertheless, tumor-associated neutrophils (TANs) had a two-sided effect in the progression of tumor (Uribe-Querol and Rosales, 2015). Some previous reports demonstrated that neutrophils directly destroyed tumor cells both *in vitro* and *in vivo* (Uribe-Querol and Rosales, 2015). In metastatic breast cancer and renal carcinoma, the tumor cells produced CCL2 and IL-8 that induced neutrophil recruitment to inhibit lung metastasis, respectively (Granot et al., 2011; López-Lago et al., 2013).

Similar to the M1 and M2 phenotypes of macrophages, neutrophils also have N1 and N2 polarization states. N1 neutrophils have anti-tumor function by secreting type I interferon and inducing NK cells to secret IL-18. N2 neutrophils secrete multiple molecules such as arginase and peroxidase to inhibit T cells and NK cells functions, which promote tumor metastasis. TGF-β derived from tumor microenvironment can induce the activation of N2 neutrophils (Fridlender et al., 2009). PA has been demonstrated to inhibit the expression of TGF-β in tumor tissue (da Silva Alves et al., 2020), which attenuates the polarization of N2 neutrophils.

4.1.4 Dendritic cells

DCs play a key role in eliminating and controlling tumor progression. In human exercise studies, PA can increase the number of DCs in the peripheral blood circulation (Ho et al., 2001; LaVoy et al., 2015). Further study showed that exercise upregulated the expression of MHC II and IL-12 on DCs in animal models (Liao et al., 2006; Chiang et al., 2007). A previous study investigated the composition of DCs subpopulations mobilized in response to acute aerobic exercise. The findings showed that exercise preferentially mobilized plasmacytoid DCs into peripheral blood to enhance immune surveillance (Brown et al., 2018b). However, there are few studies investigating the effects of exercise on DCs in cancer patients, and more research is needed in the future.

4.1.5 Myeloid-derived suppressor cells

MDSCs are effective inhibitory factors of immune function and contribute to the immune escape. Augmented ROS produced by MDSCs induced the upregulation of Notch1 in CTCs through the ROS-NRF2-ARE axis, thus enhancing CTCs metastatic traits (Sprouse et al., 2019). Recently, a preclinical study found that PA reduced the tumor-induced accumulation of MDSCs and delayed the tumor growth in a mouse model of triple negative breast cancer (Wennerberg et al., 2020). In 4T1 tumor-bearing mice, voluntary wheel running potently relayed the accumulation of IMCs/MDSCs in the spleen, blood, and tumor. Moreover, these effects led to a reduction in the number of metastatic lung nodules in exercising mice (Garritson et al., 2020). Another

previous study also showed that the combination of PA and energy restriction decreased MDSC accumulation by restraining myelopoiesis and/or the mobilization and transportation of MDSCs to secondary sites (Turbitt et al., 2019). In a mouse model of pancreatic cancer, PA diminished MDSC *via* downregulating the expression levels of Cxcr2 and Csf3r on myeloid cells (Kurz et al., 2022). These findings suggested that PA was beneficial to inhibiting tumor progression and metastases *via* suppressing MDSCs accumulation.

4.1.6 Platelets

Platelets activation plays an essential role in elevating the survival rate of the CTCs. Activated platelets adhere to CTCs to protect the tumor cells from various stressors in circulation. Moreover, aggregates of platelets and CTCs have been shown to inhibit NK cells antitumor cytotoxicity in vitro-model. Some reports have found that PA affected the clearance of CTCs by modulating platelets activity. Compared with sedentary mice with breast cancer, exercising mice had a lower number of circulating platelets (Smeda et al., 2017). In patients with nasopharyngeal carcinoma, moderate-intensity exercise decreased the formation of platelets-CTCs aggregates and minimized the risk of metastasis (Wang et al., 2007). Another study by the same team found that warm-up exercise before severe exercise reduced platelet-impeded cytotoxicity of NK cells to nasopharyngeal carcinoma cells (Wang et al., 2009).

The activation of platelets is also critical for CTCs to extravasate. Adhesion molecules on activated platelets can gather CTCs to securely adhere to the activated vascular endothelial cells. PA might be related with the downregulation of adhesion molecules on platelets and endothelial cells (ECs), such as P-selectin and epithelial cell adhesion molecule-1 (EPCAM-1) (Wang et al., 2005; Souza et al., 2017). In P-selectin-deficient mice, lung metastasis was significantly reduced post injection of tumor cells (Borsig, 2004). Nevertheless, the positive effects of exercise might be limited by intensity. Some investigations have found that strenuous exercise promoted platelets aggregation and the capacity of CTCs to adhere to ECs for sedentary healthy humans (Chen et al., 2009), yet moderate exercise inhibited platelets aggregation and adhesiveness (Wang and Liao, 2004; Wang et al., 2005; Wang, 2006).

4.2 Physical activity and adaptive immune cells

Adaptive immune cells consist mainly of T and B lymphocytes. In general, exercise-induced lymphocytosis is proportional to the duration and intensity of exercise.

4.2.1 Cytotoxic T cells

Cytotoxic T cells recognize and diminish CTCs by specifically identifying mutation-induced neoantigens. A study using breast cancer mice found that acute exercise caused a transient increase in $CD8^+$ T cells. Exercise-induced decrease in tumor growth was contingent on the levels of $CD8^+$ T cell in circulation. And key metabolites that muscles released into the blood during exercise, including lactate, made $CD8^+$ T cells more effective. Moreover, these super-effective $CD8^+$ T cells extracted from exercising mice showed better antitumor efficacy when transferred to sedentary mice (Rundqvist et al., 2020). Recently, a preclinical study also suggested that PA can increase the infiltration and effector function of CD8 T cells in breast tumors. Further investigation showed that CXCL9/11-CXCR3 pathway is required for the $CD8^+$ T cell-mediated antitumor effect of PA (Gomes-Santos et al., 2021). In a mouse model of pancreatic cancer, PA activated IL-15/ IL15Rα pathway to promotes activation of $CD8^+$ T cells (Kurz et al., 2022). Notable, exercise-induced IL-15Rα $CD8^+$ T cells selectively upregulate checkpoint PD-1, which contributes to increase sensitivity to chemotherapy.

$CD4^+$ T cells also play a central role in antitumor immune response. Similar to $CD8^+$ T cells, a temporary increase in $CD4^+$ T cells was detected after resistance exercise (Natale et al., 2003). In a mouse model of hepatocellular carcinoma, exercise enhanced immunity by raising $CD4^+$ T lymphocytes in peripheral blood (Zhang et al., 2016b).

4.2.2 Tregs

Tregs effectually inhibit the activation and proliferation of $CD8^+$ T cells, which are considered to be the important barriers to impede the effect of anti-tumor immunity. An increased number of Tregs indicated a higher CTCs-positive rate and contributed to a poorer clinical outcome in cancer patients (Xue et al., 2018). A previous study demonstrated that endurance exercise suppressed the recruitment of Tregs and relayed the tumor growth in breast cancer. Exercise led to a greater tumor immune response by increasing the ratio of CD8/Tregs (Hagar et al., 2019). PA induced the downregulation of chemokines such as CCL5, CCL20 and CCL25, which were closely associated with the recruitment of Tregs (Turbitt et al., 2019).

4.2.3 B cells

The role of B cells in cancer progression is much less understood than that of T cells. Growing evidence suggested that tumor-infiltrating B cells may exert both tumor suppressive and tumor promoting effects (Gu et al., 2019; Xu et al., 2022). During exercise, circulating B-cell counts increased mildly immediately and in proportion to exercise duration and intensity (Ronsen et al., 2001). However, there are few studies elucidating the effects of exercise on B cells immune function in cancer patients.

4.3 Additional exercise effects

Physical exercise improves blood perfusion and hypoxia, which also affect immune function. Hypoxia induces

overexpression of connexin 43 in tumor cells, leading to degradation of NK cell immune synapses and impairing NK cell killing activity (Tittarelli et al., 2015). Improving intratumor hypoxia can indirectly increase the cytotoxicity of tumor-infiltrating NK cells. Moreover, PA promotes normalization of intratumoral vessels and blood perfusion, which can increase the accessibility of immune cells and delivery of antitumor drugs.

5 Deficiencies and prospects

Existing preclinical and clinical studies have demonstrated that PA, particularly regular moderate exercise, plays a beneficial role in tumor metastasis. The immune system is highly responsive to exercise, which may lead to beneficial effects on tumor metastasis. During exercise, a large number of cytotoxic immune cells with antitumor functions are mobilized into circulation to kill CTCs. To be sure, the mechanisms of exercise modulating immune cells are extensive and diverse. However, the exploration of the potential mechanisms underlying the beneficial effect of exercise on immune cells is still in its early stages. The review analyzed that PA can control metastasis by regulating immune function. As the understanding of the mechanisms by which PA effects tumor metastasis continues to improve, new therapeutic strategies will be identified and validated, potentially contributing to improve survival in cancer patients.

Author contributions

AZ wrote original draft and drew the figures. JY, XY, TZ, XW, and XM corrected the draft. LZ revised most of the manuscript. All authors have read and agreed to the published version of the manuscript.

Acknowledgments

We acknowledge the editors and the reviewers for insightful suggestions on this work.

Conflict of interest

The authors declare that the research was conducted in the absence of any commercial or financial relationships that could be construed as a potential conflict of interest.

Publisher's note

All claims expressed in this article are solely those of the authors and do not necessarily represent those of their affiliated organizations, or those of the publisher, the editors and the reviewers. Any product that may be evaluated in this article, or claim that may be made by its manufacturer, is not guaranteed or endorsed by the publisher.

References

Baldelli, G., De Santi, M., Gervasi, M., Annibalini, G., Sisti, D., Højman, P., et al. (2021). The effects of human sera conditioned by high-intensity exercise sessions and training on the tumorigenic potential of cancer cells. *Clin. Transl. Oncol.* 23 (1), 22–34. Epub 2020/05/25. doi:10.1007/s12094-020-02388-6

Bellocco, R., Marrone, G., Ye, W., Nyrén, O., Adami, H. O., Mariosa, D., et al. (2016). A prospective cohort study of the combined effects of physical activity and anthropometric measures on the risk of post-menopausal breast cancer. *Eur. J. Epidemiol.* 31 (4), 395–404. Epub 2015/07/02. doi:10.1007/s10654-015-0064-z

Benatti, F. B., and Pedersen, B. K. (2015). Exercise as an anti-inflammatory therapy for rheumatic diseases-myokine regulation. *Nat. Rev. Rheumatol.* 11 (2), 86–97. Epub 2014/11/26. doi:10.1038/nrrheum.2014.193

Bigley, A. B., and Simpson, R. J. (2015). Nk cells and exercise: Implications for cancer immunotherapy and survivorship. *Discov. Med.* 19 (107), 433–445. Epub 2015/07/16.

Bonilla, F. A., and Oettgen, H. C. (2010). Adaptive immunity. *J. Allergy Clin. Immunol.* 125 (2), S33–S40. Epub 2010/01/12. doi:10.1016/j.jaci.2009.09.017

Borsig, L. (2004). Selectins facilitate carcinoma metastasis and heparin can prevent them. *News Physiol. Sci.* 19, 16–21. Epub 2004/01/24. doi:10.1152/nips.01450.2003

Brown, J. C., Rhim, A. D., Manning, S. L., Brennan, L., Mansour, A. I., Rustgi, A. K., et al. (2018). Effects of exercise on circulating tumor cells among patients with resected stage I-iii colon cancer. *PLoS One* 13 (10), e0204875. Epub 2018/10/18. doi:10.1371/journal.pone.0204875

Brown, F. F., Campbell, J. P., Wadley, A. J., Fisher, J. P., Aldred, S., and Turner, J. E. (2018). Acute aerobic exercise induces a preferential mobilisation of plasmacytoid dendritic cells into the peripheral blood in man. *Physiol. Behav.* 194, 191–198. Epub 2018/05/16. doi:10.1016/j.physbeh.2018.05.012

Bull, F. C., Al-Ansari, S. S., Biddle, S., Borodulin, K., Buman, M. P., Cardon, G., et al. (2020). World health organization 2020 guidelines on physical activity and sedentary behaviour. *Br. J. Sports Med.* 54 (24), 1451–1462. Epub 2020/11/27. doi:10.1136/bjsports-2020-102955

Chen, Y. W., Chen, J. K., and Wang, J. S. (2009). Exercise affects platelet-promoted tumor cell adhesion and invasion to endothelium. *Eur. J. Appl. Physiol.* 105 (3), 393–401. Epub 2008/11/11. doi:10.1007/s00421-008-0916-2

Chiang, L. M., Chen, Y. J., Chiang, J., Lai, L. Y., Chen, Y. Y., and Liao, H. F. (2007). Modulation of dendritic cells by endurance training. *Int. J. Sports Med.* 28 (9), 798–803. Epub 2007/04/17. doi:10.1055/s-2007-964914

da Silva Alves, R., Abdalla, D. R., Iunes, D. H., Mariano, K. O. P., Borges, J. B. C., Murta, E. F. C., et al. (2020). Influence of an exergaming training program on reducing the expression of il-10 and tgf-B in cancer patients. *Games Health J.* 9 (6), 446–452. Epub 2020/06/06. doi:10.1089/g4h.2020.0022

Davis, J. M., Kohut, M. L., Jackson, D. A., Colbert, L. H., Mayer, E. P., and Ghaffar, A. (1998). Exercise effects on lung tumor metastases and *in vitro* alveolar macrophage antitumor cytotoxicity. *Am. J. Physiol.* 274 (5), R1454–R1459. Epub 1998/06/05. doi:10.1152/ajpregu.1998.274.5.R1454

Dethlefsen, C., Hansen, L. S., Lillelund, C., Andersen, C., Gehl, J., Christensen, J. F., et al. (2017). Exercise-induced catecholamines activate the Hippo tumor suppressor pathway to reduce risks of breast cancer development. *Cancer Res.* 77 (18), 4894–4904. Epub 2017/09/10. doi:10.1158/0008-5472.Can-16-3125

Dianat-Moghadam, H., Mahari, A., Heidarifard, M., Parnianfard, N., Pourmousavi-Kh, L., Rahbarghazi, R., et al. (2021). Nk cells-directed therapies target circulating tumor cells and metastasis. *Cancer Lett.* 497, 41–53. Epub 2020/09/29. doi:10.1016/j.canlet.2020.09.021

Fan, Y., Jalali, A., Chen, A., Zhao, X., Liu, S., Teli, M., et al. (2020). Skeletal loading regulates breast cancer-associated osteolysis in a loading intensity-dependent fashion. *Bone Res.* 8, 9. Epub 2020/03/05. doi:10.1038/s41413-020-0083-6

Faustino-Rocha, A. I., Gama, A., Oliveira, P. A., Vanderperren, K., Saunders, J. H., Pires, M. J., et al. (2017). A contrast-enhanced ultrasonographic study about the impact of long-term exercise training on mammary tumor vascularization. *J. Ultrasound Med.* 36 (12), 2459–2466. Epub 2017/06/25. doi:10.1002/jum.14287

Febbraio, M. A. (2017). Exercise metabolism in 2016: Health benefits of exercise - more than meets the eye. *Nat. Rev. Endocrinol.* 13 (2), 72–74. Epub 2017/01/05. doi:10.1038/nrendo.2016.218

Freidenreich, D. J., and Volek, J. S. (2012). Immune responses to resistance exercise. *Exerc. Immunol. Rev.* 18, 8–41. Epub 2012/08/11.

Fridlender, Z. G., Sun, J., Kim, S., Kapoor, V., Cheng, G., Ling, L., et al. (2009). Polarization of tumor-associated neutrophil phenotype by tgf-beta: "N1" versus "N2" tan. *Cancer Cell* 16 (3), 183–194. Epub 2009/09/08. doi:10.1016/j.ccr.2009.06.017

Friedenreich, C. M., Cook, L. S., Wang, Q., Kokts-Porietis, R. L., McNeil, J., Ryder-Burbidge, C., et al. (2020). Prospective cohort study of pre- and postdiagnosis physical activity and endometrial cancer survival. *J. Clin. Oncol.* 38 (34), 4107–4117. Epub 2020/10/08. doi:10.1200/jco.20.01336

Garritson, J., Krynski, L., Haverbeck, L., Haughian, J. M., Pullen, N. A., and Hayward, R. (2020). Physical activity delays accumulation of immunosuppressive myeloid-derived suppressor cells. *PLoS One* 15 (6), e0234548. Epub 2020/06/17. doi:10.1371/journal.pone.0234548

Genetos, D. C., Kephart, C. J., Zhang, Y., Yellowley, C. E., and Donahue, H. J. (2007). Oscillating fluid flow activation of gap junction hemichannels induces atp release from mlo-Y4 osteocytes. *J. Cell. Physiol.* 212 (1), 207–214. Epub 2007/02/16. doi:10.1002/jcp.21021

Goh, J., Kirk, E. A., Lee, S. X., and Ladiges, W. C. (2012). Exercise, physical activity and breast cancer: The role of tumor-associated macrophages. *Exerc. Immunol. Rev.* 18, 158–176. Epub 2012/08/11.

Goh, J., Tsai, J., Bammler, T. K., Farin, F. M., Endicott, E., and Ladiges, W. C. (2013). Exercise training in transgenic mice is associated with attenuation of early breast cancer growth in a dose-dependent manner. *PLoS One* 8 (11), e80123. Epub 2013/12/07. doi:10.1371/journal.pone.0080123

Gomes-Santos, I. L., Amoozgar, Z., Kumar, A. S., Ho, W. W., Roh, K., Talele, N. P., et al. (2021). Exercise training improves tumor control by increasing Cd8(+) T-cell infiltration via Cxcr3 signaling and sensitizes breast cancer to immune checkpoint blockade. *Cancer Immunol. Res.* 9 (7), 765–778. Epub 2021/04/12. doi:10.1158/2326-6066.Cir-20-0499

Gonzalez, H., Hagerling, C., and Werb, Z. (2018). Roles of the immune system in cancer: From tumor initiation to metastatic progression. *Genes Dev.* 32 (19-20), 1267–1284. Epub 2018/10/03. doi:10.1101/gad.314617.118

Granot, Z., Henke, E., Comen, E. A., King, T. A., Norton, L., and Benezra, R. (2011). Tumor entrained neutrophils inhibit seeding in the premetastatic lung. *Cancer Cell* 20 (3), 300–314. Epub 2011/09/13. doi:10.1016/j.ccr.2011.08.012

Gu, Y., Liu, Y., Fu, L., Zhai, L., Zhu, J., Han, Y., et al. (2019). Tumor-educated B cells selectively promote breast cancer lymph node metastasis by hspa4-targeting igg. *Nat. Med.* 25 (2), 312–322. Epub 2019/01/16. doi:10.1038/s41591-018-0309-y

Hagar, A., Wang, Z., Koyama, S., Serrano, J. A., Melo, L., Vargas, S., et al. (2019). Endurance training slows breast tumor growth in mice by suppressing Treg cells recruitment to tumors. *BMC Cancer* 19 (1), 536. Epub 2019/06/06. doi:10.1186/s12885-019-5745-7

Ho, C. S., López, J. A., Vuckovic, S., Pyke, C. M., Hockey, R. L., and Hart, D. N. (2001). Surgical and physical stress increases circulating blood dendritic cell counts independently of monocyte counts. *Blood* 98 (1), 140–145. Epub 2001/06/22. doi:10.1182/blood.v98.1.140

Hoffmann-Goetz, L., MacNeil, B., and Arumugam, Y. (1994). Tissue distribution of radiolabelled tumor cells in wheel exercised and sedentary mice. *Int. J. Sports Med.* 15 (5), 249–253. Epub 1994/07/01. doi:10.1055/s-2007-1021055

Idorn, M., and Hojman, P. (2016). Exercise-dependent regulation of nk cells in cancer protection. *Trends Mol. Med.* 22 (7), 565–577. Epub 2016/06/06. doi:10.1016/j.molmed.2016.05.007

Janeway, C. A., Jr., and Medzhitov, R. (2002). Innate immune recognition. *Annu. Rev. Immunol.* 20, 197–216. Epub 2002/02/28. doi:10.1146/annurev.immunol.20.083001.084359

Jones, L. W., Antonelli, J., Masko, E. M., Broadwater, G., Lascola, C. D., Fels, D., et al. (2012). Exercise modulation of the host-tumor interaction in an orthotopic model of murine prostate cancer. *J. Appl. Physiol.* 113 (2), 263–272. Epub 2012/05/19. doi:10.1152/japplphysiol.01575.2011

Ju, J., Nolan, B., Cheh, M., Bose, M., Lin, Y., Wagner, G. C., et al. (2008). Voluntary exercise inhibits intestinal tumorigenesis in apc(min/+) mice and azoxymethane/dextran sulfate sodium-treated mice. *BMC Cancer* 8, 316. Epub 2008/11/04. doi:10.1186/1471-2407-8-316

Kappel, M., Tvede, N., Galbo, H., Haahr, P. M., Kjaer, M., Linstow, M., et al. (1991). Evidence that the effect of physical exercise on nk cell activity is mediated by epinephrine. *J. Appl. Physiol.* 70 (6), 2530–2534. Epub 1991/06/01. doi:10.1152/jappl.1991.70.6.2530

Kim, M. K., Kim, Y., Park, S., Kim, E., Kim, Y., Kim, Y., et al. (2020). Effects of steady low-intensity exercise on high-fat diet stimulated breast cancer progression via the alteration of macrophage polarization. *Integr. Cancer Ther.* 19, 1534735420949678. Epub 2020/09/11. doi:10.1177/1534735420949678

Kong, G., Jiang, Y., Sun, X., Cao, Z., Zhang, G., Zhao, Z., et al. (2017). Irisin reverses the il-6 induced epithelial-mesenchymal transition in osteosarcoma cell migration and invasion through the stat3/snail signaling pathway. *Oncol. Rep.* 38 (5), 2647–2656. Epub 2017/10/20. doi:10.3892/or.2017.5973

Kurz, E., Hirsch, C. A., Dalton, T., Shadaloey, S. A., Khodadadi-Jamayran, A., Miller, G., et al. (2022). Exercise-induced engagement of the il-15/il-15rα Axis promotes anti-tumor immunity in pancreatic cancer. *Cancer Cell* 40 (7), 720–737. Epub 2022/06/07. doi:10.1016/j.ccell.2022.05.006

Landmann, R. (1992). Beta-adrenergic receptors in human leukocyte subpopulations. *Eur. J. Clin. Invest.* 22, 30–36. Epub 1992/10/01.

LaVoy, E. C., Bollard, C. M., Hanley, P. J., O'Connor, D. P., Lowder, T. W., Bosch, J. A., et al. (2015). A single bout of dynamic exercise by healthy adults enhances the generation of monocyte-derived-dendritic cells. *Cell. Immunol.* 295 (1), 52–59. Epub 2015/03/10. doi:10.1016/j.cellimm.2015.02.007

Liao, H. F., Chiang, L. M., Yen, C. C., Chen, Y. Y., Zhuang, R. R., Lai, L. Y., et al. (2006). Effect of a periodized exercise training and active recovery program on antitumor activity and development of dendritic cells. *J. Sports Med. Phys. Fit.* 46 (2), 307–314. Epub 2006/07/11.

Liu, J., Song, N., Huang, Y., and Chen, Y. (2018). Irisin inhibits pancreatic cancer cell growth via the ampk-mtor pathway. *Sci. Rep.* 8 (1), 15247. Epub 2018/10/17. doi:10.1038/s41598-018-33229-w

López-Lago, M. A., Posner, S., Thodima, V. J., Molina, A. M., Motzer, R. J., and Chaganti, R. S. (2013). Neutrophil chemokines secreted by tumor cells mount a lung antimetastatic response during renal cell carcinoma progression. *Oncogene* 32 (14), 1752–1760. Epub 2012/06/06. doi:10.1038/onc.2012.201

Lucia, A., and Ramírez, M. (2016). Muscling in on cancer. *N. Engl. J. Med.* 375 (9), 892–894. Epub 2016/09/01. doi:10.1056/NEJMcibr1606456

Lundby, C., Gassmann, M., and Pilegaard, H. (2006). Regular endurance training reduces the exercise induced hif-1alpha and hif-2alpha mrna expression in human skeletal muscle in normoxic conditions. *Eur. J. Appl. Physiol.* 96 (4), 363–369. Epub 2005/11/15. doi:10.1007/s00421-005-0085-5

Ma, X., Wang, M., Yin, T., Zhao, Y., and Wei, X. (2019). Myeloid-derived suppressor cells promote metastasis in breast cancer after the stress of operative removal of the primary cancer. *Front. Oncol.* 9, 855. Epub 2019/09/26. doi:10.3389/fonc.2019.00855

MacNeil, B., and Hoffman-Goetz, L. (1993). Chronic exercise enhances *in vivo* and *in vitro* cytotoxic mechanisms of natural immunity in mice. *J. Appl. Physiol.* 74 (1), 388–395. Epub 1993/01/01. doi:10.1152/jappl.1993.74.1.388

MacNeil, B., and Hoffman-Goetz, L. (1993). Effect of exercise on natural cytotoxicity and pulmonary tumor metastases in mice. *Med. Sci. Sports Exerc.* 25 (8), 922–928. Epub 1993/08/01. doi:10.1249/00005768-199308000-00007

Majidpoor, J., and Mortezaee, K. (2021). Steps in metastasis: An updated review. *Med. Oncol.* 38 (1), 3. Epub 2021/01/05. doi:10.1007/s12032-020-01447-w

McClellan, J. L., Steiner, J. L., Day, S. D., Enos, R. T., Davis, M. J., Singh, U. P., et al. (2014). Exercise effects on polyp burden and immune markers in the Apcmin/+ mouse model of intestinal tumorigenesis. *Int. J. Oncol.* 45 (2), 861–868. Epub 2014/05/27. doi:10.3892/ijo.2014.2457

McCullough, D. J., Stabley, J. N., Siemann, D. W., and Behnke, B. J. (2014). Modulation of blood flow, hypoxia, and vascular function in orthotopic prostate tumors during exercise. *J. Natl. Cancer Inst.* 106 (4), dju036. Epub 2014/03/15. doi:10.1093/jnci/dju036

Meyerhardt, J. A., Heseltine, D., Niedzwiecki, D., Hollis, D., Saltz, L. B., Mayer, R. J., et al. (2006). Impact of physical activity on cancer recurrence and survival in patients with stage iii colon cancer: Findings from calgb 89803. *J. Clin. Oncol.* 24 (22), 3535–3541. Epub 2006/07/11. doi:10.1200/jco.2006.06.0863

Millard, A. L., Valli, P. V., Stussi, G., Mueller, N. J., Yung, G. P., and Seebach, J. D. (2013). Brief exercise increases peripheral blood nk cell counts without immediate functional changes, but impairs their responses to *ex vivo* stimulation. *Front. Immunol.* 4, 125. Epub 2013/06/12. doi:10.3389/fimmu.2013.00125

Morrisson, M. J., Bi, F., Yang, K., Cady, S. L., Hartwich, T. M., Cerchia, A. P., et al. (2021). Effect of exercise on peritoneal microenvironment and progression of ovarian cancer. *Am. J. Cancer Res.* 11 (10), 5045–5062. Epub 2021/11/13.

Murphy, E. A., Davis, J. M., Brown, A. S., Carmichael, M. D., Mayer, E. P., and Ghaffar, A. (2004). Effects of moderate exercise and oat beta-glucan on lung tumor metastases and macrophage antitumor cytotoxicity. *J. Appl. Physiol.* 97 (3), 955–959. Epub 2004/05/18. doi:10.1152/japplphysiol.00252.2004

Murray, D. R., Irwin, M., Rearden, C. A., Ziegler, M., Motulsky, H., and Maisel, A. S. (1992). Sympathetic and immune interactions during dynamic exercise. Mediation via a beta 2-adrenergic-dependent mechanism. *Circulation* 86 (1), 203–213. Epub 1992/07/01. doi:10.1161/01.cir.86.1.203

Natale, V. M., Brenner, I. K., Moldoveanu, A. I., Vasiliou, P., Shek, P., and Shephard, R. J. (2003). Effects of three different types of exercise on blood leukocyte count during and following exercise. *Sao Paulo Med. J.* 121 (1), 9–14. Epub 2003/05/20. doi:10.1590/s1516-31802003000100003

Nelson, B. H. (2008). The impact of T-cell immunity on ovarian cancer outcomes. *Immunol. Rev.* 222, 101–116. Epub 2008/03/28. doi:10.1111/j.1600-065X.2008.00614.x

Ostrand-Rosenberg, S. (2008). Immune surveillance: A balance between protumor and antitumor immunity. *Curr. Opin. Genet. Dev.* 18 (1), 11–18. Epub 2008/03/01. doi:10.1016/j.gde.2007.12.007

Pagès, F., Galon, J., Dieu-Nosjean, M. C., Tartour, E., Sautès-Fridman, C., and Fridman, W. H. (2010). Immune infiltration in human tumors: A prognostic factor that should not Be ignored. *Oncogene* 29 (8), 1093–1102. Epub 2009/12/01. doi:10.1038/onc.2009.416

Pedersen, L., Idorn, M., Olofsson, G. H., Lauenborg, B., Nookaew, I., Hansen, R. H., et al. (2016). Voluntary running suppresses tumor growth through epinephrine- and il-6-dependent nk cell mobilization and redistribution. *Cell Metab.* 23 (3), 554–562. Epub 2016/02/21. doi:10.1016/j.cmet.2016.01.011

Regmi, S., Fu, A., and Luo, K. Q. (2017). High shear stresses under exercise condition destroy circulating tumor cells in a microfluidic system. *Sci. Rep.* 7, 39975. Epub 2017/01/06. doi:10.1038/srep39975

Robson, P. J., Blannin, A. K., Walsh, N. P., Castell, L. M., and Gleeson, M. (1999). Effects of exercise intensity, duration and recovery on *in vitro* neutrophil function in male athletes. *Int. J. Sports Med.* 20 (2), 128–135. Epub 1999/04/06. doi:10.1055/s-2007-971106

Rock, C. L., Thomson, C., Gansler, T., Gapstur, S. M., McCullough, M. L., Patel, A. V., et al. (2020). American cancer society guideline for diet and physical activity for cancer prevention. *Ca. Cancer J. Clin.* 70 (4), 245–271. Epub 2020/06/10. doi:10.3322/caac.21591

Ronsen, O., Pedersen, B. K., Øritsland, T. R., Bahr, R., and Kjeldsen-Kragh, J. (2001). Leukocyte counts and lymphocyte responsiveness associated with repeated bouts of strenuous endurance exercise. *J. Appl. Physiol.* 91 (1), 425–434. Epub 2001/06/16. doi:10.1152/jappl.2001.91.1.425

Rundqvist, H., Veliça, P., Barbieri, L., Gameiro, P. A., Bargiela, D., Gojkovic, M., et al. (2020). Cytotoxic T-cells mediate exercise-induced reductions in tumor growth. *Elife* 9, e59996. Epub 2020/10/24. doi:10.7554/eLife.59996

Schmidt, M. E., Wiskemann, J., Armbrust, P., Schneeweiss, A., Ulrich, C. M., and Steindorf, K. (2015). Effects of resistance exercise on fatigue and quality of life in breast cancer patients undergoing adjuvant chemotherapy: A randomized controlled trial. *Int. J. Cancer* 137 (2), 471–480. Epub 2014/12/09. doi:10.1002/ijc.29383

Schmitz, K. H., Campbell, A. M., Stuiver, M. M., Pinto, B. M., Schwartz, A. L., Morris, G. S., et al. (2019). Exercise is medicine in oncology: Engaging clinicians to help patients move through cancer. *Ca. Cancer J. Clin.* 69 (6), 468–484. Epub 2019/10/17. doi:10.3322/caac.21579

Shao, L., Li, H., Chen, J., Song, H., Zhang, Y., Wu, F., et al. (2017). Irisin suppresses the migration, proliferation, and invasion of lung cancer cells via inhibition of epithelial-to-mesenchymal transition. *Biochem. Biophys. Res. Commun.* 485 (3), 598–605. Epub 2016/12/18. doi:10.1016/j.bbrc.2016.12.084

Shi, Y., Shi, H., Nieman, D. C., Hu, Q., Yang, L., Liu, T., et al. (2019). Lactic acid accumulation during exhaustive exercise impairs release of neutrophil extracellular traps in mice. *Front. Physiol.* 10, 709. Epub 2019/07/03. doi:10.3389/fphys.2019.00709

Shi, Y., Liu, T., Nieman, D. C., Cui, Y., Li, F., Yang, L., et al. (2020). Aerobic exercise attenuates acute lung injury through net inhibition. *Front. Immunol.* 11, 409. Epub 2020/04/09. doi:10.3389/fimmu.2020.00409

Smeda, M., Przyborowski, K., Proniewski, B., Zakrzewska, A., Kaczor, D., Stojak, M., et al. (2017). Breast cancer pulmonary metastasis is increased in mice undertaking spontaneous physical training in the running wheel; a call for revising beneficial effects of exercise on cancer progression. *Am. J. Cancer Res.* 7 (9), 1926–1936. Epub 2017/10/06.

Smith, H. A., and Kang, Y. (2013). The metastasis-promoting roles of tumor-associated immune cells. *J. Mol. Med.* 91 (4), 411–429. Epub 2013/03/22. doi:10.1007/s00109-013-1021-5

Souza, P. S., Gonçalves, E. D., Pedroso, G. S., Farias, H. R., Junqueira, S. C., Marcon, R., et al. (2017). Physical exercise attenuates experimental autoimmune encephalomyelitis by inhibiting peripheral immune response and blood-brain barrier disruption. *Mol. Neurobiol.* 54 (6), 4723–4737. Epub 2016/07/23. doi:10.1007/s12035-016-0014-0

Sprouse, M. L., Welte, T., Boral, D., Liu, H. N., Yin, W., Vishnoi, M., et al. (2019). Pmn-mdscs enhance ctc metastatic properties through reciprocal interactions via ros/notch/nodal signaling. *Int. J. Mol. Sci.* 20 (8), E1916. Epub 2019/04/21. doi:10.3390/ijms20081916

Steeg, P. S. (2016). Targeting metastasis. *Nat. Rev. Cancer* 16 (4), 201–218. Epub 2016/03/25. doi:10.1038/nrc.2016.25

Swann, J. B., and Smyth, M. J. (2007). Immune surveillance of tumors. *J. Clin. Invest.* 117 (5), 1137–1146. Epub 2007/05/04. doi:10.1172/jci31405

Szczerba, B. M., Castro-Giner, F., Vetter, M., Krol, I., Gkountela, S., Landin, J., et al. (2019). Neutrophils escort circulating tumour cells to enable cell cycle progression. *Nature* 566 (7745), 553–557. Epub 2019/02/08. doi:10.1038/s41586-019-0915-y

Tanaka, H., Shimizu, S., Ohmori, F., Muraoka, Y., Kumagai, M., Yoshizawa, M., et al. (2006). Increases in blood flow and shear stress to nonworking limbs during incremental exercise. *Med. Sci. Sports Exerc.* 38 (1), 81–85. Epub 2006/01/06. doi:10.1249/01.mss.0000191166.81789.de

Tang, H., Yu, R., Liu, S., Huwatibieke, B., Li, Z., and Zhang, W. (2016). Irisin inhibits hepatic cholesterol synthesis via ampk-srebp2 signaling. *EBioMedicine* 6, 139–148. Epub 2016/05/24. doi:10.1016/j.ebiom.2016.02.041

Thompson, H. J., Wolfe, P., McTiernan, A., Jiang, W., and Zhu, Z. (2010). Wheel running-induced changes in plasma biomarkers and carcinogenic response in the 1-methyl-1-nitrosourea-induced rat model for breast cancer. *Cancer Prev. Res.* 3 (11), 1484–1492. Epub 2010/09/30. doi:10.1158/1940-6207.Capr-10-0078

Timmons, B. W., and Cieslak, T. (2008). Human natural killer cell subsets and acute exercise: A brief review. *Exerc. Immunol. Rev.* 14, 8–23. Epub 2009/02/11.

Tittarelli, A., Janji, B., Van Moer, K., Noman, M. Z., and Chouaib, S. (2015). The selective degradation of synaptic connexin 43 protein by hypoxia-induced autophagy impairs natural killer cell-mediated tumor cell killing. *J. Biol. Chem.* 290 (39), 23670–23679. Epub 2015/07/30. doi:10.1074/jbc.M115.651547

Turbitt, W. J., Xu, Y., Sosnoski, D. M., Collins, S. D., Meng, H., Mastro, A. M., et al. (2019). Physical activity plus energy restriction prevents 4t1.2 mammary tumor progression, mdsc accumulation, and an immunosuppressive tumor microenvironment. *Cancer Prev. Res.* 12 (8), 493–506. Epub 2019/07/04. doi:10.1158/1940-6207.Capr-17-0233

Uribe-Querol, E., and Rosales, C. (2015). Neutrophils in cancer: Two sides of the same coin. *J. Immunol. Res.* 2015, 983698. Epub 2016/01/29. doi:10.1155/2015/983698

Walsh, N. P., Gleeson, M., Shephard, R. J., Gleeson, M., Woods, J. A., Bishop, N. C., et al. (2011). Position statement. Part One: Immune function and exercise. *Exerc. Immunol. Rev.* 17, 6–63. Epub 2011/03/31.

Wang, J. S., and Liao, C. H. (2004). Moderate-intensity exercise suppresses platelet activation and polymorphonuclear leukocyte interaction with surface-adherent platelets under shear flow in men. *Thromb. Haemost.* 91 (3), 587–594. Epub 2004/02/26. doi:10.1160/th03-10-0644

Wang, J. S., Li, Y. S., Chen, J. C., and Chen, Y. W. (2005). Effects of exercise training and deconditioning on platelet aggregation induced by alternating shear stress in men. *Arterioscler. Thromb. Vasc. Biol.* 25 (2), 454–460. Epub 2004/12/01. doi:10.1161/01.Atv.0000151987.04607.24

Wang, J. S., Chang, C. Y., Chow, S. E., Chen, Y. W., and Yang, C. M. (2007). Exercise modulates platelet-nasopharyngeal carcinoma cell aggregation and subsequent tissue factor and matrix metalloproteinase activities. *J. Appl. Physiol.* 103 (3), 763–770. Epub 2007/05/15. doi:10.1152/japplphysiol.00165.2007

Wang, J. S., Chung, Y., and Chow, S. E. (2009). Exercise affects platelet-impeded antitumor cytotoxicity of natural killer cell. *Med. Sci. Sports Exerc.* 41 (1), 115–122. Epub 2008/12/19. doi:10.1249/MSS.0b013e3181831f27

Wang, J., Liu, S., Li, G., and Xiao, J. (2020). Exercise regulates the immune system. *Adv. Exp. Med. Biol.* 1228, 395–408. Epub 2020/04/29. doi:10.1007/978-981-15-1792-1_27

Wang, J. S. (2006). Exercise prescription and thrombogenesis. *J. Biomed. Sci.* 13 (6), 753–761. Epub 2006/08/26. doi:10.1007/s11373-006-9105-7

Wennerberg, E., Lhuillier, C., Rybstein, M. D., Dannenberg, K., Rudqvist, N. P., Koelwyn, G. J., et al. (2020). Exercise reduces immune suppression and breast

cancer progression in a preclinical model. *Oncotarget* 11 (4), 452–461. Epub 2020/02/18. doi:10.18632/oncotarget.27464

Wu, D., Cao, W., Xiang, D., Hu, Y. P., Luo, B., and Chen, P. (2020). Exercise induces tissue hypoxia and hif-1α redistribution in the small intestine. *J. Sport Health Sci.* 9 (1), 82–89. Epub 2020/01/11. doi:10.1016/j.jshs.2019.05.002

Wu, X., Zhang, X., Yu, L., Zhang, C., Ye, L., Ren, D., et al. (2020). Zinc finger protein 367 promotes metastasis by inhibiting the Hippo pathway in breast cancer. *Oncogene* 39 (12), 2568–2582. Epub 2020/01/29. doi:10.1038/s41388-020-1166-y

Xu, Y., Wei, Z., Feng, M., Zhu, D., Mei, S., Wu, Z., et al. (2022). Tumor-infiltrated activated B cells suppress liver metastasis of colorectal cancers. *Cell Rep.* 40 (9), 111295. Epub 2022/09/01. doi:10.1016/j.celrep.2022.111295

Xue, D., Xia, T., Wang, J., Chong, M., Wang, S., and Zhang, C. (2018). Role of regulatory T cells and Cd8(+) T lymphocytes in the dissemination of circulating tumor cells in primary invasive breast cancer. *Oncol. Lett.* 16 (3), 3045–3053. Epub 2018/08/22. doi:10.3892/ol.2018.8993

Yazdani, H. O., Kaltenmeier, C., Morder, K., Moon, J., Traczek, M., Loughran, P., et al. (2021). Exercise training decreases hepatic injury and metastases through changes in immune response to liver ischemia/reperfusion in mice. *Hepatology* 73 (6), 2494–2509. Epub 2020/09/15. doi:10.1002/hep.31552

Zhang, Q. B., Zhang, B. H., Zhang, K. Z., Meng, X. T., Jia, Q. A., Zhang, Q. B., et al. (2016). Moderate swimming suppressed the growth and metastasis of the transplanted liver cancer in mice model: With reference to nervous system. *Oncogene* 35 (31), 4122–4131. Epub 2015/12/22. doi:10.1038/onc.2015.484

Zhang, Q. B., Meng, X. T., Jia, Q. A., Bu, Y., Ren, Z. G., Zhang, B. H., et al. (2016). Herbal compound songyou Yin and moderate swimming suppress growth and metastasis of liver cancer by enhancing immune function. *Integr. Cancer Ther.* 15 (3), 368–375. Epub 2015/12/25. doi:10.1177/1534735415622011

frontiers | Frontiers in Pharmacology

TYPE Original Research
PUBLISHED 17 November 2022
DOI 10.3389/fphar.2022.1053137

OPEN ACCESS

EDITED BY
Abhimanyu Thakur,
The University of Chicago, United States

REVIEWED BY
Rui Xu,
Nanjing Medical University, China
Tianru Wang,
Tongji University, China

*CORRESPONDENCE
Xiaoping Su,
xiaopingsu2013@aliyun.com
Ziwen Long,
longzw@shmu.edu.cn
Shiyi Chen,
cshiyi@163.com

†These authors have contributed equally to this work and share first authorship

SPECIALTY SECTION
This article was submitted to Pharmacology of Anti-Cancer Drugs, a section of the journal Frontiers in Pharmacology

RECEIVED 25 September 2022
ACCEPTED 07 November 2022
PUBLISHED 17 November 2022

CITATION
Luo Z, He Z, Qin H, Chen Y, Qi B, Lin J, Sun Y, Sun J, Su X, Long Z and Chen S (2022), Exercise-induced IL-15 acted as a positive prognostic implication and tumor-suppressed role in pan-cancer. *Front. Pharmacol.* 13:1053137. doi: 10.3389/fphar.2022.1053137

Exercise-induced IL-15 acted as a positive prognostic implication and tumor-suppressed role in pan-cancer

Zhiwen Luo[1†], Zhong He[2†], Haocheng Qin[2†], Yisheng Chen[1†], Beijie Qi[3], Jinrong Lin[1], Yaying Sun[1], Junming Sun[4], Xiaoping Su[5*], Ziwen Long[6*] and Shiyi Chen[1*]

[1]Department of Sports Medicine, Huashan Hospital, Fudan University, Shanghai, China, [2]Department of Rehabilitation, Huashan Hospital, Fudan University, Shanghai, China, [3]Department of Orthopedics, Shanghai Pudong Hospital, Fudan University, Shanghai, China, [4]Laboratory Animal Center, Guangxi Medical University, Nanning, China, [5]Guangxi Key Laboratory of Oral and Maxillofacial Rehabilitation and Reconstruction, College & Hospital of Stomatology, Guangxi Medical University, Nanning, China, [6]Department of Gastric Cancer Sugery, Fudan University Shanghai Cancer Center, Shanghai, China

Objective: Exercise can produce a large number of cytokines that may benefit cancer patients, including Interleukin 15 (IL-15). IL-15 is a cytokine that has multiple functions in regulating the adaptive and innate immune systems and tumorigenesis of lung and breast cancers. However, the roles of IL-15 in other types of cancer remain unknown. In this article, we try to systematically analyze if IL-15 is a potential molecular biomarker for predicting patient prognosis in pan-cancer and its connection with anti-cancer effects of exercise.

Methods: The expression of IL-15 was detected by The Cancer Genome Atlas (TCGA) database, Human protein Atlas (HPA), and Genotype Tissue-Expression (GTEX) database. Analysis of IL-15 genomic alterations and protein expression in human organic tissues was analyzed by the cBioPortal database and HPA. The correlations between IL-15 expression and survival outcomes, clinical features, immune-associated cell infiltration, and ferroptosis/cuproptosis were analyzed using the TCGA, ESTIMATE algorithm, and TIMER databases. Gene Set Enrichment Analysis (GSEA) was performed to evaluate the biological functions of IL-15 in pan-cancer.

Results: The differential analysis suggested that the level of IL-15 mRNA expression was significantly downregulated in 12 tumor types compared with normal tissues, which is similar to the protein expression in most cancer types. The high expression of IL-15 could predict the positive survival outcome of patients with LUAD (lung adenocarcinoma), COAD (colon adenocarcinoma), COADREAD (colon and rectum adenocarcinoma), ESCA (esophageal carcinoma), SKCM (skin cutaneous melanoma), UCS (uterine carcinosarcoma), and READ (rectum adenocarcinoma). Moreover, amplification was found to be the most frequent mutation type of IL-15 genomic. Furthermore, the expression of IL-15 was correlated to the infiltration levels of various immune-associated cells in pan-cancer assessed by the ESTIMATE algorithm and TIMER database. In addition, IL-15 is positively correlated with ferroptosis/cuproptosis-related genes (ACSL4 and LIPT1) in

pan-cancer. Levels of IL-15 were reported to be elevated in humans for 10–120 min following an acute exercise. Therefore, we hypothesized that the better prognosis of pan-cancer patients with regular exercise may be achieved by regulating level of IL-15.

Conclusion: Our results demonstrated that IL-15 is a potential molecular biomarker for predicting patient prognosis, immunoreaction, and ferroptosis/cuproptosis in pan-cancer and partly explained the anti-cancer effects of exercise.

KEYWORDS

pan-cancer, IL-15, prognosis, ferroptosis/cuproptosis, immune, exercise, multi-analyses

Introduction

Over time, the global rise in cancer incidence and mortality has corresponded with an increase in a range of cancer-related lifestyle factors, such as obesity and inactivity (Bray et al., 2018); thus, optimizing lifestyles and exercise (Anand et al., 2008) have been emphasized as tools for cancer prevention and management (Bourke et al., 2016; Gunnell et al., 2017). Exercise oncology-the application of sports medicine to cancer is a rapidly growing subspecialty within the field of clinical oncology, and the quantity and quality of research in this area are increasing (Jones and Alfano, 2013). Although substantial evidence has supported a link between exercise and reduced progression and mortality in several types of cancer: Exercise-induced myokines play an important role in increasing cytotoxicity and the infiltration of immune cells into the tumour on prostate cancer. Myokines released from activated skeletal muscle impaired growth and migration of PC(Pancreatic cancer) cells and enhanced PC cell death. However, the molecular mechanism between exercise and disease progression has not been fully elucidated. (Kim et al., 2021; Schwappacher et al., 2021). Research suggests that exercise could lead to a variety of physiological alterations, thereby reducing the risk of developing chronic disease. For example, the factors such as muscle secretome and catecholamines in serum will be regulated after exercise. (Jones and Alfano, 2013; Rönn et al., 2014; Bohlen et al., 2018; Chen et al., 2022). Preclinical evidence suggested that exercise may modulate levels of systemic factors such as local growth factors (IGF1), hormones (insulin and leptin), and inflammatory cytokines (IL-6, IL-15), which are known factors that have a possible impact on the cancer process (Kim et al., 2021). It has been determined that skeletal muscle is a significant source of IL-15 (rEF.146). After a single exercise session, IL-15 mRNA expression in skeletal muscle (Bohlen et al., 2018; Kim et al., 2021; Morrisson et al., 2021) was much greater in healthy volunteers than it was before the exercise (Riechman et al., 2004; Tamura et al., 2011). It was also widely reported that circulating levels of IL-15 were significantly higher after many kinds of exercise, which may benefit human health (Riechman et al., 2004; Nielsen et al., 2007; Tamura et al., 2011; Jones and Alfano, 2013; Bazgir et al., 2015; Crane et al., 2015; Palareti et al., 2016).

Interleukin 15 (IL-15) is a cytokine of the interleukin 2 (IL-2) family that has multiple functions similar to IL-2 in regulating the adaptive and innate immune systems (Bohlen et al., 2018). Although IL-15 is released in small amounts, the alpha receptor (IL15Rα), a transmembrane protein with a high affinity for IL-15, facilitates IL-15 transport from the endoplasmic reticulum through the cytoplasm and presents the IL-15/IL-15Rα complex on the cell surface (Nadeau and Aguer, 2019). Upon cell activation, IL-15 is secreted primarily by dendritic cells (DCs), macrophages, and monocytes (Do Thi et al., 2019); however, it can also be secreted by many other cell types, including endothelial cells, mesenchymal cells, and renal epithelial cells, but not by T cells or natural killer (NK) cells (Nielsen et al., 2007; Vilsmaier et al., 2021). With improved immune cell activation and migration, IL-15 is involved in anti-tumor immunity (Morrisson et al., 2021; Schwappacher et al., 2021; Vilsmaier et al., 2021). Many studies suggested that IL-15 is involved in tumor suppression by enhancing anti-tumor immunity (Crane et al., 2015; Dethlefsen et al., 2017; Bohlen et al., 2018; Liu et al., 2021). In recent years, many studies have been conducted to investigate the oncogenesis and development of pan-cancer to reveal the similarities and differences in cancer (Xu et al., 2021; Zhang et al., 2022). Therefore, it is of interest to further explore the spectrum of oncogenes in pan-cancer, but to date, there is no association analysis between IL-15 and pan-cancer.

Ferroptosis and cuproptosis are two forms of cell death induced by unbalanced ion homeostasis, which ferroptosis is driven by iron-dependent lipid peroxidation, while cuproptosis terms to intracellular copper accumulation triggers the aggregation and destabilization of proteins (Stockwell, 2022; Tang et al., 2022). A better understanding of the molecular determinants of the two cell death modes will contribute to innovate anticancer therapies (Lei et al., 2022; Tsvetkov et al., 2022). For example, much research has revealed that drugs targeting ferroptosis could kill cancer cells both *in vitro* and *in vivo* (Lei et al., 2022). Studies have reported $CD8^+$ T cells could activate ferroptosis in tumor cells *in vivo* and further induce cancer cells death(32778143). But currently, rare

studies have discovered the association between IL-15 and ferroptosis/cuproptosis-related genes in pan-cancers, which is wealthy to explore.

We have systematically investigated the role of IL-15 in human pan-cancer. We comprehensively investigated the different expression levels of IL-15 in tumor and normal control tissues by using The Cancer Genome Atlas (TCGA), Genotype-Tissue Expression (GTEX), and tumor-related databases. The predictive value of IL-15 on prognosis was also evaluated. Meanwhile, potential relationships between IL-15 mRNA expression levels and clinical features, DNA gene mutations, immune cells infiltration, and pathway regulation were evaluated in pan-cancer. This study highlights the multifaceted role of IL-15 in pan-cancer. Combined with its correlation with exercise, we provide a theoretical basis for exercise to prevent cancer and IL-15 as a pan-cancer therapeutic target.

Methods

Data processing and IL-15 expression analysis

Transcriptomic data and clinical features of tumor tissues were analyzed using UCSC Xena (https://xena.ucsc.edu/)) software (Chen et al., 2021). The GTEx portal (https://www.gtexportal.org/) was used to obtain Human normal tissue expression matrices. Strawberry Perl scripting software was applied to get the IL-15 expression data in 33 TCGA tumors and GTEx normal tissues (http://strawberryperl.com/, version 5.30.0.1). In addition, IL-15 expression in various tumor types and cell types was also assessed from the Human Protein Atlas database (https://www.proteinatlas.org/). The expression levels of IL-15 in healthy male and female tissues were presented by the Gganatgraph R program package. Expression data were cleared using log2 (TPM) to exclude missing data and duplicate values. R version 4.0.2 software was used (https://www.Rproject.org) to conduct the analysis. The Encyclopedia of Cancer Cell Lines (https://portals.broadinstitute.org/ccle/) was utilized to extract IL-15 mRNA expression in cell lines.

Immunohistochemical tissue

The relative IL-15 protein expression data in pan-cancer were obtained in the Human Protein Atlas (https://www.proteinatlas.org/) including both normal tissue and pathology tissue (Zhang et al., 2022). The overall expression can be observed directly through tissue samples.

Correlation analysis between genes in pan-cancer

The Timer database (https://cistrome.Shinyapps.io/Timer/) was utilized to analyze the relationship between the expression level of IL-15 and ferroptosis/cuproptosis-related genes in pan-cancerous tissues (Li et al., 2017). Ferroptosis: *SLC7A11, GPX4, CISD1, NFS1*, *NRF2*, *P53*, *VDACs*, *ACSL4*, and *NCOA4*; Cuproptosis: *CDKN2A*, *FDX1*, *DLD*, *DLAT*, *LIAS*, *GLS*, *LIPT1*, *MTF1*, *PDHA1*, and *PDHB*.

Genomic alterations IL-15 in pan-cancer

The genetic alterations of IL-15 in the TCGA pan-cancer dataset were analyzed using the Bioportal database (http://www.cbioportal.org/) (Cerami et al., 2012). Data on the genetic alterations and mutation sites of IL-15 was gotten from the "OnCoprint", "Summary of Cancer Types" and "Mutations" modules.

Association analysis of IL-15 expression with tumor immune microenvironment in cancers

The lollipop plots were produced by R (3.6.3 version, GSVA packages) to show the correlation between IL-15 expression and immune cells, including aDC [activated DC]; B cells; $CD8^+$ T cells; Cytotoxic cells; DC; Eosinophils; iDC [immature DC]; Macrophages; Mast cells; Neutrophils; NK CD56bright cells; NK CD56dim cells; NK cells; pDC [Plasmacytoid DC]; T cells; T helper cells; Tcm [T central memory]; Tem [T effector memory]; Tfh [T follicular helper]; Tgd [T gamma delta]; Th1 cells; Th17 cells; Th2 cells; Treg.

The Timer database (https://cistrome.Shinyapps.io/Timer/) was utilized to analyze the relationship between the expression level of IL-15 and the abundance of various immune-related cells in pan-cancerous tissues (Li et al., 2017). The expression of IL-15 in various cancer types was assessed by the "diff Exp" module in the Timer database.

The biological functions of IL-15 were analyzed using the Gene Set Enrichment Analysis (GSEA) (Luo et al., 2022a; Luo et al., 2022b; Sun et al., 2022). The GSEA online database (https://www.gsea-msigdb.org/gsea/downloads.jsp) was used to perform Kyoto Encyclopedia of Genes and Genomes (KEGG) analysis and the biological functions of IL-15 in pan-cancer were conducted *via* GSEA analysis using the R-packages "cluster Profiler".

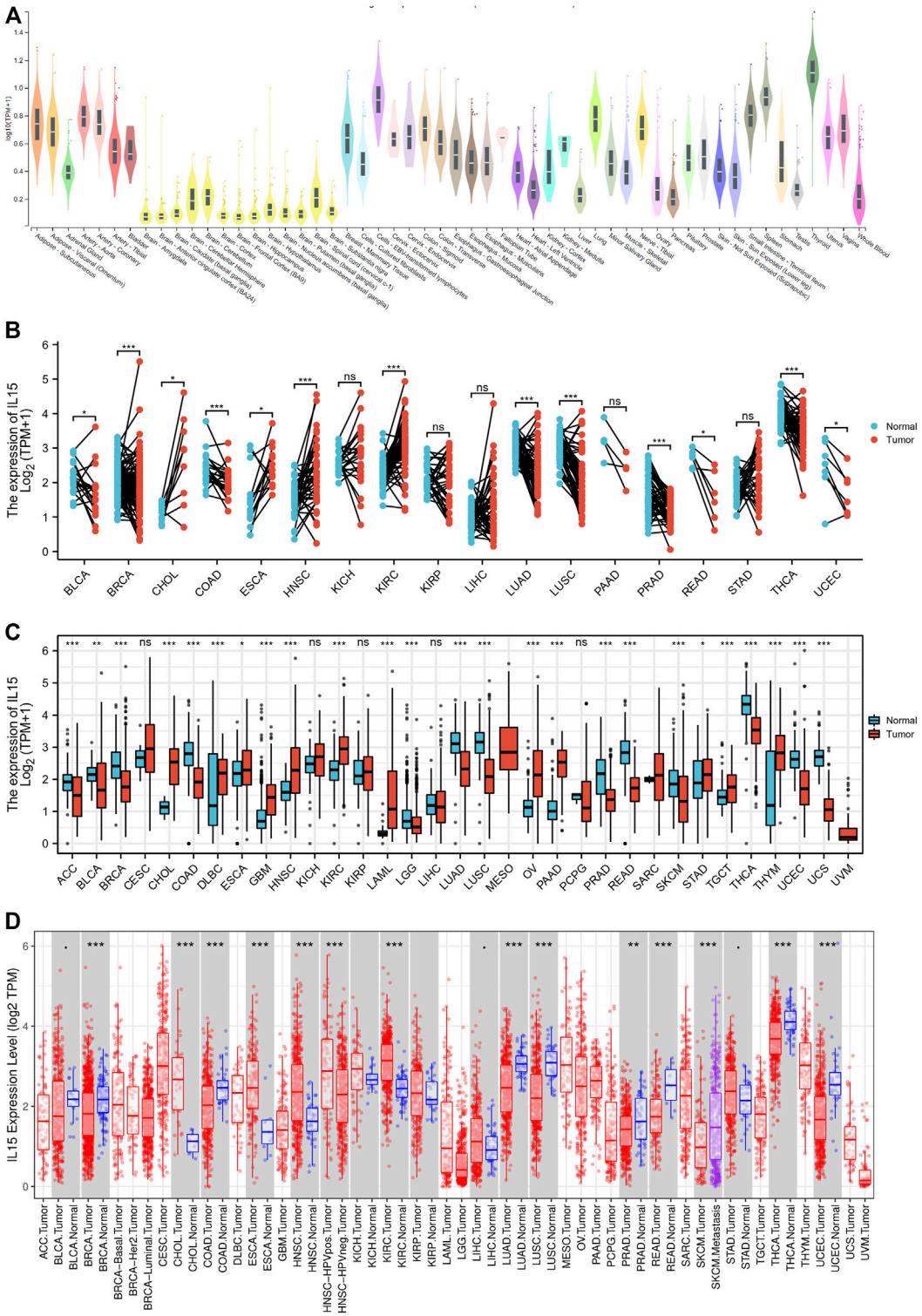

FIGURE 1
Differential expression pattern of IL-15. **(A)** IL-15 mRNA expression in normal tissues from GTEX data. **(B)** Differential IL-15 mRNA expression between paired samples in TCGA cancers. The red dot represents cancer samples, and the blue dot represents paired normal samples. **(C)** Differential IL-15 mRNA expression between TCGA cancers and GTEX normal tissues. The red column represents cancer samples, and the blue column represents normal samples. The normal group was normal tissue in TCGA and GTEX databases. **(D)** IL-15 mRNA expression in different cancer types in TIMER. The normal group was normal tissue in the TCGA database. *$p < 0.05$, **$p < 0.01$, and ***$p < 0.001$.

Statistical analysis

Differences in expression and correlation between the two groups were assessed by Wilcoxon rank-sum test and the Spearman rank-sum test. Kaplan-Meier survival curves with the log-rank test were applied to survival analysis. Besides, Hazard ratios (HR) were calculated using Cox proportional risk regression models. In addition, statistical analysis was calculated by GraphPad Prism 9.0 and R software (4.0.2). $p < 0.05$ was considered statistically significant.

Results

Expression of IL-15 in normal tissue and pan-cancer

To assess the mRNA expression of IL-15 in human normal tissue, IL-15 expression was tested in physiological tissue of the GTEX dataset. IL-15 was overexpressed in the thyroid, adipose, endocrine tissues, bone marrow, and lung tissues (Figure 1A; Supplementary Figures S1A–C). As for IL-15 in normal cell types, endometrial stromal cells and monocytes express the highest level of IL-15 mRNA (Supplementary Figure S1D). The expression abundances of IL-15 in various tissues within male and female were also observed. Generally, no significant difference was found between gender and IL-15 mRNA expression levels (Supplementary Figure S1E). According to the Atlas database, IL-15 was decreased in almost all the human cell which in lines with analysis of the CCLE database except the Lymphoid cell line (Supplementary Figure S1F).

Then, *via* analyzing the RNA-seq data of TCGA and GTex databases, the expression of IL-15 in pan-cancer was assessed deeper. A significant expression difference of IL-15 was evaluated in 33 types of cancer in paired or unpaired samples except those without normal tissue data. In paired samples (Figure 1B), IL-15 expression was downregulated in BLCA (bladder urothelial carcinoma), BRCA (breast invasive carcinoma), COAD (colon adenocarcinoma), LUAD (lung adenocarcinoma), PRAD (prostate adenocarcinoma), READ (rectum adenocarcinoma), THCA (thyroid carcinoma), and UCEC (uterine corpus endometrial carcinoma), while upregulated in CHOL (cholangiocarcinoma), ESCA (esophageal carcinoma), HNSC (head and neck squamous cell carcinoma), and KIRC (kidney renal clear cell carcinoma). In unpaired samples (Figure 1C), IL-15 expression was considerably downregulated in ACC (adrenocortical carcinoma), BLCA, BRCA, COAD, LUAD, LUSC (lung squamous cell carcinoma), PRAD, READ, THCA, LGG (brain lower grade glioma), SKCM (skin cutaneous melanoma) and UCEC, while upregulated in CHOL, DLBC (lymphoid neoplasm diffuse large B-cell lymphoma), ESCA, GBM (glioblastoma multiforme), HNSC, KIRC, LAML (acute myeloid leukemia), OV (ovarian serous cystadenocarcinoma), PAAD (pancreatic adenocarcinoma), STAD (stomach adenocarcinoma), TGCT (testicular germ cell tumors), and THYM (thymoma) compared to control tissues. Next, the mRNA expression of IL-15 in human pan-cancer was further assessed in the TIMER database. IL-15 expression was increased in CHOL, ESCA, and HNSC, while IL-15 was significantly decreased in BRCA, ESCA, LUAD, LUSC, PRAD, READ, SKCM, THCA, UCEC, and COAD (Figure 1D) compared to the control group.

Protein expression of the IL-15 in human tissues

The protein levels of IL-15 in pan-cancer were assessed by the Human Protein Atlas (HPA) (Figure 2). The protein levels of IL-15 were considerably downregulated in COADREAD (colon and rectum adenocarcinoma), LUAD, BRCA, and BLCA, while it was not obvious in LGG, SKCM, THCA, and PRAD compared with corresponding normal tissues.

Prognostic assessment value of IL-15 in pan-cancer

To investigate the prognostic assessment value of IL-15 in pan-cancer, Kaplan–Meier analysis and Cox proportional hazards model were performed to assess the relationship between IL-15 expression levels and patients' survival period (Figure 3). The expression of IL-15 was positive correlated with OS (overall survival) in LUAD ($p = 0.037$), COAD ($p = 0.045$), COADREAD ($p = 0.008$), SKCM ($p < 0.001$), PCPG ($p = 0.032$), UCS (Uterine Carcinosarcoma, $p = 0.014$) and READ ($p = 0.029$) as a good prognostic marker performed by Cox proportional hazards regression model. On the contrary, IL-15 was regarded as a high-risk factor for OS of GBM, OSCC, LGG, THYM, LIHC, LAML, PAAD, and GBMLGG (Supplementary Table S1; Supplementary Figure S2). In addition, DSS (disease-specific survival) of ESCA ($p = 0.029$), COADREAD ($p = 0.004$), COAD ($p = 0.047$), LUAD ($p = 0.037$), READ ($p = 0.017$), and SKCM ($p < 0.001$) were also positive correlated with IL-15 expression level, while that of GBM ($p = 0.005$) and LGG ($p < 0.001$) was negative correlated with IL-15 levels. For PFI (Progression-Free Interval), the overexpressed mRNA level of IL-15 showed an adverse factor in LGG ($p < 0.001$), THYM ($p = 0.019$), GBM ($p < 0.001$), PRAD ($p = 0.026$) and OV ($p = 0.022$) (Supplementary Table S1). Kaplan–Meier curves for PFI indicated a positive correlation between IL-15 overexpression and good survival outcome in patients with LUAD ($p = 0.048$), COAD ($p = 0.006$), COADREAD ($p < 0.001$), SKCM ($p < 0.001$), UCS ($p = 0.012$) and READ ($p = 0.002$) (Supplementary Table S1). Therefore, we performed the following assessments on the good-survival patients positive correlated with high IL-15 expression, including LUAD, PCPG, COAD, READ, COADREAD, ESCA, SKCM, and UCS.

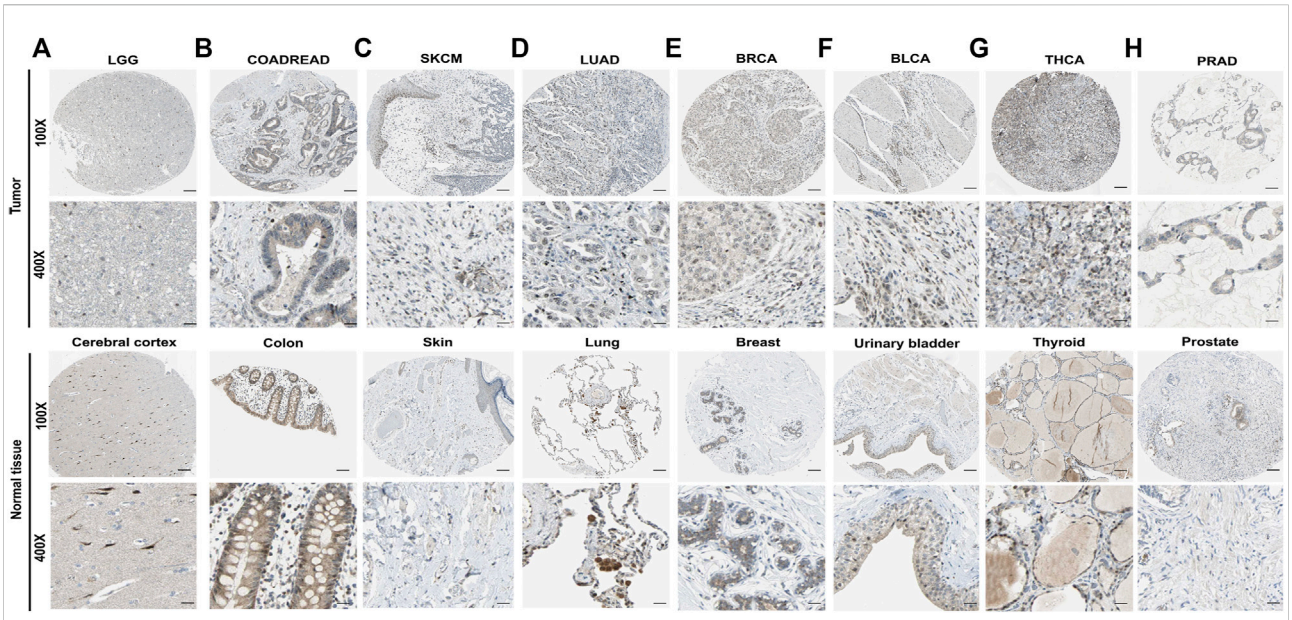

FIGURE 2
The protein expression level of IL-15 in human multiple cancer tissues **(A)** LGG, **(B)** COADREAD, **(C)** SKCM, **(D)** LUAD, **(E)** BRCA, **(F)** BLCA, **(G)** THCA, and **(H)** PRAD. Representative images of IL-15 expression in pan-cancer tissues are shown. Original magnification, ×100 and ×400. Scare bar = 200 μm or 50 μm.

Correlation analysis between IL-15 expression and clinicopathological phenotypes in pan-cancer

The correlation between the mRNA expression level of IL-15 and patients' clinicopathological features progression was further investigated in pan-cancer. IL-15 expression was negatively correlated to tumor stage in LUAD, COAD, READ, COADREAD, ESCA and SKCM (Supplementary Figures S4A–G). Higher expression of IL-15 was found in the age≥65 years group in COAD ($p < 0.05$) (Supplementary Figure S3C). It was discovered that IL-15 expression level was not significantly associated with tumor treatment response, especially between CR and PR groups (Supplementary Figure S4). Then, it was found that the overexpression of IL-15 was significantly associated with tumor status in COAD, SKCM, and COADREAD (Supplementary Figures S4C,E,G). In the three cancer types, patients with lower IL-15 expression were with higher-level tumor status. These results suggest that IL-15 expression levels could impact the prognosis in LUAD, COAD, READ, COADREAD, ESCA, and SKCM patients.

Genetic alteration analysis of IL-15 in pan-cancer

Pan-cancer patients with uterine corpus endometrial carcinoma, sarcoma, cholangiocarcinoma, and esophageal adenocarcinoma owned the highest gene alteration rate of IL-15 (>2%) compared with the primary type in the cBioPortal database (Figure 4A). Three main types of frequent genetic alterations of IL-15 were missense mutation, amplification, and deep deletion (Figure 4B). Figure 4C further presented the types, sites, and case numbers of the IL-15 gene modification. IL-15 missense mutation was the main type of alteration, while splice alteration was detected in 3 cases. Amplification, gain function, and diploid were the Top-3 frequent putative copy-number alterations of IL-15 (Figure 4D). The gene alteration of IGLVIL-66-1, ALC5A6, Lnc00189, MFSD13B, PPP1R1A, REX1BD, NUP50-DT, and SKP1P2 was more frequent in the altered group than in the unaltered group (Figure 4E).

Correlation of IL-15 expression with tumor immune microenvironment

To further assess the relationship between IL-15 and the human immune system, based on the ssGSEA algorithm and TIMER database, the relationship between IL-15 expression and the tumor immune microenvironment was evaluated (Figure 5). First of all, the relationship between IL-15 expression and immune-associated cells infiltration in pan-cancer was assessed using the ssGSEA algorithm. It was found that almost all the relative immune cells including aDC, B cells, $CD8^+$ T cells, Cytotoxic cells, DC, Eosinophils, iDC,

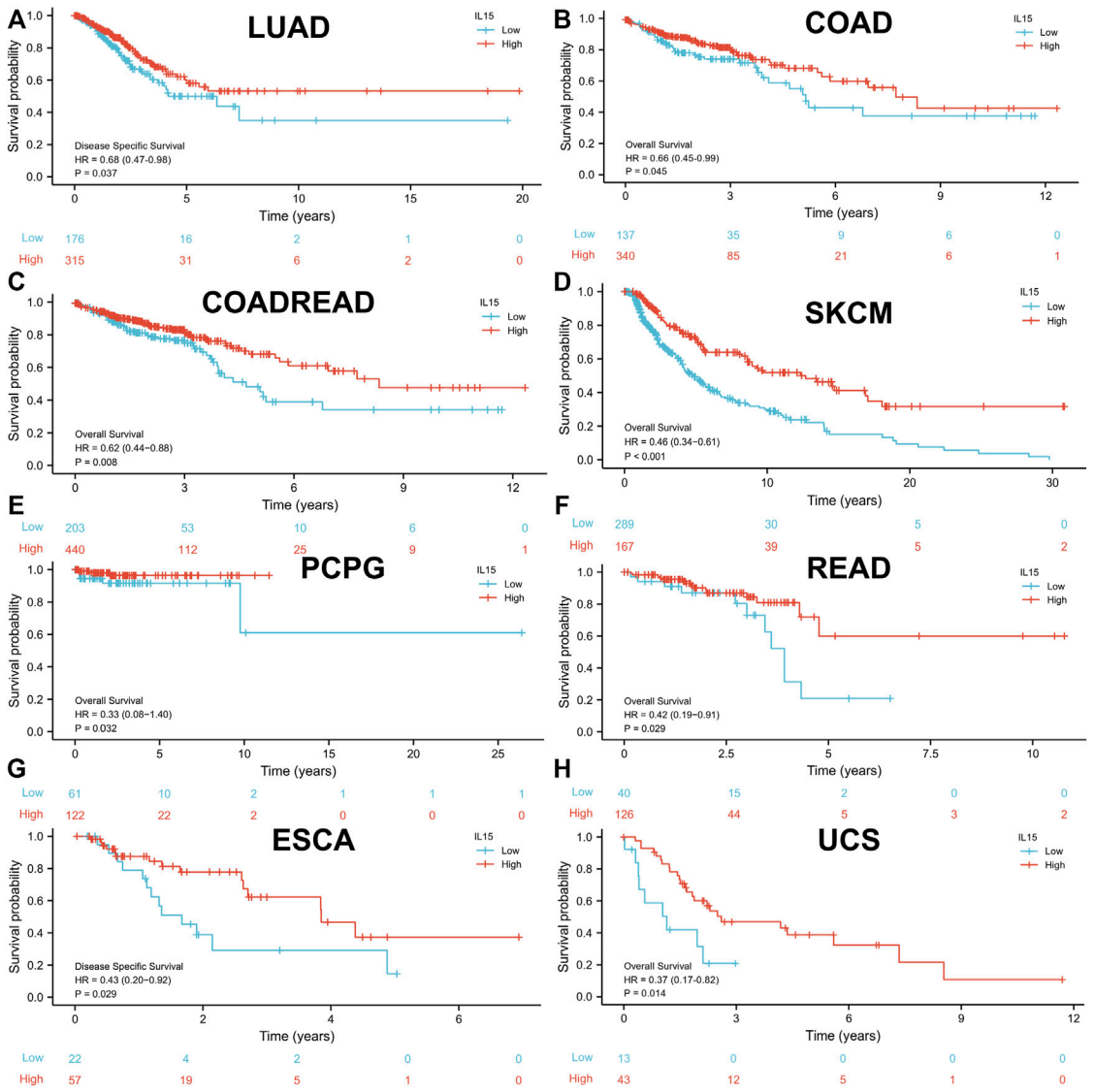

FIGURE 3
High expression of IL-15 promoted patient survival period. **(A and G)** Kaplan–Meier analysis of the association between IL-15 expression and DSS in LUAD and ESCA. **(B–F,H)** Kaplan–Meier analysis of the correlation between IL-15 expression and OS in COAD, COADREAD, SKCM, PCPG, READ, and UCS. The red line shows high IL-15 expression, and the blue line represents low IL-15 expression. OS, overall survival; DSS, disease-specific survival.

Macrophages, Neutrophils, NK CD56- cells, NK cells, T cells, T helper cells, Tcm, Tem, fh, Tgd, Th1 cells, and Treg, were positively correlated with IL-15 except Th17 cells, NK CD56$^+$ cells, Th2 cells, Mast cells, and pDC presented by Lollipop diagrams. The boxplot displayed the statistical significance of T cells, NK cells, macrophages, CD8$^+$ T cells, and B cells with low or high IL-15 expression., in which enrichment scores of the high IL-15 group were significantly higher than that of the low IL-15 group except for NK cells. Next, the TIMER database was used to further evaluate the relationship between immune-associated cells infiltration and IL-15 expression in pan-cancer. It was shown that IL-15 expression was significantly correlated with six types of infiltrating immune-associated cells including B cells, CD8$^+$T cells, CD4$^+$T cells, neutrophils, macrophages, and dendritic cells in LUAD, COAD, SKCM, ESCA, and USC, except PCPG (Supplementary Figure S4).

Biological function of IL-15 in cancer

The main (Top-5) biological processes affected by IL-15 were explored by GSEA analysis in pan-cancer. Based on KEGG gene

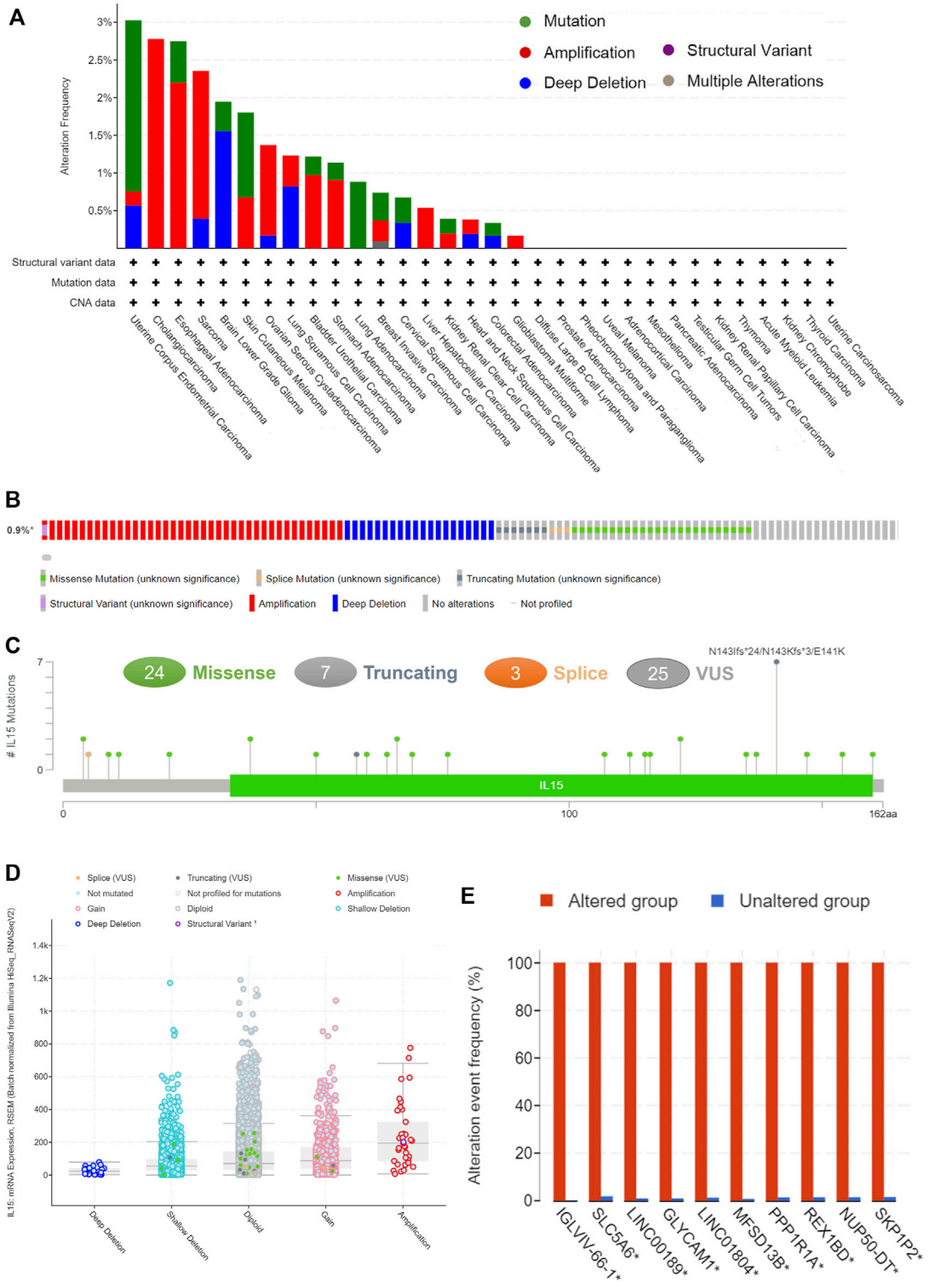

FIGURE 4
The genetic alterations of IL-15. **(A)** Alteration summary of IL-15 in TCGA pan-cancer datasets. **(B)** Summary of IL-15 structural variant, mutations, and copy-number alterations. **(C)** The mutation types, number, and sites of the IL-15 genetic alterations. **(D)** The alteration types of IL-15 in pan-cancer. **(E)**The related genes alteration frequency in the IL-15 altered group (Red) and unaltered group (blue).

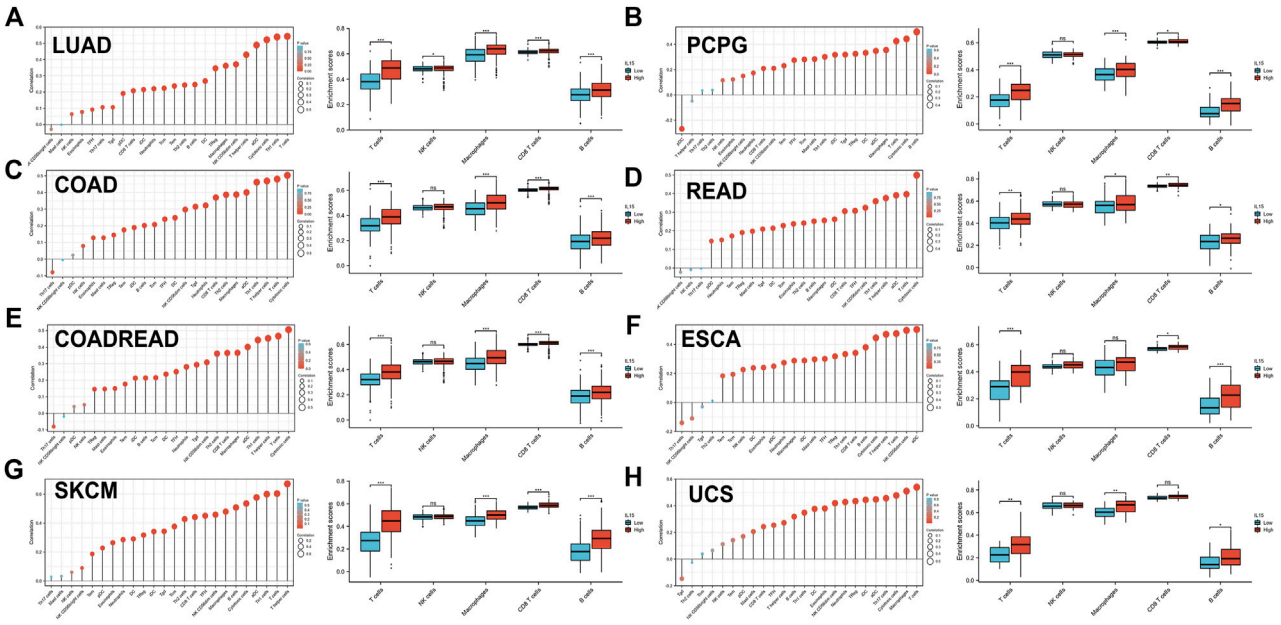

FIGURE 5
Correlation between IL-15 gene expression and tumor immune microenvironment in TCGA database. **(A–H)** Analysis of immune-associated cells infiltration with IL-15 expression in pan-cancer using lollipop diagrams and box plots. *$p < 0.05$, **$p < 0.01$, and ***$p < 0.001$.

sets analysis, the data suggested that IL-15 positively regulated signaling pathways in LUAD, PCPG, COAD, READ, COADREAD, ESCA, SKACM, and UCS (Figure 6). Cytokine receptor interaction and Gαs signaling were the most common signaling pathways of IL-15 for pan-cancer, followed by olfactory transduction, neutrophil degranulation, immunoregulatory interactions pathway. In addition, GPCR(G Protein-Coupled Receptor) ligand binding, infection, phagocytosis, and DNA damage checkpoint pathways were all involved in IL-15 biology function in pan-cancer biological analysis.

Correlation of IL-15 expression with ferroptosis-related genes and survival analysis

We first analyzed the expression of ferroptosis-related genes with IL-15 in LUAD, the largest sample size, and our results only found a correlation between *ACSL4* and IL-15 (Figure 7). We further analyzed the expression of *ACSL4* in pan-cancer, and we found a strong and significant positive correlation between ACSL4 and IL-15 in SKCM patients, and a general level of positive correlation in *PCPG, UCS, ESCA, COAD,* and *LUAD* (p less than 0.05), while the correlation was not strong in READ. Further, we analyzed the relationship between *ACSL4* and overall survival, and we found that in SKCM, high expression of *ACSL4* significantly increased patient survival (p less than 0.05). The above results suggest that the improvement of overall survival in SKCM by IL-15 may be achieved by promoting the expression of iron death-related genes. In addition, low expression of *ACSL4* protein was found in SKCM and *ACSL4* protein was relatively higher in normal skin tissue.

Correlation of IL-15 expression with cuproptosis-related genes and survival analysis

We first analyzed the expression of cuproptosis-related genes with IL-15 in LUAD and SKCM, which had the largest sample size, and our results found a correlation between *LIPT1*, *FDX1*, *MTF1*, and IL-15, and *LIPT1* was the strongest (R = 0.348) (Figure 8). Further, we analyzed the expression of LIPT14 in pan-cancer, and we found that LIPT1 and IL-15 had a strong and significant positive correlation in SKCM and READ, and a general level of positive correlation in LUAD, ESCA, PCPG (p less than 0.05), but not with UCS, COAD. We further analyzed the relationship between *ACSL4* and overall survival, and we found that in SKCM, high expression of *LIPT1* significantly increased the survival rate of patients (p less than 0.05), meanwhile, in LUAD, high expression of *LIPT1* also show general prognostic impact ($p = 0.055$). The above results suggest that IL-15 improves the overall survival of SKCM, and LUAD may be reached by promoting the expression of

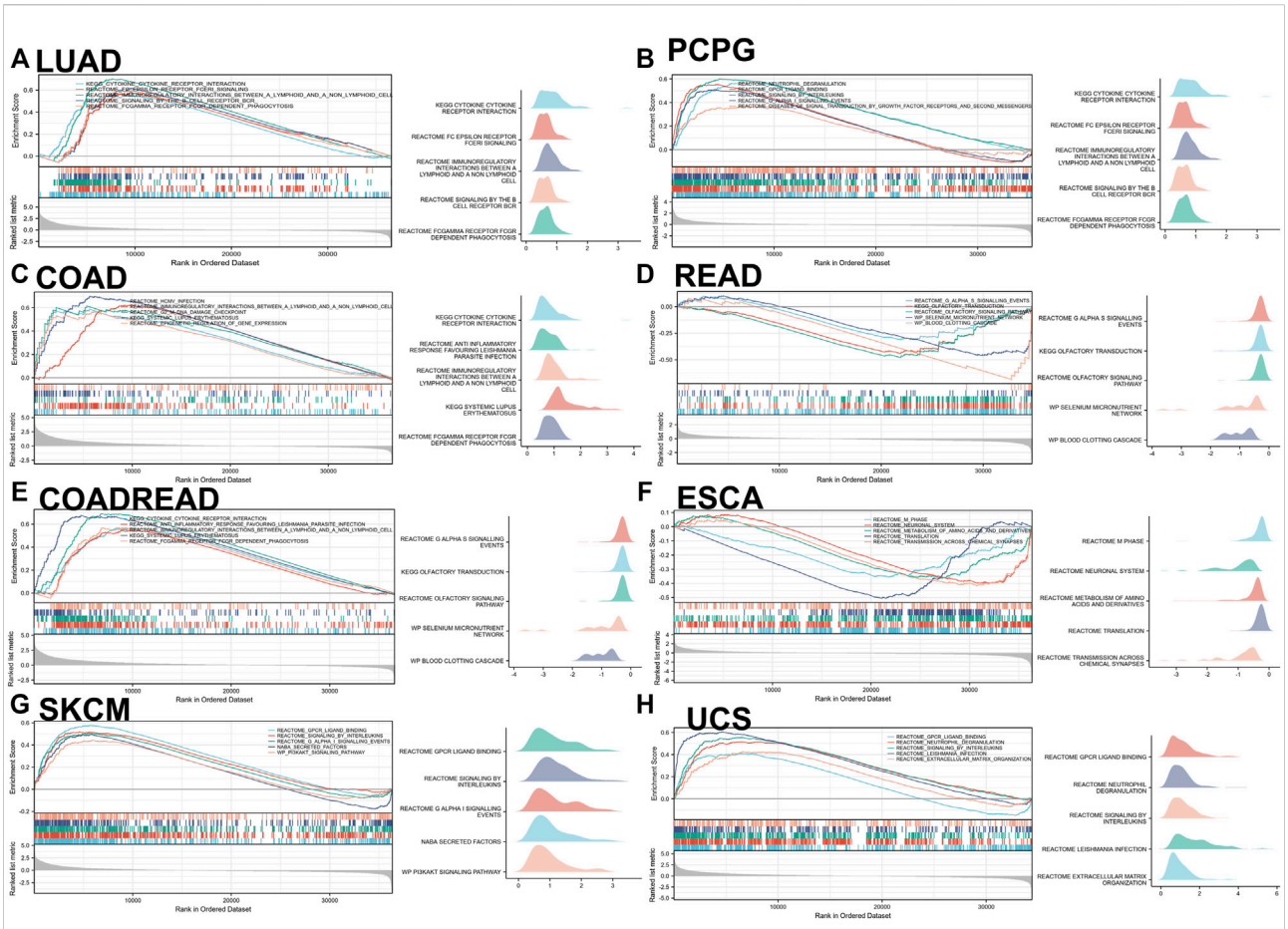

FIGURE 6
GSEA analysis in KEGG signature of IL-15 in LUAD **(A)**, PCPG **(B)**, COAD **(C)**, READ **(D)**, COADREAD **(E)**, ESCA **(F)**, SKCM **(G)**, and UCS **(H)**. The left panel: Different color curves show different functions or pathways (Top 5). The peak of the upward and downward curve represents the positive and negative regulation of IL-15, respectively. Score, enrichment score. The right panel: Summary of GSEA plots of representative data is presented. The horizontal axis is the degree of correlation, and the vertical axis is the corresponding pathway.

cuproptosis-related genes. Furthermore, low expression of *LIPT1* protein was found in SKCM and *LIPT1* protein was relatively higher in normal skin tissue.

Discussion

Numerous studies have shown that circulating levels of IL-15 are elevated in humans for 10–120 min following an acute exercise (Riechman et al., 2004; Tamura et al., 2011; Crane et al., 2015). For example, Regular endurance training for 12 weeks led to a 40% rise in the amount of IL-15 protein in the basal skeletal muscle (Rinnov et al., 2014). Weightlifting increased circulating IL-15 levels in untrained and trained young subjects during and immediately after exercise (Nielsen et al., 2007; Bazgir et al., 2015; Nadeau and Aguer, 2019; Kim et al., 2021). Recently, IL-15 has emerged as a promising cytokine for the treatment of cancer (Berger et al., 2019; Ligibel et al., 2019; Xiao et al., 2019; Schwappacher et al., 2021; Pereira et al., 2022). IL-15 is also a key factor in the development, proliferation, and activation of NK cells and $CD8^+$ T cells (Berger et al., 2019; Do Thi et al., 2019; Fiore et al., 2020; Liu et al., 2021), which are able to destroy cancer cells in the tumor microenvironment. Several current products include ALT-803 ALT-803 (Hu et al., 2018), P22339 (Hu et al., 2018), chimeric IL-15 apolipoprotein A-I (Ochoa et al., 2018), or NKTR-255 (Miyazaki et al., 2021), illustrating the promise of IL-15 in cancer therapy. Recently, some completed clinical trials have reported usage of recombinant human single-chain IL-15 and IL-15 superagonist in cancer treatment (Zhang et al., 2021). Conlon et al. utilized recombinant human single-chain IL-15 to treat metastatic malignant melanoma or renal cell cancer patient with maximum tolerated dose 0.3 ug/kg (Conlon et al., 2015). The results indicated IL-15 could dramatically mediate the NK cells in blood. In the following study by Conlon et al.and Miller et al., the results showed a better mediated effect to NK cells and $CD8^+$ cells

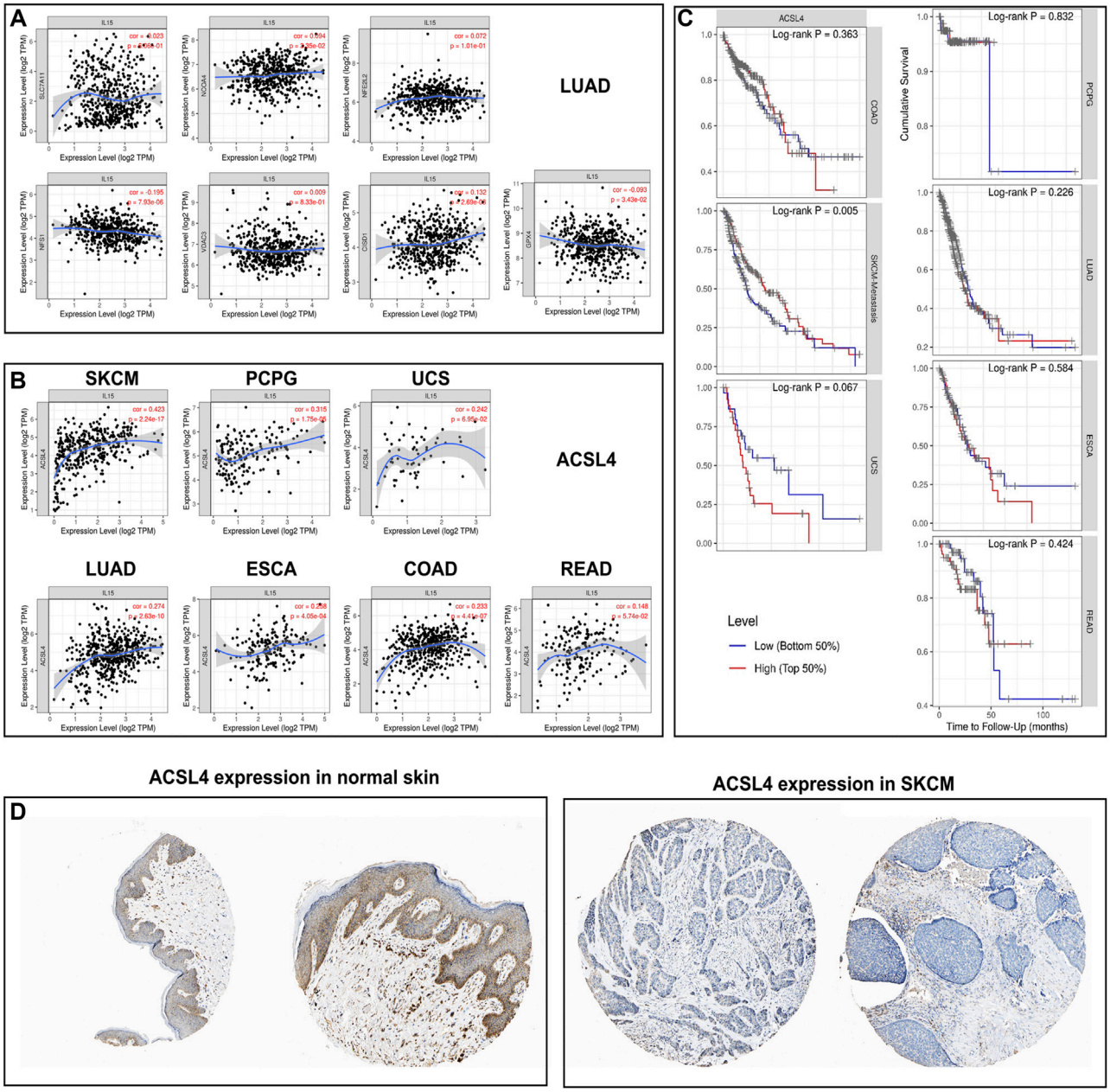

FIGURE 7
Correlation and survival analysis for IL-15 and ferroptosis-related genes in pan-cancers **(A)** Correlation between IL-15 and ferroptosis-related genes in LUAD. **(B)** Correlation between IL-15 and *ACSL4* in pan-cancers. **(C)** Survival analysis for *ACSL4* in pan-cancers. **(D)** Protein expression of *ACSL4* in SKCM and normal skin tissue.

when the maximum tolerated dose up to 2 ug/kg (Miller et al., 2018; Conlon et al., 2019). However, no studies have explored IL-15 in pan-cancer, limiting its possible clinical application, and the present study has explored the relevance by focusing on both prognostic and immunological directions.

It was found in this study that IL-15 is highly expressed in the thyroid, intestine, bone marrow, and lymphatic system, while it is less expressed in tissues such as skin and pancreas and varies independently of sex. It was also decreased in most tumor cell lines and was highly expressed in epithelial cells and monocytes, which are similar to the previous reports (Van Acker et al., 2018; Nadeau and Aguer, 2019; Xiao et al., 2019; Liu et al., 2021). IL-15 gene expression was found to be downregulated in BLCA, BRCA, COAD, LUAD, PRAD, READ, THCA, and UCEC in both

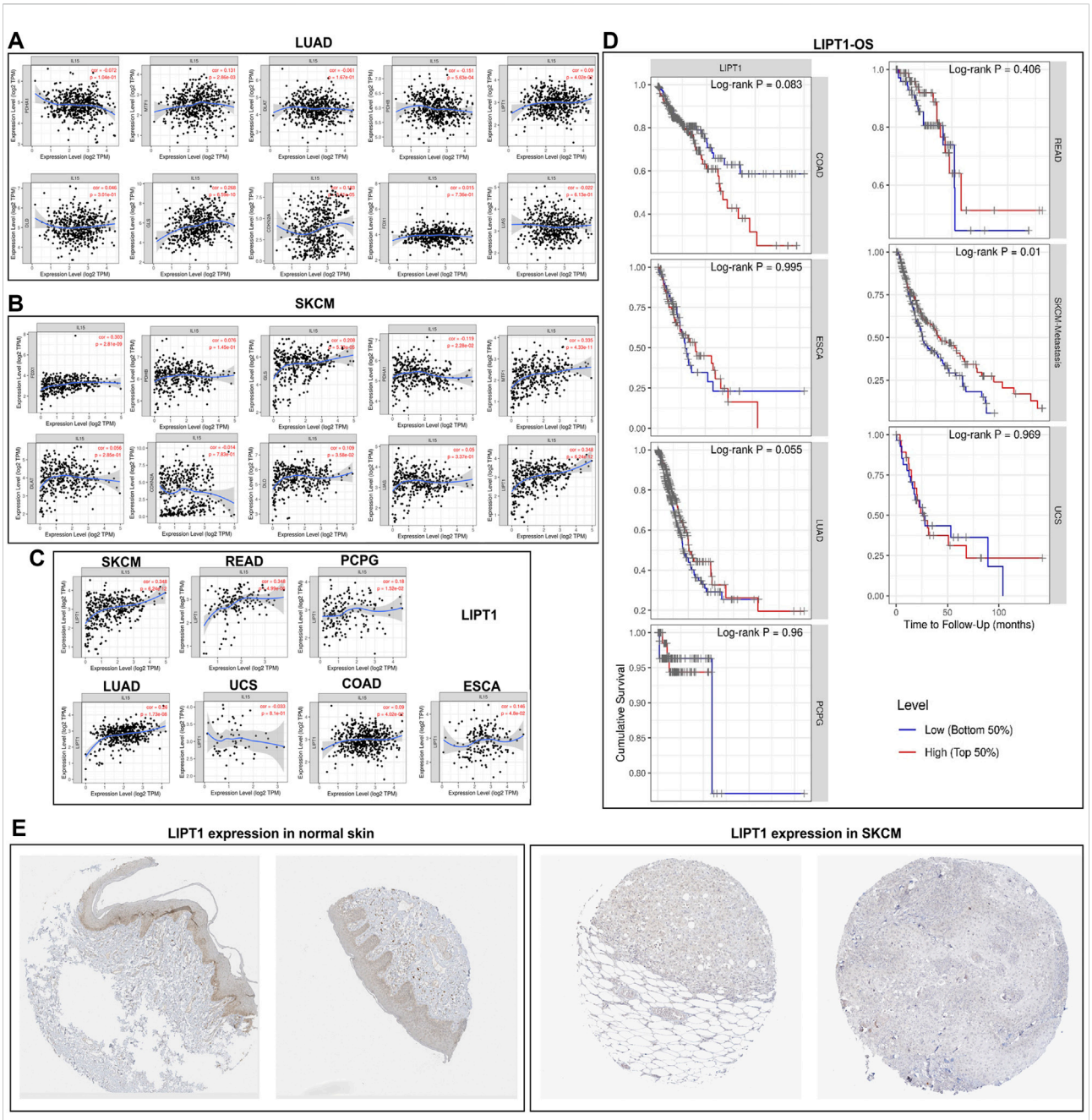

FIGURE 8
Correlation and survival analysis for IL-15 and cuproptosis-related genes in pan-cancers **(A)** Correlation between IL-15 and cuproptosis-related genes in LUAD. **(B)** Correlation between IL-15 and cuproptosis -related genes in SKCM. **(C)** Correlation between IL-15 and *LIPT1* in pan-cancers. **(D)** Survival analysis for *LIPT1* in pan-cancers. **(E)** Protein expression of *LIPT1* in SKCM and normal skin tissue.

matched and unmatched specimens in the TCGA database, GTex database, and TIMER database. We further examined IL-15 expression in tissues and found that the relative expression of IL-15 protein was downregulated in COADREAD, LUAD, BRCA, and BLCA. Currently, rare studies have checked the IL-15 expression in pan-cancer using tissue microassays except in those databases. Cierna et al. (2021) found that decreased levels of circulating IL-15 suggested PD-L1 overexpression in tumors of primary breast cancer patients and poor prognosis. Krizia et al. (Cierna et al., 2021) reported that higher IL-15 levels would lead to better outcomes in prostate cancer, which is consistent with our findings. Margolin et al. (2018) recently found that the injection of IL-15N72D: IL-15RαSu/IgG1 Fc complex could reduce cancer growth, induce

NK cell expansion and improve survival in patients with incurable advanced melanoma, renal cell, non-small cell lung, and head and neck cancer. The above results suggest that IL-15 plays an important role in the development of human cancers.

Next, we sought to analyze the relationship between mRNA expression levels of IL-15 and the prognosis of patients with cancer. Kaplan-Meier survival analysis showed that OS in LUAD, COAD, COADREAD, SKCM, UCS, and READ, OS in LUAD, COAD, COADREAD, SKCM, UCS and READ, PFI in ESCA, COADREAD, COAD, LUAD, READ, and DSS in SKCM were positively correlated with IL-15 expression, with statistically significant differences. In addition, we found that IL-15 was significantly lower in COAD, SKCM, and COADREAD with worse clinical staging compared to patients with lower staging. These results may confirm that IL-15 plays a protective role in human cancers. However, we also found that mRNA expression levels of IL-15 played a cancer-promoting role in GBM, OSCC, LGG, THYM, LIHC, LAML, PAAD, and GBMLGG. These suggest that the mechanism of IL-15 in cancers are complex and IL-15 may play a negative role in certain cancer types in a specific condition, which will need to be further tested in the future (Waldmann, 2014; Fiore et al., 2020; Cierna et al., 2021). For example, overexpression of IL-15 mRNA is associated with clinical staging and metastasis in cutaneous T-cell lymphoma (Döbbeling et al., 1998), but we found from the Kaplan-Meier database that IL-15 is more likely to be a protective factor for patients with SKCM. In addition, clinical studies have reported a correlation between high intra-tumor IL-15 concentrations and poor clinical outcomes in patients with lung cancer (Seike et al., 2007), which is contrary to our results. We suspect that the discrepancy between our online database results and the reported data may be due to the different methods used to detect IL-15 expression. Gene expression of IL-15 in lung adenocarcinoma, whereas mRNA and protein expression of IL-15 was detected in the Kaplan-Meier and Atlas databases. Therefore, the result of this study should be further validated in corresponding cancer samples for deeper investigation.

The IL-15 gene is located on chromosome 4q31 and encoded the 14–15 kDa glycoprotein-IL-15(54). IL-15 deficiency, due to mutations in its gene, has been extensively studied in many diseases, such as liver injury (Hou et al., 2012), diabetes (Liu et al., 2017) and allergy (Mathias et al., 2017). However, there are rare studies on the alteration of the IL-15 gene in human tumors. Therefore, we used the cBio-portal database to reveal the fact that amplification is the greatest frequency of IL-15 changes in pan-cancer. Alterations in IGLVIL-66-1, ALC5A6, Lnc00189, MFSD13B, PPP1R1A, REX1BD, NUP50-DT, and SKP1P2 were found to co-exist among IL-15 mutations. However, by our assay, we found that IL-15 variants do not seem to affect the prognosis of cancer patients (data not presented). Furthermore, studies have reported that if IL-15 deficiency leads to a range of problems (Gillgrass et al., 2014; Mathias et al., 2017; Van Acker et al., 2018; Schwappacher et al., 2021), suggesting that these variants may not affect the functional profile of IL-15 in cancer.

Due to a marked reduction in the number of peripheral lymphocytes, NK cells, T cells in IL-15-deficient mice (Grabstein et al., 1994; Miller et al., 2018), we believed that IL-15 may play an important role in the immune regulation of human tumors. Firstly, we used the ssGSEA algorithm in the TCGA database and found that IL-15 was positively associated with a range of immune cells including aDC, B cells, $CD8^+$ T cells, Cytotoxic cells, DC, Eosinophils, iDC, Macrophages, Neutrophils, NK $CD56^-$ cells, NK cells, T cells, T helper cells, Tcm, Tem, fh, Tgd, Th1 cells, and Treg. Only NK $CD56^+$ cells, Th2 cells, Mast cells, and pDC were not significantly positively correlated with IL-15 expression. Timer database mining further revealed that IL-15 expression was significantly correlated with infiltration levels of a variety of immune-related cells, including B cells, $CD8^+$T cells, $CD4^+$T cells, neutrophils, macrophages, and dendritic cells in LUAD, COAD, SKCM, ESCA, and USC. The role of IL-15 in the human immune system has been studied in recent years. In mouse models, exogenous IL-1t5 treatment can reverse the downregulation of NK cell and T cell activity in IL-15 deficient mice (Kennedy et al., 2000). In terms of the cancer microenvironment, systemic IL-15 treatment reduced tumor growth, metastasis, and recurrence by increasing the cytotoxic effects of NK cells in mice inoculated with a lung and breast cancer models (Tang et al., 2008; Gillgrass et al., 2014). A preclinical study showed reduced tumor growth and increased immune cell infiltration in a mouse model of prostate cancer with IL-15 overexpression 2.5-fold and 2.7-fold higher numbers of $CD8^+$ T cells and NK cells, respectively than in mice in the model without IL-15 injection (Morris et al., 2014). Our study suggested that IL-15 could also be useful in LUAD, COAD, SKCM, ESCA, and USC by improving the infiltration of the immune cells in tumors.

Furthermore, it has been suggested that IL-15 plays an important role in modulating lipid metabolism and glucose metabolism (Nadeau and Aguer, 2019; Kim et al., 2021). In mice, high levels of circulating IL-15 prevented abnormal glucose tolerance and insulin resistance induced by the high-fat diet. Overexpression of muscle-specific IL-15 in mice and supraphysiological IL-15 treatment in rats resulted in lower respiratory exchange rates and higher whole-body fatty acid oxidation, showing a greater tendency to use lipids as a high-energy fuel (Almendro et al., 2006; Morris et al., 2014). The series of abnormal expressions of lipid metabolism and gluconeogenic signaling pathways that may be induced by the reduction of IL-15 in pan-cancer may lead to the metabolic dysfunction of the body in the development of cancer (Crane et al., 2015; Bohlen et al., 2018; Nadeau and Aguer, 2019). This can at least partly explain why the upregulated IL-15 gene expression can be a risk factor in OS of GBM, OSCC, LGG, THYM, LIHC, LAML, PAAD, and GBMLGG in our results. Moreover, GPCR ligand binding, infection, phagocytosis, and DNA damage checkpoints were found to be IL-15 mediated pathways in pan-cancer, which deserved further investigation.

Finally, we analyzed the relationship between IL-15 and ion-induced death and their impact on clinical prognosis. Our results show that IL-15 is positively associated with ferroptosis/cuproptosis-related genes in various types of tumors, such as *LIPT1, ACSL4*. High expression of these genes can improve the prognosis of patients with SKCM and LUAD, which suggests that IL-15 may be able to kill cancer cells by activating the process of ferroptosis/cuproptosis. The literature reports that loss *ACSL4* will promote cancer progress and enhanced *ACSL4* expression will result in better clinical outcomes in tumors (Liao et al., 2022). Furthermore, high LIPT1 expression was reported to be a good prognostic factor in SKCM (Lv et al., 2022), which is in line with our work. IL-15 may be in synergy with ferroptosis/cuproptosis inducers for tumor treatment in the future.

Further studies can continue to delve into the evidence of potential associations between IL-15 expression and DNA mismatch repair system, microsatellite instability, ferroptosis/cuproptosis, or tumor mutation burden, and explore the possibility that IL-15 may influence the response of cancer patients to immune checkpoint therapy, which will contribute to further understanding of the mechanisms of immunotherapy for cancer treatment. In addition, pharmacological target exploration can be performed to search for drugs that can target or synergize IL-15 and contribute to clinical cancer treatment.

Conclusion

This study systematically evaluated the characteristics of IL-15 in various aspects, including expression pattern, survival prognosis, genetic mutation, tumor immune microenvironment, ferroptosis/cuproptosis, and signaling pathway. Exercise-induced IL-15 might serve as a potential candidate for multiple-cancer treatments since it showed low expression in multiple cancers and predicted a better prognosis in cancer patients. Moreover, the aberrant IL-15 expression may be related to the tumour immune microenvironment in multiple types of cancer. This study highlights the positive roles of IL-15 in pan-cancer and provides data-based insights for the application of IL-15 in cancer treatment.

Data availability statement

The original contributions presented in the study are included in the article/Supplementary Material, further inquiries can be directed to the corresponding authors.

Author contributions

ZWLu, ZH, and YC came out with the idea and designed the study. HQ, JL, BQ, ZH, and ZWLu analysed the data. ZWLu and YS was the major contributor to writing the manuscript. SC, JS, ZWLo and XS supervised the study and edited the manuscript. All authors have confirmed and approved the final version of the manuscript.

Funding

Supported by the project of the National Natural Science Foundation of China (grant number 82102634; 82172509; 81772419; 81972062); and Healthy Shanghai Project, No. JKSHZX-2022-02.

Acknowledgments

The authors thank all of the members of the laboratory of the Shanghai Institute of Nutrition and Health (CAS) for their encouragement and assistance in this study.

Conflict of interest

The authors declare that the research was conducted in the absence of any commercial or financial relationships that could be construed as a potential conflict of interest.

Publisher's note

Supplementary material

The Supplementary Material for this article can be found online at: https://www.frontiersin.org/articles/10.3389/fphar.2022.1053137/full#supplementary-material

References

Almendro, V., Busquets, S., Ametller, E., Carbó, N., Figueras, M., Fuster, G., et al. (2006). Effects of interleukin-15 on lipid oxidation: Disposal of an oral [(14)C]-triolein load. *Biochim. Biophys. Acta* 1761, 37–42. doi:10.1016/j.bbalip.2005.12.006

Anand, P., Kunnumakara, A. B., Sundaram, C., Harikumar, K. B., Tharakan, S. T., Lai, O. S., et al. (2008). Cancer is a preventable disease that requires major lifestyle changes. *Pharm. Res.* 25, 2097–2116. doi:10.1007/s11095-008-9661-9

Bazgir, B., Salesi, M., Koushki, M., and Amirghofran, Z. (2015). Effects of eccentric and concentric emphasized resistance exercise on IL-15 serum levels and its relation to inflammatory markers in athletes and non-athletes. *Asian J. Sports Med.* 6, e27980. doi:10.5812/asjsm.27980

Berger, A., Colpitts, S. J., Seabrook, M. S. S., Furlonger, C. L., Bendix, M. B., Moreau, J. M., et al. (2019). Interleukin-15 in cancer immunotherapy: IL-15 receptor complex versus soluble IL-15 in a cancer cell-delivered murine leukemia model. *J. Immunother. Cancer* 7, 355–413. doi:10.1186/s40425-019-0777-8

Bohlen, J., McLaughlin, S. L., Hazard-Jenkins;Infante, H. A. M., Montgomery, C., Davis, M., Pistilli, E. E., et al. (2018). Dysregulation of metabolic-associated pathways in muscle of breast cancer patients: Preclinical evaluation of interleukin-15 targeting fatigue. *J. Cachexia Sarcopenia Muscle* 9, 701–714. doi:10.1002/jcsm.12294

Bourke, L., Smith, D., Steed, L., Hooper, R., Carter, A., Catto, J., et al. (2016). Exercise for men with prostate cancer: A systematic review and meta-analysis. *Eur. Urol.* 69, 693–703. doi:10.1016/j.eururo.2015.10.047

Bray, F., Ferlay, J., Soerjomataram, I., Siegel, R. L., Torre, L. A., and Jemal, A. (2018). Global cancer statistics 2018: GLOBOCAN estimates of incidence and mortality worldwide for 36 cancers in 185 countries. *Ca. Cancer J. Clin.* 68, 394–424. doi:10.3322/caac.21492

Cerami, E., Gao, J., Dogrusoz, U., Gross, B. E., Sumer, S. O., Aksoy, B. A., et al. (2012). The cBio Cancer Genomics Portal: An open platform for exploring multidimensional cancer genomics data. *Cancer Discov.* 2, 401–404. doi:10.1158/2159-8290.CD-12-0095

Chen, Y., Sun, Y., Luo, Z., Chen, X., Wang, Y., Qi, B., et al. (2022). Exercise modifies the transcriptional regulatory features of monocytes in alzheimer's patients: A multi-omics integration analysis based on single cell technology. *Front. Aging Neurosci.* 14. doi:10.3389/fnagi.2022.881488

Chen, Y., Sun, Y., Xu, Y., Lin, W-W., Luo, Z., Han, Z., et al. (2021). Single-cell integration analysis of heterotopic ossification and fibrocartilage developmental lineage: Endoplasmic reticulum stress effector Xbp1 transcriptionally regulates the notch signaling pathway to mediate fibrocartilage differentiation. *Oxid. Med. Cell. Longev.* 2021, 7663366–7663429. doi:10.1155/2021/7663366

Cierna, Z., Smolkova, B., Cholujova, D., Gronesova, P., Miklikova, S., Cihova, M., et al. (2021). Decreased levels of circulating cytokines VEGF, TNF-β and IL-15 indicate PD-L1 overexpression in tumours of primary breast cancer patients. *Sci. Rep.* 11, 1294–1311. doi:10.1038/s41598-020-80351-9

Conlon, K. C., Lugli, E., Welles, H. C., Rosenberg, S. A., Fojo, A. T., Morris, J. C., et al. (2015). Redistribution, hyperproliferation, activation of natural killer cells and CD8 T cells, and cytokine production during first-in-human clinical trial of recombinant human interleukin-15 in patients with cancer. *J. Clin. Oncol.* 33, 74–82. doi:10.1200/JCO.2014.57.3329

Conlon, K. C., Potter, E. L., Pittaluga, S., Lee, C. R., Miljkovic, M. D., Fleisher, T. A., et al. (2019). IL15 by continuous intravenous infusion to adult patients with solid tumors in a phase I trial induced dramatic NK-cell subset expansion. *Clin. Cancer Res.* 25, 4945–4954. doi:10.1158/1078-0432.CCR-18-3468

Crane, J. D., Macneil, L. G., Lally, J. S., Ford, R. J., Bujak, A. L., Brar, I. K., et al. (2015). Exercise-stimulated interleukin-15 is controlled by AMPK and regulates skin metabolism and aging. *Aging Cell* 14, 625–634. doi:10.1111/acel.12341

Dethlefsen, C., Hansen, L. S., Lillelund, C., Andersen, C., Gehl, J., Christensen, J. F., et al. (2017). Exercise-induced catecholamines activate the Hippo tumor suppressor pathway to reduce risks of breast cancer development. *Cancer Res.* 77, 4894–4904. doi:10.1158/0008-5472.CAN-16-3125

Do Thi, V. A., Jeon, H. M., Park, S. M., Lee, H., and Kim, Y. S. (2019). Cell-based Il-15:Il-15rα secreting vaccine as an effective therapy for CT26 colon cancer in mice. *Mol. Cells* 42, 869–883. doi:10.14348/molcells.2019.0188

Döbbeling, U., Dummer, R., Laine, E., Potoczna, N., Qin, J. Z., Burg, G., et al. (1998). Interleukin-15 is an autocrine/paracrine viability factor for cutaneous T-cell lymphoma cells. *Blood* 92, 252–258. doi:10.1182/blood.v92.1.252.413k08_252_258

Fiore, P. F., Di Matteo, S., Tumino, N., Mariotti, F. R., Pietra, G., Ottonello, S., et al. (2020). Interleukin-15 and cancer: Some solved and many unsolved questions. *J. Immunother. Cancer* 8, e001428. doi:10.1136/jitc-2020-001428

Gillgrass, A., Gill, N., Babian, A., and Ashkar, A. A. (2014). The absence or overexpression of IL-15 drastically alters breast cancer metastasis via effects on NK cells, CD4 T cells, and macrophages. *J. Immunol.* 193, 6184–6191. doi:10.4049/jimmunol.1303175

Grabstein, K. H., Eisenman, J., Shanebeck, K., Rauch, C., Srinivasan, S., Fung, V., et al. (1994). Cloning of a T cell growth factor that interacts with the β chain of the interleukin-2 receptor. *Science* 264 (80-), 965–968. doi:10.1126/science.8178155

Gunnell, A. S., Joyce, S., Tomlin, S., Taaffe, D. R., Cormie, P., Newton, R. U., et al. (2017). Physical activity and survival among long-term cancer survivor and non-cancer cohorts. *Front. Public Heal* 5, 19. doi:10.3389/fpubh.2017.00019

Hou, H-S., Liao, C-L., Sytwu, H-K., Liao, N-S., Huang, T-Y., Hsieh, T-Y., et al. (2012). Deficiency of interleukin-15 enhances susceptibility to acetaminophen-induced liver injury in mice. *PLoS One* 7, e44880. doi:10.1371/journal.pone.0044880

Hu, Q., Ye, X., Qu, X., Cui, D., Zhang, L., Xu, Z., et al. (2018). Discovery of a novel IL-15 based protein with improved developability and efficacy for cancer immunotherapy. *Sci. Rep.* 8, 7675–7711. doi:10.1038/s41598-018-25987-4

Jones, L. W., and Alfano, C. M. (2013). Exercise-oncology research: Past, present, and future. *Acta Oncol.* 52, 195–215. doi:10.3109/0284186X.2012.742564

Kennedy, M. K., Glaccum, M., Brown, S. N., Butz, E. A., Viney, J. L., Embers, M., et al. (2000). Reversible defects in natural killer and memory CD8 T cell lineages in interleukin 15-deficient mice. *J. Exp. Med.* 191, 771–780. doi:10.1084/jem.191.5.771

Kim, J. S., Galvão, D. A., Newton, R. U., Gray, E., and Taaffe, D. R. (2021). Exercise-induced myokines and their effect on prostate cancer. *Nat. Rev. Urol.* 18, 519–542. doi:10.1038/s41585-021-00476-y

Lei, G., Zhuang, L., and Gan, B. (2022). Targeting ferroptosis as a vulnerability in cancer. *Nat. Rev. Cancer* 22, 381–396. doi:10.1038/s41568-022-00459-0

Li, T., Fan, J., Wang, B., Traugh, N., Chen, Q., Liu, J. S., et al. (2017). Timer: A web server for comprehensive analysis of tumor-infiltrating immune cells. *Cancer Res.* 77, e108–e110. doi:10.1158/0008-5472.CAN-17-0307

Liao, P., Wang, W., Wang, W., Kryczek, I., Li, X., Bian, Y., et al. (2022). CD8+ T cells and fatty acids orchestrate tumor ferroptosis and immunity via ACSL4. *Cancer Cell* 40, 365–378.e6. doi:10.1016/j.ccell.2022.02.003

Ligibel, J. A., Dillon, D., Giobbie-Hurder, A., McTiernan, A., Frank, E., Cornwell, M., et al. (2019). Impact of a pre-operative exercise intervention on breast cancer proliferation and gene expression: Results from the pre-operative health and body (PreHAB) study. *Clin. Cancer Res.* 25, 5398–5406. doi:10.1158/1078-0432.CCR-18-3143

Liu, B., Zhu, X., Kong, L., Wang, M., Spanoudis, C., Chaturvedi, P., et al. (2021). Bifunctional TGF-β trap/IL-15 protein complex elicits potent NK cell and CD8+ T cell immunity against solid tumors. *Mol. Ther.* 29, 2949–2962. doi:10.1016/j.ymthe.2021.06.001

Liu, Z., Liang, G., Gui, L., Li, Y., Liu, M., Bai, Y., et al. (2017). Weakened IL-15 production and impaired mTOR activation alter dendritic epidermal T cell homeostasis in diabetic mice. *Sci. Rep.* 7, 6028. doi:10.1038/s41598-017-05950-5

Luo, Z., Qi, B., Sun, Y., Chen, Y., Lin, J., Qin, H., et al. (2022). Engineering bioactive M2 macrophage-polarized, anti-inflammatory, miRNA-based liposomes for functional muscle repair: From exosomal mechanisms to biomaterials. *Small* 18, 2201957. doi:10.1002/smll.202201957

Luo, Z., Sun, Y., Qi, B., Lin, J., Chen, Y., Xu, Y., et al. (2022). Human bone marrow mesenchymal stem cell-derived extracellular vesicles inhibit shoulder stiffness via let-7a/Tgfbr1 axis. *Bioact. Mat.* 17, 344–359. doi:10.1016/j.bioactmat.2022.01.016

Lv, H., Liu, X., Zeng, X., Liu, Y., Zhang, C., Zhang, Q., et al. (2022). Comprehensive analysis of cuproptosis-related genes in immune infiltration and prognosis in melanoma. *Front. Pharmacol.* 13, 930041. doi:10.3389/fphar.2022.930041

Margolin, K., Morishima, C., Velcheti, V., Miller, J. S., Lee, S. M., Silk, A. W., et al. (2018). Phase I trial of ALT-803, a novel recombinant IL15 complex, in patients with advanced solid tumors. *Clin. Cancer Res.* 24, 5552–5561. doi:10.1158/1078-0432.CCR-18-0945

Mathias, C. B., Schramm, C. M., Guernsey, L. A., Wu, C. A., Polukort, S. H., Rovatti, J., et al. (2017). IL-15-deficient mice develop enhanced allergic responses to airway allergen exposure. *Clin. Exp. Allergy* 47, 639–655. doi:10.1111/cea.12886

Miller, J. S., Morishima, C., McNeel, D. G., Patel, M. R., Kohrt, H. E. K., Thompson, J. A., et al. (2018). A first-in-human phase I study of subcutaneous outpatient recombinant human IL15 (rhIL15) in adults with advanced solid tumors. *Clin. Cancer Res.* 24, 1525–1535. doi:10.1158/1078-0432.CCR-17-2451

Miyazaki, T., Maiti, M., Hennessy, M., Chang, T., Kuo, P., Addepalli, M., et al. (2021). NKTR-255, a novel polymer-conjugated rhIL-15 with potent antitumor efficacy. *J. Immunother. Cancer* 9, 0020244–e2112. doi:10.1136/jitc-2020-002024

Morris, J. C., Ramlogan-Steel, C. A., Yu, P., Black, B. A., Mannan, P., Allison, J. P., et al. (2014). Vaccination with tumor cells expressing IL-15 and IL-15R inhibits murine breast and prostate cancer. *Gene Ther.* 21, 393–401. doi:10.1038/gt.2014.10

Morrisson, M. J., Bi, F., Yang, K., Cady, S. L., Hartwich, T. M., Cerchia, A. P., et al. (2021). Effect of exercise on peritoneal microenvironment and progression of ovarian cancer. *Am. J. Cancer Res.* 11, 5045–5062.

Nadeau, L., and Aguer, C. (2019). Interleukin-15 as a myokine: Mechanistic insight into its effect on skeletal muscle metabolism. *Appl. Physiol. Nutr. Metab.* 44, 229–238. doi:10.1139/apnm-2018-0022

Nielsen, A. R., Mounier, R., Plomgaard, P., Mortensen, O. H., Penkowa, M., Speerschneider, T., et al. (2007). Expression of interleukin-15 in human skeletal muscle - effect of exercise and muscle fibre type composition. *J. Physiol.* 584, 305–312. doi:10.1113/jphysiol.2007.139618

Ochoa, M. C., Minute, L., López, A., Pérez-Ruiz, E., Gomar, C., Vasquez, M., et al. (2018). Enhancement of antibody-dependent cellular cytotoxicity of cetuximab by a

chimeric protein encompassing interleukin-15. *Oncoimmunology* 7, e1393597. doi:10.1080/2162402X.2017.1393597

Palareti, G., Legnani, C., Cosmi, B., Antonucci, E., Erba, N., Poli, D., et al. (2016). Comparison between different D-Dimer cutoff values to assess the individual risk of recurrent venous thromboembolism: Analysis of results obtained in the DULCIS study. *Int. J. Lab. Hematol.* 38, 42–49. doi:10.1111/ijlh.12426

Pereira, M. G., Voltarelli, V. A., Tobias, G. C., de Souza, L., Borges, G. S., de Almeida, N. R., et al. (2022). Aerobic exercise training and *in vivo* akt activation counteract cancer cachexia by inducing a hypertrophic profile through eif-2α modulation. *Cancers (Basel)* 14, 28. doi:10.3390/cancers14010028

Riechman, S. E., Balasekaran, G., Roth, S. M., and Ferrell, R. E. (2004). Association of interleukin-15 protein and interleukin-15 receptor genetic variation with resistance exercise training responses. *J. Appl. Physiol.* 97, 2214–2219. doi:10.1152/japplphysiol.00491.2004

Rinnov, A., Yfanti, C., Nielsen, S., Akerström, T. C. A., Peijs, L., Zankari, A., et al. (2014). Endurance training enhances skeletal muscle interleukin-15 in human male subjects. *Endocrine* 45, 271–278. doi:10.1007/s12020-013-9969-z

Rönn, T., Volkov, P., Tornberg, A., Elgzyri, T., Hansson, O., Eriksson, K. F., et al. (2014). Extensive changes in the transcriptional profile of human adipose tissue including genes involved in oxidative phosphorylation after a 6-month exercise intervention. *Acta Physiol.* 211, 188–200. doi:10.1111/apha.12247

Schwappacher, R., Dieterich, W., Reljic, D., Pilarsky, C., Mukhopadhyay, D., Chang, D. K., et al. (2021). Muscle-Derived cytokines reduce growth, viability and migratory activity of pancreatic cancer cells. *Cancers (Basel)* 13, 3820. doi:10.3390/cancers13153820

Seike, M., Yanaihara, N., Bowman, E. D., Zanetti, K. A., Budhu, A., Kumamoto, K., et al. (2007). Use of a cytokine gene expression signature in lung adenocarcinoma and the surrounding tissue as a prognostic classifier. *J. Natl. Cancer Inst.* 99, 1257–1269. doi:10.1093/jnci/djm083

Stockwell, B. R. (2022). Ferroptosis turns 10: Emerging mechanisms, physiological functions, and therapeutic applications. *Cell* 185, 2401–2421. doi:10.1016/j.cell.2022.06.003

Sun, Y., Luo, Z., Chen, Y., Lin, J., Zhang, Y., Qi, B., et al. (2022). si-Tgfbr1-loading liposomes inhibit shoulder capsule fibrosis via mimicking the protective function of exosomes from patients with adhesive capsulitis. *Biomater. Res.* 26, 39. doi:10.1186/s40824-022-00286-2

Tamura, Y., Watanabe, K., Kantani, T., Hayashi, J., Ishida, N., and Kaneki, M. (2011). Upregulation of circulating IL-15 by treadmill running in healthy individuals: Is IL-15 an endocrine mediator of the beneficial effects of endurance exercise? *Endocr. J.* 58, 211–215. doi:10.1507/endocrj.k10e-400

Tang, D., Chen, X., and Kroemer, G. (2022). Cuproptosis: A copper-triggered modality of mitochondrial cell death. *Cell Res.* 32, 417–418. doi:10.1038/s41422-022-00653-7

Tang, F., Zhao, L., Jiang, Y., Ba, D., Cui, L., and He, W. (2008). Activity of recombinant human interleukin-15 against tumor recurrence and metastasis in mice. *Cell. Mol. Immunol.* 5, 189–196. doi:10.1038/cmi.2008.23

Tsvetkov, P., Coy, S., Petrova, B., Dreishpoon, M., Verma, A., Abdusamad, M., et al. (2022). Copper induces cell death by targeting lipoylated TCA cycle proteins. *Science* 375, 1254–1261. doi:10.1126/science.abf0529

Van Acker, H. H., Anguille, S., De Reu, H., Berneman, Z. N., Smits, E. L., and Van Tendeloo, V. F. (2018). Interleukin-15-cultured dendritic cells enhance anti-tumor gamma delta T cell functions through IL-15 secretion. *Front. Immunol.* 9, 658. doi:10.3389/fimmu.2018.00658

Vilsmaier, T., Heidegger, H. H., Schröder, L., Trapp, E., zehni, A. Z., Rack, B., et al. (2021). Interleukin 15 and Eotaxin correlate with the outcome of breast cancer patients vice versa independent of CTC status. *Arch. Gynecol. Obstet.* 303, 217–230. doi:10.1007/s00404-020-05793-y

Waldmann, T. A. (2014). Interleukin-15 in the treatment of cancer. *Expert Rev. Clin. Immunol.* 10, 1689–1701. doi:10.1586/1744666X.2014.973856

Xiao, R., Mansour, A. G., Huang, W., Chrislip, L. A., Wilkins, R. K., Queen, N. J., et al. (2019). Adipocytes: A novel target for IL-15/IL-15rα cancer gene therapy. *Mol. Ther.* 27, 922–932. doi:10.1016/j.ymthe.2019.02.011

Xu, B., Lu, M., Yan, L., Ge, M., Ren, Y., Wang, R., et al. (2021). A pan-cancer analysis of predictive methylation signatures of response to cancer immunotherapy. *Front. Immunol.* 12, 796647–796713. doi:10.3389/fimmu.2021.796647

Zhang, L., Li, X., Zhang, J., and Xu, G. (2022). Prognostic implication and oncogenic role of PNPO in pan-cancer. *Front. Cell Dev. Biol.* 9, 763674–763715. doi:10.3389/fcell.2021.763674

Zhang, S., Zhao, J., Bai, X., Handley, M., and Shan, F. (2021). Biological effects of IL-15 on immune cells and its potential for the treatment of cancer. *Int. Immunopharmacol.* 91, 107318. doi:10.1016/j.intimp.2020.107318

Glossary

ACC Adrenocortical carcinoma
BLCA Bladder urothelial carcinoma
BRCA Breast invasive carcinoma
CHOL Cholangiocarcinoma
COAD Colon adenocarcinoma
COADREAD Colon and rectum adenocarcinoma
DCs Dendritic cells
DLBC Lymphoid neoplasm diffuse large B-cell lymphoma
DSS Disease-specific survival
ESCA Esophageal carcinoma
GBM Glioblastoma multiforme
GSEA Gene Set Enrichment Analysis
GTEX Genotype Tissue-Expression
HNSC Head and neck squamous cell carcinoma
HPA Human protein Atlas
HR Hazard ratios
IL-15 Interleukin 15
KEGG Kyoto Encyclopedia of Genes and Genomes
KIRC Kidney renal clear cell carcinoma
LAML Acute myeloid leukemia
LGF Local growth factors
LGG Brain lower grade glioma
LUAD Lung adenocarcinoma
LUSC Lung squamous cell carcinoma
NK Natural killer
OS Overall survival
OV Ovarian serous cystadenocarcinoma
PAAD Pancreatic adenocarcinoma
PFI Progression-Free Interval
PRAD Prostate adenocarcinoma
READ Rectum adenocarcinoma
SKCM Skin cutaneous melanoma
STAD Stomach adenocarcinoma
TCGA The Cancer Genome Atlas
TGCT Testicular germ cell tumors
THCA Thyroid carcinoma
THYM Thymoma
UCEC Uterine corpus endometrial carcinoma
UCS Uterine carcinosarcoma

frontiers | Frontiers in Pharmacology

TYPE Original Research
PUBLISHED 17 November 2022
DOI 10.3389/fphar.2022.1072253

OPEN ACCESS

EDITED BY
Kui Zhang,
The University of Chicago, United States

REVIEWED BY
Zeyuan Wang,
Merck, United States
Chiwei Xu,
The Rockefeller University,
United States
Enchao Qiu,
Thomas Jefferson University,
United States
Yuanning Zheng,
Stanford University, United States
Guangzhao Pan,
Institute of Cancer and Basic Medicine (CAS), China

*CORRESPONDENCE
Yuan Yang,
yangyuan@wchscu.cn
Yanhui Liu,
liuyh@scu.edu.cn

†These authors have contributed equally to this work

SPECIALTY SECTION
This article was submitted to Pharmacology of Anti-Cancer Drugs, a section of the journal Frontiers in Pharmacology

RECEIVED 17 October 2022
ACCEPTED 07 November 2022
PUBLISHED 17 November 2022

CITATION
Chen S, Zhang S, Feng W, Li J, Yuan Y, Li W, Wang Z, Yang Y and Liu Y (2022), Serine and glycine metabolism-related gene expression signature stratifies immune profiles of brain gliomas, and predicts prognosis and responses to immunotherapy.
Front. Pharmacol. 13:1072253.
doi: 10.3389/fphar.2022.1072253

Serine and glycine metabolism-related gene expression signature stratifies immune profiles of brain gliomas, and predicts prognosis and responses to immunotherapy

Siliang Chen[1†], Shuxin Zhang[1,2†], Wentao Feng[1], Junhong Li[3], Yunbo Yuan[1], Wenhao Li[1], Zhihao Wang[1], Yuan Yang[1*] and Yanhui Liu[1*]

[1]Department of Neurosurgery, West China Hospital of Sichuan University, Chengdu, China, [2]Department of Head and Neck Surgery, Sichuan Cancer Hospital and Institute, Sichuan Cancer Hospital, School of Medicine, University of Electronic Science and Technology of China, Chengdu, China, [3]Department of Neurosurgery, Chengdu Second People's Hospital, Chengdu, China

Glioma is one of the most lethal cancers and causes more than 200,000 deaths every year. Immunotherapy was an inspiring therapy for multiple cancers but failed in glioma treatment. The importance of serine and glycine and their metabolism has been well-recognized in the physiology of immune cells and microenvironment in multiple cancers. However, their correlation with prognosis, immune cells, and immune microenvironment of glioma remains unclear. In this study, we investigated the relationships between the expression pattern of serine and glycine metabolism-related genes (SGMGs) and clinicopathological features, prognosis, and tumor microenvironment in glioma based on comprehensive analyses of multiple public datasets and our cohort. According to the expression of SGMGs, we conducted the consensus clustering analysis to stratify all patients into four clusters with remarkably distinctive clinicopathological features, prognosis, immune cell infiltration, and immune microenvironment. Subsequently, a serine and glycine metabolism-related genes signature (SGMRS) was constructed based on five critical SGMGs in glioma to stratify patients into SGMRS high- and low-risk groups and tested for its prognostic value. Higher SGMRS expressed genes associated with the synthesis of serine and glycine at higher levels and manifested poorer prognosis. Besides, we confirmed that SGMRS was an independent prognostic factor and constructed nomograms with satisfactory prognosis prediction performance based on SGMRS and other factors. Analyzing the relationship between SGMRS and immune landscape, we found that higher SGMRS correlated with 'hotter' immunological phenotype and more immune cell infiltration. Furthermore, the expression levels of multiple immunotherapy-related targets, including PD-1, PD-L1, and B7-H3, were positively correlated with SGMRS, which was validated by the better predicted response to immune checkpoint inhibitors. In conclusion, our

study explored the relationships between the expression pattern of SGMGs and tumor features and created novel models to predict the prognosis of glioma patients. The correlation of SGMRS with immune cells and microenvironment in gliomas suggested an essential role of serine and glycine metabolism in reforming immune cells and microenvironment. Finally, the results of our study endorsed the potential application of SGMRS to guide the selection of immunotherapy for gliomas.

KEYWORDS

serine, glycine, metabolism, glioma, prognosis, immune infiltration, tumor microenvironment, immune checkpoint inhibitor

Introduction

Glioma is one of the most life-threatening tumors and accounts for approximately 80% of malignant tumors in the central nervous system (Ostrom et al., 2021). The prognosis of glioma patients remains poor even after a complete standard treatment regime consisting of surgery, chemotherapy, and radiotherapy (Stupp et al., 2005). For example, the median overall survival of patients with glioblastoma, which is the most aggressive glioma and accounts for nearly 50% of all gliomas, is fewer than two years after thorough treatment (Chinot et al., 2014; Gilbert et al., 2014; Stupp et al., 2015; Omuro et al., 2022). Therefore, exploring novel therapy to improve the prognosis of glioma patients is urgently needed and attracts abundant researchers to devote themselves to it. In recent years, the applications of immunotherapy, which aims to enhance anti-tumor immunity delivered by immune cells, have been endorsed by lots of studies in multiple cancers, including melanoma (Larkin et al., 2015), non-small-cell lung cancer (Reck et al., 2016), gastric cancer (Janjigian et al., 2021), and renal cell carcinoma (Choueiri et al., 2021a). Multiple randomized clinical trials were also devoted to evaluating the efficacy of immune checkpoint inhibitors (ICIs) in the treatment of glioblastoma, but all these attempts eventually failed (Reardon et al., 2020; Lim et al., 2022; Omuro et al., 2022). The immunologically quiescent environment of the brain is considered an important reason for these failures. The blood-brain barrier not only prevents the majority of antitumor drugs out of brain, but also blocks most peripheral immune cells from entering central nervous system. Besides, regulatory T (Treg) cells in tumor microenvironment of glioma functions to deliver immunosuppressive effects by exhausting cytotoxic T cells, which is another reason for the failure of immunotherapy to activate T cells (Colombo and Piconese, 2007). However, metastatic brain tumors located in similar environments with gliomas can benefit from ICIs therapy (Tawbi et al., 2018; Hendriks et al., 2019), indicating that the unique immune microenvironment of gliomas may result in resistance to ICIs. Adjuvant ICIs for glioblastoma would reshape the immune microenvironment and enhance anti-tumor immunity (Cloughesy et al., 2019; Schalper et al., 2019). Therefore, investigating potential pathways that influence the immune microenvironment of gliomas can provide novel methods to reshape the immune landscape and subsequently enhance anti-tumor immunity, reinforce the efficacy of immunotherapy, and improve prognosis.

Serine and glycine, two non-essential amino acids, play critical roles in multiple cell physiological processes (Sullivan and Vander Heiden, 2017). Cells require serine and glycine *via* intracellular synthesis and uptake from the extracellular environment. The synthesis process of serine and glycine consists of two steps: *de novo* synthesis of serine branched from glycolysis and reversible interconversion from serine to glycine (Geeraerts et al., 2021), indicating the tight relationship between the metabolism processes of these two amino acids. The function of serine, glycine, and their metabolism in cancers attracted significant attention in recent years. Upregulated synthesis of serine and glycine has been demonstrated in multiple cancers, including lung cancer and glioma (Kim et al., 2015; Liao et al., 2019b). The important physiological roles of serine and glycine synthesis in tumors, including fueling nucleotide biosynthesis (Fan et al., 2019), regulating lipid metabolism (Gao et al., 2018), altering sphingolipid diversity (Muthusamy et al., 2020), and maintaining cellular redox homeostasis (Ye et al., 2014), were potential causes that drive the tumors to upregulate the synthesis of serine and glycine to meet the aberrant demand. The process of serine and glycine synthesis can generate abundant one-carbon units and replenish carbon sources for one-carbon metabolism in cancer cells (Locasale, 2013; Newman and Maddocks, 2017; Fan et al., 2019). Besides, serine and glycine are critical for the survival and growth of cancer cells (DeBerardinis, 2011; DeBerardinis and Chandel, 2016). Downregulation of serine and glycine synthesis has been shown to inhibit cancer cell proliferation (Mullarky et al., 2016; Pacold et al., 2016). Cancer cells can not only upregulate serine and glycine synthesis, but also secret extra serine and glycine to extracellular spaces to reshape tumor microenvironment (Geeraerts et al., 2021). In glioma, glycine concentration was determined as a biomarker of aggressiveness (Tiwari et al., 2020). Serine and

glycine in tumor microenvironment enhanced nucleotide production and cell proliferation in brain metastasis (Ngo et al., 2020). Furthermore, serine and glycine synthesized and secreted by cancer cells play multiple roles in tumor immune microenvironment. Serine in extracellular environments inhibits the functions of macrophages and neutrophils (He et al., 2019). A high level of phosphoglycerate dehydrogenase (PHGDH), an essential enzyme for serine and glycine synthesis, can induce macrophages to immunosuppressive M2-like macrophages (Wilson et al., 2020). Serine and glycine synthesis can also switch the phenotype of macrophages to express immunosuppressive programmed death-ligand (PD-L1) by inducing the production of IL-1β (Su et al., 2018; Rodriguez et al., 2019). These findings suggest that the metabolism of serine and glycine is involved in tumorigenesis and related to the aggressiveness and immune microenvironment of cancers. However, the role of serine and glycine metabolism in malignant features and the immune landscape of glioma remains unclear and need to be further elucidated.

In this study, we comprehensively analyzed the RNA-sequence data from multiple glioma patient cohorts, including TCGA, CGGA325, CGGA693, and our institution, to investigate the relationship between serine and glycine metabolism-related genes (SGMGs) expression and clinicopathological characteristics of glioma. Moreover, we constructed a serine and glycine metabolism-related gene risk signature (SGMRS) to evaluate the clinical significance of SGMGs expression profile. Additionally, we also conducted several analyses to investigate the correlation between the expression of SGMGs and the tumor immune microenvironment landscape of glioma.

Materials and methods

Data sources

Gene expression profile (fragments per kilobase million, FPKM) and clinicopathological features in this study were obtained from three public databases and an own cohort. Those patients with primary oligodendroglioma, astrocytoma, and glioblastoma were included in this study. Those patients with recurrent gliomas or age <18 were exclude from this study, because these tumors occupied minority of the data set with distinctive biological features (Louis et al., 2021). The three cohorts of public databases were from the Cancer Genome Atlas (TCGA, https://portal.gdc.cancer.gov/) and the Chinese Glioma Genome Atlas (CGGA, http://www.cgga.org.cn/). The TCGA cohort contained 662 primary glioma samples, and 655 of which had complete survival data. There are two cohorts from the CGGA database, CGGA325 and CGGA 693 cohorts. The CGGA325 cohort contained 226 adult primary gliomas, and the CGGA693 cohort contained 415 primary gliomas. FPKM data of these two cohorts were downloaded from the CGGA website.

Our own cohort consisted of 77 primary glioma patients from West China Hospital (WCH). The tumor samples were obtained during tumor resection surgery and subsequently sequenced for mRNA. After that, the mRNA sequencing data was quantified and normalized to FPKM by STAR. Prognosis information of these 77 patients was obtained through regular follow-up and telephone interview. The overall survival (OS) was calculated as the time length from surgery to death or last follow-up (censored value). In preprocessing procedure, we exclude the genes with too low FPKM values (maximum FPKM <0.1 or standard deviation < 0.01, which may represent sequencing/mapping artifacts) from further analyses. Detailed clinicopathological information of these four cohorts was showed in Table 1.

Consensus clustering analyses based on serine and glycine metabolism-related genes

The serine and glycine metabolism-related genes (SGMGs) were identified based on the serine and glycine metabolism pathway from PathBank (https://pathbank.org/, pathway No. SMP0000004), which contained 24 SGMGs. After excluding the genes with low expression levels, 21 SGMGs were eventually enrolled in the following analyses. The list of these 24 SGMGs was downloaded from the PubChem website (https://pubchem.ncbi.nlm.nih.gov/pathway/PathBank:SMP0000004/), and the list of SGMGs before and after exclusion was given in Supplementary Table S1. Subsequently, unsupervised consensus clustering analyses were conducted based on expression patterns of SGMGs to represent the different serine and glycine metabolism patterns in gliomas. Consensus clustering analysis was conducted using the R package 'ConsensusClusterPlus'. Briefly, for number of clusters (k) from 2 to 10, hierarchical clustering of k clusters was performed over 1,000 random subsets of samples based on Pearson correlation. The consensus index was calculated as the frequency for which two samples were stratified into the same cluster. The optimal k was determined when gain in area under the cumulated distribution function (CDF) curve of the consensus index converged with the increase of k, under the restriction that the sample size of each cluster should not too small to study its implications. Furthermore, we performed the t-Distributed Stochastic Neighbor Embedding (tSNE) analysis to visualize the different expression patterns of SGMGs in each cluster. Besides, a naïve Bayes classifier was constructed based on the SGMGs expression and cluster labels of the TCGA cohort to classify the patients of the other three cohorts into distinctive clusters.

TABLE 1 Clinicopathological characteristics of patients in TCGA, CGGA325, CGGA693, and WCH cohorts.

Characteristics	TCGA (N = 662)	CGGA325 (N = 226)	CGGA693 (N = 415)	WCH (N = 77)
Age: mean (range)	46 (18–89)	52 (22–87)	43 (19–76)	46 (19–77)
Gender				
Female	282 (42.6%)	87 (38.5%)	176 (42.4%)	30 (39.0%)
Male	380 (57.4%)	139 (61.5%)	239 (57.6%)	47 (77.0%)
NA	0	0	0	0
Histology				
Astrocytoma	341 (51.5%)	82 (36.3%)	182 (43.9%)	22 (28.6%)
Oligodendroglioma	167 (25.2%)	60 (26.6%)	94 (22.7%)	21 (27.3%)
Glioblastoma	154 (23.3%)	84 (37.2%)	139 (33.5%)	34 (44.2%)
Grade				
G2	214 (32.3%)	94 (41.6%)	134 (32.3%)	29 (37.7%)
G3	237 (35.8%)	48 (21.2%)	142 (34.2%)	14 (18.2%)
G4	154 (23.3%)	84 (37.2%)	139 (33.5%)	34 (44.2%)
NA	57 (8.6%)	0	0	0
IDH status				
Mutant	421 (63.6%)	115 (50.9%)	169 (40.7%)	42 (54.5%)
WT	236 (35.6%)	110 (48.7%)	207 (49.9%)	35 (45.5%)
NA	5 (0.8%)	1 (0.4%)	39 (9.4%)	0
1p19q Codeletion				
Codel	167 (25.2%)	54 (23.9%)	267 (64.3%)	19 (24.7%)
Non-codel	488 (73.7%)	169 (74.8%)	88 (21.2%)	43 (55.8%)
NA	7 (1.1%)	3 (1.3%)	60 (14.5%)	15 (19.5%)
TERT promoter status				
Mutant	340 (51.4%)	NA	NA	30 (39.0%)
WT	156 (23.6%)	NA	NA	23 (29.9%)
NA	166 (25.1%)	NA	NA	24 (31.2%)
MGMT promoter status				
Methylated	472 (71.3%)	97 (42.9%)	141 (34.0%)	35 (45.5%)
Unmethylated	157 (23.7%)	115 (50.9%)	195 (47.0%)	13 (16.9%)
NA	33 (5.0%)	14 (6.2%)	79 (19.0%)	29 (37.7%)
ATRX status				
Mutant	192 (29.0%)	NA	NA	22 (28.6%)
WT	459 (69.3%)	NA	NA	53 (68.8%)
NA	11 (1.7%)	NA	NA	2 (2.6%)

Abbreviation: TCGA, the cancer genome atlas; CGGA, chinese glioma genome atlas; WCH, west china hospital; IDH, isocitrate dehydrogenase; TERT, telomerase reverse transcriptase; MGMT, O6-methylguanine-DNA, methyltransferase; ATRX, alpha-thalassemia x-linked intellectual disability syndrome; WT, wild type; NA, not available.

Construction and validation of the serine and glycine metabolism-related genes risk signature

To elucidate the relationship between serine and glycine metabolism and glioma, we constructed a gene risk signature based on the expression of SGMGs, the serine and glycine metabolism-related genes risk signature (SGMRS). In the first step, patients of TCGA cohort were split into training and validation sets with a ratio of 6:4, and all the other three cohorts were defined as validation sets. Subsequently, we utilized the Least Absolute Shrinkage and Selection Operator (LASSO) Cox regression analysis to filter the 21 SGMGs in the training set. The SGMG was determined as critical SGMG if its coefficient was not zero at the optimal model with maximum C-indices in over 80 random repetitions of LASSO Cox regression out of 100. Moreover, we fitted a concluding multivariate Cox regression model to the training set with critical SGMGs. The serine and glycine metabolism-related genes risk signature (SGMRS) was calculated using the following formula:

$$SGMRS = \sum_{i=1} \left(\beta_i * Exp_i \right)$$

In this formula, β represented the coefficient of each critical SGMG when fitted by the concluding multivariate Cox regression model. *Exp* standed for the expression level of each essential SGMG. Furthermore, the optimal SGMRS cut-off value was settled by the function 'surv_cutpoint' of the R package 'survminer' with each group proportion ≥0.3. According to the optimal cut-off value, all patients were allocated into SGMRS low-risk or high-risk group. Eventually, to validate the efficacy of prognostic prediction, we illustrated the receiver operating characteristic (ROC) curves in validation sets of 1-, 2-, and 3-year survival rates and used the R package 'time ROC' to calculate the area under the ROC curve (AUC).

Assessments of gene alterations and copy number variation

We obtained the data of gene alterations and copy number variation (CNVs) from the cBioPortal database (https://www.cbioportal.org/) for the TCGA cohort to assess the gene alterations and CNVs between different clusters and SGMRS risk groups. Subsequently, the R package 'maftools' was used to depict the different patterns of gene alterations and tumor mutation burdens (TMBs). Moreover, the CNV levels were represented as the Genomic Identification of Significant Targets in Cancer (GISTIC) score.

Gene set enrichment analyses

In the section of gene set enrichment analyses, we used the R package 'clusterProfiler' to conduct the over-representation and gene set enrichment analysis (GSEA) to assess the differentially expressed genes (DEGs). Besides, we used the R package 'limma' to determine the DEGs between clusters and risk groups. DEGs were defined as those genes with $|\log2FC| > 0.5$ and adjusted p-value < 0.05. In the GSEA, the DEGs were arranged according to their log2FC values and a Running Enrichment Score for each gene set was computed by adding 1/(number of DEGs) when a DEG was found in the gene set and subtracting 1/(number of DEGs) if not. Moreover, we converted the logFPKM matrix of genes to the pathway expression matrix using the R package 'GSVA'. The differentially expressed pathways between clusters and risk groups were identified with the 'limma' package.

Comprehensive characterization of tumor immune microenvironment based on serine and glycine metabolism

To explore the impact of serine and glycine metabolism on the tumor immune cells and immune microenvironment, we conducted multiple analyses to characterize the differences in the tumor immune microenvironment between different clusters and risk groups. Firstly, we applied the website of CIBERSORTx (https://cibersortx.stanford.edu/). Subsequently, we utilized the Estimation of Stromal and Immune Cells in Malignant Tumor issues using Expression data (ESTIMATE) to calculate the stromal, immune, and ESTIMATE scores in glioma, contributing to evaluating the infiltration of stromal and immune cells in the tumor microenvironment (Yoshihara et al., 2013). In this algorithm, the non-hematopoiesis-related genes that were differentially expressed between tumor cells and matched stromal cells separated by laser capture microdissection in multiple cancers were screened. The stromal related genes were selected from these genes. Besides, we also integrated the tumor purity data based on the ESTIMATE score and consensus purity estimation (CPE) previously published by D.Aran et al. (Aran et al., 2015). To identify the tumor immunological phenotype (TIP), we applied another previously published algorithm (Wang et al., 2021) to compute the TIP gene signature. According to the TIP gene signature, we could identify the immunological phenotype of tumor as either relatively 'cold' or 'hot' tumors. Additionally, the Tumor Immune Dysfunction and Exclusion (TIDE) suite (http://tide.dfci.harvard.edu/) was applied to predict potential response to therapy with ICIs.

Nomogram construction based on SGMRS and other prognostic factors

To construct a nomogram that could effectively predict glioma patients' prognosis, we initially identified independent prognostic factors using univariate and multivariate Cox regression analyses. Firstly, the SGMRS, together with other potential prognostic factors, including age, gender, tumor grade, radiotherapy, chemotherapy, Karnofsky Performance Scale (KPS), isocitrate dehydrogenase (IDH) mutation, and 1p/19q codeletion, were enrolled into univariate Cox regression analysis. Then those prognostic factors with p-value < 0.05 in univariate Cox regression analysis entered the following multivariate analysis. Eventually, those prognostic factors with p-value < 0.05 in multivariate Cox regression analysis were determined as independent prognostic factors.

The nomograms were constructed based on these independent prognostic factors using the R package 'rms'. To assess the efficacy of nomograms in the prediction of prognosis, we computed calibration curves for each nomogram.

Statistical analyses

The R software (version 4.2.1) was used to perform the above bioinformatic analyses unless otherwise specified. For

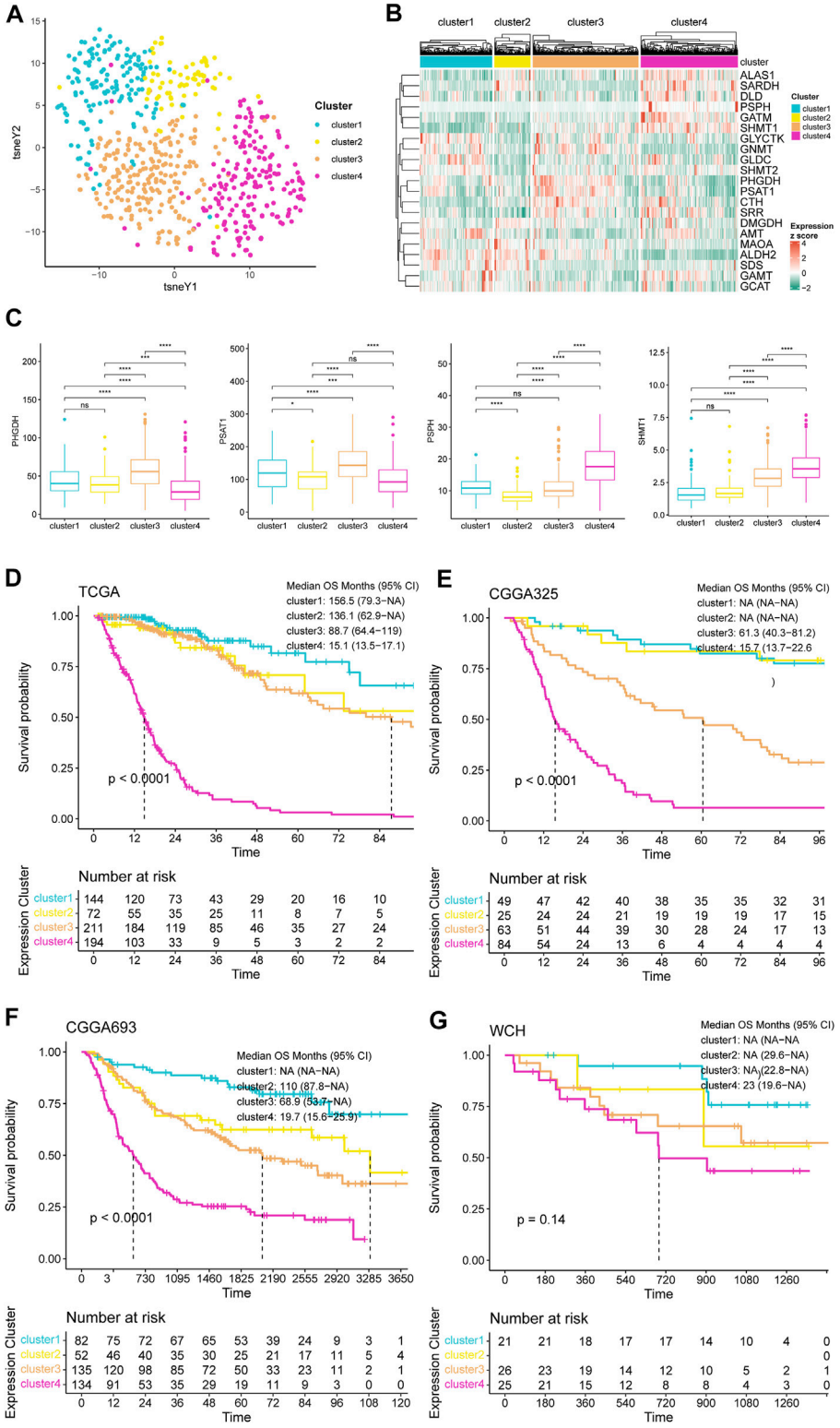

FIGURE 1
Clustering of gliomas based on expression pattern of SGMGs. **(A)** tSNE map for SGMGs expression patterns of four consensus clusters. **(B)** Heatmap for expression of 21 SGMGs based on four clusters. **(C)** The expression levels of PHGDH, PSAT1, PSPH, and SHMT1 among four clusters. **(D)** K-M curves based on four consensus clusters in **(D)** TCGA, **(E)** CGGA325, **(F)** CGGA693, and **(G)** WCH cohorts.

continuous variables, the Wilcoxon rank sum test was used to evaluate the differences between different clusters and risk groups. For categorical variables, the chi-square test was used to evaluate the differences. All the survival analyses were performed using the R package 'survminer'. The differences between Kaplan-Meier (K-M) curves were tested by log-rank test. Univariate and multivariate Cox regression analyses were conducted using the 'coxph' function of the R package 'survival'. The LASSO Cox regression analysis was performed using the R package 'glmnet'. In linear regression analysis, the T Iterative Grubbs test was utilized to exclude the outliers.

Ethic approval and data availability

The collection processes of clinical data and tumor samples were approved by the institutional review board of West China Hospital (No. 2018.569) following the 1964 Helsinki declaration and its later amendments. Besides, every patient signed written consent for collecting and using tumor tissue and clinical information. All the tumor tissue sequencing data from West China Hospital were available at the Genome Sequence Archive for Humans with accession code: HRA002839 (https://ngdc.cncb.ac.cn/gsa-human/s/JQssVoV1).

Results

Unsupervised consensus clustering analyses based on serine and glycine metabolism-related genes

Based on the expression patterns of 21 serine and glycine metabolism-related genes (SGMGs), we performed an unsupervised consensus clustering analysis in patients of TCGA cohort. According to the clustering algorithm explained in Material and Method section, the delta area of CDF dropped significantly when k increased from 3 to 4, which suggest convergence of within-cluster similarity over between-cluster similarity with increased k over 4. Therefore, 4 was chosen to be the optimal number of clusters, and patients of TCGA cohort were classified into four consensus clusters (Supplementary Figure S1). The different expression patterns of SGMGs among these four clusters were illustrated using tSNE analysis (Figure 1A). Besides, the expression levels of four important genes involved in serine and glycine synthesis were illustrated (Figure 1B). Notably, cluster 3 significantly highly expressed PHGDH and PSAT1, and cluster 4 significantly highly expressed PSPH and SHMT1 (Figure 1C). The expression levels of all SGMGs in different clusters are illustrated in Supplementary Figure S1.

The survival analysis demonstrated that the prognosis of cluster 4 was overwhelmingly worse than the other three clusters in TCGA cohort (Figure 1D). Based on the naïve Bayes clustering classifier trained by the TCGA cohort, patients of the other three cohorts were also classified into four clusters. In survival analyses, the other three cohorts also exhibited the same trend (Figures 1E, F), indicating that the expression pattern of SGMGs was related to the prognosis of glioma patients even in independent glioma cohorts.

To investigate the distinctive patterns of pathway alterations related to serine and glycine metabolism, we conducted functional enrichment analyses between cluster 1 and cluster 4, which showed the most differential SGMGs expression profiles and prognosis. In GSEA, the cytokine signaling in immune system pathway (NES = 2.739, adjusted p-value < 0.001) and the extracellular matrix organization pathway (NES = 3.165, adjusted p-value < 0.001) ranked among the top five REACTOME gene sets in the differentially expressed genes (DEGs) between cluster 1 and 4 (Figure 2A), suggesting the potential impact of serine and glycine metabolism on the tumor microenvironment and immunity. Besides, the extracellular matrix receptor interaction pathway (NES = 2.869, adjusted p-value <0.001) and the asthma pathway (NES = 2.983, adjusted p-value < 0.001) were also among the top 5 most significantly enriched Kyoto Encyclopedia of Genes and Genomes (KEGG) gene sets in the cluster 1/4 DEGs (Figure 2B), indicating the potential effect on inflammation and neurogenesis in glioma.

The results of gene mutation analysis revealed different gene mutation models of each cluster (Figure 2C). IDH1 mutation, a critical marker for diagnosis and prognosis of gliomas, was frequently observed in cluster 1, 2, and 3 but hardly occurred in cluster 4. Moreover, the mutation rates of TP53 and ATRX in cluster 3 were remarkably higher than the other 3 clusters. Moreover, most CIC mutations occurred in cluster 1. The analysis of CNVs also suggested distinctive characteristics among the four clusters. The gain of chromosome 7 and loss of chromosome 10 (+7/-10), which was recognized as a diagnostic marker for glioblastoma, predominantly occurred in cluster 4.1p/19q codeletion, which was indispensable for diagnosis of oligodendroglioma, mainly occurred in cluster 1, in line with the best prognosis of cluster 1. In clinicopathological features, the proportion of WHO grade 4 tumors grew from cluster 1 to cluster 4, which were characterized by glioblastomas and gliomas with unmethylated MGMT promoter, while TERT promoter wild-type tumors occupied the majority of cluster 3 gliomas, suggesting a potential connection between these tumors and alternative telomere lengthening (Figures 2E–H). Additionally, the differences in other clinicopathological features among these four clusters were also illustrated in Supplementary Figure S2.

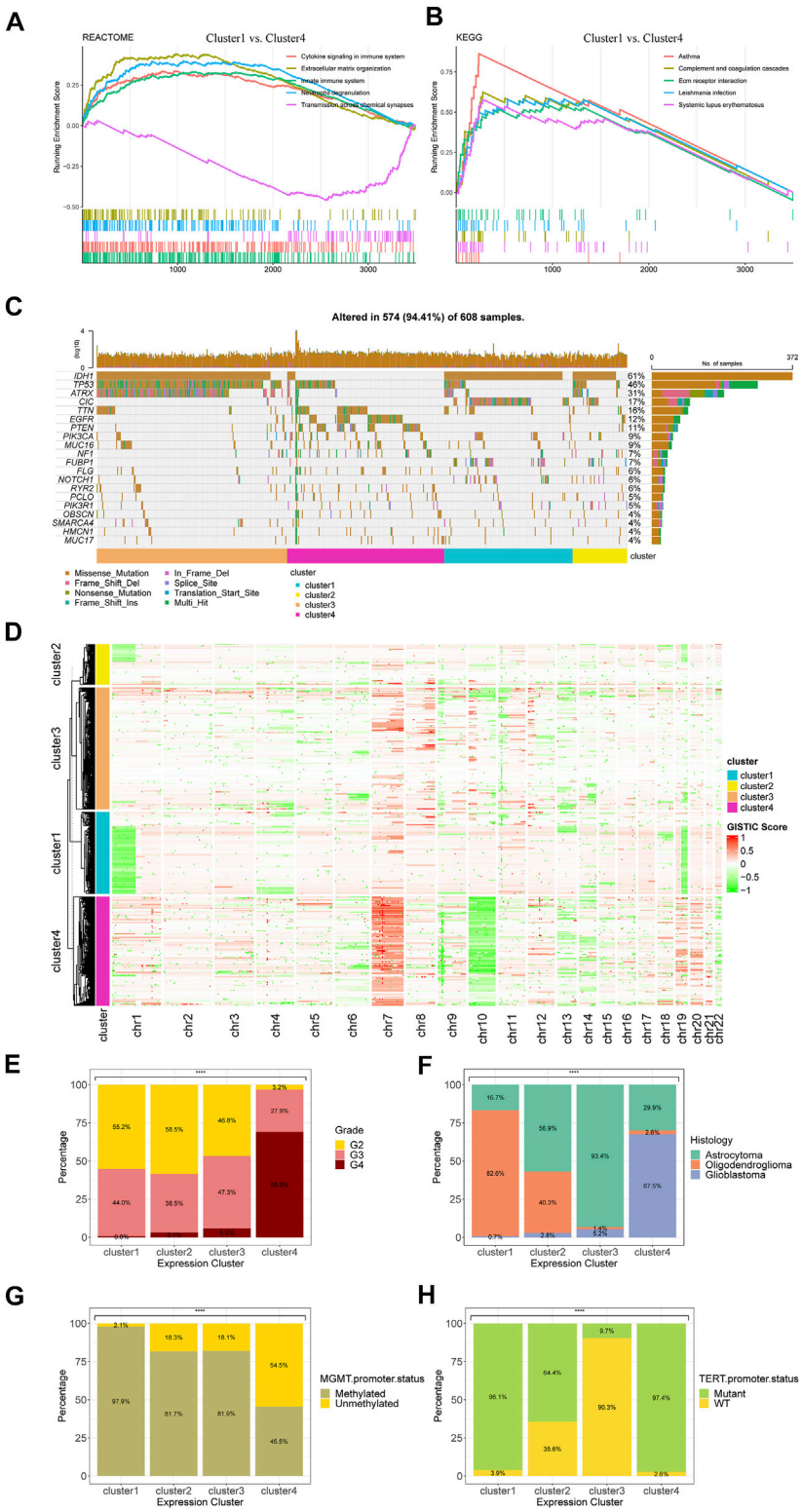

FIGURE 2
Functional enrichment and clinicopathological characteristics of the four consensus clusters in TCGA cohort. **(A)** Top five pathways with the highest NES in the REACTOME gene set between cluster 1 and cluster 4. **(B)** Top five pathways with the highest NES in the KEGG gene set between cluster 1 and cluster 4. **(C)** Top 20 mutated genes of the four consensus clusters. **(D)** Heatmap for copy number variations of the four clusters. **(E)** The differences in **(E)** tumor grade, **(F)** histological diagnosis, **(G)** MGMT promoter status, and **(H)** TERT promoter status among four clusters. *p < 0.05; **p < 0.01; ***p < 0.001; ****p < 0.0001.

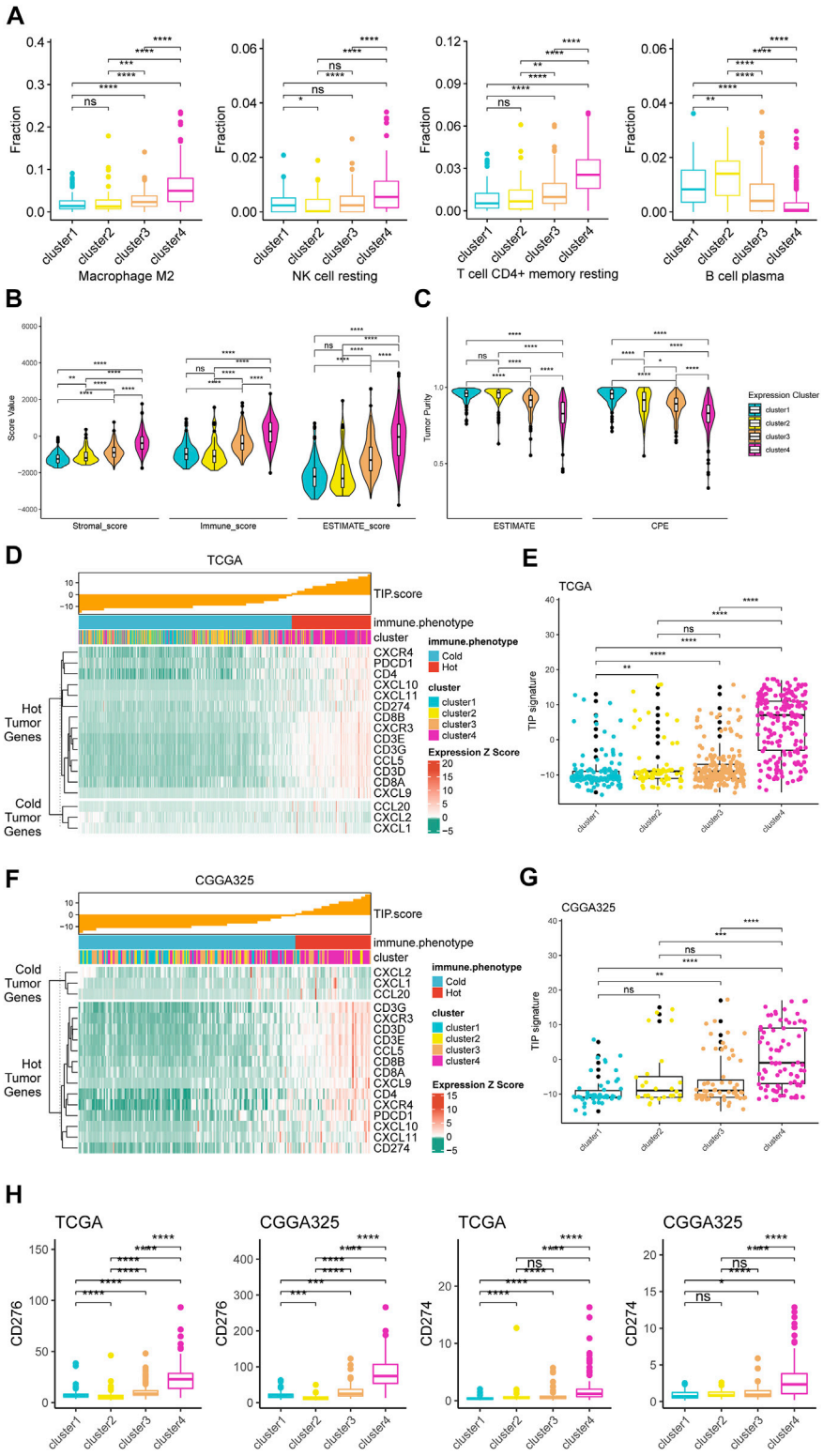

FIGURE 3
Different immunological landscapes of tumor microenvironment among four clusters. **(A)** Boxplots for infiltration fraction of four types of immune cells based on CIBERSORTx in TCGA cohort. **(B)** Differences in stromal, immune, and ESTIMATE scores among four clusters in TCGA cohort. **(C)** Difference in tumor purity among four clusters in TCGA cohort. **(D)** TIP score and related gene expression heatmap among four clusters in TCGA cohort. **(E)** Difference in TIP score among four clusters in TCGA cohort. **(F)** TIP score and related gene expression heatmap among four clusters in CGGA325 cohort. **(G)** Difference in TIP score among four clusters in CGGA325 cohort. **(H)** Differences in expression levels of CD274 and CD276 among four clusters in TCGA and CGGA 325 cohorts. *$p < 0.05$; **$p < 0.01$; ***$p < 0.001$; ****$p < 0.0001$.

Analyses of immune cells infiltration and tumor microenvironment based on consensus clusters

Based on the consensus clusters, we performed comprehensive analyses to explore the impact of serine and glycine metabolism on the immune cells and immune microenvironment in glioma. The analyses of immune cell infiltration in the tumor microenvironment revealed that there were more abundant M2 macrophages, resting NK cells, and resting memory $CD4^+$ T cells but fewer plasma B cells in the tumor microenvironment of cluster 4 (Figure 3A). Besides, the calculation of stromal, immune, and ESTIMATE scores based on the ESTIMATE algorithm demonstrated that cluster 4 had remarkably higher scores than the other three clusters. Higher stromal, immune, and ESTIMATE scores represented for more stromal cells and more immune infiltration in the tumor microenvironment. In comparison, cluster 3 gliomas also had significantly higher scores than cluster 1 and 2, suggesting that these tumor microenvironment-related scores were related to serine and glycine metabolism and prognosis in glioma (Figure 3B). Furthermore, for the analysis of tumor purity, cluster 4 was manifested with significantly lower tumor purity than other clusters, indicating a more complex tumor microenvironment of cluster 4 (Figure 3C). Moreover, based on the computation of the TIP score, cluster 4 was demonstrated with higher expression of genes related to the 'hot' immunological phenotype of tumor than other clusters in TCGA cohort (Figure 3D). The resulting TIP score of cluster 4 was significantly higher than other clusters, suggesting cluster 4 could be a relatively 'hotter' tumor compared to those in other clusters (Figure 3E). These findings were also validated in CGGA325 cohort (Figure 3F, G), suggesting a robust association between the expression of serine/glycine metabolism-related genes and the immune landscape of gliomas. Additionally, analyses of markers related to immunotherapy revealed that expression levels of CD274 (PD-L1) and CD276 (B7-H3), which were essential targets for immunotherapy, expressed at remarkably higher levels in cluster 4 compared to other clusters in TCGA and CGGA325 cohorts (Figure 3H). Combined results of TIP score and the expression levels of immunotherapy-related targets demonstrated that cluster 4, which exhibited 'hotter' immunological phenotype and expressed more immunotherapy-related targets, might be more likely to response to immunotherapy than patients of other clusters.

Construction and validation of serine and glycine metabolism-related genes risk signature

In this section, we filtered the 21 SGMGs with the LASSO Cox regression in training set to identify critical genes for the construction of serine and glycine metabolism-related genes risk signature (SGMRS). Five SGMGs, including SHMT1, PSPH, GNMT, SARDH, and ALDH2, were identified as critical genes for the construction of SGMRS (Figure 4A), and the formula of the SGMRS was derived by fitting a final multivariate Cox regression model to the expression of the 5 critical SGMGs in the training dataset. The SGMRS was calculated using the following formula:

$$0.505*SARDH+0.243*SHMT1-1.77e-4*PSPH-0.050*ALDH2-0.209*GNMT$$

Further univariate analysis demonstrated that SHMT1, SARDH, and PSPH were hazardous prognostic factors for glioma (Figure 4B). GNMT and ALDH2 were protective factors for glioma (Figure 4B). Moreover, to validate these results, we obtained representative immunohistochemical staining for SARDH and PSPH from the Human Protein Atlas (https://www.proteinatlas.org/) (Pontén et al., 2008). The staining figures revealed that the protein levels of SARDH and PSPH were higher in high-grade gliomas compared to low-grade gliomas (Supplementary Figure 3A-B), which was consistent with the results of the univariate analysis. Subsequently, the 'surv_cutpoint' algorithm was used to identify the optimal SGMRS cut-off for all these four cohorts, and the patients were classified into SGMRS high- and low-risk groups based on this cut-off (Figure 4C). Further survival analyses revealed that the patients in SGMRS high-risk group had an enormously poorer prognosis than low-risk group in the TCGA validation cohort (Figure 4D), which was also confirmed by the other three cohorts (Figures 4E,F). We also conducted ROC analyses to examine the efficacy of SGMRS to predict survival rates at 1, 2, and 3 years. AUCs of the ROC curves of SGMRS in TCGA validation cohort at 1, 2, and 3 years was 0.815, 0.842, and 0.848, endorsing the effectiveness of SGMRS on prognosis prediction (Figure 4H). In the other three cohorts, the performances of SGMRS on prognosis prediction were similar (Figure 4H).

To illustrate the expression pattern of these five critical SGMGs, we aligned a heatmap of the expression level of each patient in order of SGMRS. Besides, the clinicopathological features, including tumor grade, histology diagnosis, IDH status, 1p/19q codeletion, TERT promoter status, ATRX status, and MGMT promoter status, were also integrated (Figure 5A). As for the analysis of gene mutations, the SGMRS high-risk group manifested with a lower incidence of IDH1 and TP53 mutation (Figure 5B) and a higher incidence of EGFR and PTEN mutation. Furthermore, the tumor mutation burden (TMB) analysis between SGMRS high- and low-risk groups revealed a significantly higher TMB in high-risk groups (Figure 5C). Additionally, the analysis of CNVs demonstrated that most of chromosome +7/-10 occurred in SGMRS high-risk group (Figure 5D), and most of the 1p/19q codeletion occurred in the low-risk group.

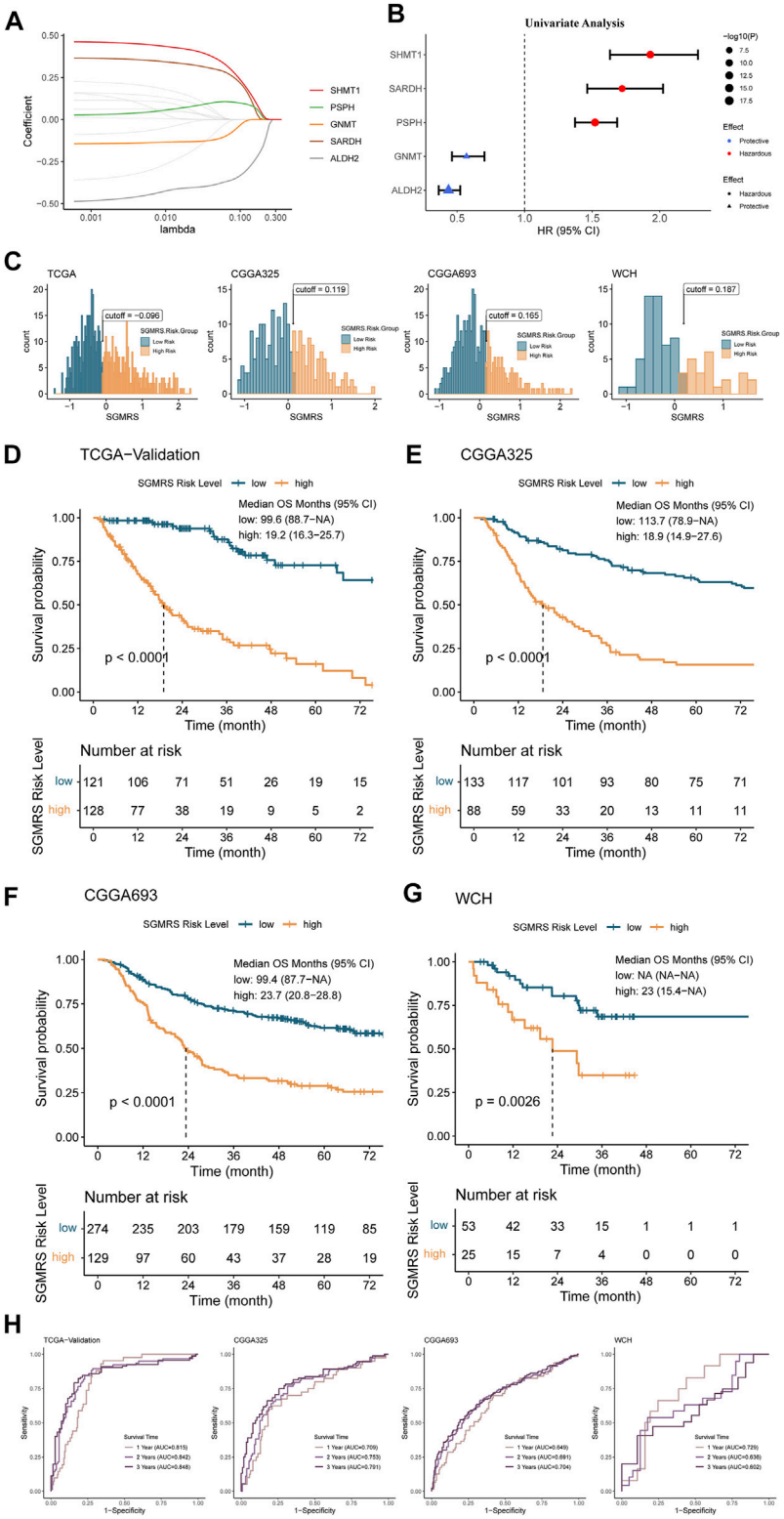

FIGURE 4
Construction of SGMRS and its relationship with prognosis. **(A)** Average of coefficients of five critical SGMGs in the LASSO Cox regression at each lambda value. **(B)** The prognostic effect of each critical SGMG in glioma. **(C)** Optima cutoff value of SGMRS in all four cohorts. **(D)** K-M curves of the **(D)** TCGA, **(E)** CGGA325, **(F)** CGGA693, and **(G)** WCH cohorts based on SGMRS high- and low-risk groups. **(H)** ROC curves and matched AUC of 1-, 2-, 3-year survival rate in all four cohorts.

FIGURE 5
Clinicopathological features of SGMRS risk groups. **(A)** Expression level of five critical SGMGs and its relationship with clinicopathological features. **(B)** Gene mutations of five critical SGMGs and top eight frequently mutated genes in gliomas ordered by SGMRS risk groups. **(C)** Difference in tumor mutation burden between SGMRS high- and low-risk groups. **(D)** Copy number variation and its relationship with clinicopathological features ordered by SGMRS risk groups. *$p < 0.05$; **$p < 0.01$; ***$p < 0.001$; ****$p < 0.0001$.

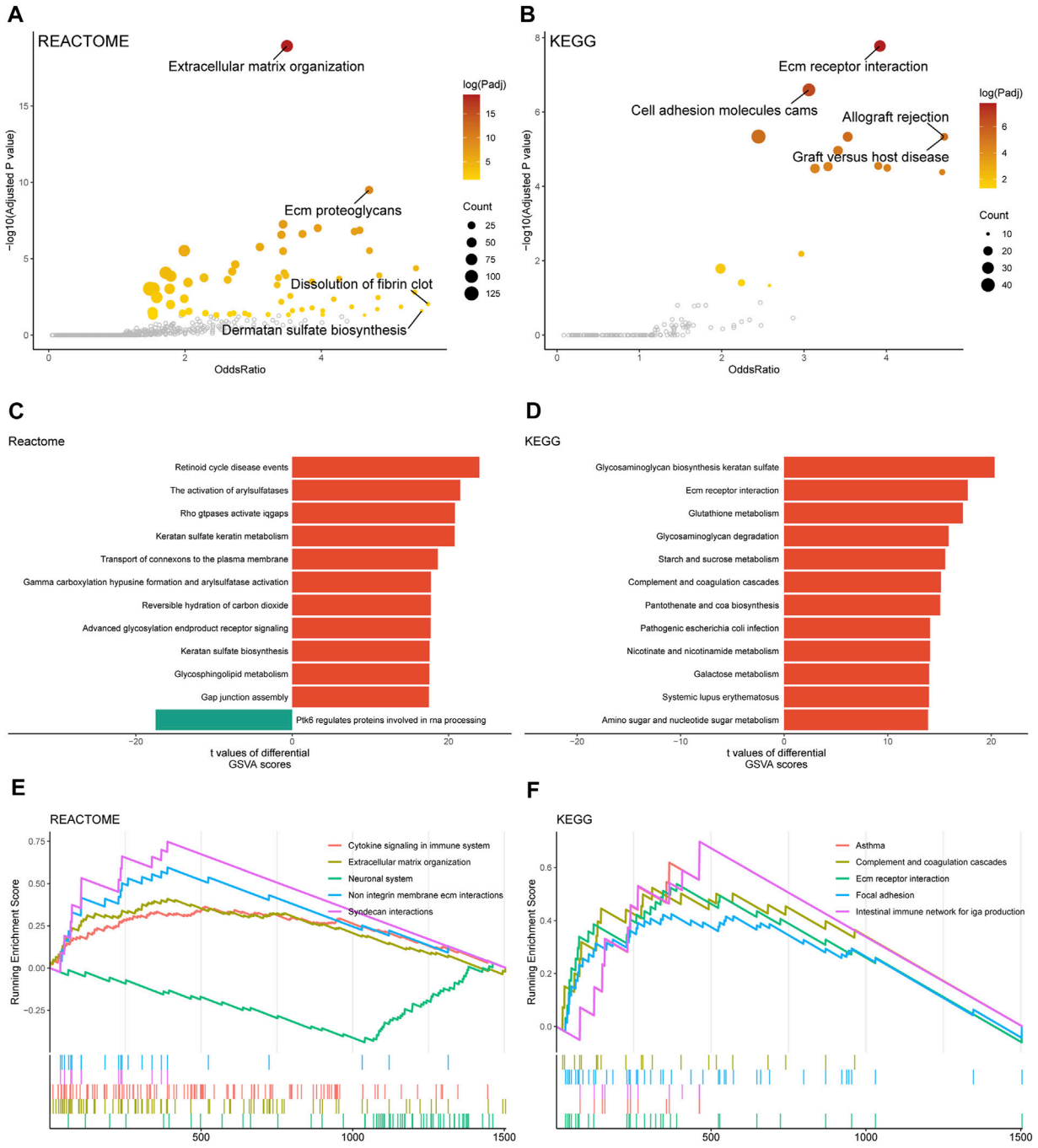

FIGURE 6
Functional enrichment analyses between two SGMRS risk groups. **(A)** Pathways with high confidence and odds ratio in REACTOME gene sets. **(B)** Pathways with high confidence and odds ratio in KEGG gene sets. **(C)** Top 12 pathways in REACTOME gene set with the highest GSVA scores. **(D)** Top 12 pathways in KEGG gene set with the highest GSVA scores. **(E)** Top five pathways in REACTOME gene set with the highest normalized enrichment scores. **(F)** Top five pathways in KEGG gene set with the highest normalized enrichment scores.

Functional enrichment analyses based on SGMRS risk groups

In this section, we performed multiple functional enrichment analyses to investigate the pathway alterations in different SGMRS risk groups. The extracellular matrix organization of REACTOME gene sets and the extracellular matrix receptor interaction of KEGG gene sets were identified with high odds ratio and *p*-value between high- and low-risk groups (Figures 6A,B). The retinoid cycle disease events pathway was listed in the

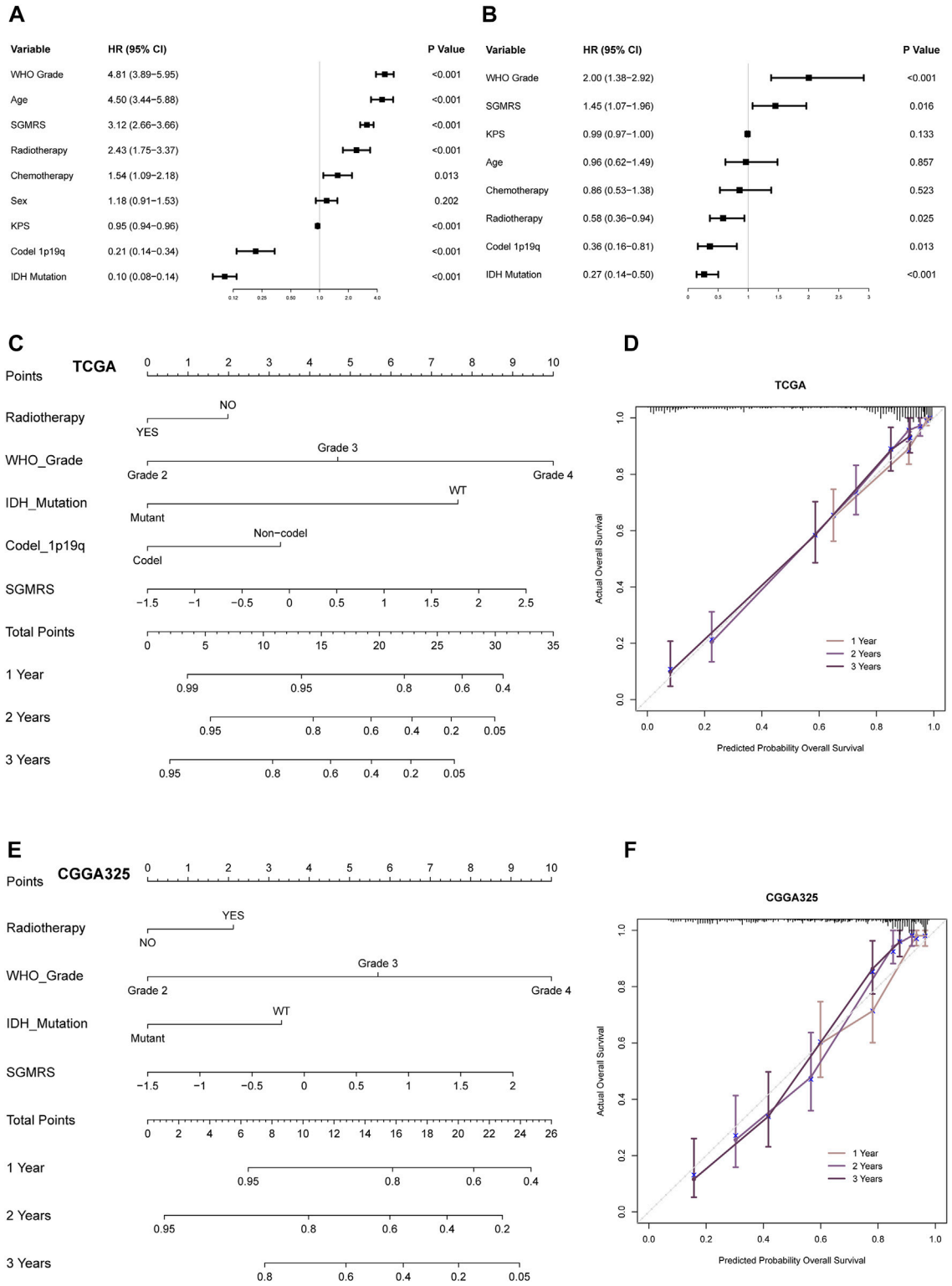

FIGURE 7
Prognostic value of SGMRS and construction of SGMRS-based nomograms. **(A)** Univariate analysis of potential prognostic factors in glioma. **(B)** Multivariate analysis to identify independent prognostic factors in glioma. **(C)** Nomogram of 1-, 2-, and 3-year survival rate of glioma patients in TCGA cohort. **(D)** Calibration plots for the nomogram of TCGA cohort. **(E)** Nomogram of 1-, 2-, and 3-year survival rate of glioma patients in CGGA325 cohort. **(F)** Calibration plots for the nomogram of CGGA325 cohort.

top 12 dysregulated pathways in the REACTOME gene set (Figure 6C). The glutathione metabolism pathway, which was regulated by serine and glycine synthesis (Geeraerts et al., 2021), was listed in the top 12 pathways with highest GSVA scores in the KEGG gene set (Figure 6D). Besides, the cytokine signaling in immune system pathway (NES = 2.568, adjusted *p*-value <0.001) and extracellular matrix organization pathway (NES = 2.718, adjusted *p*-value <0.001) of REACTOME gene sets were ranked in the top five pathways in comparison between two SGMRS risk groups using GSEA (Figure 6E). The complement and coagulation cascades pathway (NES = 2.223, adjusted *p*-value <0.001) and the focal adhesion pathway (NES = 2.354, adjusted *p*-value <0.001) of KEGG gene sets were ranked in the top five (Figure 6F).

Construction of nomograms based on SGMRS to predict prognosis in glioma patients

We firstly conducted univariate and multivariate Cox regression analyses to identify independent prognostic factors for the subsequent construction of nomograms. The SGMRS, together with other potential prognostic factors, including tumor grade, patient age, radiotherapy, chemotherapy, sex, KPS, 1p/19q codeletion, and IDH mutation, were enrolled into univariate Cox regression analysis in TCGA cohort (Figure 7A). Subsequently, those prognostic factors (*p*-value < 0.05 in univariate analysis) were enrolled into multivariate Cox regression analysis. Eventually, the SGMRS, together with tumor grade, radiotherapy, 1p/19q codeletion, and IDH mutation, were identified as independent prognostic factors in glioma (*p*-value < 0.05, Figure 7B). These factors were utilized to construct a nomogram to achieve individualized survival rate prediction (Figure 7C). The corrected C-index of this nomogram based on TCGA cohort was 0.848. This nomogram's efficacy in predicting the prognosis of glioma patients was validated by the 1-, 2-, and 3-year calibration curves (Figure 7D). For the CGGA325 and cohort, the corrected C-index of the nomogram was 0.765 (Figure 7E). For the CGGA693 cohort and WCH cohort, it is 0.772 and 0.696 respectively. The 1-, 2-, and 3-year calibration curves derived from CGGA325 dataset also endorsed performance of the nomogram (Figure 7F).

Correlation of SGMRS with immune cells and immune microenvironment

To investigate the connection between SGMRS and the immune landscape of gliomas, we performed comprehensive analyses to elucidate the correlation between SGMRS and multiple immunity-related indexes. Firstly, we computed the infiltration fraction of 22 types of immune cells in the tumor microenvironment using the CIBERSORTx algorithm. The results revealed that gliomas of SGMRS high-risk group harbored more macrophages (including M0, M1, and M2), resting NK cells, and resting memory $CD4^+$ T cells infiltrated into the tumor microenvironment, and fewer plasma cells and activated NK cells (Figure 8A), depicting distinctive immune cell infiltration models between SGMRS high- and low-risk groups. Subsequently, we utilized the ESTIMATE algorithm to analyze immune-related scores and tumor purity. The SGMRS high-risk group manifested with higher stromal, immune, and ESTIMATE scores compared to the low-risk group in TCGA, CGGA325, and WCH cohorts (Figure 8B), indicating a significantly more complex tumor microenvironment in gliomas with higher SGMRS. The analysis of tumor purity also confirmed that gliomas of the high-risk group had remarkably lower tumor purity than those of the low-risk group, which was in accordance with the results of immune-related scores (Figure 8C). Further correlation analysis confirmed that the stromal score, immune score, and ESTIMATE score were strongly positively correlated with the value of SGMRS in these three cohorts (Figures 8D–F). The tumor purity was negatively correlated with the value of SGMRS in these three cohorts (Figure 8G).

To explore potential applications of SGMRS in the guidance of immunotherapy, we analyzed the relationship between multiple immunotherapy-related markers and SGMRS. In gliomas of SGMRS high-risk group, the expression levels of CD274 (PD-L1), CD276 (B7-H3), and CD279 (PD-1) were remarkably higher compared to the low-risk group in TCGA cohort (Figure 9A). In the CGGA325 cohort, this result was also confirmed (Figure 9B), indicating that gliomas with high SGMRS would overexpress multiple targets for immunotherapy. Furthermore, to validate the potential ability of SGMRS to direct the use of immunotherapy, we calculated the TIP score to identify the relationship between the immunological phenotype and SGMRS in glioma. The result demonstrated that gliomas of SGMRS high-risk group would highly express immunological 'hot' tumor genes (Figure 9C) in TCGA cohort. And the TIP scores of gliomas in the high-risk group were enormously higher than low-risk group (Figure 9D). Correlation analysis confirmed the positive correlation between TIP score and SGMRS (Figure 9E). These findings were also validated in the CGGA325 cohort (Figures 9F–H). Additionally, the analysis of cytotoxic T cells (CTLs) revealed that the gliomas of SGMRS high-risk group harbored more CTLs infiltration compared to the low-risk group in TCGA and CGGA325 cohort (Figure 9I). It is also demonstrated that patients of the high-risk group would respond better to immune checkpoint inhibitors compared to low risk in TCGA cohort (Figure 9J). Most of these findings can be validated in other cohorts (Supplementary Figure S4).

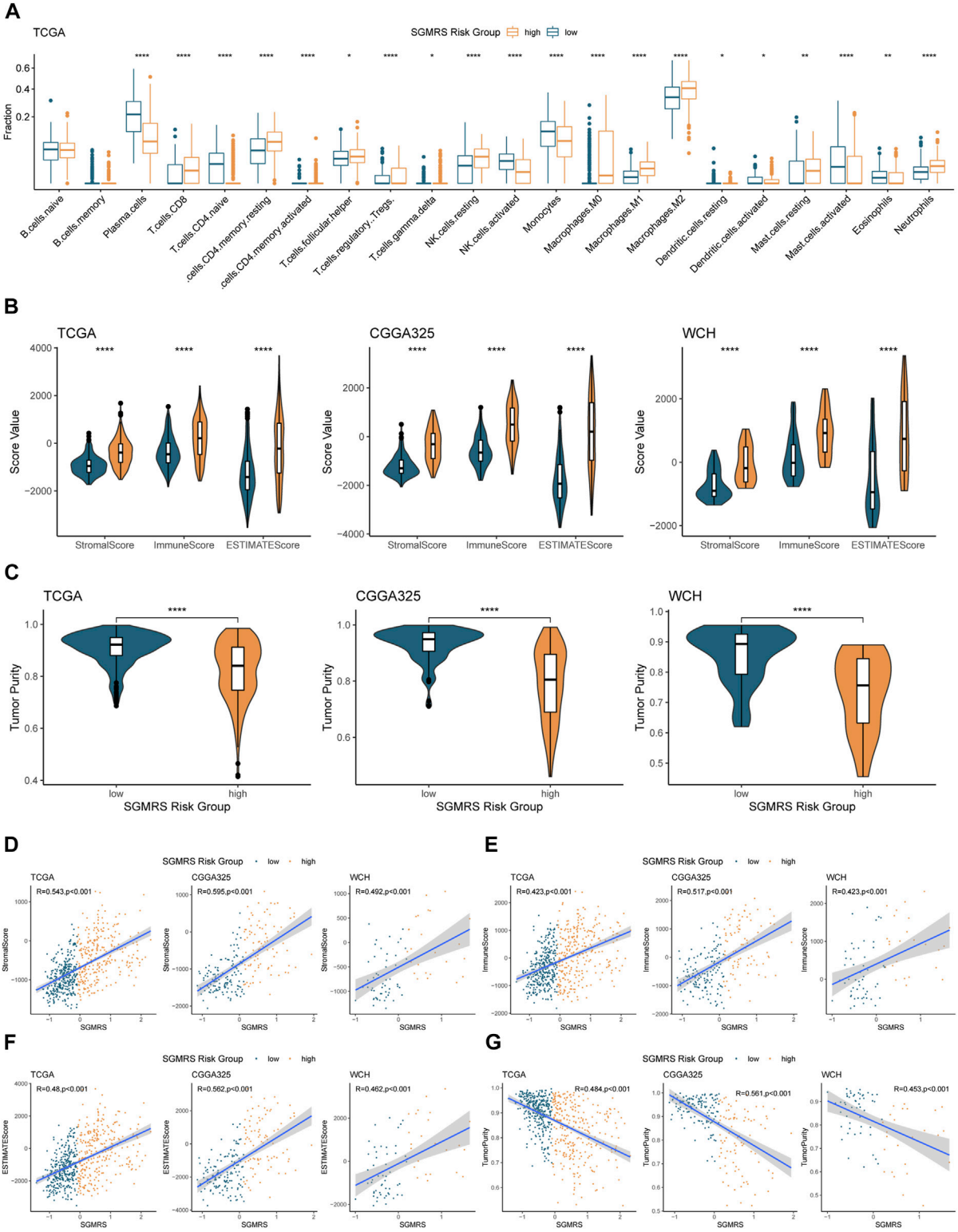

FIGURE 8
Analyses on immune landscapes of tumor microenvironment between SGMRS high- and low-risk groups. **(A)** Boxplot for the estimated infiltration fraction of 22 types of immune cells in tumors. **(B)** Differences in the stromal, immune, and ESTIMATE scores between two risk groups in TCGA, CGGA325, and WCH cohorts. **(C)** Differences in tumor purity between two risk groups in TCGA, CGGA325, and WCH cohorts. **(D)** Analyses of correlations of SGMRS with the **(D)** stromal score, **(E)** immune score, **(F)** ESTIMATE score, and **(G)** tumor purity in TCGA, CGGA325, and WCH cohorts. *$p < 0.05$; **$p < 0.01$; ***$p < 0.001$; ****$p < 0.0001$.

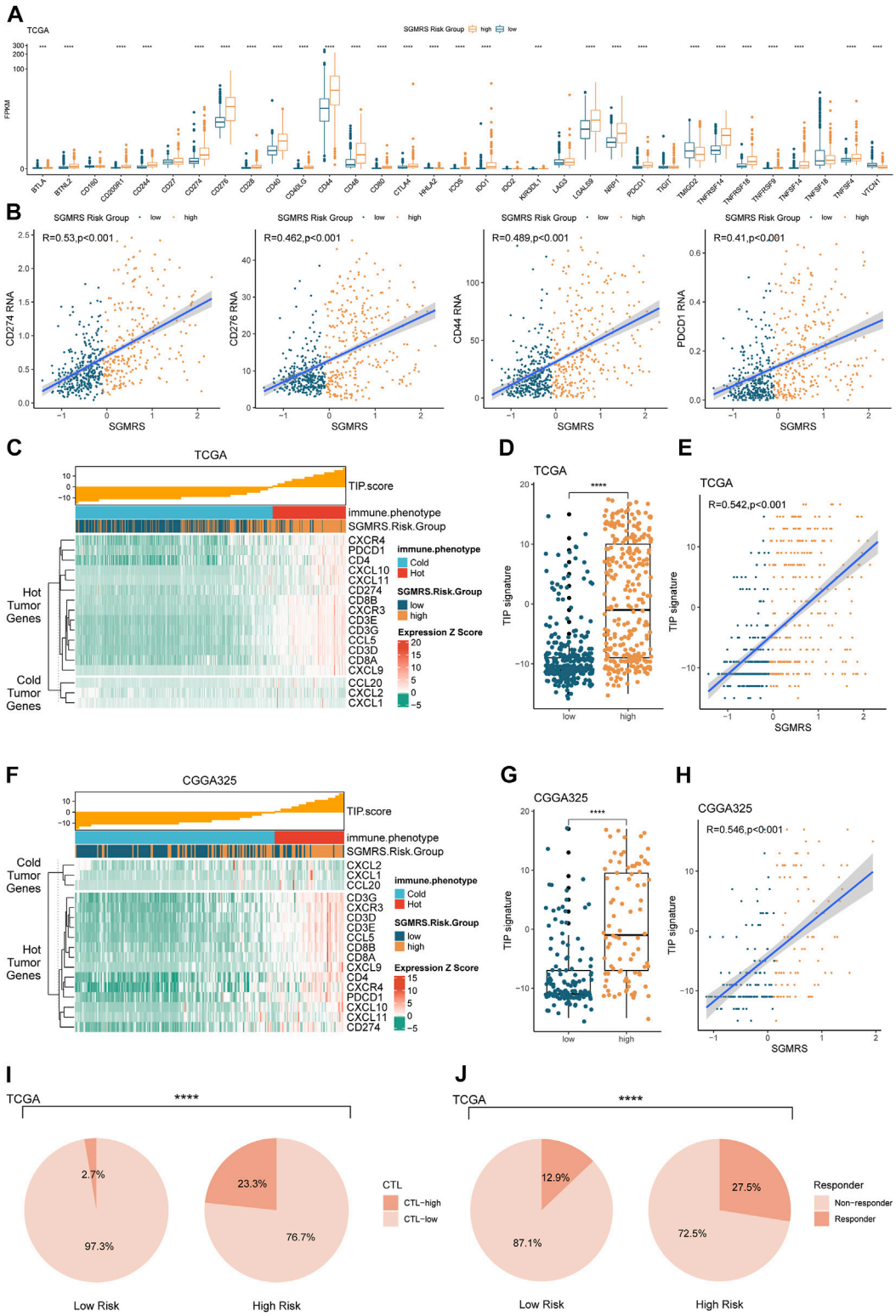

FIGURE 9
Differences in expression of immunotherapy-related genes, immunological phenotype, and response to ICIs between two SGMRS risk groups. **(A)** Boxplot for the expression level of 33 immunotherapy-related genes in two risk groups in TCGA cohort. **(B)** Analyses of correlations between SGMRS and the expression levels of CD274, CD276, CD44, and PD-1 in TCGA cohort. **(C)** Analysis of TIP score and related gene expression levels ordered by SGMRS in TCGA cohort. **(D)** Difference in TIP score between two risk groups in TCGA cohort. **(E)** Analysis of correlation between

(*Continued*)

FIGURE 9 (Continued)
SGMRS and TIP score in TCGA cohort. **(F)** Analysis of TIP score and related gene expression levels ordered by SGMRS in CGGA325 cohort. **(G)** Difference in TIP score between two risk groups in CGGA325 cohort. **(H)** Analysis of correlation between SGMRS and TIP score in CGGA325 cohort. **(I)** Difference in proportion of patients with high cyto-toxic T lymphocytes infiltration between two risk groups in TCGA cohort. **(J)** Difference in proportion of patients with predictive response to immune checkpoint inhibitors between two risk groups in TCGA cohort.

Discussion

As one of the most lethal cancer, glioma causes more than 200 thousand deaths worldwide every year (Sung et al., 2021). Due to its heavy burden and direct threats to human health, countless researchers devoted themselves to exploring novel therapies to improve the prognosis of glioma patients. However, there is hardly inspiring breakthrough in the field of glioma, especially for glioblastoma, which accounts for 50% of gliomas and presented with only a median overall survival of 22 months after the complete treatment process, including surgery resection, radiotherapy, chemotherapy, and even tumor treating field (Stupp et al., 2005; Stupp et al., 2017). Immunotherapy, emerging under the spotlight as a novel therapy for cancers, has been proven effective in multiple types of cancer (Eggermont et al., 2018; Gandhi et al., 2018; Choueiri et al., 2021b; Cortes et al., 2022). Hence, several studies have concentrated on the potential therapeutic effects of immunotherapy in glioma. However, almost all these attempts at the application of immunotherapy failed to improve the overall survival of glioma patients in phase 3 clinical trials (Weller et al., 2017; Wakabayashi et al., 2018; Reardon et al., 2020; Lim et al., 2022; Omuro et al., 2022). The blood-brain barrier (BBB), which functions to block most peripheral immune cells out of the central nervous system (CNS), was recognized as an important reason for these failures. However, inspiringly, a novel lymphatic pathway permitting antigen-presenting cells to escape from CNS was introduced in recent years (Louveau et al., 2015). Further research proved that lymphocytes outside CNS could be primed by these antigen-presenting cells and then infiltrate into the brain and execute immune responses (Lim et al., 2018). These studies suggest that brain is not a closed area for applications of immunotherapy. If we can further investigate and understand the mechanisms of immune cell infiltrations and reshaped immune landscapes of the tumor microenvironment, immunotherapy might become another robust weapon for us to fight against glioma. Therefore, our present study devoted to investigating the underlying mechanisms of the unique immune landscape of glioma, aiming to provide potential help to the application of immunotherapy.

In the field of tumor immunity, the relationship between unique metabolic patterns and immunological characteristics of tumors has become an attractive topic (Xia et al., 2021). Many studies have suggested that serine and glycine metabolism has critical effects on cancers (DeBerardinis, 2011; DeBerardinis and Chandel, 2016). As two non-essential amino acid, cells can gain serine and glycine through intracellular synthesis and uptake from the environment (de Koning et al., 2003; Sullivan and Vander Heiden, 2017). The upregulation of serine and glycine synthesis has been observed in many cancers (Kim et al., 2015; Liao et al., 2019b). As a side-branch of glycolysis, serine and glycine synthesis was tightly regulated by the activity of glycolysis. Due to the Warburg effect, cancer cells could fulfil the requirement of glycolytic intermediates in the synthesis of serine and glycine through activated aerobic glycolysis (DeBerardinis and Chandel, 2020). Upregulating the activity of M2 isoform of pyruvate kinase (PKM2), an enzyme functioned to catalyze conversion of phosphoenolpyruvate into pyruvate, can restrict 3-PG, the initial compound of serine and glycine synthesis, channeling into serine and glycine synthesis (Chaneton et al., 2012). In cancer cells, activation of PKM2 can reduce the synthesis of serine and glycine and render cancer cells dependent on uptake from environment (Kung et al., 2012). On the other way, restriction of dietary serine and glycine, which functioned to decrease serine and glycine uptake from environment, can reduce tumor growth (Maddocks et al., 2013; Gravel et al., 2014). But this effect was alleviated in those cancer models with upregulated serine and glycine synthesis, suggesting that the synthesis of serine and glycine can compensate the lack of uptake from environment (Maddocks et al., 2017). Therefore, the simultaneous application of inhibiting serine and glycine synthesis and uptake exhibited a promising effect and called for more studies.

Moreover, in glioma, the concentration of glycine was also proved with a positive correlation with aggressiveness (Tiwari et al., 2020). Furthermore, serine and glycine were manifested as immunosuppressive metabolites (He et al., 2019). Cancer cells can overproduce abundant serine and glycine, which delivers robust immunosuppressive effects and might contributes to the immune evasion of cancer cells (Hanahan and Weinberg, 2011). Extracellular serine can suppress the function of macrophages and neutrophils (He et al., 2019). High activity of PHGDH would promote macrophages to differentiate into M2-like (Wilson et al., 2020). Hence, investigating the relationship between serine and glycine metabolism and the immune landscape of glioma may contribute to the application of immunotherapy.

In the present study, to explore the relationship between SGMGs and clinicopathological features and the immune landscape of gliomas, we firstly classified all patients into four consensus clusters based on their distinctive expression patterns of SGMGs. Compared to the other clusters, gliomas in cluster 4 expresses significantly higher levels of PSPH and

SHMT1 which were known culprits of aberrant serine and glycine production in malignant cancers (Geeraerts et al., 2021). Additionally, the strong immunohistochemistry signal of PSPH in high grade gliomas presented as an example that the dysregulated SMGMs could be used as pathological biomarkers to identify the most aggressive gliomas (Supplementary Figure S3). Among these four clusters, different clinicopathological features and prognosis patterns were depicted. Furthermore, the incidences of gene alterations also differed among these four clusters. For instance, IDH mutation, a critical diagnostic and prognostic marker for glioma would lead to abnormal tricarboxylic acid (TCA) cycle (Yan et al., 2009; Pirozzi and Yan, 2021). Besides, the serine and glycine synthesis pathway was reported to provide approximately 50% of the total anaplerotic flux of glutamine into the TCA cycle (Possemato et al., 2011), indicating potential interaction between serine and glycine metabolism and IDH mutation. Nevertheless, even with potential interaction with other prognostic factors, the SGMRS was still proved as an independent prognostic factor in multivariate analysis, which included SGMRS and other potential prognostic factors, indicating the satisfactory potential of SGMRS as a prognostic factor.

After filtering SGMGs, five SGMGs were identified as critical genes for the prognosis of glioma, suggesting the strong interaction between these five genes and glioma. For example, phosphoserine phosphatase (PSPH), an essential enzyme of serine and glycine metabolism, catalyzes the dephosphorylation of phosphoserine to serine. In multiple cancers, PSPH promotes tumor growth and metastasis (Liao et al., 2019a; Rawat et al., 2021). In our study, the hazardous effect of PSPH was illustrated. Serine hydroxymethyl transferase 1 (SHMT1) is a critical enzyme that converts serine to glycine (Hebbring et al., 2012). Upregulation of SHMT1 would increase the concentration of glycine. Several studies have found that SHMT1 can promote tumor growth and progression (Pandey et al., 2014; Gupta et al., 2017). The activity of SHMT1 was strongly negatively correlated with the overall survival in both clustering analysis and SGMRS analysis, which was accordance with previous study and endorsed the critical role of SHMT1 on the prognosis of glioma patients. Compared to other three essential enzymes of serine and glycine synthesis, SHMT1 showed significantly stronger correlation with prognosis both in consensus clustering analysis and in SGMRS analysis, suggesting that SHMT1 was the essential enzyme of serine and glycine synthesis to regulate the malignancy of glioma. Besides, glycine N-methyltransferase (GNMT) catalyzes the methylation of glycine to form sarcosine (Yeo and Wagner, 1994), which might decrease glycine concentration in the tumor. GNMT has been proven to have tumor suppression function in hepatocellular carcinoma (Chen et al., 1998). However, there is no study to elucidate the effects of GNMT in glioma. Our study suggested the protective effects of GNMT in glioma, inspiring further research on it.

Further analyses of immune cell infiltration and immune landscapes depicted the relationship between serine and glycine metabolism and the immune microenvironment of glioma. The CIBERSORTx analyses estimated the infiltration fraction of multiple types of immune cells. The results demonstrated that the infiltration of many immune cells was correlated with SGMRS. For example, the infiltration of M2 macrophages into the tumor microenvironment was strongly positively correlated with SGMRS. Circulating monocytes and neighboring macrophages can be recruited by tumor cells and then infiltrated into the tumor microenvironment. Subsequently, these macrophages were polarized from M1-like to M2-like, forming tumor-associated macrophages (TAMs) (Anderson et al., 2021). TAMs can synthesize cytokines to suppress the function of T lymphocytes and upregulated immunosuppressive surface proteins (Curiel et al., 2004; Colombo and Piconese, 2007; Yang and Zhang, 2017). These immunosuppressive functions of TAMs became an important reason for the immune evasion of tumors. The correlation between high SGMRS and high infiltration of TAMs suggests the role of serine and glycine metabolism in immune evasion, inspiring that serine and glycine metabolism could be another target to suppress immune evasion of glioma. The expression levels of multiple immunotherapy-related genes, including PD-1 and PD-L1, were also strongly positively correlated with SGMRS. The serine and glycine synthesis was also reported to induce macrophages to overexpress PD-L1 by promoting the release of IL-1β (Su et al., 2018; Rodriguez et al., 2019; Yu et al., 2019), according to our study. Additionally, higher SGMRS was correlated with immunological 'hotter' features and more potential responders to ICIs. These findings suggested the potential ability of SGMRS to predict the expression of targets for immunotherapy and the consequent ability to guide the selection and use of immunotherapy in glioma.

Although comprehensive analyses were conducted in our present study, there are still some limitations. First, protocols used for data preprocessing and sequencing were different among these four cohorts. Next, compared to metabolic and proteomic data, the abundance of public RNA-sequencing datasets allows more robust analysis and validation of the results in multiple independent cohorts. However, the results derived from transcriptome analysis as performed here would be still more impactful if validated in future experiments. Besides, all the analyses and related genes were about serine and glycine metabolism, in other word, in the scope of pharmacodynamics of serine and glycine. The disposition of serine and glycine in different organs or tissues might also influence their effects, which remains to be explored. In addition, due to lack of transcriptomic data from gliomas patients receiving immunotherapy, the implications of our findings are confined to estimated ICI responses rather than actual response. The application of the prediction results should be evaluated with a clinical study design. Finally, the underlying mechanism of how serine and glycine metabolism impacted immune cell infiltration and the immune landscape remains unclear and calls for further investigation.

Conclusion

In conclusion, we demonstrated that expression patterns of SGMGs were closely related to clinicopathological features, immune cell infiltration, and the immune landscape of glioma. A novel serine and glycine metabolism assessment score system, SGMRS, exhibited with robust ability to predict the prognosis of glioma patients. Besides, higher SGMRS, standing for more glycine synthesis and less glycine catabolism, predicts more immune cells infiltration, a more complex tumor microenvironment, and more expression of targets for immunotherapy, endorsing the application of SGMRS to guide the choice and use of immunotherapy in glioma.

Data availability statement

The datasets presented in this study can be found in online repositories. The names of the repository/repositories and accession number(s) can be found in the article/Supplementary Material.

Ethics statement

The studies involving human participants were reviewed and approved by the institutional review board of West China Hospital (No. 2018.569). The patients/participants provided their written informed consent to participate in this study.

Author contributions

Study design: SC, SZ, YL, and YY. Data retrieve: SC, ZW Statistical Analysis: SC, YY. Result interpretation: SC, SZ, WF, and WL Writing-original draft: all authors. Writing-revise: YL, SC, SZ, and JL.

Funding

This work was supported by a grant from Sichuan Province Science and Technology Support Program (2017SZ0006 to YL), the Clinical Research Innovation Project, West China Hospital, Sichuan University (19HXCX009 to YL), the National Natural Science Young Foundation of China (Grant No.81902532 to YY), and Post-Doctor Research Project, West China Hospital, Sichuan University (Grant No.20HXBH035 to SZ).

Conflict of interest

The authors declare that the research was conducted in the absence of any commercial or financial relationships that could be construed as a potential conflict of interest.

Publisher's note

All claims expressed in this article are solely those of the authors and do not necessarily represent those of their affiliated organizations, or those of the publisher, the editors and the reviewers. Any product that may be evaluated in this article, or claim that may be made by its manufacturer, is not guaranteed or endorsed by the publisher.

Supplementary material

The Supplementary Material for this article can be found online at: https://www.frontiersin.org/articles/10.3389/fphar.2022.1072253/full#supplementary-material

References

Anderson, N. R., Minutolo, N. G., Gill, S., and Klichinsky, M. (2021). Macrophage-based approaches for cancer immunotherapy. *Cancer Res.* 81 (5), 1201–1208. doi:10.1158/0008-5472.Can-20-2990

Aran, D., Sirota, M., and Butte, A. J. (2015). Systematic pan-cancer analysis of tumour purity. *Nat. Commun.* 6, 8971. doi:10.1038/ncomms9971

Chaneton, B., Hillmann, P., Zheng, L., Martin, A. C. L., Maddocks, O. D. K., Chokkathukalam, A., et al. (2012). Serine is a natural ligand and allosteric activator of pyruvate kinase M2. *Nature* 491 (7424), 458–462. doi:10.1038/nature11540

Chen, Y. M., Shiu, J. Y., Tzeng, S. J., Shih, L. S., Chen, Y. J., Lui, W. Y., et al. (1998). Characterization of glycine-N-methyltransferase-gene expression in human hepatocellular carcinoma. *Int. J. Cancer* 75 (5), 787–793. doi:10.1002/(sici)1097-0215(19980302)75:5<787::aid-ijc20>3.0.co;2-2

Chinot, O. L., Wick, W., Mason, W., Henriksson, R., Saran, F., Nishikawa, R., et al. (2014). Bevacizumab plus radiotherapy-temozolomide for newly diagnosed glioblastoma. *N. Engl. J. Med.* 370 (8), 709–722. doi:10.1056/NEJMoa1308345

Choueiri, T. K., Powles, T., Burotto, M., Escudier, B., Bourlon, M. T., Zurawski, B., et al. (2021a). Nivolumab plus cabozantinib versus sunitinib for advanced renal-cell carcinoma. *N. Engl. J. Med.* 384 (9), 829–841. doi:10.1056/NEJMoa2026982

Choueiri, T. K., Tomczak, P., Park, S. H., Venugopal, B., Ferguson, T., Chang, Y. H., et al. (2021b). Adjuvant pembrolizumab after nephrectomy in renal-cell carcinoma. *N. Engl. J. Med.* 385 (8), 683–694. doi:10.1056/NEJMoa2106391

Cloughesy, T. F., Mochizuki, A. Y., Orpilla, J. R., Hugo, W., Lee, A. H., Davidson, T. B., et al. (2019). Neoadjuvant anti-PD-1 immunotherapy promotes a survival benefit with intratumoral and systemic immune responses in recurrent glioblastoma. *Nat. Med.* 25 (3), 477–486. doi:10.1038/s41591-018-0337-7

Colombo, M. P., and Piconese, S. (2007). Regulatory-T-cell inhibition versus depletion: The right choice in cancer immunotherapy. *Nat. Rev. Cancer* 7 (11), 880–887. doi:10.1038/nrc2250

Cortes, J., Rugo, H. S., Cescon, D. W., Im, S. A., Yusof, M. M., Gallardo, C., et al. (2022). Pembrolizumab plus chemotherapy in advanced triple-negative breast cancer. *N. Engl. J. Med.* 387 (3), 217–226. doi:10.1056/NEJMoa2202809

Curiel, T. J., Coukos, G., Zou, L., Alvarez, X., Cheng, P., Mottram, P., et al. (2004). Specific recruitment of regulatory T cells in ovarian carcinoma fosters immune privilege and predicts reduced survival. *Nat. Med.* 10 (9), 942–949. doi:10.1038/nm1093

de Koning, T. J., Snell, K., Duran, M., Berger, R., Poll-The, B. T., and Surtees, R. (2003). L-serine in disease and development. *Biochem. J.* 371 (3), 653–661. doi:10.1042/bj20021785

DeBerardinis, R. J., and Chandel, N. S. (2016). Fundamentals of cancer metabolism. *Sci. Adv.* 2 (5), e1600200. doi:10.1126/sciadv.1600200

DeBerardinis, R. J., and Chandel, N. S. (2020). We need to talk about the Warburg effect. *Nat. Metab.* 2 (2), 127–129. doi:10.1038/s42255-020-0172-2

DeBerardinis, R. J. (2011). Serine metabolism: Some tumors take the road less traveled. *Cell Metab.* 14 (3), 285–286. doi:10.1016/j.cmet.2011.08.004

Eggermont, A. M. M., Blank, C. U., Mandala, M., Long, G. V., Atkinson, V., Dalle, S., et al. (2018). Adjuvant pembrolizumab versus placebo in resected stage III melanoma. *N. Engl. J. Med.* 378 (19), 1789–1801. doi:10.1056/NEJMoa1802357

Fan, T. W. M., Bruntz, R. C., Yang, Y., Song, H., Chernyavskaya, Y., Deng, P., et al. (2019). De novo synthesis of serine and glycine fuels purine nucleotide biosynthesis in human lung cancer tissues. *J. Biol. Chem.* 294 (36), 13464–13477. doi:10.1074/jbc.RA119.008743

Gandhi, L., Rodríguez-Abreu, D., Gadgeel, S., Esteban, E., Felip, E., De Angelis, F., et al. (2018). Pembrolizumab plus chemotherapy in metastatic non-small-cell lung cancer. *N. Engl. J. Med.* 378 (22), 2078–2092. doi:10.1056/NEJMoa1801005

Gao, X., Lee, K., Reid, M. A., Sanderson, S. M., Qiu, C., Li, S., et al. (2018). Serine availability influences mitochondrial dynamics and function through lipid metabolism. *Cell Rep.* 22 (13), 3507–3520. doi:10.1016/j.celrep.2018.03.017

Geeraerts, S. L., Heylen, E., De Keersmaecker, K., and Kampen, K. R. (2021). The ins and outs of serine and glycine metabolism in cancer. *Nat. Metab.* 3 (2), 131–141. doi:10.1038/s42255-020-00329-9

Gilbert, M. R., Dignam, J. J., Armstrong, T. S., Wefel, J. S., Blumenthal, D. T., Vogelbaum, M. A., et al. (2014). A randomized trial of bevacizumab for newly diagnosed glioblastoma. *N. Engl. J. Med.* 370 (8), 699–708. doi:10.1056/NEJMoa1308573

Gravel, S. P., Hulea, L., Toban, N., Birman, E., Blouin, M. J., Zakikhani, M., et al. (2014). Serine deprivation enhances antineoplastic activity of biguanides. *Cancer Res.* 74 (24), 7521–7533. doi:10.1158/0008-5472.Can-14-2643-t

Gupta, R., Yang, Q., Dogra, S. K., and Wajapeyee, N. (2017). Serine hydroxymethyl transferase 1 stimulates pro-oncogenic cytokine expression through sialic acid to promote ovarian cancer tumor growth and progression. *Oncogene* 36 (28), 4014–4024. doi:10.1038/onc.2017.37

Hanahan, D., and Weinberg, R. A. (2011). Hallmarks of cancer: The next generation. *Cell* 144 (5), 646–674. doi:10.1016/j.cell.2011.02.013

He, F., Yin, Z., Wu, C., Xia, Y., Wu, M., Li, P., et al. (2019). l-Serine lowers the inflammatory responses during pasteurella multocida infection. *Infect. Immun.* 87 (12), e00677. doi:10.1128/iai.00677-19

Hebbring, S. J., Chai, Y., Ji, Y., Abo, R. P., Jenkins, G. D., Fridley, B., et al. (2012). Serine hydroxymethyltransferase 1 and 2: Gene sequence variation and functional genomic characterization. *J. Neurochem.* 120 (6), 881–890. doi:10.1111/j.1471-4159.2012.07646.x

Hendriks, L. E. L., Henon, C., Auclin, E., Mezquita, L., Ferrara, R., Audigier-Valette, C., et al. (2019). Outcome of patients with non-small cell lung cancer and brain metastases treated with checkpoint inhibitors. *J. Thorac. Oncol.* 14 (7), 1244–1254. doi:10.1016/j.jtho.2019.02.009

Janjigian, Y. Y., Shitara, K., Moehler, M., Garrido, M., Salman, P., Shen, L., et al. (2021). First-line nivolumab plus chemotherapy versus chemotherapy alone for advanced gastric, gastro-oesophageal junction, and oesophageal adenocarcinoma (CheckMate 649): A randomised, open-label, phase 3 trial. *Lancet* 398 (10294), 27–40. doi:10.1016/s0140-6736(21)00797-2

Kim, D., Fiske, B. P., Birsoy, K., Freinkman, E., Kami, K., Possemato, R. L., et al. (2015). SHMT2 drives glioma cell survival in ischaemia but imposes a dependence on glycine clearance. *Nature* 520 (7547), 363–367. doi:10.1038/nature14363

Kung, C., Hixon, J., Choe, S., Marks, K., Gross, S., Murphy, E., et al. (2012). Small molecule activation of PKM2 in cancer cells induces serine auxotrophy. *Chem. Biol.* 19 (9), 1187–1198. doi:10.1016/j.chembiol.2012.07.021

Larkin, J., Chiarion-Sileni, V., Gonzalez, R., Grob, J. J., Cowey, C. L., Lao, C. D., et al. (2015). Combined nivolumab and ipilimumab or monotherapy in untreated melanoma. *N. Engl. J. Med.* 373 (1), 23–34. doi:10.1056/NEJMoa1504030

Liao, L., Ge, M., Zhan, Q., Huang, R., Ji, X., Liang, X., et al. (2019a). PSPH mediates the metastasis and proliferation of non-small cell lung cancer through MAPK signaling pathways. *Int. J. Biol. Sci.* 15 (1), 183–194. doi:10.7150/ijbs.29203

Liao, L., Yu, H., Ge, M., Zhan, Q., Huang, R., Ji, X., et al. (2019b). Upregulation of phosphoserine phosphatase contributes to tumor progression and predicts poor prognosis in non-small cell lung cancer patients. *Thorac. Cancer* 10 (5), 1203–1212. doi:10.1111/1759-7714.13064

Lim, M., Weller, M., Idbaih, A., Steinbach, J., Finocchiaro, G., Raval, R. R., et al. (2022). Phase III trial of chemoradiotherapy with temozolomide plus nivolumab or placebo for newly diagnosed glioblastoma with methylated MGMT promoter. *Neuro. Oncol.* 24, 1935–1949. doi:10.1093/neuonc/noac116

Lim, M., Xia, Y., Bettegowda, C., and Weller, M. (2018). Current state of immunotherapy for glioblastoma. *Nat. Rev. Clin. Oncol.* 15 (7), 422–442. doi:10.1038/s41571-018-0003-5

Locasale, J. W. (2013). Serine, glycine and one-carbon units: Cancer metabolism in full circle. *Nat. Rev. Cancer* 13 (8), 572–583. doi:10.1038/nrc3557

Louis, D. N., Perry, A., Wesseling, P., Brat, D. J., Cree, I. A., Figarella-Branger, D., et al. (2021). The 2021 WHO classification of tumors of the central nervous system: A summary. *Neuro. Oncol.* 23 (8), 1231–1251. doi:10.1093/neuonc/noab106

Louveau, A., Smirnov, I., Keyes, T. J., Eccles, J. D., Rouhani, S. J., Peske, J. D., et al. (2015). Structural and functional features of central nervous system lymphatic vessels. *Nature* 523 (7560), 337–341. doi:10.1038/nature14432

Maddocks, O. D., Berkers, C. R., Mason, S. M., Zheng, L., Blyth, K., Gottlieb, E., et al. (2013). Serine starvation induces stress and p53-dependent metabolic remodelling in cancer cells. *Nature* 493 (7433), 542–546. doi:10.1038/nature11743

Maddocks, O. D. K., Athineos, D., Cheung, E. C., Lee, P., Zhang, T., van den Broek, N. J. F., et al. (2017). Modulating the therapeutic response of tumours to dietary serine and glycine starvation. *Nature* 544 (7650), 372–376. doi:10.1038/nature22056

Mullarky, E., Lucki, N. C., Beheshti Zavareh, R., Anglin, J. L., Gomes, A. P., Nicolay, B. N., et al. (2016). Identification of a small molecule inhibitor of 3-phosphoglycerate dehydrogenase to target serine biosynthesis in cancers. *Proc. Natl. Acad. Sci. U. S. A.* 113 (7), 1778–1783. doi:10.1073/pnas.1521548113

Muthusamy, T., Cordes, T., Handzlik, M. K., You, L., Lim, E. W., Gengatharan, J., et al. (2020). Serine restriction alters sphingolipid diversity to constrain tumour growth. *Nature* 586 (7831), 790–795. doi:10.1038/s41586-020-2609-x

Newman, A. C., and Maddocks, O. D. K. (2017). One-carbon metabolism in cancer. *Br. J. Cancer* 116 (12), 1499–1504. doi:10.1038/bjc.2017.118

Ngo, B., Kim, E., Osorio-Vasquez, V., Doll, S., Bustraan, S., Liang, R. J., et al. (2020). Limited environmental serine and Glycine confer brain metastasis sensitivity to PHGDH inhibition. *Cancer Discov.* 10 (9), 1352–1373. doi:10.1158/2159-8290.Cd-19-1228

Omuro, A., Brandes, A. A., Carpentier, A. F., Idbaih, A., Reardon, D. A., Cloughesy, T., et al. (2022). Radiotherapy combined with nivolumab or temozolomide for newly diagnosed glioblastoma with unmethylated *MGMT* promoter: An international randomized phase III trial. *Neuro. Oncol.*, noac099. doi:10.1093/neuonc/noac099

Ostrom, Q. T., Cioffi, G., Waite, K., Kruchko, C., and Barnholtz-Sloan, J. S. (2021). CBTRUS statistical report: Primary brain and other central nervous system tumors diagnosed in the United States in 2014-2018. *Neuro. Oncol.* 23, iii1–iii105. doi:10.1093/neuonc/noab200

Pacold, M. E., Brimacombe, K. R., Chan, S. H., Rohde, J. M., Lewis, C. A., Swier, L. J., et al. (2016). A PHGDH inhibitor reveals coordination of serine synthesis and one-carbon unit fate. *Nat. Chem. Biol.* 12 (6), 452–458. doi:10.1038/nchembio.2070

Pandey, S., Garg, P., Lee, S., Choung, H. W., Choung, Y. H., Choung, P. H., et al. (2014). Nucleotide biosynthesis arrest by silencing SHMT1 function via vitamin B6-coupled vector and effects on tumor growth inhibition. *Biomaterials* 35 (34), 9332–9342. doi:10.1016/j.biomaterials.2014.07.045

Pirozzi, C. J., and Yan, H. (2021). The implications of IDH mutations for cancer development and therapy. *Nat. Rev. Clin. Oncol.* 18 (10), 645–661. doi:10.1038/s41571-021-00521-0

Pontén, F., Jirström, K., and Uhlen, M. (2008). The human protein atlas--a tool for pathology. *J. Pathol.* 216 (4), 387–393. doi:10.1002/path.2440

Possemato, R., Marks, K. M., Shaul, Y. D., Pacold, M. E., Kim, D., Birsoy, K., et al. (2011). Functional genomics reveal that the serine synthesis pathway is essential in breast cancer. *Nature* 476 (7360), 346–350. doi:10.1038/nature10350

Rawat, V., Malvi, P., Della Manna, D., Yang, E. S., Bugide, S., Zhang, X., et al. (2021). PSPH promotes melanoma growth and metastasis by metabolic deregulation-mediated transcriptional activation of NR4A1. *Oncogene* 40 (13), 2448–2462. doi:10.1038/s41388-021-01683-y

Reardon, D. A., Brandes, A. A., Omuro, A., Mulholland, P., Lim, M., Wick, A., et al. (2020). Effect of nivolumab vs bevacizumab in patients with recurrent glioblastoma: The CheckMate 143 phase 3 randomized clinical trial. *JAMA Oncol.* 6 (7), 1003–1010. doi:10.1001/jamaoncol.2020.1024

Reck, M., Rodríguez-Abreu, D., Robinson, A. G., Hui, R., Csőszi, T., Fülöp, A., et al. (2016). Pembrolizumab versus chemotherapy for PD-L1-positive non-small-cell lung cancer. *N. Engl. J. Med.* 375 (19), 1823–1833. doi:10.1056/NEJMoa1606774

Rodriguez, A. E., Ducker, G. S., Billingham, L. K., Martinez, C. A., Mainolfi, N., Suri, V., et al. (2019). Serine metabolism supports macrophage IL-1β production. *Cell Metab.* 29 (4), 10031003–10031011. doi:10.1016/j.cmet.2019.01.014

Schalper, K. A., Rodriguez-Ruiz, M. E., Diez-Valle, R., López-Janeiro, A., Porciuncula, A., Idoate, M. A., et al. (2019). Neoadjuvant nivolumab modifies the tumor immune microenvironment in resectable glioblastoma. *Nat. Med.* 25 (3), 470–476. doi:10.1038/s41591-018-0339-5

Stupp, R., Mason, W. P., van den Bent, M. J., Weller, M., Fisher, B., Taphoorn, M. J., et al. (2005). Radiotherapy plus concomitant and adjuvant temozolomide for glioblastoma. *N. Engl. J. Med.* 352 (10), 987–996. doi:10.1056/NEJMoa043330

Stupp, R., Taillibert, S., Kanner, A. A., Kesari, S., Steinberg, D. M., Toms, S. A., et al. (2015). Maintenance therapy with tumor-treating fields plus temozolomide vs temozolomide alone for glioblastoma: A randomized clinical trial. *Jama* 314 (23), 2535–2543. doi:10.1001/jama.2015.16669

Stupp, R., Taillibert, S., Kanner, A., Read, W., Steinberg, D., Lhermitte, B., et al. (2017). Effect of tumor-treating fields plus maintenance temozolomide vs maintenance temozolomide alone on survival in patients with glioblastoma: A randomized clinical trial. *Jama* 318 (23), 2306–2316. doi:10.1001/jama.2017.18718

Su, S., Zhao, J., Xing, Y., Zhang, X., Liu, J., Ouyang, Q., et al. (2018). Immune checkpoint inhibition overcomes ADCP-induced immunosuppression by macrophages. *Cell* 175 (2), 442–457. e423. doi:10.1016/j.cell.2018.09.007

Sullivan, M. R., and Vander Heiden, M. G. (2017). When cancer needs what's non-essential. *Nat. Cell Biol.* 19 (5), 418–420. doi:10.1038/ncb3523

Sung, H., Ferlay, J., Siegel, R. L., Laversanne, M., Soerjomataram, I., Jemal, A., et al. (2021). Global cancer statistics 2020: GLOBOCAN estimates of incidence and mortality worldwide for 36 cancers in 185 countries. *Ca. Cancer J. Clin.* 71 (3), 209–249. doi:10.3322/caac.21660

Tawbi, H. A., Forsyth, P. A., Algazi, A., Hamid, O., Hodi, F. S., Moschos, S. J., et al. (2018). Combined nivolumab and ipilimumab in melanoma metastatic to the brain. *N. Engl. J. Med.* 379 (8), 722–730. doi:10.1056/NEJMoa1805453

Tiwari, V., Daoud, E. V., Hatanpaa, K. J., Gao, A., Zhang, S., An, Z., et al. (2020). Glycine by MR spectroscopy is an imaging biomarker of glioma aggressiveness. *Neuro. Oncol.* 22 (7), 1018–1029. doi:10.1093/neuonc/noaa034

Wakabayashi, T., Natsume, A., Mizusawa, J., Katayama, H., Fukuda, H., Sumi, M., et al. (2018). JCOG0911 INTEGRA study: A randomized screening phase II trial of interferonβ plus temozolomide in comparison with temozolomide alone for newly diagnosed glioblastoma. *J. Neurooncol.* 138 (3), 627–636. doi:10.1007/s11060-018-2831-7

Wang, H., Li, S., Wang, Q., Jin, Z., Shao, W., Gao, Y., et al. (2021). Tumor immunological phenotype signature-based high-throughput screening for the discovery of combination immunotherapy compounds. *Sci. Adv.* 7 (4), eabd7851. doi:10.1126/sciadv.abd7851

Weller, M., Butowski, N., Tran, D. D., Recht, L. D., Lim, M., Hirte, H., et al. (2017). Rindopepimut with temozolomide for patients with newly diagnosed, EGFRvIII-expressing glioblastoma (ACT IV): A randomised, double-blind, international phase 3 trial. *Lancet. Oncol.* 18 (10), 1373–1385. doi:10.1016/s1470-2045(17)30517-x

Wilson, J. L., Nägele, T., Linke, M., Demel, F., Fritsch, S. D., Mayr, H. K., et al. (2020). Inverse data-driven modeling and multiomics analysis reveals phgdh as a metabolic checkpoint of macrophage polarization and proliferation. *Cell Rep.* 30 (5), 1542–1552. doi:10.1016/j.celrep.2020.01.011

Xia, L., Oyang, L., Lin, J., Tan, S., Han, Y., Wu, N., et al. (2021). The cancer metabolic reprogramming and immune response. *Mol. Cancer* 20 (1), 28. doi:10.1186/s12943-021-01316-8

Yan, H., Parsons, D. W., Jin, G., McLendon, R., Rasheed, B. A., Yuan, W., et al. (2009). IDH1 and IDH2 mutations in gliomas. *N. Engl. J. Med.* 360 (8), 765–773. doi:10.1056/NEJMoa0808710

Yang, L., and Zhang, Y. (2017). Tumor-associated macrophages: From basic research to clinical application. *J. Hematol. Oncol.* 10 (1), 58. doi:10.1186/s13045-017-0430-2

Ye, J., Fan, J., Venneti, S., Wan, Y. W., Pawel, B. R., Zhang, J., et al. (2014). Serine catabolism regulates mitochondrial redox control during hypoxia. *Cancer Discov.* 4 (12), 1406–1417. doi:10.1158/2159-8290.Cd-14-0250

Yeo, E. J., and Wagner, C. (1994). Tissue distribution of glycine N-methyltransferase, a major folate-binding protein of liver. *Proc. Natl. Acad. Sci. U. S. A.* 91 (1), 210–214. doi:10.1073/pnas.91.1.210

Yoshihara, K., Shahmoradgoli, M., Martínez, E., Vegesna, R., Kim, H., Torres-Garcia, W., et al. (2013). Inferring tumour purity and stromal and immune cell admixture from expression data. *Nat. Commun.* 4, 2612. doi:10.1038/ncomms3612

Yu, W., Wang, Z., Zhang, K., Chi, Z., Xu, T., Jiang, D., et al. (2019). One-carbon metabolism supports S-adenosylmethionine and histone methylation to drive inflammatory macrophages. *Mol. Cell* 75 (6), 1147–1160. doi:10.1016/j.molcel.2019.06.039

frontiers | Frontiers in Pharmacology

TYPE Original Research
PUBLISHED 18 November 2022
DOI 10.3389/fphar.2022.1069204

OPEN ACCESS

EDITED BY
Kui Zhang,
The University of Chicago, United States

REVIEWED BY
Yuan Yao,
Mayo Clinic, United States
Zeyuan Wang,
Merck, United States
Fu Yang,
Duke University, United States
Yongjin Liu,
Texas A&M University, United States
Man Zhao,
Stanford University, United States
Jiannan Huang,
University of South Dakota, United States
Roushu Zhang,
Institute for Protein Innovation (IPI), United States

*CORRESPONDENCE
Yue Wang,
wangyue0512@163.com
Jianhua Jin,
jianhuajin88@sina.com

‡These authors have contributed equally to this work

SPECIALTY SECTION
This article was submitted to Pharmacology of Anti-Cancer Drugs, a section of the journal Frontiers in Pharmacology

RECEIVED 13 October 2022
ACCEPTED 07 November 2022
PUBLISHED 18 November 2022

CITATION
Zeng C, He R, Dai Y, Lu X, Deng L, Zhu Q, Liu Y, Liu Q, Lu W, Wang Y and Jin J (2022), Identification of TGF-β signaling-related molecular patterns, construction of a prognostic model, and prediction of immunotherapy response in gastric cancer.
Front. Pharmacol. 13:1069204.
doi: 10.3389/fphar.2022.1069204

Identification of TGF-β signaling-related molecular patterns, construction of a prognostic model, and prediction of immunotherapy response in gastric cancer

Cheng Zeng [1,2‡], Rong He [3‡], Yuyang Dai [4‡], Xiaohuan Lu [5], Linghui Deng [1,2,6], Qi Zhu [1,2], Yu Liu [7], Qian Liu [1,2], Wenbin Lu [1,2], Yue Wang [8*] and Jianhua Jin [1,2*]

[1]Department of Oncology, Wujin Hospital Affiliated with Jiangsu University, Changzhou, Jiangsu, China, [2]Department of Oncology, Wujin Clinical College of Xuzhou Medical University, Changzhou, Jiangsu, China, [3]Department of Medical Oncology, Shanghai Tenths People's Hospital, School of Medicine, Tongji University, Shanghai, China, [4]School of Medicine, Jiangsu University, Zhenjiang, Jiangsu, China, [5]Department of Gastrointestinal Surgery, Union Hospital, Tongji Medical College, Huazhong University of Science and Technology, Wuhan, Hubei, China, [6]Department of Oncology, The First Affiliated Hospital of Soochow University, Suzhou, Jiangsu, China, [7]Department of Internal Medicine, School of Medicine, Dalian Medical University, Dalian, Liaoning, China, [8]Cancer Institute, Xuzhou Medical University, Xuzhou, Jiangsu, China

Background: TGF-β signaling pathway plays an essential role in tumor progression and immune responses. However, the link between TGF-β signaling pathway-related genes (TSRGs) and clinical prognosis, tumor microenvironment (TME), and immunotherapy in gastric cancer is unclear.

Methods: Transcriptome data and related clinical data of gastric cancer were downloaded from the Cancer Genome Atlas (TCGA) and Gene Expression Omnibus (GEO) databases, and 54 TSRGs were obtained from the Molecular Signatures Database (MSigDB). We systematically analyzed the expression profile characteristics of 54 TSRGs in 804 gastric cancer samples and examined the differences in prognosis, clinicopathological features, and TME among different molecular subtypes. Subsequently, TGF-β-related prognostic models were constructed using univariate and least absolute shrinkage and selection operator (LASSO) Cox regression analysis to quantify the degree of risk in each patient. Patients were divided into two high- and low-risk groups based

Abbreviations: CNV, copy number variation; CR, Complete response; DEGs, differentially expressed genes; EMT, epithelial-mesenchymal transition; FPKM, fragments per kilobase million; GEO, gene expression omnibus; GO, gene ontology; GSVA, gene set variation analysis; ICIs, immune checkpoint inhibitors; IC50, half inhibitory centration; IPS, immunophenoscore; KEGG, kyoto encyclopedia of genes and genomes; LASSO, least absolute shrinkage and selection operator; MSigDB, molecular signatures database; MSI-H, high microsatellite instability; OS, overall survival; PD, Progressive disease; PR, Partial response; SD, Stable disease; ssGSEA, single sample gene set enrichment analysis; TCGA, the cancer genome atlas; TIDE, tumor immune dysfunction and exclusion; TILs, tumor-infiltrating lymphocytes; TMB, tumor mutation burden; TME, tumor microenvironment; TPM, transcripts per kilobase million; TSRGs, TGF-β signaling pathway-related genes.

on the median risk score. Finally, sensitivity to immune checkpoint inhibitors (ICIs) and anti-tumor agents was assessed in patients in high- and low-risk groups.

Results: We identified two distinct TGF-β subgroups. Compared to TGF-β cluster B, TGF-β cluster A exhibits an immunosuppressive microenvironment with a shorter overall survival (OS). Then, a novel TGF-β-associated prognostic model, including SRPX2, SGCE, DES, MMP7, and KRT17, was constructed, and the risk score was demonstrated as an independent prognostic factor for gastric cancer patients. Further studies showed that gastric cancer patients in the low-risk group, characterized by higher tumor mutation burden (TMB), the proportion of high microsatellite instability (MSI-H), immunophenoscore (IPS), and lower tumor immune dysfunction and exclusion (TIDE) score, had a better prognosis, and linked to higher response rate to immunotherapy. In addition, the risk score and anti-tumor drug sensitivity were strongly correlated.

Conclusion: These findings highlight the importance of TSRGs, deepen the understanding of tumor immune microenvironment, and guide individualized immunotherapy for gastric cancer patients.

KEYWORDS

gastric cancer, TGF-β, molecular pattern, prognosis, tumor microenvironment, immunotherapy

Introduction

Gastric cancer is a highly heterogeneous malignant tumor of the digestive system, ranking fifth in incidence and third in mortality worldwide (Smyth et al., 2020). As the early symptoms of gastric cancer are not obvious, some patients have already entered the middle and late stages with poor prognostic when diagnosed (Wei et al., 2020). In recent years, with the application of targeted drugs such as trastuzumab in clinical treatment, the prognosis of HER-2-positive patients with advanced gastric cancer has improved (Zhu et al., 2021). However, the overall prognosis of gastric cancer is still disappointing (Patel and Cecchini, 2020).

Immune checkpoint inhibitors (ICIs) bring new hope to tumor patients due to their significant efficacy and low side effects. However, the response rate of immunotherapy for patients with advanced gastric cancer is less than 30% (Chen et al., 2022), which limits their use in clinical treatment. Studies have shown that the tumor microenvironment (TME) plays a vital role in tumor development and can influence the response rate of ICIs(Zhang and Zhang, 2020). Several biomarkers reflecting the TME, such as tumor mutation burden (TMB), microsatellite instability (MSI), the density of tumor-infiltrating lymphocytes (TILs), and PD-L1 expression, have been found to correlate with the therapeutic efficacy of ICIs(Rizzo et al., 2021; Niu et al., 2022). Tumor cells with high microsatellite instability (MSI-H) have an increased TMB and generate new antigens due to unrepaired mis-replicated DNA, which allows more TILs to infiltrate and thus respond better to ICIs(Lizardo et al., 2020). In addition, patients with high PD-L1 expression have higher response rates to ICIs and longer survival time in most tumors (Ni et al., 2021). Most biomarkers reflect only one aspect of the TME. Recently, some investigators have used transcriptomic data to systematically assess the TME with the help of bioinformatics approaches to screen for different immune phenotypes and thus predict the response rate to ICIs. For example, Zhang et al. (2020) used transcriptomic data from multiple m6A regulators to identify three m6A modification patterns associated with immune phenotypes and to construct an m6A scoring system to predict immunotherapy response.

TGF-β can be produced by most cells through autocrine and paracrine forms, such as tumor cells, stromal cells, and immune cells (Ungefroren, 2019). TGF-β signaling pathway plays a vital role in embryonic development, tumor progression, and immune response (Morikawa et al., 2016; Kim et al., 2021). In early tumor cells, the TGF-β signaling pathway can inhibit proliferation, induce cell cycle arrest and apoptosis, and is considered a tumor suppressor (Colak and Ten Dijke, 2017; Garcia-Rendueles et al., 2017). However, in advanced tumor cells, the TGF-β signaling pathway regulates tumor recurrence and metastasis through mechanisms such as promoting angiogenesis, inducing epithelial-mesenchymal transition (EMT), regulating genomic instability, and immune escape (Colak and Ten Dijke, 2017; Garcia-Rendueles et al., 2017). In addition, the collagen fibers induced by activation of the TGF-β signaling pathway in fibroblasts in the TME restrict the infiltration of T cells into tumor cells, which in turn inhibits the body's anti-cancer immune response and is regarded as an immunosuppressive cytokine (Batlle and Massagué, 2019; Zhao et al., 2020a). Currently, most studies focus on only one or two

genes in the TGF-β signaling pathway, while tumor development is often the result of a large number of genes interacting together. Therefore, it is necessary to systematically analyze the relationship between multiple genes in the TGF-β signaling pathway and the TME to discover new and different immune phenotypes and screen people sensitive to immunotherapy for more precise treatment.

In this study, 804 gastric cancer samples were obtained from TCGA and GEO databases, and 54 TSRGs were collected from MSigDB. We analyzed the expression levels and gene mutation characteristics of 54 TSRGs in gastric cancer and classified gastric cancer patients into two distinct TGF-β subgroups based on the expression levels of the 54 TSRGs. Subsequently, three gene subgroups were identified based on the differentially expressed genes (DEGs) between the two distinct TGF-β subgroups. Next, we constructed and validated a prognostic model, which can predict the prognosis of gastric cancer patients, paint a picture of immune infiltration, and predict ICIs response rates and antitumor drug sensitivity.

Materials and methods

Data collection

Gene expression data, somatic mutation data, copy number variation (CNV) data, and corresponding clinicopathological information of gastric cancer patients were downloaded from the TCGA database (https://portal.gdc.cancer.gov/). The GSE84337 dataset was obtained from the GEO database (https://www.ncbi.nlm.nih.gov/geo/). After excluding patients with missing survival time, 804 samples were included in this study, 371 from the TCGA-STAD dataset and 433 from the GSE84437 dataset. To eliminate batch effects of different datasets, we converted fragments per kilobase million (FPKM) values of the TCGA-STAD dataset to transcripts per kilobase million (TPM) and merged two datasets using the ComBat algorithm of the R package sva (Leek et al., 2012). 54 TSRGs were obtained from the MSigDB (HALLMARK_TGF_BETA_SIGNALING) (Supplementary Table S1) (Yu et al., 2022).

Differential expression and mutational analysis of TSRGs

We performed differential expression analysis of 54 TSRGs in gastric cancer samples and normal samples using R package limma with the adjusted $p < 0.05$ and $|\log2\ FC)|>1$ (Ritchie et al., 2015). The protein-protein interaction network of 54 TSRGs was constructed in the STRING database (https://string-db.org/). R package maftools was utilized to map the somatic mutation waterfall of 54 TSRGs in gastric cancer patients (Mayakonda et al., 2018). Lastly, we calculated the CNV gain or loss percentage of 54 TSRGs in gastric cancer patients and analyzed the chromosomal location using the R package RCircos (Zhang et al., 2013).

Consensus clustering analysis of TSRGs

We first extracted the expression of 54 TSRGs in 804 samples and then performed consensus unsupervised clustering analysis based on 54 TSRGs expression levels using the R package ConsensusClusterPlus (Wilkerson and Hayes, 2010). PCA was performed to visualize the distribution between the two different TGF-β subgroups. To explore the clinical significance of different TGF-β subgroups, we performed Kaplan–Meier survival analysis using the R package survival and survminer (Wang et al., 2020). In addition, we mapped the expression heat map of 54 TSRGs using the R package pheatmap in conjunction with the clinicopathological features of the patients.

TGF-β-based subtype TME analysis

To explore the differences in TME between TGF-β subgroups, we first analyzed the stromal score, immune score, and ESTIMATE score between two subgroups using the ESTIMATE algorithm. We analyzed the differences in the expression of critical immune checkpoints such as PD-1, PD-L1, and CTLA-4 between the two subgroups. Subsequently, we calculated the infiltration level of 22 immune cells in each sample using the CIBERSORT algorithm (Newman et al., 2015) and analyzed the abundance of immune cell infiltrates between the two subgroups using the single sample gene set enrichment analysis (ssGSEA) algorithm (Zeng et al., 2022). In addition, gene set variation analysis (GSVA) was performed with the hallmark gene set (h.all.v7.5.1.symbols) to investigate the differences in TGF-β subgroups in signaling pathways (Hänzelmann et al., 2013).

Gene consensus clustering analysis of TGF-β pattern-related DEGs

To identify DEGs in the distinct TGF-β subgroups, R package limma was utilized with $|\log2\text{-fold change (FC)}| \geq 1$ and adjusted $p < 0.05$. Based on the DEGs, we performed gene ontology (GO) enrichment analysis and kyoto encyclopedia of genes and genomes (KEGG) signaling pathway analysis. We performed a clustering analysis based on the expression of DEGs and performed a Kaplan–Meier survival analysis among gene subgroups. In addition, we combined TGF-β subgroups, gene subgroups, and clinicopathological features of patients to map the expression heat map of DEGs.

Construction and validation of the risk model for gastric cancer

To quantify the degree of risk for each patient, we constructed a risk model based on DEGs. First, we performed univariate regression analysis to screen DEGs associated with the prognosis of gastric cancer patients. Second, we randomly divided the patients into training and testing sets in a 1:1 ratio (Qing et al., 2022). The training set is used to construct the risk model, and the testing set and the entire set are used to validate the risk model. Third, the LASSO Cox regression analysis was executed in the training set to reduce overfitting genes with 10-fold cross-validation and 1000 repeated times (Tibshirani, 1997). Finally, we performed a multivariate regression analysis using the genes screened by the LASSO regression analysis and calculated the risk score for each patient according to expression levels and regression coefficients of genes. The formula was as follows: Risk score = $\beta_{gene1} \times \exp_{gene1} + \beta_{gene2} \times \exp_{gene2} + \ldots + \beta_{genen} \times \exp_{genen}$ (Qing et al., 2022). Patients were divided into high- and low-risk groups based on the median risk score. Furthermore, we analyzed the relationship between the TGF-β cluster, gene cluster, risk score, and survival status using the R package ggalluvial and the differences in risk scores between distinct subgroups (Zeng et al., 2022). In the training and validation sets, we performed Kaplan-Meier survival analysis with the R package survminer and survival (Wang et al., 2020) and ROC curve analysis with the R package timeROC (Zeng et al., 2022), respectively.

Subgroup analysis based on available clinicopathological characteristics

To explore the performance power of the risk score among different subgroups of clinicopathological characteristics, we first analyzed the correlation between risk scores and clinicopathological characteristics using the Student's *t*-test. In addition, Kaplan–Meier survival analysis was performed in different subgroups stratified by age (≤65 years or >65 years), sex (female or male), T stage (T1-2 or T3-4), and N stage (N0 or N1-3).

Independent prognostic and nomogram analysis

Univariate and multivariate Cox regression analyses were performed to explore whether the risk score could be an independent prognostic factor for gastric cancer patients in the training, testing, and entire set, respectively. Age, gender, tumor size (T), lymph node metastasis (N), and risk score were included for analysis. In addition, we constructed a nomogram integrated the risk score and clinicopathological factors to predict the survival of gastric cancer patients at 1-, 3-, and 5-year using R package rms in the training set, testing set, and entire set, respectively (Zeng et al., 2022). Calibration curves were plotted to determine the performance of the nomograms in predicting OS.

Investigation of the immune landscape

To explore the differences in the tumor immune microenvironment between high- and low-risk groups of gastric cancer patients based on the risk model, we first analyzed the stromal score, immune score, and ESTIMATE score between the two groups using the ESTIMATE algorithm. Then, we analyzed the Spearman correlation between the risk score and immune cells using seven methods, including the XCELL, TIMER, QUANTISEQ, MCPCOUNTER, EPIC, CIBERSORT-ABS, and CIBERSORT algorithms (Zeng et al., 2022). We further analyzed the Spearman correlation between the expression of 5 genes in the model and immune cells. In addition, the ssGSEA was subjected to calculate the infiltrating immune cells' scores and assess the activity of immune-related pathways between high- and low-risk groups using the R package gsva (Hänzelmann et al., 2013). Finally, we analyzed the expression levels of immune checkpoint-related genes between high- and low-risk groups.

Immunotherapy response and antitumor drug sensitivity

TMB(Rizzo et al., 2021), MSS(Rizzo et al., 2021), IPS(Wu et al., 2021), and TIDE (Zeng et al., 2022) scores were considered markers to predict immunotherapy response. First, we downloaded the mutation data of gastric cancer patients in MAF format from the TCGA database and annotated them using the R package maftools (Mayakonda et al., 2018), and subsequently analyzed the correlation between the risk score and TMB as well as the mutated genes common to patients in high- and low-risk groups. Second, we downloaded IPS and MSS data from the TCIA database (http://tcia.at/) for gastric cancer patients and analyzed the differences between patients in high- and low-risk groups. Finally, we analyzed the response rate of gastric cancer patients to immunotherapy based on the TIDE website (http://tide.dfci.harvard.edu/).

Next, we used the R package pRRophetic to calculate the half inhibitory centration (IC50) of antitumor drugs for each patient and analyzed the differences in sensitivity to antitumor drugs between patients in high- and low-risk groups (Geeleher et al., 2014).

Statistical analysis

R software (version 4.1.2) and related R packages were utilized for statistical analyses. The Wilcoxon test was used to compare clinicopathological characteristics, immune status,

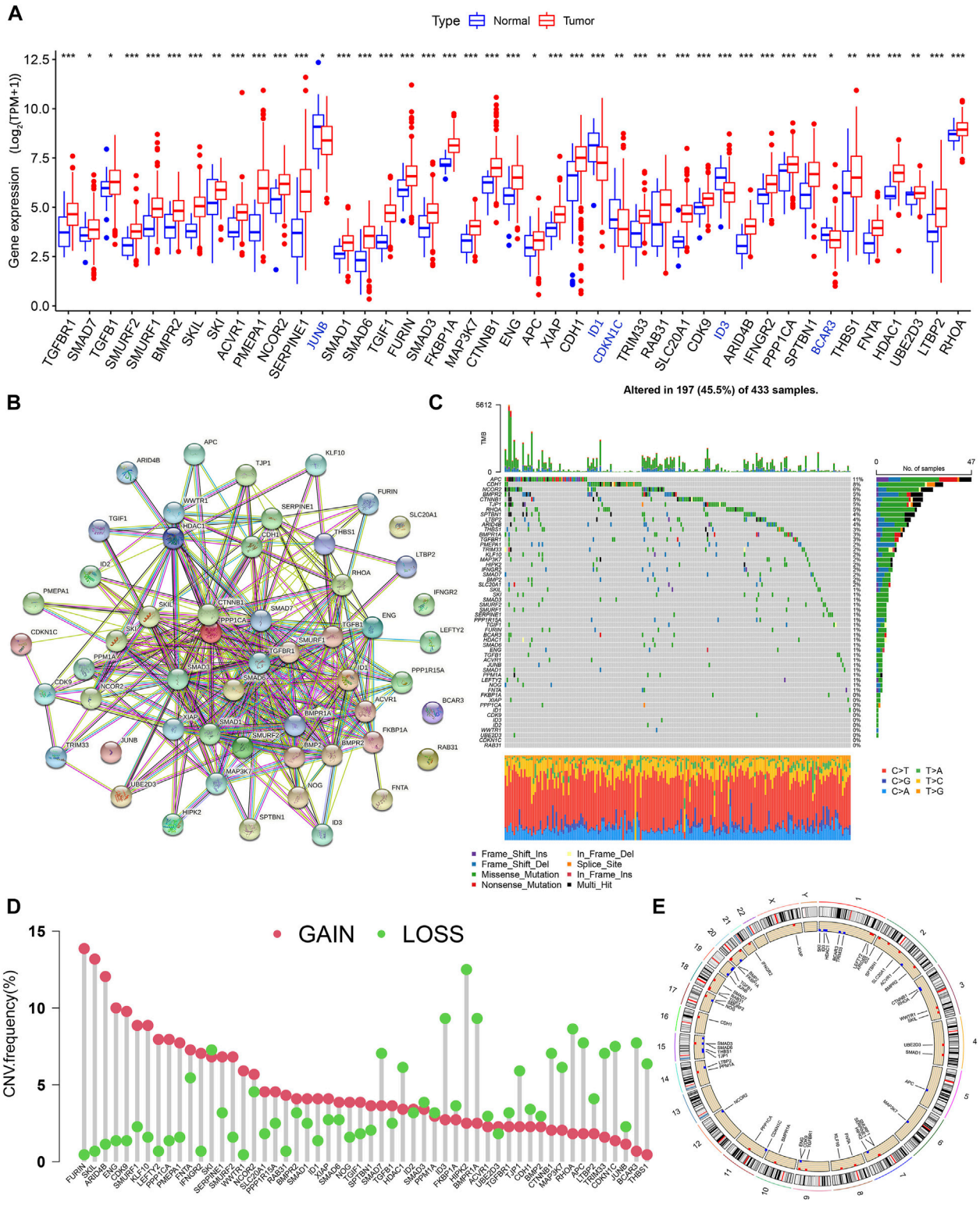

FIGURE 1
Genetic mutational characteristics of TSRGs in gastric cancer, **(A)** Differential expression analysis of TSRGs in gastric cancer and normal tissues. **(B)** Protein-protein interaction network analysis of TSRGs in the STRING database. **(C)** Mutation frequency analysis of TSRGs in gastric cancer. **(D)** Frequencies of CNV gain, loss, and non-CNV among TSRGs. **(E)** Locations of CNV alterations in TSRGs on chromosomes. TSRGs, TGF-β signaling related genes; CNV, copy number variant; *p < 0.05; **p < 0.01; ***p < 0.001.

TMB, IPS, TIDE scores, and IC50 values between different groups. Kaplan-Meier curves were used to compare OS between different groups. Univariate and multivariate Cox regression analyses were used to analyze independent prognostic factors. ROC curves and nomograms were used to evaluate the predictive power of the risk model. $p < 0.05$ was considered statistically significant. $^{*}p < 0.05$; $^{**}p < 0.01$; $^{***}p < 0.001$.

Results

Differential expression and genetic variation landscape of TSRGs in gastric cancer

The design idea of this study is shown in Supplementary Figure S1. We first performed differential expression analysis of 54 TSRGs in gastric cancer tissues and normal gastric tissues. We obtained 43 DEGs with the adjusted $p < 0.05$ and $|\log2\ FC)|>1$, of which JUNB, ID1, CDKN1C, ID3, and BCAR3 were lowly expressed in gastric cancer tissues, and the remaining DEGs were highly expressed in gastric cancer tissues (Figure 1A). Protein-protein interaction network analysis based on the String database revealed a close linkage between most genes (Figure 1B). Next, we explored the somatic mutation levels and the frequency of CNVs alteration in 54 TSRGs in gastric cancer patients. The waterfall plot in Figure 1C shows that 197 (45.5%) of the 433 samples had TSRG mutations. Among them, APC (11%) had the highest mutation frequency, followed by CDH1 (8%) and NCOR2 (6%). Missense mutations are the most common form of mutation in TSRGs. We also investigated the frequency of CNVs alterations of TSRGs and found that FURIN, SKIL, and ARID4B had the most significant copy number increase, while HIPK2, ID3, and BMPR1A had the most significant copy number deletion (Figure 1D). Figure 1E shows the site of CNVs of TSRGs on chromosomes.

Identification of TGF-β subgroups in gastric cancer

To understand the expression pattern of TSRGs involved in tumorigenesis, data from 804 gastric cancer samples from TCGA-STAD and GSE84437 datasets were enrolled in our study for further analysis (Supplementary Table S2). To explore the characteristics of 54 TSRGs expression profiles in gastric cancer, we performed unsupervised clustering analysis to identify gastric cancer subtypes based on 54 TSRGs expression levels. The results showed that $K = 2$ was the most appropriate cluster, and 804 gastric cancer patients were classified into TGF-β cluster A ($n = 443$) and TGF-β cluster B ($n = 361$) (Figures 2A–C and Supplementary Table S3). The PCA results further demonstrate the excellent grouping effect (Figure 2D). Kaplan-Meier survival analysis showed a more significant survival advantage for TGF-β cluster B ($p < 0.001$, Figure 2E). In addition, we combined TGF-β subgroups and clinicopathological features of gastric cancer patients to map 54 TSRGs expression heatmaps and found that 54 TSRGs were expressed at higher levels in TGF-β cluster A compared to TGF-β cluster B (Figure 2F).

Characteristics of the TME in two distinct TGF-β subgroups

To explore the correlation between TSRGs and TME in gastric cancer, we first performed an ESTIMATE analysis. The results showed that patients in TGF-β cluster A had a higher stromal score, immune score, and ESTIMATE score (Figures 3A–C), suggesting that gastric cancer patients in the TGF-β cluster A have higher immune activity and lower tumor purity. Then, expression analysis of three crucial immune checkpoint genes (PD1, PD-L1, and CTLA4) showed higher expression levels of PD1, PD-L1, and CTLA4 in gastric patients in the TGF-β cluster A compared to patients in TGF-β cluster B (Figures 3D–F). We further analyzed the level of infiltration of 23 immune cells in patients with two distinct TGF-β clusters using the CIBERSORT algorithm. As shown in Figure 3G, the infiltration levels of activated B cell, activated dendritic cell, CD56 bright natural killer cell, eosinophil, gamma delta T cell, immature B cell, immature dendritic cell, MDSC, macrophage, mast cell, natural killer T cell, natural killer cell, plasmacytoid dendritic cell, regulatory T cell, T follicular helper cell, type 1 T helper cell, and type 2 T helper cell were higher in the TGF-β cluster A than those in the TGF-β cluster B, while activated CD4 T cell and neutrophil had significantly lower infiltration in TGF-β cluster A than those in the TGF-β cluster B. In addition, GSVA enrichment analysis revealed multiple tumor-associated signaling pathways enriched in TGF-β cluster A, including KRAS, IL2/STAT5, inflammatory response, hypoxia, apoptosis, and wnt/β-catenin signaling pathways (Figure 3H).

Identification of gene clusters based on TGF-β pattern-related DEGs

To further explore the potential biological functions of the TGF-β clusters, we obtained 202 TGF-β clusters-related DEGs (Supplementary Table S4) using R package limma and performed functional enrichment analysis. These TGF-β cluster-related DEGs are mainly enriched in biological processes associated with the extracellular matrix (Figure 4A). KEGG analysis showed that DEGs were associated with metastasis and tumor-related signaling pathways (Figure 4B), suggesting that

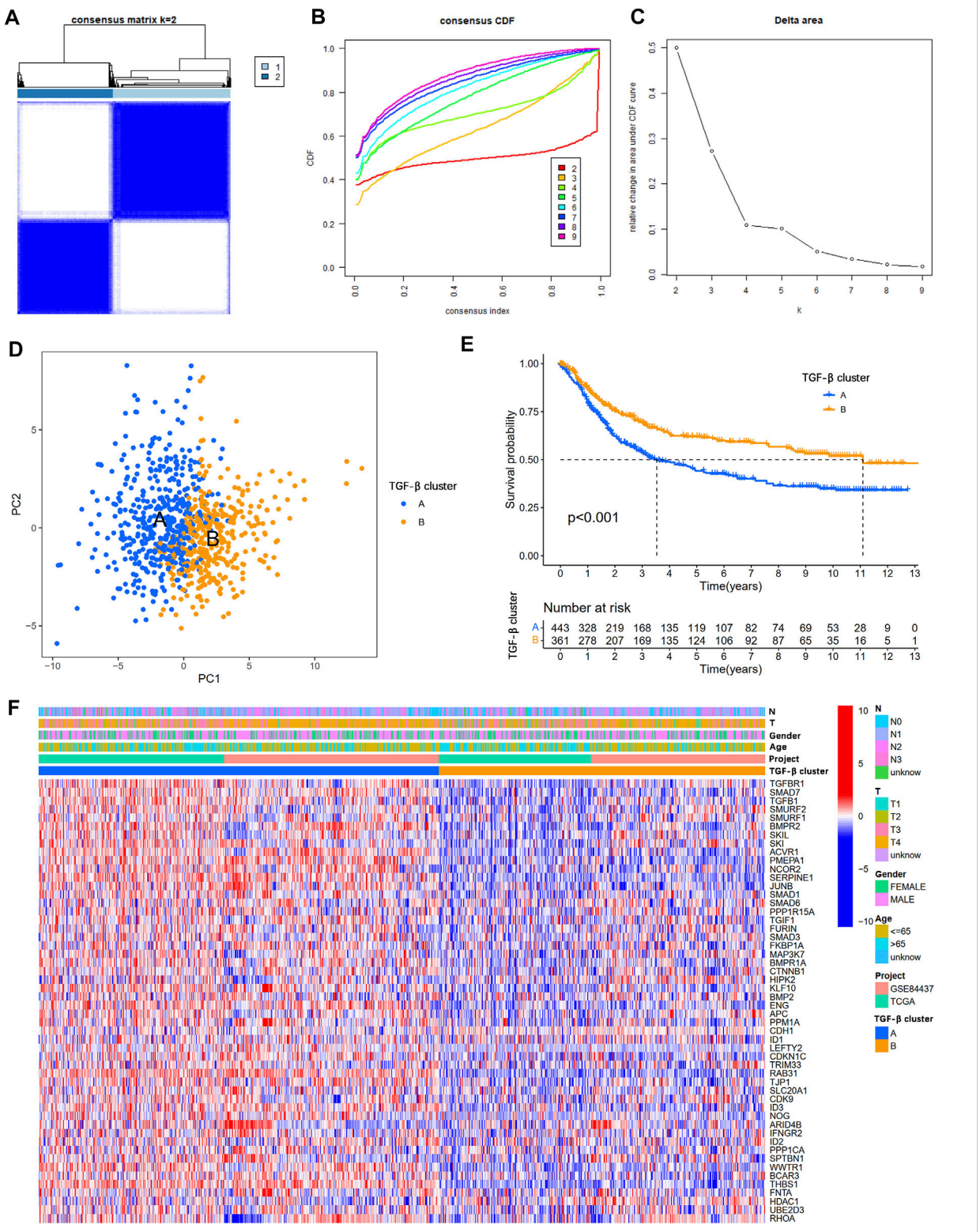

FIGURE 2
Overall survival and clinicopathological characteristics of two different TSRG subgroups. **(A)** Consensus matrix heatmap defining two clusters (*k* = 2). **(B)** The cumulative distribution function (CDF) from *k* = 2 to 9. **(C)** Relative variation of the area under the CDF region at *k* = 2–9. **(D)** PCA shows different distributions between the two subgroups. **(E)** Kaplan-Meier survival analysis between two different TSRG subgroups. **(F)** Differences in clinicopathologic characteristics and expression levels of TSRGs between the two distinct TSRG subgroups. TSRGs, TGF-β signaling related genes; CDF, cumulative distribution function; PCA, principal components analysis.

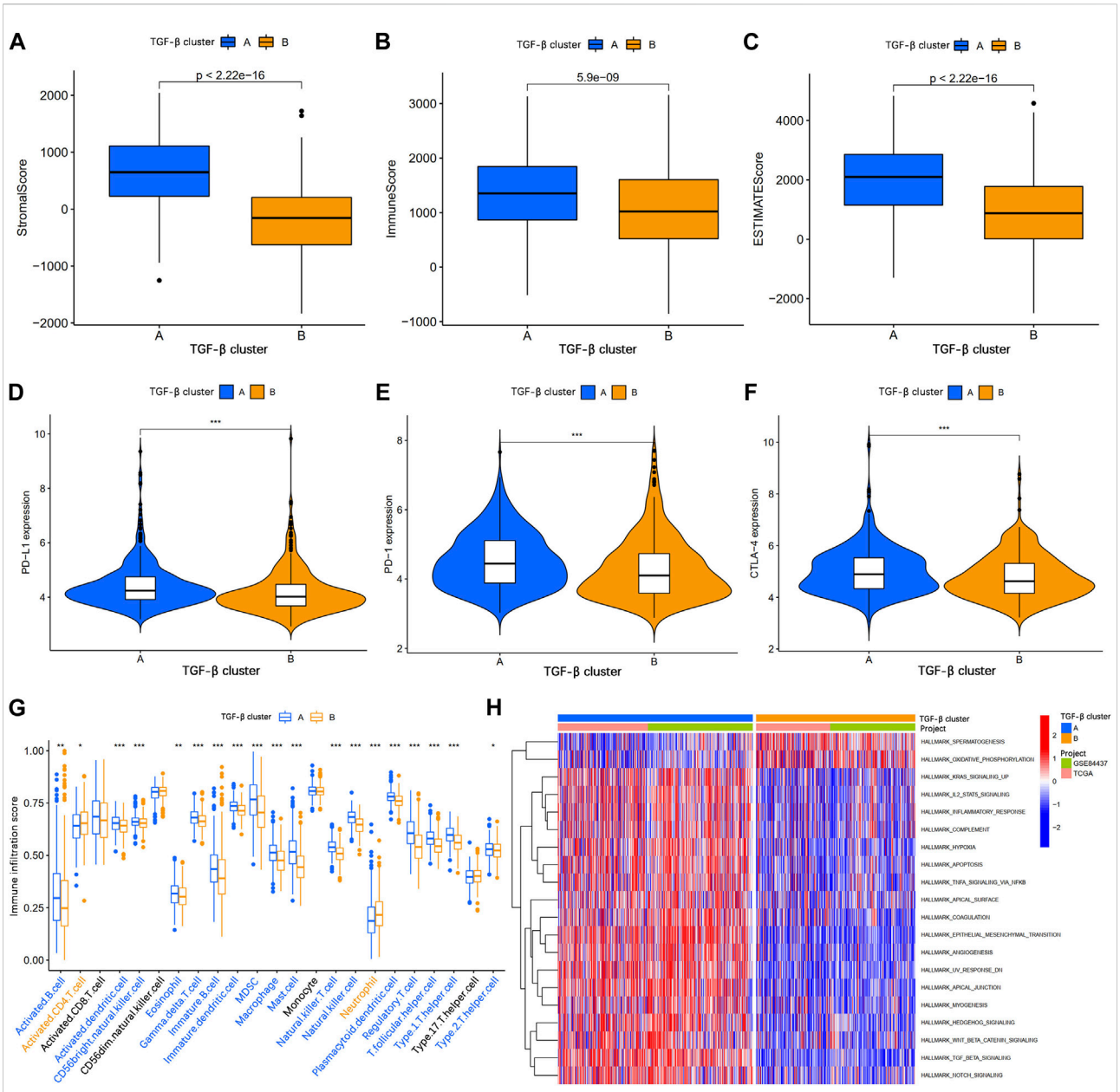

FIGURE 3
Analysis of the tumor immune microenvironment between two different TGF-β subgroups. **(A–C)** Stromal score, immune score, and ESTIMATE score analyses between two subgroups. **(D–F)** Expression levels of PD-1, PD-L1, and CTLA-4 in the two subgroups. **(G)** The abundance of 23 infiltrating immune cell types in the two different TGF-β subgroups. **(H)** GSVA of biological pathways between two subgroups. GSVA, gene set variation analysis; PD-1, programmed cell death 1; PD-L1, programmed cell death 1 ligand 1; CTLA-4, cytotoxic T-lymphocyte associated protein 4; *p < 0.05; **p < 0.01; ***p < 0.001.

TSRGs play an essential role in tumorigenesis and metastasis. Then, 202 TGF-β cluster-related DEGs were subjected to univariate Cox regression analysis to screen for genes associated with OS in gastric cancer. We obtained 199 genes related to the prognosis of gastric cancer patients at $p < 0.05$ (Supplementary Table S5). To further explore the potential mechanisms of prognosis-related DEGs in gastric cancer, based on the expression level of 199 prognostic genes, unsupervised consensus clustering analysis was utilized to classify gastric cancer patients into three different gene clusters, namely gene cluster A, gene cluster B, and gene cluster C (Supplementary Table S6). Kaplan-Meier survival analysis showed that patients in gene cluster A had the worst OS, whereas patients in gene cluster C showed a superior OS

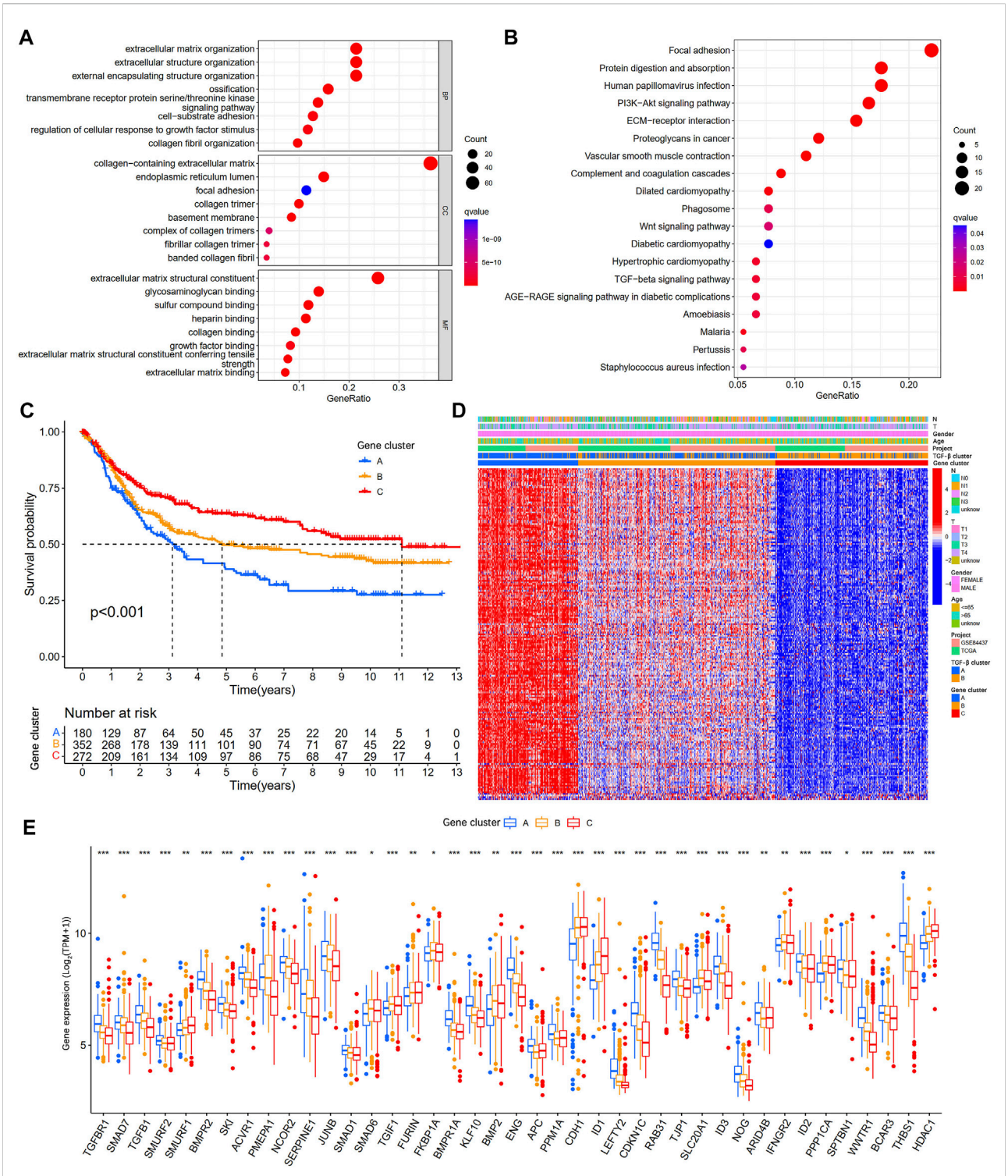

FIGURE 4
Identification of gene subgroups based on DEGs among two TGF-β subgroups. **(A,B)** GO and KEGG enrichment analyses of DEGs among two TGF-β subgroups. **(C)** Kaplan-Meier survival analysis between three different gene subgroups. **(D)** Heatmap of clinicopathologic characteristics and DEGs expressions among the three gene subgroups. **(E)** Differences in the expression of 54 TSRGs among the three gene subgroups. DEGs, differentially expressed genes; GO, Gene Ontology; KEGG, Kyoto Encyclopedia of Genes and Genomes; TSRGs, TGF-β signaling related genes; *p < 0.05; **p < 0.01; ***p < 0.001.

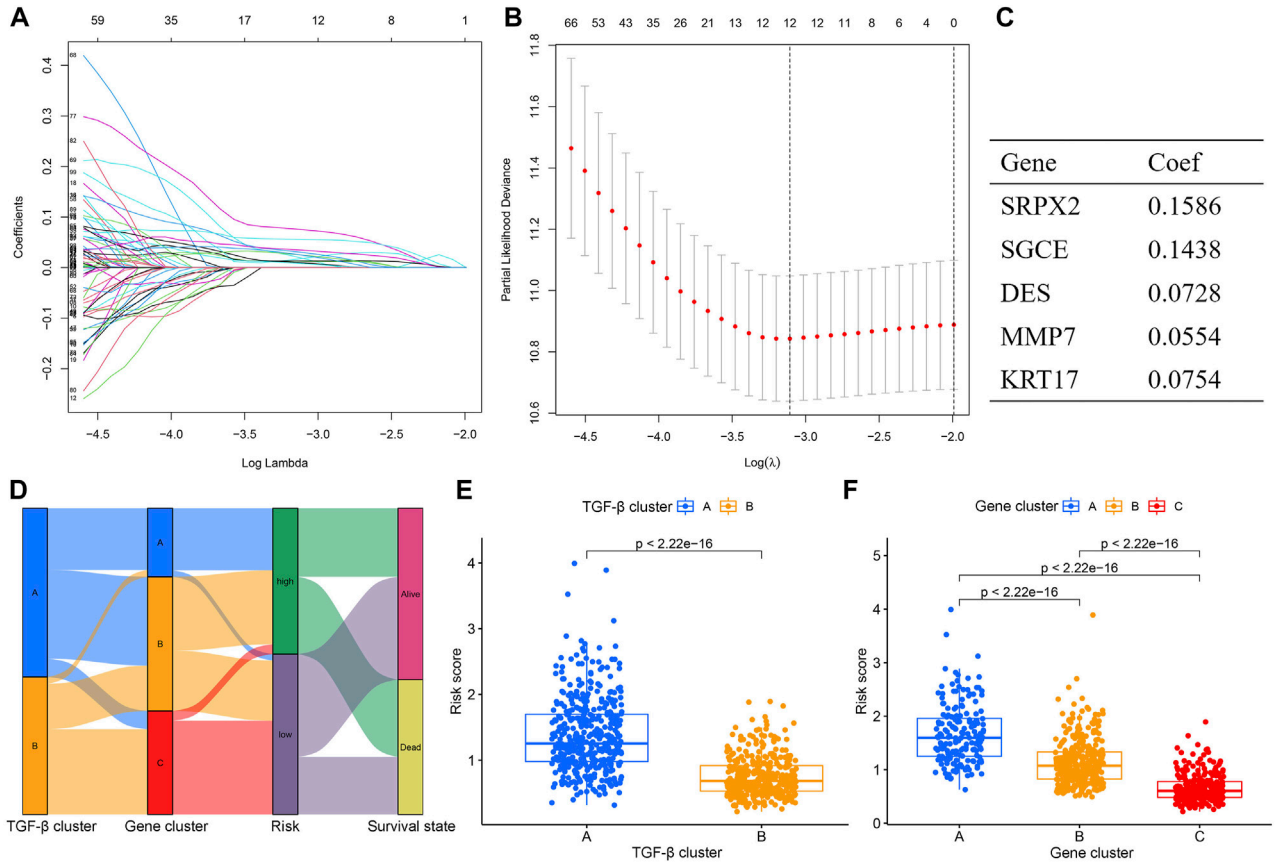

FIGURE 5
Construction of the TGF-β cluster-related DEGs prognostic model. **(A,B)** Twelve optimal TGF-β cluster-related DEGs were found using the LASSO cox regression. **(C)** Five optimal TGF-β cluster-related DEGs were found using the multivariate Cox analysis. **(D)** Sankey diagram of TGF-β cluster, gene cluster, risk score, and survival status. **(E)** Differences in risk score between two TGF-β clusters. **(F)** Differences in risk score between three gene clusters. DEGs, differentially expressed genes; LASSO, least absolute shrinkage and selection operator; Coef, coefficient.

(Figure 4C). In addition, we combined the TGF-β cluster, gene cluster, and clinicopathological features of gastric cancer patients to map heat maps and found significant expression differences among gene clusters (Figure 4D). The three gene clusters showed significance in TSRGs expression, as expected from the TGF-β clusters (Figure 4E).

Construction and validation of the risk model

To quantify the risk of each gastric cancer patient, we constructed a prognostic risk model based on TGF-β cluster-related prognostic DEGs. First, the R package caret was used to randomize patients into a training set (n = 402) (Supplementary Table S7). And a testing set (n = 402) (Supplementary Table S8) at a ratio of 1:1. Second, in the training set, LASSO and multivariate Cox regression analyses were used to construct an appropriate risk model. Based on the minimum partial likelihood deviance, 12 potential candidate genes were screened by LASSO regression analysis (Figures 5A,B; Supplementary Table S9). Subsequent multivariate Cox regression of 12 prognosis-related genes yielded five genes used to construct the risk model, namely SRPX2, SGCE, DES, MMP7, and KRT17. We calculated the risk score for each patient based on the formula. Risk score= (0.1586×expression of SRPX2) + (0.1438×expression of SGCE) + (0.0728×expression of DES) + (0.0554×expression of MMP7) + (0.0754×expression of KRT17) (Figure 5C). The Sankey diagram showed the correlation between risk score and TGF-β clusters, gene clusters, and survival status (Figure 5D). In addition, we observed an obvious difference in the risk score of the TGF-β clusters and gene clusters (Figures 5E,F). The previous survival analysis showed shorter OS in the TGF-β cluster A and gene cluster A groups, and our model showed

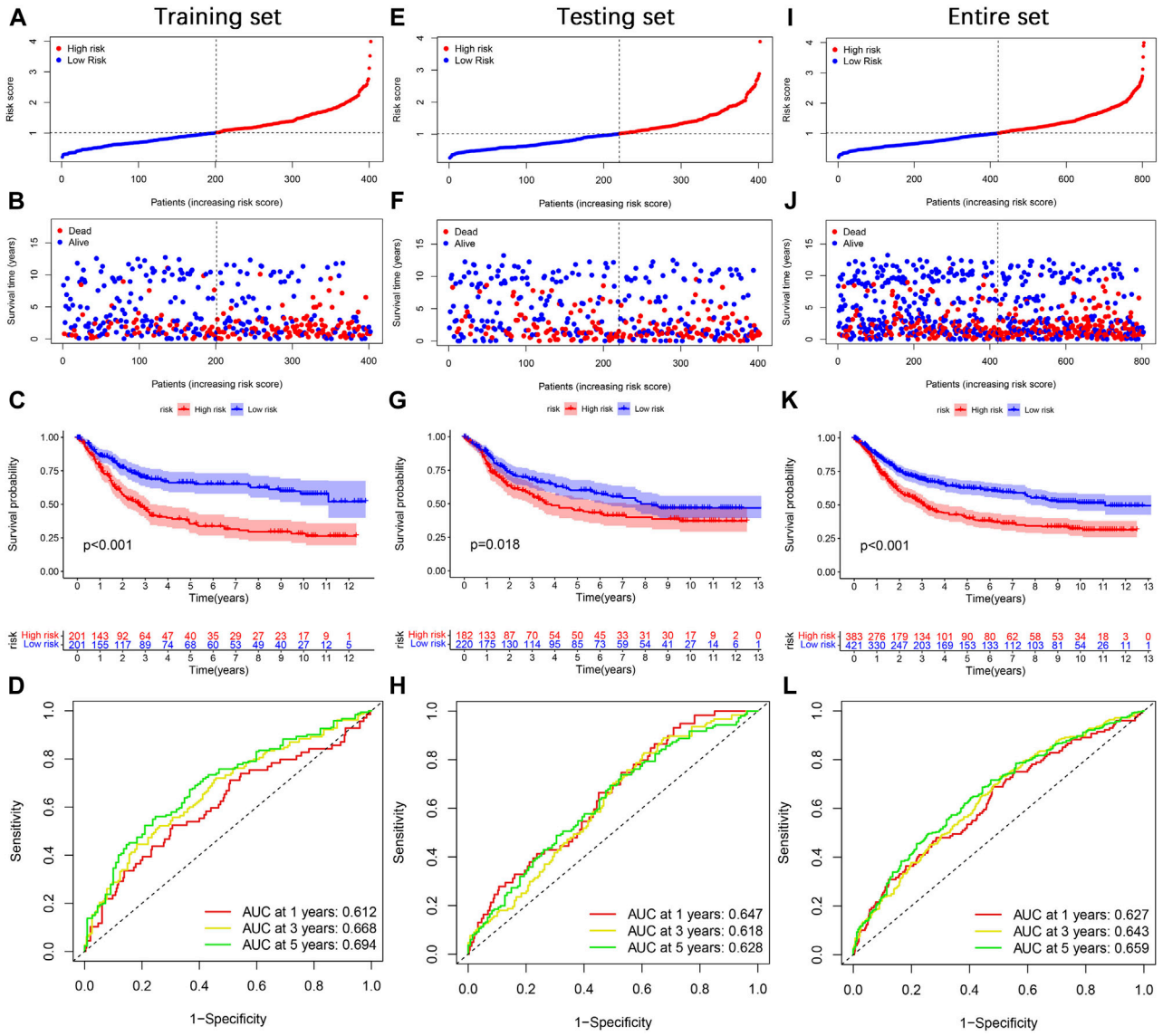

FIGURE 6
Prognosis value of the TGF-β cluster-related DEGs prognostic model. **(A)** The distribution of risk score, **(B)** survival status, **(C)** Kaplan–Meier survival curves, **(D)** the 1-, 3-, and 5-year ROC curves. **(E–L)** The validation sets, including the testing set and the entire set, were analyzed similarly.

the highest risk scores in TGF-β cluster A and gene cluster A groups, which further demonstrated the excellent performance of our risk model.

Next, we divided gastric cancer patients into high- and low-risk groups based on the median risk score. The risk score curve and survival status scatter plots show that the number of deaths in gastric cancer patients increases as the risk score increases (Figures 6A,B). Kaplan-Meier survival analysis showed that patients in the high-risk group had worse OS than those in the low-risk group (Figure 6C). The risk score's 1-, 3-, and 5-year AUC values were 0.612, 0.668, and 0.694, respectively (Figure 6D). Meanwhile, we did the same analysis in two validation sets (the testing set and the entire set), respectively, and we obtained similar results (Figures 6E–L). In the IMvigor210 cohort, patients in the high-risk group had significantly lower survival than the low-risk group (Supplementary Figure S2A), which further validates the accuracy of our constructed prognostic model. Taken together, our established risk model has an excellent performance in predicting the survival outcome of gastric cancer patients.

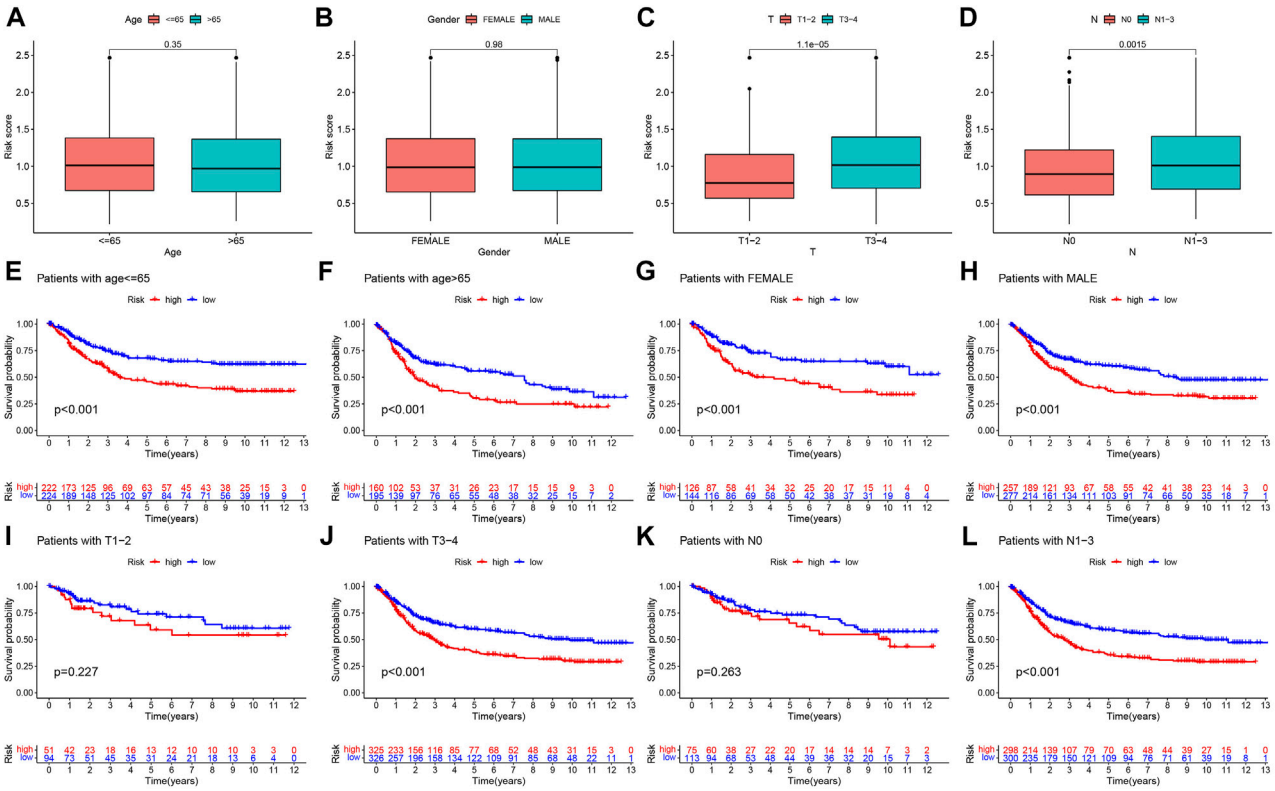

FIGURE 7
Prognostic model-based clinicopathological characteristics and survival subgroup analysis, Differential analysis of the risk score for **(A)** age, **(B)** gender, **(C)** T stage, and **(D)** N stage subgroups. Kaplan-Meier survival analysis for **(E)** age ≤65 years, **(F)** age >65 years, **(G)** female, **(H)** male, **(I)** T1-2, **(J)** T3-4, **(K)** N0, and **(L)** N1-3 between high- and low-risk groups.

Clinical correlation analysis and stratification analysis of the risk model

To explore the correlation between the risk score and available clinicopathological characteristics, we first analyzed differences in risk scores across clinical subgroups. The subgroups were divided by age (≤65 years or >65 years), sex (female or male), T stage (T1-2 or T3-4), and N stage (N0 or N1-3). The results showed that the risk scores were not statistically different across age and gender subgroups (Figures 7A,B), while patients in the T3-4 and N1-3 subgroups had higher risk scores (Figures 7C,D). In addition, we performed Kaplan-Meier survival analysis for different subgroups. We found that in the age ≤65 years (Figure 7E), age >65 years (Figure 7F), female (Figure 7G), male (Figure 7H), T3-4 (Figure 7J), N1-3 (Figure 7L) subgroups of gastric cancer patients, the OS of patients in the high-risk group was significantly lower than that of low-risk patients, while no significant differences were seen for T1-2 (Figure 7I), N0 (Figure 7K) subgroups.

Independent prognostic and nomogram analysis

To explore whether the risk score is an independent prognostic factor for patients with gastric cancer, we performed univariate and multivariate Cox regression analyses in the training set and two validation sets (testing set and entire set) in combination with clinicopathological characteristics. In the training set, univariate Cox regression analysis displayed that age (HR = 1.025, 1.011–1.039, $p < 0.001$), T stage (HR = 1.233, 1.011–1.505, $p = 0.039$), N stage (HR = 1.472, 1.256–1.725, $p < 0.001$), and risk score (HR = 2.122, 1.675–2.690, $p < 0.001$) predicted worse OS (Figure 8A). Multivariate Cox regression analysis showed that the age (HR = 1.028, 1.018–1.038, $p < 0.001$), N stage (HR = 1.392, 1.181–1.604, $p < 0.001$) and risk score (HR = 2.005, 1.562–2.574, $p < 0.001$) were independent prognostic factors in gastric cancer patients (Figure 8B). In the testing set, univariate Cox regression analysis displayed that age (HR = 1.027, 1.012–1.042, $p < 0.001$), T stage (HR = 1.276, 1.051–1.550, $p = 0.014$), N stage (HR = 1.633, 1.387–1.923, $p <$

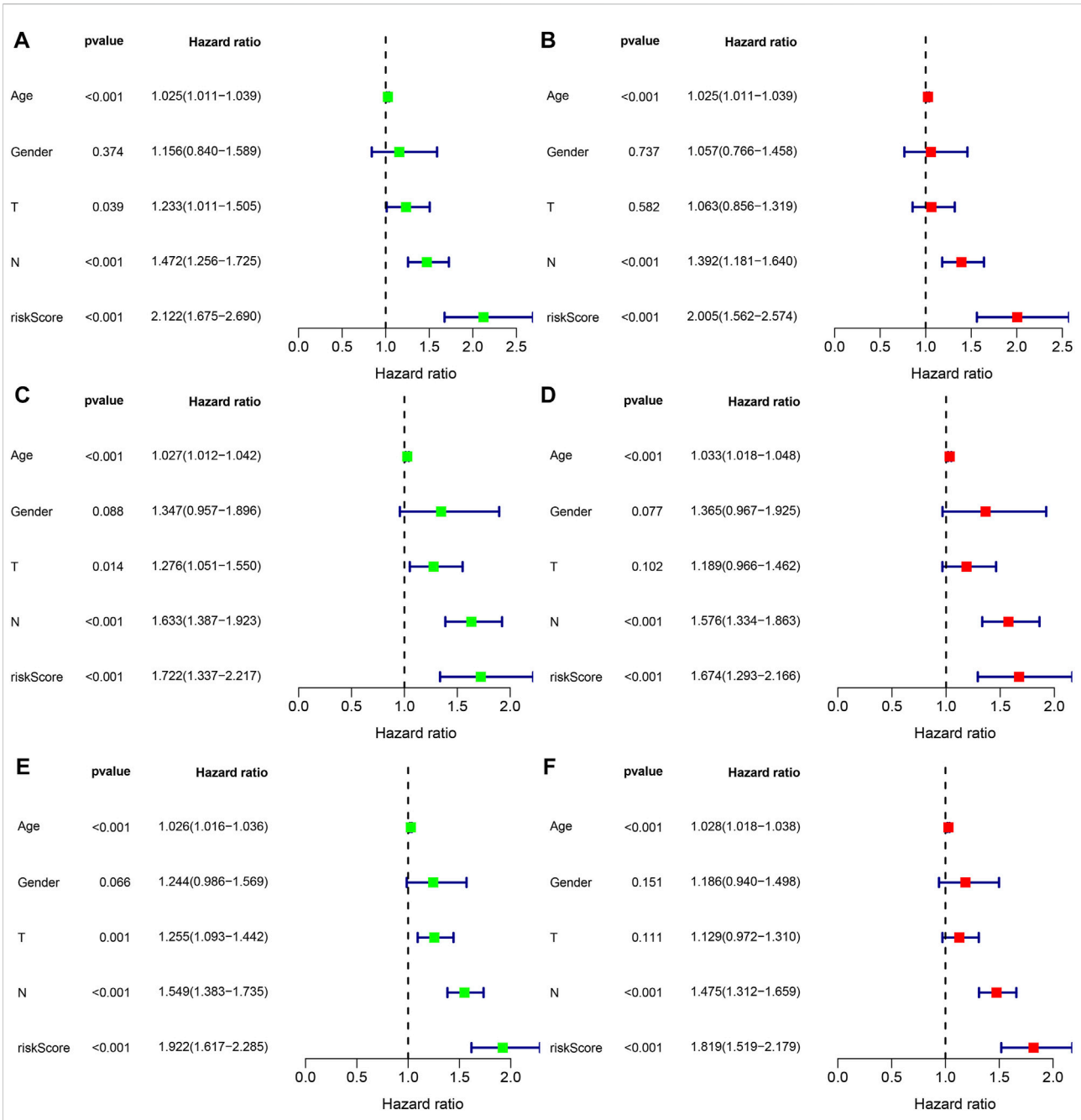

FIGURE 8
The independent prognosis analysis of the risk score and clinicopathological variables in gastric cancer. **(A,B)** Univariate and multivariate Cox regression analyses of clinicopathological variables and risk scores with OS in the training set, **(C,D)** testing set, and **(E,F)** entire set.

0.001), and risk score (HR = 1.722, 1.337–2.217, $p < 0.001$) predicted worse OS (Figure 8C). Multivariate Cox regression analysis showed that the age (HR = 1.033, 1.018–1.048, $p < 0.001$), N stage (HR = 1.576, 1.334–1.863, $p < 0.001$) and risk score (HR = 1.674, 1.293–2.166, $p < 0.001$) were independent prognostic factors in gastric cancer patients (Figure 8D). In the entire set, univariate Cox regression analysis displayed that age (HR = 1.026, 1.016–1.036, $p < 0.001$), T stage (HR = 1.255, 1.093–1.442, $p = 0.001$), N stage (HR = 1.549, 1.383–1.735, $p < 0.001$), and risk score (HR = 1.922, 1.617–2.285, $p < 0.001$) predicted worse OS (Figure 8E). Multivariate Cox regression analysis showed that the age (HR = 1.028, 1.018–1.038, $p < 0.001$), N stage (HR = 1.475, 1.312–1.659, $p < 0.001$) and risk score (HR = 1.819, 1.519–2.179, $p < 0.001$) were independent

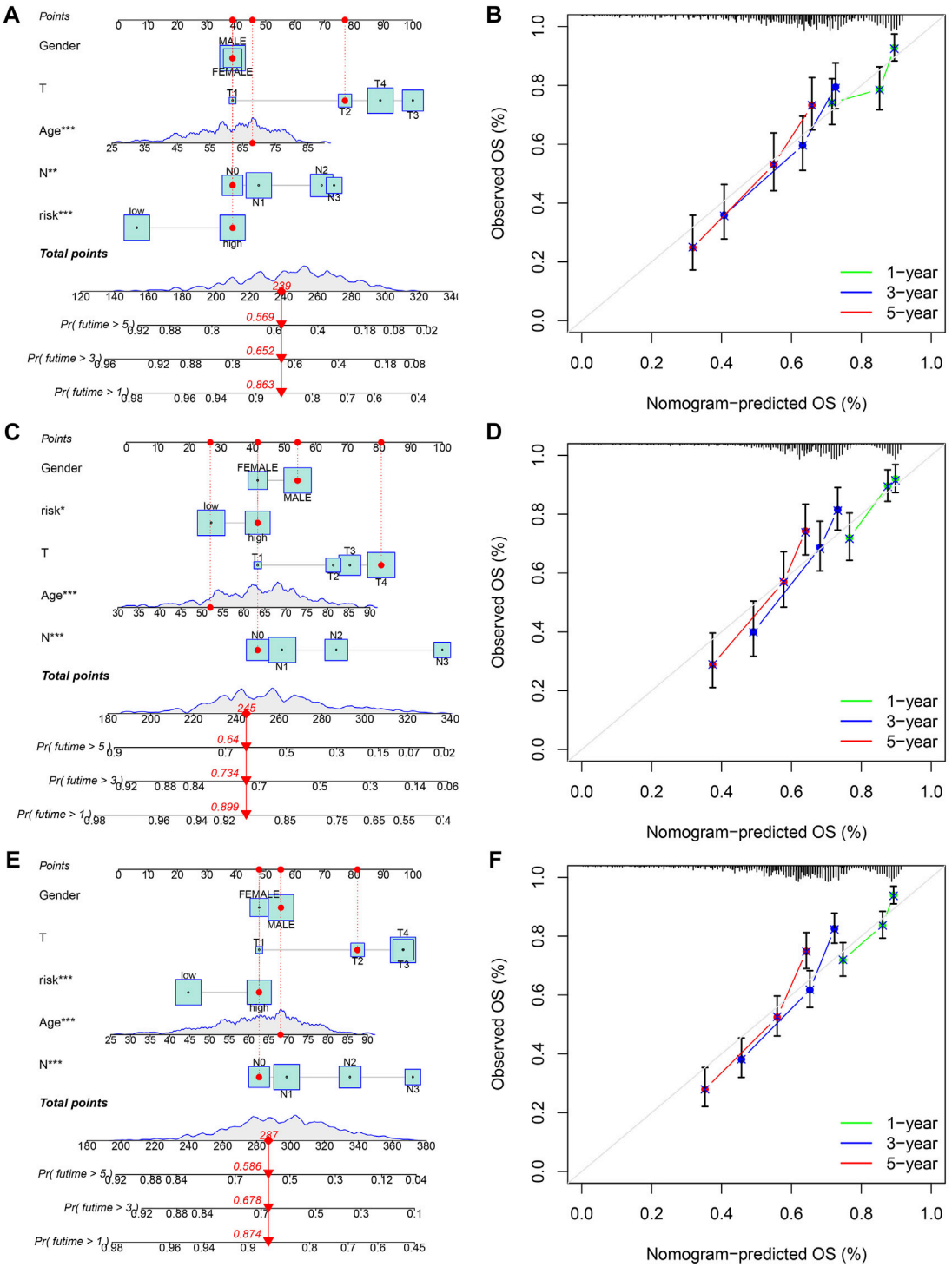

FIGURE 9
Construction and validation of a nomogram for predicting OS in gastric cancer. **(A,B)** The nomogram combining gender, age, T stage, N stage, and risk score for predicting gastric cancer patient OS at 1-, 3-, and 5- years in the training set, **(C,D)** testing set, and **(E,F)** entire set. *p < 0.05; **p < 0.01; ***p < 0.001.

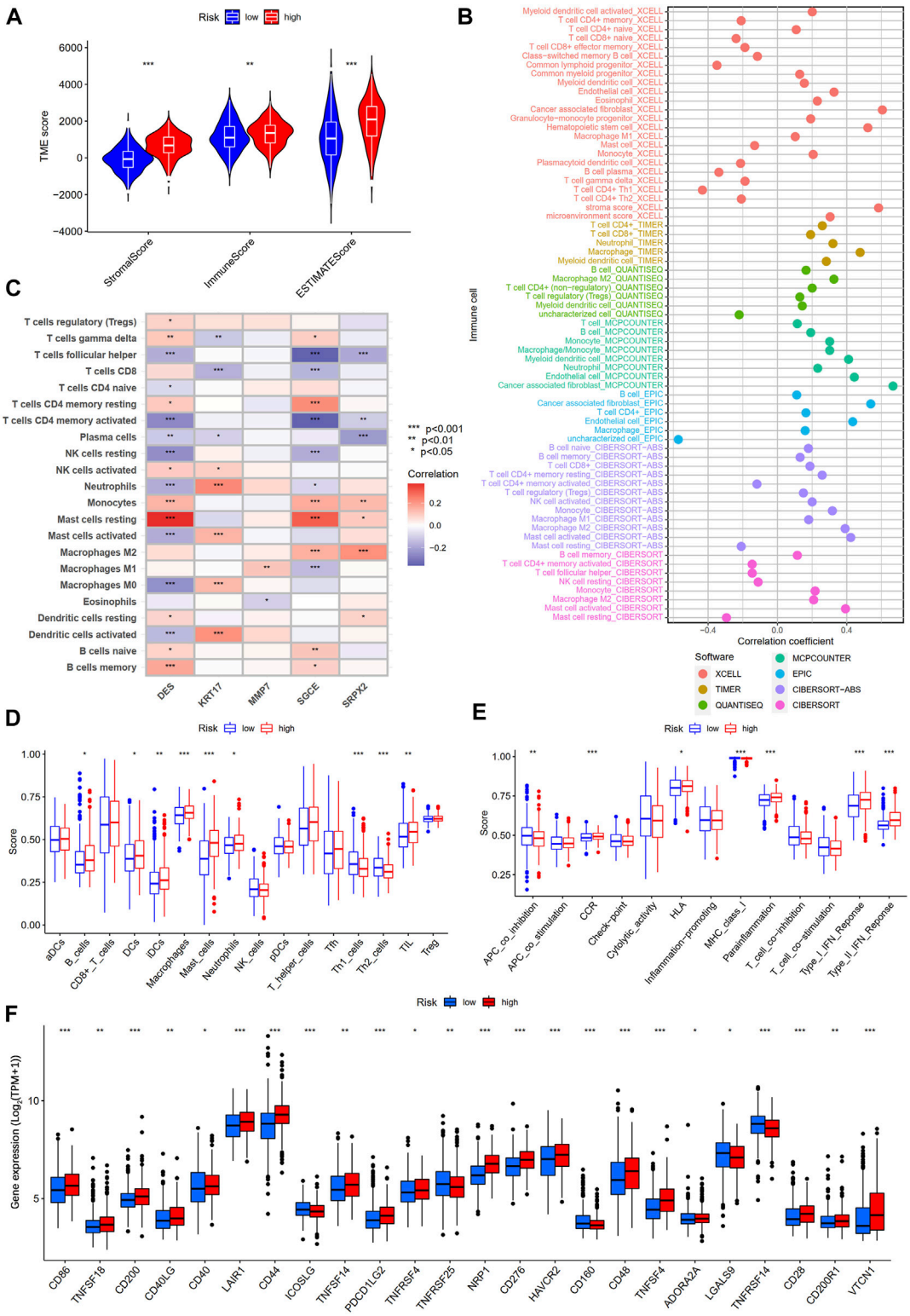

FIGURE 10
Differential analysis of tumor immune microenvironment between high- and low-risk groups. **(A)** TME score between high- and low-risk groups. **(B)** Spearman correlation analysis of immune components and risk scores based on XCELL, TIMER, QUANTISEQ, MCPCOUNTER, EPIC, CIBERSORT-ABS, and CIBERSORT algorithms. **(C)** Spearman correlations between the abundance of immune cells and five genes in the prognostic model. **(D)** 16 immune cells and **(E)** 13 immune-related functions between the high- and low-risk groups by ssGSEA. **(F)** The expression of immune checkpoint-related genes between the high- and low-risk groups.

prognostic factors in gastric cancer patients (Figure 8F). Taken together, the risk score is an independent prognostic factor for patients with gastric cancer.

Given the close correlation between the risk score and prognosis of gastric cancer patients, we integrated gender, age, T stage, N stage, and risk score to plot a nomogram to predict the 1-, 3-, and 5-year survival rates in the training set and two validation sets (testing set and entire set) (Figures 9A,C,E). Furthermore, the 1-, 3-, and 5-year calibration curves showed great accuracy between the nomogram-predicted OS and the actual observed OS (Figures 9B,D,F).

Analysis of tumor immune microenvironment between high- and low-risk groups

To explore the differences in tumor immune microenvironment between high- and low-risk groups of gastric cancer patients, we first performed ESTIMATE analysis. The results showed that gastric patients in the high-risk group had a higher stromal score, immune score, and ESTIMATE score (Figure 10A). Subsequently, seven algorithms were used to assess the correlation between the level of immune cell infiltration and the risk score. As shown in Figure 10B, the risk score was positively correlated with myeloid dendritic cell, $CD4^+$ T cell, $CD8^+$ T cell, cancer-associated fibroblast, hematopoietic stem cell, neutrophil, and macrophage M2, while negatively correlated with T cell $CD4^+$ memory activated, T cell follicular helper, NK cell resting, and mast cell resting (Supplementary Table S10). We also performed a correlation analysis between the five genes in our prognostic model and the immune cells. We found that DES, KRT17, SGCE, and SRPX2 were significantly correlated with most immune cells, while MMP7 only correlated with macrophages M1 and eosinophils (Figure 10C). In addition, we further explored the difference of 16 immune cells and 13 immune-related pathways between the two subgroups using ssGSEA. We found that B cells, DCs, iDCs, macrophages, mast cells, neutrophils, TIL, CCR, HLA, parainflammation, type I IFN response, and type II IFN response were more enriched in the high-risk group, while the Th1 cells, Th2 cells, APC co inhibition, and MHC class I is less enriched in the high-risk group (Figures 10D,E). Finally, we analyzed the expression levels of immune checkpoint-related genes between two subgroups. Figure 10F showed that 24 immune checkpoint-related genes were differentially expressed in the high- and low-risk groups.

Immunotherapy response analysis

TMB and MSI are considered biomarkers of tumor immunotherapy response rate (Rizzo et al., 2021), and patients with high TMB and MSI-H benefit from immunotherapy and have more prolonged survival. Therefore, we first analyzed the correlation between the TMB and risk score. The results showed a negative correlation between the TMB and risk score (Figure 11A), and the TMB of gastric cancer patients in the low-risk group was significantly higher than that of gastric cancer patients in the high-risk group (Figure 11B). Kaplan-Meier survival analysis showed that the risk score diminished the prognostic advantage of patients with gastric cancer in the high TMB group (Figure 11C). We further analyzed the somatic mutations in the high- and low-risk groups of gastric cancer patients. The results showed that the most common form of mutation was missense mutation, and the top five mutated genes were TTN, TP53, MUC16, ARID1A, and LRP1B, and the frequency of mutations was higher in the low-risk group (Figure 11D), which was consistent with the results of the above study. In addition, we analyzed the correlation between the MSI and risk scores and showed that patients in the low-risk group had a higher proportion of MSI-H and that patients with MSI-H had lower risk scores (Figure 11E).

IPS and TIDE scores are novel tumor immunotherapy response rate biomarkers that better assess the efficacy of anti-PD1 and anti-CTLA4 therapies. A high IPS score represents higher immunogenicity, and a high TIDE score represents a greater likelihood of tumor immune escape (Wu et al., 2021; Zeng et al., 2022); therefore, the higher the IPS and the lower the TIDE score, the better the patient's outcome to immunotherapy. Our results showed that gastric cancer patients in the low-risk group had higher IPS (Ips_ctla4_neg_pd1_neg, ips_ctla4_pos_pd1_neg, and ips_ctla4_pos_pd1_pos scores) than those in the high-risk group, but there was no statistically significant difference between the two groups in the ips_ctla4_neg_pd1_pos score (Figures 11F–I). Furthermore, the TIDE, dysfunction, and exclusion scores of gastric cancer patients in the low-risk group were lower than those in the high-risk group (Figures 11J–L). In addition, analysis of immunotherapy response based on the IMvigor210 cohort showed that patients in the immunotherapy-responsive group (complete response (CR)/partial response (PR) group) had significantly lower risk scores than the immunotherapy non-responsive group (stable disease (SD)/progressive disease (PD) group) (Supplementary Figure S2B). The above results suggest that patients with gastric cancer in the low-risk group may be may be more sensitive to immunotherapy.

Antitumor drug sensitivity analysis

To explore the potential role of our established risk model for clinical treatment, we analyzed the differences in IC50 of common antitumor drugs between high- and low-risk groups. We found that gastric cancer patients in the low-risk group were more sensitive to ATRA, cytarabine, gefitinib, gemcitabine,

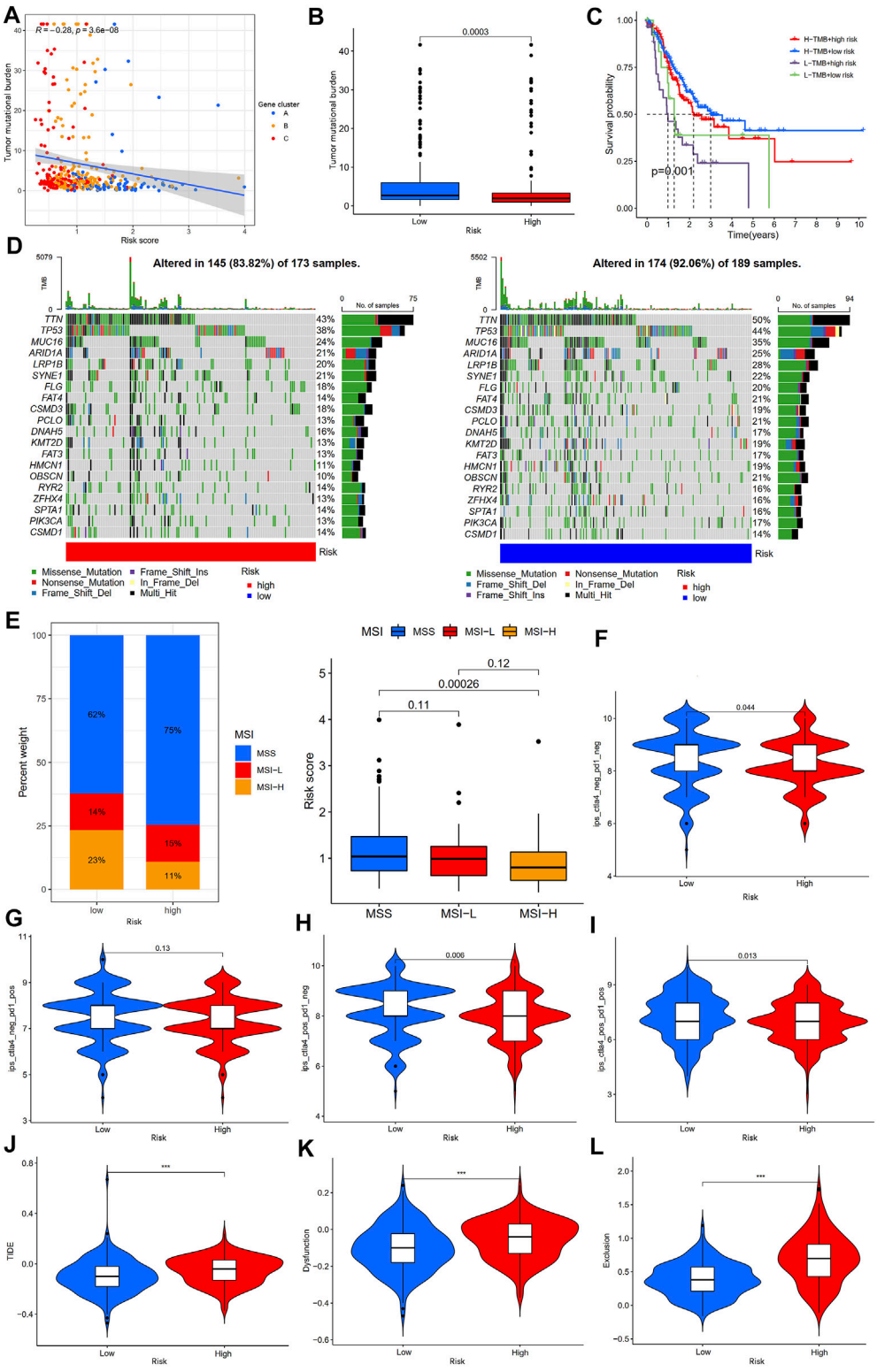

FIGURE 11
Analysis of immunotherapy response rates between high- and low-risk groups. **(A)** Spearman correlation analysis of the risk score and TMB. **(B)** Analysis of TMB differences between high- and low-risk groups. **(C)** Kaplan–Meier survival analysis among four subgroups stratified by both TMB and risk score. **(D)** The waterfall plot of somatic mutation landscape high- and low-risk groups. **(E)** Relationships between risk score and MSI. **(F)** The ips_ctla4_neg_pd1_neg, **(G)** ips_ctla4_neg_pd1_pos, **(H)** ips_ctla4_pos_pd1_neg, and **(I)** ips_ctla4_pos_pd1_pos analyses between the high- and low-risk groups. **(J–L)** The TIDE, dysfunction, and exclusion score analyses between the high- and low-risk groups. TMB, tumor mutation burden; IPS, immunophenoscore; TIDE, tumor immune dysfunction and exclusion; ***p < 0.001.

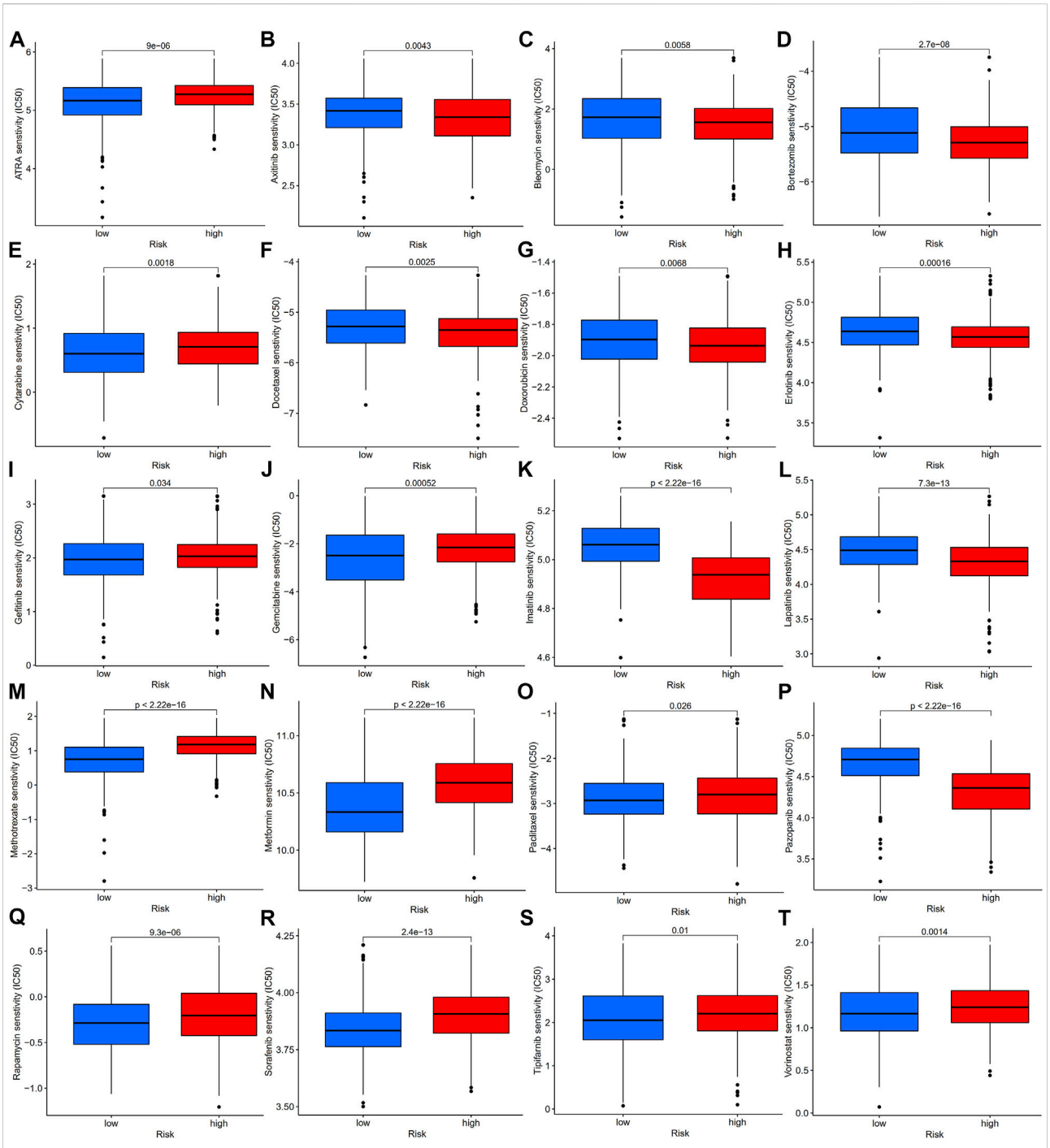

FIGURE 12
Antitumor drug sensitivity analysis of gastric patients in high- and low-risk groups, IC50 analysis of ATRA **(A)**, axitinib **(B)**, bleomycin **(C)**, bortezomib **(D)**, cytarabine **(E)**, docetaxel **(F)**, doxorubicin **(G)**, erlotinib **(H)**, gefitinib **(I)**, gemcitabine **(J)**, imatinib **(K)**, lapatinib **(L)**, methotrexate **(M)**, metformin **(N)**, paclitaxel **(O)**, pazopanib **(P)**, rapamycin **(Q)**, sorafenib **(R)**, tipifarnib **(S)**, and vorinostat **(T)** in the high- and low-risk groups, which were classified by the prognostic model. IC50, half-maximal inhibitory concentration.

methotrexate, metformin, paclitaxel, rapamycin, sorafenib, tipifarnib, and vorinostat than those in the high-risk group, while gastric cancer patients in the low-risk group were less sensitive to axitinib, bleomycin, bortezomib, docetaxel, doxorubicin, erlotinib, imatinib, lapatinib, and pazopanib than those in the high-risk group (Figure 12). The above results

suggest that our prognostic model can be an essential indicator of antitumor drugs for patients with gastric cancer.

Discussion

Numerous studies have shown that the TGF-β signaling pathway plays an essential role in the tumor immune microenvironment and can exert both pro- and anti-tumor effects (Morikawa et al., 2016; Colak and Ten Dijke, 2017; Garcia-Rendueles et al., 2017; Batlle and Massagué, 2019; Kim et al., 2021). However, most studies focus on one or two TGF-β signaling pathway genes or a single TME cell, and the overall TME infiltration characteristics mediated by the multiple TGF-β signaling pathway genes have not been comprehensively understood. Discovering the role of different TGF-β-related subtypes in the TME will help improve our understanding of the antitumor immune microenvironment and guide more precise individualized immune therapy.

In this study, we first analyzed the differential expression levels and genetic mutation characteristics of 54 TSRGs using the TCGA-STAD dataset. Although the mutation frequency of 54 TSRGs was low, most were highly expressed and closely related in gastric cancer. Subsequently, we identified two distinct TGF-β subgroups, TGF-β cluster A and TGF-β cluster B, based on 54 TSRGs transcriptome expression levels using an unsupervised clustering approach. Compared to gastric cancer patients with TGF-β cluster B, gastric cancer patients with TGF-β cluster A had shorter OS, higher expression levels of 54 TSRGs, higher stromal scores, immune scores, ESTIMATE scores, higher levels of PD1, PD-L1, CTLA4 expression levels, and higher infiltration levels of MDSC, macrophage, and regulatory T cells. The above results imply that TGF-β cluster A has a more active immunosuppressive TME. Tumor cells in the immunosuppressive TME can evade the killing effect of immune cells and have a high degree of malignancy, which in turn leads to a shorter survival of patients (Lei et al., 2020). And the patients with TGF-β cluster A in this study had shorter survival, which is consistent with this phenomenon. Next, we identified the DEGs between two distinct TGF-β subgroups and further identified three gene subgroups based on DEGs. There was a significant difference in OS between the three gene subgroups. In addition, 41 of the 54 TSRGs were significantly differentially expressed among the three gene subgroups. This demonstrated a close association between gene subgroups and TGF-β subgroups.

Next, we constructed a TGF-β-related prognostic model to calculate the risk score for each patient. We first screened prognosis-related genes by univariate Cox regression analysis for differentially expressed genes between two TGF-β subgroups. Next, LASSO Cox regression analysis was used to construct a prognostic model containing five genes, and each patient's risk score was calculated. We found that TGF-β cluster A and gene cluster A were mainly concentrated in the high-risk group, while TGF-β cluster B and gene cluster C were primarily concentrated in the low-risk group. Patients in the high-risk group had a poor prognosis, consistent with the previous results of poor prognosis in the TGF-β cluster A and gene cluster A groups. The five genes in the prognostic model were SRPX2, SGCE, DES, MMP7, and KRT17. Studies have shown that SRPX2 is highly expressed in gastric cancer and can promote migration and adhesion of gastric cancer cells, which is closely associated with poor prognosis of gastric cancer patients (Tanaka et al., 2009). The present study showed that SRPX2 is a risk factor for the prognosis of gastric cancer patients, which is consistent with the above findings. SGCE has a hazard ratio greater than 1 in gastric cancer and is considered a poor prognostic marker (Hou et al., 2017), which is consistent with the results of this study. SGCE is a sponge molecule of EGFR and its E3 ubiquitination ligase (c-Cbl). High expression of SGCE inhibits EGFR degradation *via* the ubiquitin lysosomal pathway, increases tumor cell drug resistance, and promotes metastasis (Zhao et al., 2020b). Studies have shown that desmin (DES) protein is more advantageous than elastin protein in detecting vascular invasion in gastric cancer and is considered one of the markers of tumor invasion (Ekinci et al., 2018; Shin et al., 2020). MMP7 expression was significantly associated with poor clinicopathological features of gastric cancer patients, including vascular invasion, undifferentiated histological types, higher TNM stage, and high CEA levels (Wattanawongdon et al., 2022), and was considered one of the prognostic markers of gastric cancer (Chang et al., 2014). It was shown that silencing KRT inhibited the proliferation, migration, and invasion of gastric cancer cells, induced apoptosis, and stalled the gastric cancer cell cycle at the G1/S phase by decreasing the expression of cyclin E1 and cyclin D (Hu et al., 2018). In addition, Zhou et al. constructed a prognostic signature based on multiple gastric cancer datasets in the GEO database, including MMP7 and KRT17 (Zhou et al., 2021), which indirectly demonstrated the reliability of our prognostic model. Next, we performed a survival analysis between high- and low-risk groups, which showed that OS was worse in the high-risk group of gastric cancer patients. This result was also confirmed in both validation sets (testing set and entire set). The risk scores also had excellent performance across clinicopathological characteristics subgroups. Univariate and multifactorial Cox regression analyses demonstrated that the risk score was an independent prognostic factor for patients with gastric cancer. In addition, the nomograms constructed by the risk score combined with clinicopathological characteristics also excelled in predicting the overall survival of gastric cancer patients at 1-, 3-, and 5-year. Overall, the TGF-β-related prognostic model we constructed could excellently predict the prognosis of gastric cancer patients.

The TME is the internal environment on which tumor cells depend for survival. Under normal circumstances, immune cells in the TME can recognize and remove tumor cells on time, but tumor

cells can create an immunosuppressive TME through a complex regulatory network to produce immune escape (Joyce and Fearon, 2015; Jiang et al., 2019). The immunosuppressive TME consists of immunosuppressive cells such as regulatory T cells (Tregs), tumor-associated macrophages (TAMs), tumor-associated neutrophils (TANs), myeloid-derived suppressor cells (MDSCs), tumor-associated fibroblasts (CAFs), extracellular matrix, suppressive cytokines such as interleukin 10, interleukin 17, TGF-β exosomes and immune checkpoint molecules such as PD1, PD-L1, and CTLA4 (Zhang et al., 2019; Li et al., 2020; Nakamura and Smyth, 2020). Studies have shown that increased MDSCs in tumor tissues promote the production of Tregs and deplete activated T cells (Davis et al., 2016). Furthermore, Tregs can inhibit CD80 and CD86 co-stimulatory signaling *via* CTLA4, secrete suppressive cytokines, and kill effector T cells (Tekguc et al., 2021). TAMs can enhance the immunosuppressive TME in several ways. In gastric cancer, TAMs promote PD-L1 expression through the secretion of CXCL8, thereby suppressing the antitumor effects of $CD8^+$ T cells (Lin et al., 2019). TAMs can also recruit Tregs through the secretion of chemokines such as CCL2, CCL3, CCL20, and CCL22, which in turn form immunosuppressive TMEs(Cassetta and Pollard, 2020; Pan et al., 2020). In addition, TAMs-derived TGF-β can promote its secretion of CCL22 to recruit Tregs, which in turn can secrete IL-8 to promote TGF-β secretion by TAMs, thereby enhancing immunosuppressive TME (Wang et al., 2019). This study showed higher MDSC, macrophage, and regulatory T cell infiltration levels and more active signaling pathways such as TGF-β, and Wnt/β-catenin signaling pathways in the TGF-β cluster A, suggesting a more active immunosuppressive microenvironment. Spearman correlation analysis of immune cells and risk scores showed a positive correlation between risk scores and myeloid dendritic cells, M2 macrophages, and CAFs, suggesting that the TME of patients in the high-risk group was immunosuppressive. Patients with gastric cancer of TGF-β cluster A were mainly concentrated in the high-risk group, and the results of the before-and-after study were consistent.

ICIs offer new hope for patients with advanced cancer due to their significant efficacy and fewer side effects. However, only a small number of patients can benefit from them. Therefore, there is an urgent need to screen the population with a high response rate for more precise treatment. Currently, common biomarkers to predict the efficacy of ICIs include TMB, microsatellite status, IPS, and TIDE score. Tumor cells with MSI-H have an increased TMB and generate new antigens due to unrepaired mis-replicated DNA, which allows more TILs to infiltrate and thus respond better to ICIs (Lizardo et al., 2020). This study showed that the low-risk group had a higher TMB and a higher percentage of MSI-H than the high-risk group, suggesting that low-risk gastric cancer patients may have a better treatment effect on ICIs. IPS and TIDE scores are novel immunotherapy biomarkers with good predictive power for response rates to ICIs (Wu et al., 2021). A high IPS represents higher immunogenicity, and a high TIDE score represents a greater likelihood of tumor immune escape (Wu et al., 2021; Zeng et al., 2022); therefore, the higher the IPS and the lower the TIDE score, the better the patient's outcome to ICIs. This study showed that patients with gastric cancer in the low-risk group had higher IPS scores and lower TIDE scores, suggesting that patients in the low-risk group are highly immunogenic, again demonstrating that patients in the low-risk group are a potentially highly beneficial population for ICIs treatment. In addition, we analyzed the differences in sensitivity of common antitumor drugs between high- and low-risk groups to provide a new perspective on clinical antitumor drug combination strategies.

Our study also has some limitations. This study is a retrospective study based on public data and needs to be further validated in a large, multicenter prospective study. Second, this study needs to incorporate more clinicopathological features for a more comprehensive analysis of the clinical value of the risk model. In addition, *in vivo and in vitro* experiments are needed to further explore the specific mechanisms of risk scores in the TME.

Conclusion

In this study, we found that TGF-β cluster A presented an immunosuppressive microenvironment with shorter OS. Second, we constructed a risk model associated with TSRGs to predict the prognosis of gastric cancer patients. In addition, gastric cancer patients in the low-risk group, characterized by higher TMB, the proportion of MSI-H, IPS, and lower TIDE score, may be more sensitive to immunotherapy.

Data availability statement

The original contributions presented in the study are included in the article/Supplementary Material, further inquiries can be directed to the corresponding authors.

Author contributions

All authors participated in the conception and design of the study; protocol/project development—YW and JJ; data collection or management—CZ, RH, YD, and XL; data analysis—CZ, LD, QZ, YL, QL, and WL; manuscript writing/editing—CZ. All authors read and approved the paper.

Funding

The work was supported by the National Natural Science Foundation of China (81872275); by the Open Project of

Jiangsu Provincial Key Laboratory of Tumor Biotherapy (XZSYSKF2020005); by the Scientific Research Project of Jiangsu Commission of Health (M2020002); by the Changzhou Sci and Tech Program (CJ20220006, CJ20210015, CJ20220007); by the Science and Technology Project of Changzhou Health Commission (WZ202224); by Changzhou High-Level Medical Talents Training Project (2016CZBJ054, 2022CZBJ110).

Acknowledgments

The authors gratefully acknowledge the multiple databases which made the data available.

Conflict of interest

The authors declare that the research was conducted in the absence of any commercial or financial relationships that could be construed as a potential conflict of interest.

Publisher's note

Supplementary material

The Supplementary Material for this article can be found online at: https://www.frontiersin.org/articles/10.3389/fphar.2022.1069204/full#supplementary-material

SUPPLEMENTARY FIGURE S1
Schematic diagram of the study design.

SUPPLEMENTARY FIGURE S2
Risk model validation on the imvigor210 cohort. **(A)** Kaplan–Meier survival analysis between high- and low-risk groups. **(B)** Immunotherapy response analysis. CR: Complete response; PR: Partial response; SD: Stable disease; PD: Progressive disease.

References

Batlle, E., and Massagué, J. (2019). Transforming growth factor-β signaling in immunity and cancer. *Immunity* 50 (4), 924–940. doi:10.1016/j.immuni.2019.03.024

Cassetta, L., and Pollard, J. W. (2020). Tumor-associated macrophages. *Curr. Biol.* 30 (6), R246–R248. doi:10.1016/j.cub.2020.01.031

Chang, W.-J., Du, Y., Zhao, X., Ma, L.-Y., and Cao, G.-W. (2014). Inflammation-related factors predicting prognosis of gastric cancer. *World J. Gastroenterol.* 20 (16), 4586–4596. doi:10.3748/wjg.v20.i16.4586

Chen, Y., Jia, K., Sun, Y., Zhang, C., Li, Y., Zhang, L., et al. (2022). Predicting response to immunotherapy in gastric cancer via multi-dimensional analyses of the tumour immune microenvironment. *Nat. Commun.* 13 (1), 4851. doi:10.1038/s41467-022-32570-z

Colak, S., and Ten Dijke, P. (2017). Targeting TGF-β signaling in cancer. *Trends Cancer* 3 (1), 56–71. doi:10.1016/j.trecan.2016.11.008

Davis, R. J., Van Waes, C., and Allen, C. T. (2016). Overcoming barriers to effective immunotherapy: MDSCs, TAMs, and Tregs as mediators of the immunosuppressive microenvironment in head and neck cancer. *Oral Oncol.* 58, 59–70. doi:10.1016/j.oraloncology.2016.05.002

Ekinci, Ö., Öğüt, B., Çelik, B., and Dursun, A. (2018). Compared with elastin stains, h-caldesmon and desmin offer superior detection of vessel invasion in gastric, pancreatic, and colorectal adenocarcinomas. *Int. J. Surg. Pathol.* 26 (4), 318–326. doi:10.1177/1066896917752442

Garcia-Rendueles, A. R., Rodrigues, J. S., Garcia-Rendueles, M. E. R., Suarez-Fariña, M., Perez-Romero, S., Barreiro, F., et al. (2017). Rewiring of the apoptotic TGF-β-SMAD/NFκB pathway through an oncogenic function of p27 in human papillary thyroid cancer. *Oncogene* 36 (5), 652–666. doi:10.1038/onc.2016.233

Geeleher, P., Cox, N., and Huang, R. S. (2014). pRRophetic: an R package for prediction of clinical chemotherapeutic response from tumor gene expression levels. *PloS One* 9 (9), e107468. doi:10.1371/journal.pone.0107468

Hänzelmann, S., Castelo, R., and Guinney, J. (2013). Gsva: Gene set variation analysis for microarray and RNA-seq data. *BMC Bioinforma.* 14, 7. doi:10.1186/1471-2105-14-7

Hou, J.-Y., Wang, Y.-G., Ma, S.-J., Yang, B.-Y., and Li, Q.-P. (2017). Identification of a prognostic 5-Gene expression signature for gastric cancer. *J. Cancer Res. Clin. Oncol.* 143 (4), 619–629. doi:10.1007/s00432-016-2324-z

Hu, H., Xu, D.-H., Huang, X.-X., Zhu, C.-C., Xu, J., Zhang, Z.-Z., et al. (2018). Keratin17 promotes tumor growth and is associated with poor prognosis in gastric cancer. *J. Cancer* 9 (2), 346–357. doi:10.7150/jca.19838

Jiang, X., Wang, J., Deng, X., Xiong, F., Ge, J., Xiang, B., et al. (2019). Role of the tumor microenvironment in PD-L1/PD-1-mediated tumor immune escape. *Mol. Cancer* 18 (1), 10. doi:10.1186/s12943-018-0928-4

Joyce, J. A., and Fearon, D. T. (2015). T cell exclusion, immune privilege, and the tumor microenvironment. *Sci. (New York, N.Y.)* 348 (6230), 74–80. doi:10.1126/science.aaa6204

Kim, B.-G., Malek, E., Choi, S. H., Ignatz-Hoover, J. J., and Driscoll, J. J. (2021). Novel therapies emerging in oncology to target the TGF-β pathway. *J. Hematol. Oncol.* 14 (1), 55. doi:10.1186/s13045-021-01053-x

Leek, J. T., Johnson, W. E., Parker, H. S., Jaffe, A. E., and Storey, J. D. (2012). The sva package for removing batch effects and other unwanted variation in high-throughput experiments. *Bioinforma. Oxf. Engl.* 28 (6), 882–883. doi:10.1093/bioinformatics/bts034

Lei, X., Lei, Y., Li, J.-K., Du, W.-X., Li, R.-G., Yang, J., et al. (2020). Immune cells within the tumor microenvironment: Biological functions and roles in cancer immunotherapy. *Cancer Lett.* 470, 126–133. doi:10.1016/j.canlet.2019.11.009

Li, L., Yu, R., Cai, T., Chen, Z., Lan, M., Zou, T., et al. (2020). Effects of immune cells and cytokines on inflammation and immunosuppression in the tumor microenvironment. *Int. Immunopharmacol.* 88, 106939. doi:10.1016/j.intimp.2020.106939

Lin, C., He, H., Liu, H., Li, R., Chen, Y., Qi, Y., et al. (2019). Tumour-associated macrophages-derived CXCL8 determines immune evasion through autonomous PD-L1 expression in gastric cancer. *Gut* 68 (10), 1764–1773. doi:10.1136/gutjnl-2018-316324

Lizardo, D. Y., Kuang, C., Hao, S., Yu, J., Huang, Y., and Zhang, L. (2020). Immunotherapy efficacy on mismatch repair-deficient colorectal cancer: From bench to bedside. *Biochim. Biophys. Acta. Rev. Cancer* 1874 (2), 188447. doi:10.1016/j.bbcan.2020.188447

Mayakonda, A., Lin, D.-C., Assenov, Y., Plass, C., and Koeffler, H. P. (2018). Maftools: Efficient and comprehensive analysis of somatic variants in cancer. *Genome Res.* 28 (11), 1747–1756. doi:10.1101/gr.239244.118

Morikawa, M., Derynck, R., and Miyazono, K. (2016). TGF-B and the TGF-β family: Context-dependent roles in cell and tissue physiology. *Cold Spring Harb. Perspect. Biol.* 8 (5), a021873. doi:10.1101/cshperspect.a021873

Nakamura, K., and Smyth, M. J. (2020). Myeloid immunosuppression and immune checkpoints in the tumor microenvironment. *Cell. Mol. Immunol.* 17 (1), 1–12. doi:10.1038/s41423-019-0306-1

Newman, A. M., Liu, C. L., Green, M. R., Gentles, A. J., Feng, W., Xu, Y., et al. (2015). Robust enumeration of cell subsets from tissue expression profiles. *Nat. Methods* 12 (5), 453–457. doi:10.1038/nmeth.3337

Ni, Y., Soliman, A., Joehlin-Price, A., Rose, P. G., Vlad, A., Edwards, R. P., et al. (2021). High TGF-β signature predicts immunotherapy resistance in gynecologic cancer patients treated with immune checkpoint inhibition. *NPJ Precis. Oncol.* 5 (1), 101. doi:10.1038/s41698-021-00242-8

Niu, X., Chen, L., Li, Y., Hu, Z., and He, F. (2022). Ferroptosis, necroptosis, and pyroptosis in the tumor microenvironment: Perspectives for immunotherapy of SCLC. *Semin. Cancer Biol.* 86, 273–285. doi:10.1016/j.semcancer.2022.03.009

Pan, Y., Yu, Y., Wang, X., Zhang, T., and Devadas, S. (2020). iCa2+ flux, ROS and IL-10 determines cytotoxic, and suppressor T cell functions in chronic human viral infections. *Front. Immunol.* 11, 83. doi:10.3389/fimmu.2020.00083

Patel, T. H., and Cecchini, M. (2020). Targeted therapies in advanced gastric cancer. *Curr. Treat. Options Oncol.* 21 (9), 70. doi:10.1007/s11864-020-00774-4

Qing, X., Xu, W., Liu, S., Chen, Z., Ye, C., and Zhang, Y. (2022). Molecular characteristics, clinical significance, and cancer immune interactions of angiogenesis-associated genes in gastric cancer. *Front. Immunol.* 13, 843077. doi:10.3389/fimmu.2022.843077

Ritchie, M. E., Phipson, B., Wu, D., Hu, Y., Law, C. W., Shi, W., et al. (2015). Limma powers differential expression analyses for RNA-sequencing and microarray studies. *Nucleic Acids Res.* 43 (7), e47. doi:10.1093/nar/gkv007

Rizzo, A., Ricci, A. D., and Brandi, G. (2021). PD-L1, TMB, MSI, and other predictors of response to immune checkpoint inhibitors in biliary tract cancer. *Cancers* 13 (3), 558. doi:10.3390/cancers13030558

Shin, J., Wood, L. D., Hruban, R. H., and Hong, S.-M. (2020). Desmin and CD31 immunolabeling for detecting venous invasion of the pancreatobiliary tract cancers. *PloS One* 15 (11), e0242571. doi:10.1371/journal.pone.0242571

Smyth, E. C., Nilsson, M., Grabsch, H. I., van Grieken, N. C., and Lordick, F. (2020). Gastric cancer. *Lancet (London, Engl.* 396 (10251), 635–648. doi:10.1016/S0140-6736(20)31288-5

Tanaka, K., Arao, T., Maegawa, M., Matsumoto, K., Kaneda, H., Kudo, K., et al. (2009). SRPX2 is overexpressed in gastric cancer and promotes cellular migration and adhesion. *Int. J. Cancer* 124 (5), 1072–1080. doi:10.1002/ijc.24065

Tekguc, M., Wing, J. B., Osaki, M., Long, J., and Sakaguchi, S. (2021). Treg-expressed CTLA-4 depletes CD80/CD86 by trogocytosis, releasing free PD-L1 on antigen-presenting cells. *Proc. Natl. Acad. Sci. U. S. A.* 118 (30), e2023739118. doi:10.1073/pnas.2023739118

Tibshirani, R. (1997). The lasso method for variable selection in the Cox model. *Stat. Med.* 16 (4), 385–395. doi:10.1002/(sici)1097-0258(19970228)16:4<385:aid-sim380>3.0.co;2-3

Ungefroren, H. (2019). Blockade of TGF-β signaling: A potential target for cancer immunotherapy? *Expert Opin. Ther. Targets* 23 (8), 679–693. doi:10.1080/14728222.2019.1636034

Wang, D., Yang, L., Yue, D., Cao, L., Li, L., Wang, D., et al. (2019). Macrophage-derived CCL22 promotes an immunosuppressive tumor microenvironment via IL-8 in malignant pleural effusion. *Cancer Lett.* 452, 244–253. doi:10.1016/j.canlet.2019.03.040

Wang, S., Su, W., Zhong, C., Yang, T., Chen, W., Chen, G., et al. (2020). An eight-CircRNA assessment model for predicting biochemical recurrence in prostate cancer. *Front. Cell Dev. Biol.* 8, 599494. doi:10.3389/fcell.2020.599494

Wattanawongdon, W., Bartpho, T. S., Tongtawee, T., Paoin, C., Kangwantas, K., and Dechsukhum, C. (2022). Precancerous gastric lesions with *Helicobacter pylori* vacA +/babA2+/oipA + genotype increase the risk of gastric cancer. *Biomed. Res. Int.* 2022, 7243029. doi:10.1155/2020/7243029

Wei, L., Sun, J., Zhang, N., Zheng, Y., Wang, X., Lv, L., et al. (2020). Noncoding RNAs in gastric cancer: Implications for drug resistance. *Mol. Cancer* 19 (1), 62. doi:10.1186/s12943-020-01185-7

Wilkerson, M. D., and Hayes, D. N. (2010). ConsensusClusterPlus: A class discovery tool with confidence assessments and item tracking. *Bioinforma. Oxf. Engl.* 26 (12), 1572–1573. doi:10.1093/bioinformatics/btq170

Wu, J., Li, L., Zhang, H., Zhao, Y., Zhang, H., Wu, S., et al. (2021). A risk model developed based on tumor microenvironment predicts overall survival and associates with tumor immunity of patients with lung adenocarcinoma. *Oncogene* 40 (26), 4413–4424. doi:10.1038/s41388-021-01853-y

Yu, Q., Zhao, L., Yan, X.-X., Li, Y., Chen, X.-Y., Hu, X.-H., et al. (2022). Identification of a TGF-β signaling-related gene signature for prediction of immunotherapy and targeted therapy for lung adenocarcinoma. *World J. Surg. Oncol.* 20 (1), 183. doi:10.1186/s12957-022-02595-1

Zeng, C., Liu, Y., He, R., Lu, X., Dai, Y., Qi, G., et al. (2022). Identification and validation of a novel cellular senescence-related lncRNA prognostic signature for predicting immunotherapy response in stomach adenocarcinoma. *Front. Genet.* 13, 935056. doi:10.3389/fgene.2022.935056

Zhang, B., Wu, Q., Li, B., Wang, D., Wang, L., and Zhou, Y. L. (2020). m6A regulator-mediated methylation modification patterns and tumor microenvironment infiltration characterization in gastric cancer. *Mol. Cancer* 19 (1), 53. doi:10.1186/s12943-020-01170-0

Zhang, H., Meltzer, P., and Davis, S. (2013). RCircos: an R package for Circos 2D track plots. *BMC Bioinforma.* 14, 244. doi:10.1186/1471-2105-14-244

Zhang, Y., Xu, J., Zhang, N., Chen, M., Wang, H., and Zhu, D. (2019). Targeting the tumour immune microenvironment for cancer therapy in human gastrointestinal malignancies. *Cancer Lett.* 458, 123–135. doi:10.1016/j.canlet.2019.05.017

Zhang, Y., and Zhang, Z. (2020). The history and advances in cancer immunotherapy: Understanding the characteristics of tumor-infiltrating immune cells and their therapeutic implications. *Cell. Mol. Immunol.* 17 (8), 807–821. doi:10.1038/s41423-020-0488-6

Zhao, H., Wei, J., and Sun, J. (2020a). Roles of TGF-β signaling pathway in tumor microenvirionment and cancer therapy. *Int. Immunopharmacol.* 89, 107101. doi:10.1016/j.intimp.2020.107101

Zhao, L., Qiu, T., Jiang, D., Xu, H., Zou, L., Yang, Q., et al. (2020b). SGCE promotes breast cancer stem cells by stabilizing EGFR. *Adv. Sci.* 7 (14), 1903700. doi:10.1002/advs.201903700

Zhou, L., Lu, H., Zeng, F., Zhou, Q., Li, S., Wu, Y., et al. (2021). Constructing a new prognostic signature of gastric cancer based on multiple data sets. *Bioengineered* 12 (1), 2820–2835. doi:10.1080/21655979.2021.1940030

Zhu, Y., Zhu, X., Wei, X., Tang, C., and Zhang, W. (2021). HER2-targeted therapies in gastric cancer. *Biochim. Biophys. Acta. Rev. Cancer* 1876 (1), 188549. doi:10.1016/j.bbcan.2021.188549

frontiers | Frontiers in Pharmacology

TYPE Original Research
PUBLISHED 09 December 2022
DOI 10.3389/fphar.2022.1079566

OPEN ACCESS

EDITED BY
Kui Zhang,
The University of Chicago, United States

REVIEWED BY
Nian Ma,
University of Pennsylvania, United States
Lunda Shen,
Texas A&M University, United States
Lei Huang,
Microsoft, United States
Yujuan Su,
University of California, San Diego, United States

*CORRESPONDENCE
Jun Huang,
huangjun@zzu.edu.cn
Liping Chen,
lpchen14@fudan.edu.cn
Guifu Dai,
daiguifu@zzu.edu.cn

SPECIALTY SECTION
This article was submitted to Pharmacology of Anti-Cancer Drugs, a section of the journal Frontiers in Pharmacology

RECEIVED 25 October 2022
ACCEPTED 30 November 2022
PUBLISHED 09 December 2022

CITATION
Huang J, Zhao C, Zhang X, Zhao Q, Zhang Y, Chen L and Dai G (2022), Hepatitis B virus pathogenesis relevant immunosignals uncovering amino acids utilization related risk factors guide artificial intelligence-based precision medicine.
Front. Pharmacol. 13:1079566.
doi: 10.3389/fphar.2022.1079566

Hepatitis B virus pathogenesis relevant immunosignals uncovering amino acids utilization related risk factors guide artificial intelligence-based precision medicine

Jun Huang[1]*, Chunbei Zhao[1], Xinhe Zhang[1], Qiaohui Zhao[1], Yanting Zhang[1], Liping Chen[2,3]* and Guifu Dai[1]*

[1]School of Life Sciences, Zhengzhou University, Zhengzhou, Henan, China, [2]Key Laboratory of Gastroenterology and Hepatology, State Key Laboratory for Oncogenes and Related Genes, Department of Gastroenterology and Hepatology, Ministry of Health, Shanghai Institute of Digestive Disease, Renji Hospital, School of Medicine, Shanghai Jiaotong University, Shanghai, China, [3]Shanghai Public Health Clinical Center, Fudan University, Shanghai, China

Background: Although immune microenvironment-related chemokines, extracellular matrix (ECM), and intrahepatic immune cells are reported to be highly involved in hepatitis B virus (HBV)-related diseases, their roles in diagnosis, prognosis, and drug sensitivity evaluation remain unclear. Here, we aimed to study their clinical use to provide a basis for precision medicine in hepatocellular carcinoma (HCC) *via* the amalgamation of artificial intelligence.

Methods: High-throughput liver transcriptomes from Gene Expression Omnibus (GEO), NODE (https://www.bio.sino.org/node), the Cancer Genome Atlas (TCGA), and our in-house hepatocellular carcinoma patients were collected in this study. Core immunosignals that participated in the entire diseases course of hepatitis B were explored using the "Gene set variation analysis" R package. Using ROC curve analysis, the impact of core immunosignals and amino acid utilization related gene on hepatocellular carcinoma patient's clinical outcome were calculated. The utility of core immunosignals as a classifier for hepatocellular carcinoma tumor tissue was evaluated using explainable machine-learning methods. A novel deep residual neural network model based on immunosignals was constructed for the long-term overall survival (LS) analysis. *In vivo* drug sensitivity was calculated by the "oncoPredict" R package.

Results: We identified nine genes comprising chemokines and ECM related to hepatitis B virus-induced inflammation and fibrosis as CLST signals. Moreover, CLST was co-enriched with activated CD4+ T cells bearing harmful factors (aCD4) during all stages of hepatitis B virus pathogenesis, which was also verified by our hepatocellular carcinoma data. Unexpectedly, we found that hepatitis B virus-hepatocellular carcinoma patients in the $CLST^{high}aCD4^{high}$ subgroup had the shortest overall survival (OS) and were characterized by a

risk gene signature associated with amino acids utilization. Importantly, characteristic genes specific to CLST/aCD4 showed promising clinical relevance in identifying patients with early-stage hepatocellular carcinoma *via* explainable machine learning. In addition, the 5-year long-term overall survival of hepatocellular carcinoma patients can be effectively classified by CLST/aCD4 based GeneSet-ResNet model. Subgroups defined by CLST and aCD4 were significantly involved in the sensitivity of hepatitis B virus-hepatocellular carcinoma patients to chemotherapy treatments.

Conclusion: CLST and aCD4 are hepatitis B virus pathogenesis-relevant immunosignals that are highly involved in hepatitis B virus-induced inflammation, fibrosis, and hepatocellular carcinoma. Gene set variation analysis derived immunogenomic signatures enabled efficient diagnostic and prognostic model construction. The clinical application of CLST and aCD4 as indicators would be beneficial for the precision management of hepatocellular carcinoma.

KEYWORDS

hepatitis B virus, hepatocellular carcinoma, tumor microenvironment (TME), artificial inteligence-AI, anti-tumor drug, prognosis, amino acids utilization

Introduction

Chronic hepatitis B virus (HBV) infection remains a major health concern worldwide (Kramvis et al., 2022). First-line anti-HBV drugs approved by FDA including PEG IFN-α and nucleoside (acid) analogs (NAs) are not yet effective in achieving functional cure referring to hepatitis B surface antigen (HBsAg) and covalently closed circular DNA (cccDNA) elimination (Levrero et al., 2018; Fanning et al., 2019; Yang et al., 2019; Tout et al., 2020). Over 200 million people are afflicted with chronic hepatitis B (CHB) and are at a high risk of developing liver fibrosis (LF), liver cirrhosis, and hepatocellular carcinoma (HCC) (Wangensteen and Chang, 2021). HBV-related diseases cause heavy economic pressure and psychological burden to many families, especially in the Asia-Pacific region, where HBV is highly prevalent (Wang et al., 2017; Wong et al., 2019; Howell et al., 2020; Sarin et al., 2020). Considerable evidence suggests that chemokines, the extracellular matrix (ECM), parenchymal hepatic cells, tissue-resident lymphocytes, and extrahepatic immune cells in the liver microenvironment are associated with HBV-related diseases progression (Yuen et al., 2018). CXCR3-related chemokines (CXCL9 and CXCL10), directly produced by hepatocytes or liver sinusoidal endothelial cells at the early stage of HBV infection, can result in intrahepatic lymphocyte infiltration (Rehermann, 2013). SPP1(the CD44 ligand) derived from activated hepatic stellate cells (HSC) serves as a stimulator for KLRG1+ NK cells that can mediate liver scarring limitation in CHB pathogenesis (Wijaya et al., 2019) and has predictive value in the prognosis of HCC (Shang et al., 2012; da Costa et al., 2015). SOX9, which can be directly induced in HBV-infected human hepatoma cells (Yang et al., 2020) has been identified as a risk factor for cirrhosis and HCC (Chen et al., 2021; Damrauer et al., 2021). However, these previous studies are performed just through flow cytometry (FCM), immune fluorescence (IF), and immunohistochemistry (IHC) with limited subpopulations of liver-infiltrating lymphocytes (LILs) and a small samples size; the orchestra of multiple chemokines and ECM related genes with a variety of LILs during HBV pathogenesis are not globally indicated.

The core mechanism underlying amino acid metabolic adaptations in cancer cells to grow in a nutrient-deficient tumor microenvironment (TME) was recently reported, and LYSET (TMEM251) and other amino acid utilization-associated genes (ATF4, TSC2, VPS18, RAB7A, SLC7A5, SLC3A2, TGFBRAP1, GNPTAB, and GCN2) have been primarily screened out mainly through CRISPR-Cas9 based high-throughput method (Pechincha et al., 2022). Although these key players essential for tumor cell proliferation in harsh TME conditions and LYSET invovled in lysosomal biogenesis have been uncovered in the latest studies (Pechincha et al., 2022; Richards et al., 2022), their impact on pan-cancer clinical outcomes remains unknown. The metabolic status of amino acids in HCC patients with different immune subtypes according to HBV pathogenesis-relevant immunosignals is worthy of further study.

Currently, precise diagnosis and prognosis of HBV-related liver diseases have attracted much attention (Petrizzo et al., 2018; Zheng et al., 2020). The main obstacle to artificial intelligence (AI) models' establishment in genome medicine is that neither gene microarray nor RNA-seq data are suitable for direct learning (Oh et al., 2021). Although several AI models based on these high-dimensional biological data have been constructed to detect liver cancer at an early stage and assess the prognosis

(Long et al., 2019; Tao et al., 2020; Christou and Tsoulfas, 2021; Liu W. et al., 2021; Liu X. et al., 2021), the input data used in these models are relatively complex and not easy to follow. Until now, the optimal model with a promising predictive value for clinical utilization has been far from reaching a general consensus (Le Berre et al., 2020; Christou and Tsoulfas, 2021; Liu X. et al., 2021; Oh et al., 2021; Wang et al., 2022). "Gene set variation analysis (GSVA)" R package (GSVA, for short) (Aran et al., 2017; Charoentong et al., 2017), CIBERSORT (Newman et al., 2015), MCP-counter and TIMER were primarily developed and used for novel immune cell subtype identification and concentration evaluation using tissue transcriptome data (Aran et al., 2017; Charoentong et al., 2017; Danaher et al., 2017; Finotello and Trajanoski, 2018; Thakur et al., 2022). Among these tools, GSVA has been widely used in tumor (Charoentong et al., 2017; Deng et al., 2019; Shen et al., 2019; Xiao et al., 2020; Gong et al., 2021; Zhuang et al., 2021) and non-tumor researches (Hu et al., 2021; Shen et al., 2021; Yu et al., 2021) for core module identification at the gene-set level. AI-based models constructed using low-dimensional biological pathway data generated by GSVA as inputs have become popular and demonstrate promising effects (Chawla et al., 2022; Martinez et al., 2022). However, the application of GSVA-derived core immunosignals with even lower dimensionality for efficient feature selection, which benefits machine learning and deep learning in precision oncology, has not been researched.

In this study, immunogenomic profiling of liver transcriptomes was performed to explore the core immunosignals involved in the entire disease course of hepatitis B and their extended clinical applications in early diagnosis, prognostic assessment, and precision usage of anti-cancer drugs. First, we employed GSVA to identify a meaningful HBV pathogenic gene module, named CLST. The potential role of CLST in predicting liver injury and detecting HBV-LF was uncovered. Co-enrichment of CLST and activated CD4+T cells (aCD4) in liver tissue from HCC patients was identified and experimentally verified in our in-house RNA-seq data. Next, a high enrichment score for nutritional utilization of amino acid-related genes was demonstrated as a predictive factor for poor overall survival (OS). The link between nutritional utilization of amino acids and CLST/aCD4 dysregulation in patients with HBV-HCC was explored. Powerful and explainable machine learning methods were then incorporated to construct tools for tumor tissue identification. Simultaneously, a novel deep residual neural network model (GeneSet-ResNet) based on CLST and aCD4 was proposed for long OS(LS) status prediction. Finally, the utility of aCD4 and CLST for evaluating anti-HCC drug sensitivity was evaluated. A new strategy for the construction of novel gene set-based AI models will be helpful for precision medicine.

Materials and methods

Raw data collection and proceeding

A total of 11 Gene Expression Omnibus (GEO) datasets were downloaded from the GEO database (https://www.ncbi.nlm.nih.gov/geo/). The CHCC cohort comprising Chinese patients with HBV-HCC was obtained from NODE (https://www.bio.sino.org/node). The TCGA-LIHC cohort, consisting of HCC patients, was collected from The Cancer Genome Atlas (TCGA). Brief information about the 13 cohorts and workflow of this study are provided in Additional files (Supplementary Table S1; Supplementary Figure S1). R Studio (Version 1.4.1103) was used to obtain raw data (normalization, gene ID convention, clinical information collection) based on the recommended R packages. The CHCC-GSE14520 dataset comprising 396 tumor tissue samples from HBV-HCC patients was cross-technology combined. The non-biological effects across CHCC and GSE14520 were corrected through "SVA" R package (Tang et al., 2021).

Collection and sequencing of liver cancer tissue

Fresh liver cancer tissue specimens from HBV-HCC patients surgically resected from the Shanghai Public Health Clinical Center affiliated with Fudan University (SPHCC) were collected, aliquoted, and stored in a liquid nitrogen tank at −80°C within 2 h. Total tissue RNA was extracted and sent for transcriptome high-throughput sequencing (RiboBio Co., Ltd.) to compare changes in the transcript mRNA levels of related genes in liver cancer.

Identification of differentially expressed genes (DEGs)

Grading (G) and staging (S) systems have been utilized for the efficient evaluation of inflammation and fibrosis in chronic liver diseases, respectively. DEGs (S1/S0, S2/S0, S3/S0, and S4/S0) of GSE84044 were downloaded from the supplementary materials provided in a previous study (Wang et al., 2017) and visualized using GraphPad Prism. DEGs (G1/G0, G2/G0, G3/G0, and G4/G0) of GSE84044 were screened primarily *via* "Limma" R package and visualized *via* "ggplot2" R package, "pheatmap" R package or "EnhancedVolcano" R package. As for the "Enhanced Volcano" R package, upregulated genes with fold change (FC) > 1.5 and p-value < 0.05 were considered statistically significant. Venn analysis was used to identify overlapping DEGs.

Functional annotation and hub genes screening

Gene Ontology (GO) analyses were performed to investigate the biological function annotation of overlapping DEGs of GSE84044 using "clusterProfiler" R package and visualized *via* the "ggplot2" R package. Kyoto Encyclopedia of Genes and Genomes (KEGG) signaling pathway analyses were based on "clusterProfiler" R package and also visualized *via* the "ggplot2" R package. A PPI network of overlapping DEGs from GSE84044, containing 57 nodes and 89 edges, was constructed using the STRING database. Cytoscape software was used to visualize and screen the hub genes. Protein and protein interaction (PPI) analyses of member genes of aCD4 were conducted and visualized using online tools provided by the STRING database.

ssGSEA score calculation

The enrichment scores (ES) of 28 LILs and CLST in liver samples from the GEO database or NODE were calculated primarily *via* the "GSVA" R package with single sample gene set enrichment analysis (ssGSEA) algorithm (Hanzelmann et al., 2013; Charoentong et al., 2017; Yu et al., 2021). A total of 28 gene sets consisting of cell-specific marker genes represent 28 LILs (Charoentong et al., 2017). CLST and amino acid utilization-associated gene signatures were defined in this study according to previous studies (Subramanian et al., 2005; Barbie et al., 2009).

Correlation and comparison

The heatmap showing spearman comparison among hub genes and grading (or staging) was calculated and drawn by using the "Hmisc" R package. The "Hmisc" R package was utilized to calculate the correlations between selected genes and LILs. The R package "ggcorrplot" was used to calculate correlations between CLST and LILs. The results were visualized using the "pheatmap" R package. Comparisons of differences between the two groups were performed and visualized as box plots or dot plots *via* the "ggplot2" R package, and heatmap *via* the "pheatmap" R package, respectively according to the guidelines. Statistical significance was set at $p < 0.05$.

Diagnostic values evaluation and overall survival analysis

The diagnostic values of CLST and LILs immune signals for identifying whether CHB patients are living with liver injury or liver fibrosis were calculated through COX analysis using the "pROC" R package based on liver transcriptomes of GSE83148 and GSE84044, respectively. OS analysis was performed using the Kaplan-Meier survival" R package based on expression values of hub genes or ES of identified immunogenomic signals in tumor tissues of GSE14520 and/or CHCC with available survival information. Kaplan-Meier curves were drawn and plotted *via* the "survminer" R package. Statistical significance was set at $p < 0.05$.

Explainable machine learning algorithms for tumor tissue detection

Nine powerful AI algorithms, including logistic regression (LR), linear discriminant analysis (LDA), K neighbors (KNN), Gaussian naive Bayes (GNB), support vector machine (SVM), random forest (RF), decision tree (CRAT), gradient boosting decision tree (GBDT), and LightGBM (LGBM, leaf-wise GBDT) were evaluated for tumor detection. The area under the curve (AUC) was calculated to quantify predictive performance. Shapley additive explanation method (SHAP) was implemented to provide the model-level quantitative interpretation by evaluating the importance of each feature to the classification.

Long term OS analysis *via* GeneSet-ResNet

A two-dimensional (2-D) ResNet-18 model, called GeneSet-ResNet, was proposed in this study, where the input layers receiving 2-D pseudo-images were converted by the expression values of unique feature genes of both CLST and aCD4 that could be detected in the liver transcriptomes of HCC patients. The sample imbalance between HCC patients with long-term overall survival (LS) and those with short-term overall survival (SS) was solved using Borderline SMOTE. Repeated stratified K-fold cross-validations (splits = 10, repeats = 30, and random state = 2022) were used in the GeneSet-ResNet model. In each 10-fold cross-validation, the dataset was randomly divided into a training set (70% of the samples) for batch training and a test set (10% of the samples) for performance evaluation. The model performance was also validated using a validation set comprising 20% of the samples. In addition, excellent training results and generalization ability were achieved by employing the root-mean-square propagation (RMsprop) optimization algorithm and the learning rate decay method. Accuracy (ACC) were calculated as follows:

$$ACC = (TP + TN)/(TP + TN + FN + FP)$$

TP, true positive; FP, false positive; TN, true negative; FN, false negative.

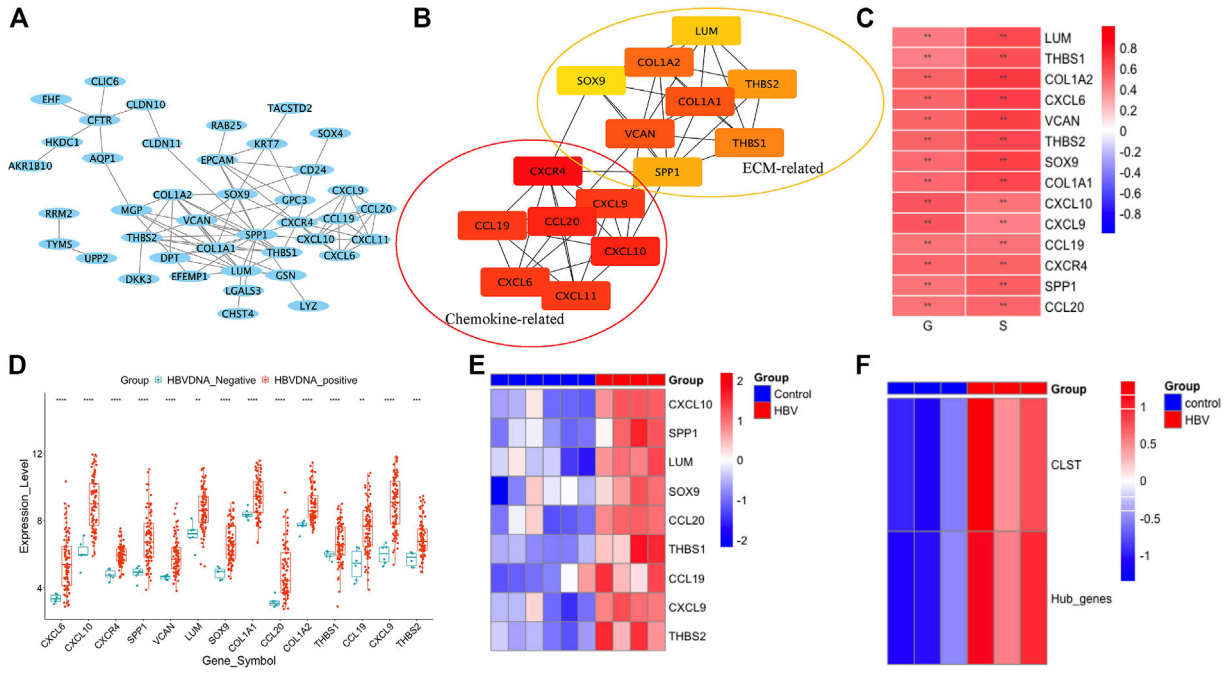

FIGURE 1
CLST identification. **(A)** PPI network of overlapping DEGs by STRING (GSE84044). **(B)** Seven chemokine-related genes and eight ECM-related genes in two groups were further identified using Cytoscape of MCODE plug-in. **(C)** Correlations among expression values of 14 hub genes, G scores, and S scores. **(D)** Dot plots of 14 GS-associated hub genes in liver samples of CHB group and control group. **(E)** Heatmap of nine hub genes in HBV-infected mice and control mice. **(F)** Heatmap showing ES of gene set comprised of 14 GS-associated hub genes and CLST in HBV-PHH and control PHH.

The area under the curve (AUC) was calculated to quantify predictive performance.

Chemotherapy sensitivity prediction

The half-maximal inhibitory concentration (IC50) for patients with HCC based on liver transcriptomes was predicted using the "calcPhenotype" algorithm provided by a ridge regression model ("oncoPredict" R package) (Maeser et al., 2021). The differences in sensitivity between first-line and emerging drugs used for HCC treatment between HBV-HCC patients in the CLST ^{high} aCD4 ^{high} subgroup and those in the CLST^{low}aCD4 ^{low} subgroup were analyzed using the Wilcoxon test. Statistical significance was set at $p < 0.05$.

Results

CLST definition

The gene expression profiles of HBV-LF were re-analyzed according to a previous study. Overlapping DEGs upregulated in S2, S3, and S4 when compared to the S0 group were selected (Supplementary Figures S2A, S2B). Chemokine signaling pathways in which cargo-carrying genes encoding CXC subfamily ligands and CCL subfamily ligands were observed to be primarily enriched (Supplementary Figures S2C, S2D). Of the overlapping DEGs, 15 hub genes belonging to the chemokine-related gene cluster and ECM-related gene cluster with the highest maximal clique centrality (MCC) score were screened (Figures 1A,B). The majority of 15 hub genes were also significantly upregulated in the G2, G3, and G4 groups compared to the G0 group (Supplementary Figures S3A–D). Fourteen hub genes that were positively associated with G and S were listed in this study as GS-associated hub genes (Figure 1C). These genes were confirmed to be upregulated in the liver tissues of HBV-infected patients (Figure 1D) and CHB patients with liver injury (Supplementary Figures S3D–E) compared to normal controls. All GS-associated hub genes were highly enriched in CHB patients at immune active (IA) phases (Liu et al., 2018) and displayed a similar expression pattern in CHB patients at immune tolerance phases (IT) and immune carrier phases (IC) (Supplementary Figure S3F). To further uncover the original inducers of GS-associated hub genes, the liver transcriptomes of HBV-infected human hepatocyte chimeric mice were analyzed. We found that GS-associated hub genes that could be detected in liver tissues of human hepatocyte

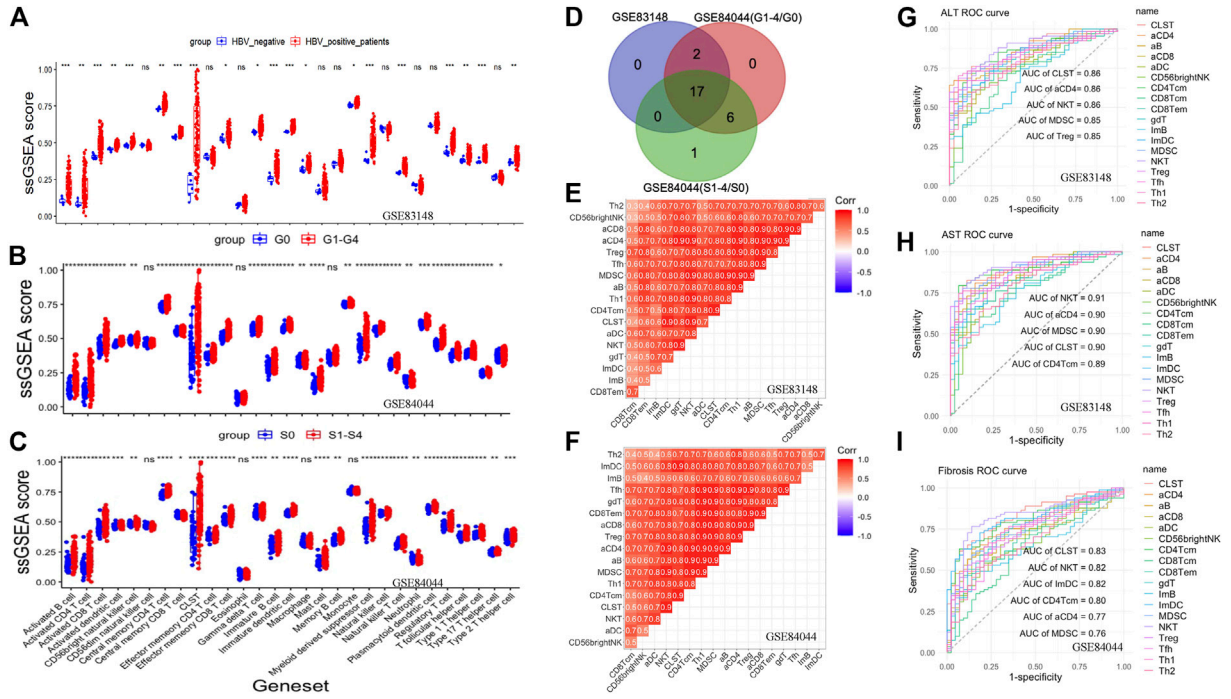

FIGURE 2
Co-enrichment and diagnostic values of CLST, NKT, MDSC, and aCD4 in CHB and HBV-LF. **(A)** Boxplot comparing immune signals between patients with chronic HBV infection and normal tissues from patients without HBV infection. **(B)** Boxplot comparing immune signals between patients with inflammation (G ≥ 1) and those without inflammation (G = 0). **(C)** Boxplot comparing immune signals between patients with liver fibrosis (S ≥ 1) and those without liver fibrosis (S = 0). **(D)** Venn diagram of upregulated LILs. **(E,F)** Correlation heatmap showing the co-enrichment pattern of CLST and LILs in CHB and HBV-LF. **(G–I)** ROC curves of CLST and LILs for predicting liver injury and LF.

chimeric mice were upregulated upon HBV infection (Figure 1E) and significantly expanded in *ex vivo* HBV-infected human primary hepatocytes (PHH) (Figure 1F). Therefore, in our study, we defined GS-associated hub genes as a gene set, including CCL19, CCL20, CXCL9, CXCL10, LUM, SOX9, SPP1, THBS1, and THBS2, named CLST.

CLST, co-expanded with LILs, could effectively predict HBV-liver inflammation and fibrosis

The host immune response plays an important role in HBV pathogenesis. Therefore, the landscape of CLST and LILs in CHB and LF is presented in this section. Both CLST and LILs were highly enriched in HBV-infected patients (Figure 2A), CHB patients with a higher score of liver inflammation that was characterized by G (Figure 2B), and with a higher score of LF that was characterized by S (Figure 2C). As shown in Figure 2D, 17 overlapping LILs, including NKT, MDSC, and activated T cells bearing CCL20 (aCD4), were screened from 28 LILs. Overlapping LILs were co-expressed with CLST in liver samples of CHB (Figure 2E) and HBV-LF (Figure 2F). Generally, we can conclude that CLST can be directly induced upon initial HBV infection and is associated with liver inflammation (G) and LF (S). All AUCs of CLST, NKT, MDSC, and activated T cells bearing CCL20 (aCD4) in predicting abnormal serum ALT/AST levels were above 0.85 (Figures 2G,H). Moreover, CLST was ranked as the leading gene set, followed by NKT, aCD4, and MDSC, which effectively segregated LF from normal liver samples (Figure 2I).

CLST synergizing with aCD4 were risk signals in HBV-HCC

The batch effect among GSE83148, GSE84044, and GSE14520 was removed by using the SVA algorithm (Supplementary Figures S4A,B). Enrichment Scores of CLST, NKT, aCD4, and MDSC were identified to be significantly higher in tumor tissues of HBV-HCC than in those without HBV in the integrated gene microarray dataset (Supplementary Figure S4C). Correlation analyses were performed in normal and tumor tissue mixed samples of two independent HBV-HCC cohorts (Figures 3A,B) and our HBV-HCC data (Figure 3C), and severe positive relationships between CLST and aCD4 were verified. In addition,

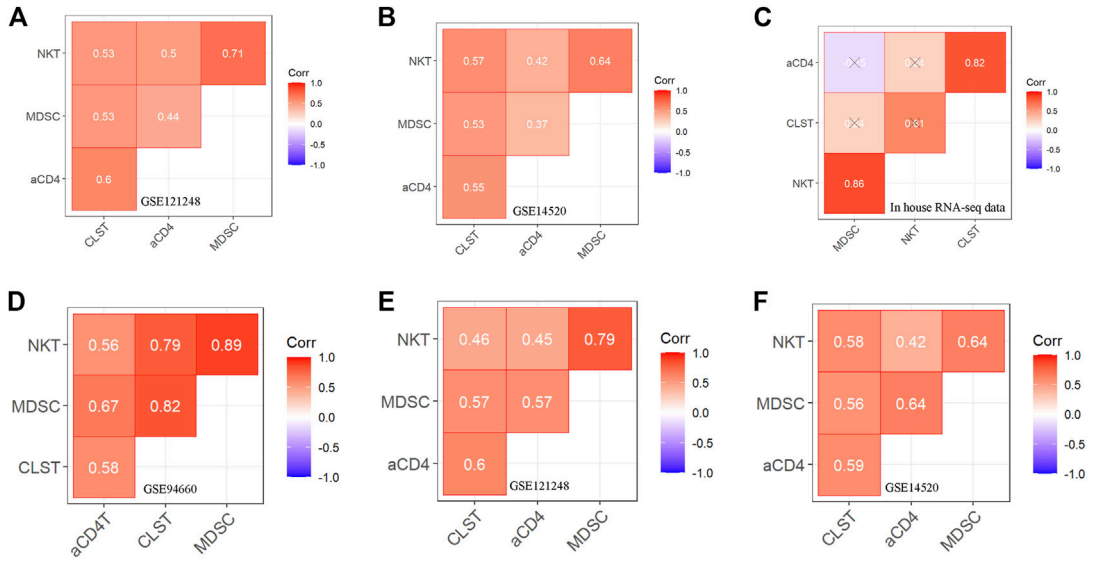

FIGURE 3
Correlation between CLST and LILs in tumor tissues of patients with HBV-HCC **(A–C)** Pearson correlation analysis showing co-enrichment among CLST, aCD4, NKT, and MDSC in liver tissues of GSE121248, GSE14520, and our in-house RNA-seq data. **(D–F)** Pearson correlation analysis showing co-enrichment among CLST, aCD4, NKT, and MDSC signals in liver tumor tissues of three independent GSE datasets.

CLST and aCD4 were significantly co-enriched in the tumor tissues of the three independent HBV-HCC cohorts (Figures 3D–F). Interestingly, positive correlations among CLST, liver-resident CD4$^+$ T naïve-like cells (CD4+$T_{LR\text{-}NL}$), acquisition of a TH17 polarization state (CD4+$T_{LR\text{-}NL}$), CD4+$T_{EM\text{-}TH1/TH17}$, and immune checkpoints (ICs) indicated their cross-talk in the tumor tissue of HBV-HCC (Figure 4A).

Additionally, PPI analysis revealed that CCL20 was the leading gene exhibiting the closest relationship with aCD4 in HBV-HCC patients (Figure 4B). Further survival analysis suggested that a higher aCD4/CLST/CCL20 was associated with significantly shorter OS (Supplementary Figure S5). The CLST^{high}aCD4^{high} (Figure 4C) and aCD4^{high}CCL20^{high} (Figure 4D) subgroups showed worse OS probabilities, highlighting the application of CLST and aCD4 for the establishment of diagnostic and prognostic models in HCC patients.

Patients with HBV-HCC in the CLST^{high}aCD4^{high} subgroup were characterized by an unfavorable status of excess nutritional usage of amino acids

As shown in Figure 5A, LYSET, ATF4, VPS18, RAB7A, SLC7A5, TGFBRAP1, and GNPTAB were previously identified as proteins involved in the nutritional utilization of amino acids (Pechincha et al., 2022; Richards et al., 2022). Surprisingly, survival analysis showed that a higher gene expression level of LYSET/ATF4/VPS18/RAB7A/SLC7A5/TGFBRAP1/GNPTAB was associated with a significantly shorter OS in HBV-HCC patients (Figures 5B–H). HBV-HCC patients in the CLST^{high}aCD4^{high} and CLST^{low}aCD4^{low} subgroups exhibited a distinct pattern of GSVA-based amino acid utilization-associated gene signature. Consistently, a higher ES of the amino acid utilization-associated gene signature represented a worse OS probability (Figure 5I). The ES of amino acid utilization-associated gene signature was found to increase in the CLST^{high}aCD4^{high} subgroup, reflecting a shorter OS (Figure 5J).

An explainable machine learning model based on feature genes belonging to CLST and aCD4 was powerful for tumor tissue detection

Nearly half of the feature genes belonging to aCD4 at higher levels were associated with a significantly shorter OS in the CHCC cohort (Supplementary Figure S6). Among them, seven genes (KIF11, CCNB1, EXO1, KNTC1, PRC1, RGS1, and CCL20) were identified as overlapping risk factors for survival in the GSE14520 cohort (data not shown). Thus, fifteen feature genes comprised of nine genes from CLST and seven genes from aCD4 were ultimately used to construct a diagnostic model for tumor tissue detection.

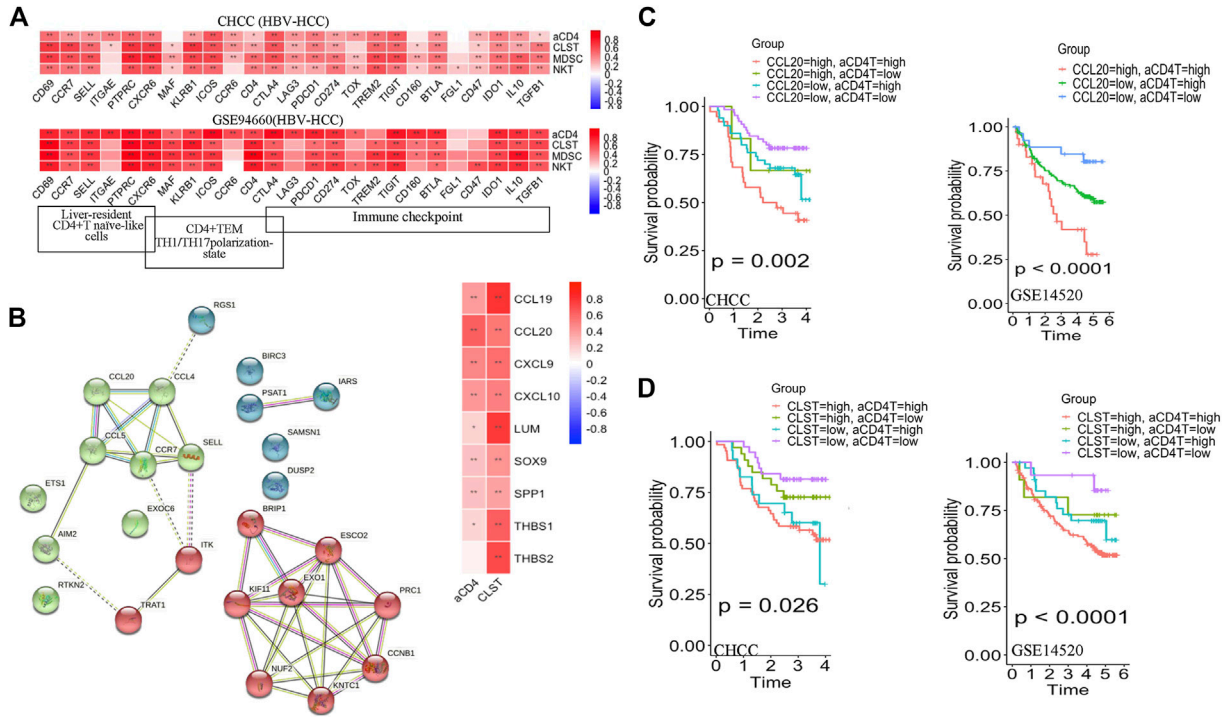

FIGURE 4
Prognostic values of CLST and aCD4 for OS prediction in HBV-HCC. **(A)** Heatmaps showing correlations between CLST, aCD4, MDSC, NKT, and specific immune genes in HBV-HCC. **(B)** PPI analysis of member genes belonging to aCD4 and correlations among aCD4, CLST, and hub gene expression values. CCL20 was an overlapping gene in both aCD4 and CLST (GSE14520). **(C,D)** KM survival analysis of OS in tumor tissues with a higher ES of both aCD4 and CCL20 or a higher ES of both aCD4 and CLST in two independent HBV-HCC cohorts. Time was calculated in years. The log-rank test for *p*-value and *p*-value <0.05 was considered significant.

Briefly, nine AI algorithms were trained and validated to separate tumor tissues from the normal liver, cirrhosis, and tumor tissues in the GSE25097 cohort. Of the nine AI algorithms, SVM outperformed in terms of the highest ACC (Supplementary Figure S7A), showed potent robustness with stratified K-fold cross-validations, and achieved the highest average AUC that could accurately separate tumor tissue from any other type of liver sample (Figures 6A,B). The efficiency of SVM was further tested in an independent HCC cohort (TCGA-LIHC), with an AUC of 0.97 (Figure 6C). SVM also was powerful in separating tumor tissues at early stage (BCLC stage 0-A) from non-tumor tissues (GSE14520) among nine AI algorithms (Supplementary Figure S7B) and achieved an average AUC of 0.99 and 0.99 with stratified K fold cross-validations (splits = 5 and 10), respectively (Figures 6D,E). The diagnostic power of SVM was also excellent in an independent test set (CHCC), with an AUC of 0.98 (Figure 6F). The SHAP summary plot suggested that CCNB1, PRC1, CCL20, KIF11, and EXO1 were the top five variables that had important impacts on the performance of SVM in the CHCC cohort (Figures 6G,H).

Deep learning model fed by feature genes from CLST and aCD4 was efficient for LS prediction

The process of generating gene expression pseudo-images and the GeneSet-ResNet architecture using resnet-18 as the backbone for LS prediction is illustrated in Figure 7A. In brief, there were 26 small squares (rows = 2, columns = 13) in each pseudo-image representing the expression value of 26 unique feature genes from one HBV-HCC sample. The sample imbalance between the LS and SS subgroups was solved using borderline SMOTE generated synthetic minority samples. The LS and SS subgroups in HBV-HCC were further classified using the GeneSet-ResNet model with gene expression pseudo-images as inputs. Model performance was evaluated in 30 repeated stratified 10-fold cross-validations. As shown in Figure 7B, an average AUC of 0.907 and ACC of 0.919 over 30 repeats of the stratified 10-fold cross-validation for LS (survival time >5 years) prediction were achieved in the CHCC-GSE14520 dataset. Interestingly, the GeneSet-ResNet model outperformed the TCGA-LIHC dataset in LS prediction (Figure 7C). These results suggest that GeneSet-ResNet, based on

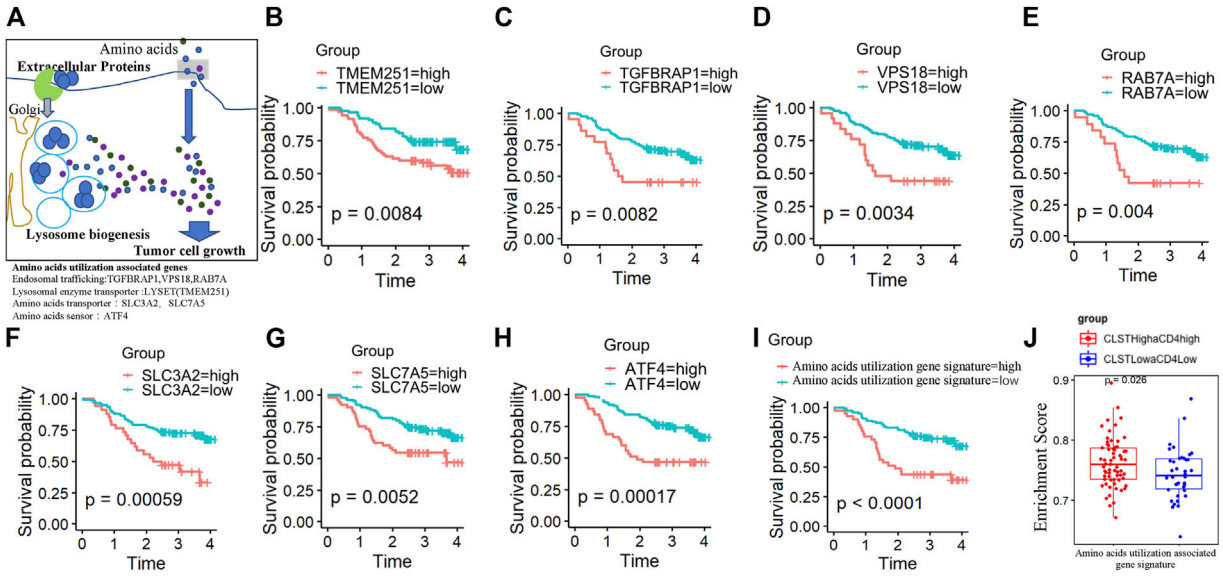

FIGURE 5
The prognostic value of nutritional utilization of the amino acid-associated gene signature in HBV-HCC **(A)** Lysosomal nutrient generation and nutritional utilization of amino acids for tumor cell growth. LYSET (TEME251), ATF4, VPS18, RAB7A, SLC7A5, TGFBRAP1, and GNPTAB were involved in this process. **(B–H)** Plots depict the KM survival curves for each nutritional utilization of amino acid-associated genes in HBV-HCC patients from the CHCC cohort divided into low and high expression groups according to the gene expression value. **(I)** KM survival curves for OS in tumor tissues of HBV-HCC patients from CHCC cohort with a high ES of the "nutritional utilization of amino acid-associated gene" signature and a low ES of the "nutritional utilization of amino acid-associated gene" signature. **(J)** Differences in the enrichment levels of the "nutritional utilization of amino acid-associated gene" signature between HBV-HCC patients from the CHCC cohort in the $CLST^{high}aCD4^{high}$ subgroup and those in the $CLST^{low}aCD4^{low}$ subgroup.

CLST and aCD4, is a robust deep learning model for 5 years LS prediction in HCC.

CLST and aCD4 guided precision anti-HBV immunotherapy and anti-cancer chemotherapy

The ESs of CLST and aCD4 in liver transcriptomes from a CHB cohort treated with IFN-α therapy were calculated, and the results indicated that CLST and aCD4 were remarkably upregulated in treatment responders (Figure 8A). These results suggest that the sensitivity of anti-HBV immunotherapy can be predicted using CLST and aCD4. The ESs of CLST and 28 LILs in the liver tissues of treatment responders pre- and post-IFN-α were also evaluated. CLST and LILs tended to be downregulated in responders after receiving PEG IFN-α (Figure 8B). Both CLST and aCD4 were significantly suppressed in paired samples with the engagement of PEG IFN-α (Figure 8C). Moreover, only aCD4 and CLST levels showed a significant positive correlation in these responders (Figure 8D). The sensitivities of the $CLST^{high}aCD4^{high}$ and $CLST^{low}aCD4^{low}$ subgroups in HBV-HCC patients to 198 anticancer chemotherapies from a resource for therapeutic biomarker discovery in cancer cells (Genomics of Drug Sensitivity in Cancer, GDSC) were compared (Supplementary Table S2; Figure 8E). HBV-HCC patients in the $CLST^{high}aCD4^{high}$ subgroup were more sensitive to the majority of anticancer drugs (167/198) than those in the $CLST^{low}aCD4^{low}$ subgroup (Figure 8E). In terms of first-line chemotherapy selection, patients in the $CLST^{high}aCD4^{high}$ subgroup were more sensitive to sorafenib (Figure 8F). Patients in the $CLST^{low}aCD4^{low}$ subgroup were more sensitive to two emerging chemotherapies: SB505124 (TGF-β receptor inhibitor) and dihydrorotenone (Figure 8F).

Discussion

Although most of the feature genes in CLST, including intrahepatic mRNA for CXCL9 (Wang et al., 2017; Jiang et al., 2021), CXCL10 (Wang et al., 2017; Singh et al., 2020; Jiang et al., 2021), CCL20 (Zhao et al., 2014), SOX9 (Xu et al., 2016; Yang et al., 2020), SPP1 (Shang et al., 2012), and LUM (Xu et al., 2016) have been reported involved in several HBV-related diseases, there are no reports systemically describing their landscape during all the stages of HBV related diseases even less the integration of these genes as a gene set for predicting liver

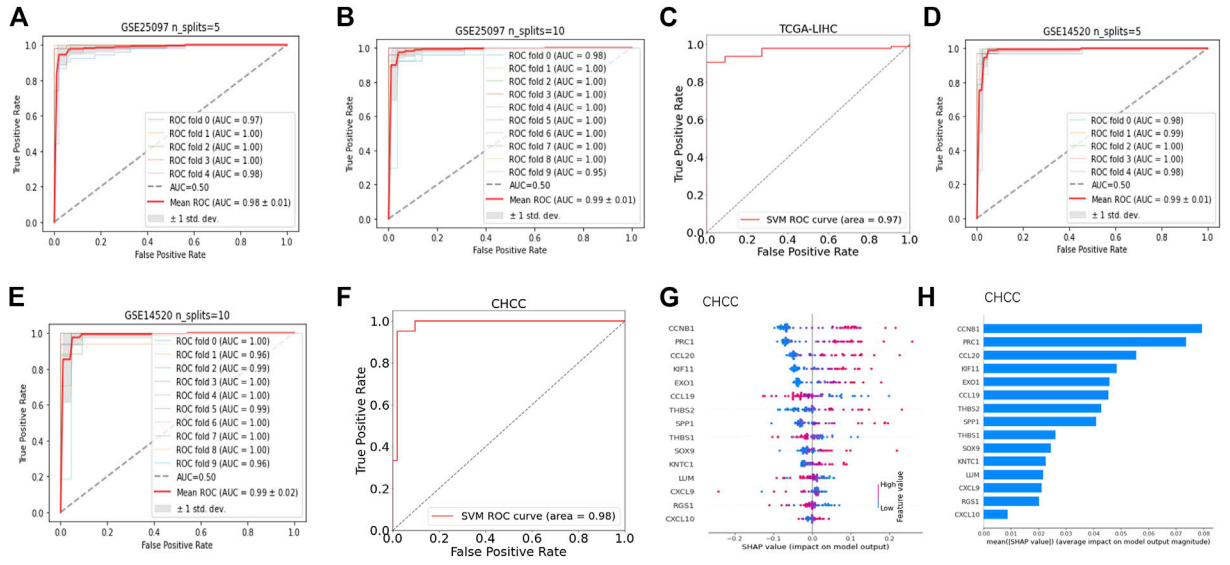

FIGURE 6
Fifteen feature genes of CLST and aCD4 were promising diagnostic signals for tumor tissue identification. **(A,B)** ROC curves of expression values of 15 feature genes for HCC tumor prediction among HCC tumor, adjacent non-tumor, cirrhotic, and normal liver samples using SVM with stratified K-fold cross-validations (n_splits = 5 and 10). **(C)** ROC curves of expression values of 15 feature genes as a diagnostic set for the separation of HCC tumors from non-tumor liver samples *via* SVM. **(D,E)** AUC of ROC curves of expression values of 15 feature genes as diagnostic markers for early-stage HBV-HCC tumor identification from non-tumor liver samples *via* SVM with stratified K-fold cross-validations (n_splits = 5 and 10). **(F)** ROC curves of expression values of 15 feature genes as diagnostic markers for separation of tumor tissues at the early stage of HBV-HCC from non-tumor liver samples in the CHCC cohort *via* SVM. **(G,H)** SHAP profiles of 15 feature genes of the outperformed SVM model in the CHCC cohort. The dot plot shows the effect of the expression value of the feature gene on the model output. The bar plot shows the decreasing average feature importance of the expression value of the 15 feature genes on the influence of the final model output for predicting tumor tissues at an early stage.

injury and LF, to our best knowledge. Host-encoding genes can serve as prognostic biomarkers in LF, and a fibrosis risk score (FRS) has been established; however, none of these studies considered global immunogenomic information in consideration (Xu et al., 2016; Zhou et al., 2017; Singh et al., 2018). "GSVA" R package is a powerful tool for analyzing and exploring the complex involvement of the immune microenvironment in larger samples (Moeini et al., 2019; Chawla et al., 2022; Martin-Serrano et al., 2022). Through GSVA, we identified hub genes associated with HBV pathogenicity and demonstrated that the CLST signal initially induced by HBV infection was co-enriched with the majority of LILs in CHB and HBV-LF patients. CLST was ranked as the leading factor for efficient diagnosis of CHB patients living with LF compared to those without LF. Interestingly, CLST and aCD4 exhibited the strongest correlation in the largest HBV-HCC cohort among multiple independent cohorts and were verified in our in-house HBV-HCC patients. These observations suggest that the CLST-aCD4 axis plays an important role in HCC pathogenesis. Mechanistically, CLST and aCD4 were found to be highly associated with both Th1/Th17 polarization and ICs in tumor tissues.

TH17 has been widely reported to be an important inflammatory factor in HCC (Bansal, 2020; Ma et al., 2020; Li et al., 2021). Recently, the expansion of liver-resident CD4+T naïve-like cells (CD4+$T_{LR\text{-}NL}$) acquiring a TH17 polarization state has been proven to be a candidate contributor to primary sclerosing cholangitis (PSC) pathogenesis (Poch et al., 2021). Immune checkpoints (ICs) are associated with poor clinical outcomes in HCC (Ma et al., 2019; Wang et al., 2019; Shen et al., 2022). Interestingly, in this study, positive correlations among CLST, CD4+$T_{LR\text{-}NL}$, CD4+$T_{EM\text{-}TH1/TH17}$, and ICs indicated their crosstalk in the tumor tissue of HBV-HCC. Th17 cells recruited *via* the CCL20-CCR6 axis in the tumor microenvironment (TME) are drivers of worse clinical outcomes (Zhang et al., 2009; Liao et al., 2013; Li et al., 2016; Li et al., 2017) and ICs have been well demonstrated to account for immunosuppressive microenvironment formation that favors anti-tumor immune evasion (Sangro et al., 2021). Our study leads to the hypothesis that CLST and aCD4 bearing CCL20 are important causes of damaged immune surveillance and TME generation. Actually, a recent study provides a solid foundation for the association between CCL20 and TME and it will be promising for further study in HBV related diseases (Fan et al., 2022). Correspondingly, a higher ES of CLST or aCD4 implies a shorter OS. We provide insights into the 25 member genes of aCD4 and highlight that nearly half of these genes are significantly associated with worse survival rates. Obviously, aCD4 could be referred to as a special CD4+T cell subset at the station of activation. Currently, novel functional immune

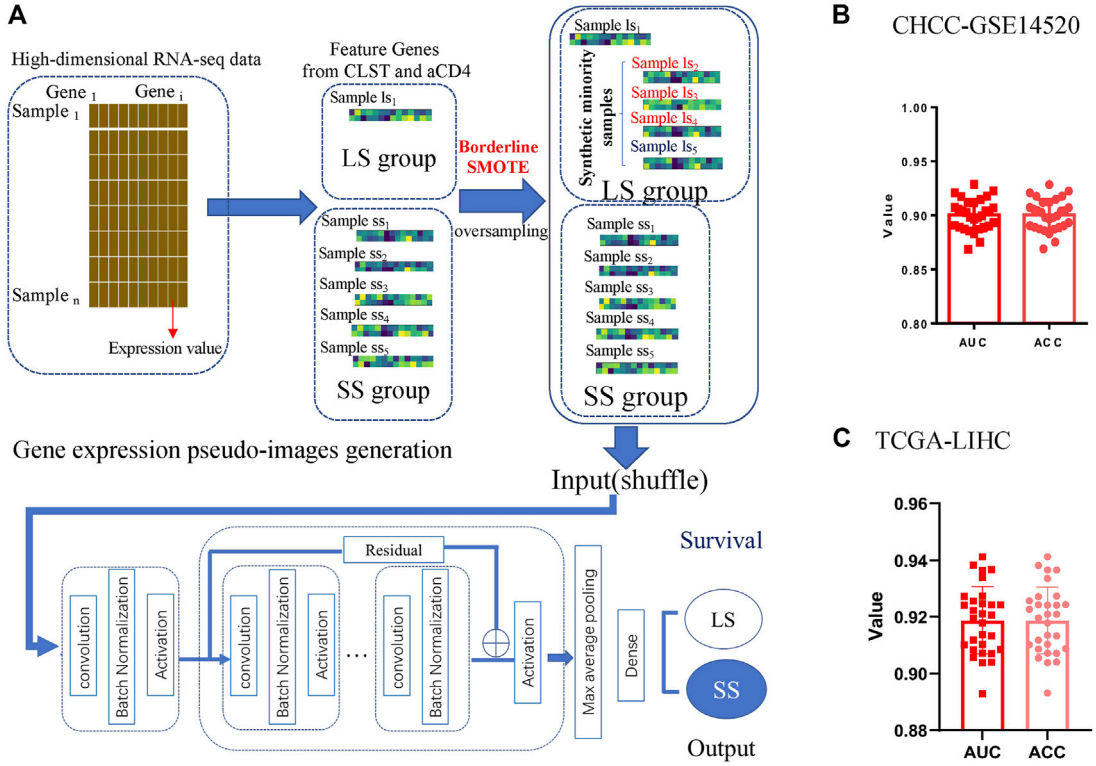

FIGURE 7
Unique feature genes belonging to CLST and aCD4 were promising prognostic signals in LS prediction. **(A)** Process of LS prediction in HCC patients (generation of gene expression pseudo-images with CLST and aCD4, oversampling with synthetic minority samples, input layer, detailed architecture of the deep residual network module, and output layer for LS status prediction). **(B)** The average AUC and ACC values of 30 repeats for LS status (>5 years) prediction in HBV-HCC patients. **(C)** The average AUC and ACC values of 30 repeats for LS status (>5 years) prediction in HCC patients.

subsets at the single-cell level resolution have been studied (Song et al., 2020; Lian et al., 2022) and the definition of aCD4 in HBV-related diseases is worthy of further exploration.

Further research in this study also highlights that HBV-HCC patients with dual higher ES of both CLST and aCD4 predict worse overall survival. To uncover the underlying mechanism, we focused on the characteristics of the amino acid utilization system in $CLST^{high}aCD4^{high}$ and $CLST^{low}aCD4^{low}$ subgroups. Non-glucose nutrients, such as amino acids, lactate, acetate, and macromolecules, can also be absorbed by cancer cells as alternative energy sources (Kamphorst et al., 2015; Pechincha et al., 2022). Both the macropinocytosis and lysosomal catabolic signaling pathways in malignant tumor cells are activated in nutrient-deficient environments (Commisso et al., 2013; Kamphorst et al., 2015; Palm et al., 2015; Pechincha et al., 2022). The increased activity of extracellular protein uptake and lysosomal breakdown constitute an alternative source of amino acids that enables cancer cell growth (Pechincha et al., 2022). Interestingly, we found that each amino acid utilization-associated gene represents a risk factor that affects the clinical outcome of HBV-HCC patients. A lower ES of amino acid utilization associated gene signature in HBV-HCC patients is beneficial for improving survival. We propose that unfavorable nutritional utilization of amino acids may be a potent carcinogenic factor for HCC progression, and the potential link between excess amino acid usage and a dysregulated immune microenvironment according to CLST and aCD4 still requires further experimental exploration.

Dual higher ES of both CLST and aCD4 was critical for the poor progression of HBV-HCC, implying the potential role of CLST/aCD4 interaction in promoting poor clinical outcomes. To test the potential value of CLST and aCD4 in the construction of prognostic models, we present a methodology to compare survival rates for the first time. The survival-sensitive deep residual neural network model based on these two gene sets, named GeneSet-ResNet, outperformed the deep residual neural network classifier in 5 years of LS prediction in liver cancer. This model takes the expression values of low-dimensional feature genes belonging to immunogenomic gene sets as inputs. The gene expression pseudo-images generated in this study were simpler than ever (Hao et al., 2018; Oh et al., 2021; Wang et al., 2022) and hold promising predictive values, thus providing a perspective on their future use in other cancer types.

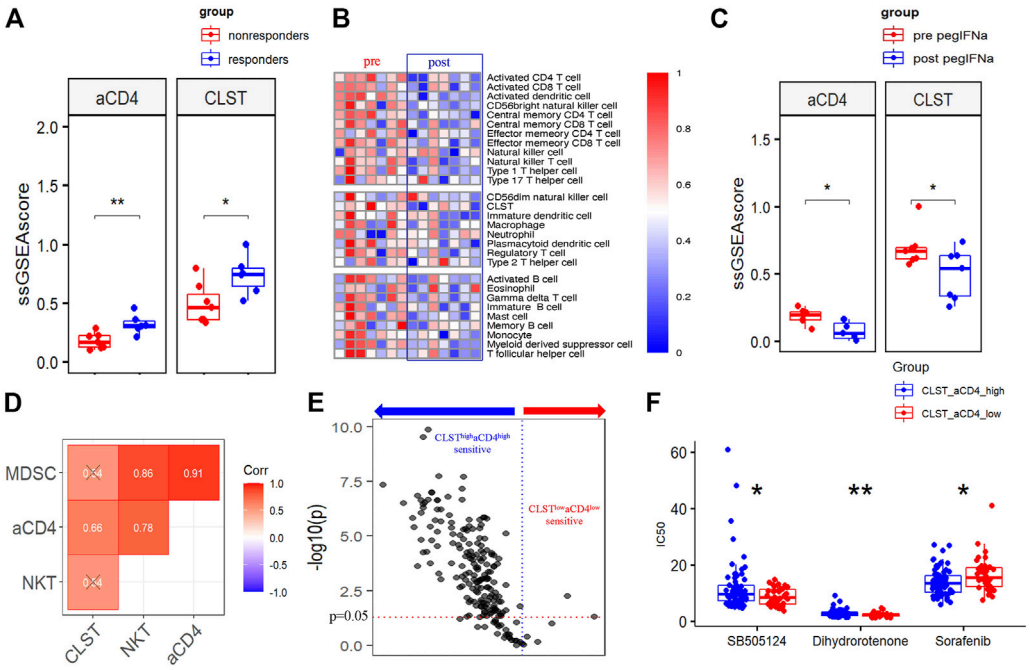

FIGURE 8
CLST and aCD4 were involved in drug sensitivity to anti-HBV immunotherapy and anti-cancer chemotherapies. **(A)** Comparisons of CLST and aCD4 between PEG IFN-α treatment responders and non-responders (GSE27555). **(B)** Heatmaps showing differences in liver samples from HBV-infected patients pre and post PEG-IFN-α treatment (GSE66698). **(C)** Boxplot of pairwise comparisons of CLST, aCD4, NKT, and MDSC between the control group and PEG IFN-α-treated group (GSE66698). **(D)** Correlations among CLST, aCD4, NKT, and MDSC in PEG IFN-α-treated liver samples (GSE66698). **(E)** Volcano plot of the sensitivity of HBV-HCC patients in the $CLST^{high}aCD4^{high}$ subgroup and $CLST^{low}aCD4^{low}$ subgroup to 198 anti-cancer drugs. **(F)** Comparisons of the sensitivity to first-line chemotherapy (sorafenib) and emerging chemotherapies (SB505124, dihydrorotenone) between the $CLST^{high}aCD4^{high}$ subgroup and $CLST^{low}aCD4^{low}$ subgroup (CHCC).

Fifteen feature genes from CLST and aCD4 were incorporated to perform nine AI algorithms with K-fold cross-validation to detect tumor tissues in HCC. The SVM-derived model was built and worked robustly with high accuracy and a powerful AUC in both training cohorts and independent test cohorts. Our bioinformatics analysis indicated that CLST and aCD4 are powerful diagnostic and prognostic signals across all stages of HBV infection that are suitable for constructing AI models in HCC. There is an urgent need for robust tools to detect tumors at an early stage and predict tumor-related death due to the limitation of efficient HCC treatments, and the AI models developed in this study will facilitate the improvement of clinical management and precision medicine.

PEG IFN-α treatment has the potential to prevent advanced HBV-LF and HBV-HCC occurrence in responders (Liang et al., 2016; Ye and Chen, 2021). The liver transcriptomes of HBV patients receiving standard PEG IFN-α were analyzed to test whether first-line therapy exerts an anti-HBV effect by modulating CLST and aCD4 signals. Correspondingly, CLST and aCD4 were significantly suppressed in responders to PEG IFN-α. These findings suggest that the impact of PEG-IFN-α on improving liver function and inhibiting disease progression during HBV infection is closely related to the CLST-aCD4 axis, which requires further experimental verification. HCC is resistant to current therapies (Song et al., 2021; Rai and Mukherjee, 2022; Xia et al., 2022; Zhang et al., 2022), and a novel strategy that considers the immunology of the disease to improve treatment remains important (Donne and Lujambio, 2022; Rai and Mukherjee, 2022; Shen et al., 2022). Significant differences in sorafenib response between the $CLST^{high}aCD4^{high}$ and $CLST^{low}aCD4^{low}$ subgroups illustrated that CLST and aCD4 might be important biomarkers for optimizing the use of multi-kinase inhibitors for precision HCC treatment. More importantly, TGF-β inhibition therapies may constitute a promising option for treating HCC in the future. Employing the CLST-aCD4 signal as a predictor allows the appropriate selection of HCC patients that could benefit from interrupting the TGF-β/TβR signaling pathway.

In conclusion, *via* GSVA and AI, our study provides a comprehensive understanding of immune microenvironment-related gene characteristics involved in HBV infection and detect subtle clues for clinical management of HBV-related HCC, providing basis for precision medicine.

There are still limitations in our current study. Although a large number of web accessible high throughput data were enrolled in this

study, more experiments are needed for further validation before clinical application of CLST/aCD4 signals in HBV related diseases. The current study only focuses on the clinical application of immunosignals in precision medicine of HBV-related liver diseases, and their specific in HCC at pan-cancer level are promising in further research.

Data availability statement

The original contributions presented in the study are included in the article/Supplementary Material, further inquiries can be directed to the corresponding authors.

Ethics statement

The studies involving human participants were reviewed and approved by the Ethics Committee of Shanghai Public Health Clinical Center affiliated to Fudan University (SPHCC). The patients/participants provided their written informed consent to participate in this study.

Author contributions

JH, LC, and GD supervised the project. JH and CZ designed the workflow of the research. CZ, XZ, QZ, and LC collected the web accessible data from GEO, NODE, and TCGA databases. JH, CZ, YZ, and QZ performed the analysis and interpretation of original date. JH, GD, CZ, and LC were participated in writing and editing the manuscript.

Funding

This work was funded by National Natural Science Foundation of China (No. 8190120757) and Key Research and Development Program of Henan Province (No. 222102310622).

Acknowledgments

We thank Jiaming Zeng (University of Macau) and all the members of his bioinformatics team for generously sharing their experiences.

Conflict of interest

The authors declare that the research was conducted in the absence of any commercial or financial relationships that could be construed as a potential conflict of interest.

Publisher's note

Supplementary material

The Supplementary Material for this article can be found online at: https://www.frontiersin.org/articles/10.3389/fphar.2022.1079566/full#supplementary-material

SUPPLEMENTARY FIGURE S1
Detailed steps of the study.

SUPPLEMENTARY FIGURE S2
Venn diagram and functional annotation of DEGs in HBV-LF. **(A)** Histogram bar chart of upregulated DEGs at differential S were drawn using GraphPad Prism (GSE84044). **(B)** The Venn diagram of overlapping upregulated DEGs among S2/S0, S3/S0, and S4/S0 performed by online tool http://bioinformatics.psb.ugent.be/webtools/Venn/. **(C)** Visualization of GO analysis of 64 DEGs and extracellular matrix (ECM) with the most counts and lowest p value. MF: molecular function. CC, cellular component; BP,biological process. **(D)** Visualization of KEGG pathway analysis. Chemokine signaling pathway was highly enriched.

SUPPLEMENTARY FIGURE S3
Validation of GS associated hub genes in HBV-LF and CHB. **(A-C)** Volcano plots illustrate hub genes that upregulated in G2, G3, and G4 when compared to the G0 group (GSE84044). **(D,E)** Volcano plot performed by "EnhancedVolcano" R package showing 14 GS associated hub genes were upregulated in HBV patients with abnormal ALT and AST when compared to HBV patients with normal ALT and AST, respectively (GSE83148). **(F)** Heatmap of GS associated hub genes in CHB patients at IC, IT, and IA phases (GSE65359).

SUPPLEMENTARY FIGURE S4
Comparisons of immune signals in tumor tissues with HBV and normal tissues without HBV. "SVA" R package was utilized to merge and normalize three microarray datasets (GSE83148, GSE84044, and GSE14520). Batch effects were visualized using PCA algorithm before **(A)** and after removing **(B)** *via* the ComBat function provided by "SVA" R package. **(C)** Boxplot of comparisons of immune signals in HBV-tumor tissue samples and normal samples without HBV infection in combined data.

SUPPLEMENTARY FIGURE S5
Kaplan-Meier (KM) survival analysis. Kaplan-Meier (KM) survival plot for patients according to aCD4 and CLST in HCC (GSE14520).KM analysis of CCL20 in tumor tissues from HBV-HCC patients for OS in two independent cohorts (CHCC, left; GSE14520, right).

SUPPLEMENTARY FIGURE S6
OS analysis of feature genes belonging to aCD4. The association between each of feature genes belonging to aCD4 and OS probability in HBV-HCC tumor tissues (CHCC). Time was calculated by year.

SUPPLEMENTARY FIGURE S7
SVM outperformed in nine AI algorithms for HCC tumor tissue identification. **(A)**Comparison of nine AI algorithms based on expression value of 15 feature genes as a prognostic set with ACC calculation for HCC tumor identification among HCC tumor, adjacent non-tumor, cirrhotic and healthy liver samples (GSE25097). **(B)** Comparison expression value of fifteen feature genes based on nine AI algorithms with ACC calculation for predicting tumor tissue at early stage of HCC (GSE14520).

References

Aran, D., Hu, Z., and Butte, A. J. (2017). xCell: digitally portraying the tissue cellular heterogeneity landscape. *Genome Biol.* 18 (1), 220. doi:10.1186/s13059-017-1349-1

Bansal, R. (2020). Battling IL-17, the troublemaker in alcohol-induced hepatocellular carcinoma. *J. Hepatol.* 72 (5), 809–812. doi:10.1016/j.jhep.2020.02.011

Barbie, D. A., Tamayo, P., Boehm, J. S., Kim, S. Y., Moody, S. E., Dunn, I. F., et al. (2009). Systematic RNA interference reveals that oncogenic KRAS-driven cancers require TBK1. *Nature* 462 (7269), 108–112. doi:10.1038/nature08460

Charoentong, P., Finotello, F., Angelova, M., Mayer, C., Efremova, M., Rieder, D., et al. (2017). Pan-cancer immunogenomic analyses reveal genotype-immunophenotype relationships and predictors of response to checkpoint blockade. *Cell Rep.* 18 (1), 248–262. doi:10.1016/j.celrep.2016.12.019

Chawla, S., Rockstroh, A., Lehman, M., Ratther, E., Jain, A., Anand, A., et al. (2022). Gene expression based inference of cancer drug sensitivity. *Nat. Commun.* 13 (1), 5680. doi:10.1038/s41467-022-33291-z

Chen, Y., Qian, B., Sun, X., Kang, Z., Huang, Z., Ding, Z., et al. (2021). Sox9/INHBB axis-mediated crosstalk between the hepatoma and hepatic stellate cells promotes the metastasis of hepatocellular carcinoma. *Cancer Lett.* 499, 243–254. doi:10.1016/j.canlet.2020.11.025

Christou, C. D., and Tsoulfas, G. (2021). Challenges and opportunities in the application of artificial intelligence in gastroenterology and hepatology. *World J. Gastroenterol.* 27 (37), 6191–6223. doi:10.3748/wjg.v27.i37.6191

Commisso, C., Davidson, S. M., Soydaner-Azeloglu, R. G., Parker, S. J., Kamphorst, J. J., Hackett, S., et al. (2013). Macropinocytosis of protein is an amino acid supply route in Ras-transformed cells. *Nature* 497 (7451), 633–637. doi:10.1038/nature12138

da Costa, A. N., Plymoth, A., Santos-Silva, D., Ortiz-Cuaran, S., Camey, S., Guilloreau, P., et al. (2015). Osteopontin and latent-TGF beta binding-protein 2 as potential diagnostic markers for HBV-related hepatocellular carcinoma. *Int. J. Cancer* 136 (1), 172–181. doi:10.1002/ijc.28953

Damrauer, J. S., Smith, M. A., Walter, V., Thennavan, A., Mose, L. E., Selitsky, S. R., et al. (2021). Genomic characterization of rare molecular subclasses of hepatocellular carcinoma. *Commun. Biol.* 4 (1), 1150. doi:10.1038/s42003-021-02674-1

Danaher, P., Warren, S., Dennis, L., D'Amico, L., White, A., Disis, M. L., et al. (2017). Gene expression markers of tumor infiltrating leukocytes. *J. Immunother. Cancer* 5, 18. doi:10.1186/s40425-017-0215-8

Deng, L., Lu, D., Bai, Y., Wang, Y., Bu, H., and Zheng, H. (2019). Immune profiles of tumor microenvironment and clinical prognosis among women with triple-negative breast cancer. *Cancer Epidemiol. Biomarkers Prev.* 28 (12), 1977–1985. doi:10.1158/1055-9965.EPI-19-0469

Donne, R., and Lujambio, A. (2022). The liver cancer immune microenvironment: Therapeutic implications for hepatocellular carcinoma. *Hepatology*. Epub ahead of print. doi:10.1002/hep.32740

Fan, T., Li, S., Xiao, C., Tian, H., Zheng, Y., Liu, Y., et al. (2022). CCL20 promotes lung adenocarcinoma progression by driving epithelial-mesenchymal transition. *Int. J. Biol. Sci.* 18 (11), 4275–4288. doi:10.7150/ijbs.73275

Fanning, G. C., Zoulim, F., Hou, J., and Bertoletti, A. (2019). Therapeutic strategies for Hepatitis B virus infection: Towards a cure. *Nat. Rev. Drug Discov.* 18 (11), 827–844. doi:10.1038/s41573-019-0037-0

Finotello, F., and Trajanoski, Z. (2018). Quantifying tumor-infiltrating immune cells from transcriptomics data. *Cancer Immunol. Immunother.* 67 (7), 1031–1040. doi:10.1007/s00262-018-2150-z

Gong, J., Li, R., Chen, Y., Zhuo, Z., Chen, S., Cao, J., et al. (2021). HCC subtypes based on the activity changes of immunologic and hallmark gene sets in tumor and nontumor tissues. *Brief. Bioinform.* 22 (5), bbaa427. doi:10.1093/bib/bbaa427

Hanzelmann, S., Castelo, R., and Guinney, J. (2013). Gsva: Gene set variation analysis for microarray and RNA-seq data. *BMC Bioinforma.* 14, 7. doi:10.1186/1471-2105-14-7

Hao, J., Kim, Y., Kim, T. K., and Kang, M. (2018). PASNet: Pathway-associated sparse deep neural network for prognosis prediction from high-throughput data. *BMC Bioinforma.* 19 (1), 510. doi:10.1186/s12859-018-2500-z

Howell, J., Pedrana, A., Schroeder, S. E., Scott, N., Aufegger, L., Atun, R., et al. (2020). A global investment framework for the elimination of Hepatitis B. *J. Hepatol.* 74, 535–549. doi:10.1016/j.jhep.2020.09.013

Hu, X., Ni, Y., Wang, F., Ni, Z., Jin, T., Li, Y., et al. (2021). Identification of molecular mechanisms for achieving HIV-1 control in the absence of antiretroviral therapy. *Life Sci.* 265, 118857. doi:10.1016/j.lfs.2020.118857

Jiang, Y., Qin, S., Wei, X., Liu, X., Guan, J., Zhu, H., et al. (2021). Highly activated TRAIL(+) CD56(bright) NK cells are associated with the liver damage in HBV-LC patients. *Immunol. Lett.* 232, 9–19. doi:10.1016/j.imlet.2020.12.008

Kamphorst, J. J., Nofal, M., Commisso, C., Hackett, S. R., Lu, W., Grabocka, E., et al. (2015). Human pancreatic cancer tumors are nutrient poor and tumor cells actively scavenge extracellular protein. *Cancer Res.* 75 (3), 544–553. doi:10.1158/0008-5472.CAN-14-2211

Kramvis, A., Chang, K. M., Dandri, M., Farci, P., Glebe, D., Hu, J., et al. (2022). A roadmap for serum biomarkers for Hepatitis B virus: Current status and future outlook. *Nat. Rev. Gastroenterol. Hepatol.* 19 (11), 727–745. doi:10.1038/s41575-022-00649-z

Le Berre, C., Sandborn, W. J., Aridhi, S., Devignes, M. D., Fournier, L., Smail-Tabbone, M., et al. (2020). Application of artificial intelligence to gastroenterology and hepatology. *Gastroenterology* 158 (1), 76–94. doi:10.1053/j.gastro.2019.08.058

Levrero, M., Subic, M., Villeret, F., and Zoulim, F. (2018). Perspectives and limitations for nucleo(t)side analogs in future HBV therapies. *Curr. Opin. Virol.* 30, 80–89. doi:10.1016/j.coviro.2018.04.006

Li, J., Sung, C. Y., Lee, N., Ni, Y., Pihlajamaki, J., Panagiotou, G., et al. (2016). Probiotics modulated gut microbiota suppresses hepatocellular carcinoma growth in mice. *Proc. Natl. Acad. Sci. U. S. A.* 113 (9), E1306–E1315. doi:10.1073/pnas.1518189113

Li, K., Liu, H., and Guo, T. (2017). Th17/Treg imbalance is an indicator of liver cirrhosis process and a risk factor for HCC occurrence in HBV patients. *Clin. Res. Hepatol. Gastroenterol.* 41 (4), 399–407. doi:10.1016/j.clinre.2016.12.004

Li, N., Yamamoto, G., Fuji, H., and Kisseleva, T. (2021). Interleukin-17 in liver disease pathogenesis. *Semin. Liver Dis.* 41 (4), 507–515. doi:10.1055/s-0041-1730926

Lian, Q., Zhang, K., Zhang, Z., Duan, F., Guo, L., Luo, W., et al. (2022). Differential effects of macrophage subtypes on SARS-CoV-2 infection in a human pluripotent stem cell-derived model. *Nat. Commun.* 13 (1), 2028. doi:10.1038/s41467-022-29731-5

Liang, K. H., Hsu, C. W., Chang, M. L., Chen, Y. C., Lai, M. W., and Yeh, C. T. (2016). Peginterferon is superior to nucleos(t)ide analogues for prevention of hepatocellular carcinoma in chronic hepatitis B. *J. Infect. Dis.* 213 (6), 966–974. doi:10.1093/infdis/jiv547

Liao, R., Sun, J., Wu, H., Yi, Y., Wang, J. X., He, H. W., et al. (2013). High expression of IL-17 and IL-17RE associate with poor prognosis of hepatocellular carcinoma. *J. Exp. Clin. Cancer Res.* 32, 3. doi:10.1186/1756-9966-32-3

Liu, H., Li, F., Zhang, X., Yu, J., Wang, J., Jia, J., et al. (2018). Differentially expressed intrahepatic genes contribute to control of hepatitis B virus replication in the inactive carrier phase. *J. Infect. Dis.* 217 (7), 1044–1054. doi:10.1093/infdis/jix683

Liu, W., Liu, X., Peng, M., Chen, G. Q., Liu, P. H., Cui, X. W., et al. (2021). Artificial intelligence for hepatitis evaluation. *World J. Gastroenterol.* 27 (34), 5715–5726. doi:10.3748/wjg.v27.i34.5715

Liu, X., Lu, J., Zhang, G., Han, J., Zhou, W., Chen, H., et al. (2021). A machine learning approach yields a multiparameter prognostic marker in liver cancer. *Cancer Immunol. Res.* 9 (3), 337–347. doi:10.1158/2326-6066.CIR-20-0616

Long, J., Wang, A., Bai, Y., Lin, J., Yang, X., Wang, D., et al. (2019). Development and validation of a TP53-associated immune prognostic model for hepatocellular carcinoma. *EBioMedicine* 42, 363–374. doi:10.1016/j.ebiom.2019.03.022

Ma, H. Y., Yamamoto, G., Xu, J., Liu, X., Karin, D., Kim, J. Y., et al. (2020). IL-17 signaling in steatotic hepatocytes and macrophages promotes hepatocellular carcinoma in alcohol-related liver disease. *J. Hepatol.* 72 (5), 946–959. doi:10.1016/j.jhep.2019.12.016

Ma, J., Zheng, B., Goswami, S., Meng, L., Zhang, D., Cao, C., et al. (2019). PD1(Hi) CD8(+) T cells correlate with exhausted signature and poor clinical outcome in hepatocellular carcinoma. *J. Immunother. Cancer* 7 (1), 331. doi:10.1186/s40425-019-0814-7

Maeser, D., Gruener, R. F., and Huang, R. S. (2021). oncoPredict: an R package for predicting *in vivo* or cancer patient drug response and biomarkers from cell line screening data. *Brief. Bioinform.* 22 (6), bbab260. doi:10.1093/bib/bbab260

Martin-Serrano, M. A., Kepecs, B., Torres-Martin, M., Bramel, E. R., Haber, P. K., Merritt, E., et al. (2022). Novel microenvironment-based classification of intrahepatic cholangiocarcinoma with therapeutic implications. *Gut* 2021, 326514. doi:10.1136/gutjnl-2021-326514

Martinez, B. A., Shrotri, S., Kingsmore, K. M., Bachali, P., Grammer, A. C., and Lipsky, P. E. (2022). Machine learning reveals distinct gene signature profiles in lesional and nonlesional regions of inflammatory skin diseases. *Sci. Adv.* 8 (17), eabn4776. doi:10.1126/sciadv.abn4776

Moeini, A., Torrecilla, S., Tovar, V., Montironi, C., Andreu-Oller, C., Peix, J., et al. (2019). An immune gene expression signature associated with development of human hepatocellular carcinoma identifies mice that respond to chemopreventive agents. *Gastroenterology* 157 (5), 1383–1397. doi:10.1053/j.gastro.2019.07.028

Newman, A. M., Liu, C. L., Green, M. R., Gentles, A. J., Feng, W., Xu, Y., et al. (2015). Robust enumeration of cell subsets from tissue expression profiles. *Nat. Methods* 12 (5), 453–457. doi:10.1038/nmeth.3337

Oh, J. H., Choi, W., Ko, E., Kang, M., Tannenbaum, A., and Deasy, J. O. (2021). PathCNN: Interpretable convolutional neural networks for survival prediction and pathway analysis applied to glioblastoma. *Bioinformatics* 37 (1), i443–i450. doi:10.1093/bioinformatics/btab285

Palm, W., Park, Y., Wright, K., Pavlova, N. N., Tuveson, D. A., and Thompson, C. B. (2015). The utilization of extracellular proteins as nutrients is suppressed by mTORC1. *Cell* 162 (2), 259–270. doi:10.1016/j.cell.2015.06.017

Pechincha, C., Groessl, S., Kalis, R., de Almeida, M., Zanotti, A., Wittmann, M., et al. (2022). Lysosomal enzyme trafficking factor LYSET enables nutritional usage of extracellular proteins. *Science* 378 (6615), eabn5637. doi:10.1126/science.abn5637

Petrizzo, A., Mauriello, A., Tornesello, M. L., Buonaguro, F. M., Tagliamonte, M., and Buonaguro, L. (2018). Cellular prognostic markers in hepatitis-related hepatocellular carcinoma. *Infect. Agent. Cancer* 13, 10. doi:10.1186/s13027-018-0183-8

Poch, T., Krause, J., Casar, C., Liwinski, T., Glau, L., Kaufmann, M., et al. (2021). Single-cell atlas of hepatic T cells reveals expansion of liver-resident naive-like CD4(+) T cells in primary sclerosing cholangitis. *J. Hepatol.* 75 (2), 414–423. doi:10.1016/j.jhep.2021.03.016

Rai, V., and Mukherjee, S. (2022). Targets of immunotherapy for hepatocellular carcinoma: An update. *World J. Hepatol.* 14 (1), 140–157. doi:10.4254/wjh.v14.i1.140

Rehermann, B. (2013). Pathogenesis of chronic viral hepatitis: Differential roles of T cells and NK cells. *Nat. Med.* 19 (7), 859–868. doi:10.1038/nm.3251

Richards, C. M., Jabs, S., Qiao, W., Varanese, L. D., Schweizer, M., Mosen, P. R., et al. (2022). The human disease gene LYSET is essential for lysosomal enzyme transport and viral infection. *Science* 378 (6615), eabn5648. doi:10.1126/science.abn5648

Sangro, B., Sarobe, P., Hervas-Stubbs, S., and Melero, I. (2021). Advances in immunotherapy for hepatocellular carcinoma. *Nat. Rev. Gastroenterol. Hepatol.* 18 (8), 525–543. doi:10.1038/s41575-021-00438-0

Sarin, S. K., Kumar, M., Eslam, M., George, J., Al Mahtab, M., Akbar, S. M. F., et al. (2020). Liver diseases in the asia-pacific region: A lancet gastroenterology & hepatology commission. *Lancet. Gastroenterol. Hepatol.* 5 (2), 167–228. doi:10.1016/S2468-1253(19)30342-5

Shang, S., Plymoth, A., Ge, S., Feng, Z., Rosen, H. R., Sangrajrang, S., et al. (2012). Identification of osteopontin as a novel marker for early hepatocellular carcinoma. *Hepatology* 55 (2), 483–490. doi:10.1002/hep.24703

Shen, S., Wang, G., Zhang, R., Zhao, Y., Yu, H., Wei, Y., et al. (2019). Development and validation of an immune gene-set based Prognostic signature in ovarian cancer. *EBioMedicine* 40, 318–326. doi:10.1016/j.ebiom.2018.12.054

Shen, W., Chen, Y., Lei, P., Sheldon, M., Sun, Y., Yao, F., et al. (2022). Immunotherapeutic approaches for treating hepatocellular carcinoma. *Cancers (Basel)* 14 (20), 5013. doi:10.3390/cancers14205013

Shen, Y., Xu, L.-r., Tang, X., Lin, C.-p., Yan, D., Xue, S., et al. (2021). Identification of potential therapeutic targets for atherosclerosis by analysing the gene signature related to different immune cells and immune regulators in atheromatous plaques. *BMC Med. Genomics* 14 (1), 145. doi:10.1186/s12920-021-00991-2

Singh, A. K., Rooge, S. B., Varshney, A., Vasudevan, M., Bhardwaj, A., Venugopal, S. K., et al. (2018). Global microRNA expression profiling in the liver biopsies of Hepatitis B virus-infected patients suggests specific microRNA signatures for viral persistence and hepatocellular injury. *Hepatology* 67 (5), 1695–1709. doi:10.1002/hep.29690

Singh, K. P., Zerbato, J. M., Zhao, W., Braat, S., Deleage, C., Tennakoon, G. S., et al. (2020). Intrahepatic CXCL10 is strongly associated with liver fibrosis in HIV-Hepatitis B co-infection. *PLoS Pathog.* 16 (9), e1008744. doi:10.1371/journal.ppat.1008744

Song, G., Shi, Y., Zhang, M., Goswami, S., Afridi, S., Meng, L., et al. (2020). Global immune characterization of HBV/HCV-related hepatocellular carcinoma identifies macrophage and T-cell subsets associated with disease progression. *Cell Discov.* 6 (1), 90. doi:10.1038/s41421-020-00214-5

Song, J. S., Chang, C. C., Wu, C. H., Dinh, T. K., Jan, J. J., Huang, K. W., et al. (2021). A highly selective and potent CXCR4 antagonist for hepatocellular carcinoma treatment. *Proc. Natl. Acad. Sci. U. S. A.* 118 (13), e2015433118. doi:10.1073/pnas.2015433118

Subramanian, A., Tamayo, P., Mootha, V. K., Mukherjee, S., Ebert, B. L., Gillette, M. A., et al. (2005). Gene set enrichment analysis: A knowledge-based approach for interpreting genome-wide expression profiles. *Proc. Natl. Acad. Sci. U. S. A.* 102 (43), 15545–15550. doi:10.1073/pnas.0506580102

Tang, K., Ji, X., Zhou, M., Deng, Z., Huang, Y., Zheng, G., et al. (2021). Rank-in: Enabling integrative analysis across microarray and RNA-seq for cancer. *Nucleic Acids Res.* 49 (17), e99. doi:10.1093/nar/gkab554

Tao, K., Bian, Z., Zhang, Q., Guo, X., Yin, C., Wang, Y., et al. (2020). Machine learning-based genome-wide interrogation of somatic copy number aberrations in circulating tumor DNA for early detection of hepatocellular carcinoma. *EBioMedicine* 56, 102811. doi:10.1016/j.ebiom.2020.102811

Thakur, A., Liang, L., Ghosh, D., Cili, A., and Zhang, K. (2022). Identification and functional analysis of exosomal miR-16-5p, miR-6721-5p, and miR-486-5p associated with immune infiltration for potential vitiligo theranostics. *Clin. Immunol. Commun.* 2, 110–117. doi:10.1016/j.clicom.2022.08.002

Tout, I., Loureiro, D., Mansouri, A., Soumelis, V., Boyer, N., and Asselah, T. (2020). Hepatitis B surface antigen seroclearance: Immune mechanisms, clinical impact, importance for drug development. *J. Hepatol.* 73 (2), 409–422. doi:10.1016/j.jhep.2020.04.013

Wang, M., Gong, Q., Zhang, J., Chen, L., Zhang, Z., Lu, L., et al. (2017). Characterization of gene expression profiles in HBV-related liver fibrosis patients and identification of ITGBL1 as a key regulator of fibrogenesis. *Sci. Rep.* 7, 43446. doi:10.1038/srep43446

Wang, S., Zhang, H., Liu, Z., and Liu, Y. (2022). A novel deep learning method to predict lung cancer long-term survival with biological knowledge incorporated gene expression images and clinical data. *Front. Genet.* 13, 800853. doi:10.3389/fgene.2022.800853

Wang, X., He, Q., Shen, H., Xia, A., Tian, W., Yu, W., et al. (2019). TOX promotes the exhaustion of antitumor CD8(+) T cells by preventing PD1 degradation in hepatocellular carcinoma. *J. Hepatol.* 71 (4), 731–741. doi:10.1016/j.jhep.2019.05.015

Wangensteen, K. J., and Chang, K. M. (2021). Multiple roles for hepatitis B and C viruses and the host in the development of hepatocellular carcinoma. *Hepatology* 73 (1), 27–37. doi:10.1002/hep.31481

Wijaya, R. S., Read, S. A., Schibeci, S., Eslam, M., Azardaryany, M. K., El-Khobar, K., et al. (2019). KLRG1+ natural killer cells exert a novel antifibrotic function in chronic Hepatitis B. *J. Hepatol.* 71 (2), 252–264. doi:10.1016/j.jhep.2019.03.012

Wong, M. C. S., Huang, J. L. W., George, J., Huang, J., Leung, C., Eslam, M., et al. (2019). The changing epidemiology of liver diseases in the Asia-Pacific region. *Nat. Rev. Gastroenterol. Hepatol.* 16 (1), 57–73. doi:10.1038/s41575-018-0055-0

Xia, Z., Kong, F., Wang, K., and Zhang, X. (2022). Role of N6-methyladenosine methylation regulators in the drug therapy of digestive system tumours. *Front. Pharmacol.* 13, 908079. doi:10.3389/fphar.2022.908079

Xiao, B., Liu, L., Li, A., Xiang, C., Wang, P., Li, H., et al. (2020). Identification and verification of immune-related gene prognostic signature based on ssGSEA for osteosarcoma. *Front. Oncol.* 10, 607622. doi:10.3389/fonc.2020.607622

Xu, M. Y., Qu, Y., Li, Z., Li, F., Xiao, C. Y., and Lu, L. G. (2016). A 6 gene signature identifies the risk of developing cirrhosis in patients with chronic Hepatitis B. *Front. Biosci.* 21, 479–486. doi:10.2741/4403

Yang, H., Zhou, Y., Mo, J., Xiang, Q., Qin, M., Liu, W., et al. (2020). SOX9 represses Hepatitis B virus replication through binding to HBV EnhII/Cp and inhibiting the promoter activity. *Antivir. Res.* 177, 104761. doi:10.1016/j.antiviral.2020.104761

Yang, L., Liu, F., Tong, X., Hoffmann, D., Zuo, J., and Lu, M. (2019). Treatment of chronic hepatitis B virus infection using small molecule modulators of nucleocapsid assembly: Recent advances and perspectives. *ACS Infect. Dis.* 5 (5), 713–724. doi:10.1021/acsinfecdis.8b00337

Ye, J., and Chen, J. (2021). Interferon and hepatitis B: Current and future perspectives. *Front. Immunol.* 12, 733364. doi:10.3389/fimmu.2021.733364

Yu, B., Yin, Y. X., Tang, Y. P., Wei, K. L., Pan, Z. G., Li, K. Z., et al. (2021). Diagnostic and predictive value of immune-related genes in crohn's disease. *Front. Immunol.* 12, 643036. doi:10.3389/fimmu.2021.643036

Yuen, M. F., Chen, D. S., Dusheiko, G. M., Janssen, H. L. A., Lau, D. T. Y., Locarnini, S. A., et al. (2018). Hepatitis B virus infection. *Nat. Rev. Dis. Prim.* 4, 18035. doi:10.1038/nrdp.2018.35

Zhang, J. P., Yan, J., Xu, J., Pang, X. H., Chen, M. S., Li, L., et al. (2009). Increased intratumoral IL-17-producing cells correlate with poor survival in hepatocellular carcinoma patients. *J. Hepatol.* 50 (5), 980–989. doi:10.1016/j.jhep.2008.12.033

Zhang, X., Luo, M., Zhang, J., Guo, B., Singh, S., Lin, X., et al. (2022). The role of lncRNA H19 in tumorigenesis and drug resistance of human Cancers. *Front. Genet.* 13, 1005522. doi:10.3389/fgene.2022.1005522

Zhao, J., Zhang, Z., Luan, Y., Zou, Z., Sun, Y., Li, Y., et al. (2014). Pathological functions of interleukin-22 in chronic liver inflammation and fibrosis with Hepatitis B virus infection by promoting T helper 17 cell recruitment. *Hepatology* 59 (4), 1331–1342. doi:10.1002/hep.26916

Zheng, R., Wang, G., Pang, Z., Ran, N., Gu, Y., Guan, X., et al. (2020). Liver cirrhosis contributes to the disorder of gut microbiota in patients with hepatocellular carcinoma. *Cancer Med.* 9 (12), 4232–4250. doi:10.1002/cam4.3045

Zhou, W., Ma, Y., Zhang, J., Hu, J., Zhang, M., Wang, Y., et al. (2017). Predictive model for inflammation grades of chronic Hepatitis B: Large-scale analysis of clinical parameters and gene expressions. *Liver Int.* 37 (11), 1632–1641. doi:10.1111/liv.13427

Zhuang, W., Zhang, Z., Zhang, S., Ao, J., Weng, W., Wu, B., et al. (2021). An immunogenomic signature for molecular classification in hepatocellular carcinoma. *Mol. Ther. Nucleic Acids* 25, 105–115. doi:10.1016/j.omtn.2021.06.024

frontiers | Frontiers in Pharmacology

TYPE Original Research
PUBLISHED 13 January 2023
DOI 10.3389/fphar.2022.1097197

OPEN ACCESS

EDITED BY
Zhijie Xu,
Central South University, China

REVIEWED BY
Qu Song,
Guangxi Medical University Cancer Hospital, China
Xin Jiang,
First Affiliated Hospital of Jilin University, China

*CORRESPONDENCE
Xiaoshen Wang,
xiaoshen.wang@fdeent.org
Yi Zhu,
zhuyi1113@hotmail.com
Shu Tian,
shu.tian@fdeent.org

†These authors have contributed equally to this work

SPECIALTY SECTION
This article was submitted to Pharmacology of Anti-Cancer Drugs, a section of the journal Frontiers in Pharmacology

RECEIVED 13 November 2022
ACCEPTED 28 December 2022
PUBLISHED 13 January 2023

CITATION
Li R, Yan L, Tian S, Zhao Y, Zhu Y and Wang X (2023), Increased response to TPF chemotherapy promotes immune escape in hypopharyngeal squamous cell carcinoma.
Front. Pharmacol. 13:1097197.
doi: 10.3389/fphar.2022.1097197

Increased response to TPF chemotherapy promotes immune escape in hypopharyngeal squamous cell carcinoma

Ruichen Li†, Li Yan†, Shu Tian*†, Yang Zhao, Yi Zhu* and Xiaoshen Wang*

Department of Radiation Oncology, Eye and ENT Hospital of Fudan University, Shanghai, China

Background: There is an urgent need to identify which patients would benefit from TPF chemotherapy in hypopharyngeal squamous cell carcinoma (HPSCC) and to explore new combinations to improve the treatment effect.

Materials and methods: Gene-expression profiles in 15 TPF-sensitive patients were compared to 13 resistant patients. Immunohistochemistry (IHC) was performed to detect $CD8^+$ T cells in 28 samples. Patient-Derived Tumor Xenograft (PDX) model and IHC were used to verify markers that optimize treatment for HPSCC.

Results: Through RNA sequencing 188 genes were up-regulated in TPF chemotherapy-resistant (CR) tissues were involved in T cell activation, while 60 down-regulated genes were involved in glycolysis. Gene set enrichment analysis (GSEA) showed that chemotherapy-sensitive (CS) group upregulation of the pathways of glycolysis, while immune response was downregulated. CIBERSORT, MCP-counter, and IHC proved that most immune cells including $CD8^+$ T cells in the CR significantly higher than that in CS group. Among the 16 up-regulated genes in CS had close associations, the most significant negative correlation between the gene level and $CD8^+$ T cells existed in SEC61G. SEC61G was related to glycolysis, which was transcriptionally regulated by E2F1, and participated in antigen degradation through ubiquitin-dependent protein catabolic process. Palbociclib, combined with Cetuximab decreased the tumor burden and significantly suppressed the expression of E2F1 and SEC61G while activating MHC-I in PDX model.

Conclusion: Enhanced glycolysis promoted immune escape, but increased response to TPF chemotherapy. SEC61G was the center of the molecular network and targeting the E2F1/SEC61G pathway increased the expression level of MHC-I.

KEYWORDS

hypopharyngeal squamous cell carcinoma, TPF, chemotherapeutic sensitivity, glycolysis, immune response, SEC61G

Abbreviations: BP, biological processes; B2M, β2-microglobulin; DEGs, differently expressed genes; CR, chemo-resistant; CS, chemo-sensitive; CT, computed tomography; HNSCC, head and neck squamous cell carcinoma; ER, endoplasmic reticulum membrane; HPSCC, hypopharyngeal squamous cell carcinoma; DDP, cisplatin; PD-L1, programmed death-ligand 1; PDX, patient-Derived Tumor Xenograft; MRI, Magnetic resonance imaging; GO, gene ontology; KEGG, Kyoto encyclopedia of genes and genomes; GSEA, Gene Set Enrichment Analysis; IHC, immunohistochemistry; GLUT1, glucose transporter 1; PKM2, Pyruvate Kinase M2; TME, tumor microenvironment.

Introduction

Head and neck squamous cell carcinoma (HNSCC) is one of the most common malignant tumors in the world. Hypopharyngeal squamous cell carcinoma (HPSCC) is relatively rare and accounts for roughly 3% of all head and neck cancers (Garneau et al., 2018; Zhang et al., 2021). Patients with HPSCC frequently present at an advanced stage which is characterized by extensive local spread and early metastasis (Uzcudun et al., 2001; Eckel and Bradley, 2019). HPSCC has a poor prognosis with an overall 5-year survival rate of only 25%–35% (Liu et al., 2020; Visini et al., 2021; Marzouki et al., 2022). Therefore, exploring effective targets to improve the prognosis of HPSCC is urgently required.

Surgery combined with radiotherapy and chemotherapy is the main treatment method, among which cisplatin (DDP)-based chemotherapy is widely applied in HPSCC (Yu et al., 2014; Li et al., 2022). However, chemotherapeutic resistance resulted in treatment failure, including recurrence and distant metastasis in various human tumors (Yu et al., 2014). Based on molecular mechanism, resistance to first-line chemotherapy agents, such as TPF as the most effective therapeutic management in HPSCC is a multifactorial event (Arora et al., 2010; Galluzzi et al., 2012; Mukhtar et al., 2014; Azwar et al., 2021).

Immunotherapy has dramatically changed the treatment landscape for patients with different tumors. Programmed death-ligand 1 (PD-L1) expression by tumor cells is a mechanism for down-regulation of antitumor T-cell responses and is a target for immunotherapy in various cancers. PD-1+ T lymphocytes were wildly infiltrated in HPSCC tissues, whose positivity in combination with CD8 high expression has been reported to present predictive potential in HPSCC (Hu et al., 2020; Wang et al., 2021). However, relevant large-scale and randomized clinical studies are lacking. There is an urgent need to identify which patients would benefit from chemotherapy or immunotherapy based on target markers, to optimize treatment for HPSCC patients in the future.

In previous study (Li et al., 2022), we have reported that modified TPF chemotherapy was an effective approach for laryngeal preservation in HPSCC. However, there were still 35%–45% of patients who showed no response after chemotherapy (Li et al., 2022). In present study, we further identify the differentially expressed genes that are closely related to the TPF-chemotherapy-sensitivity (CS) in HPSCC by RNA sequencing. Patient-Derived Tumor Xenograft (PDX) model and immunohistochemistry (IHC) staining were used to verify markers that optimize treatment for HPSCC.

Materials and methods

Patient source and inclusion criteria

Between April 2014 and December 2018, patients with a pathological diagnosis of HPSCC who were treated in the Eye and ENT Hospital of Fudan University were enrolled. The inclusion criteria were as follows: 1) Patients with a confirmed pathological diagnosis of primary HPSCC in our hospital, and the tumor specimens from the biopsy are available; 2) Patients were not exposed to any treatment before they got a biopsy; 3) Locally advanced HPSCC with confirmed clinical stages of III, IVA, and IVB as defined by the eighth edition of the American Joint Committee on Cancer; 4) Patients received at least 2 cycles of TPF induction chemotherapy, and the tumor regression could be evaluated; 5) Patients with complete clinical and follow-up data.

TPF induction chemotherapy and treatment efficacy

We performed at least two 21-day cycles of TPF neoadjuvant chemotherapy with docetaxel (75 mg/m^2, day 1), cisplatin (25 mg/m^2, days 1–3), 5-fluorouracil (500 mg/m^2, days 1–4) or capecitabine (825 mg/m^2, twice daily, days 1–14). Treatment efficacy was evaluated based on Response Evaluation Criteria in Solid Tumors (RECIST, V1.1). The efficacy of induction chemotherapy was evaluated on days 14–21 of the second cycle of chemotherapy. According to the RECIST, a total of 28 patients met the screening criteria, and were divided into two groups: fifteen patients proved to be sensitive to treatment, while the rest thirteen patients were grouped into chemotherapy-resistant (CR). The clinical features are summarized in Supplementary Table S1.

Gene quantitative profiling and bioinformatic analysis

The research was approved by the Clinical Ethics Committee and we obtained written informed consent from the patient. RNA sequencing was conducted by Shanghai oebiotech Co. (Shanghai, China). Very low expression genes were filtered out firstly (sum (FPKM) < 6, FPKM means Fragments Per Kilobase of transcript per Million fragments mapped), fold change (FC) combined with T-test were conducted to analyze the differentially expressed genes (DEGs). Compared to the gene expression from the sensitive group, FC < 1 in the resistant group was regarded as a down-regulated gene, while FC > 1 was up-regulated gene. Genes with a FC > 2, or <.5 compared to the sensitive group and $p <$ .05 were subjected to further verification.

The gene ontology (GO), Kyoto encyclopedia of genes and genomes (KEGG) were analyzed using the online system "Metascape" (https://metascape.org) for enrichment analysis. R package clusterProfiler (3.8.0) (Yu et al., 2012) was used to carry out Gene Set Enrichment Analysis (GSEA) to elaborate on the significant pathway between drug-resistant and sensitive samples. C5.go.bp.v7.5.1.symbols.gmt, c2.cp.kegg.v7.5.1.symbols.gmt, and h.all.v7.5.1.symbols.gmt in the MsigDB Collections were used as the reference gene collection. FDR <.25, adjusted p-value <.05, and |NSE| > 1 was considered as statistically significant. Two methods were used to analyze the components of immune cells. Method 1: the relative proportions of 22 types of immune cells were analyzed by online tool CIBERSORT (https://cibersort.stanford.edu). Method 2: Based on the FPKM expression profile, the following cell abundance was analyzed using MCP-counter (https://zenodo.org/record/61372#.XVPIB6276qB) of R language: T cells, Monocytic lineage, B lineage, Neutrophils, Cytotoxic lymphocytes, NK cells, CD8$^+$T cells, Myeloid dendritic cells, Fibroblasts, and Endothelial cells. The significance of different types of immune cells in the two groups was analyzed by Mann-Whitney U test. The online system "STRING (https://cn.string-db.org/)" was conducted to build the functional protein association network.

Enrichment analysis of SEC61G

The correlation between the expression of different genes and $CD8^+$T cells infiltration, or MHC-I molecular antigen presentation was explored by TIMER 2.0 (https://cistrome.shinyapps.io/timer/). The correlation between SEC61G expression and EGFR expression in HNSC normal and tumor was explored by GEPIA (http://gepia.cancer-pku.cn/). Datasets of Head and Neck Squamous Cell Carcinoma (TCGA, Firehose Legacy) was acquired from cBioportal (https://www.cbioportal.org/). Spearman's correlation coefficient (r) was calculated to assess the correlation between co-expressed genes and SEC61G, of which $p < .001$ and $|r| > .35$ were selected. "Transcription Factor Target" analysis for 2275 co-expressed genes related to SEC61G in HNSCC (Head and Neck Squamous Cell Carcinoma (TCGA, Firehose Legacy)) was carried out through Webgestalt (http://www.webgestalt.org/). The gene expression data of SEC61G and the HPV status in TCGA-HNSC project were acquired from UCSC Xena browser (http://xenabrowser.net/datapages/). Cases without complete gene expression data and HPV status were excluded. Patients with HNSCC were classified into low- and high-expression groups according to the mean SEC61G expression value.

Exploring the immune-related functional relationship network

ImmuNet (https://immunet.princeton.edu/) was utilized to predict the related molecular network in antigen processing and presentation, natural killer cell mediated cytotoxicity, B cell receptor signaling pathway, T cell receptor signaling pathway, and chemokine signaling pathway.

In vivo study

Animal studies were performed in compliance with the International Animal Care and Use Committee-approved protocol (IACUC). PDX model, was derived from a patient with HPSCC who had never received systemic therapy. The study was approved by the Ethics Committee and the patient agreed with written informed consent. Small pieces ($5 \times 5 \times 5\ mm^3$) of tumor samples were obtained from the patient and subcutaneously injected into NOD-SCID mice. When tumor sizes reached 1,000 mm^3, it was removed and divided into small pieces and transplanted into another mouse. We defined patient-oriented mice model as P0 generation, and subsequently generations were numbered consecutively (P1, P2, and P3). After P1 generation, the tumor was engrafted into BALB/c male nude mice. P3 generation model was utilized for drug response. The mice were randomly grouped and treatment started when tumor sizes reached 70 mm^3. Each group included 6 mice.

Mice were treated with 100 mg/kg Palbociclib (daily), 1 mg Cetuximab (weekly), or a combination of Palbociclib and Cetuximab. Palbociclib was administrated by oral gavage and Cetuximab was administrated by intraperitoneal injection. Tumor size and body weight were measured twice weekly. After 28 days of drug treatment, tumors were removed, weighed, photographed, fixed, and kept at −80°C. (Palbociclib (PD-0332991) was obtained from Selleck Chemicals and dissolved in water. Cetuximab was obtained from Merck kGaA.)

Immunohistochemistry

Antibodies against E2F1 (sc-251): Santa Cruz Biotechnology. SEC61G (11147-2-AP) and HLA class I ABC (15240-1-AP): Proteintech. CD8 (GTX16696): GeneTex. IHC staining was performed as described previously (Hu et al., 2020).

Statistical analysis

Statistical analyses were conducted using GraphPad Prism (version 9.0, San Diego, CA, United States). Mann-Whitney U or ANOVA was used to compare the difference between groups. Fisher's exact probability method was used for comparison between groups of categorical variables. All tests were on two sides, and $p < .05$ was considered statistically significant.

Results

Molecular profiles in TPF-responsive patients relative to resistant patients

The drug-sensitive one was defined as tumor volume reduced more than 50% after treatment. Among 15,671 protein-coding genes with a sum (FPKM) greater than 6, 1,310 genes exhibited statistically differentiated expression in the CR compared to CS ($p < .05$) (Supplementary Figure S1). Furthermore, of these 1,310 genes, 188 genes with an FC > 2 presented a higher expression in the tissue from the CR, while 60 with an FC < .5 were down-regulated (Supplementary Figure S1).

Functional annotation of differentially expressed genes

From the identified 1,310 differentially expressed genes, pathway enrichment analysis was performed. As shown in Figure 1A, "T cell activation", and "Central carbon metabolism in cancer" attracted our attention. Next, the 188 up-regulated genes in resistant group (Figure 1B) were involved in "inflammatory response", "regulation of leukocyte activation", "positive regulation of immune response", "adaptive immune response", and "T cell activation". On the contrary, 60 down-regulated genes were involved in "HIF-1 signaling pathway", "Glycolysis/Gluconeogenesis", and "regulation of proteolysis" (Figure 1C).

A GSEA analysis (Figure 2) was also conducted to explore the potential pathways correlated with the CS group. GSEA analyses showed that CS group upregulation of the pathways involving glycolysis, oxidative phosphorylation, protein secretion, and unfolded protein response (UPR). However, B cell activation involved in immune response, positive regulation of natural killer cell mediated immunity, complement, interferon gamma response, allograft rejection, and T cell receptor signaling pathway were downregulated.

The correlation between chemosensitivity and immune cell infiltration

Due to the pathways related to immune response being downregulated in CS group (Figures 1, 2), firstly, as shown in

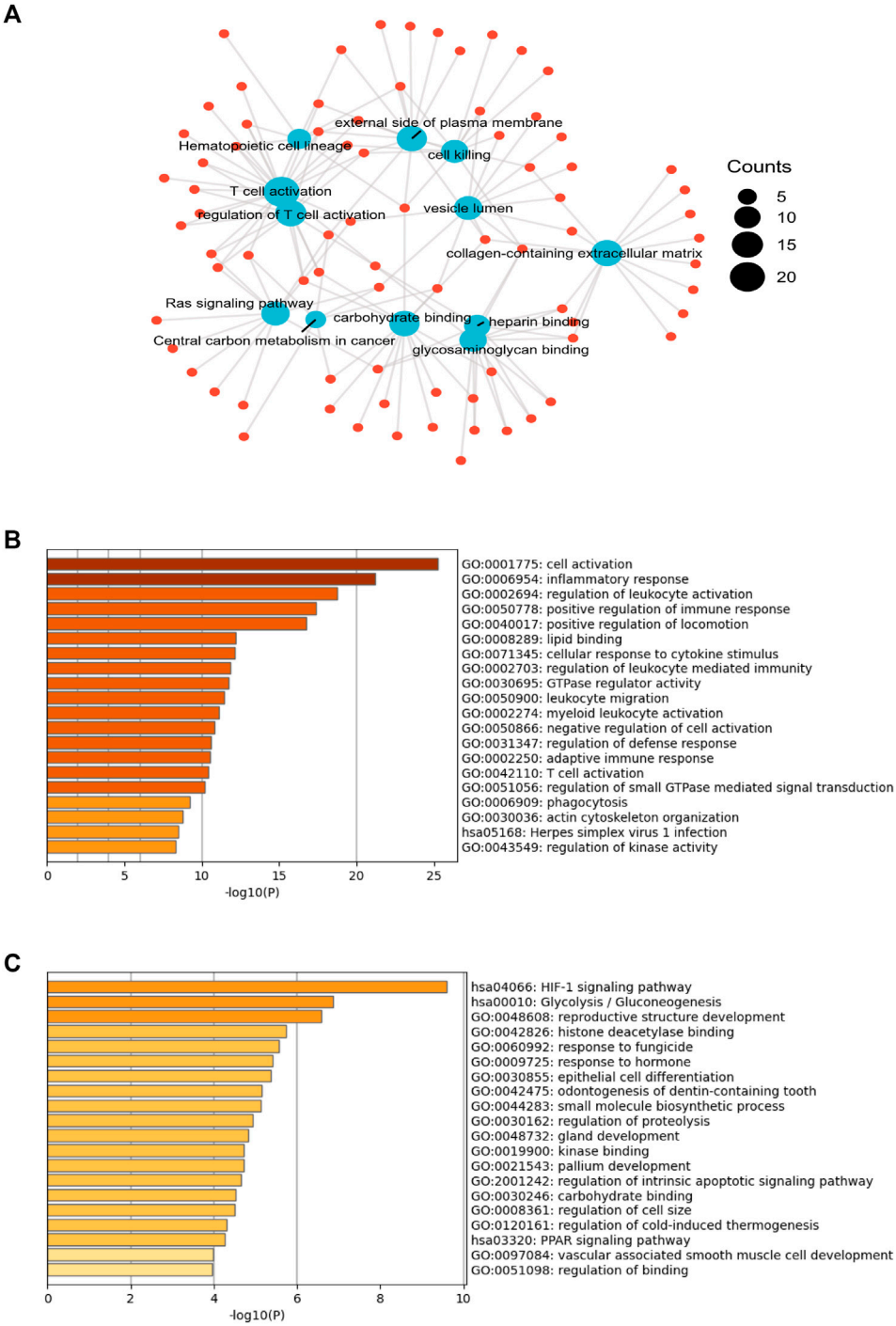

FIGURE 1
The gene expression profiles in chemotherapy-sensitive and resistant hypopharyngeal cancer patient tissues. **(A)** Gene oncology (GO)-biological processes (BP), GO-molecular functions (MF) and Kyoto encyclopedia of genes and genomes (KEGG) analysis of 1,310 genes showed significant differences in the expression levels of tissues from the non-sensitive group compared to the sensitive group ($p < .05$) based on mRNA-targeted genes. **(B)** The GO enrichment analysis and KEGG pathway analysis for evaluating 188 up-regulated genes in the resistant group. **(C)** The GO enrichment analysis and KEGG pathway analysis for evaluating 60 up-regulated genes in the sensitive group.

Figure 3A, CIBERSORT showed that the proportions of naïve CD4$^+$T cells and monocytes significantly increased in the CR group ($p < .05$), while neutrophils significantly increased in the CS group ($p < .05$). Secondly, the absolute abundance of 8 types of immune cells, endothelial cells, and fibroblasts were analyzed by MCP-counter. As shown in Figure 3B, T cells, B cells, monocytes, and endothelial cells were significantly increased in the CR group ($p < .05$).

We further performed IHC to detect CD8$^+$ T cells in 28 samples (Figure 3C). Consistent with our hypothesis, CD8$^+$ T cells were significantly lower in resistant patients' samples than in sensitive

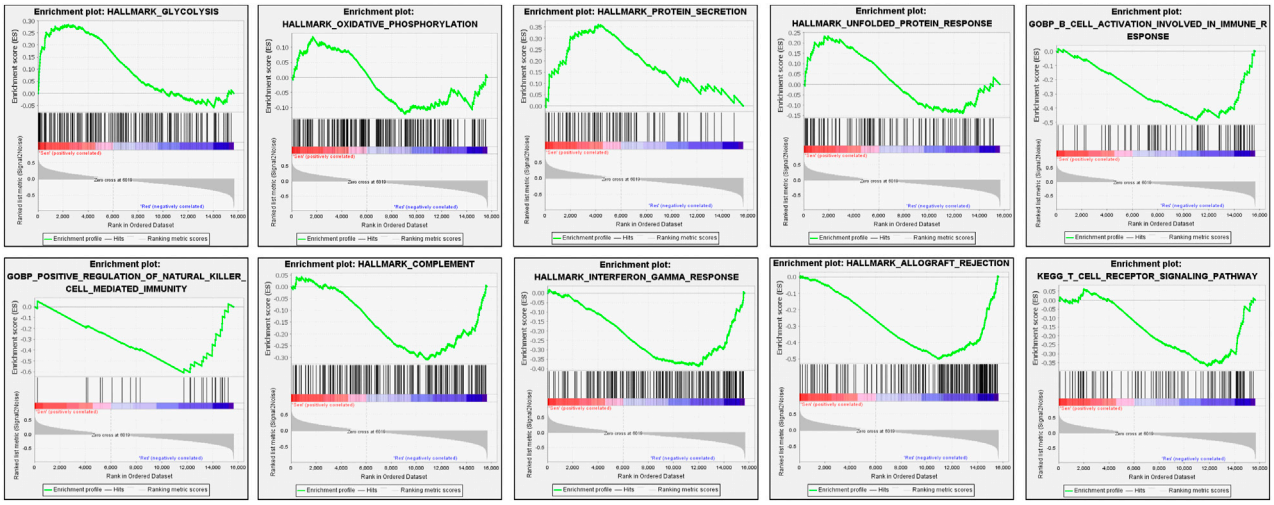

FIGURE 2
Enrichment plots derived from the gene set enrichment analysis (GSEA) related to drug-sensitive group.

ones (p = .046). Supplementary Table S2 shows the correlation between CD8$^+$lymphocyte subsets and clinicopathological parameters of 28 patients. The increased infiltration density of CD8$^+$ T cells was significantly associated with CR (p = .002) but not other factors (p > .05).

Key factor in HPSCC chemosensitivity

STRING web platform was used to predict the protein association network related to 60 up-regulated genes in the CS group and we found that 16 proteins had functional and physical associations (Figure 4A). The 16 related proteins closely related to the regulation of glucose metabolic pathway and signaling (Figure 4B). Owing to the infiltration of CD8$^+$ T cells being significantly decreased in CS group, among the 16 genes, CA12, EGFR, FABP4, FABP5, HK2, MAGEA3, MAGEA6, SEC61G, SLC2A1, SLC5A1, and TMEM45A were significantly negatively correlated with CD8$^+$ T cells infiltration (Supplementary Figure S2), while the most significant negative correlation existed in SEC61G (partial correlation: −.273, p = 1.52e-09), also known as endoplasmic reticulum (ER) SEC61 gamma subunit.

Functional enrichment analysis of SEC61G in HNSCC

A total of 2275 co-expressed genes related to SEC61G in HNSCC (Head and Neck Squamous Cell Carcinoma (TCGA, Firehose Legacy)) were identified, of which 1,041 genes were positively correlated. Then the functions of positively co-expression in patients with HNSCC were predicted (Figure 5A). The GO-biological processes (BP), molecular functions (MF) items, and KEGG pathway were including “ribosome”, “oxidative phosphorylation”, “protein folding”, “UPR”, “proteasome”, “ubiquitin mediated proteolysis”.

Next, we divided HPV-negative and HPV-positive patients respectively into high- and low-expression groups based on the mean SEC61G expression. In HPV-negative HNSCC (Figure 5B), GSEA showed that high SEC61G expression positively upregulated the pathways including E2F targets, UPR, G2M checkpoint, glycolysis, ribosome, oxidative phosphorylation, and translation. However, B/T cell receptor signaling pathway, natural killer cell mediated cytotoxicity, antigen presentation folding assembly and peptide loading of class I MHC, and interferon gamma signaling were downregulated. Surprisingly, in HPV-positive HNSCC (Figure 5C), UPR, protein secretion, hypoxia, and glycolysis were downregulated.

CDK4/6 inhibitor and EGFR inhibitor increase MHC-I expression by targeting E2F1/SEC61G axis

SEC61G acted a significant role in MHC-I mediated antigen processing and presentation (Figure 5). Thus, ImmuNet was utilized to explore the immune-related molecular network involving. As shown in Figures 6A,B, SEC61G was the center of the molecular network in relation to “antigen processing and presentation” and “natural killer cell mediated cytotoxicity”. Functional enrichment showed that endoplasmic reticulum protein-containing complex and ubiquitin-dependent protein catabolic process were enriched. However, neither molecular network nor enrichment was obtained regarding SEC61G in B/T cell receptor and chemokine signaling pathway (Figures 6C–E), which means that SEC61G is not directly involved in the inhibition of T cells signaling pathway. Figure 6F illustrated that SEC61G expression significantly negatively correlated with HLA-A, HLA-B, HLA-C, and β2-microglobulin (B2M) in HNSCC.

A “Transcription Factor Target” analysis was performed using the 2275 co-expressed genes related to SEC61G in HNSCC and predicted that SEC61G was transcriptionally regulated by E2F (Figure 7A). The result was consistent with the study in breast cancer, E2F1 bound to the promoter of SEC61G directly and controlled its expression (Ma et al., 2021). Previous reports have shown that SEC61G and EGFR were encompassed in the minimal overlapped regions of amplification

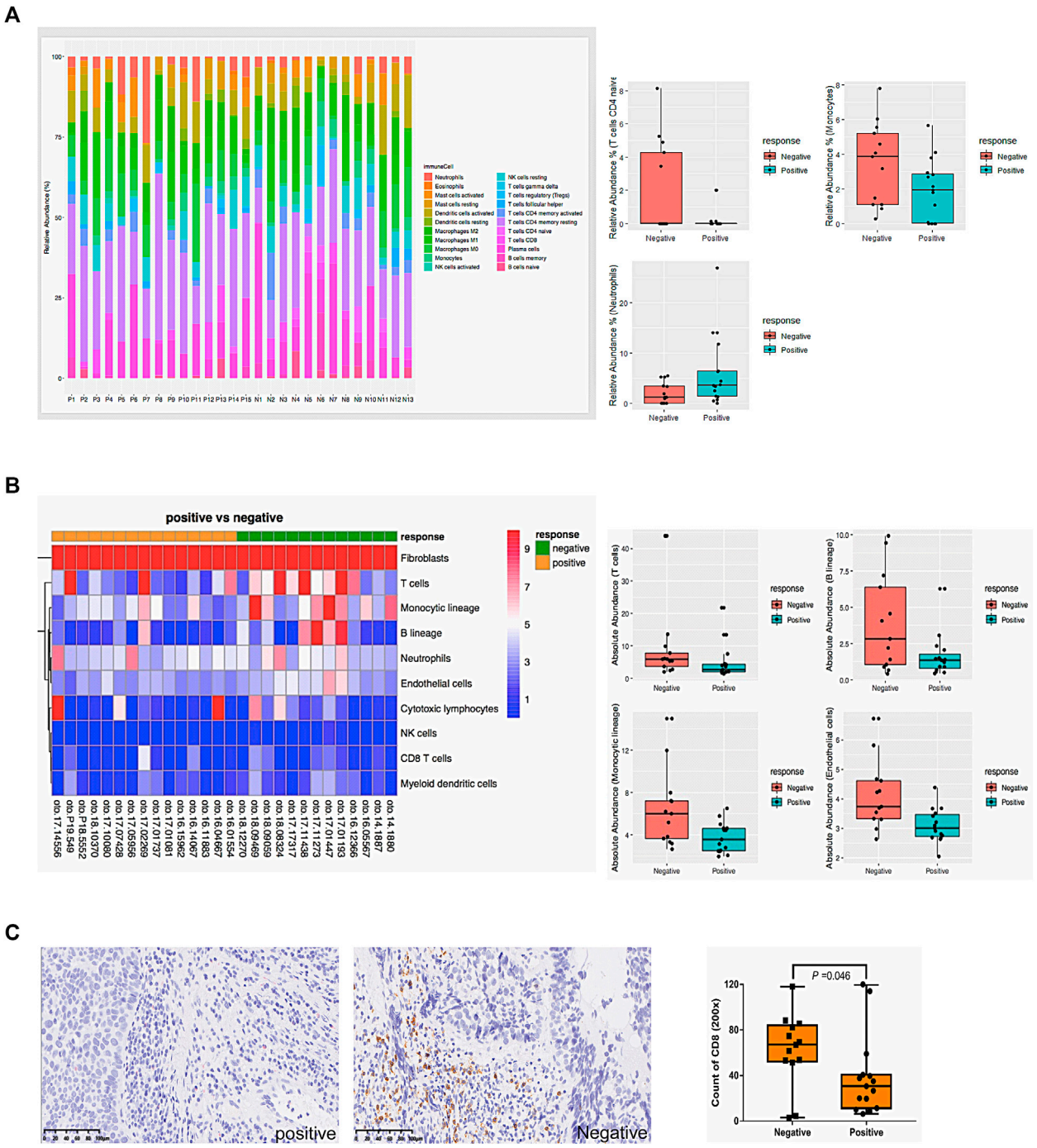

FIGURE 3
The correlation between chemosensitivity and immune cell infiltration. **(A)** The relative proportions of 22 types of immune cells in 28 samples were analyzed by online tool CIBERSORT. **(B)** The absolute abundance of 8 types of immune cells, endothelial cells, and fibroblasts in 28 samples was analyzed by MCP-counter. **(C)** Representative CD8 immunohistochemistry staining and the count of CD8 positive cells in hypopharyngeal cancer tissues. Mann-Whitney U was used to compare the difference between groups. Negative: drug-resistant; Positive: drug-sensitive.

(Lu et al., 2009), and inhibition of EGFR could decrease downstream E2F1 transcriptional activity (Nishioka et al., 2011; Wang et al., 2020). As illustrated in Figure 7B, SEC61G expression significantly positively correlated with EGFR in HNSC tumor but not in HNSC normal. Therefore, we believe that targeting E2F1/SEC61G by CDK4/6 inhibitor or EGFR inhibitor to improve the expression of MHC-I in HNSCC is feasible. To verify our hypothesis, we analyzed the potential application of Palbociclib/Cetuximab in PDX model of HPSCC (Figure 7C). Palbociclib monotherapy surprisingly exhibited a comparable effect to that in Cetuximab monotherapy. We observed a significant reduction in tumor growth in combination treatment. In the combination group, the mean tumor weight was lower (90 mg) compared to Palbociclib (230 mg), Cetuximab (170 mg) and vehicle control (600 mg). Next, the tumors in PDX model were

10.3389/fphar.2022.1097197

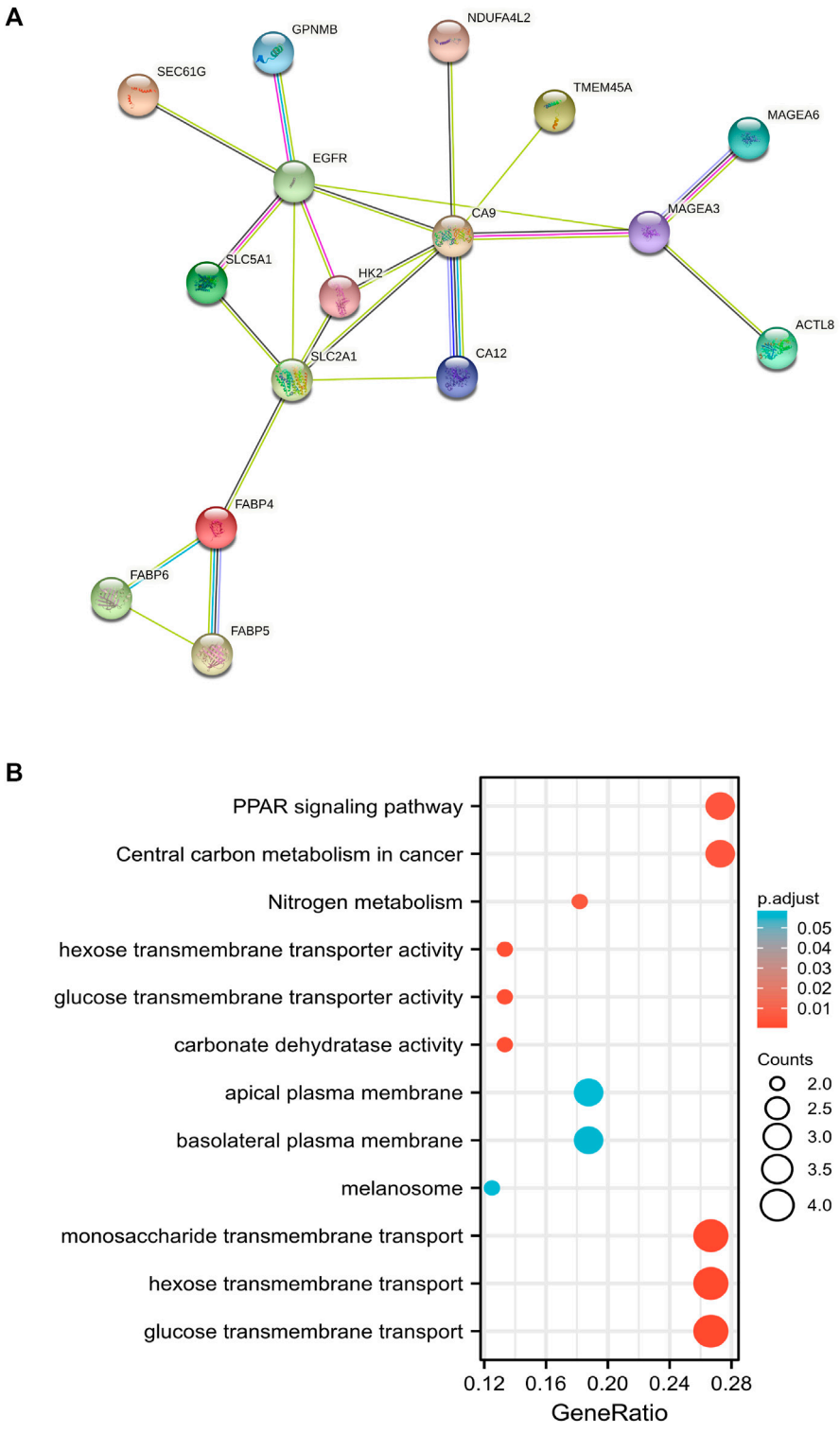

FIGURE 4
The protein association network related to up-regulated genes in chemotherapy-sensitive group. **(A)** Sixteen proteins among 60 up-regulated proteins in sensitive group which had functional and physical associations were predicted by STRING web platform. **(B)** GO and KEGG analyses of 16 related genes in functional protein association network.

analyzed by IHC. As expected, the levels of E2F1 and SEC61G were substantially diminished in Palbociclib-treated group when compared to control, while the expression of MHC-I was correspondingly increased (Figure 7D). Similarly, Cetuximab monotherapy or the combination therapy also effectively decreased the expression of E2F1 and SEC61G but activated MHC-I (Figure 7D).

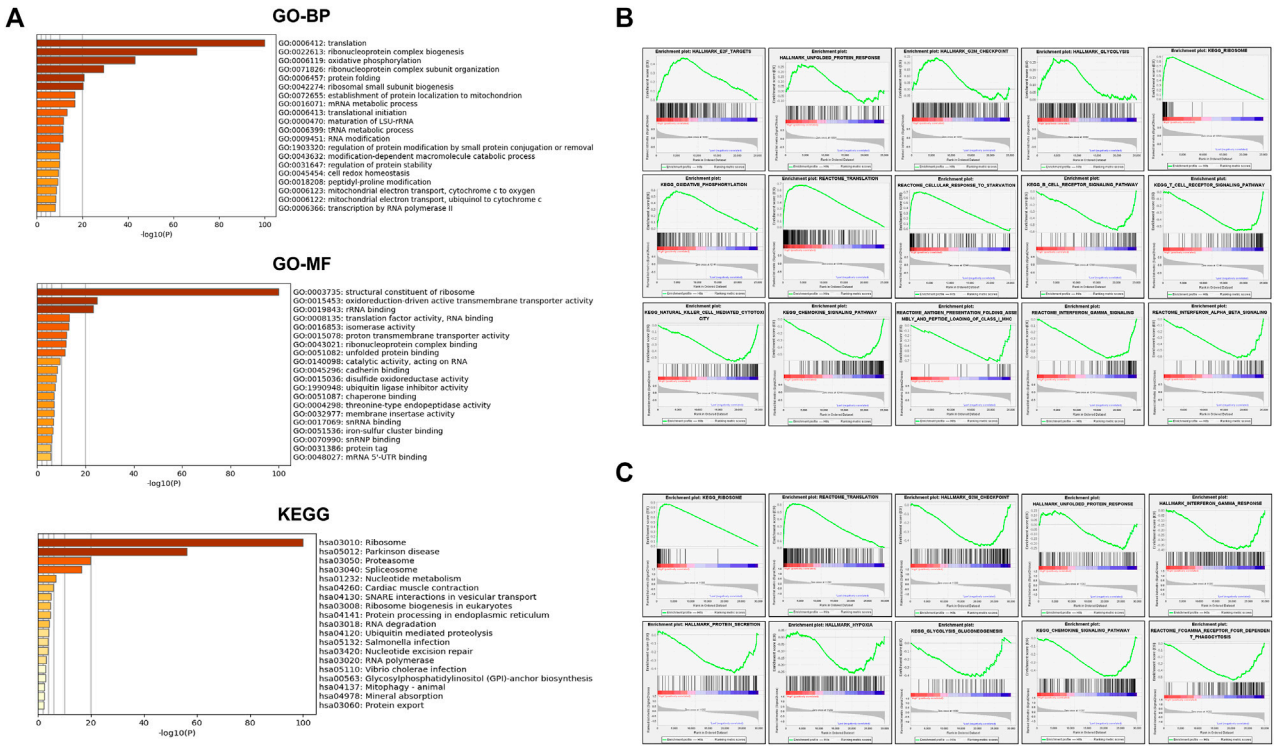

FIGURE 5
SEC61G-associated gene enrichment analysis. **(A)** Gene oncology (GO)-biological processes (BP), GO-molecular functions (MF) and Kyoto encyclopedia of genes and genomes (KEGG) analysis of 1041 SEC61G positive co-expression genes in HNSCC (Head and Neck Squamous Cell Carcinoma (TCGA, Firehose Legacy)). **(B)** Enrichment plots derived from the gene set enrichment analysis (GSEA) related to high SEC61G expression in HPV-negative HNSCC based on TCGA-HNSC database. **(C)** GSEA related to high SEC61G expression in HPV-positive HNSCC based on TCGA-HNSC database.

Discussion

The prognosis of HPSCC is extremely poor, especially metastasis is the main factor of poor prognosis which is widely known at present (Kuo et al., 2016). Chemotherapy plays a very important role, commonly used chemotherapy regimens for HPSCC include TPF. However, resistance to drugs is a common clinical issue in the treatment of patients with HPSCC. Many studies have confirmed single genetic markers associated with chemotherapy sensitivity in HPSCC. For instance, COX-2 expression has been found to be associated with chemoresistance through the cancer stemness property (Saito et al., 2021). The ctDNA might play a significant role in DDP resistance in HPSCC by amplifying related functional genes (Lin et al., 2022). However, genome-wide analysis associated with chemotherapy resistance HPSCC is lacking.

In this study, the main DEGs involving the BPs including "regulation of immune response" and "Glycolysis/Gluconeogenesis". Glycolysis has been confirmed to be significantly associated with the development of certain diseases (Ganapathy-Kanniappan and Geschwind, 2013). The genetic modifications could influence metabolism and induced aerobic glycolysis (Van den Bossche et al., 2022). HNSCC presents a high rate of glycolysis to fulfill their metabolic requirements (Raj et al., 2021). Glycolysis provides ATP, NADPH, and carbon skeletons for the growth and construction of tumor cells (Dang, 2012; Alfarouk et al., 2014). As to the correlation between glycolysis and the response to the chemotherapy, most evidence illustrated that enhanced glycolysis contributed to resistance to cisplatin-based chemotherapy in many tumors (Simons et al., 2007; Xintaropoulou et al., 2018; Zhang et al., 2018; Sawayama et al., 2019; Dai et al., 2020; Varghese et al., 2020). However, in our study, we surprisingly found that DEGs significantly clustered in glycolysis which is associated with TPF-chemotherapy sensitivity in HPSCC patients. For example, SLC5A1, which was one of the 16 related up-regulated genes in CS group in our study, facilitates glucose transport (Mueckler and Thorens, 2013). A risk model found that SLC5A1 is one of the three hub genes that related to cisplatin therapy response in ovarian cancer (Chen et al., 2022). Several studies have also proved that an increased glycolysis rate can enhance the sensitivity to chemotherapy. As a key driver of aerobic glycolysis, upregulation of Pyruvate Kinase M2 (PKM2) facilitates the response to chemotherapy in gastric cancer, breast cancer and intestinal cancer (Zhu et al., 2016). Knockdown of PFKFB2 increased the glycolysis rate and enhanced the effect of paclitaxel-based chemotherapy in breast and ovarian cancers (Yang et al., 2019). Metformin suppressed Nrf2 and decreased cisplatin resistance through enhanced glucose metabolism (Cai et al., 2020). Hypoxia improved the response of retinoblastoma cells to chemotherapy by activation of glycolysis (Yang et al., 2017). Together, glycolysis is a complex process, which may display completely opposite effects in different settings.

Another case that surprised us was that most immune cells including $CD8^+$ T cells in the CS group significantly lower than that in CR group. Glycolysis can transform the efficacy of immune cells and contributes to cancer cells to escape immunological

10.3389/fphar.2022.1097197

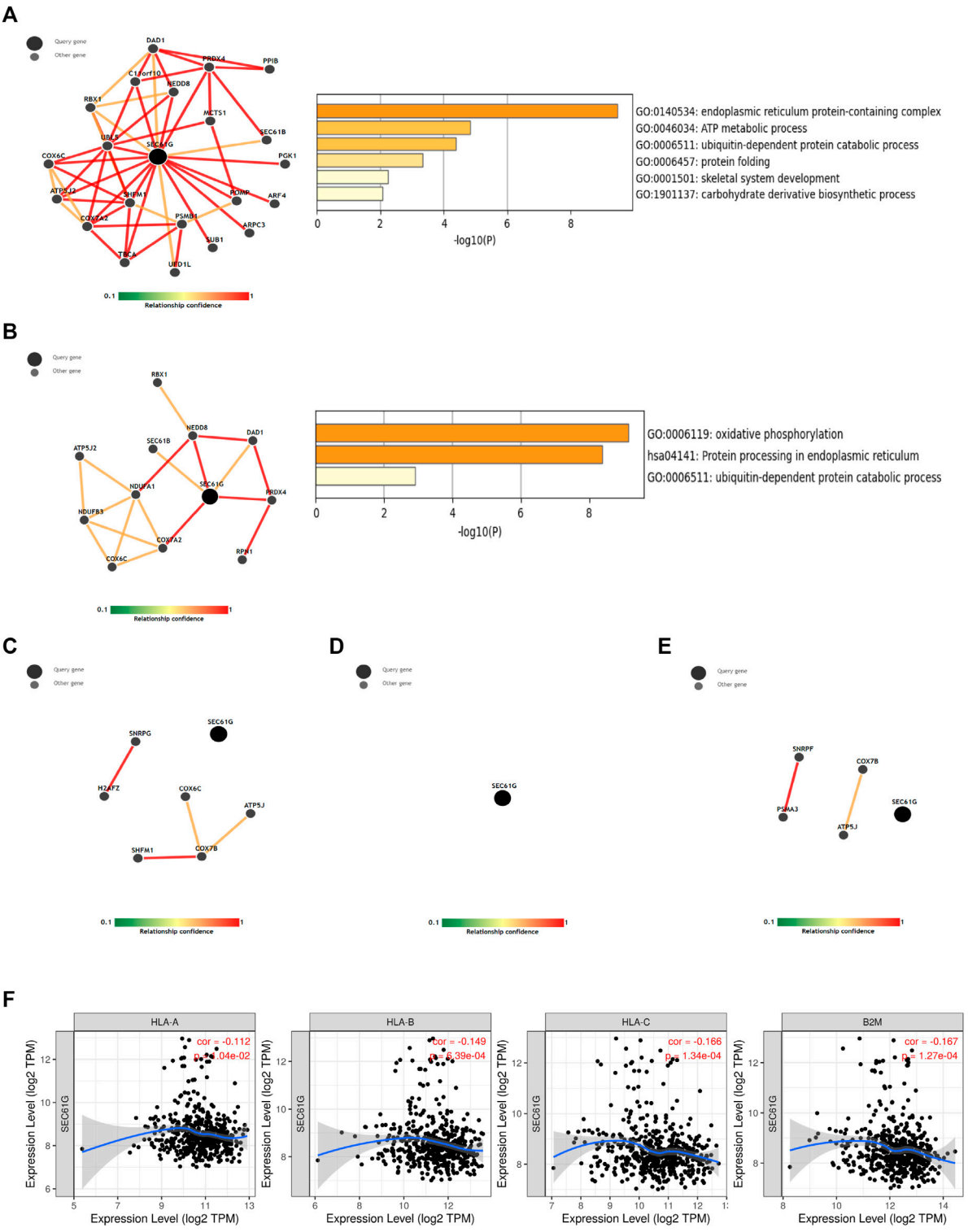

FIGURE 6
The immune-related analysis involving SEC61G. **(A)** A molecular network involving SEC61G in antigen processing and presentation based on ImmuNet analysis. **(B)** A molecular network involving SEC61G in natural killer cell mediated cytotoxicity based on ImmuNet analysis. **(C)** No molecular network was built related to B cell receptor signaling pathway. **(D)** No molecular network was built related to T cell receptor signaling pathway. **(E)** No molecular network was built related to chemokine signaling pathway. **(F)** The correlation between SEC61G expression and key components in MHC-I presentation in HNSCC *via* TIMER.

10.3389/fphar.2022.1097197

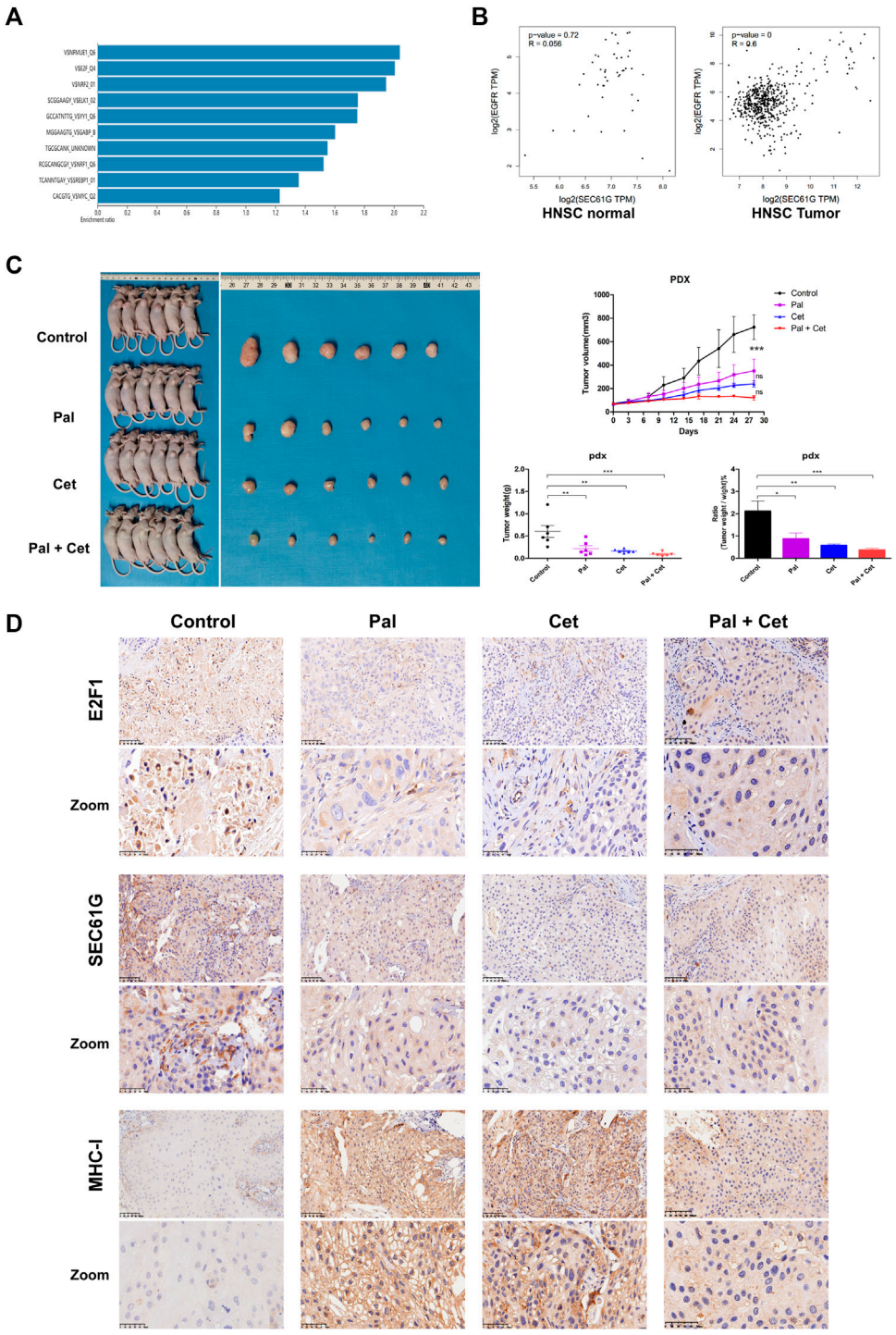

FIGURE 7
CDK4/6 inhibitor and EGFR inhibitor increase MHC-I expression by targeting E2F1/SEC61G axis. **(A)** "Transcription Factor Target" analysis for 2275 co-expressed genes related to SEC61G in HNSCC (Head and Neck Squamous Cell Carcinoma (TCGA, Firehose Legacy)) through webgestalt approach. **(B)** The correlation between the expression of SEC61G and EGFR in HNSC normal and HNSC tumor based on TCGA-HNSC database. **(C)** Combination Palbociclib and Cetuximab in Patient-Derived Tumor Xenograft (PDX) model related to hypopharyngeal squamous cell carcinoma. Hypopharyngeal cancer PDX models were treated with control, Palbociclib (100 mg/kg/day), Cetuximab (1 mg/week) or Cetuximab plus Palbociclib for 28 days (n = 6 per group). The growth curves of xenografts are shown. After 28 days, the mice were killed, and tumors were dissected, weighed and photographed. One-way ANOVA and Tukey's multiple comparisons test. *$p < .05$, **$p < .01$, ***$p < .001$. Pal, Palbociclib; Cet, Cetuximab; ns, not significant. **(D)** Immunohistochemistry staining of E2F1, SEC61G, and HLA class I ABC (MHC-I) in PDX models after treatments. Pal, Palbociclib treatment mouse; Cet, Cetuximab treatment mouse; Pal + Cet, Palbociclib plus Cetuximab treatment mouse.

surveillance within the tumor microenvironment (TME) (Gill et al., 2016). Disturbance of intracellular pH due to the lactate produced by glycolysis inhibits the proliferation and the activity of immune cells in the TME (Ganapathy-Kanniappan, 2017). Such low-pH TME has been proved to decrease the physiology of antigen-presenting cells (Romero-Garcia et al., 2016). Xie (Xie et al., 2021) proved that lactate produced by Notch1 signaling inhibits the activity of T cell and NK cell and leads to the immune escape of lung cancer. Aerobic glycolysis enhanced by EGFR signaling inhibits the efficacy of cytotoxic T cell in triple negative breast cancer cells (Lim et al., 2016). Thus, alteration of TME to reduce glycolysis and acidity may improve the effect of immunotherapy.

Immunotherapy, including anti-PD-1/PD-L1 and CTLA-4 has been more and more widely used in HNSCC (Pitt et al., 2016; Dogan et al., 2018; Fasano et al., 2022). And its combination with chemotherapy is currently under investigation to improve long-term survival prognosis for tumor patients due to the synergism mechanism such as activation of various innate immune pathways. Pembrolizumab plus chemotherapy has been the preferred choice for recurrent HNSCC, based on the bulky disease or CPS scores from patients (Burtness et al., 2019). In this study, the correlation between DEGs and infiltrating immune cells was verified, and interestingly in CR patients the DEGs significantly clustered in the immune-related GO terms involving T cells, B cells, and monocytes, while not in CS group. The IHC results also validated that $CD8^+$ T cells in the CR group significantly increased. Previous studies showed that with certain types of cancer, patients have been resistant to chemotherapy could be rescued by immunotherapy (Naoum et al., 2018; Yang et al., 2020), and our study probably provided the potential mechanism to identify the better immunotherapy combinations for patients based on different chemo-respond and different proportions of immunological cells infiltration.

The SEC61 complex forms a transmembrane channel where proteins are translocated across and integrated into the ER membrane (Hartmann et al., 1994; Greenfield and High, 1999). For kidney cancer SEC61G knockdown significantly promoted cell apoptosis in a caspase-dependent manner (Meng et al., 2021). Upregulation of SEC61G also promote cell invasion, and migration *via* modulating glycolysis in breast cancer (Ma et al., 2021). SEC61G expression is also elevated in head and neck cancer based on TCGA database, which is found to be significantly correlated with clinical stage, genetic mutation status, and poorer prognosis (Liang et al., 2021). However, its role in chemotherapy of HPSCC is unclear. In this study, SEC61G was up-regulated remarkably in CS group, meanwhile, the expression level of SEC61G was significantly negatively correlated with the infiltration of $CD8^+$ T cells in our study. SEC61G is significantly involved in antigen processing. However, neither molecular network nor enrichment was obtained regarding SEC61G in B/T cell receptor signaling. It means that SEC61G is not directly involved in the inhibition of T cells infiltration. Without MHC-I molecules, ineffectively immune cell recruitment and activation would lead to tumor immune escape (Garrido et al., 2016). The study furtherly examined that Palbociclib, as the selective CDK4/6 inhibitor, combined with Cetuximab decreased the tumor burden in PDX model. E2F1, as the transcription factor directly bound to the promoter and regulate the expression of SEC61G, has been validated in breast cancer (Ma et al., 2021). Here we demonstrated that the expression of E2F1 and SEC61G were remarkably reduced, while the expression of MHC-I was increased. The combination therapy of immunotherapy and CDK4/6 inhibitors or EGFR inhibitors is rational. The role and mechanism of SEC61G modulating the chemosensitivity of HPSCC through metabolic and immune-related signaling pathways deserves further study.

Although this study enhanced a better understanding of the relationship between immune escape and the response to TPF chemotherapy, some limitations really existed. The exploration of the role of SEC61G was mainly based on RNA sequencing analysis and bioinformatic analysis, which lacks verification from samples, and the relevant pathways are still needed for further validation.

Conclusion

In conclusion, enhanced glycolysis promoted immune escape, but increased response to TPF chemotherapy. SEC61G was the center of the molecular network and targeting the E2F1/SEC61G pathway increased the expression level of MHC-I, which potentially in turn affects the difference in tumor drug sensitivity. The molecular mechanisms that affect drug sensitivity in HPSCC deserve further exploration.

Data availability statement

The data presented in the study are deposited in the Genome Sequence Archive (GSA) repository (http://bigd.big.ac.cn/gsa-human), accession number HRA005361.

Ethics statement

The studies involving human participants were reviewed and approved by Clinical Ethics Committee in the Eye and ENT Hospital of Fudan University. The patients/participants provided their written informed consent to participate in this study. The animal study was reviewed and approved by Clinical Ethics Committee in the Eye and ENT Hospital of Fudan University.

Author contributions

RL: Conceptualization, Methodology, Software, Formal analysis, Investigation, Visualization, Writing-Original Draft; LY: Methodology, Software, Formal analysis, Validation, Writing-Original Draft; ST: Resources, Data Curation, Methodology, Visualization; YZ: Investigation, Formal analysis; YZ: Conceptualization, Methodology, Supervision, Writing-Review and Editing; XW: Conceptualization, Supervision, Project administration, Funding acquisition, Writing-Review and Editing.

Funding

This study was supported by the Medical Guidance Project of the Shanghai Science and Technology Commission [number 21Y11900300] and the National Key R&D Program of China [number 2020YFE0205500].

Conflict of interest

The authors declare that the research was conducted in the absence of any commercial or financial relationships that could be construed as a potential conflict of interest.

Publisher's note

All claims expressed in this article are solely those of the authors and do not necessarily represent those of their affiliated organizations, or those of the publisher, the editors and the reviewers. Any product that may be evaluated in this article, or claim that may be made by its manufacturer, is not guaranteed or endorsed by the publisher.

Supplementary material

The Supplementary Material for this article can be found online at: https://www.frontiersin.org/articles/10.3389/fphar.2022.1097197/full#supplementary-material

References

Alfarouk, K. O., Verduzco, D., Rauch, C., Muddathir, A. K., Adil, H. H., Elhassan, G. O., et al. (2014). Glycolysis, tumor metabolism, cancer growth and dissemination. A new pH-based etiopathogenic perspective and therapeutic approach to an old cancer question. *Oncoscience* 1, 777–802. doi:10.18632/oncoscience.109

Arora, S., Kothandapani, A., Tillison, K., Kalman-Maltese, V., and Patrick, S. M. (2010). Downregulation of XPF-ERCC1 enhances cisplatin efficacy in cancer cells. *DNA Repair (Amst)* 9, 745–753. doi:10.1016/j.dnarep.2010.03.010

Azwar, S., Seow, H. F., Abdullah, M., Faisal, J. M., and Mohtarrudin, N. (2021). Recent updates on mechanisms of resistance to 5-Fluorouracil and reversal strategies in colon cancer treatment. *Biol. (Basel)* 10, 854. doi:10.3390/biology10090854

Burtness, B., Harrington, K. J., Greil, R., Soulieres, D., Tahara, M., de Castro, G. J., et al. (2019). Pembrolizumab alone or with chemotherapy versus cetuximab with chemotherapy for recurrent or metastatic squamous cell carcinoma of the head and neck (KEYNOTE-048): A randomised, open-label, phase 3 study. *Lancet* 394, 1915–1928. doi:10.1016/S0140-6736(19)32591-7

Cai, L., Jin, X., Zhang, J., Li, L., and Zhao, J. (2020). Metformin suppresses Nrf2-mediated chemoresistance in hepatocellular carcinoma cells by increasing glycolysis. *Aging (Albany NY)* 12, 17582–17600. doi:10.18632/aging.103777

Chen, S., Wu, Y., Wang, S., Wu, J., Wu, X., and Zheng, Z. (2022). A risk model of gene signatures for predicting platinum response and survival in ovarian cancer. *J. Ovarian Res.* 15, 39. doi:10.1186/s13048-022-00969-3

Dai, S., Peng, Y., Zhu, Y., Xu, D., Zhu, F., Xu, W., et al. (2020). Glycolysis promotes the progression of pancreatic cancer and reduces cancer cell sensitivity to gemcitabine. *Biomed. Pharmacother.* 121, 109521. doi:10.1016/j.biopha.2019.109521

Dang, C. V. (2012). Links between metabolism and cancer. *Genes Dev.* 26, 877–890. doi:10.1101/gad.189365.112

Dogan, V., Rieckmann, T., Munscher, A., and Busch, C. J. (2018). Current studies of immunotherapy in head and neck cancer. *Clin. Otolaryngol.* 43, 13–21. doi:10.1111/coa.12895

Eckel, H. E., and Bradley, P. J. (2019). Natural history of treated and untreated hypopharyngeal cancer. *Adv. Otorhinolaryngol.* 83, 27–34. doi:10.1159/000492305

Fasano, M., Corte, C., Liello, R. D., Viscardi, G., Sparano, F., Iacovino, M. L., et al. (2022). Immunotherapy for head and neck cancer: Present and future. *Crit. Rev. Oncol. Hematol.* 174, 103679. doi:10.1016/j.critrevonc.2022.103679

Galluzzi, L., Senovilla, L., Vitale, I., Michels, J., Martins, I., Kepp, O., et al. (2012). Molecular mechanisms of cisplatin resistance. *Oncogene* 31, 1869–1883. doi:10.1038/onc.2011.384

Ganapathy-Kanniappan, S., and Geschwind, J. F. (2013). Tumor glycolysis as a target for cancer therapy: Progress and prospects. *Mol. Cancer* 12, 152. doi:10.1186/1476-4598-12-152

Ganapathy-Kanniappan, S. (2017). Linking tumor glycolysis and immune evasion in cancer: Emerging concepts and therapeutic opportunities. *Biochim. Biophys. Acta Rev. Cancer* 1868, 212–220. doi:10.1016/j.bbcan.2017.04.002

Garneau, J. C., Bakst, R. L., and Miles, B. A. (2018). Hypopharyngeal cancer: A state of the art review. *Oral Oncol.* 86, 244–250. doi:10.1016/j.oraloncology.2018.09.025

Garrido, F., Aptsiauri, N., Doorduijn, E. M., Garcia, L. A., and van Hall, T. (2016). The urgent need to recover MHC class I in cancers for effective immunotherapy. *Curr. Opin. Immunol.* 39, 44–51. doi:10.1016/j.coi.2015.12.007

Gill, K. S., Fernandes, P., O'Donovan, T. R., McKenna, S. L., Doddakula, K. K., Power, D. G., et al. (2016). Glycolysis inhibition as a cancer treatment and its role in an anti-tumour immune response. *Biochim. Biophys. Acta* 1866, 87–105. doi:10.1016/j.bbcan.2016.06.005

Greenfield, J. J., and High, S. (1999). The Sec61 complex is located in both the ER and the ER-Golgi intermediate compartment. *J. Cell Sci.* 112 (10), 1477–1486. doi:10.1242/jcs.112.10.1477

Hartmann, E., Sommer, T., Prehn, S., Gorlich, D., Jentsch, S., and Rapoport, T. A. (1994). Evolutionary conservation of components of the protein translocation complex. *Nature* 367, 654–657. doi:10.1038/367654a0

Hu, C., Tian, S., Lin, L., Zhang, J., and Ding, H. (2020). Prognostic and clinicopathological significance of PD-L1 and tumor infiltrating lymphocytes in hypopharyngeal squamous cell carcinoma. *Oral Oncol.* 102, 104560. doi:10.1016/j.oraloncology.2019.104560

Kuo, P., Sosa, J. A., Burtness, B. A., Husain, Z. A., Mehra, S., Roman, S. A., et al. (2016). Treatment trends and survival effects of chemotherapy for hypopharyngeal cancer: Analysis of the National Cancer Data Base. *Cancer-Am Cancer Soc.* 122, 1853–1860. doi:10.1002/cncr.29962

Li, R., Ye, L., Zhu, Y., Ding, H., Wang, S., Ying, H., et al. (2022). Induction chemotherapy of modified docetaxel, cisplatin, 5-fluorouracil for laryngeal preservation in locally advanced hypopharyngeal squamous cell carcinoma. *Head. Neck* 44, 2018–2029. doi:10.1002/hed.27119

Liang, L., Huang, Q., Gan, M., Jiang, L., Yan, H., Lin, Z., et al. (2021). High SEC61G expression predicts poor prognosis in patients with head and neck squamous cell carcinomas. *J. Cancer* 12, 3887–3899. doi:10.7150/jca.51467

Lim, S. O., Li, C. W., Xia, W., Lee, H. H., Chang, S. S., Shen, J., et al. (2016). EGFR signaling enhances aerobic glycolysis in Triple-Negative breast cancer cells to promote tumor growth and immune escape. *Cancer Res.* 76, 1284–1296. doi:10.1158/0008-5472.CAN-15-2478

Lin, C., Chen, Y., Zhang, F., Liu, B., Xie, C., and Song, Y. (2022). Encoding gene RAB3B exists in linear chromosomal and circular extrachromosomal DNA and contributes to cisplatin resistance of hypopharyngeal squamous cell carcinoma via inducing autophagy. *Cell Death Dis.* 13, 171. doi:10.1038/s41419-022-04627-w

Liu, Y. P., Zheng, C. C., Huang, Y. N., He, M. L., Xu, W. W., and Li, B. (2020). Molecular mechanisms of chemo- and radiotherapy resistance and the potential implications for cancer treatment. *MedComm* 2, 315–340. doi:10.1002/mco2.55

Lu, Z., Zhou, L., Killela, P., Rasheed, A. B., Di, C., Poe, W. E., et al. (2009). Glioblastoma proto-oncogene SEC61gamma is required for tumor cell survival and response to endoplasmic reticulum stress. *Cancer Res.* 69, 9105–9111. doi:10.1158/0008-5472.CAN-09-2775

Ma, J., He, Z., Zhang, H., Zhang, W., Gao, S., and Ni, X. (2021). SEC61G promotes breast cancer development and metastasis via modulating glycolysis and is transcriptionally regulated by E2F1. *Cell Death Dis.* 12, 550. doi:10.1038/s41419-021-03797-3

Marzouki, H., Addas, M. A., Nujoom, M., Zawawi, F., Almarzouki, H. Z., and Merdad, M. (2022). Hypopharyngeal reconstruction: Possibilities, outcomes, and updates for improving the human health for quality of life. *Comput. Intell. Neurosci.* 2022, 6132481. doi:10.1155/2022/6132481

Meng, H., Jiang, X., Wang, J., Sang, Z., Guo, L., Yin, G., et al. (2021). SEC61G is upregulated and required for tumor progression in human kidney cancer. *Mol. Med. Rep.* 23, 427. doi:10.3892/mmr.2021.12066

Mueckler, M., and Thorens, B. (2013). The SLC2 (GLUT) family of membrane transporters. *Mol. Asp. Med.* 34, 121–138. doi:10.1016/j.mam.2012.07.001

Mukhtar, E., Adhami, V. M., and Mukhtar, H. (2014). Targeting microtubules by natural agents for cancer therapy. *Mol. Cancer Ther.* 13, 275–284. doi:10.1158/1535-7163.MCT-13-0791

Naoum, G. E., Morkos, M., Kim, B., and Arafat, W. (2018). Novel targeted therapies and immunotherapy for advanced thyroid cancers. *Mol. Cancer* 17, 51. doi:10.1186/s12943-018-0786-0

Nishioka, T., Kim, H. S., Luo, L. Y., Huang, Y., Guo, J., and Chen, C. Y. (2011). Sensitization of epithelial growth factor receptors by nicotine exposure to promote breast cancer cell growth. *Breast Cancer Res.* 13, R113. doi:10.1186/bcr3055

Pitt, J. M., Marabelle, A., Eggermont, A., Soria, J. C., Kroemer, G., and Zitvogel, L. (2016). Targeting the tumor microenvironment: Removing obstruction to anticancer immune responses and immunotherapy. *Ann. Oncol.* 27, 1482–1492. doi:10.1093/annonc/mdw168

Raj, S., Kumar, A., and Kumar, D. (2021). Regulation of glycolysis in head and neck cancer. *Adv. Exp. Med. Biol.* 1280, 219–230. doi:10.1007/978-3-030-51652-9_15

Romero-Garcia, S., Moreno-Altamirano, M. M., Prado-Garcia, H., and Sanchez-Garcia, F. J. (2016). Lactate contribution to the tumor microenvironment: Mechanisms, effects on immune cells and therapeutic relevance. *Front. Immunol.* 7, 52. doi:10.3389/fimmu.2016.00052

Saito, S., Ozawa, H., Imanishi, Y., Sekimizu, M., Watanabe, Y., Ito, F., et al. (2021). Cyclooxygenase-2 expression is associated with chemoresistance through cancer stemness property in hypopharyngeal carcinoma. *Oncol. Lett.* 22, 533. doi:10.3892/ol.2021.12794

Sawayama, H., Ogata, Y., Ishimoto, T., Mima, K., Hiyoshi, Y., Iwatsuki, M., et al. (2019). Glucose transporter 1 regulates the proliferation and cisplatin sensitivity of esophageal cancer. *Cancer Sci.* 110, 1705–1714. doi:10.1111/cas.13995

Simons, A. L., Ahmad, I. M., Mattson, D. M., Dornfeld, K. J., and Spitz, D. R. (2007). 2-Deoxy-D-glucose combined with cisplatin enhances cytotoxicity via metabolic oxidative stress in human head and neck cancer cells. *Cancer Res.* 67, 3364–3370. doi:10.1158/0008-5472.CAN-06-3717

Uzcudun, A. E., Bravo, F. P., Sanchez, J. J., Garcia, G. A., Rabanal, R. I., Gonzalez, B. M., et al. (2001). Clinical features of pharyngeal cancer: A retrospective study of 258 consecutive patients. *J. Laryngol. Otol.* 115, 112–118. doi:10.1258/0022215011907703

Van den Bossche, V., Zaryouh, H., Vara-Messler, M., Vignau, J., Machiels, J. P., Wouters, A., et al. (2022). Microenvironment-driven intratumoral heterogeneity in head and neck cancers: Clinical challenges and opportunities for precision medicine. *Drug Resist Updat* 60, 100806. doi:10.1016/j.drup.2022.100806

Varghese, E., Samuel, S. M., Liskova, A., Samec, M., Kubatka, P., and Busselberg, D. (2020). Targeting glucose metabolism to overcome resistance to anticancer chemotherapy in breast cancer, *Cancers (Basel)*. 12, 2252. doi:10.3390/cancers12082252

Visini, M., Giger, R., Shelan, M., Elicin, O., and Anschuetz, L. (2021). Predicting factors for oncological and functional outcome in hypopharyngeal cancer. *Laryngoscope* 131, E1543–E1549. doi:10.1002/lary.29186

Wang, J., Lun, L., Jiang, X., Wang, Y., Li, X., Du, G., et al. (2021). APE1 facilitates PD-L1-mediated progression of laryngeal and hypopharyngeal squamous cell carcinoma. *Int. Immunopharmacol.* 97, 107675. doi:10.1016/j.intimp.2021.107675

Wang, Z. J., Chang, L. L., Wu, J., Pan, H. M., Zhang, Q. Y., Wang, M. J., et al. (2020). A novel rhynchophylline analog, y396, inhibits endothelial dysfunction induced by oxidative stress in diabetes through epidermal growth factor receptor. *Antioxid. Redox Signal* 32, 743–765. doi:10.1089/ars.2018.7721

Xie, M., Fu, X. G., and Jiang, K. (2021). Notch1/TAZ axis promotes aerobic glycolysis and immune escape in lung cancer. *Cell Death Dis.* 12, 832. doi:10.1038/s41419-021-04124-6

Xintaropoulou, C., Ward, C., Wise, A., Queckborner, S., Turnbull, A., Michie, C. O., et al. (2018). Expression of glycolytic enzymes in ovarian cancers and evaluation of the glycolytic pathway as a strategy for ovarian cancer treatment. *Bmc Cancer* 18, 636. doi:10.1186/s12885-018-4521-4

Yang, C., Xia, B. R., Zhang, Z. C., Zhang, Y. J., Lou, G., and Jin, W. L. (2020). Immunotherapy for ovarian cancer: Adjuvant, combination, and neoadjuvant. *Front. Immunol.* 11, 577869. doi:10.3389/fimmu.2020.577869

Yang, H., Shu, Z., Jiang, Y., Mao, W., Pang, L., Redwood, A., et al. (2019). 6-Phosphofructo-2-Kinase/Fructose-2, 6-Biphosphatase-2 regulates TP53-Dependent paclitaxel sensitivity in ovarian and breast cancers. *Clin. Cancer Res.* 25, 5702–5716. doi:10.1158/1078-0432.CCR-18-3448

Yang, Q., Tripathy, A., Yu, W., Eberhart, C. G., and Asnaghi, L. (2017). Hypoxia inhibits growth, proliferation, and increases response to chemotherapy in retinoblastoma cells. *Exp. Eye Res.* 162, 48–61. doi:10.1016/j.exer.2017.07.001

Yu, G., Wang, L. G., Han, Y., and He, Q. Y. (2012). ClusterProfiler: An R package for comparing biological themes among gene clusters. *Omics* 16, 284–287. doi:10.1089/omi.2011.0118

Yu, L., Gu, C., Zhong, D., Shi, L., Kong, Y., Zhou, Z., et al. (2014). Induction of autophagy counteracts the anticancer effect of cisplatin in human esophageal cancer cells with acquired drug resistance. *Cancer Lett.* 355, 34–45. doi:10.1016/j.canlet.2014.09.020

Zhang, X., Zhang, Y., Yu, X., Sun, Y., Miao, S., Liu, S., et al. (2021). Different primary sites of hypopharyngeal cancer have different lymph node metastasis patterns: A retrospective analysis from multi-center data. *Front. Oncol.* 11, 727991. doi:10.3389/fonc.2021.727991

Zhang, X. Y., Zhang, M., Cong, Q., Zhang, M. X., Zhang, M. Y., Lu, Y. Y., et al. (2018). Hexokinase 2 confers resistance to cisplatin in ovarian cancer cells by enhancing cisplatin-induced autophagy. *Int. J. Biochem. Cell Biol.* 95, 9–16. doi:10.1016/j.biocel.2017.12.010

Zhu, H., Wu, J., Zhang, W., Luo, H., Shen, Z., Cheng, H., et al. (2016). PKM2 enhances chemosensitivity to cisplatin through interaction with the mTOR pathway in cervical cancer. *Sci. Rep.* 6, 30788. doi:10.1038/srep30788

frontiers | Frontiers in Pharmacology

TYPE Original Research
PUBLISHED 25 January 2023
DOI 10.3389/fphar.2023.1102277

OPEN ACCESS

EDITED BY
Zhi-Yao He,
Sichuan University, China

REVIEWED BY
Huandi Zhou,
Second Hospital of Hebei Medical University, China
Hua Zhu,
Renmin Hospital of Wuhan University, China

*CORRESPONDENCE
Yongwei Zhu,
zhuyongwei@csu.edu.cn
Xuejun Li,
lxjneuro@csu.edu.cn

SPECIALTY SECTION
This article was submitted to Pharmacology of Anti-Cancer Drugs, a section of the journal Frontiers in Pharmacology

RECEIVED 18 November 2022
ACCEPTED 16 January 2023
PUBLISHED 25 January 2023

CITATION
Li Y, Zhu Y, Chen L, Xia S, Adegboro AA, Wanggou S and Li X (2023), Transcription factor ZBTB42 is a novel prognostic factor associated with immune cell infiltration in glioma.
Front. Pharmacol. 14:1102277.
doi: 10.3389/fphar.2023.1102277

Transcription factor ZBTB42 is a novel prognostic factor associated with immune cell infiltration in glioma

Yanwen Li[1,2], Yongwei Zhu[1,2]*, Long Chen[1,2], Shunjin Xia[1,2], Abraham Ayodeji Adegboro[1,2], Siyi Wanggou[1,2] and Xuejun Li[1,2]*

[1]Department of Neurosurgery, Xiangya Hospital, Central South University, Changsha, China, [2]Hunan International Scientific and Technological Cooperation Base of Brain Tumor Research, Xiangya Hospital, Central South University, Changsha, China

Background: ZBTB42 is a transcription factor that belongs to the ZBTB transcript factor family and plays an important role in skeletal muscle development. Dysregulation of ZBTB42 expression can lead to a variety of diseases. However, the function of ZBTB42 in glioma development has not been studied by now.

Methods: We analyzed the expression of ZBTB42 in LGG and GBM *via* the The Cancer Genome Atlas CGA and Chinese Glioma Genome Atlas database. Gene Ontology, KEGG, and GSVA analyses were performed to illustrate ZBTB42-related pathways. ESTIMATE and CIBERSORT were applied to calculate the immune score and immune cell proportion in glioma. One-class logistic regression OCLR algorithm was used to study the stemness of glioma. Multivariate Cox analysis was employed to detect the prognostic value of five ZBTB42-related genes.

Results: Our results show that ZBTB42 is highly expressed in glioma and may be a promising prognostic factor for Low Grade Glioma and GBM. In addition, ZBTB42 is related to immune cell infiltration and may play a role in the immune suppression microenvironment. What's more, ZBTB42 is correlated with stem cell markers and positively associated with glioma stemness. Finally, a five genes nomogram based on ZBTB42 was constructed and has an effective prognosis prediction ability.

Conclusion: We identify that ZBTB42 is a prognostic biomarker for Low Grade Glioma and GBM and its function is related to the suppressive tumor microenvironment and stemness of glioma.

KEYWORDS

glioma, ZBTB42, microenvironment, immune suppression, stemness

Introduction

Glioma is the most lethal cancer among brain tumors which have a complex pathogenetic mechanism and characteristic that is prone to relapse (Taga and Tabu, 2020). WHO (World Health Organization) classified glioma as grades I to IV based on histopathological characteristics and prognostic factors. Glioblastoma (GBM) is the most aggressive, invasive, and malignant brain tumor and has been defined as grade IV by WHO (Hanif et al., 2017). There is no effective strategy to cure this malignant disease. After surgery and radiotherapy with concomitant temozolomide treatment, 5-year survival in patients with glioblastoma is only 4.1% (Stupp et al., 2009). One reason is the intricate tumor microenvironment (TME) in glioma. In addition to tumor cells, the TME also harbors stromal cells, extracellular proteins, chemokines, growth factors, etc. These stromal cells and

extracellular matrix can facilitate tumor proliferation and help tumor cells resist hypoxia, radiotherapy, and chemotherapy (Nijkamp et al., 2013; Wu and Dai, 2017). In the meanwhile, the chemokines, cytokines, and growth factors secreted by tumor and stromal cells can induce immune cell infiltration in solid glioma tissue. The immune cells are usually reprogrammed into immunosuppressive phenotype and regulate the interaction between host and tumor, which can promote glioma development (Gieryng et al., 2017; Quail and Joyce, 2017). On the other hand, the immune checkpoints such as the programmed cell death 1 (PD-1) and the Cytotoxic T-lymphocyte associated protein 4 (CTLA4) expressed on the surface of the immune cells can decrease the T cell activation and proliferation (Huang et al., 2020). Therefore, immune therapy and immune checkpoint inhibitor (ICI) therapy have drawn much attention and brought hope to glioma patients.

ZBTB (Zinc finger and BTB domain-containing) transcript factors are a family of members, which is highly conserved in mammals and plays a crucial role in the development of the hemopoietic system and central neural system (Okado, 2021). Many ZBTB family genes such as Bcl6(ZBTB27), PLZF (ZBTB16), and Rp58 (ZBTB18, ZNF238), regulate neuronal cell's fate lineage decision, migration, maturation, and maintenance (Tiberi et al., 2012; Xiang et al., 2012; Gaber et al., 2013). Whereas, deregulation of these genes promotes multiple kinds of tumor progression, especially glioma. Bcl6 and cofactor NCoR complex repress the MEK-ERK and S6K-RPS6 pathway *via* regulating the expression of AXL to promote glioma proliferation (Xu et al., 2017). PLZF can stimulate cellular transformation and proliferation in glioma and increase tumor growth by repressing the transcription of CDKN1A (Choi et al., 2014). Low expression of Rp58 is associated with the epithelial-mesenchymal transition (EMT) and cell survival in glioma (Tatard et al., 2010; Xiang et al., 2021).

Here, we find that ZBTB42, a member of the ZBTB transcription factor family, is a new biomarker for glioma. ZBTB42 is known to be expressed in skeletal muscle and testis and mutation of ZBTB42 leads to Lethal congenital contracture syndrome (LCCS) (Takahashi et al., 2008; Patel et al., 2014). ZBTB42 expression knockdown with shRNA in glioma cells induced decreased growth ability (Xu et al., 2017). More interestingly, ZBTB42 is almost never expressed in the normal brain while highly expressed in glioma tissue, but its mechanism of regulating glioma progression is still unknown. In this study, we found abnormally high expression of ZBTB42 in glioma and verified this discovery with clinical glioma samples and cultured cells. Then we demonstrated that increased expression of ZBTB42 leads to an immunosuppressive microenvironment and a worse prognosis, and ZBTB42 is highly related to immune checkpoint genes. On the other hand, glioma patients with high expression of ZBTB42 usually comprise higher stemness of glioma which may be another aspect of ZBTB42 potential function in glioma.

Materials and methods

Data collection

The transcriptome expression of glioma, LGG and GBM was downloaded from the TCGA data portal (https://tcga-data.nci.nih.gov/tcga/) and CGGA database (http://www.cgga.org.cn/). The patients without clinical information were excluded. The expression of ZBTB42 in pan-cancer and GTEx was downloaded from GEPIA2. The mRNA expression and methylation of ZBTB42 from the TCGA database and GSE databases were obtained from the Brainbase website tool.

Clinical tissue collection and cell culture

15 glioma tissues and 11 normal brain samples were collected from Xiangya Hospital, Central South University between January 2016 and January 2022. Gliomas were classified according to 2016 WHO classification: five WHO II cases, four WHO III cases, and six WHO IV cases. The glioma tissues of different WHO grades and normal brain tissues were analyzed by immunohistochemistry staining (IHC) and 11 pairs of glioma samples and normal brain samples were analyzed by RT-qPCR. This study was approved by the Ethics Committee of Xiangya Hospital of Center South University. Human glioma cells HA 1,800, A172, U87, U251, HS683, and LN229 were purchased from Shanghai Cell bank. All cells were cultured in a humidified atmosphere containing 5% CO_2/95% air at 37°C. Dulbecco's Modified Eagle's Medium (high glucose) with 10% fetal bovine serum (Bovogen) and 1% penicillin/streptomycin was applied to culture cells.

Real-time quantitative polymerase chain reaction

The samples were kept at −80°C freezer until RNA extraction. We used Total RNA Extractor (Sangon Biotech, China) to extract RNA from clinical samples and cultured cells. The Prime Script® RT reagent Kit (Takara) was applied to synthesize RNA into cDNAs. RT-qPCR was performed in the 7,500 Real-time PCR System (Applied Biosystems) with SYBR Premix Ex Taq (Takara, Japan). The primers are ZBTB42: 5′-GCCGCCTACTGGACTTCATGTAC-3′(Forward), 5′-GCCCTTGCAGACCTTGACGATG -3′(Reverse) and GAPDH: 5′- TGACATCAAGAAGGTGGTGAAGCAG-3′(Forward), 5′-GTGTCGCTGTTGAAGTCAGAGGAG-3′(Reverse). Each assay was carried out in triplicate and $2^{-\triangle\triangle Ct}$ was calculated to analyze the gene expression difference.

Immunohistochemistry

Glioma tissues of different WHO grades and normal brain tissues were fixed with 4% paraformaldehyde and embedded in paraffin. Then, the tissues were sectioned into 4 μm and rehydrated with gradient concentration ethanol. Citrate buffer was used for antigen retrieval and 3% hydrogen peroxide (H_2O_2) was applied to quench endogenous peroxidase. After blocking in 10% normal goat serum, the sections were incubated with ZBTB42 antibody (1:500, HPA, HPA066961) overnight at 4°. Then, the sections were incubated by secondary antibody (goat anti-rabbit IgG, 1:5,000, Proteintech) for 1 h at room temperature. Finally, the sections were stained with diaminobenzidine tetrahydrochloride (DAB) and hematoxylin. The quantification of ZBTB42 immunohistochemistry staining was performed by the software ImageJ.

Gene set enrichment analysis and protein-protein interaction (PPI) network

The Differential Expression Genes (DEGs) were generated by "limma" package from the high ZBTB42 expression group and low expression group. The Gene Ontology (GO) and Kyoto

10.3389/fphar.2023.1102277

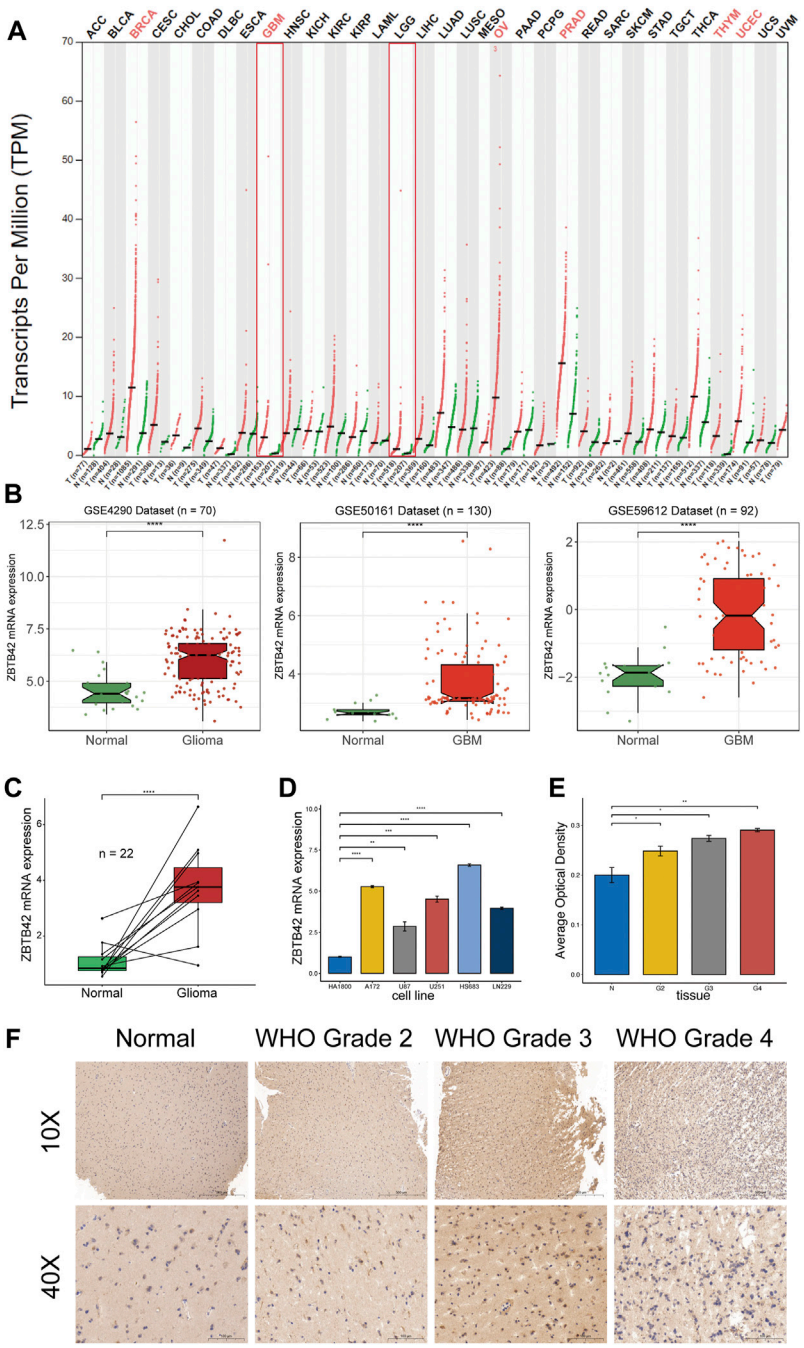

FIGURE 1
ZBTB42 expression profile in pan-cancer and glioma. **(A)** ZBTB42 mRNA expression of pan-cancer in TCGA dataset. **(B)** ZBTB42 is highly expressed in glioma compared with normal tissue in three different GEO datasets. **(C)** ZBTB42 mRNA expression in normal brain and glioma tissues. **(D)** ZBTB42 mRNA expression in human glia cell line and different glioma cell lines. **(E)** Quantification of ZBTB42 IHC staining between different WHO grades of gliomas and normal tissues (n = 12). **(F)** Immunohistochemistry staining of ZBTB42 in normal brain and glioma samples (n = 12). *p < 0.05; **p < 0.01; ***p < 0.001; ****p < 0.0001.

Encyclopedia of Genes and Genomics (KEGG) enrichment were then performed *via* the R package "clusterProfiler." The GSVA Reactome and Hallmark gene sets were obtained from the Molecular Signatures Database (MSigDB). The PPI was generated from the website tools STRING (https://string-db.org/).

Immune-related analysis

ESTIMATE algorithms were applied to calculate the immune score, stromal score, and ESTIMATE score of the high ZBTB42 expression and low expression groups. The proportion of immune cell infiltration was generated by "CIBERSORT." Correlation

10.3389/fphar.2023.1102277

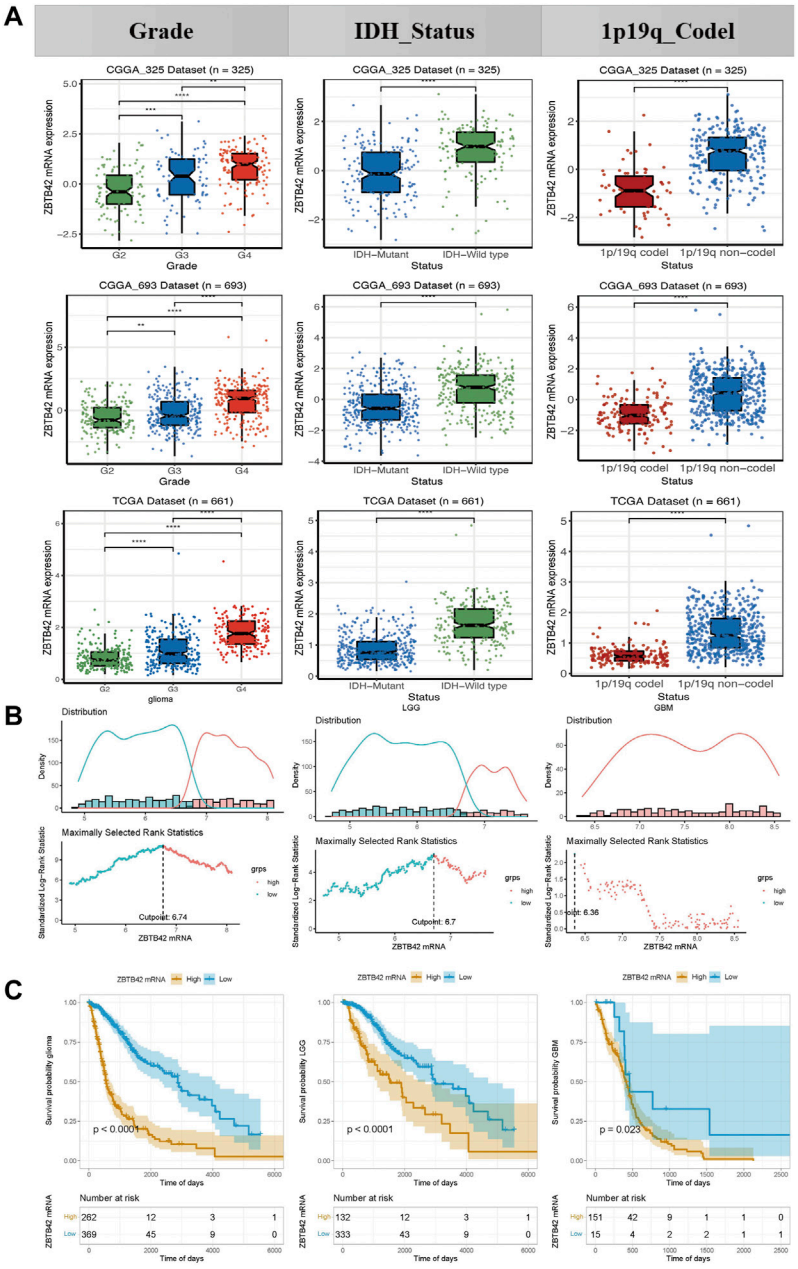

FIGURE 2
ZBTB42 expression in different subgroups of glioma and correlated with tumor progression. **(A)** Expression of ZBTB42 in clinical subgroups of glioma. **(B)** Optimal cut point determination in glioma, LGG, and GBM. **(C)** High expression of ZBTB42 leads to poor prognosis in both LGG and GBM. *$p < 0.05$; **$p < 0.01$; ***$p < 0.001$; ****$p < 0.0001$.

analysis of ZBTB42 with immune-related genes and stemness signature genes was carried out by R package "corrplot."

Statistical analysis

All statistical analyses were performed on R studio version 4.2.0. The Wilcoxon rank-sum test was applied to analyze the expression of ZBTB42 in cultured cells, AOD of normal tissue and glioma samples, and different clinicopathological subgroups. All statistical tests were two-sided. The $p < .05$ was regarded as a significant difference. The optimal cutting point was determined by the R package "Survminer" to separate glioma, LGG, and GBM patients into high ZBTB42 expression and low expression groups. The Kaplan-Meier plotter was utilized to illustrate the overall survival of glioma, LGG, and GBM patients between the high ZBTB42 expression and low expression groups. Least Absolute Shrinkage and Selection Operator (LASSO) regression filtrated DEGs between the high ZBTB42 expression and low expression groups into five prognostic genes. Multivariate cox regression analysis was performed to detect the independent prognostic performance of these genes. The nomogram based on prognostic genes was constructed by R package "rms." The

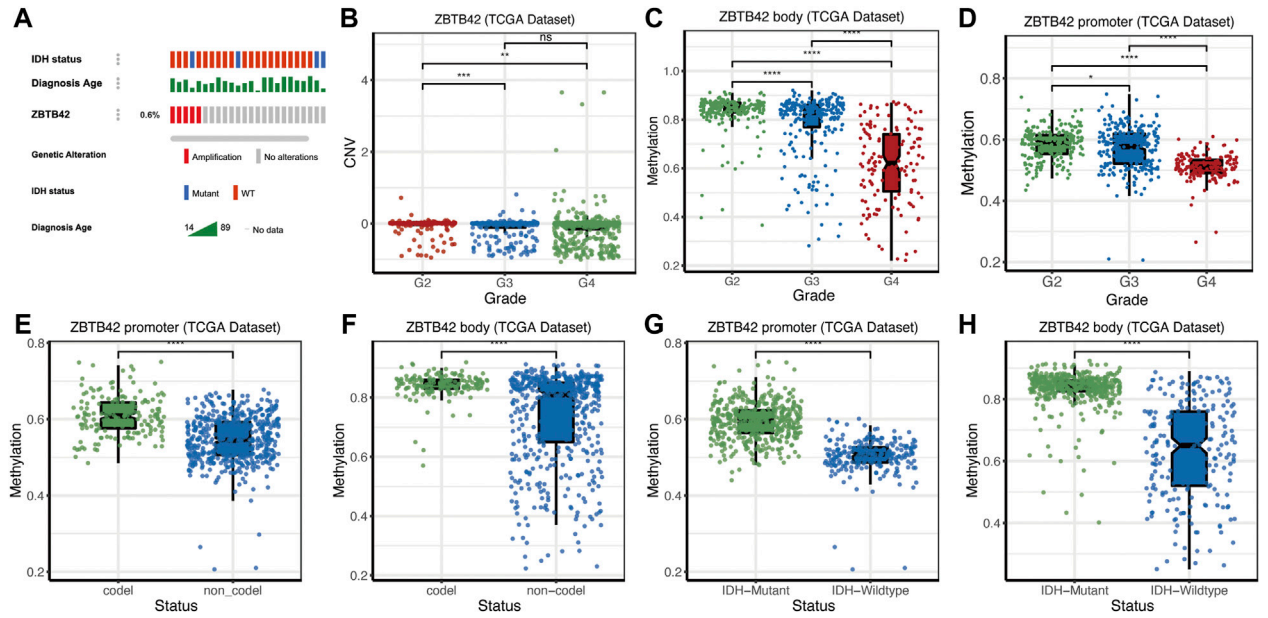

FIGURE 3
The copy number variations, mutation and epigenetic modification of ZBTB42 **(A)** Amplification state of ZBTB42 in glioma. **(B)** Copy number variations (CNVs) changes of ZBTB42. **(C,D)** Methylation of ZBTB42 promoter and ZBTB42 body in different WHO grades glioma. **(E,F)** Methylation of ZBTB42 promoter and ZBTB42 body in 1p19q codel and 1p19q non-codel subgroups. **(G,H)** Methylation of ZBTB42 promoter and ZBTB42 body in IDH wild type and mutant subgroups. *$p < 0.05$; **$p < 0.01$; ***$p < 0.001$; ****$p < 0.0001$.

area under curve (AUC) was generated by the R package "survivalROC" to evaluate the predictive ability of the model.

Result

ZBTB42 expression analysis in pan-cancer and glioma

To investigate the expression of ZBTB42 in normal tissue and tumors, we used the online tool GEPIA2 to analyze this gene in 34 tumors versus adjacent tissues (or GTEX). According to Figure 1A, the expression of ZBTB42 is slightly increased in breast invasive carcinoma (BRCA), glioblastoma multiforme (GBM), ovarian serous cystadenocarcinoma (OV), Prostate adenocarcinoma (PRAD), thymoma (THYM), and uterine corpus endometrial carcinoma (UCEC), while it is also increased in many other tumors including Brain Low Grade Glioma (LGG). To further verify ZBTB42 expression in glioma, especially in GBM, Brainbase was used to analyze multiple glioma GSE datasets. In GSE4290, GSE50161, and GSE59612, ZBTB42 expression is highly elevated in glioma and GBM (Figure 1B). Furthermore, we performed ZBTB42 RT-qPCR on glioma and normal brain tissue. The increased expression of ZBTB42 was observed and the difference was significant (Figure 1C). Compared with normal human glia cells, the A172, U87, U251, HS683, and LN229 shows increasing expression of ZBTB42 (Figure 1D). The immunohistochemistry staining showed an evident ZBTB42 signal in different WHO grades of glioma samples (Figure 1F). The quantification analysis of area optical density (AOD) indicated that ZBTB42 is higher expressed in glioma tissues compared with normal brain tissue (Figure 1E). The graphic schematic and immunofluorescence on the U-2 OS and MCF7 cell lines showed that ZBTB42 is expressed in the nucleus and cell membrane (Supplementary Figures S1A, B). Meanwhile, we found that in the GTEx dataset, ZBTB42 is lowly expressed in brain tissue (Supplementary Figures S1C, D) which indicated that ZBTB42 may play a role in the development of glioma.

ZBTB42 shows expression preference in malignant subtypes of glioma and is correlated with tumor progression

To further understand the distribution of ZBTB42 in glioma with different clinical parameters, we analyzed the glioma patients from the CGGA-325 cohort, CGGA-693 cohort, and the TCGA dataset by the Brainbase website. Interestingly, the level of ZBTB42 expression increased with the improvement of the WHO grade in all glioma datasets (Figure 2A). Remarkably, compared with the IDH mutant and 1p/19q codeletion subgroup, a higher expression of ZBTB42 was observed in the IDH wild type and 1p/19q non-codeletion subgroup (Figure 2A). These data suggested that ZBTB42 may be involved in glioma malignancy progression. Then we asked does ZBTB42 deregulation plays a role in the progression of glioma. We divided the 631 TCGA glioma patients into high ZBTB42 expression and low expression groups by optimal cutoff point (Figure 2B). Kaplan-Meier plotter analysis showed that the patients in the high expression group, have poor overall survival (Figure 2C). When we analyzed the LGG and GBM separately, the conclusions were the same (Figure 2C).

To answer why the expression of ZBTB42 is elevated, we moved to the genetic alterations, copy number variation (CNV), and

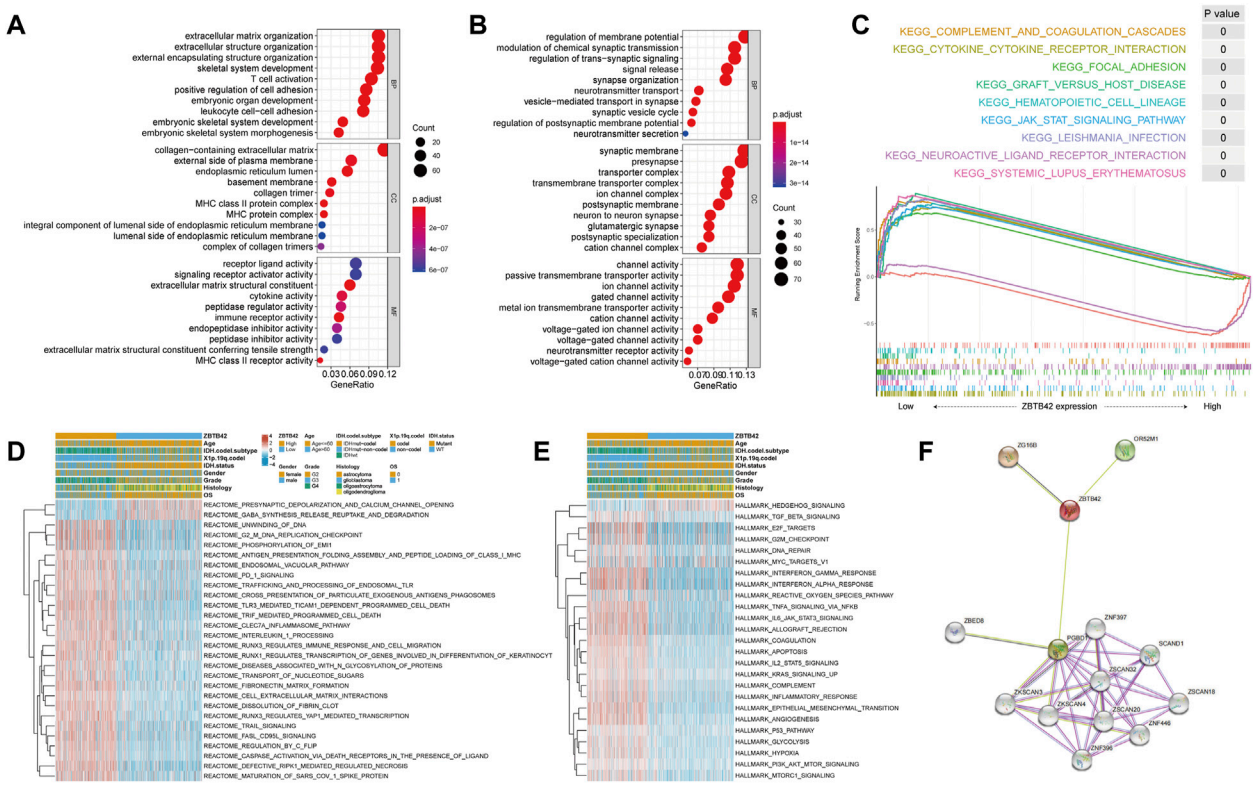

FIGURE 4
Pathway enrichment analysis of dysregulation of ZBTB42 in TCGA cohort. **(A,B)** Biological process analysis on upregulated genes **(A)** and downregulated genes **(B)** between the ZBTB42 high expression group and low expression group. **(C)** The pathways related to upregulated genes and downregulated genes by KEGG enrichment analysis. **(D)** GSVA analysis on Reactome gene set between glioma patients with high ZBTB42 expression and low expression. **(E)** GSVA analysis on Hallmark gene set between glioma patients with high ZBTB42 expression and low expression. **(F)** Protein-protein interaction network based on ZBTB42-related genes by STRING database. The lines between genes represent protein-protein associations and different colors represent how these relationships were validated. The green line represents two genes are neighborhood genes; The pink line represents the relationship that has been experimentally determined by existing papers. The black line represents two genes that are co-expressed. The purple line represents protein homology.

methylation modification of ZBTB42 in the TCGA dataset. Firstly, we check the genetic alterations state. ZBTB42 is amplified in .6% of glioma patients and most of which are IDH wild-type glioma (Figure 3A). The CNV decreased in Grade 3 glioma compared with Grade 2 while there was no significant difference between Grade 3 and Grade 4 (Figure 3B). In terms of epigenetics, we found that the methylation of ZBTB42 promoter and body decreases accompanied by Grade 2 to Grade 4 (Figures 3C, D). A similar demethylation of ZBTB42 also appeared in the IDH wild-type and 1p19q non-codeletion subgroup (Figures 3E–H). Therefore, the demethylation of the promoter and body may result in the increased expression of ZBTB42, and abnormal expression of ZBTB42 reveals a more severe tumor progression.

Pathway enrichment analysis of dysregulation of ZBTB42 in TCGA cohort

To elucidate the effect of ZBTB42 alteration on biological functions in glioma, we compared the high ZBTB42 expression group and low expression group in glioma and filtered out upregulated and downregulated genes. After that, GO and KEGG enrichment analyses were performed. In GO analysis of upregulated genes, we found that except for skeletal system development which we already know, most related pathways were focusing on extracellular matrix and immune-related pathways such as T cell activation, MHC class II protein complex, and immune receptor activity (Figure 4A). Spearman correlation analysis showed that ZBTB42 was highly related to the T cell activation-related genes, such as CD28, CD247, AKT1, etc., (Supplementary Figure S2). In terms of downregulated genes, the pathways were focusing on the channel activity of the cell member (Figure 4B). In the KEGG analysis, the upregulated genes were in the hematopoietic cell lineage, cytokine-cytokine receptor, and JAK-STAT signaling pathway (Figure 4C). Taken all together, we speculated that dysregulation of ZBTB42 in glioma affects glioma progression *via* the tumor microenvironment, especially the immune microenvironment.

To verify this hypothesis, we performed GSVA analysis with DEGs between the high ZBTB42 expression group and low expression group on Reactome and Hallmark gene sets from MSigDB. The GSVA Reactome analysis suggests multiple pathways such as PD1 signaling, CLEC7A inflammasome, and immune response were positively related to upregulated genes. Besides that, the cell-extracellular matrix, cell cycle, and cell death pathways were also highly related to these genes (Figure 4D). In GSVA hallmark analysis, a similar result was detected (Figure 4E), which confirmed the

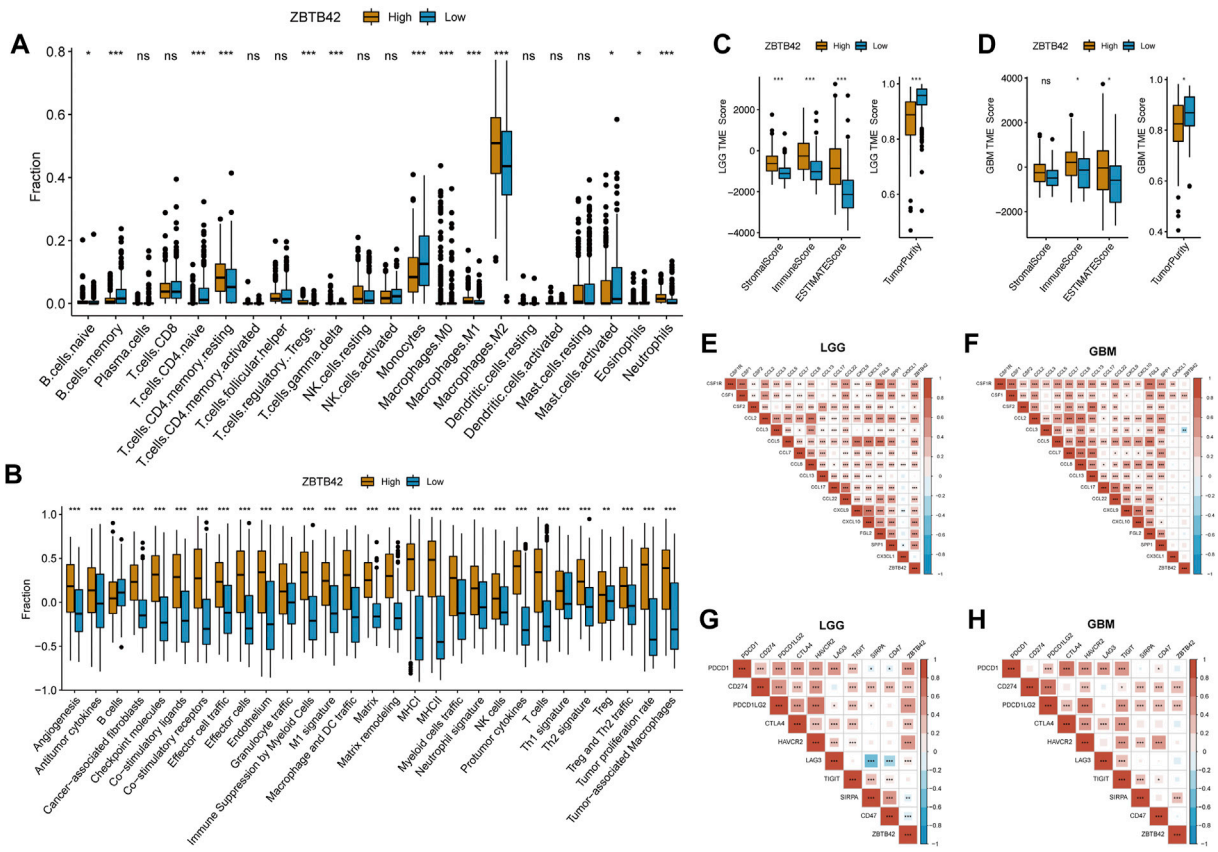

FIGURE 5
High ZBTB42 expression group is associated with immune suppression in glioma. **(A)** The fraction of 22 immune cell infiltration in high ZBTB42 expression group and low expression group of gliomas. **(B)** Immune-related signature scores between high ZBTB42 expression group and low expression group of gliomas by ssGSEA analysis. **(C,D)** Stromal score, Immune score, and ESTIMATE score, and tumor purity of LGG **(C)** and GBM **(D)** in the TCGA dataset. **(E–H)** Map of ZBTB42 correlation with cytokine genes, chemokine genes, and immune checkpoint genes in LGG **(E, G)** and GBM **(F, H)**. $*p < 0.05$; $**p < 0.01$; $***p < 0.001$.

relativity between ZBTB42 and the glioma microenvironment. In addition, protein-protein interaction suggested that ZBTB42 potentially interacted with PGBD1, ZSCAN20, and ZNF396. These genes are all associated with glioma prognosis and ZSCAN20 is related to the immune infiltration of tumors (Figure 4F).

The high ZBTB42 expression group is associated with immune suppression in glioma

To further investigate the interaction between the high ZBTB42 expression group with the immune microenvironment in glioma, the CIBERSORT algorithm was applied to detect immune cell proportion in glioma from the TCGA dataset. Interestingly, compared with the low expression group, the high expression group had more immune cell infiltration, such as resting $CD4^+$ memory T cells, Treg cells, M1 Macrophages, and M2 Macrophages (Figure 5A). In contrast, the number of memory B cells, naïve T cells, and monocytes in the high expression group decreased. Increasing T reg cells and M2 macrophages suggested that there was immune suppression in the high expression group microenvironment. Then, we performed ssGSEA analysis to explore the immune-related signature variations. The results showed that checkpoint molecules, immune suppression by myeloid cells, protumor cytokines, and Treg signature were increased in the high expression group (Figure 5B). To calculate immune scores and verify the presence of infiltrating immune cells, ESTIMATE algorithms were employed in LGG and GBM patients from the TCGA dataset. In LGG, the result showed that all three scores were increased and the tumor purity was decreased in the high expression group, predicting the existence of more stroma cells and immune cells (Figure 5C). In GBM, the Stromal score, Immune score, and ESTIMATE score were higher and the tumor purity was lower in the high ZBTB42 expression group. However, the difference in stromal score wasn't significant (Figure 5D). In addition, we found that ZBTB42 was positively related to chemokines and cytokines, such as FGL2, SPP1, and CCL, CXCL subfamilies (Figure 5E). In both LGG and GBM, ZBTB42 was positively related to CSF1, which is known for promoting glioma immune suppression (Figures 5E, F). On the other hand, the immune checkpoint gene like PD1 was reported to inhibit T cell effects, induce T cell inactivity and make T cells exhausted. Correlation analysis showed that ZBTB42 was positively related to PD1, PD-L1, PD-L2, CTLA4, TIM3, and LAG3 in LGG (Figure 5G) and positively related to PD-L1, PD-L2, SIRPA in GBM (Figure 5H), suggesting that the high expression of ZBTB42 may promote glioma progression *via* immune suppression microenvironment.

10.3389/fphar.2023.1102277

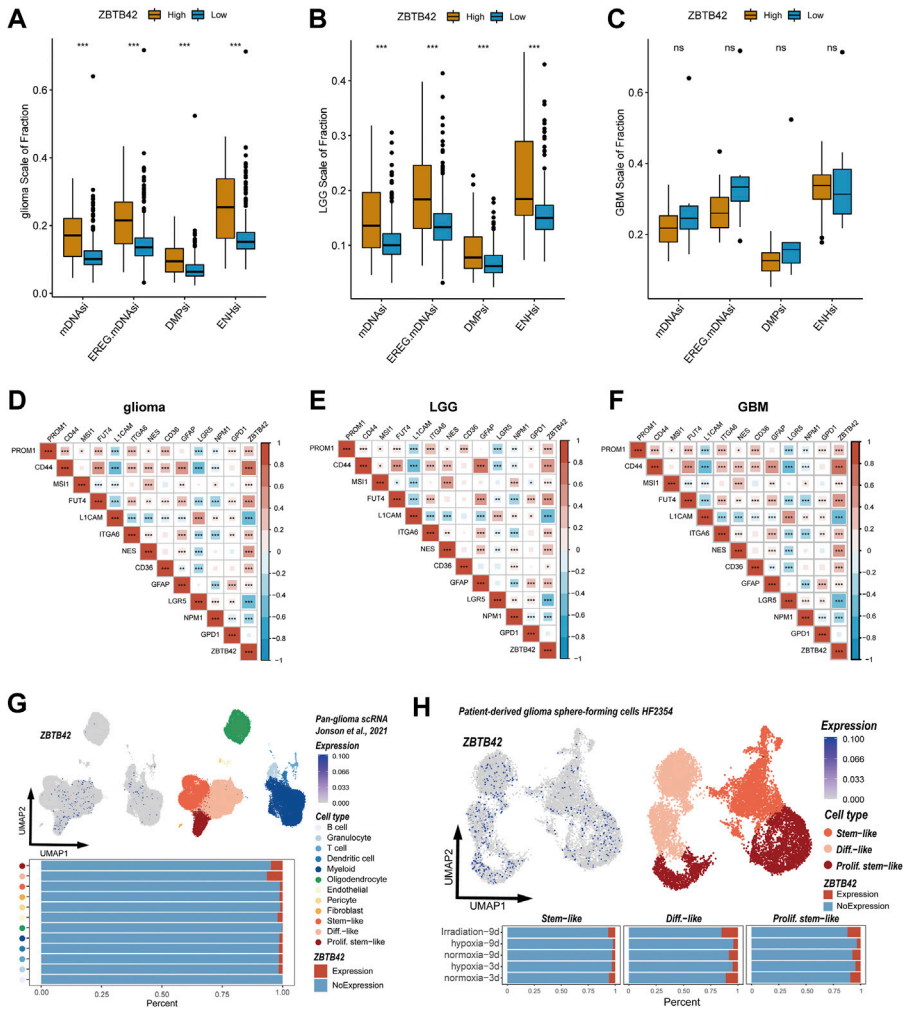

FIGURE 6
High ZBTB42 expression is related to the stronger tumor-stemness feature of glioma. **(A,B)** mDNAsi, EREG.mDNAsi, DMPsi, and ENHsi of high ZBTB42 expression and low expression group in glioma **(A)**, LGG **(B)** and GBM **(C)**. **(D–F)** Map of ZBTB42 correlation with stemness characteristic genes in glioma **(D)**, LGG **(E)**, and GBM **(F)**. **(G,H)** ZBTB42 was expressed in stem-like and proliferation stem-like cell subtypes analyzed by single cell sequencing data. *$p < 0.05$; **$p < 0.01$; ***$p < 0.001$.

High ZBTB42 expression is related to the stronger tumor-stemness feature of glioma

Interestingly, in the GO and KEGG analysis, the upregulation genes were enriched in the cell cycle, and cytokines (Figure 4A). In ssGSEA analysis, tumor proliferation-related signatures and extracellular matrix signatures such as angiogenesis, protumor cytokines, tumor proliferation rate, and matrix remodeling were also significantly improved in the high ZBTB42 expression group (Figure 5B). Therefore, we asked if ZBTB42 is related to the stemness of glioma. To answer this question, four stemness indices were calculated by the one-class logistic regression (OCLR) algorithm in glioma, LGG, and GBM. We found that the stemness indices of the high expression group were significantly higher than the low expression group in glioma and LGG (Figures 6A, B). However, we didn't get the same conclusion in GBM (Figure 6C). To further validate our assumption, correlation analysis was performed between ZBTB42 and stemness markers. ZBTB42 was positively related to stem cell markers like PROM1, CD44, MSI1, FUT4, ITGA6, NES, CD36, and GFAP in glioma, LGG, and GBM (Figures 6D–F). In addition, we collected the single cell sequence data of glioma. As a result, we found ZBTB42 was mainly expressed in stem-like cells and differentiation-like cells (Figure 6G). We also detected the expression of ZBTB42 in sphere-forming cells which received radiation and a hypoxia culture environment. Interestingly, the expression of ZBTB42 was increased in stem-like, differentiation-like, and proliferation stem-like cells after radiation, indicating that ZBTB42 wasn't only related to the stemness of glioma but also may play a role in radiation resistance in glioma treatment (Figure 6H). These data suggested that increased expression of ZBTB42 was also associated with the stemness of glioma and may play a role in glioma stem cells.

Construction of a ZBTB42-related prognostic model

To further illustrate the potential role of ZBTB42 in glioma, we applied Lasso regression on the DEGs between the high ZBTB42 expression group and low expression group in LGG patients (Figures 7A, B). 5 genes were detected which were mostly

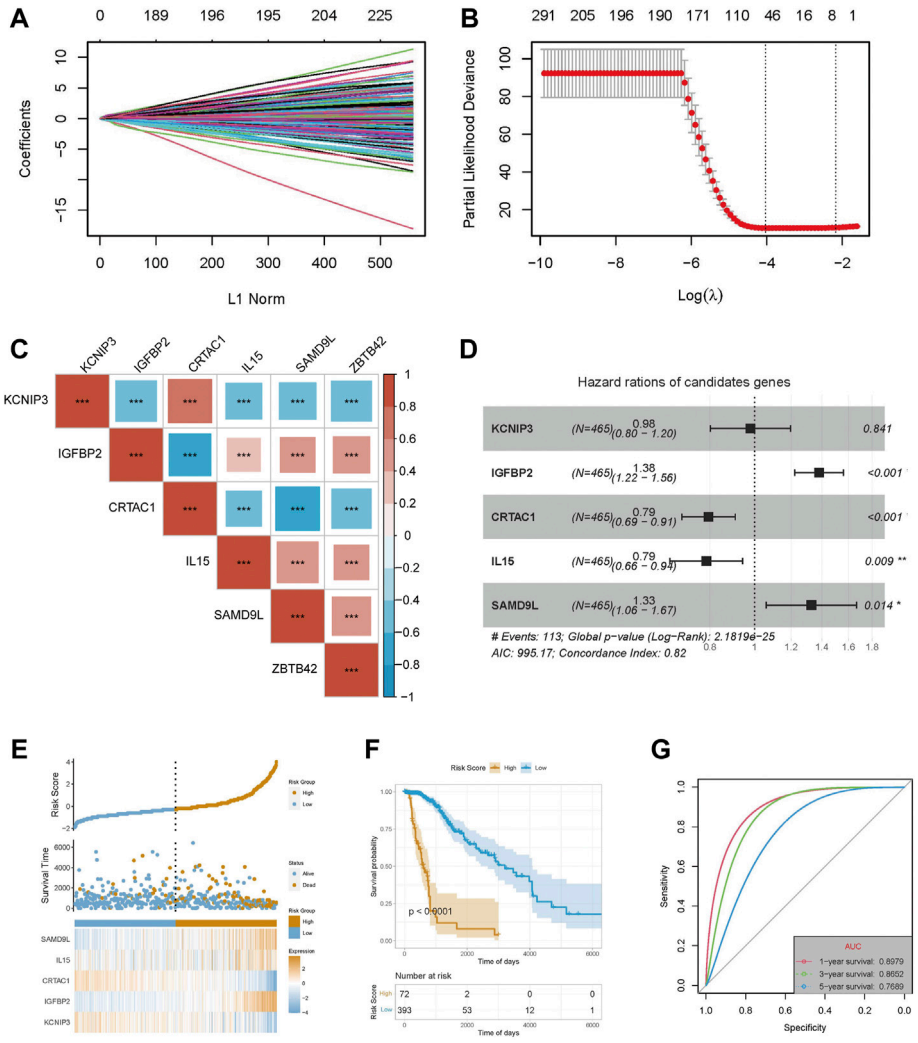

FIGURE 7
Construction of a prognostic model with ZBTB42-related genes in LGG. **(A)** LASSO coefficients profiles of DEG between high ZBTB42 expression group and low expression group in LGG. **(B)** LASSO regression with cross-validation obtained optimal prognostic-related genes in LGG. **(C)** Map of ZBTB42 correlation with prognostic related genes in LGG. **(D)** Multivariate Cox analysis of KCNIP3, IGFBP2, CRTAC1, IL15, and SAMD9L with clinical outcomes for LGG. **(E)** The risk score, survival time, and expression distribution of the five genes in the LGG cohort. **(F)** Kaplan-Meier survival analysis of high-risk model and low-risk model. **(G)** Prediction sensitivity validation of the prognostic model by receiver operating characteristic (ROC) curve analysis in 1, 3, and 5 years for LGG patients. *$p < 0.05$; **$p < 0.01$; ***$p < 0.001$.

related to the clinical prognosis. Interestingly, all these genes were related to the expression of ZBTB42 in LGG (Figure 7C). Multivariate Cox analysis confirmed that these genes were independent prognostic factors for LGG patients (Figure 7D). The risk score and survival time showed that the high risk group had a poor clinical outcome (Figure 7E). Kaplan-Meier plotter analysis showed that the low-risk group of the patients had a better prognosis (Figure 7F). The area under the curve (AUC) of 1 year, 3 years, and 5 years were 0.898, 0.865, and 0.769 indicating that this model can predict the survival of glioma patients efficiently (Figure 7G). Furthermore, we verified the prognostic value of these genes in GBM and glioma *via* multivariate Cox analysis (Supplementary Figures S3A, B). The result suggested that KCNIP, IGFBP2, IL5, and SAMD9L were independent poor prognostic factors for GBM and glioma. On the other hand, CRTAC1 was associated with good clinical outcomes. The patients were divided into high risk group and low risk group based on the distribution of expression of five genes and the high risk group was associated with a bad prognosis (Supplementary Figures S3C, D, G, H). The Kaplan-Meier plotter and ROC analysis confirmed the good performance of these genes in the clinical prediction (Supplementary Figures S3E, F, I, J). The same analysis was also performed in the CGGA-325 cohort and CGGA-693 and the results support that 5 ZBTB42-related genes have good prognostic prediction ability (Supplementary Figure S4).

Discussion

ZBTB42 was found in the testes, and regulates the development of skeletal muscle, while its function in tumors hasn't been well described (Takahashi et al., 2008). Here we first illustrated the ZBTB42 expression profile in pan-cancer and investigated its

potential relationship with glioma. High expression is detected in glioma and leads to a poor prognosis. The epigenetic modification of glioma plays a crucial role in tumor cell plasticity and resistance to hypoxia, chemotherapy, and radiotherapy (Johnson et al., 2021). The most common epigenetic alteration in malignant tumors is methylation. The methylation of intergenic regions, gene bodies, and DNA repetitive sequences in DNA repair and tumor suppressor genes is an important part of tumor formation and progression (Aoki and Natsume, 2019; Ehrlich, 2019). In glioma, the methylation status of the O6-methylguanine-DNA methyltransferase (MGMT) promotor is associated with the response to temozolomide treatment (Aoki and Natsume, 2019; Mathur et al., 2020). Our data show increased ZBTB42 promotor and gene body methylation preference in benign subtypes of glioma, which is negatively related to ZBTB42 expression. In addition, a high level of ZBTB42 methylation leads to better overall survival in LGG patients. Collectively, ZBTB42 is a prognostic biomarker of glioma and the hypomethylation of ZBTB42 is, at least partly, the reason for the promotion of ZBTB42 expression.

In our present study, we performed GO, KEGG, and GSVA analysis on the DEGs. The pathways enriched are mainly focused on immune response, T cell activation, cytokines, and JAK-STAT signaling. The tumor microenvironment is a complicated cellular milieu constructed during tumorigenesis which consists of tumor cells, immune cells, stromal cells, and extracellular matrix molecules (Hanahan and Coussens, 2012; Senga, 2021). The immune cells such as macrophages, T cells, B cells, natural killer cells, dendritic cells, and myeloid-derived suppressor cells (MDSCs) interact with stromal cells, tumor cells, cytokines and decide the immune characteristics and tumor progression (Nagarsheth et al., 2017). The tumor-associatediated macrophages (TAMs), which contain M1 and M2 subgroups, take up the largest proportion of the immune cells and usually play an immunosuppressive role in microenviroment regulation (Grabowski et al., 2021). M1 macrophages are antineoplastic because of their enhanced antitumor inflammatory reactions and intrinsic phagocytosis function while M2 macrophages behave as immune-suppressor with immunosuppressive factors secretion and decreased antigen-presentingenting ability (Ruffell et al., 2014; Zhou et al., 2017; Liu et al., 2021). Besides the antiinflammation, the M2 macrophages can also induce angiogenesis to promote tumor growth and metastasis (Martinez et al., 2008; Fleetwood et al., 2009). In the tumor microenvironment, T reg cells are a subset of $CD4^+$ T cells and they can curtail the function of multiple immune cells by decreasing the production of interleukin (IL)-2 and interferon (IFN)-γ, increasing Th2 cytokine skewing, and directly inhibiting of endogenous generation and expansion (Humphries et al., 2010). Our immune cell infiltration analysis shows increasing M2 macrophages and T-reg cells in the high ZBTB42 expression group. In the contrast, the number of memory B cells, naïve T cells, and monocytes decreased. Colony-stimulating factor-1(CSF-1) plays an important role in the differentiation and survival of TAM (Pyonteck et al., 2013). Several experiments were performed to target glioma-associated macrophage populations by colony-stimulating factor-1 receptor (CSF-1R). In mice, inhibition of CSF-1R can either block the transformation of M2 macrophages or deplete TAMs to prevent glioma progression and invasion (Yan et al., 2017). The survival in the preclinical model was enhanced efficiently in the treatment group (Pyonteck et al., 2013; Sun et al., 2019; Akkari et al., 2020). In the correlation analysis, ZBTB42 is positively related to the expression of CSF-1 in both LGG and GBM indicating ZBTB42 is associated with immune suppression in glioma and this feature may be related to the increased expression of CSF-1.

Moreover, the immune checkpoint genes can induce immune suppression and anti-immune checkpoint inhibitors (ICI) have been wildly studied both in basic research and clinical trials (Qi et al., 2020). Programmed Cell Death Protein 1 (PD-1), which has become the most comprehensively immune checkpoint molecule, is a transmembrane protein on the T and B cells and plays a crucial role in inducing immunosuppression. PD-1 can modulate the activity of T-cells, activate apoptosis of antigen-specific T cells, and inhibit apoptosis of Treg cells (Han et al., 2020). Cytotoxic T-lymphocyte-associated protein 4 (CTLA-4) express on the activated T cells and Treg cells and belongs to the immunoglobulin superfamily. CTLA4 can inhibit T cell co-stimulatory by combining with the ligands CD80 and CD86 which are expressed on antigen-presenting cells (APCs) (Fong et al., 2012). We found that ZBTB42 is associated with PD1, and PD-L1. PD-L2, CTLA4 HAVCR2, LAG3. Considering that ZBTB42 is expressed in the nucleus and cell membrane, targeting ZBTB42 may help people precisely kill cells with immune checkpoints and promote the overall survival of patients.

On the other hand, glioma stem cells (GSCs) are an important part of the glioma microenvironment and regulate glioma initiation, progression, and recurrence (Folkins et al., 2007). In the tumor microenvironment, the GSCs can secret cytokines such as fibroblast growth factor 2 (FGF2), hypoxia-inducing factor (HIF), and vascular endothelial growth factor (VEGF) to promote tumor invasion, recruit immune cells, induce angiogenesis, and self-renew (Hambardzumyan and Bergers, 2015). ZBTB42 is positively related to glioma stem cells marker genes such as CD44, MSI1, Fut4, and NES and the high expression group has a stronger relationship with glioma stemness. Interestingly, we found that ZBTB42 was expressed in the stem-like, proliferation stem-like, and differentiation-like cells based on the download single cell sequencing data (Johnson et al., 2021). After radiation, the percentage of ZBTB42 in the above tumor cells was increased, indicating that ZBTB42 may play a role in the radiation resistance of glioma cells.

Finally, we sorted out 5 genes which highly related to ZBTB42 and they showed potent prognostic value. Based on these genes, we constructed a nomogram model which has a sensitive prognosis prediction ability in LGG, GBM, and glioma patients. This model may help clinicians make clinical prognosis predictions and decide on treatment strategies.

Conclusion

In summary, we have identified ZBTB42 as a novel prognostic biomarker for glioma. ZBTB42 is related to immune suppression and glioma stemness in the microenvironment. Targeting ZBTB42 treatment may help glioma patients have better overall survival.

Data availability statement

The original contributions presented in the study are included in the article/Supplementary Material, further inquiries can be directed to the corresponding authors.

Ethics statement

The studies involving human participants were reviewed and approved by The Ethics Committee of the Xiangya Hospital Central South University. The patients/participants provided their written informed consent to participate in this study.

Author contributions

YL authored drafts of the paper. AA helped with the draft preparation. YZ analyzed the data and prepared the figures. YL and LC collected clinical samples. YL, LC, and SX performed cell culture, qPCR and IHC. XL, SW, and YZ conceived the experiments and reviewed drafts of the paper. All authors approved the final draft.

Funding

This work was funded by National Natural Science Foundation of China (grant no. 81770781, 81472594).

Conflict of interest

The authors declare that the research was conducted in the absence of any commercial or financial relationships that could be construed as a potential conflict of interest.

Publisher's note

All claims expressed in this article are solely those of the authors and do not necessarily represent those of their affiliated organizations, or those of the publisher, the editors and the reviewers. Any product that may be evaluated in this article, or claim that may be made by its manufacturer, is not guaranteed or endorsed by the publisher.

Supplementary material

The Supplementary Material for this article can be found online at: https://www.frontiersin.org/articles/10.3389/fphar.2023.1102277/full#supplementary-material

References

Akkari, L., Bowman, R. L., Tessier, J., Klemm, F., Handgraaf, S. M., De Groot, M., et al. (2020). Dynamic changes in glioma macrophage populations after radiotherapy reveal CSF-1R inhibition as a strategy to overcome resistance. *Sci. Transl. Med.* 12, eaaw7843. doi:10.1126/scitranslmed.aaw7843

Aoki, K., and Natsume, A. (2019). Overview of DNA methylation in adult diffuse gliomas. *Brain Tumor Pathol.* 36, 84–91. doi:10.1007/s10014-019-00339-w

Choi, W. I., Kim, M. Y., Jeon, B. N., Koh, D. I., Yun, C. O., Li, Y., et al. (2014). Role of promyelocytic leukemia zinc finger (PLZF) in cell proliferation and cyclin-dependent kinase inhibitor 1A (p21WAF/CDKN1A) gene repression. *J. Biol. Chem.* 289, 18625–18640. doi:10.1074/jbc.M113.538751

Ehrlich, M. (2019). DNA hypermethylation in disease: Mechanisms and clinical relevance. *Epigenetics* 14, 1141–1163. doi:10.1080/15592294.2019.1638701

Fleetwood, A. J., Dinh, H., Cook, A. D., Hertzog, P. J., and Hamilton, J. A. (2009). GM-CSF- and M-CSF-dependent macrophage phenotypes display differential dependence on type I interferon signaling. *J. Leukoc. Biol.* 86, 411–421. doi:10.1189/jlb.1108702

Folkins, C., Man, S., Xu, P., Shaked, Y., Hicklin, D. J., and Kerbel, R. S. (2007). Anticancer therapies combining antiangiogenic and tumor cell cytotoxic effects reduce the tumor stem-like cell fraction in glioma xenograft tumors. *Cancer Res.* 67, 3560–3564. doi:10.1158/0008-5472.CAN-06-4238

Fong, B., Jin, R., Wang, X., Safaee, M., Lisiero, D. N., Yang, I., et al. (2012). Monitoring of regulatory T cell frequencies and expression of CTLA-4 on T cells, before and after DC vaccination, can predict survival in GBM patients. *PLoS One* 7, e32614. doi:10.1371/journal.pone.0032614

Gaber, Z. B., Butler, S. J., and Novitch, B. G. (2013). PLZF regulates fibroblast growth factor responsiveness and maintenance of neural progenitors. *PLoS Biol.* 11, e1001676. doi:10.1371/journal.pbio.1001676

Gieryng, A., Pszczolkowska, D., Walentynowicz, K. A., Rajan, W. D., and Kaminska, B. (2017). Immune microenvironment of gliomas. *Lab. Invest.* 97, 498–518. doi:10.1038/labinvest.2017.19

Grabowski, M. M., Sankey, E. W., Ryan, K. J., Chongsathidkiet, P., Lorrey, S. J., Wilkinson, D. S., et al. (2021). Immune suppression in gliomas. *J. Neurooncol* 151, 3–12. doi:10.1007/s11060-020-03483-y

Hambardzumyan, D., and Bergers, G. (2015). Glioblastoma: Defining tumor niches. *Trends Cancer* 1, 252–265. doi:10.1016/j.trecan.2015.10.009

Han, Y., Liu, D., and Li, L. (2020). PD-1/PD-L1 pathway: Current researches in cancer. *Am. J. Cancer Res.* 10, 727–742.

Hanahan, D., and Coussens, L. M. (2012). Accessories to the crime: Functions of cells recruited to the tumor microenvironment. *Cancer Cell* 21, 309–322. doi:10.1016/j.ccr.2012.02.022

Hanif, F., Muzaffar, K., Perveen, K., Malhi, S. M., and Simjee, S. H. U. (2017). Glioblastoma multiforme: A review of its epidemiology and pathogenesis through clinical presentation and treatment. *Asian Pac J. Cancer Prev.* 18, 3–9. doi:10.22034/APJCP.2017.18.1.3

Huang, B., Li, X., Li, Y., Zhang, J., Zong, Z., and Zhang, H. (2020). Current immunotherapies for glioblastoma multiforme. *Front. Immunol.* 11, 603911. doi:10.3389/fimmu.2020.603911

Humphries, W., Wei, J., Sampson, J. H., and Heimberger, A. B. (2010). The role of tregs in glioma-mediated immunosuppression: Potential target for intervention. *Neurosurg. Clin. N. Am.* 21, 125–137. doi:10.1016/j.nec.2009.08.012

Johnson, K. C., Anderson, K. J., Courtois, E. T., Gujar, A. D., Barthel, F. P., Varn, F. S., et al. (2021). Single-cell multimodal glioma analyses identify epigenetic regulators of cellular plasticity and environmental stress response. *Nat. Genet.* 53, 1456–1468. doi:10.1038/s41588-021-00926-8

Liu, J. Y., Geng, X. F., Hou, J. X., and Wu, G. S. (2021). New insights into M1/M2 macrophages: Key modulators in cancer progression. *Cancer Cell Int.* 21, 389. doi:10.1186/s12935-021-02089-2

Martinez, F. O., Sica, A., Mantovani, A., and Locati, M. (2008). Macrophage activation and polarization. *Front. Biosci.* 13, 453–461. doi:10.2741/2692

Mathur, R., Zhang, Y., Grimmer, M. R., Hong, C., Zhang, M., Bollam, S., et al. (2020). MGMT promoter methylation level in newly diagnosed low-grade glioma is a predictor of hypermutation at recurrence. *Neuro Oncol.* 22, 1580–1590. doi:10.1093/neuonc/noaa059

Nagarsheth, N., Wicha, M. S., and Zou, W. (2017). Chemokines in the cancer microenvironment and their relevance in cancer immunotherapy. *Nat. Rev. Immunol.* 17, 559–572. doi:10.1038/nri.2017.49

Nijkamp, M. M., Span, P. N., Bussink, J., and Kaanders, J. H. (2013). Interaction of EGFR with the tumour microenvironment: Implications for radiation treatment. *Radiother. Oncol.* 108, 17–23. doi:10.1016/j.radonc.2013.05.006

Okado, H. (2021). Nervous system regulated by POZ domain Kruppel-like zinc finger (POK) family transcription repressor RP58. *Br. J. Pharmacol.* 178, 813–826. doi:10.1111/bph.15265

Patel, N., Smith, L. L., Faqeih, E., Mohamed, J., Gupta, V. A., and Alkuraya, F. S. (2014). ZBTB42 mutation defines a novel lethal congenital contracture syndrome (LCCS6). *Hum. Mol. Genet.* 23, 6584–6593. doi:10.1093/hmg/ddu384

Pyonteck, S. M., Akkari, L., Schuhmacher, A. J., Bowman, R. L., Sevenich, L., Quail, D. F., et al. (2013). CSF-1R inhibition alters macrophage polarization and blocks glioma progression. *Nat. Med.* 19, 1264–1272. doi:10.1038/nm.3337

Qi, Y., Liu, B., Sun, Q., Xiong, X., and Chen, Q. (2020). Immune checkpoint targeted therapy in glioma: Status and hopes. *Front. Immunol.* 11, 578877. doi:10.3389/fimmu.2020.578877

Quail, D. F., and Joyce, J. A. (2017). The microenvironmental landscape of brain tumors. *Cancer Cell* 31, 326–341. doi:10.1016/j.ccell.2017.02.009

Ruffell, B., Chang-Strachan, D., Chan, V., Rosenbusch, A., Ho, C. M., Pryer, N., et al. (2014). Macrophage IL-10 blocks CD8+ T cell-dependent responses to chemotherapy by suppressing IL-12 expression in intratumoral dendritic cells. *Cancer Cell* 26, 623–637. doi:10.1016/j.ccell.2014.09.006

Senga, S. (2021). Hallmarks of cancer. *Eur. J. Cancer Prev.* 31, S11. doi:10.1097/01.cej.0000816704.67680.d7

Stupp, R., Hegi, M. E., Mason, W. P., Van Den Bent, M. J., Taphoorn, M. J., Janzer, R. C., et al. (2009). Effects of radiotherapy with concomitant and adjuvant temozolomide versus radiotherapy alone on survival in glioblastoma in a randomised phase III study: 5-year

analysis of the EORTC-NCIC trial. *Lancet Oncol.* 10, 459–466. doi:10.1016/S1470-2045(09)70025-7

Sun, L., Liang, H., Yu, W., and Jin, X. (2019). Increased invasive phenotype of CSF-1R expression in glioma cells via the ERK1/2 signaling pathway. *Cancer Gene Ther.* 26, 136–144. doi:10.1038/s41417-018-0053-y

Taga, T., and Tabu, K. (2020). Glioma progression and recurrence involving maintenance and expansion strategies of glioma stem cells by organizing self-advantageous niche microenvironments. *Inflamm. Regen.* 40, 33. doi:10.1186/s41232-020-00142-7

Takahashi, A., Hirai, S., Ohtaka-Maruyama, C., Miwa, A., Hata, Y., Okabe, S., et al. (2008). Co-localization of a novel transcriptional repressor simiRP58 with RP58. *Biochem. Biophys. Res. Commun.* 368, 637–642. doi:10.1016/j.bbrc.2008.01.147

Tatard, V. M., Xiang, C., Biegel, J. A., and Dahmane, N. (2010). ZNF238 is expressed in postmitotic brain cells and inhibits brain tumor growth. *Cancer Res.* 70, 1236–1246. doi:10.1158/0008-5472.CAN-09-2249

Tiberi, L., Van Den Ameele, J., Dimidschstein, J., Piccirilli, J., Gall, D., Herpoel, A., et al. (2012). BCL6 controls neurogenesis through Sirt1-dependent epigenetic repression of selective Notch targets. *Nat. Neurosci.* 15, 1627–1635. doi:10.1038/nn.3264

Wu, T., and Dai, Y. (2017). Tumor microenvironment and therapeutic response. *Cancer Lett.* 387, 61–68. doi:10.1016/j.canlet.2016.01.043

Xiang, C., Baubet, V., Pal, S., Holderbaum, L., Tatard, V., Jiang, P., et al. (2012). RP58/ZNF238 directly modulates proneurogenic gene levels and is required for neuronal differentiation and brain expansion. *Cell Death Differ.* 19, 692–702. doi:10.1038/cdd.2011.144

Xiang, C., Frietze, K. K., Bi, Y., Li, Y., Dal Pozzo, V., Pal, S., et al. (2021). RP58 represses transcriptional programs linked to nonneuronal cell identity and glioblastoma subtypes in developing neurons. *Mol. Cell Biol.* 41, e0052620. doi:10.1128/MCB.00526-20

Xu, L., Chen, Y., Dutra-Clarke, M., Mayakonda, A., Hazawa, M., Savinoff, S. E., et al. (2017). BCL6 promotes glioma and serves as a therapeutic target. *Proc. Natl. Acad. Sci. U. S. A.* 114, 3981–3986. doi:10.1073/pnas.1609758114

Yan, D., Kowal, J., Akkari, L., Schuhmacher, A. J., Huse, J. T., West, B. L., et al. (2017). Inhibition of colony stimulating factor-1 receptor abrogates microenvironment-mediated therapeutic resistance in gliomas. *Oncogene* 36, 6049–6058. doi:10.1038/onc.2017.261

Zhou, D., Yang, K., Chen, L., Zhang, W., Xu, Z., Zuo, J., et al. (2017). Promising landscape for regulating macrophage polarization: Epigenetic viewpoint. *Oncotarget* 8, 57693–57706. doi:10.18632/oncotarget.17027

frontiers | Frontiers in Pharmacology

TYPE Original Research
PUBLISHED 09 February 2023
DOI 10.3389/fphar.2023.1138452

OPEN ACCESS

EDITED BY
Zhijie Xu,
Xiangya Hospital, Central South University, China

REVIEWED BY
Wei Shenyu,
Zhejiang Chinese Medical University, China
Liu Yunfei,
Ludwig Maximilian University of Munich, Germany

*CORRESPONDENCE
Deping Dong,
depingdong123@sina.com
Songtao Yuan,
yuansongtao@vip.163.com
Xinyuan Zhao,
zhaoxinyuan@ntu.edu.cn

†These authors have contributed equally to this work

SPECIALTY SECTION
This article was submitted to Pharmacology of Anti-Cancer Drugs, a section of the journal Frontiers in Pharmacology

RECEIVED 05 January 2023
ACCEPTED 30 January 2023
PUBLISHED 09 February 2023

CITATION
Meng S, Zhu T, Fan Z, Cheng Y, Dong Y, Wang F, Wang X, Dong D, Yuan S and Zhao X (2023), Integrated single-cell and transcriptome sequencing analyses develops a metastasis-based risk score system for prognosis and immunotherapy response in uveal melanoma. *Front. Pharmacol.* 14:1138452. doi: 10.3389/fphar.2023.1138452

Integrated single-cell and transcriptome sequencing analyses develops a metastasis-based risk score system for prognosis and immunotherapy response in uveal melanoma

Shuting Meng[1†], Tianye Zhu[2†], Zhiwei Fan[3], Yulan Cheng[4], Yefeng Dong[1], Fengxu Wang[4], Xuehai Wang[4], Deping Dong[1*], Songtao Yuan[2*] and Xinyuan Zhao[4*]

[1]Hai an People's Hospital, Nantong, China, [2]Department of Ophthalmology, The First Affiliated Hospital of Nanjing Medical University, Nanjing, China, [3]School of Medicine, Nantong University, Nantong, China, [4]Nantong Key Laboratory of Environmental Toxicology, Department of Occupational Medicine and Environmental Toxicology, School of Public Health, Nantong University, Nantong, China

Background: Uveal melanoma (UM) is the most frequent ocular neoplasm with a strong metastatic ability. The prognostic value of metastasis-associated genes (MAGs) of UM remains unclear. It is urgent to develop a prognostic score system according to the MAGs of UM.

Methods: Unsupervised clustering was used to identify MAGs-based molecular subtypes. Cox methods were utilized to generate a prognostic score system. The prognostic ability of the score system was detected by plotting ROC and survival curves. The immune activity and underlying function were depicted by CIBERSORT GSEA algorithms.

Results: Gene cluster analysis determined two MAGs-based subclusters in UM, which were remarkably different in clinical outcomes. A risk score system containing six MAGs (COL11A1, AREG, TIMP3, ADAM12, PRRX1 and GAS1) was set up. We employed ssGSEA to compare immune activity and immunocyte infiltration between the two risk groups. Notch, JAK/STAT and mTOR pathways were greatly enriched in the high-risk group. Furthermore, we observed that knockdown of AREG could inhibit UM proliferation and metastasis by *in vitro* assays.

Conclusion: The MAGs-based subtype and score system in UM can enhance prognosis assessment, and the core system provides valuable reference for clinical decision-making.

KEYWORDS

uveal melanoma, metastasis, prognosis, immunotherapy response, drug sensitivity, areg

Introduction

Uveal melanoma (UM), the major primary intraocular malignancy in adults, accounts for 83% of intraocular melanomas. Among them, choroidal, ciliary and iris melanomas account for 85%–90%, 5%–8%, and 3%–5%, respectively (Singh et al., 2011). Patients mostly complain of decreased visual acuity, visual distortion, and loss of visual field, and 30% of patients may not

have any ocular symptom, making them highly susceptible to underdiagnosis and misdiagnosis. This highly malignant disease is prone to invasive metastasis, mainly in the liver (89%) (Diener-West et al., 2005). Once metastasized, the prognosis is extremely poor. Currently, UM is mainly treated by ophthalmopexy, local tumor resection, local radiation therapy (external scleral dressing or stereotactic radiation therapy, proton beam treatment) and laser photocoagulation treatment (transpupillary thermal or photodynamic therapy) (Carvajal et al., 2017). The high proliferative activity of UM cells and the extreme susceptibility to extraocular metastasis are the main reasons for the therapeutic difficulty and high mortality of this tumor. However, the current treatments for UM are ineffective against tumor metastasis (Augsburger et al., 2009), so most studies have diverted to immunotherapy. Identification of probable biomarkers of UM may offer key data for early recurrence monitoring or treatment (Bol et al., 2016). Currently, though some key genes and pathways in UM are identified, the prognosis remains unsatisfactory (Xue et al., 2019). Hence, new markers are urgently needed to evaluate the prognosis of UM.

With the fast advancement of immunotherapy recently, the tumor microenvironment (TME) is reportedly pivotal in cancer growth and therapeutic response (Arneth, 2019). Prognostic or predictive biomarkers related to TME may largely help assess tumor prognosis and advance oncology therapies.

TME is a complicated and integrated system consisting of various stromal cells, such as fibroblasts, smooth muscle cells, immune and inflammatory cells, glial cells, adipocytes, and some vascular cells (Song et al., 2021a; Liu et al., 2022a). These cells can be initiated by tumor cells to produce abundant growth factors, cytokines, and stromal degrading enzymes around them, which facilitate the division and invasion of tumor cells (Song et al., 2021b). TME is the material basis for the survival and development of tumor cells, and TME and tumor cells are an interdependent and mutually promoting whole (Chen et al., 2021; Liu et al., 2022b). TME is physiologically characteristic of low oxygen, low pH and high interstitial hydraulic pressure, which provide the necessary material basis for tumor formation, development, invasion, metastasis, drug therapy resistance, and immune response (Watnick, 2012).

Tumor metastasis is a major factor contributing to the poor prognostic outcome of various cancers. There are several theoretical models about the mechanism of tumor metastasis, and the most prevalent one is the epithelial-mesenchymal transition (EMT) theory (Mittal, 2018). This theory suggests that first some cells during tumor metastasis undergo EMT, which causes tumor cells to lose their cell-to-cell adhesion and fall off from the tumor tissues into the blood circulation system. Then the cells flow with the blood to other suitable places for growth (Song et al., 2021c). EMT leads to tumor cytoskeleton rearrangement, reduced cellular rigidity and cell/cellular connectivity, facilitating tumor metastasis and invasion (Davis et al., 2014).

Diverse developmental signaling pathways, such as tumor growth factor (TGF)-β, WNT, NOTCH and growth factor receptor tyrosine kinase, are associated with the induction of EMT in certain physiological circumstances. TGF-β, a cytokine released by tumor cells and stromal fibroblasts in the TME, is regarded a main cause of EMT (Katsuno et al., 2013). Other signaling pathways involved in EMT induction are inflammatory cytokines such as TNF-a *via* NF-jB (Wu et al., 2009), IL-6/STAT pathways (Lo et al., 2007) and extracellular matrix (ECM) stiffness (Wei et al., 2015). Then these signaling molecules can stimulate various EMT transcribing factors EMT-(tf) to start the EMT program, including inhibition of epithelial markers and stimulation of mesenchymal markers.

The occurrence of $CD4^+$ T lymphocyte inflammatory infiltration in UM has been reported. Moreover, the ability of $CD4^+$CD25+FoxP3+ Treg cells to suppress Th1 or cytotoxic T lymphocyte reactions is a main principle of tumor escape in many cancers (Amaro et al., 2017). In cardiomyocyte studies, fibroblast growth factor (FGF)-2 generation can be modulated transcriptionally (Jin et al., 2000) and FGF-2 prevents UM cells from growth restriction by bromodomain and extra-terminal protein inhibitors (Chua et al., 2019). In addition, EMT may contribute to the transdifferentiation of epithelial tumor cells, conferring their migration and invasiveness (Smolkova et al., 2018).

In present academic research, two independent UM cohorts were utilized explore the significance of metastasis-associated genes (MAGs) in UM in order to explore new prognostic biomarkers. We set up a MAGs-based risk score system for forecasting prognosis of UM cases. Our data disclosed potential function and prognostic power of MAGs in UM. Furthermore, AREG was selected to confirm the model accuracy by various wet lab experiments.

Materials and methods

Data collection

The gene expression profile and relevant clinical data were acquired from the GEO (https://www.ncbi.nlm.nih.gov/geo/) and TCGA (https://portal.gdc.cancer.gov/) databases, respectively. The TCGA-UM cohort including the gene expressions and clinical data of 80 UM patients was chosen as the training set to build a prognostic model. The GSE22138 with RNA sequencing of 63 UM samples was used as the validating set. The metastasis-associated genes (MAGs) obtained from MSigDB website (https://www.gsea-msigdb.org/gsea/index.jsp) are provided in Supplementary Table S1.

Construction of MAGs-based risk score system (MBRSS)

Prognostic genes in the training set were identified through univariate Cox analysis. Then the coefficients of these model genes were computed to construct a prognostic model *via* multivariate analysis. The equation is: risk score = $\sum_{i=1}^{n}(coef \times Exp_i)$, where Exp_i and coef are the expression level and risk coefficient of each gene respectively. The patients were classified by the median risk score into high- and low-risk groups. An external dataset GSE68465 was adopted to validate the predictive ability of signature.

Functional enrichment analysis

GSEA was done to uncover the probable molecular mechanisms of the prognostic genes at the cutoff value of adjusted $p < 0.05$. The signaling pathways for UM were recognized using the Kyoto Encyclopedia of Genes and Genomes (KEGG) on R clusterProfiler and visualized on R ggplot2 (Yu et al., 2012).

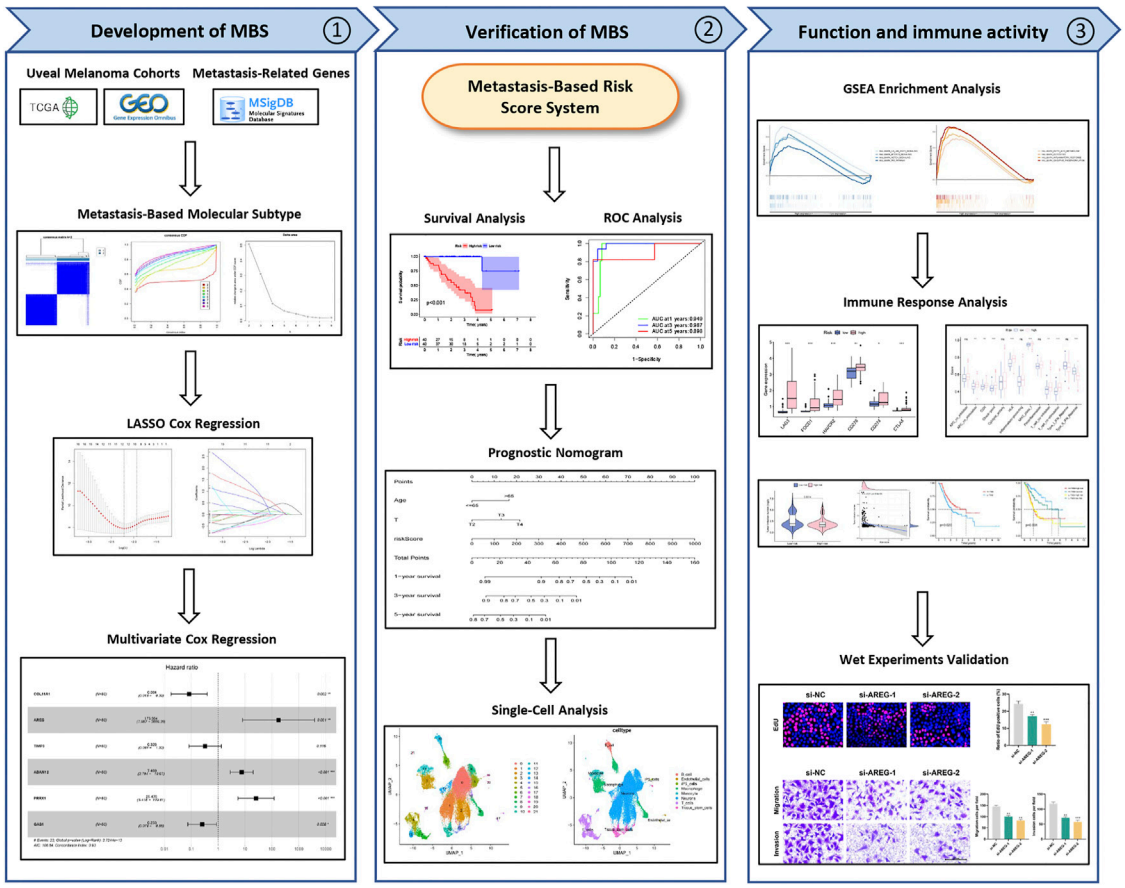

FIGURE 1
The flowchart of the present research.

Determination of a prognostic nomogram

The independence of the model was determined *via* Cox regression analyses. Then a nomogram was set up to strengthen the predictive ability of the model based on diverse clinical traits. The nomogram was verified *via* a calibration curves.

Immune activity analysis

Relative infiltration levels of 21 types of immune cells were quantified using the CIBERSORT algorithm as described before (Subramanian et al., 2005). The immune activities between groups, as de-scribed by the normalized enrichment score (NES), were compared with single sample gene set enrichment analysis (ssGSEA).

Single-cell analysis

To investigate the expression pattern of genes at single-cell level, GSE139829 dataset including 11 samples was collected from GEO database. We applied "Seurat" R package to conduct data quality control and normalization. The UMAP algorithm was employed to reduce the dimension of data. Next, cells were annotated according to surface markers.

Cell culture and transfection

Human UM cell line (MUM-2B) was obtained from the Fuheng Biology Inc., (Fuheng, Shanghai, China). For MUM-2B cell culture, DMEM (keyGEN bioTECH, China) with 10% fetal bovine serum (FBS) was used. Cells were transfected with the synthesized siRNAs (GenePharma, China) targeting AREG by the Lipofectamine3000 based on the manufacturer's protocol. The siRNA-AREG sequences are provided in Supplementary Table S2.

Quantitative real-time PCR

The cell total RNA of was collected using RNA easy reagent (Vazyme, China) and cDNA was obtained using a PrimeScript RT

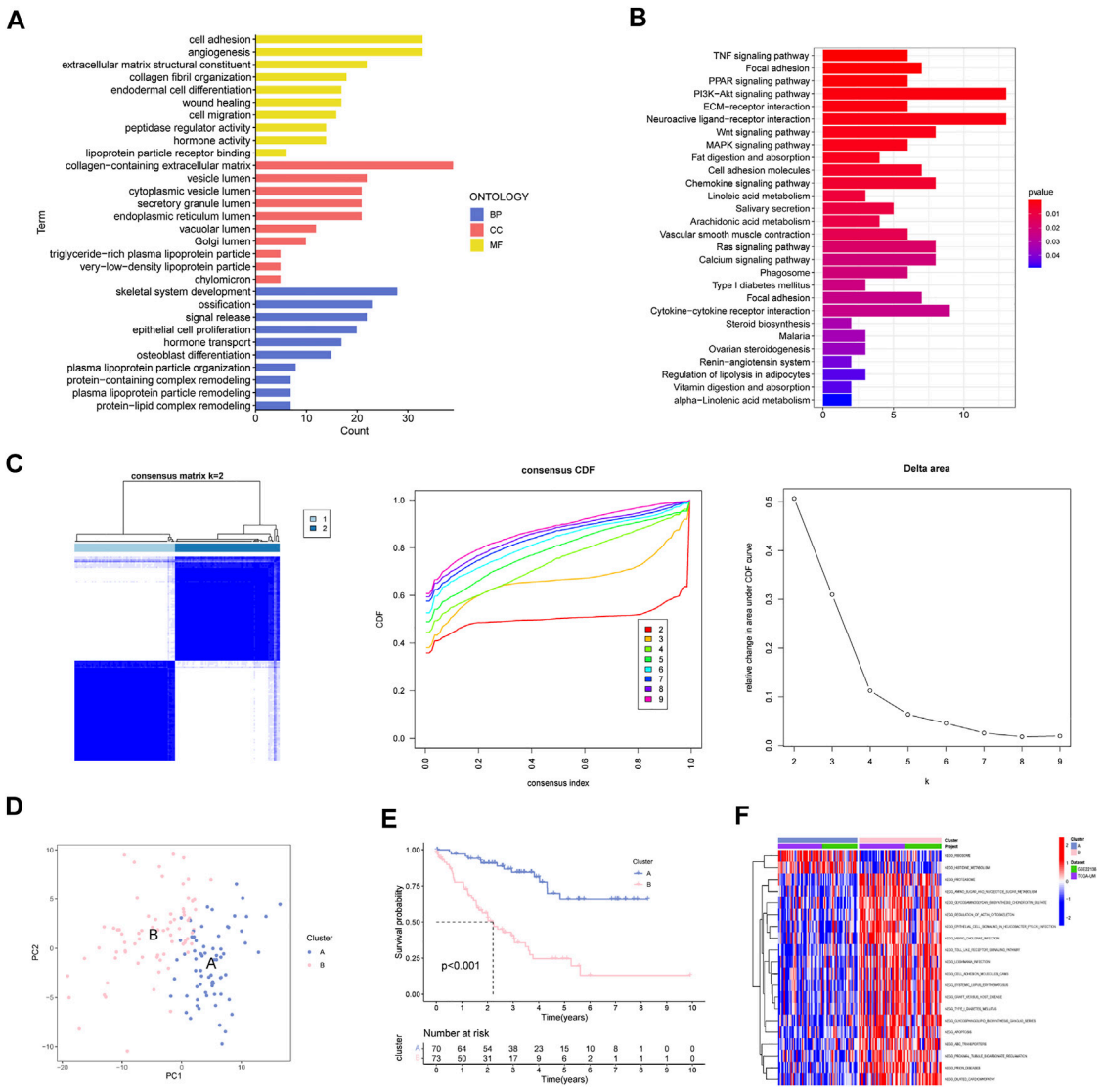

FIGURE 2
Determination of MAGs-based Molecular Subtype in UM. **(A)** GO analysis, **(B)** KEGG enrichment and **(C)** Consensus clustering analysis of MAGs. **(D)** PCA, **(E)** survival analysis and **(F)** GSVA analysis of two subclusters.

Reagent Kit (Takara, Japan). Then, qRT-PCR was performed through a ChamQ SYBR qPCR Master Mix (Vazyme, China). The relative expression levels of m RNA were normalized to GAPDH. The primer sequences of AREG and GAPDH are shown in Supplementary Table S1.

Cell capability assay

The transfected cells were seeded in a 96-well plate. Cell capability was measured by CellTiter-Glo luminescent cell viability assay (CTG, Promega, Germany). After CTG kit incubation, the luminescence was detected multifunctional enzyme marker.

EdU assay

The transfected cells were seeded in a 96-well plate. Following incubation in EdU reagent (Ribobio, China) for 2 h, cells were fixed and permeated, and stained with Apollo reagent for half hour. Nuclei were stained with Hoechst 33342.

Migration and invasion assays

A transwell insert with 8 mm pores (Millipore) was utilized. In the upper chamber, 1×10^4 cells were seeded in 200 mL media without serum, while 500 mL complete medium was supplied in the lower chamber. Based on the manufacturer's instructions, we performed Matrigel for the invasion detection (BD Biosciences, United States).

Immunofluorescence (IF) assay

After 30 min of treatment with the blocking solution, cells were incubated with primary antibody (E-cadherin and N-cadherin) overnight. Fluorescence-labeled secondary antibodies and DAPI were then applied for staining.

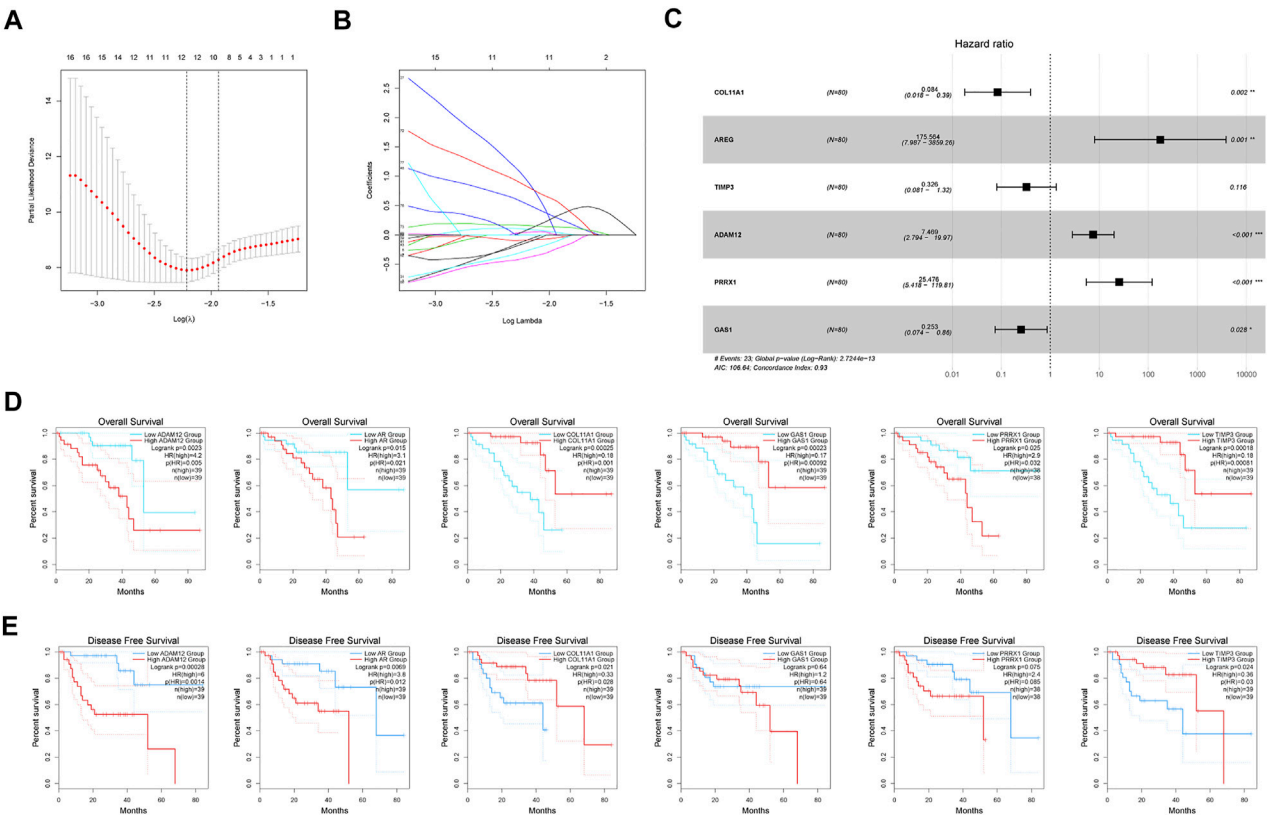

FIGURE 3
Development of the MAGs-based score system. **(A–B)** LASSO coefficient profile analysis. **(C)** Six MAGs identified for score system (*$p < 0.05$, **$p < 0.01$, ***$p < 0.001$). Kaplan-Meier curves of **(D)** OS and **(E)** DFS.

Statistical analysis

All statistical analyses were finished on R 4.0.5. The outcomes of UM cases were compared between groups through Kaplan-Meier (KM) analysis. The area under the curve (AUC) generated by ROC analysis was computed to test the modeling accuracy. The AUCs for 1-, 3-, and 5-year survival rates were estimated.

Results

MAGs-based molecular subtype in UM

The flowchart of the present research is shown in Figure 1.

Totally 200 MAGs were collected from MSigDB portal. GO and KEGG analyses were employed to better understand the functions of these MAGs. Results revealed that MAGs were mainly involved in EMT-related biological process, including cell adhesion, wound healing and cell migration (Figure 2A). As shown in Figure 2B, MAGs may regulate TNF, PPAR, and Wnt pathways.

Next, we applied consensus cluster analysis of the 200 MAGs and identified a novel molecular subtype. The UM cases were clustered into two optimal subsets at k = 2 (Figure 2C). PCA demonstrated that the two subsets can be effectively separated by MAGs (Figure 2D). Survival curves suggest that cluster A has a favorable survival outcome compared to cluster B (Figure 2E). In addition, epithelial cell signaling and cell adhesion pathways were great in cluster B (Figure 2F).

Establishment and validation of the MBRSS

The training cohort (TCGA-UM) was utilized to screen out prognostic factors. Uni-variate Cox analysis was first applied to determine a total of 94 MAGs with prognostic values. LASSO regression was conducted to shrink the overfitting value of the signature and screened out 12 candidate genes for next analysis (Figures 3A, B). Finally, we obtained six MAGs (COL11A1, AREG, TIMP3, ADAM12, PRRX1, and GAS1) from multivariate Cox analysis to create the MBRSS: [COL11A1 × (−2.4808)] + [AREG × (5.1680)] + [TIMP3 × (−1.1211)] + [ADAM12× (2.0108)] + [PRRX1 × (3.2377)] + [GAS1 × (−1.3746)] (Figure 3C). Depending on the median risk score, all UM samples were divided into high-risk and low-risk groups. KM survival analysis disclosed three protective indicators and three risky indicators (Figure 3D). Except for GAS1 and PRRX1, all other genes were significant in DFS (Figure 3E).

In the training set, K-M curves illustrated that the MBRSS-low subgroup presented favorable survival outcome (Figure 4A). The AUCs of 1-, 3-, and 5-year survival were 0.949, 0.987, and 0.898, respectively (Figure 4B). The risk score and clinical status of each case from two risk groups were shown in Figure 4C. Moreover, we confirmed the forecasting ability of MBRSS in the testing set

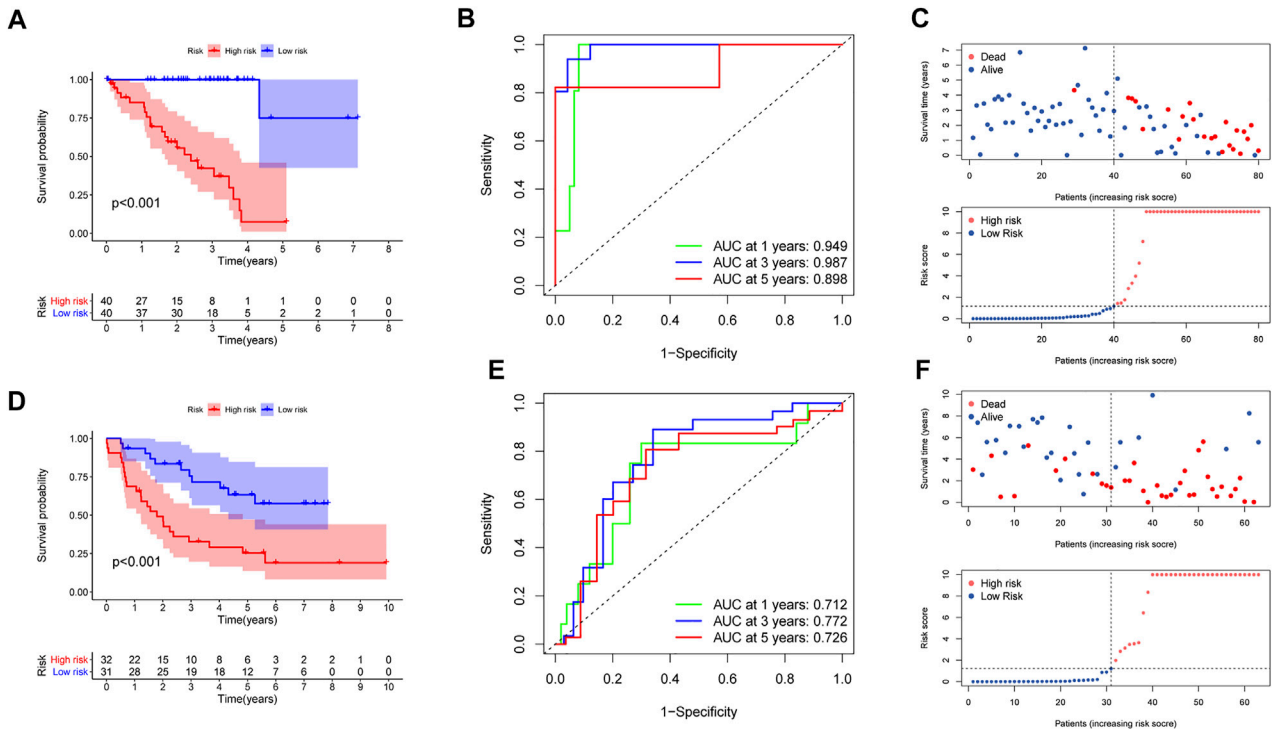

FIGURE 4
Evaluation of the MAGs-based score system. **(A,D)** Survival analysis for patients in the two subgroups. **(B,E)** ROC curves displayed the favorable ability of the model. **(C,F)** Distribution of the risk score and survival status.

(Figures 4D–F). The difference in clinical outcome be-tween groups was further verified in the testing cohort. The AUCs were 0.712, 0.772 and 0.726 for 1-, 3-, and 5-year survival, respectively (Figure 4E).

Development t of an MBRSS-Associated nomogram

Cox regression analysis was performed to confirm the independent value of the MBRSS. Univariate regression unearthed that age, stage and risk score were closely corre-lated to the survival outcome (Figure 5A). After multivariate analysis, the risk score was still an independent prognosis indicator in UM (Figure 5B). Then we set up an MBRSS-based nomogram to enhance its capability of prognosis assessment (Figure 5C). Calibration curves were plotted to demonstrate the optimal forecasting effectiveness of the nomogram (Figure 5D).

GSEA enrichment of MBRSS

GSEA with hallmark gene sets was applied to better understand the underlying functions in the MBRSS-high group. Results disclosed that the high-risk UM samples were related to hallmarks including IL6/JAK/STAT5, mTOR, Notch, and P53 signaling pathways (Figure 6A). In addition, fatty acid metabolism, glycolysis, inflammatory response and oxidative phosphorylation were remarkably enriched in the MBRSS-high group (Figure 6B).

Characterization of Immune Landscape in UM

Given the essential effect of immune checkpoints in anti-tumor immunotherapy, their correlation with MBRSS was detected. LAG3, PDCD1, HAVCR2, CD276, CD274 and CTLA4 were highly expressed in the high-MBRSS group (Figures 7A, B). Figure 7C presents the differences in immunocyte infiltration level between the two groups. As for the immune function of UM samples, APC stimulation, checkpoint, HLA, II-IFN response were activated in the high-MBRSS group (Figure 7D).

Clinical potency analysis of MBRSS

We further explored the relationship between TMB and MBRSS and found that TMB value was lower in the high-MBRSS group (Figures 8A, B). Survival curves illustrated that the high-TMB UM patients presented favorable survival outcome (Figure 8C). The UM cases with low TMB and high risk had the lowest 5-year survival rate (Figure 8D). In addition, the relationship between MBRSS and m6A regulators was analyzed. Results revealed that YTHDF2, YTHDC2, ALKBH5 and YTHDF1 were upregulated, and ZC3H13 was low expressed in high-MBRSS group (Figure 8E). Drug sensitivity analysis demonstrated that High-MBRSS group displayed high IC50 value of Camptothecin, Doxorubicin, Etoposide and Tipifarnib (Figure 8F).

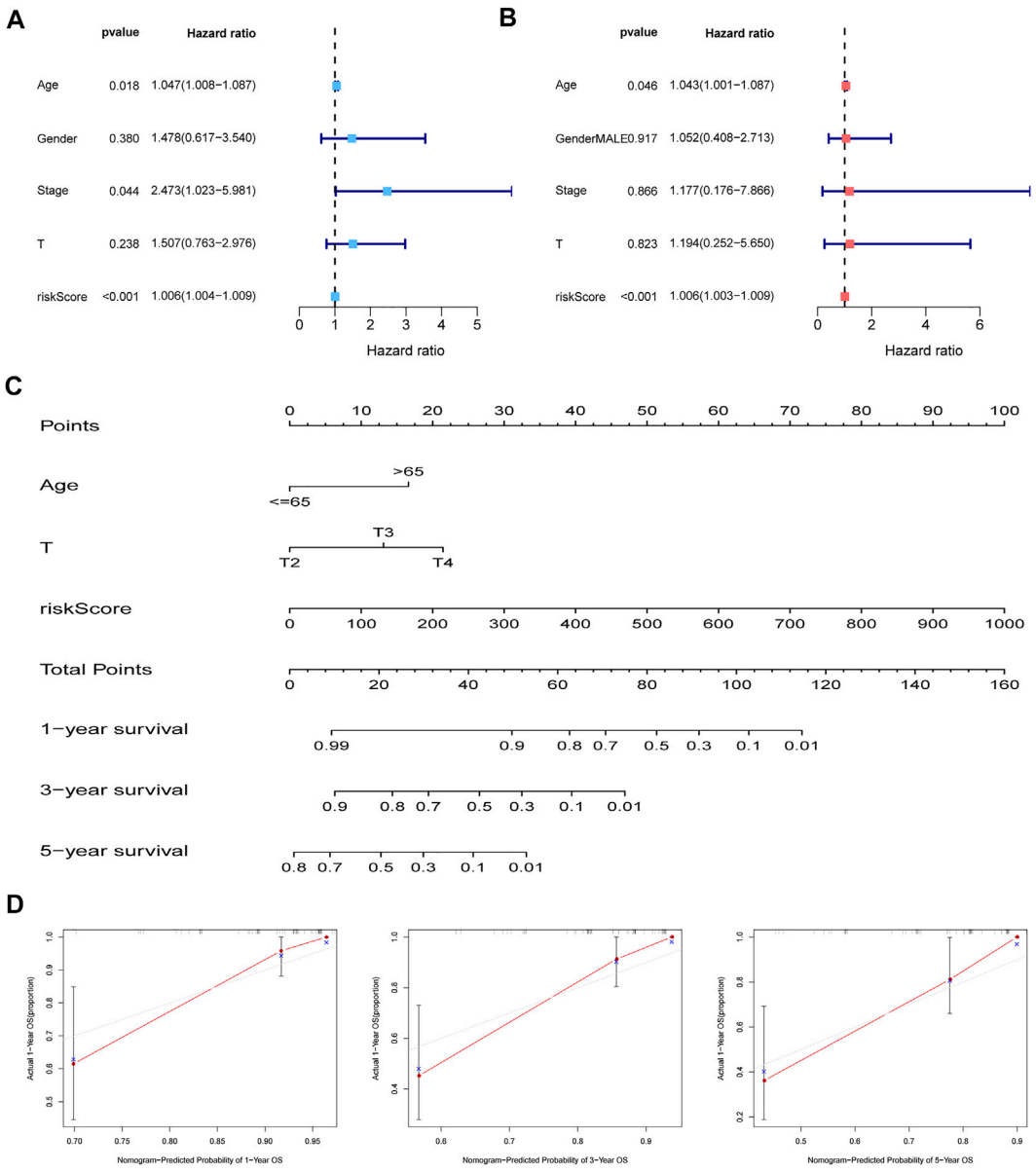

FIGURE 5
Establishment of the nomogram. **(A–B)** independent prognosis analysis by univariate and multivariate analyses. **(C)** Nomogram for improving prognosis assessment. **(D)** Calibration curves of the nomogram.

Single-cell analysis of MBRSS

A total of 11 UM samples were collected from GSE139829. Figure 9A presents a favorable integration effect of 11 samples, suggesting this data can be utilized for next analysis. After dimension reduction and the t-SNE clustering, all cells were divided into 22 different clusters (Figure 9B). According to different cell markers, 22 cell clusters were classified into 8 cell populations including B cells, endothelial cells, iPS cells, macrophage cells, monocyte cells, neurons, T cells and stem cells (Figure 9C). Then, we explored the cell location of each model genes. The results indicated that ADAM12 highly expressed in macrophage cells, AREG mainly located in T cells and TIMP3 highly expressed in neurons (Figure 9D).

Knockdown of AREG blocks UM proliferation and metastasis

We selected AREG for *in vitro* experiments since it has the highest HR score. Figure 10A shows the favorable silencing efficiency by qRT-PCR assay. Then, we observed that MuM-2B cells proliferation was greatly inhibited by silencing AREG based on the results of CTG and EdU assays (Figures 10B–D). To evaluate

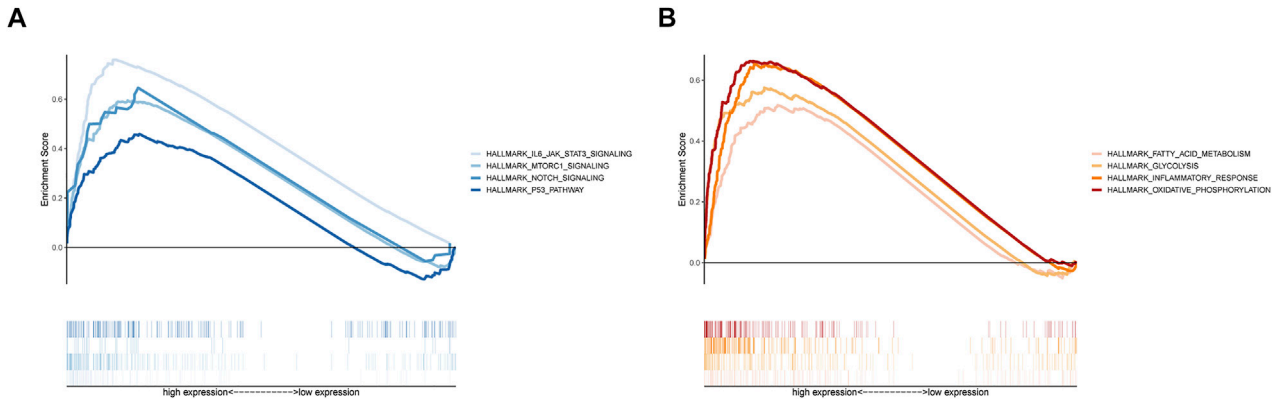

FIGURE 6
GSEA of MBRSS. **(A)** Tumor-related pathways of hallmark. **(B)** Cellular biological process of hallmark.

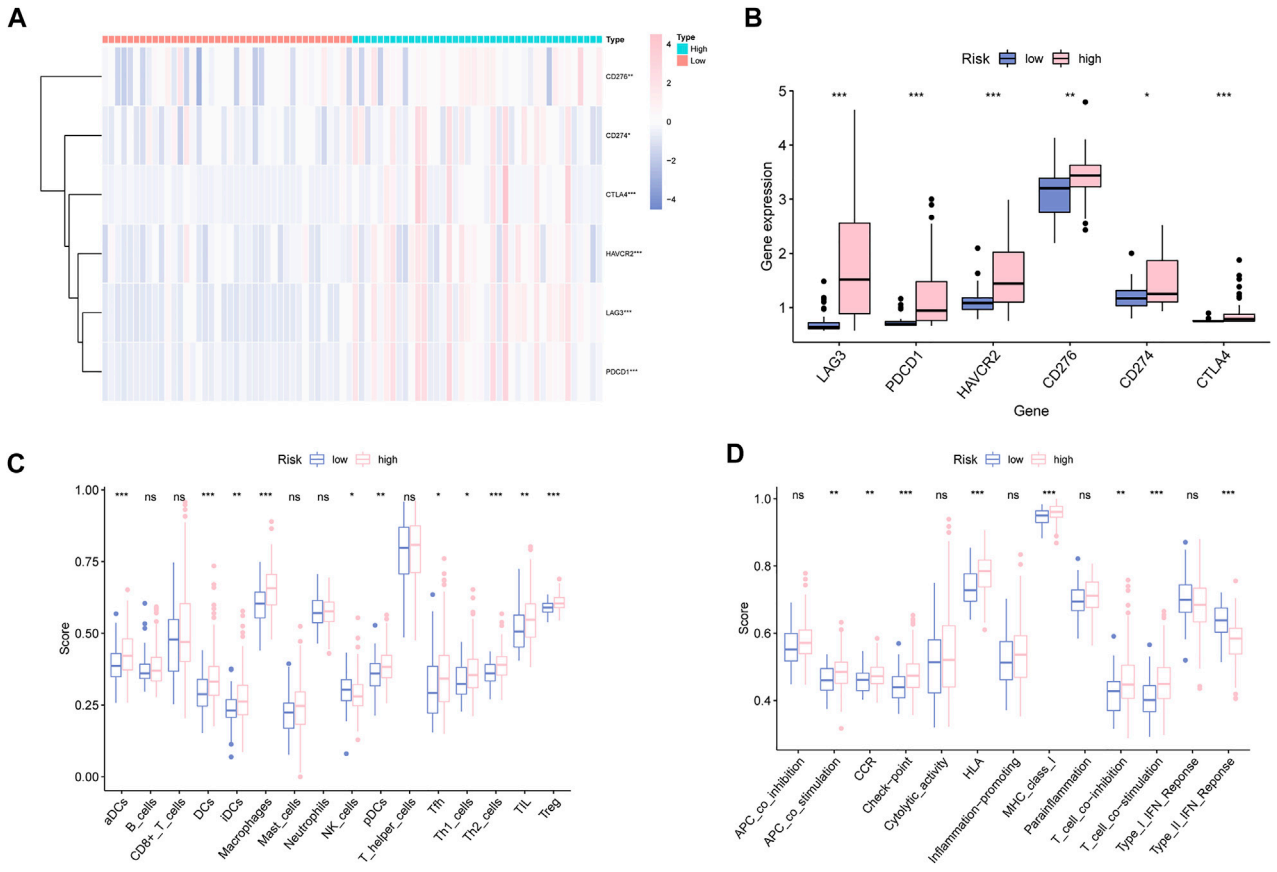

FIGURE 7
Characterization of Immune Landscape in UM. **(A–B)** Immune checkpoints analysis. **(C)** Immunocyte infiltration analysis. **(D)** The relationship between immune function analysis and MBRSS (ns > 0.05, *p < 0.05, **p < 0.01, ***p < 0.001).

the role of AREG on MuM-2B cell metastasis, transwell assay was conducted. The results indicated that cell migration and invasion ability were remarkably suppressed in AREG knockdown group (Figures 10E, F). Then, we explore the role of AREG in regulation of cell metastatic ability by IF assay. The results disclosed that silencing AREG blocked E-cadherin expression whereas enhanced N-cadherin levels, indicating that AREG affects UM cell metastasis through meditation of EMT process (Figure 10G).

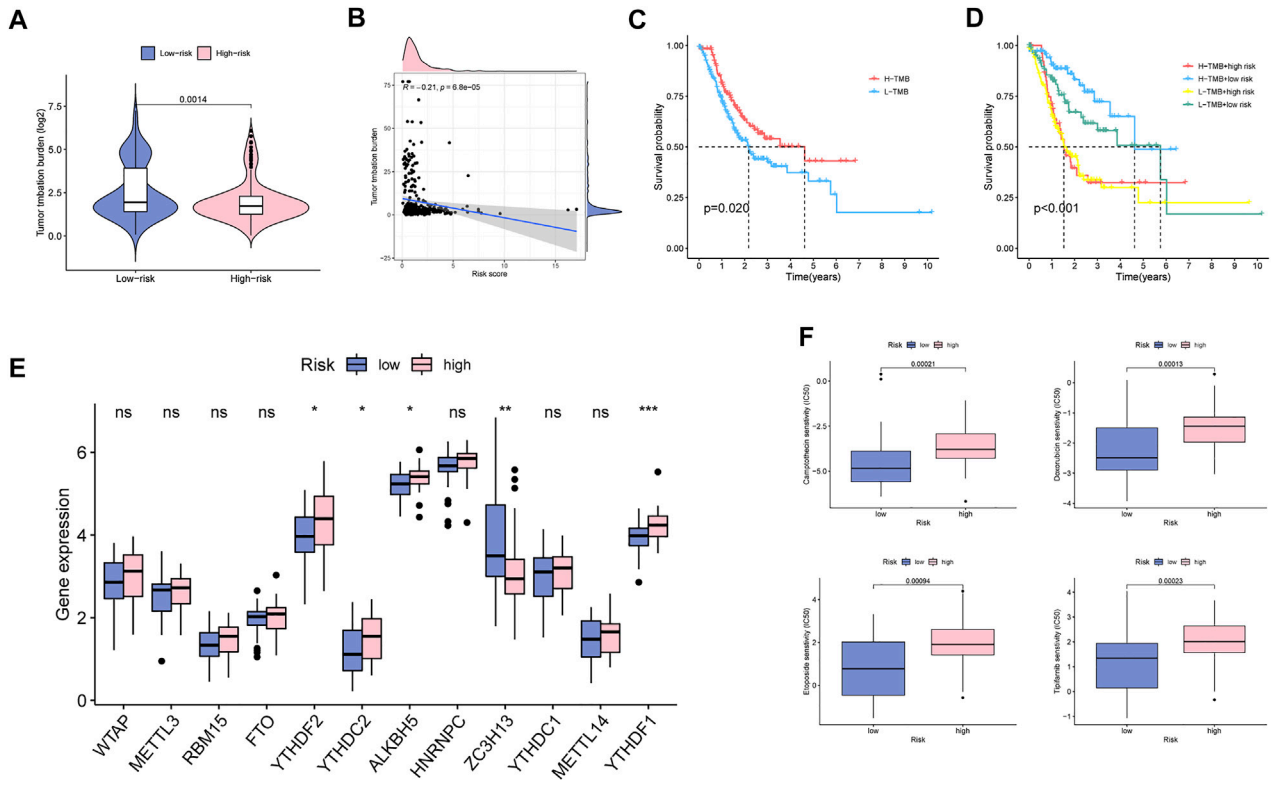

FIGURE 8
Clinical potency analysis of MBS. **(A–B)** The relationship between TMB and MBRSS. Survival analysis of different groups **(C)** with TMB and **(D)** with TMB and risk score. **(E)** The relationship between m6A regulators and MBRSS (ns > 0.05, *p < 0.05, **p < 0.01, ***p < 0.001). **(F)** Drug sensitivity analysis of MBS.

Discussion

We probed into the prognostic characteristics of UM based on comprehensive assay of TCGA and GEO. To investigate the relationship between patient prognosis and gene expression in the training set, we applied KM, univariate Cox analysis, and LASSO Cox regression, which found 10 genetic features associated with prognosis. Applying this signature to the training group, we found significant differences in Cox regression, ROC, and KM analyses between the high- and low-risk groups. The prognostic power of the ten-gene markers was similarly verified in the validation set, which fully demonstrated the validity of the ten-gene signature in forecasting the prognosis of UM. GSEA and immune infiltration analysis suggested that the ten-gene marker risk scores of UM patients may be associated with the TME. This study plays a positive role in guiding the further clinical treatment of UM.

Here, six genes were found to be strongly associated with tumor development. Amphiregulin (AREG) gene, which belongs to the epidermal growth factor (EGF) family, is overexpressed in many cancer tissues. AREG participates in EMT in pancreatic cancer cells through NF-κB signaling and facilitates the movement and spread of pancreatic cancer cells (Wang et al., 2020). AREG upregulates ICAM-1 expression *via* EGFR/PI3K/Akt/NF-κB signaling and promotes the cancer cell viability of osteosarcoma (Liu et al., 2015). Paired related homeobox 1 (PRRX1), is a key member of the homomeric protein pairing family located at the nucleus. PRRX1 mediates cancer cell invasion and metastasis by starting EMT (Meng et al., 2022). In addition, PRRX1 impacts the division and metastasis of various tumor cells *via* Wnt/β-catenin and Notch pathways, and maintains the characteristics of tumor stem cells to promote EMT (Du et al., 2021). A disintegrin and metalloprotease12 (ADAM12) is implied in the starting and advancement of many tumors. ADAM12 is significantly more expressed in hepatocellular carcinoma (HCC) tissues than in surrounding tissues, and a signal pathway related to ADAM12 is found. The high ADAM12 gene expression in HCC tissues is remarkably positively related with T stage, pathological stage and residual tumor (Du et al., 2022). In breast cancer, hypoxia starts HIF-dependent expression of ADAM12, which cleaves the extracellular domain of membrane-bound heparin-bound EGF-like growth factor (HB-EGF). The released extracellular domain of HB-EGF connects to EGF receptor and triggers signal transduction pathways that endow breast cancer cells with enhanced cell migrating and invading abilities, resulting in distant metastasis (Wang et al., 2021). TIMP3 is a main component of the tissue inhibitors of the metalloproteinase (TIMP) family. It is mainly enclosed in the extracellular matrix (ECM) of tissues and inhibits abscission enzymes, transmembrane MMPs and membrane-bound MMPs. TIMP3 promoter methylation is recently recognized as an epigenetic candidate for the treatment of brca1 breast cancer. Knockdown of lncRNA ROR regulates the division, death and invasion of breast cancer cells by inhibiting TIMP3 (Hu et al., 2021). Growth arrest specific 1 (Gas1) plays a key role in growth inhibition. Gas1 negatively regulates glycolysis and provides energy for tumor progression and metastasis. Gas1 negatively regulates the

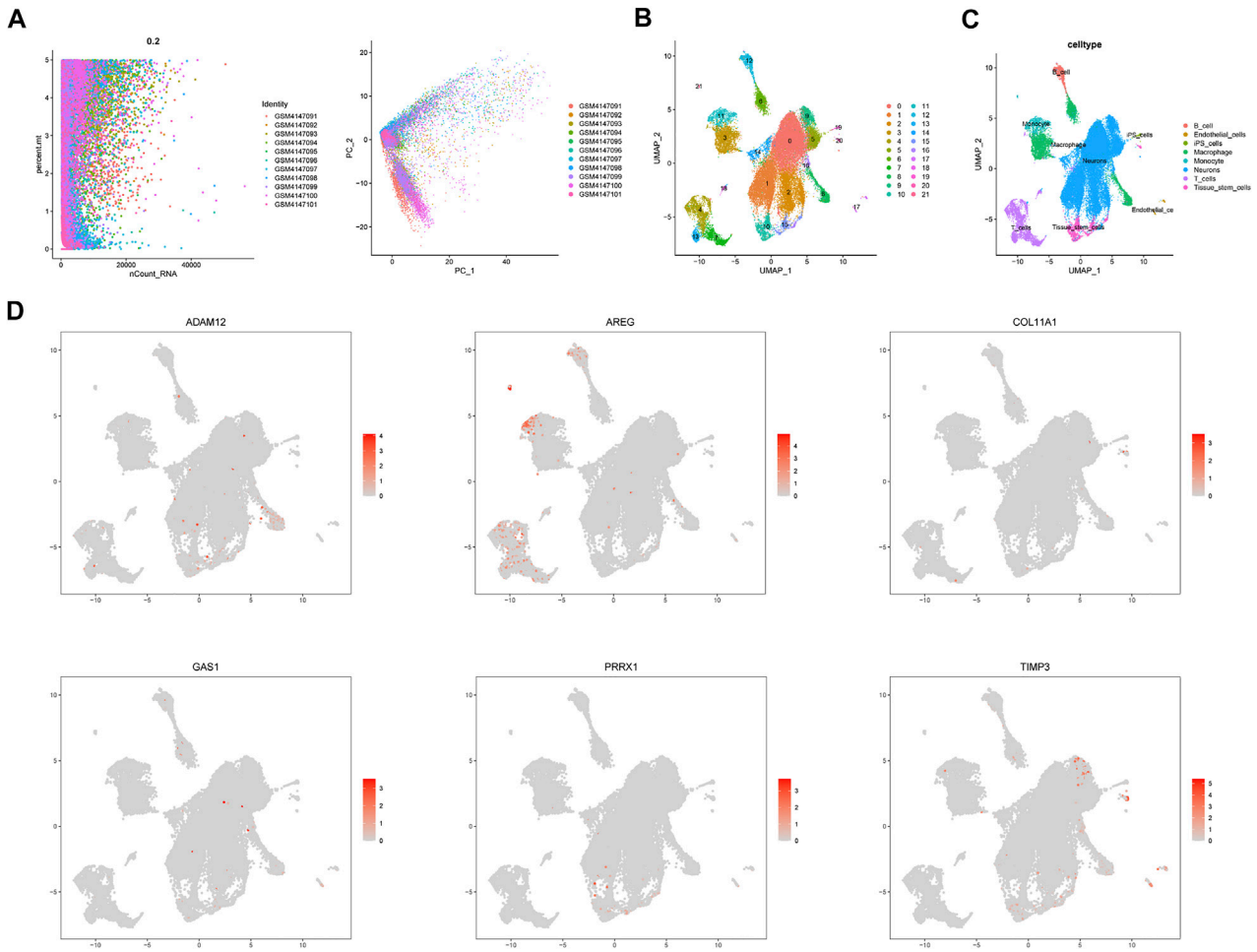

FIGURE 9
Single cell sequencing analysis. **(A)** Data integration of 11 samples. **(B)** Dimensionality reduction and cluster analysis. **(C)** The cells were classified into approximately 8 cell types, including B cells, endothelial cells, iPS cells, macrophage cells, monocyte cells, neurons, T cells and stem cells. **(D)** Cell location of each model gene.

AMPK/mTOR/p70S6K signaling axis and modulates the proliferation, metastasis and abnormal metabolism of malignant tumor cells (Li et al., 2016). Collagen type X1 alpha 1 (COL11A1), from the collagen family, is mostly expressed and released by cancer-related fibroblast subsets, and modulates matrix-tumor interaction and the mechanical characteristics of ECM. It is up-expressed in most human tumor cell lines and tissues and can regulate cell cycle to promote cancer and affect tumor cell proliferation. In ovarian cancer cells, COL11A1 modulates TGF-β3 *via* the NF-κB/IGFBP2 axis, thereby activating cancer-associated fibroblasts and influencing tumor development and migration (Wu et al., 2021).

Immune checkpoints (ICPs), a class of immune-resisting molecules, are expressed on immune cells and mediate the level of immune stimulation. They are pivotal in avoiding autoimmunity (Zhu et al., 2021). ICP molecules enable the immune system to be activated within the normal range. Tumor cells express substances that activate ICPs, which, upon activation, prevent antigen presentation to T cells and in tumor immunity, thereby inhibiting the immune role of T cells and allowing them to avoid surveillance and survive. Immunotherapy through ICPs modulates T cell activity to kill tumor cells through a series of pathways, such as co-inhibition or co-stimulatory signals. UM is a highly metastatic cancer for which ICP therapy is largely ineffective compared to cutaneous melanoma. ICPs are epigenetically mediated *via* DNA methylation. Luka de Vos et al. found that DNA methylation of CTLA4, PD-1, PDL1, PD-L2, LAG3, TIGIT and TIM-3 was remarkably associated with mRNA expressions, BAP1-apoptosis and prognosis of UM. Therefore, the application of ICP gene DNA methylation assays to the biomarker program of the ICP blockade (ICB) trial may help better explain the underlying mechanisms of UM to ICB (de Vos et al., 2022).

The tumor immune microenvironment (TIME) consists of a diverse array of cell types, including T lymphocytes, B lymphocytes, tumor-associated macrophages (TAMs), natural killer cells (NKs), dendritic cells (DCs), tumor-associated neutrophils (TANs), and myeloid-derived suppressor cells (MDSCs). Various biochemical molecules released by the abnormal metabolism of cancer cells reshape the TME and affect the normal immune response of immune cells (Domblides et al., 2019).

Macrophages are important intrinsic immune cells that function mainly through phagocytosis and intake of cellular debris and pathogens, and activation of other immune cells against pathogen invasion. TAMs infiltrating tumor tissues are highly plastic and heterogeneous (Biswas et al., 2013). In the early tumor stage, pro-

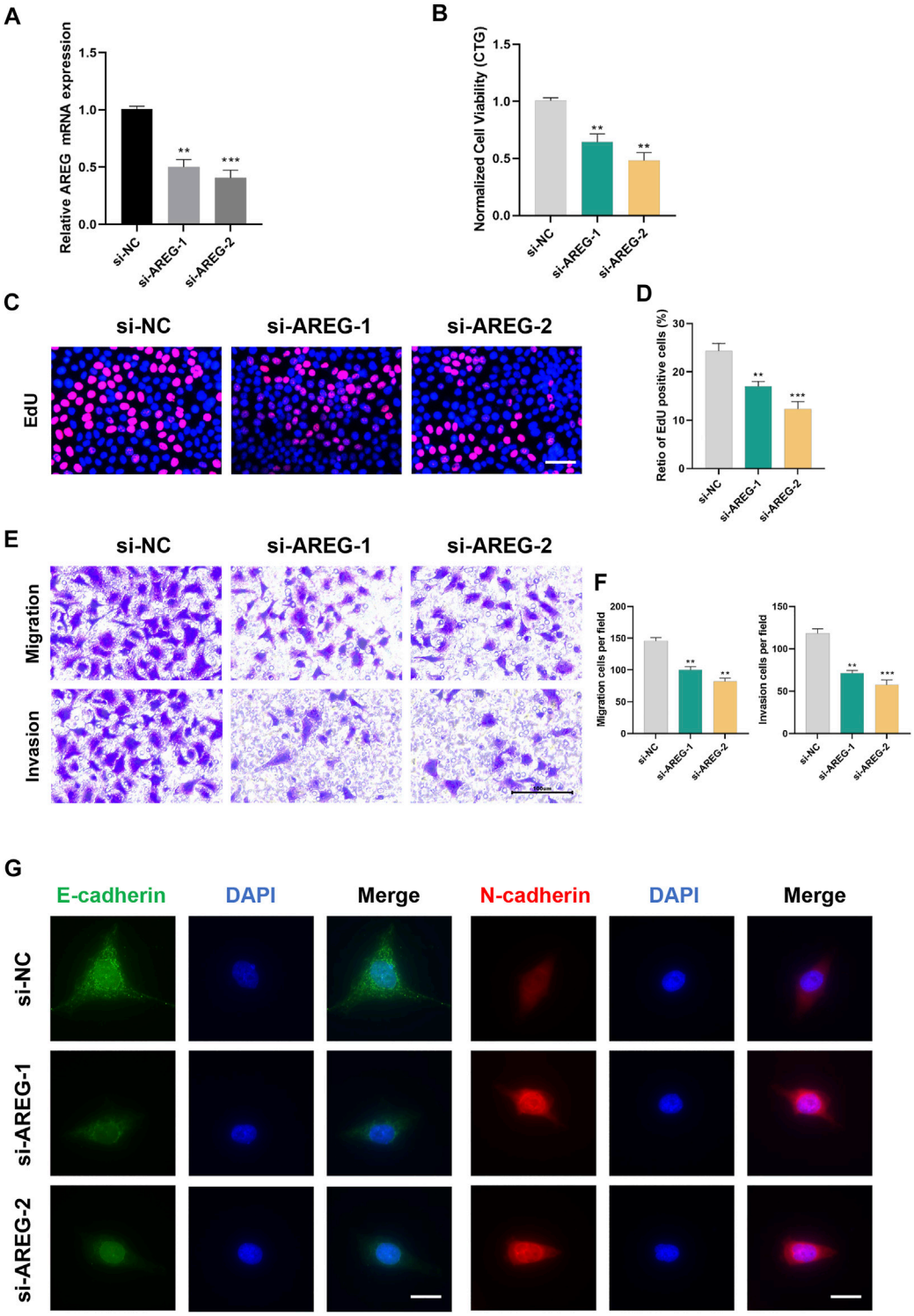

FIGURE 10
Silencing AREG inhibits UM proliferation and metastasis. **(A)** Transfection efficiency was detected by qRT-PCR. Cell proliferation was detected by **(B)** CTG and **(C,D)** EdU assays. Scale bar, 50 mm. **(E,F)** The role of AREG on cell metastasis was tested by transwell assay. **(G)** Downregulation of AREG enhanced N-cadherin and inhibited E-cadherin by Immunofluorescence. Scale bar, 50 mm (**$p < 0.01$, ***$p < 0.001$).

inflammatory cytokines such as toll-like receptor (TLR) agonists can promote TAM polarization to M-type, and NO and reactive oxygen species (ROS) produced by M macrophages can considerably restrict tumor cell division and kill tumor cells. The tumor cells are killed by NO and ROS (Mantovani and Allavena, 2015). During tumor progression, interleukin (IL)-4 and colony-stimulating factor (CSF)-1 induce TAMs to polarize to M2 macrophages. M2 macrophages secrete EGF, matrix metalloprotein 9 (MMP-9), and other proteins to suppress antitumor effects and promote tumor progression (Mantovani et al., 2017).

Tregs differentiate from initial $CD4^+$ T cells, which are a class of immunosuppressive T cells that highly express FOXP3, CD25, and CD4. Tregs often accumulate in tumors, supply energy for immune responses through lipid metabolism and the OXPHOS pathway, maintain the immunosuppression of the TME, and promote tumor infiltration and metastasis (Sharma et al., 2017).

As the first line of antitumor defense in the body, NKs can release perforin on the surface of target cells, resulting in cell perforation, allowing granzyme b to enter tumor cells to induce apoptosis and thus non-specifically kill tumor cells. It also promotes the anti-tumor behaviors of adaptive immune cells by secreting cytokines. Defective transcription factor c-Myc protein (Loftus et al., 2018), accumulation of lactate in the TME (Harmon et al., 2019), and excessive lipid metabolism (Michelet et al., 2018) inhibit the metabolic activity of NKs and affect their normal function.

Type 2 IFN, the main cytokine regulating the immune system, mainly functions to upregulate the expression of MHC molecules and activate macrophages. Type 2 IFN can intensify the activity of NK cells and T cells, promoting the secretion of Thl cytokines, which is conducive to the activation of anti-tumor immune pathway. Additionally, high concentration of type 2 IFN or continuous low dose of type 2 IFN is conducive to the formation of tumor cell immune escape microenvironment. Our results show that type 2 IFN is lowly expressed in the high-risk group and is potentially an early tumor detection and molecular target (Corrales et al., 2017).

Furthermore, we selected AREG to confirm our proposed score system in UM by a variety of *in vitro* experiments. In line with previous studies (Wang et al., 2020; Bolitho et al., 2021), we observed that downregulation of AREG remarkably blocked UM cell growth and metastatic ability, further demonstrating the ability of AREG to regulate proliferation, migration and invasion in tumors.

Nevertheless, there are some shortcomings in our project. Although we performed experiments for validation, the main results were derived from bioinformatics analyses based on public UM datasets. More clinical data from multiple centers need to confirm the ability and accuracy of our proposed MBRSS. Moreover, animal experiments and patient specimens need to further test the role of AREG in UM.

Conclusion

In conclusion, we successfully identified metastatic molecular subtype in UM and further created a risk score system based on MAGs with single-cell and transcriptome analyses bioinformatics prediction and experimental validation. Further, we found that RRM2 might be a future biomarker and a reference to predict immune response. These findings may aid in understanding the role of RRM2 and its clinical application in cancers.

Data availability statement

The original contributions presented in the study are included in the article/Supplementary Material, further inquiries can be directed to the corresponding authors.

Author contributions

SM and DD contributed to the design of the study; TZ and SY conducted the data analyses and wrote the manuscript; ZF, YC, YD, and FW contributed significantly to analysis and manuscript preparation; XW, DD, and XZ helped review and editing preparation.

Conflict of interest

The authors declare that the research was conducted in the absence of any commercial or financial relationships that could be construed as a potential conflict of interest.

Publisher's note

Supplementary material

The Supplementary Material for this article can be found online at: https://www.frontiersin.org/articles/10.3389/fphar.2023.1138452/full#supplementary-material

References

Amaro, A., Gangemi, R., Piaggio, F., Angelini, G., Barisione, G., Ferrini, S., et al. (2017). The biology of uveal melanoma. *Cancer Metastasis Rev.* 36, 109–140. doi:10.1007/s10555-017-9663-3

Arneth, B. (2019). Tumor microenvironment. *Med. Kaunas.* 56, 15. doi:10.3390/medicina56010015

Augsburger, J. J., Corrêa, Z. M., and Shaikh, A. H. (2009). Effectiveness of treatments for metastatic uveal melanoma. *Am. J. Ophthalmol.* 148, 119–127. doi:10.1016/j.ajo.2009.01.023

Biswas, S. K., Allavena, P., and Mantovani, A. (2013). Tumor-associated macrophages: Functional diversity, clinical significance, and open questions. *Semin. Immunopathol.* 35, 585–600. doi:10.1007/s00281-013-0367-7

Bol, K. F., van den Bosch, T., Schreibelt, G., Mensink, H. W., Keunen, J. E., Kiliç, E., et al. (2016). Adjuvant dendritic cell vaccination in high-risk uveal melanoma. *Ophthalmology* 123, 2265–2267. doi:10.1016/j.ophtha.2016.06.027

Bolitho, C., Moscova, M., Baxter, R. C., and Marsh, D. J. (2021). Amphiregulin increases migration and proliferation of epithelial ovarian cancer cells by inducing its own expression via PI3-kinase signaling. *Mol. Cell Endocrinol.* 533, 111338. doi:10.1016/j.mce.2021.111338

Carvajal, R. D., Schwartz, G. K., Tezel, T., Marr, B., Francis, J. H., and Nathan, P. D. (2017). Metastatic disease from uveal melanoma: Treatment options and future prospects. *Br. J. Ophthalmol.* 101, 38–44. doi:10.1136/bjophthalmol-2016-309034

Chen, F., Song, J., Ye, Z., Xu, B., Cheng, H., Zhang, S., et al. (2021). Integrated analysis of cell cycle-related and immunity-related biomarker signatures to improve the prognosis prediction of lung adenocarcinoma. *Front. Oncol.* 11, 666826. doi:10.3389/fonc.2021.666826

Chua, V., Orloff, M., Teh, J. L., Sugase, T., Liao, C., Purwin, T. J., et al. (2019). Stromal fibroblast growth factor 2 reduces the efficacy of bromodomain inhibitors in uveal melanoma. *EMBO Mol. Med.* 11, e9081. doi:10.15252/emmm.201809081

Corrales, L., Matson, V., Flood, B., Spranger, S., and Gajewski, T. F. (2017). Innate immune signaling and regulation in cancer immunotherapy. *Cell Res.* 27, 96–108. doi:10.1038/cr.2016.149

Davis, F. M., Stewart, T. A., Thompson, E. W., and Monteith, G. R. (2014). Targeting EMT in cancer: Opportunities for pharmacological intervention. *Trends Pharmacol. Sci.* 35, 479–488. doi:10.1016/j.tips.2014.06.006

de Vos, L., Carrillo Cano, T. M., Zarbl, R., Klümper, N., Ralser, D. J., Franzen, A., et al. (2022). , CTLA4, PD-1, PD-L1, PD-L2 , TIM-3, TIGIT, and LAG3 DNA methylation is associated with BAP1 -aberrancy, transcriptional activity, and overall survival in uveal melanoma. *J. Immunother.* 45, 324–334. doi:10.1097/CJI.0000000000000429

Diener-West, M., Reynolds, S. M., Agugliaro, D. J., Caldwell, R., Cumming, K., Earle, J. D., et al. (2005). Development of metastatic disease after enrollment in the COMS trials for treatment of choroidal melanoma: Collaborative Ocular Melanoma Study Group Report No. 26. *Arch. Ophthalmol.* 123, 1639–1643.

Domblides, C., Lartigue, L., and Faustin, B. (2019). Control of the antitumor immune response by cancer metabolism. *Cells* 8, 104. doi:10.3390/cells8020104

Du, S., Sun, L., Wang, Y., Zhu, W., Gao, J., Pei, W., et al. (2022). ADAM12 is an independent predictor of poor prognosis in liver cancer. *Sci. Rep.* 12, 6634. doi:10.1038/s41598-022-10608-y

Du, W., Liu, X., Yang, M., Wang, W., and Sun, J. (2021). The regulatory role of PRRX1 in cancer epithelial-mesenchymal transition. *Onco Targets Ther.* 14, 4223–4229. doi:10.2147/OTT.S316102

Harmon, C., Robinson, M. W., Hand, F., Almuaili, D., Mentor, K., Houlihan, D. D., et al. (2019). Lactate-mediated acidification of tumor microenvironment induces apoptosis of liver-resident NK cells in colorectal liver metastasis. *Cancer Immunol. Res.* 7, 335–346. doi:10.1158/2326-6066.CIR-18-0481

Hu, A., Hong, F., Li, D., Jin, Y., Kon, L., Xu, Z., et al. (2021). Long non-coding RNA ROR recruits histone transmethylase MLL1 to up-regulate TIMP3 expression and promote breast cancer progression. *J. Transl. Med.* 19, 95. doi:10.1186/s12967-020-02682-5

Jin, Y., Sheikh, F., Detillieux, K. A., and Cattini, P. A. (2000). Role for early growth response-1 protein in alpha(1)-adrenergic stimulation of fibroblast growth factor-2 promoter activity in cardiac myocytes. *Mol. Pharmacol.* 57, 984–990.

Katsuno, Y., Lamouille, S., and Derynck, R. (2013). TGF-β signaling and epithelial-mesenchymal transition in cancer progression. *Curr. Opin. Oncol.* 25, 76–84. doi:10.1097/CCO.0b013e32835b6371

Li, Q., Qin, Y., Wei, P., Lian, P., Li, Y., Xu, Y., et al. (2016). Gas1 inhibits metastatic and metabolic phenotypes in colorectal carcinoma. *Mol. Cancer Res.* 14, 830–840. doi:10.1158/1541-7786.MCR-16-0032

Liu, J. F., Tsao, Y. T., and Hou, C. H. (2015). Amphiregulin enhances intercellular adhesion molecule-1 expression and promotes tumor metastasis in human osteosarcoma. *Oncotarget* 6, 40880–40895. doi:10.18632/oncotarget.5679

Liu, J., Geng, R., Ni, S., Cai, L., Yang, S., Shao, F., et al. (2022). Pyroptosis-related lncRNAs are potential biomarkers for predicting prognoses and immune responses in patients with UCEC. *Mol. Ther. Nucleic Acids* 27, 1036–1055. doi:10.1016/j.omtn.2022.01.018

Liu, J., Geng, R., Zhong, Z., Zhang, Y., Ni, S., Liu, W., et al. (2022). N1-Methyladenosine-Related lncRNAs are potential biomarkers for predicting prognosis and immune response in uterine corpus endometrial carcinoma. *Oxid. Med. Cell Longev.* 2022, 2754836. doi:10.1155/2022/2754836

Lo, H. W., Hsu, S. C., Xia, W., Cao, X., Shih, J. Y., Wei, Y., et al. (2007). Epidermal growth factor receptor cooperates with signal transducer and activator of transcription 3 to induce epithelial-mesenchymal transition in cancer cells via up-regulation of TWIST gene expression. *Cancer Res.* 67, 9066–9076. doi:10.1158/0008-5472.CAN-07-0575

Loftus, R. M., Assmann, N., Kedia-Mehta, N., O'Brien, K. L., Garcia, A., Gillespie, C., et al. (2018). Amino acid-dependent cMyc expression is essential for NK cell metabolic and functional responses in mice. *Nat. Commun.* 9, 2341. doi:10.1038/s41467-018-04719-2

Mantovani, A., and Allavena, P. (2015). The interaction of anticancer therapies with tumor-associated macrophages. *J. Exp. Med.* 212, 435–445. doi:10.1084/jem.20150295

Mantovani, A., Marchesi, F., Malesci, A., Laghi, L., and Allavena, P. (2017). Tumour-associated macrophages as treatment targets in oncology. *Nat. Rev. Clin. Oncol.* 14, 399–416. doi:10.1038/nrclinonc.2016.217

Meng, Z., Chen, Y., Wu, W., Yan, B., Zhang, L., Chen, H., et al. (2022). PRRX1 is a novel prognostic biomarker and facilitates tumor progression through epithelial-mesenchymal transition in uveal melanoma. *Front. Immunol.* 13, 754645. doi:10.3389/fimmu.2022.754645

Michelet, X., Dyck, L., Hogan, A., Loftus, R. M., Duquette, D., Wei, K., et al. (2018). Metabolic reprogramming of natural killer cells in obesity limits antitumor responses. *Nat. Immunol.* 19, 1330–1340. doi:10.1038/s41590-018-0251-7

Mittal, V. (2018). Epithelial mesenchymal transition in tumor metastasis. *Annu. Rev. Pathol.* 13, 395–412. doi:10.1146/annurev-pathol-020117-043854

Sharma, P., Hu-Lieskovan, S., Wargo, J. A., and Ribas, A. (2017). Primary, adaptive, and acquired resistance to cancer immunotherapy. *Cell* 168, 707–723. doi:10.1016/j.cell.2017.01.017

Singh, A. D., Turell, M. E., and Topham, A. K. (2011). Uveal melanoma: Trends in incidence, treatment, and survival. *Ophthalmology* 118, 1881–1885. doi:10.1016/j.ophtha.2011.01.040

Smolkova, B., Horvathova Kajabova, V., Zmetakova, I., Kalinkova, L., Czanner, G., Markova, A., et al. (2018). Role of epigenetic deregulation in hematogenous dissemination of malignant uveal melanoma. *Neoplasma* 65, 840–854. doi:10.4149/neo_2018_180420N261

Song, J., Liu, Y., Guan, X., Zhang, X., Yu, W., and Li, Q. (2021). A novel ferroptosis-related biomarker signature to predict overall survival of esophageal squamous cell carcinoma. *Front. Mol. Biosci.* 8, 675193. doi:10.3389/fmolb.2021.675193

Song, J., Sun, Y., Cao, H., Liu, Z., Xi, L., Dong, C., et al. (2021). A novel pyroptosis-related lncRNA signature for prognostic prediction in patients with lung adenocarcinoma. *Bioengineered* 12, 5932–5949. doi:10.1080/21655979.2021.1972078

Song, J., Zhang, S., Sun, Y., Gu, J., Ye, Z., Sun, X., et al. (2021). A radioresponse-related lncRNA biomarker signature for risk classification and prognosis prediction in non-small-cell lung cancer. *J. Oncol.* 2021, 4338838. doi:10.1155/2021/4338838

Subramanian, A., Tamayo, P., Mootha, V. K., Mukherjee, S., Ebert, B. L., Gillette, M. A., et al. (2005). Gene set enrichment analysis: A knowledge-based approach for interpreting genome-wide expression profiles. *Proc. Natl. Acad. Sci. U. S. A.* 102, 15545–15550. doi:10.1073/pnas.0506580102

Wang, L., Wang, L., Zhang, H., Lu, J., Zhang, Z., Wu, H., et al. (2020). AREG mediates the epithelial-mesenchymal transition in pancreatic cancer cells via the EGFR/ERK/NF-κB signalling pathway. *Oncol. Rep.* 43, 1558–1568. doi:10.3892/or.2020.7523

Wang, R., Godet, I., Yang, Y., Salman, S., Lu, H., Lyu, Y., et al. (2021). Hypoxia-inducible factor-dependent ADAM12 expression mediates breast cancer invasion and metastasis. *Proc. Natl. Acad. Sci. U. S. A.* 118, e2020490118. doi:10.1073/pnas.2020490118

Watnick, R. S. (2012). The role of the tumor microenvironment in regulating angiogenesis. *Cold Spring Harb. Perspect. Med.* 2, a006676. doi:10.1101/cshperspect.a006676

Wei, S. C., Fattet, L., Tsai, J. H., Guo, Y., Pai, V. H., Majeski, H. E., et al. (2015). Matrix stiffness drives epithelial-mesenchymal transition and tumour metastasis through a TWIST1-G3BP2 mechanotransduction pathway. *Nat. Cell Biol.* 17, 678–688. doi:10.1038/ncb3157

Wu, Y., Deng, J., Rychahou, P. G., Qiu, S., Evers, B. M., and Zhou, B. P. (2009). Stabilization of snail by NF-kappaB is required for inflammation-induced cell migration and invasion. *Cancer Cell* 15, 416–428. doi:10.1016/j.ccr.2009.03.016

Wu, Y. H., Huang, Y. F., Chang, T. H., Chen, C. C., Wu, P. Y., Huang, S. C., et al. (2021). COL11A1 activates cancer-associated fibroblasts by modulating TGF-β3 through the NF-κB/IGFBP2 axis in ovarian cancer cells. *Oncogene* 40, 4503–4519. doi:10.1038/s41388-021-01865-8

Xue, M., Shang, J., Chen, B., Yang, Z., Song, Q., Sun, X., et al. (2019). Identification of prognostic signatures for predicting the overall survival of uveal melanoma patients. *J. Cancer* 10, 4921–4931. doi:10.7150/jca.30618

Yu, G., Wang, L. G., Han, Y., and He, Q. Y. (2012). clusterProfiler: an R package for comparing biological themes among gene clusters. *OMICS* 16, 284–287. doi:10.1089/omi.2011.0118

Zhu, Z., Song, J., Gu, J., Xu, B., Sun, X., and Zhang, S. (2021). FMS-related tyrosine kinase 3 ligand promotes radioresistance in esophageal squamous cell carcinoma. *Front. Pharmacol.* 12, 659735. doi:10.3389/fphar.2021.659735

frontiers | Frontiers in Pharmacology

TYPE Original Research
PUBLISHED 01 March 2023
DOI 10.3389/fphar.2023.1136184

OPEN ACCESS

EDITED BY
Kui Zhang,
The University of Chicago, United States

REVIEWED BY
Sen Li,
Jilin Agriculture University, China
Demeng Xia,
Shanghai University, China

*CORRESPONDENCE
Wenchao Zhang,
2204140314@csu.edu.cn
Zhi-Hong Li,
lizhihong@csu.edu.cn

SPECIALTY SECTION
This article was submitted to Pharmacology of Anti-Cancer Drugs, a section of the journal Frontiers in Pharmacology

RECEIVED 02 January 2023
ACCEPTED 16 February 2023
PUBLISHED 01 March 2023

CITATION
Qi L, Chen F, Wang L, Yang Z, Zhang W and Li Z-H (2023), Identification of anoikis-related molecular patterns to define tumor microenvironment and predict immunotherapy response and prognosis in soft-tissue sarcoma. *Front. Pharmacol.* 14:1136184. doi: 10.3389/fphar.2023.1136184

Identification of anoikis-related molecular patterns to define tumor microenvironment and predict immunotherapy response and prognosis in soft-tissue sarcoma

Lin Qi[1,2], Fangyue Chen[3], Lu Wang[1,2], Zhimin Yang[1,2,4], Wenchao Zhang[1,2]* and Zhi-Hong Li[1,2]*

[1]Department of Orthopedics, The Second Xiangya Hospital, Central South University, Changsha, China, [2]Hunan Key Laboratory of Tumor Models and Individualized Medicine, The Second Xiangya Hospital, Changsha, China, [3]Department of General Surgery, Changhai Hospital, Navy Military Medical University, Shanghai, China, [4]Department of Microbiology, Immunology & Molecular Genetics, University of Texas Long School of Medicine, UT Health Science Center, San Antonio, TX, United States

Background: Soft-tissue sarcoma (STS) is a massive threat to human health due to its high morbidity and malignancy. STS also represents more than 100 histologic and molecular subtypes, with different prognosis. There is growing evidence that anoikis play a key role in the proliferation and invasion of tumors. However, the effects of anoikis in the immune landscape and the prognosis of STS remain unclear.

Methods: We analyzed the genomic and transcriptomic profiling of 34 anoikis-related genes (ARGs) in patient cohort of pan-cancer and STS from The Cancer Genome Atlas (TCGA) database. Single-cell transcriptome was used to disclose the expression patterns of ARGs in specific cell types. Gene expression was further validated by real-time PCR and our own sequencing data. We established the Anoikis cluster and Anoikis subtypes by using unsupervised consensus clustering analysis. An anoikis scoring system was further built based on the differentially expressed genes (DEGs) between Anoikis clusters. The clinical and biological characteristics of different groups were evaluated.

Results: The expressions of most ARGs were significantly different between STS and normal tissues. We found some common ARGs profiles across the pan-cancers. Network of 34 ARGs demonstrated the regulatory pattern and the association with immune cell infiltration. Patients from different Anoikis clusters or Anoikis subtypes displayed distinct clinical and biological characteristics. The scoring system was efficient in prediction of prognosis and immune cell infiltration. In addition, the scoring system could be used to predict immunotherapy response.

Conclusion: Overall, our study thoroughly depicted the anoikis-related molecular and biological profiling and interactions of ARGs in STS. The Anoikis score model could guide the individualized management.

KEYWORDS

soft-tissue sarcoma, anoikis, immune cell infiltration, tumor microenvironment, scoring system

Introduction

Soft-tissue sarcoma (STS) is rare and accounts for approximate 1% of all adult malignancies (Gamboa et al., 2020), most commonly occurring in the extremities. In 2022, 13,190 people were newly diagnosed with STS and 5,130 people died of STS in United States (Siegel et al., 2022). STS was known as its heterogeneity which includes at least 100 different histologic and molecular subtypes. Genomic study has indicated that STS was mainly characterized by copy number variations but low mutation loads (Cancer Genome Atlas Research Network. Electronic address and Cancer Genome Atlas Research Network, 2017). However, a few genes (TP53, ATRX, RB1) showed highly recurrent mutations across different sarcoma types. These findings highlighted the importance of genetic alterations in STS, corresponding to its heterogeneity. Meanwhile, transcriptomic profiling of STS enhanced our understanding of STS biology and provided potential therapeutic targets. Transcriptomics can identify patients among different histological subtypes (Nielsen et al., 2002; Linn et al., 2003). Expression of some gene signatures were associated with prognosis of STS, such as hypoxia-inducible factor alpha (HIFA) and its targets (Francis et al., 2007).

In recent years, multiple molecular processes have been introduced to cancer biology and treatment such as the anoikis. Anoikis is a programmed cell death manner, happening when cells detached from appropriate extracellular matrix, which is a crucial mechanism in maintenance of plastic cell growth and attachment (Taddei et al., 2012). Cancer cells are characterized by insensitivity to anoikis since its survival and proliferation do not rely on adhesion to extracellular matrix (Cai et al., 2015). Thus, cancers represent a feature of anoikis resistance. In this scenario, figuring out the anoikis regulators of cancers contributes to the discovery of novel therapeutics, especially for cancer metastasis (Sakamoto and Kyprianou, 2010). For instance, in LKB1-deficient lung cancer, the PLAG1-GDH1 axis was reported to accelerate anoikis resistance through the CamKK2-AMPK pathway (Jin et al., 2018). Nuclear MYH9-induced CTNNB1 expression could facilitate gastric cancer cell anoikis resistance and induce metastasis. Similarly, it was reported that anoikis resistance in gastric cancer was regulated by TCF7L2 through transcriptionally activating PLAUR (Zhang et al., 2022), resulting in enhancement of metastasis. IQGAP1, a scaffolding protein that regulates cellular motility and extracellular signals, also reported to modulate the anoikis resistance and metastasis of hepatocellular carcinoma by accumulation of Rac1-dependent ROS and activation of Src/FAK signaling (Mo et al., 2021). These researches highlighted the critical role of anoikis profiling in various cancers.

Specifically, anoikis resistance also participate in the biology of STS. Recently, a study has conducted proteomic screens to identify suppressors of anoikis in Ewing sarcoma. The result indicated that the upregulation of IL1 receptor accessory protein (IL1RAP) significantly suppressed anoikis, which could be a new cell-surface target in Ewing sarcoma (Zhang et al., 2021). In a previous study, E-cadherin cell-cell adhesion was demonstrated to mediate suppression of anoikis by activating the ErbB4 tyrosine kinase in Ewing sarcoma (Kang et al., 2007).

Together, these findings have depicted a potential but limited role of anoikis in STS. More comprehensive studies are required to reveal the muti-omic profiling, regulator networks, microenvironments, targetable molecules, and prognostic predictors for STS. Further genotyping based on anoikis-related genes would help to understand the heterogeneity of STS, which is important to the personalized medicine. Therefore, in this study, we comprehensively analyzed the cross-talk of the anoikis-related genes (ARGs) and their molecular profiling in STS. We also focused on the impact of ARGs on tumor microenvironment, especially on the immune cell infiltration. Meanwhile, the stratification system and prognostic scoring model were established based on ARGs to guide the therapeutics for STS.

Materials and methods

Data collection and processing

The gene expression matrices of STS were downloaded from UCSC Xena (https://xenabrowser.net/) and GEO database (https://www.ncbi.nlm.nih.gov/geo/). Normal adipose and muscle tissue sample from Genotype-Tissue Expression (GTEx) database were used as normal control (https://gtexportal.org/home/). UCSC Xena has co-analyzed the TCGA data and GTEx data using UCSC bioinformatic pipeline (TOIL RNA-seq) for gene expression comparison. The copy number variations (CNVs), somatic mutation, and clinical information were downloaded from TCGA-SARC cohort. For pan-cancer analysis, data was derived from the TARGET Pan-Cancer (PANCAN) cohort. In GEO database, we identified two cohort of STS (GSE17674 and GSE63157) with prognosis data and one dataset of single-cell RNA-seq for STS (GSE131309). Moreover, we introduced a cohort of immunotherapy, in which the patients were treated with the combination of anti-PD-1 and anti-CTLA-4 therapy (Gide et al., 2019). By using this cohort, we analyzed the association between immunotherapy response and Anoikis score.

Unsupervised clustering of ARGs

We identified the ARGs from GOBP_ANOIKIS term of Gene Set Variation Analysis (GSVA) database (http://www.gsea-msigdb.org/gsea/msigdb/cards/GOBP_ANOIKIS). Chromosome location of ARGs was plotted by the package "Rcircos" (version 1.2.1). Next, we conducted unsupervised clustering analysis using the 34 ARGs to define distinct clusters of patients. We set the key parameters of maxK = 9 and repetitions = 1,000 for algorithm packaged in "ConsensusClusterPlus" (Wilkerson and Hayes, 2010). Further, we recognized the differentially expressed genes (DEGs) ($\log2|FC|\geq3$, adjp <0.05) between Anoikis clusters by using the R package "limma" (version 3.48.3). Univariate COX regression analysis was utilized to recognize DEGs with significant prognostic relevance in STS.

As the prognostic DEGs were identified, we further input them into unsupervised clustering analysis and stratified patients into different Anoikis subtypes. These subtypes were more applicative and accurate since the DEGs reflected more comprehensive and common gene profiling.

GSVA and Gene Ontology (GO) annotation

For the above defined clusters or subtypes, GSVA analysis was conducted to probe their biological characteristics by using the R package "GSVA" (version 1.40.1) (Hanzelmann et al., 2013). Meanwhile, biological differences between subgroups with high and low Anoikis score were also analyzed by GSVA. The h.all.v7.5.1 and c2.cp.kegg.v7.4 gene sets were downloaded from the Molecular Signatures Database (MSigDB). The R package "limma" (version 3.48.3) was utilized when comparing the differential expressed hallmark gene sets and tested using moderated t-statistics. The results were plotted using the R package "ggplot2" (version 3.3.5). Additionally, the R package "clusterProfiler" (version 4.0.5) was adopted for GO annotation. The significant enrichment was determined by false discovery rate (FDR) < 0.05.

Evaluation of tumor immune infiltration

To assess the immune cell infiltration in tumor microenvironment, we applied the single-sample gene set enrichment analysis (ssGSEA), the marker genes of multiple types of immune cells were downloaded from previous study (Bindea et al., 2013). Infiltration level was normalized ranging from 0 to 1. Tumor mutation burden (TMB) signatures from published data (Mariathasan et al., 2018) were utilized to estimate the association between tumor microenvironment and biological processes. Moreover, we extracted signatures related to immunotherapy-predicted pathways and cancer-immunity cycles as previously reported (Chen and Mellman, 2013; Hu et al., 2021). Specifically, the cancer-immunity cycles containing seven steps: step one and two: cancer antigen release and presentation, step three: T-cell priming and activation, step four: immune cell recruitment, step five: immune cell infiltration into tumors, step six: T-cell recognition of cancers, step seven: killing of cancer cells. These cycles were applied to guide frameworks for immunotherapy. We used GSVA to calculate the signatures scores of immunotherapy-predicted pathway and cancer-immunity cycles as previously described. The associations between Anoikis score and GSVA scores of different gene sets were compared by using the R package "ggcor" (version 0.9.4.3).

Establishment of the anoikis scoring model

In order to applied the above findings in more patients, we next generated the anoikis scoring system based on our previous established Anoikis clusters. DEGs between Anoikis cluster C1 and C2 were identified and Univariate COX regression analysis was conducted to recognize prognosis relevant DEGs. The prognostic DEGs were then analyzed using principal component analysis (PCA) and calculated for signature scores. This method was advantageous in identification of the score of the set with most significant correlation and elimination of unrelated blocks. To calculate the Anoikis score, the formula of $\Sigma(PC1_i + PC2_i)$ was applied where i was the expression of the enrolled prognostic DEGs. On this basis, patients were divided into the high and low Anoikis score group according to a cut-off value determined by the algorithm.

Single-cell transcriptome analysis

In this study, we used a single-cell RNA-seq dataset (GSE131309) from published study (Jerby-Arnon et al., 2021). The data were analyzed following standard pipeline of the package "Seurat" (version 4.0.5). Gene expression was normalized by LogNormalize (scale factor = 10,000). 2,000 highly variable genes (HVGs) were then recognized within the function of FindVariableGenes. 25 PC were picked up based on the result of ElbowPlot. Subsequently, we performed the cell clustering and t-distributed stochastic neighbor embedding (t-SNE) to figure out the cell subpopulations. The same labels from the data resource were used for specific cell cluster annotation, as described in previous study (Jerby-Arnon et al., 2021). Expression of specific genes was illustrated in t-SNE plots.

Prediction of chemotherapeutic sensitivity

Drug response data were retrieved from the Genomics of Drug Sensitivity in Cancer (GDSC) (https://www.cancerrxgene.org/downloads/anova). The GDSC database provides the drug sensitivity data and genetic correlation for more than 1,000 genetically characterized human cell lines (Yang et al., 2013). Drug response data of 518 compounds targeting 24 pathways were identified. IC50 and drug sensitivity score were utilized to assess the chemotherapeutic sensitivity, as calculated by the R packages "pRRophetic" (version 0.5) and "oncoPredict" (version 0.2) (Iorio et al., 2016; Maeser et al., 2021).

Cell lines and real-time PCR

The human synovial sarcoma (SW-982) and liposarcoma cell line (SW-872) were purchased from the Procell Life Science & Technology Co., Ltd. Primary human skin fibroblast cell line (HSF) was acquired from Fenghui Biotechnology Co., Ltd. The primary hSS-005R cell line was established by our laboratory. They were cultured in Dulbecco's modified Eagle medium (DMEM) completed with 10% fetal bovine serum (FBS) and 1% Penicillin-Streptomycin at 37 °C and 5% CO_2.

For real-time PCR analysis of mRNA expression, 2×10^5 cells were cultured in six well plates for 24 h and the RNA Express Total RNA Kit (M050, NCM Biotech, China) was used for subsequent total RNA extraction. RevertAid First Strand cDNA Synthesis kit (K1622, Thermo Fisher Scientific, United States) was utilized for cDNA synthesis. For each sample, 50 ng cDNA was mixed with Hieff® qPCR SYBR Green Master Mix (11201ES03, YEASEN, China) and gene specific primers following the manufacturer's protocol. Reactions were performed on the Applied Biosystems QuantStudio (Thermo Fisher Laboratories). Real-time PCR experiments were repeated using three biological replicates. The primer sequences were as follow: GAPDH, 5′- CAG GAGGCATTGCTGATGAT -3' (forward), 5′- GAAGGCTGGGGC TCATTT-3' (reverse); E2F1, 5′- ACGTGACGTGTCAGGACCT -3' (forward), 5′- GATCGGGCCTTGTTTGCTCTT -3' (reverse); SNAI2,

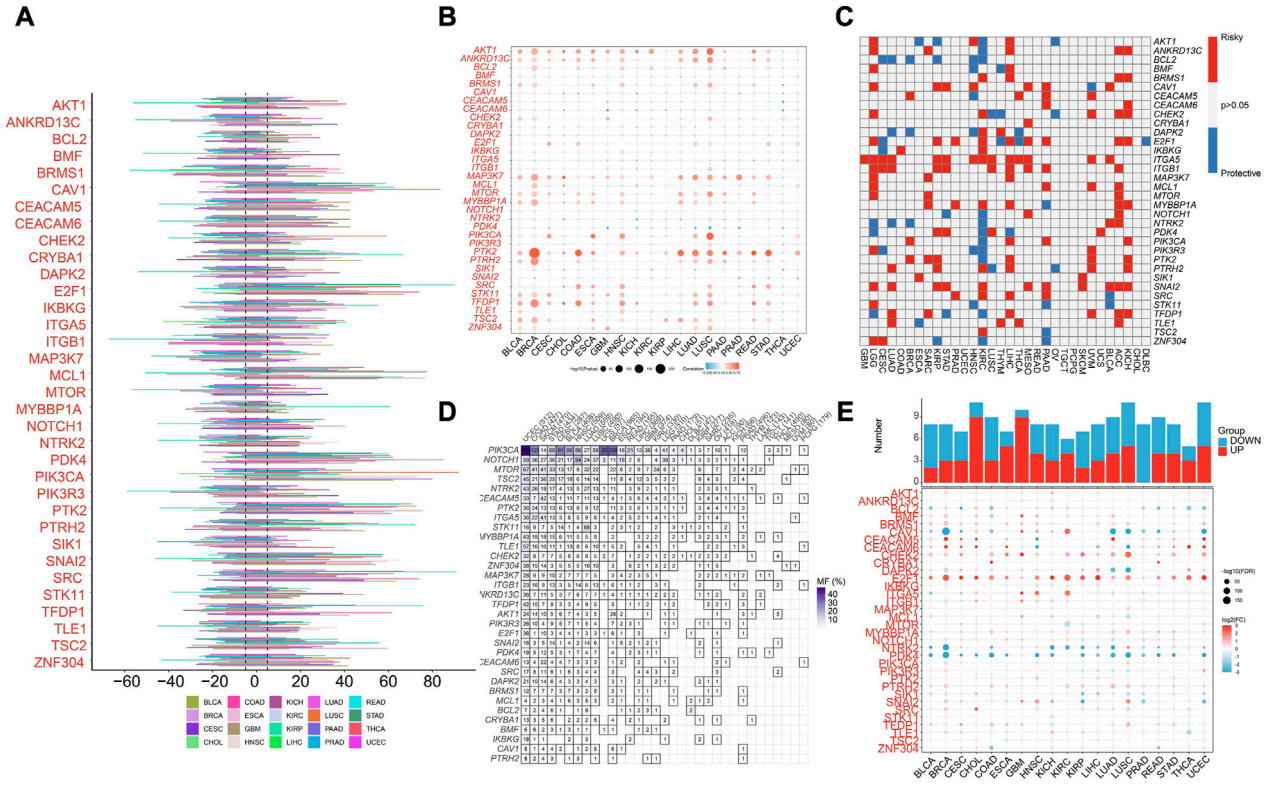

FIGURE 1
Pan-cancer analysis of Anoikis-related genes (ARGs) in pan-cancer TCGA data. **(A)** The illustration of somatic copy number variance (SCNV) of ARGs in different cancer types. The percentage of amplification and deletion was annotated. **(B)** The correlation of SCNV and expression of ARGs within different cancer types. **(C)** The prognostic effects of the expression of ARGs across different cancer types. Red indicates the risk factor, and blue indicated the protective factor. **(D)** The mutation frequency of ARGs in different cancer types. **(E)** The expression patterns of ARGs between tumor and normal samples in different cancer types. The upper histograms illustrate the number of significantly differentially upregulated (red) and downregulated (blue) genes.

5′- TGTGACAAGGAATATGTGAGCC -3’ (forward), 5′- TGAGCC CTCAGATTTGACCTG -3’ (reverse); DAPK2, 5′- GGGACGCCG GAATTTGTTG -3’ (forward), 5′- TTCCTGCTTCGTGTCTCCCA -3’ (reverse).

Full-length transcriptome analysis

We performed full-length mRNA-seq on four STS samples and four paired normal tissues (GSE198568). Total RNA was extracted from fresh frozen samples for full-length transcriptome analysis. The sequencing was performed by Biomarker Technologies (Biomarker Technologies Ltd., Beijing, China) following the operation protocols of Oxford Nanopore Technologies (Oxford Nanopore Technologies, Oxford, United Kingdom). Data were analyzed in accordance with the pipeline provided by Biomarker Technologies Ltd.

Statistical analysis

R software (version 4.1.0) was used for statistical analysis. We conducted the spearman correlation test when calculating the correlations of ARGs. Student’s t-tests and Wilcoxon signed-rank test were conducted for parametric comparisons and non-parametric comparisons. Multiple groups comparisons were tested by one-way ANOVA or Kruskal–Wallis test. Log-rank test was applied in survival analysis. The prognostic factors were determined by Univariate and multivariate Cox regression. To assess the accuracy of model, Receiver operating characteristic (ROC) curves were plotted and area under the curve (AUC) was calculated by using R package “timeROC” (version 0.4). The optimal cut-off value of Anoikis scores was determined by using the package “survminer” (version 0.4.9). Besides, chi-square or Fisher exact tests was adopted to compare clinical characteristics in different groups. p-value <0.05 was defined as statistical significance.

Results

Pan-cancer analysis of ARGs

We first analyzed the profiling of ARGs in pan-cancer level. Copy number variance (CNV) analysis of ARGs indicated CNV gain of CVA1, E2F1, MCL1, PDK4, PIK3CA, PTK2, SNAI2, and

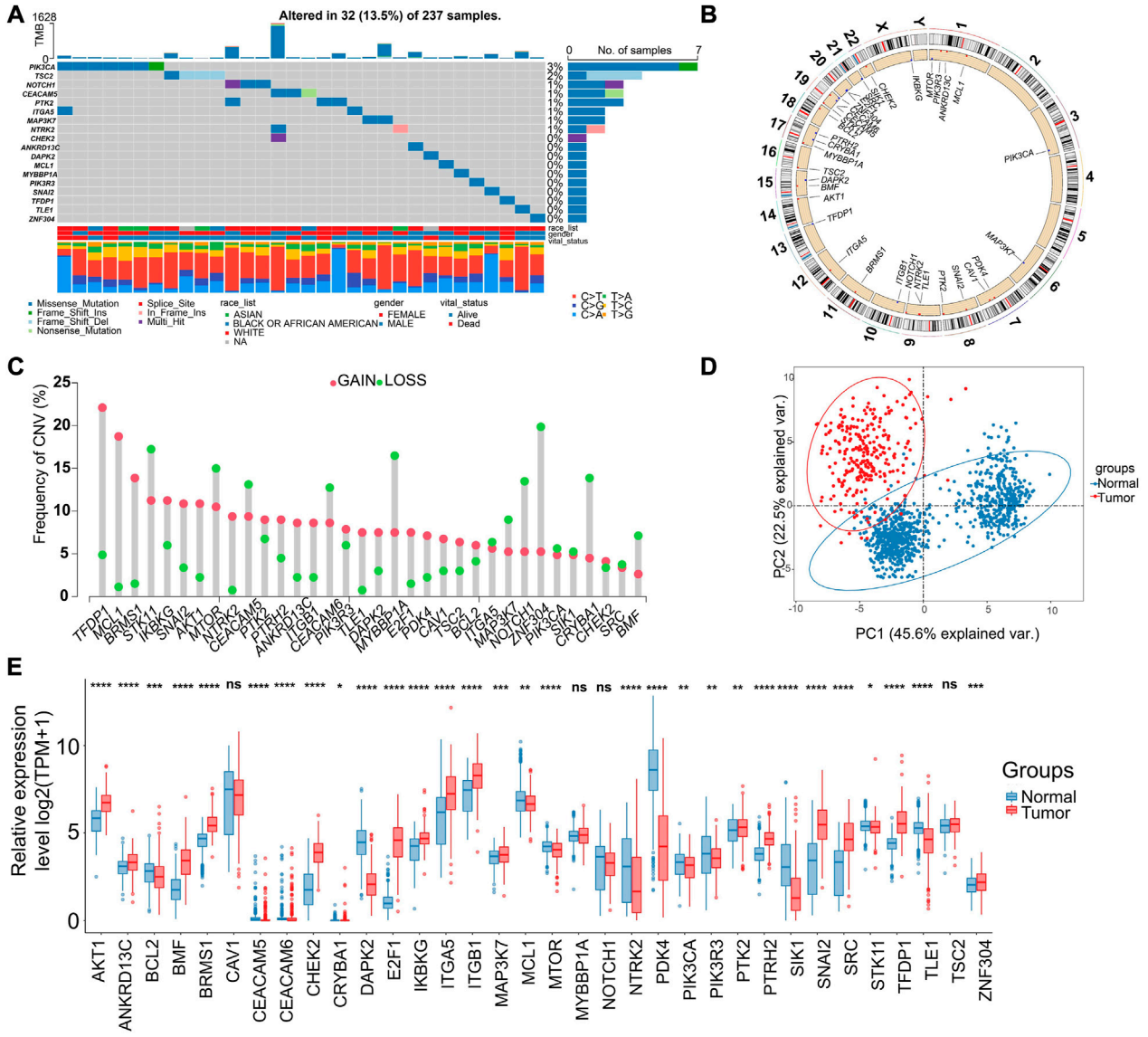

FIGURE 2
Genomic and transcriptional landscapes of ARGs in soft-tissue sarcoma (STS) in TCGA database. **(A)** The mutation frequency of ARGs (Top 18) in 237 patients with STS in TCGA database. **(B)** The specific location of ARGs on the human chromosomes. **(C)** The SCNV of ARGs in patients with STS in TCGA database. Red indicates CNV gain, and green indicates CNV loss. **(D)** The principal component analysis (PCA) of ARGs expression to identify tumor among normal samples based on the TCGA-GTEx database. Red indicates tumor samples, blue indicate normal tissues. **(E)** The expression of ARGs between tumor (red) and normal samples (blue) based on the TCGA-GTEx database. *, $0.01 \le p < 0.05$; **, $0.001 \le p < 0.01$; ***, $0.0001 \le p < 0.001$; ****, $p < 0.0001$; ns, $p \ge 0.05$.

SRC in various cancer types (Figure 1A). Significant correlation between SCNV and expression of PTK2 was found in different cancer types (Figure 1B). As reveled by survival analysis, high expression of most ARGs suggested high risk effect for LGG, LIHC, ACC and KICH but protective effect for KIRC (Figure 1C). Besides, ITGA5 and ITGB1 were risk factors for multiple cancer types (Figure 1C). Among the 34 ARGs, PIK3CA showed the highest mutation frequency in different cancer types (Figure 1D). E2F1 and CHEK2 were highly expressed across most cancer types compared to normal samples, while PDK4 and NTRK2 were decreased in various cancers (Figure 1E).

Genomic and transcriptional landscapes of ARGs in STS

More specifically, the ARGs were analyzed in STS cohort. Only 32 (13.5%) of 237 samples showed ARGs-related mutations, concentrating within 18 ARGs (Figure 2A). Most ARGs located in chromosome 1, 9, 17, 19 (Figure 2B). The SCNV frequency of ARGs were depicted in Figure 2C. Notably, the expression profiling of 34 ARGs could discriminate against tumor and normal tissues (Figure 2D) since most of them showed significant differential expression (Figure 2E). In order to specialize the expression

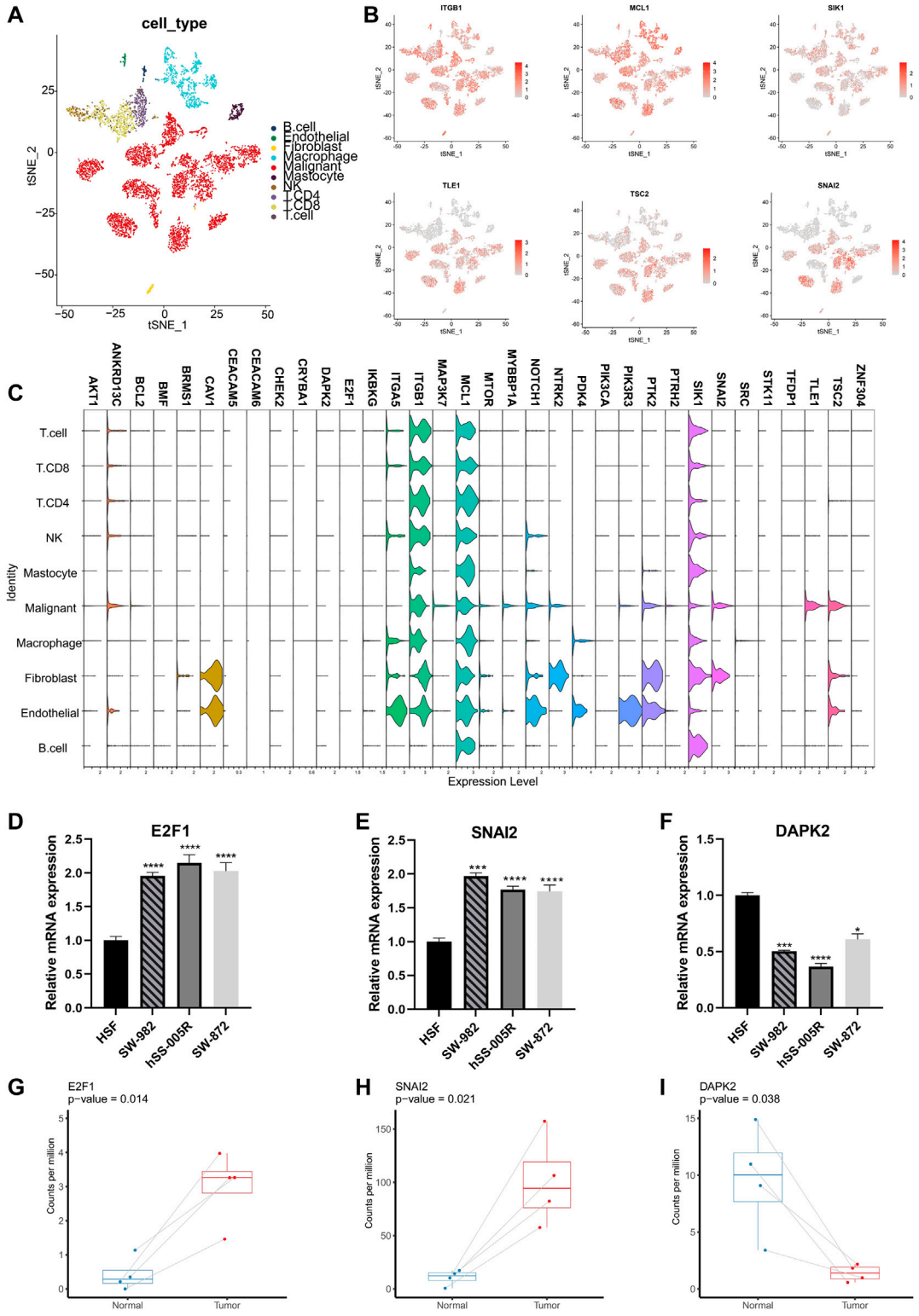

FIGURE 3
Validation of expression patterns of ARGs at single-cell resolution. **(A)** The t-distributed stochastic neighbor embedding (t-SNE) plot showing specific cell types of STS. **(B)** The t-SNE plots showing the expression of ARGs in different cell types. **(C)** The violin plots illustrating expression levels of ARGs across different cell types. **(D–F)** Validation of expression of ARGs between STS cell lines and the control cell line by the real-time PCR. Real-time PCR experiments were repeated using three biological replicates. **(G–I)** The box plots illustrating the expression of ARGs between STS and matched adjacent normal tissues based on our own sequencing data. *, $0.01 \leq p < 0.05$; ***, $0.0001 \leq p < 0.001$; ****, $p < 0.0001$.

10.3389/fphar.2023.1136184

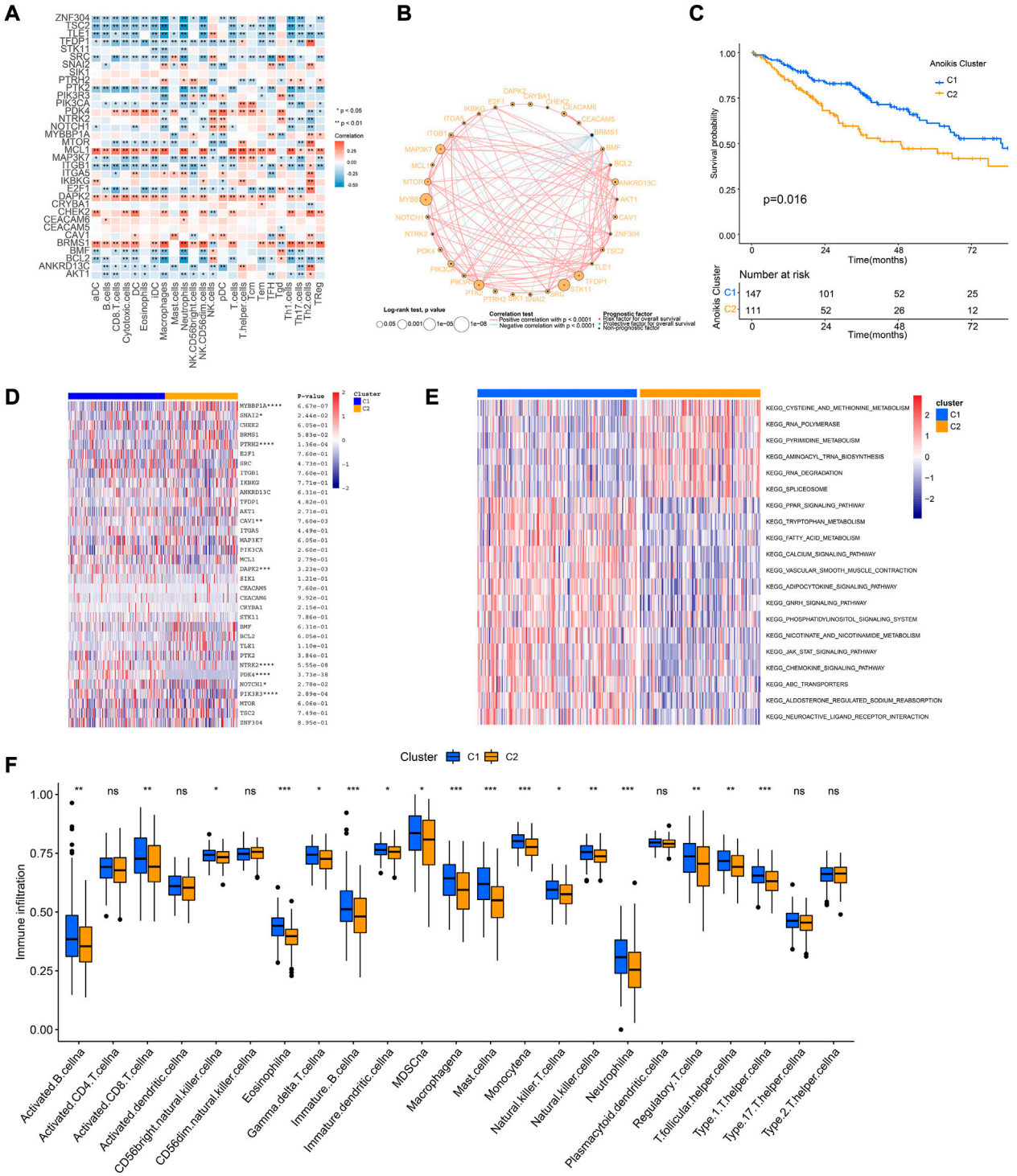

FIGURE 4
Cross-talk of ARGs and identification of Anoikis clusters. **(A)** The correlation analysis of the expression of ARGs and signatures of immune cells. Red indicated positively associated and blue indicated negatively associated. **(B)** The correlation network of ARGs in the TCGA-SARC cohort. The significance of the prognostic effects was illustrated by the circle size. **(C)** The Kaplan-Meier curve comparing the survival between different Anoikis clusters. **(D)** The heatmap of ARGs between different Anoikis clusters. **(E)**The gene set variation analysis (GSVA) illustrating pathways significantly enriched between different Anoikis clusters. **(F)** The infiltrations of different immune cells between different Anoikis clusters. *, $0.01 \le p < 0.05$; **, $0.001 \le p < 0.01$; ***, $0.0001 \le p < 0.001$; ****, $p < 0.0001$; ns, $p \ge 0.05$.

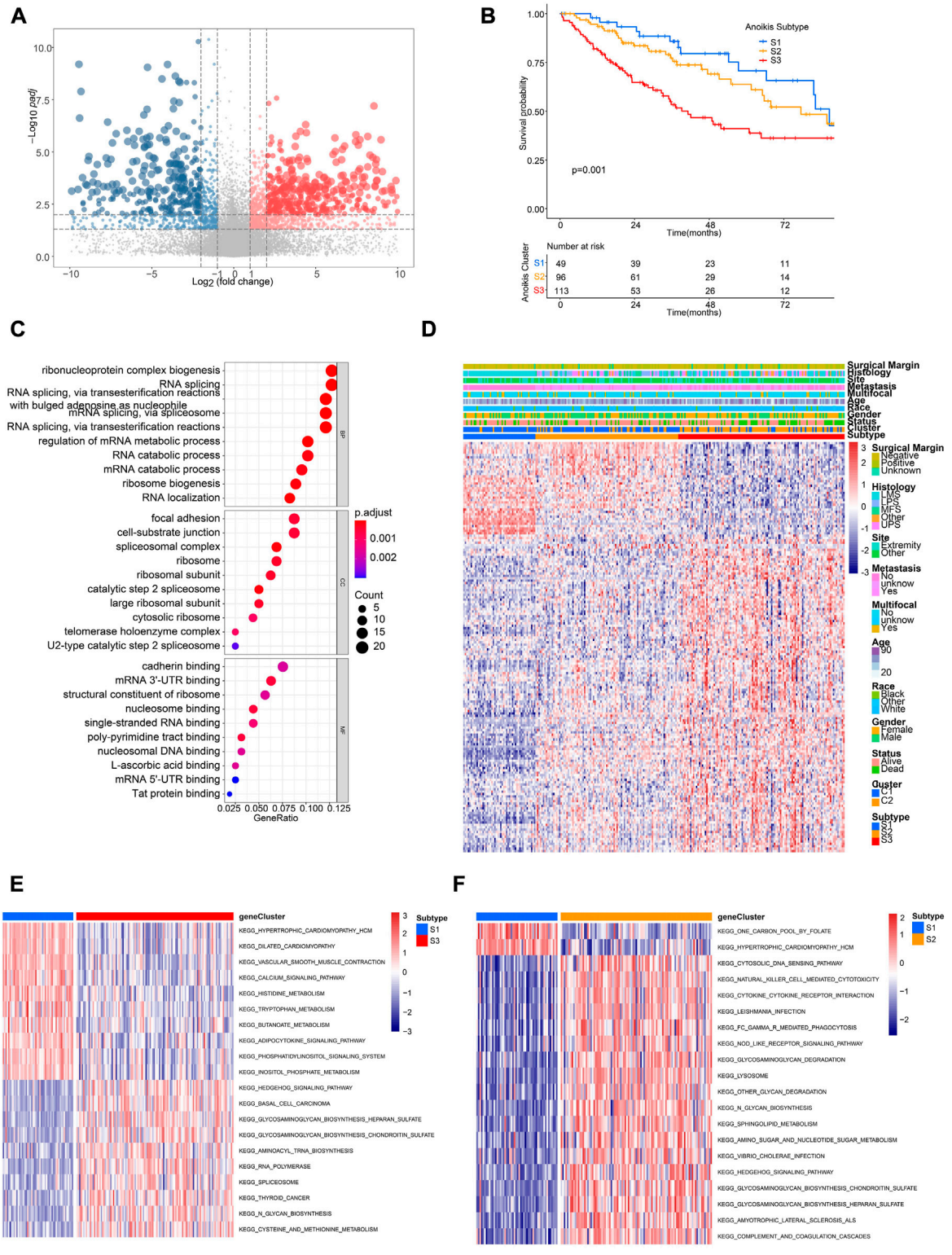

FIGURE 5
Identification of distinct Anoikis subtypes and related biological characteristics. **(A)** The volcano plot showing significantly differentially expressed genes (DEGs) between different Anoikis clusters (C2 versus C1). Genes significantly upregulated were marked in red, while genes significantly downregulated were marked in blue. **(B)** The Kaplan-Meier curve comparing the survival between different Anoikis subtypes. **(C)** Gene Ontology (GO) enrichment analysis of DEGs identified in the above resulted. BP, biological process; CC, cellular component; MF, molecular function. **(D)** The unsupervised clustering of TCGA-SARC cohort based on the ARGs-related DEGs. **(E, F)** The GSVA comparing pathways significantly enriched among distinct Anoikis subtypes.

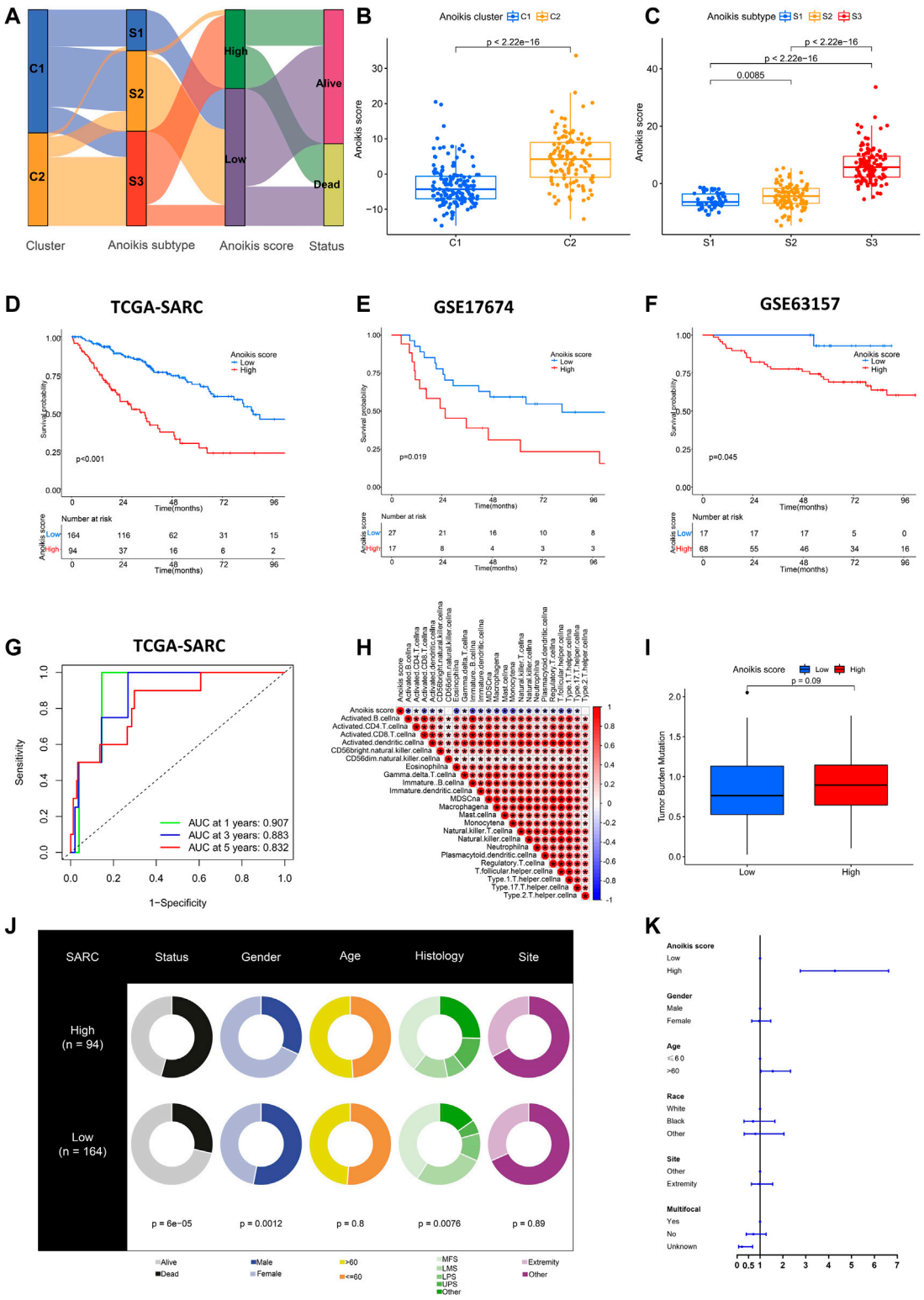

FIGURE 6
Establishment and validation of Anoikis score. **(A)** Alluvial diagram showing the relations among Anoikis clusters, Anoikis subtypes and Anoikis score groups. **(B, C)** The box plots illustrating the Anoikis score in different Anoikis clusters and Anoikis subtypes. **(D–F)** The Kaplan-Meier curves comparing the survival between low (blue) and high (red) Anoikis score groups in TCGA-SARC cohort **(D)**, GSE17674 **(E)** and GSE63157 **(F)**. **(G)** The time-dependent receiver operating characteristic curve (ROC) assessing the predictive performance of Anoikis score in TCGA-SARC cohort. **(H)** The correlation analysis between Anoikis score and signatures of immune cells. Red indicated positively associated and blue indicated negatively associated. **(I)** The box plot of tumor mutation burden (TMB) between low and high Anoikis score groups in TCGA-SARC cohort. **(J)** The pie plots showing proportions of different clinical characteristics between low and high Anoikis score groups in TCGA-SARC cohort. **(K)** The forest plot illustration multi-variate Cox analysis including clinical information and Anoikis score. *, $p < 0.05$.

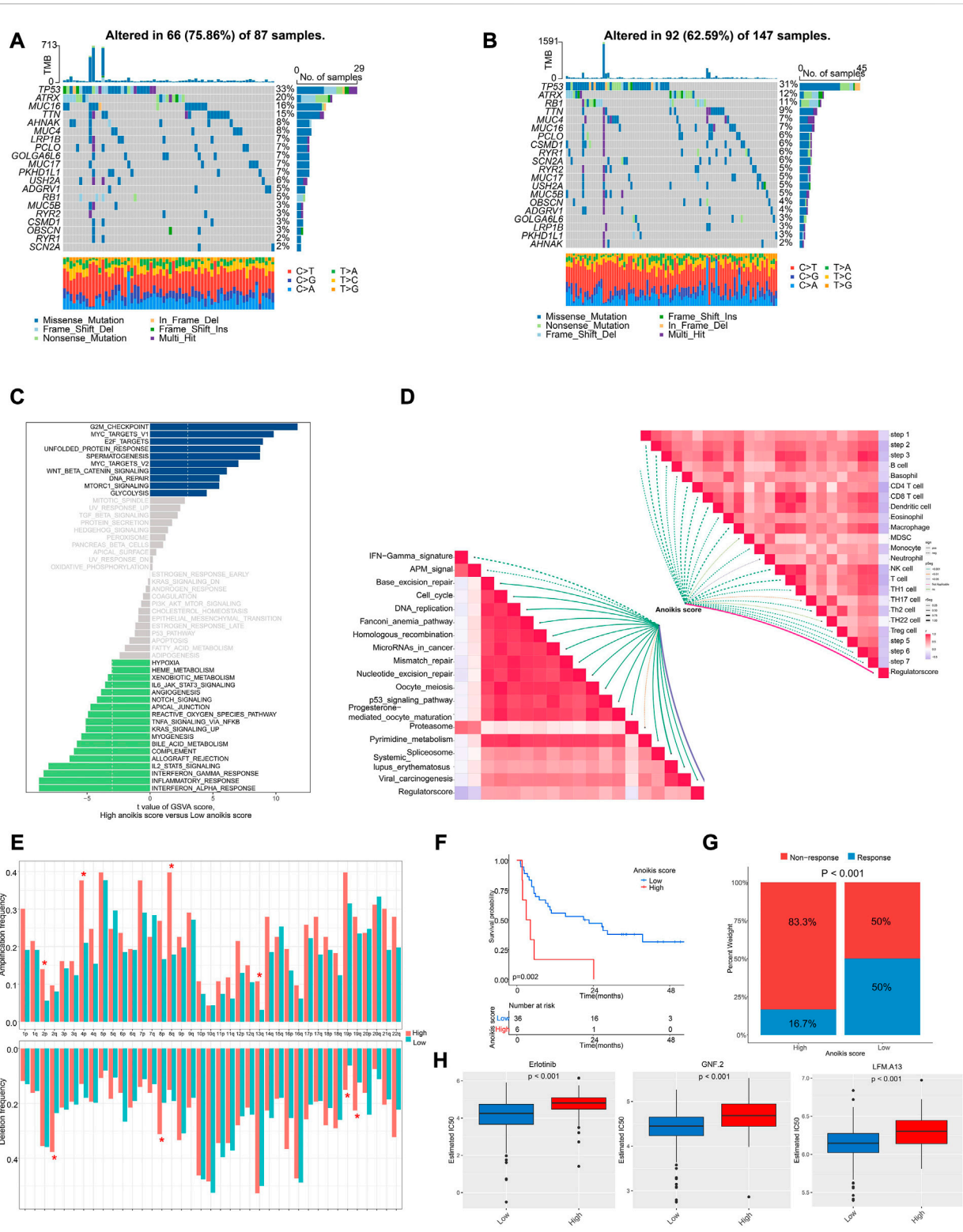

FIGURE 7
The genomic and transcriptional characteristics between Anoikis score groups. **(A, B)** The differences in mutation frequency between high **(A)** and low **(B)** Anoikis score groups. **(C)** The GSVA illustrating significantly differently enriched pathways between Anoikis score groups. **(D)** The correlation analysis of Anoikis score with immunotherapy-predicted pathways and cancer immunity cycles. **(E)** The frequency of arm-level amplification and deletion between Anoikis score groups. **(F)** The Kaplan-Meier curve comparing the survival between low and high Anoikis score groups in an immunotherapy cohort. **(G)** The rates of clinical response between Anoikis score groups in an immunotherapy cohort. **(H)** The box plots showing significant differences in the estimated IC50 of several drugs between Anoikis score groups in TCGA-SARC cohort. *, $p < 0.05$.

pattern of ARGs, we next visualized their expression in single cell transcriptomics from GSE131309 (Figures 3A, B). We noticed that ITGB1, MCL1, and SIK1 broadly expressed in all cell types while TLE1, TSC2, and SNAI2 were mainly clustered in malignant subtypes (Figures 3B, C; Supplementary Figure S1). As validated by real-time PCR, the expression of E2F1 and SNAI2 were significantly higher in STS cell lines including SW-982, hss-005R, and SW-872 compared to HSF cell line, while DAPK2 was lower in STS cell lines (Figures 3D–F). Additionally, the consistent results were identified in our own sequencing data of four pairs of STS and normal samples (Figures 3G–I).

Cross-talk of ARGs and identification of anoikis clusters

Tumor immune microenvironment is a key regulator of tumor progression, in which the immune cells cross-talk with other cell types and impact their predestination. Through correlation analysis of the expression pattern of ARGs and signatures of immune cells, we found that expression of MCL1, DAPK2, PDK4, and BRMS1 were positively correlated with most immune cells (Figure 4A). The network of 34 ARGs displayed a comprehensive landscape of the interactions (Figure 4B). Among them, most ARGs such as BMF, BCL2, ANKRD13C, AKT1, ZNF304, TSC2 showed positive correlation with other genes, but BRMS1 negatively correlated with most ARGs (Figure 4B). These findings indicated the interactive patterns of ARGs.

Further, we conducted unsupervised consensus clustering to identify distinct expression patterns of ARGs in different patients (Supplementary Figure S2). Consequently, 258 patients were clustered into two clusters by using K = 2 as the optimal index based on elbow method (Krolak-Schwedt and Eckes, 1992), named as C1 and C2 containing 147 and 111 patients respectively. The two clusters showed distinct prognosis (p = 0.016), ARGs expression patterns, and pathway enrichment patterns (Figures 4C–E), indicating the different characteristics between them. Specifically, patients of cluster C1 showed better survival and improved immune infiltration patterns (Figures 4C, F). GSVA showed that Cluster C1 were positively enriched in chemokine signaling and JAK-STAT signaling pathways (Figure 4E).

Identification of distinct anoikis subtypes and related biological characteristics

In order to further identify distinct patient groups based on the characteristic of Anoikis clusters, we performed unsupervised consensus clustering using DEGs between cluster C1 and C2 (Figure 5A; Supplementary Figures 3A–F). As a result, three subtypes (S1, S2, S3) were identified, with the patient number of 49, 96, 113 respectively. Patients of the three subtypes were significantly different in survival (Figure 5B). Besides, the DEGs were enriched in GO terms of ribonucleoprotein complex biogenesis, RNA splicing, focal adhesion, cell-subtract junction, cadherin binding, etc. (Figure 5C). Gene expression patterns of three subtypes were distinct but the clinical characteristics were irregular (Figure 5D). Pathway analysis of different subtypes were conducted to identify corresponding characteristics. GSVA suggested the enrichment of hedgehog signaling, basal cell carcinoma, and glycosaminoglycan biogenesis in S3 subtype (Figure 5E), while the pathways of cytosolic DNA sensing, natural killing cell mediated cytotoxicity, and cytokine-cytokine receptor interaction were enriched in S2 subtype (Figure 5F). Interestingly, subtype S2 showed higher infiltration of most immune cells compared to S1 and S2 (Supplementary Figure S3G).

Establishment and validation of anoikis score

As displayed above, the identification of Anoikis clusters (C1, C2) and Anoikis subtypes (S1, S2, S3) helped to classify patients with different gene expression patterns. Nevertheless, they were limited within the TCGA-SARC cohort. Therefore, we further established the Anoikis score based on DEGs between Anoikis clusters C1 and C2 to apply this model in external cohorts. The flow diagram was illustrated in Figure 6A. The Anoikis score was significantly different among Anoikis clusters or Anoikis subtypes (Figures 6B, C). Patients were then divided into the high Anoikis score and low Anoikis score group by an algorithm calculated cut-off value. Patients with high Anoikis score showed poor prognosis in TCGA-SARC cohort (p < 0.001) (Figure 6D). External validation using GSE17674 (p = 0.019) and GSE63157 (p = 0.045) data further confirmed this result (Figures 6E, F). The AUC also suggested the reliability of Anoikis score in 1-, 3-, and 5-year survival prediction, with the values of 0.907, 0.883, and 0.832 respectively (Figure 6G). Notably, the Anoikis score was negatively correlated with multiple types of innate immune cells and adoptive immune cells including B cells, Macrophages, and various subtypes of T cells (Figure 6H), suggesting the potential of Anoikis score in STS immune infiltration prediction. There was a slight difference in TMB between high and low Anoikis score group (Figure 6I). Additionally, groups with high and low Anoikis score showed differences in clinical characteristics including survival status (p < 0.001), gender (p < 0.001), and histology (p < 0.001), but not in age and tumor site (Figure 6J). Multivariate Cox regression analysis indicated that high Anoikis score was a significant risk factor for STS (Figure 6K; Supplementary Figure S4). Together, these findings demonstrated the reliability of our Anoikis score model in prognostic prediction for STS.

The genomic and transcriptional characteristics between anoikis score groups

Next, we interrogated the genomic and transcriptional profiling between high and low Anoikis score groups. We observed a higher frequency of mutation in high Anoikis score group with alteration in 66 (75.86%) of 87 samples (Figure 7A), compared with low Anoikis score group with mutations in 92 (62.59%) of 147 samples (Figure 7B). Noteworthily, the frequency of arm-level amplification and deletion seems to be higher in high Anoikis score group compared to low group (Figure 7E). Considering the

enriched pathways in different Anoikis score groups, we found positive enrichment of pathways including G2M checkpoint, MYC targets, and E2F targets in high Anoikis score group but negative enrichment of pathways including interferon alpha response, inflammation response, and interferon gamma response (Figure 7C). This result was consistent with previous finding (Figure 6H) that high Anoikis score indicated poor immune infiltration. Moreover, we analyzed the correlation of Anoikis score with immunotherapy-predicted pathways and cancer immunity cycles. As a result, the Anoikis score was significantly negative associated with various immune cells including B cell, $CD4^+$ T cells, $CD8^+$ T cells, dendritic cells, etc. Meanwhile, Anoikis score was positively correlated with most immunotherapy-predicted pathways such as Base excision repair, cell cycle, and DNA replication (Figure 7D).

Because of the close relationship of Anoikis score and immune status, we further analyzed the Anoikis score in an immunotherapy cohort. Interestingly, patients with high Anoikis score showed poor survival ($p = 0.002$) (Figure 7F) and poor response to immunotherapy ($p < 0.001$) (Figure 7G). Additionally, we utilized the GDSC database to screen for drugs with different response in high and low Anoikis score groups. Surprisingly, we identified three drugs with higher IC50 in high Anoikis score group compared to low score group, namely, erlotinib ($p < 0.001$), GNF.2 ($p < 0.001$) and LFM.A13 ($p < 0.001$) (Figure 7H). These findings could provide potential methods for individualized immunotherapy of STS patients.

Discussion

STS is an uncommon and heterogeneous tumor with limited treatment currently (Linch et al., 2014). Several studies have explored the genomic and transcriptomic characteristics of STS to uncover the molecular profiling and find new therapeutic targets. Anoikis, a critical process of cell death, has shown great impact on STS biology, predominantly through a mechanism of anoikis resistance, which could create a microenvironment suitable for tumor metastasis (Kang et al., 2007; Zhang et al., 2021). Although the intriguing conclusions have been made, there is a lack of comprehensive analysis and applicable predictive model for ARGs in STS. The interactions between ARGs and tumor microenvironment, especially the immune cell infiltration, have not been recognized for STS. In the present study, we conducted comprehensive analysis of the 34 ARGs in STS.

In spite of the fact that all cancers are molecularly distinct, many of them share common driver mutations or characteristics of transcriptional regulation (Ciriello et al., 2013). We first analyzed the profiles of ARGs at pan-cancer level. Several ARGs showed gain of CNVs such as E2F1, MCL1, and PIK3CA across multiple cancers. CNVs of E2F1 were reported previously in various type of cancers to be associated with cancer susceptibility (Nelson et al., 2006; Rocca et al., 2017; Rocca et al., 2019; Rocca et al., 2021). MCL1 also displayed CNVs in non-small lung cancer and uterine cervix adenocarcinoma and impact on survival of patients (Yin et al., 2016; Lin et al., 2020). Similarly, PIK3CA acquired CNVs in a wide-range of cancers which regulated the cancer progression and prognosis (Yamamoto et al., 2008; Brauswetter et al., 2016; Migliaccio et al., 2022). Interestingly, PIK3CA showed the highest frequency of mutations among all ARGs in different cancers, which was consistent with previous studies (Mei et al., 2016; Mosele et al., 2020).

In STS, mutation frequency of PIK3CA was also at the top of ARGs list, indicating its critical role in STS biology. Despite this, the overall mutation burden of ARGs in STS was relatively low. The expression of most ARGs were differentially expressed so that the expression pattern could discriminate between STS and normal tissues. Differential expression of some ARGs was further confirmed by real-time PCR and our own sequencing data. For unbiased high-resolution snapshots of gene expression programs, single-cell RNA sequencing is the preferred method. Single-cell resolved gene expression profiles offer several key advantages over bulk population sequencing (Kanev et al., 2021). Notably, by single-cell transcriptomic analysis, we found that the expression of ARGs showed cell-type specificity, e.g., ITGB1, MCL1, and SIK1 highly expressed in multiple cell types while TLE1, TSC2, and SNAI2 were predominantly identified in malignant subtypes. This characteristic could help guiding the discovery of new therapeutic targets. Single-cell transcriptomics in prostate cancer revealed the high expression of MCL1 in persistent senescent tumor cells, a kind of metabolically active cell that promoted tumor proliferation and metastatic dissemination (Troiani et al., 2022). Hence, MCL1 maybe a potential indicator for cancer malignancy.

Next, we established the clustering system for STS based on 34 ARGs by using unsupervised consensus clustering. Two clusters were recognized (C1 and C2), in which the cluster C1 was characterized by better prognosis and improved immune cell infiltration. We speculated that the distinct ARGs patterns in cluster C1 resulted in a tumor microenvironment suitable for immune cell response. As expected, pathway analysis indicated the enrichment of chemokine signaling and JAK-STAT signaling in cluster C1. Increase of chemokine contributed to the improvement of immune cell engraftment, such as T cells (Dangaj et al., 2019). The IFNγ-JAK-STAT signaling was also a determinant for chemokine expression (Xu et al., 2019). To further classify patients based on Anoikis clusters, we performed unsupervised consensus clustering based on DEGs between C1 and C2. Subsequently, three Anoikis subtypes with different characteristics were established (S1, S2, S3). We noticed that S1 showed the best prognosis while S2 was characterized by optimal immune infiltration. Compared with S3, the S1 subtype was enriched in several metabolic pathways such as histidine metabolism, tryptophan metabolism, butanoate metabolism, and adipocytokine signaling pathway. Among them, the histidine metabolism was associated with good response of cancer therapy (Frezza, 2018). However, the tryptophan metabolism and adipocytokine signaling pathway could promote cancer progression in other cancers (Rose et al., 2004; Platten et al., 2019). This inconsistent conclusion may be explained by the heterogeneity in different cancer types, further studies are required for exploration of the metabolism-related mechanisms and the cancer suppression metabolic niche in specific STS subtype. Not surprisingly, we also observed the enrichment of cytokine-cytokine receptor interaction in S2. It was reported that higher level of TMB was associated with poorer in cancer patients, and the risk scores of STS patients with higher risk score were also higher in our study, which needs further research (Valero et al., 2021).

Moreover, we built an anoikis scoring system according to the prognostic DEGs between cluster C1 and C2. The anoikis scoring system could be utilized to calculate specific score of individual patients. The system was effective in prediction of prognosis in multiple cohort which was of great potential in clinical guidance. The group of low Anoikis score showed better prognosis and immune infiltration.

Similarly, the low Anoikis score group was enriched in immune-related pathway such as IL6 JAK-STAT3 signaling, TNFA signaling, complement, INFγ response, INFα response, and inflammatory response. Further, the Anoikis score may also serve as an indicator for the response of immunotherapy. Similar findings were also reported in other cancer types, as ARGs were significantly associated with TME (Guizhen et al., 2022; Zhang et al., 2023). Although the anoikis scoring system achieved good predictive performance, high intratumor heterogeneity between samples may limit further application of this tool. Besides, larger sample size is needed to validate results in the future.

Conclusion

Taken together, this study comprehensively analyzed the anoikis profiles in STS for the first time. We unraveled the profiling and interactions of ARGs in both the pan-cancer levels and STS, figuring out the critical role of ARGs in tumor biology. The establishment of Anoikis subtypes reflected the heterogeneity of ARGs between patients regarding the prognosis and immune cell infiltration. The Anoikis scoring system further provided individualized assessment for prognosis and immune response, which could guide personalized treatment for STS.

Data availability statement

Publicly available datasets were analyzed in this study. This data can be found here: UCSC Xena (https://xena.ucsc.edu/) and GEO database (https://www.ncbi.nlm.nih.gov/geo/) with accession No. GSE17674, GSE63157, GSE131309, GSE198568.

Author contributions

LQ and WZ performed the bioinformatic analysis and wrote the manuscript; LW collected the sample and performed qRT-PCR experiments; FC and ZY organized the data; LQ, WZ, and Z-HL conceived and designed the experiments; all authors read and approved the final version of the manuscript.

Funding

This work was supported by the National Natural Science Foundation of China (82172500), the Science and Technology Development Fund Guided by Central Government (2021Szvup169) and Major Project of Technology Innovation of Hunan Province (2021SK1060).

Acknowledgments

The authors are grateful to the patients whose publicly available data made this project possible.

Conflict of interest

The authors declare that the research was conducted in the absence of any commercial or financial relationships that could be construed as a potential conflict of interest.

Publisher's note

All claims expressed in this article are solely those of the authors and do not necessarily represent those of their affiliated organizations, or those of the publisher, the editors and the reviewers. Any product that may be evaluated in this article, or claim that may be made by its manufacturer, is not guaranteed or endorsed by the publisher.

Supplementary material

The Supplementary Material for this article can be found online at: https://www.frontiersin.org/articles/10.3389/fphar.2023.1136184/full#supplementary-material

SUPPLEMENTARY FIGURE S1
The t-SNE plots of the expression of ARGs in different cell types.

SUPPLEMENTARY FIGURE S2
The identification of Anoikis clusters. **(A-E)** Consensus clustering based on ARGs (K = 2-6). **(F)** Consensus cumulative distribution function (CDF) Plot based on ARGs.

SUPPLEMENTARY FIGURE S3
The identification of Anoikis subtypes. **(A-E)** Consensus clustering based on ARGs-realted DEGs (K = 2-6). **(F)** Consensus cumulative distribution function (CDF) Plot based on ARGs-realted DEGs. **(G)** The infiltrations of different immune cells between different Anoikis subtypes. ***, $0.0001 \leq p < 0.001$.

SUPPLEMENTARY FIGURE S4
Subgroup analysis of Anoikis score based on clinical characteristics. The Kaplan-Meier curves comparing the survival between low and high Anoikis score groups in different genders **(A-B)**, ages **(C-D)**, histology **(E-I)** and tumor sites **(J-K)**.

References

Bindea, G., Mlecnik, B., Tosolini, M., Kirilovsky, A., Waldner, M., Obenauf, A. C., et al. (2013). Spatiotemporal dynamics of intratumoral immune cells reveal the immune landscape in human cancer. *Immunity* 39 (4), 782–795. doi:10.1016/j.immuni.2013.10.003

Brauswetter, D., Danos, K., Gurbi, B., Felegyhazi, E. F., Birtalan, E., Meggyeshazi, N., et al. (2016). Copy number gain of PIK3CA and MET is associated with poor prognosis in head and neck squamous cell carcinoma. *Virchows Arch.* 468 (5), 579–587. doi:10.1007/s00428-016-1905-1

Cai, Q., Yan, L., and Xu, Y. (2015). Anoikis resistance is a critical feature of highly aggressive ovarian cancer cells. *Oncogene* 34 (25), 3315–3324. doi:10.1038/onc.2014.264

Cancer Genome Atlas Research Network (2017). Comprehensive and integrated genomic characterization of adult soft tissue sarcomas. *Cell* 171 (4), 950–965.e928. doi:10.1016/j.cell.2017.10.014

Chen, D. S., and Mellman, I. (2013). Oncology meets immunology: The cancer-immunity cycle. *Immunity* 39 (1), 1–10. doi:10.1016/j.immuni.2013.07.012

Ciriello, G., Miller, M. L., Aksoy, B. A., Senbabaoglu, Y., Schultz, N., and Sander, C. (2013). Emerging landscape of oncogenic signatures across human cancers. *Nat. Genet.* 45 (10), 1127–1133. doi:10.1038/ng.2762

Dangaj, D., Bruand, M., Grimm, A. J., Ronet, C., Barras, D., Duttagupta, P. A., et al. (2019). Cooperation between constitutive and inducible chemokines enables T cell engraftment and immune attack in solid tumors. *Cancer Cell* 35 (6), 885–900.e10. doi:10.1016/j.ccell.2019.05.004

Francis, P., Namlos, H. M., Muller, C., Eden, P., Fernebro, J., Berner, J. M., et al. (2007). Diagnostic and prognostic gene expression signatures in 177 soft tissue sarcomas: Hypoxia-induced transcription profile signifies metastatic potential. *BMC Genomics* 8, 73. doi:10.1186/1471-2164-8-73

Frezza, C. (2018). Histidine metabolism boosts cancer therapy. *Nature* 559 (7715), 484–485. doi:10.1038/d41586-018-05573-4

Gamboa, A. C., Gronchi, A., and Cardona, K. (2020). Soft-tissue sarcoma in adults: An update on the current state of histiotype-specific management in an era of personalized medicine. *CA Cancer J. Clin.* 70 (3), 200–229. doi:10.3322/caac.21605

Gide, T. N., Quek, C., Menzies, A. M., Tasker, A. T., Shang, P., Holst, J., et al. (2019). Distinct immune cell populations define response to anti-PD-1 monotherapy and anti-PD-1/anti-CTLA-4 combined therapy. *Cancer Cell* 35 (2), 238–255.e6. doi:10.1016/j.ccell.2019.01.003

Guizhen, Z., Weiwei, Z., Yun, W., Guangying, C., Yize, Z., and Zujiang, Y. (2022). An anoikis-based signature for predicting prognosis in hepatocellular carcinoma with machine learning. *Front. Pharmacol.* 13, 1096472. doi:10.3389/fphar.2022.1096472

Hanzelmann, S., Castelo, R., and Guinney, J. (2013). Gsva: Gene set variation analysis for microarray and RNA-seq data. *BMC Bioinforma.* 14, 7. doi:10.1186/1471-2105-14-7

Hu, J., Yu, A., Othmane, B., Qiu, D., Li, H., Li, C., et al. (2021). Siglec15 shapes a non-inflamed tumor microenvironment and predicts the molecular subtype in bladder cancer. *Theranostics* 11 (7), 3089–3108. doi:10.7150/thno.53649

Iorio, F., Knijnenburg, T. A., Vis, D. J., Bignell, G. R., Menden, M. P., Schubert, M., et al. (2016). A landscape of pharmacogenomic interactions in cancer. *Cell* 166 (3), 740–754. doi:10.1016/j.cell.2016.06.017

Jerby-Arnon, L., Neftel, C., Shore, M. E., Weisman, H. R., Mathewson, N. D., McBride, M. J., et al. (2021). Opposing immune and genetic mechanisms shape oncogenic programs in synovial sarcoma. *Nat. Med.* 27 (2), 289–300. doi:10.1038/s41591-020-01212-6

Jin, L. T., Chun, J., Pan, C., Kumar, A., Zhang, G. J., Ha, Y., et al. (2018). The PLAG1-GDH1 Axis promotes anoikis resistance and tumor metastasis through CamKK2-AMPK signaling in LKB1-deficient lung cancer. *Mol. Cell*, 69(1), 87. doi:10.1016/j.molcel.2017.11.025

Kanev, K., Roelli, P., Wu, M., Wurmser, C., Delorenzi, M., Pfaffl, M. W., et al. (2021). Tailoring the resolution of single-cell RNA sequencing for primary cytotoxic T cells. *Nat. Commun.* 12 (1), 569. doi:10.1038/s41467-020-20751-7

Kang, H. G., Jenabi, J. M., Zhang, J. S., Keshelava, N., Shimada, H., May, W. A., et al. (2007). E-cadherin cell-cell adhesion in Ewing tumor cells mediates suppression of anoikis through activation of the ErbB4 tyrosine kinase. *Cancer Res.* 67 (7), 3094–3105. doi:10.1158/0008-5472.Can-06-3259

Krolak-Schwedt, S., and Eckes, T. (1992). A graph theoretic criterion for determining the number of clusters in a data set. *Multivar. Behav. Res.* 27 (4), 541–565. doi:10.1207/s15327906mbr2704_3

Lin, Y. C., Chen, Y. C., Chen, R. Y., Huang, Y. X., Tu, S. J., Liang, J. A., et al. (2020). Genomic biomarkers of survival in patients with adenocarcinoma of the uterine cervix receiving chemoradiotherapy. *Int. J. Mol. Sci.* 21 (11), 4117. doi:10.3390/ijms21114117

Linch, M., Miah, A. B., Thway, K., Judson, I. R., and Benson, C. (2014). Systemic treatment of soft-tissue sarcoma-gold standard and novel therapies. *Nat. Rev. Clin. Oncol.* 11 (4), 187–202. doi:10.1038/nrclinonc.2014.26

Linn, S. C., West, R. B., Pollack, J. R., Zhu, S., Hernandez-Boussard, T., Nielsen, T. O., et al. (2003). Gene expression patterns and gene copy number changes in dermatofibrosarcoma protuberans. *Am. J. Pathol.* 163 (6), 2383–2395. doi:10.1016/S0002-9440(10)63593-6

Maeser, D., Gruener, R. F., and Huang, R. S. (2021). oncoPredict: an R package for predicting *in vivo* or cancer patient drug response and biomarkers from cell line screening data. *Brief. Bioinform* 22 (6), bbab260. doi:10.1093/bib/bbab260

Mariathasan, S., Turley, S. J., Nickles, D., Castiglioni, A., Yuen, K., Wang, Y., et al. (2018). TGFβ attenuates tumour response to PD-L1 blockade by contributing to exclusion of T cells. *Nature* 554 (7693), 544–548. doi:10.1038/nature25501

Mei, Z. B., Duan, C. Y., Li, C. B., Cui, L., and Ogino, S. (2016). Prognostic role of tumor PIK3CA mutation in colorectal cancer: A systematic review and meta-analysis. *Ann. Oncol.* 27 (10), 1836–1848. doi:10.1093/annonc/mdw264

Migliaccio, I., Paoli, M., Risi, E., Biagioni, C., Biganzoli, L., Benelli, M., et al. (2022). PIK3CA co-occurring mutations and copy-number gain in hormone receptor positive and HER2 negative breast cancer. *NPJ Breast Cancer* 8 (1), 24. doi:10.1038/s41523-022-00382-5

Mo, C. F., Li, J., Yang, S. X., Guo, H. J., Liu, Y., Luo, X. Y., et al. (2021). Correction: IQGAP1 promotes anoikis resistance and metastasis through rac1-dependent ROS accumulation and activation of Src/FAK signalling in hepatocellular carcinoma. *Br. J. Cancer* 125 (4), 622. doi:10.1038/s41416-021-01449-z

Mosele, F., Stefanovska, B., Lusque, A., Tran Dien, A., Garberis, I., Droin, N., et al. (2020). Outcome and molecular landscape of patients with PIK3CA-mutated metastatic breast cancer. *Ann. Oncol.* 31 (3), 377–386. doi:10.1016/j.annonc.2019.11.006

Nelson, M. A., Reynolds, S. H., Rao, U. N., Goulet, A. C., Feng, Y., Beas, A., et al. (2006). Increased gene copy number of the transcription factor E2F1 in malignant melanoma. *Cancer Biol. Ther.* 5 (4), 407–412. doi:10.4161/cbt.5.4.2512

Nielsen, T. O., West, R. B., Linn, S. C., Alter, O., Knowling, M. A., O'Connell, J. X., et al. (2002). Molecular characterisation of soft tissue tumours: A gene expression study. *Lancet* 359 (9314), 1301–1307. doi:10.1016/S0140-6736(02)08270-3

Platten, M., Nollen, E. A. A., Rohrig, U. F., Fallarino, F., and Opitz, C. A. (2019). Tryptophan metabolism as a common therapeutic target in cancer, neurodegeneration and beyond. *Nat. Rev. Drug Discov.* 18 (5), 379–401. doi:10.1038/s41573-019-0016-5

Rocca, M. S., Benna, C., Goldin, E., Di Nisio, A., De Toni, L., Cosci, I., et al. (2021). E2F1 copy number variations in germline and breast cancer: A retrospective study of 222 Italian women. *Mol. Med.* 27 (1), 26. doi:10.1186/s10020-021-00287-2

Rocca, M. S., Benna, C., Mocellin, S., Rossi, C. R., Msaki, A., Di Nisio, A., et al. (2019). E2F1 germline copy number variations and melanoma susceptibility. *J. Transl. Med.* 17 (1), 181. doi:10.1186/s12967-019-1933-0

Rocca, M. S., Di Nisio, A., Marchiori, A., Ghezzi, M., Opocher, G., Foresta, C., et al. (2017). Copy number variations of E2F1: A new genetic risk factor for testicular cancer. *Endocr. Relat. Cancer* 24 (3), 119–125. doi:10.1530/ERC-16-0514

Rose, D. P., Komninou, D., and Stephenson, G. D. (2004). Obesity, adipocytokines, and insulin resistance in breast cancer. *Obes. Rev.* 5 (3), 153–165. doi:10.1111/j.1467-789X.2004.00142.x

Sakamoto, S., and Kyprianou, N. (2010). Targeting anoikis resistance in prostate cancer metastasis. *Mol. Asp. Med.* 31 (2), 205–214. doi:10.1016/j.mam.2010.02.001

Siegel, R. L., Miller, K. D., Fuchs, H. E., and Jemal, A. (2022). Cancer statistics, 2022. *CA Cancer J. Clin.* 72 (1), 7–33. doi:10.3322/caac.21708

Taddei, M. L., Giannoni, E., Fiaschi, T., and Chiarugi, P. (2012). Anoikis: An emerging hallmark in health and diseases. *J. Pathol.* 226 (2), 380–393. doi:10.1002/path.3000

Troiani, M., Colucci, M., D'Ambrosio, M., Guccini, I., Pasquini, E., Varesi, A., et al. (2022). Single-cell transcriptomics identifies Mcl-1 as a target for senolytic therapy in cancer. *Nat. Commun.* 13, 2177. ARTN 2177. doi:10.1038/s41467-022-29824-1

Valero, C., Lee, M., Hoen, D., Wang, J., Nadeem, Z., Patel, N., et al. (2021). The association between tumor mutational burden and prognosis is dependent on treatment context. *Nat. Genet.* 53 (1), 11–15. doi:10.1038/s41588-020-00752-4

Wilkerson, M. D., and Hayes, D. N. (2010). ConsensusClusterPlus: A class discovery tool with confidence assessments and item tracking. *Bioinformatics* 26 (12), 1572–1573. doi:10.1093/bioinformatics/btq170

Xu, Y. P., Lv, L., Liu, Y., Smith, M. D., Li, W. C., Tan, X. M., et al. (2019). Tumor suppressor TET2 promotes cancer immunity and immunotherapy efficacy. *J. Clin. Invest.* 129 (10), 4316–4331. doi:10.1172/JCI129317

Yamamoto, H., Shigematsu, H., Nomura, M., Lockwood, W. W., Sato, M., Okumura, N., et al. (2008). PIK3CA mutations and copy number gains in human lung cancers. *Cancer Res.* 68 (17), 6913–6921. doi:10.1158/0008-5472.CAN-07-5084

Yang, W., Soares, J., Greninger, P., Edelman, E. J., Lightfoot, H., Forbes, S., et al. (2013). Genomics of drug sensitivity in cancer (GDSC): A resource for therapeutic biomarker discovery in cancer cells. *Nucleic Acids Res.* 41, D955–D961. doi:10.1093/nar/gks1111

Yin, J., Li, Y., Zhao, H., Qin, Q., Li, X., Huang, J., et al. (2016). Copy-number variation of MCL1 predicts overall survival of non-small-cell lung cancer in a Southern Chinese population. *Cancer Med.* 5 (9), 2171–2179. doi:10.1002/cam4.774

Zhang, H. F., Hughes, C. S., Li, W., He, J. Z., Surdez, D., El-Naggar, A. M., et al. (2021). Proteomic screens for suppressors of anoikis identify IL1RAP as a promising surface target in ewing sarcoma. *Cancer Discov.* 11 (11), 2884–2903. doi:10.1158/2159-8290.Cd-20-1690

Zhang, T., Wang, B. F., Su, F., Gu, B. H., Xiang, L., Gao, L., et al. (2022). TCF7L2 promotes anoikis resistance and metastasis of gastric cancer by transcriptionally activating PLAUR. *Int. J. Biol. Sci.* 18 (11), 4560–4577. doi:10.7150/ijbs.69933

Zhang, Z., Zhu, Z., Fu, J., Liu, X., Mi, Z., Tao, H., et al. (2023). Anoikis patterns exhibit distinct prognostic and immune landscapes in Osteosarcoma. *Int. Immunopharmacol.* 115, 109684. doi:10.1016/j.intimp.2023.109684

frontiers | Frontiers in Pharmacology

TYPE Original Research
PUBLISHED 24 March 2023
DOI 10.3389/fphar.2023.1113182

OPEN ACCESS

EDITED BY
Abhimanyu Thakur,
The University of Chicago, United States

REVIEWED BY
Shanqiang Qu,
Southern Medical University, China
Zhicheng Hu,
The First Affiliated Hospital of Sun Yat-Sen University, China

*CORRESPONDENCE
Meiqing Lou,
Meiqing_Lou2020@163.com
Anke Zhang,
theanke@163.com
Anwen Shao,
shaoanwen@zju.edu.cn

†These authors have contributed equally to this work

SPECIALTY SECTION
This article was submitted to Pharmacology of Anti-Cancer Drugs, a section of the journal Frontiers in Pharmacology

RECEIVED 01 December 2022
ACCEPTED 14 March 2023
PUBLISHED 24 March 2023

CITATION
Fang C, Zhang Z, Han Y, Xu H, Zhu Z, Du Y, Hou P, Yuan L, Shao A, Zhang A and Lou M (2023), URB2 as an important marker for glioma prognosis and immunotherapy. *Front. Pharmacol.* 14:1113182. doi: 10.3389/fphar.2023.1113182

URB2 as an important marker for glioma prognosis and immunotherapy

Chaoyou Fang[1†], Zeyu Zhang[2†], Yongquan Han[3†], Houshi Xu[1], Zhengyang Zhu[1], Yichao Du[1], Pinpin Hou[4], Ling Yuan[1], Anwen Shao[5,6]*, Anke Zhang[5,6]* and Meiqing Lou[1]*

[1]Department of Neurosurgery, Shanghai General Hospital, Shanghai Jiao Tong University School of Medicine, Shanghai, China, [2]Department of Neurosurgery, Renji Hospital, School of Medicine, Shanghai Jiao Tong University, Shanghai, China, [3]Department of Neurosurgery, The Affiliated Hospital of Guizhou Medical University, Guiyang, China, [4]Central Laboratory, Renji Hospital, School of Medicine, Shanghai Jiao Tong University, Shanghai, China, [5]Department of Neurosurgery, Second Affiliated Hospital, School of Medicine, Zhejiang University, Zhejiang, China, [6]Clinical Research Center for Neurological Diseases of Zhejiang Province, Hangzhou, China

Introduction: Glioma is the most common primary brain tumor and primary malignant tumor of the brain in clinical practice. Conventional treatment has not significantly altered the prognosis of patients with glioma. As research into immunotherapy continues, glioma immunotherapy has shown great potential.

Methods: The clinical data were acquired from the Chinese Glioma Genome Atlas (CGGA) database and validated by the Gene Expression Omnibus (GEO) database, The Cancer Genome Atlas (TCGA) dataset, Clinical Proteomic Tumor Analysis Consortium (CPTAP) database, and Western blot (WB) analysis. By Cox regression analyses, we examined the association between different variables and overall survival (OS) and its potential as an independent prognostic factor. By constructing a nomogram that incorporates both clinicopathological variables and the expression of URB2, we provide a model for the prediction of prognosis. Moreover, we explored the relationship between immunity and URB2 and elucidated its underlying mechanism of action.

Results: Our study shows that URB2 likely plays an oncogenic role in glioma and confirms that URB2 is a prognostic independent risk factor for glioma. Furthermore, we revealed a close relationship between immunity and URB2, which suggests a new approach for the immunotherapy of glioma.

Conclusion: URB2 can be used for prognosis prediction and immunotherapy of glioma.

KEYWORDS

URB2, glioma, immunity, prognosis, immunotherapy

1 Introduction

Glioma accounts for approximately thirty percent of brain tumors and eighty percent of malignant brain tumors and is the most frequent primary brain tumor (Omuro and DeAngelis, 2013; Ostrom et al., 2015). According to the criteria of the World Health Organization (WHO), glioma is classified into four different groups, which are associated with malignancy (Ostrom et al., 2017; Wesseling and Capper, 2018). Although aggressive therapies, including debulking surgery, chemotherapy, and external beam radiation therapy, are available, glioma patients

currently face a dismal prognosis (Stewart, 2002). Furthermore, systemic medications do not reach therapeutic concentrations inside solid tumors and cause systemic side effects (Blakeley, 2008; Sriraman et al., 2014). Hence, further research on the potential mechanisms of gliomas is imperative.

In recent years, glioma patients have increasingly chosen targeted therapy as a treatment option. Previous studies have revealed a high degree of immune infiltration in glioma (Bush et al., 2017). Numerous mechanisms are involved in the highly inhibited immune function in the glioma microenvironment, including immune checkpoint inhibitors (ICIs) (Ghouzlani et al., 2021). Immune checkpoints (ICs) are costimulators or cosuppressors required to produce an immune response (Korman et al., 2006). There is no doubt that the discovery of immune checkpoints such as CTLA-4 and PD-1 has exerted a significant boost in cancer immunotherapy development and has emerged as a potential treatment option for glioma (Ghouzlani et al., 2021). A breakthrough in glioma treatment by affecting immune checkpoints is being made.

In yeast, URB2 (URB2 ribosome biogenesis homolog) localizes to the nucleolus and encodes a protein measuring 135.2 kDa, which is essential for ribosome biogenesis. As it is critical for the biogenesis of the 60 S subunit, a mutation or depletion of URB2 will disrupt ribosomal subunits and rRNAs (Rosado et al., 2007). However, to date, no study has addressed the specific roles of URB2 in tumorigenesis and progression. Therefore, we investigated the predictive value of URB2 in glioma and elucidated its relationship with immunity in this study. Moreover, GSEA was conducted to confirm URB2-related biological functions and signaling pathways. To better understand the immunological correlates of URB2, we evaluated the relationship between URB2 expression and prognosis related to immune infiltration and the tumor microenvironment. This study is expected to lead to the development of novel therapies and provide effective clinical biomarkers for glioma.

2 Materials and methods

2.1 Cell culture

The U87 and U251 human malignant glioblastoma cell lines were purchased from the China Infrastructure of Cell Line Resources (Beijing, China). Cells were cultured in complete DMEM/F12 medium (2.5% certified fetal bovine serum, FBS (Vivacell, Shanghai, China), 15% horse serum, and a 1% antibiotic mixture) under 5% CO_2 and 37°C. The medium was changed every 3–4 days, and cultures were split using 0.25% trypsin. All experiments were carried out on cells with viability >95%. The cell lines were authenticated at VivaCell Shanghai using short tandem repeat analysis.

2.2 Transfection of siRNA

U87 and U251 cells in 6-well plates (about 5×10^5 cells/well) were transfected with siURB2 or corresponding negative controls. Lipo3000 transfection reagent was simultaneously added into the medium for efficient transfection. After 6 h, we replaced the culture medium. Detection was made 24 h after transfection. The human targeting siRNA of URB2 was purchased from sigama-aldrich.

2.3 Cell viability assay

The viability of glioma cells was evaluated using Cell Counting Kit-8 (CCK-8; cat. No. CK04; Dojindo Molecular Technologies, Inc.). U87 and U251 cells were seeded in 96-well plates (100 µl containing 3,000 cells/well). Cells were cultured in DMEM at 37°C under 5% CO_2 conditions for 24, 48 or 72 h. CCK-8 solution (10 µl) was then added to the cells for 4 h, and the optical density was detected at 490 nm using a Tecan microplate reader (Infinite F50; Tecan Group, Ltd.).

2.4 Western blot analysis

Human tissues and cell samples were prepared using RIPA lysis buffer. Forty nanograms of protein sample was loaded onto an SDS–PAGE gel and transferred to a nitrocellulose membrane. The membrane was blocked with 5% nonfat milk and incubated with primary antibodies overnight at 4°C: rabbit anti-URB2 (1:1000, HPA008902, Merck); rabbit anti-PCNA (ab92552; 1:1000; Abcam); and rabbit anti-β-actin (ab115777; 1:5000; Abcam). The membranes were incubated with the corresponding secondary antibody for 2 h.

2.5 Dataset acquisition and processing

To analyze the glioma patient characteristics, the clinical data were obtained from the CGGA database (http://www.cgga.org.cn/about.jsp). The protein expression profiles were obtained from the CPTAC database (https://cptac-data-portal.georgetown.edu/datasets) (Zhang et al., 2016). We considered OS as the primary outcome. Using the R programming language, the URB2 gene expression data and standardized RNA-seq data were compared. We applied box plots to display the expression difference of discrete variable visualization, and R 4.1.1 (https://www.r-project.org/) was used to perform all the analyses. To investigate the differences in URB2 mRNA expression levels in TCGA glioma patients, the R package "Limma" was applied. Additionally, an adjusted p-value (FDR) < 0.05 and |log2-fold change (FC)| ≥1 were considered statistically significant.

2.6 Chemotherapy sensitivity analysis

To evaluate NCI-60, we used the CellMiner (https://discover.nci.nih.gov/cellminer/) database (Reinhold et al., 2012). We used Pearson correlation analysis to determine whether the expression of URB2 was associated with drug sensitivity in the model.

2.7 Gene set enrichment analysis (GSEA)

By using GSEA, we can determine gene sets of hallmarks that significantly differ between the two groups (low and high

URB2 expression). We performed GSEA to examine the significance of differences in survival between the two groups. A 1000-fold permutation of gene sets was performed for each analysis to determine significant biological pathways. The pathways were considered significant when the nominal p values < 0.05 and |normalized enrichment score (NES)|>1.5.

2.8 Single-cell data analysis

We downloaded the raw data of GSE103224 and GSE148842 from the TISCH database, which were derived from two articles on single-cell sequencing of gliomas (Yuan et al., 2018; Zhao et al., 2021). After a series of dimensionality reduction clustering and corresponding cell annotation, we annotated each cell population into specific cells and showed the expression of the gene in each cell type using UMAP and violin plots, respectively.

2.9 Independent prognostic factor evaluation and nomogram construction

Cox regression analysis was applied in our model to examine the association between OS and variables and its independent prognostic value. We also confirmed the related gene URB2 expression. To visualize the relationship between survival rates and individual predictors, a nomogram-based model was constructed by the R "rms" package. Through the "survival ROC" package in R, we evaluated the prognostic ability by AUC and ROC analysis.

2.11 Immune correlation analysis

The correlation between URB2 expression and tumor mutational burden (TMB) was calculated by the Pearson correlation coefficient. The same calculation procedure was used for microsatellite instability (MSI) and tumor neoantigen burden (TNB). By analyzing the TIMER (https://cistrome.shinyapps.io/timer/) database, the relationship between URB2 expression and CD8 T-cells, B cells, macrophages, CD4 T-cells, dendritic cells, and neutrophils was determined. To explore the composition of the TME, we assessed the existence of infiltrating immune cells in glioma and calculated the ESTIMATEScore, which was estimated by expression data. To investigate the association between immunity and glioma progression, we profiled the expression of immune cells and immune checkpoints in glioma patients in TCGA datasets.

2.12 Statistical analysis

Analysis of all statistical data and figures was performed using R 4.1.1. (https://www.r-project.org/). The Pearson correlation method was used to analyze the correlation between two genes. The Wilcoxon signed rank test and logistic regression were applied to estimate the relationship between URB2 and clinicopathological characteristics. The log-rank test and Kaplan–Meier (KM) curve were applied to confirm the risk score (RS) and survival predictive ability of URB2. In this study, statistical significance was determined by $p > 0.05$.

3 Results

3.1 URB2 expression and its relationship to overall survival in glioma, as validated by other datasets

Figure 1A shows the expression levels of URB2 mRNA across all types of cancer in the TCGA study, which illustrates the high expression of URB2 either in GBM or LGG compared with normal tissue. By analyzing the GEPIA (http://gepia.cancer-pku.cn/) database, we constructed human tissue-enriched mRNA expression maps for URB2 in a more intuitive manner (Figure 1B). URB2 expression was markedly higher in both GBM and LGG than in normal tissue ($p < 0.05$; Figure 1C). Based on the median expression level, URB2 expression was divided into low and high groups. Then, the KM curves indicated that the high URB2 expression group had a worse OS than the low URB2 expression group in the TCGA database (p-value < 0.01; Figure 1D). Similar results were found in the GEO datasets GSE50161 and GSE4290 (both $p < 0.01$, Figures 1E, F). Moreover, a higher expression of URB2 was associated with worse OS, as validated in the CGGA database (Figure 1G). To further assess the diagnostic ability of URB2, we conducted a receiver operating characteristic (ROC) curve analysis, and the area under the curve (AUC) was 0.592 (1-year), 0.658 (3-year), and 0.6790 (5-year), respectively, indicating a low efficacy in diagnosing glioma based on the expression of URB2 (Figure 1H).

3.2 Protein expression of URB2 in glioblastoma multiforme in the CPTAP database

To demonstrate the difference in the protein expression level of URB2 between normal brain tissues and glioma, we further validated the CPTAC database (Figure 2). In CPTAP samples, URB2 protein expression was much higher in gliomas (Figure 2A), and similar results were found in glioma patients of different sexes (Figure 2B), ages (Figure 2C) and weights (Figure 2D).

Then, we also tested the expression of URB2 in low-grade glioma (LGG) and high-grade glioma (HGG). According to the results of Western blot, it can be observed that the expression of URB2 was significantly higher in HGG than LGG (Figure 2E). To further explore the role of URB2 in the progression of glioma, we downregulated the expression of URB2 in U87 and U251 cells. Of note, the cell proliferation was markedly inhibited after downregulation of URB2 in both cells (Figure 2F). Consistent with the results of cell viability, downregulation of URB2 in both cells can inhibited the expression of PCNA, which also indicated the inhibited cell proliferation (Figure 2G).

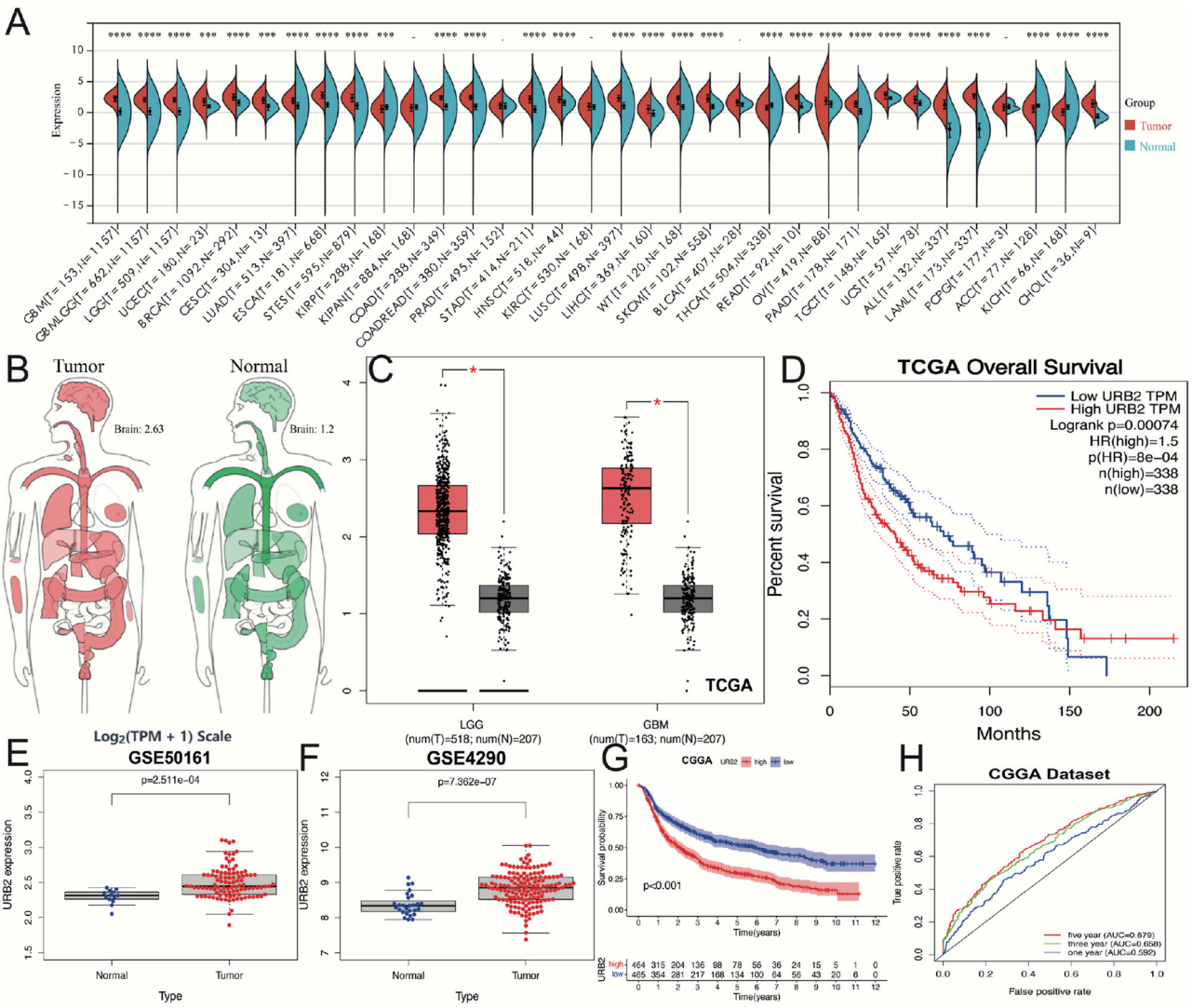

FIGURE 1
URB2 is overexpressed in glioma. Differences in the expression of URB2 in various cancers and normal tissues in the TCGA database **(A)**. Differential expression of URB2 between normal and tumor tissue in brain **(B)**. Differential expression of URB2 between LGG/GBM and normal tissue **(C)**. Overall survival of glioma patients in high and low URB2 expression groups from the TCGA database **(D)**. Differential expression of URB2 between normal and tumor tissue in GEO database **(E–F)**. KM survival curve of URB2 in CGGA dataset **(G)**. ROC curves associated with 1-, 3-, and 5-year AUC values of URB2 in CGGA dataset **(H)**. *$p < 0.05$; ***$p < 0.001$; ****$p < 0.0001$.

3.3 Clinicopathological variables and overall survival are correlated with URB2 expression

Independent-samples t tests were used to evaluate the clinical meaning of URB2 expression. We revealed that the URB2 expression level was significantly correlated with 1p/19q codeletion status (Figure 3B), Chemo status (Figure 3D), grade (Figure 3E), IDH mutation status (Figure 3F), and histology (Figure 3I) while there was no correlation in gender (Figure 3A), age (Figure 3C), RAS_type (Figure 3G), and Radio status (Figure 3H).

Cox regression analysis revealed that the URB2 expression level can be used as an independent prognostic risk factor related to OS (Supplementary Table S1). Univariate Cox analysis indicated that PRS type, histology, 1p/19q status, age, grade, IDH mutation, Chemo status, and URB2 expression were significantly related to OS in glioma patients (Figure 4A). In addition, multivariate Cox regression analysis revealed a large negative correlation between URB2 expression and OS (HR = 1.602; $p < 0.001$). Some parameters associated with worse OS included Chemo status, PRS type, IDH mutation, grade, 1p/19q status, and age (Figure 4B). The analyses suggest that URB2 expression can be used as an independent prognostic factor for OS.

3.4 Establishment of nomogram for prognosis prediction of glioma

By constructing a nomogram that incorporates both clinicopathological variables and URB2 expression, we introduced a quantitative method to predict prognostic risk (Figure 5A). ROC analysis was also performed to determine the prognostic value of

10.3389/fphar.2023.1113182

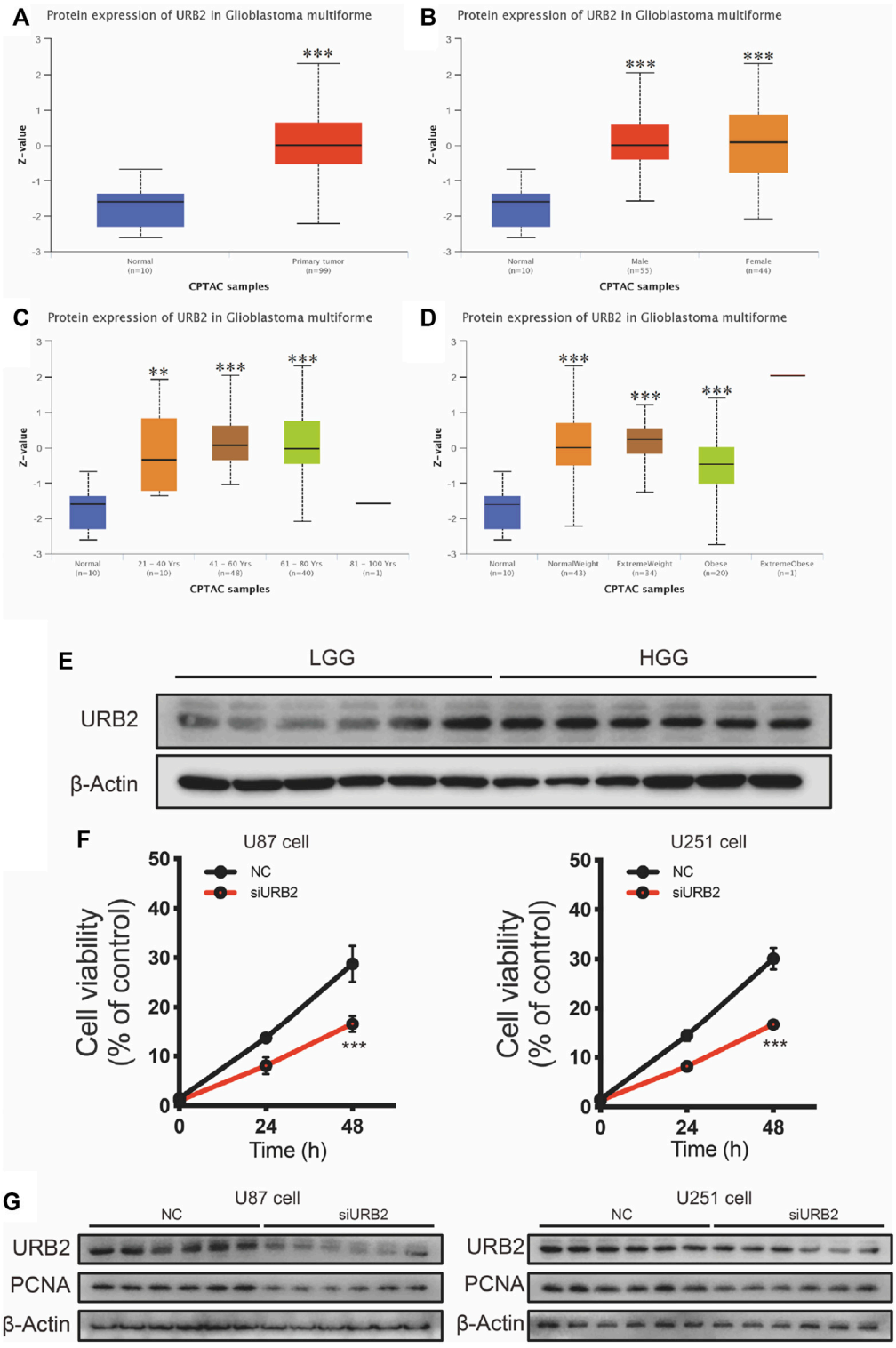

FIGURE 2
Protein expression of URB2 in Glioblastoma multiforme by CPTAP analysis and validated by Western blot. Differential expression of URB2 protein between normal tissue and primary glioblastoma multiforme **(A)**. Differential expression of URB2 protein among primary glioblastoma multiforme in different genders (male and female) and normal tissue **(B)**. Differential expression of URB2 protein among primary glioblastoma multiforme at different ages (21–40 years; 41–60 years; 61–80 years; 81–100 years) and normal tissues **(C)**. Differential expression of URB2 protein among primary glioblastoma multiforme at different weight (normal weight, extreme weight, obese, and extreme obese) **(D)**. URB2 protein expression levels in GBM and LGG **(E)**. The cell proliferation after downregulation of URB2 in U87 and U251 cells **(F)**. The expression of PCNA after downregulation of URB2 in U87 and U251 cells **(G)**. $^{**}p < 0.01$; $^{****}p < 0.001$.

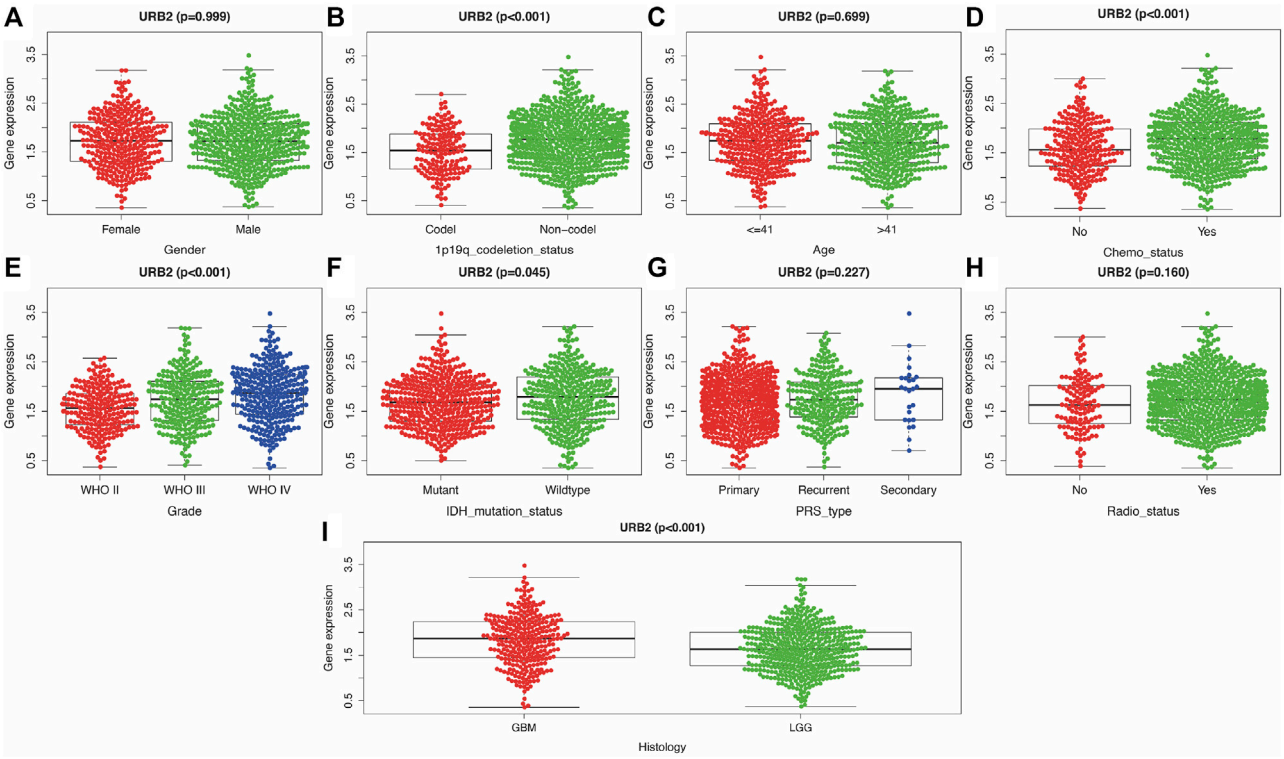

FIGURE 3
Relationship between clinicopathologic characteristics and overall survival of URB2 **(A–I)**. Correlation of URB2 expression with Gender **(A)**, 1p/19q codeletion status **(B)**, Age **(C)**, Chemo status **(D)**, Grade **(E)**, IDH mutation status **(F)**, PRS type **(G)**, Radio status **(H)**, and Histology **(I)**.

URB2 expression in gliomas, in which the AUC of URB2 expression was 0.856 (1-year; Figure 5B), 0.885 (3-year; Figure 5C), and 0.881 (5-year; Figure 5D), and the C-index was 0.8009. As shown in Figure 5E–G, the consistency between actual and ideal values is verified. These findings suggest that URB2 in combination with other parameters can be regarded as a predictor to predict the OS of glioma patients, which means that our nomogram is able to predict survival with a medium level of accuracy.

3.5 Identification of URB2-related signaling pathways

A GSEA was conducted on tissues with varying URB2 expression levels to identify pathways potentially related to URB2. Based on NES and Nom *p*-val <0.05, the pathways that were most substantially enriched were identified. High expression of URB2 was correlated with several signaling pathways, including the cell cycle, TGF beta signaling pathway, ERBB signaling pathway, RIG I-like receptor signaling pathway, and P53 signaling pathway (Figure 6) (NES, normalized enrichment score; and Nom *P*-val, normalized *p*-value).

3.6 Associations between URB2 and TMB, TNB, MSI, and PPI

The protein–protein interaction (PPI) network indicated that ten different genes (UFM1, C11orf54, SNRPC, SAV1, NOL8, URB1, NIP7, UTP15, RRS1, MAK16) were significantly related to URB2 (Figure 7A). We also revealed that URB2 was not related to MSI (GBM, $p = 0.36$; LGG, $p = 0.61$), TNB (GBM, $p = 0.59$; LGG, $p = 0.18$), or TMB in GBM ($p = 0.7$) (Figures 7B–D), while URB2 was related to TMB in LGG ($p = 0.0075$) (Figure 7D). Thus, in gliomas, TMB may play an important role in URB2 function.

3.7 Relationships among URB2 and immune infiltrations, the tumor microenvironment, and immune checkpoint molecules

We examined the possibility of a relationship between URB2 and the infiltration of six immune cell types using correlation coefficients over 0.3 and *p* values under 0.001. We found that URB2 expression is correlated with none of the six immune cell types in GBM (Figure 8A), while significantly correlated with B cells, $CD8^+$ T-cells, and Dendritic cells in LGG (Figure 8B). According to our criteria, URB2 and the immunosuppressive microenvironment of GBM were significantly correlated (Figure 8C), while no correlation was found in LGG (Figure 8D). According to our results, URB2 is significantly correlated with several immune checkpoint molecules in GBM, such as ADORA2A, BTNL2, CD160, CD200R1, and CD244, while the correlated immune checkpoint molecules in LGG include ADORA2A, BTLA,

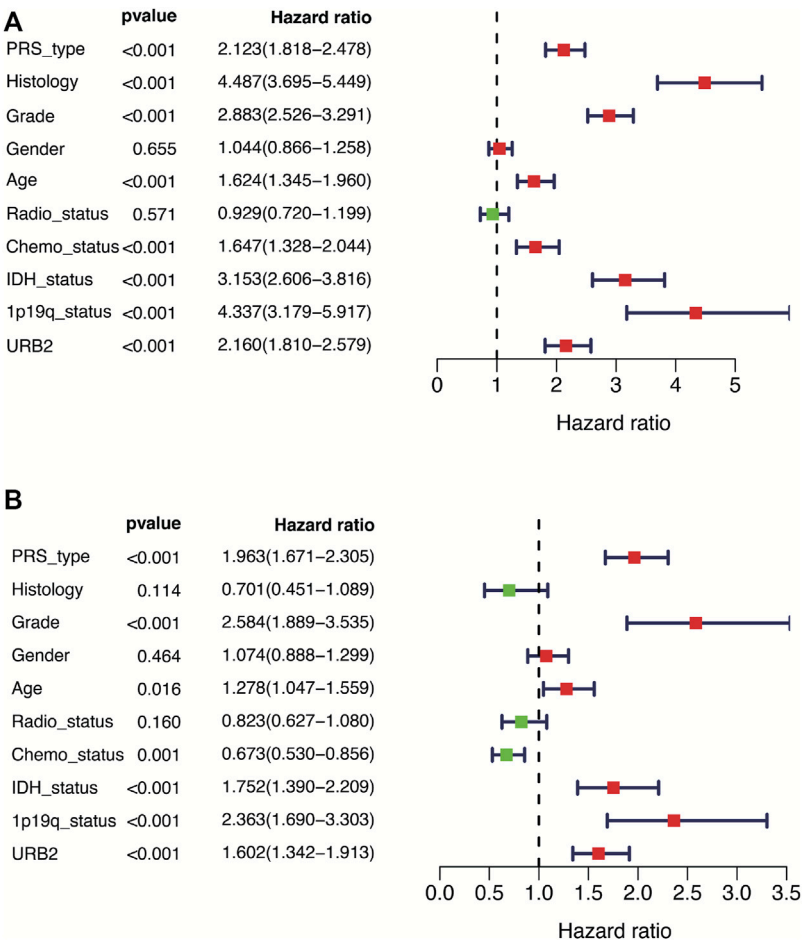

FIGURE 4
Forest plot showing univariate and multivariate cox regression analyses. Forest plot showing univariate and multivariate cox regression analyses of URB2 mRNA levels and clinicopathological variables predictive of overall survival **(A, B)**.

CD160, CD200R1, and CD27 (Figure 8E). GBM also exhibited a significant association with URB2 and several immune cells, such as activated CD8 T-cells, activated dendritic cells, and activated B cells, while it activated CD56dim natural killer cells, central memory CD4 T-cells, and CD4 T-cells in LGG (Figure 8F).

3.8 Single-cell data analysis

We downloaded the raw data of the GSE103224 and GSE148842 datasets from the TISCH database. After a series of downscaling clustering and corresponding cell annotation, a total of eight cell classes were annotated in the GSE103224 and GSE148842 datasets, which are shown in Supplementary Figures S1A, B. UMAP plots and violin plots of URB2 expression in various types of annotated cells in the GSE103224 and GSE148842 datasets are shown in Figure 9. As is shown in figures, URB2 was expressed in all types of annotated cells, including immune cells, which partially supports the close association of URB2 with immunity in glioma.

3.9 Drug sensitivity analysis

Figure 10 shows scatter plots demonstrating that drug sensitivity was significantly correlated with URB2 expression ($p < 0.05$). Notably, URB2 has a positive correlation with the sensitivity of fludarabine (correlation coefficient = 0.338, $p < 0.01$, Figure 10A) and XL-147 (correlation coefficient = 0.333, $p < 0.01$, Figure 10B).

4 Discussion

As the most frequent primary malignant brain tumor (GBD, 2016 Brain and Other CNS Cancer Collaborators, 2019), glioma claims a large number of lives every year worldwide. While GBM is one of the rarest types of glioma, its poor prognosis still makes it a critically important topic for public health concern (Iacob and Dinca, 2009). In this context, new prognostic targets must be investigated for the prediction of OS and treatment in glioma patients. URb2 is essential for the biosynthesis of 60 S ribosomal subunits. Impairment of URB2 disrupts ribosomal subunits and rRNAs. However, the prognostic role of URB2 and the specific

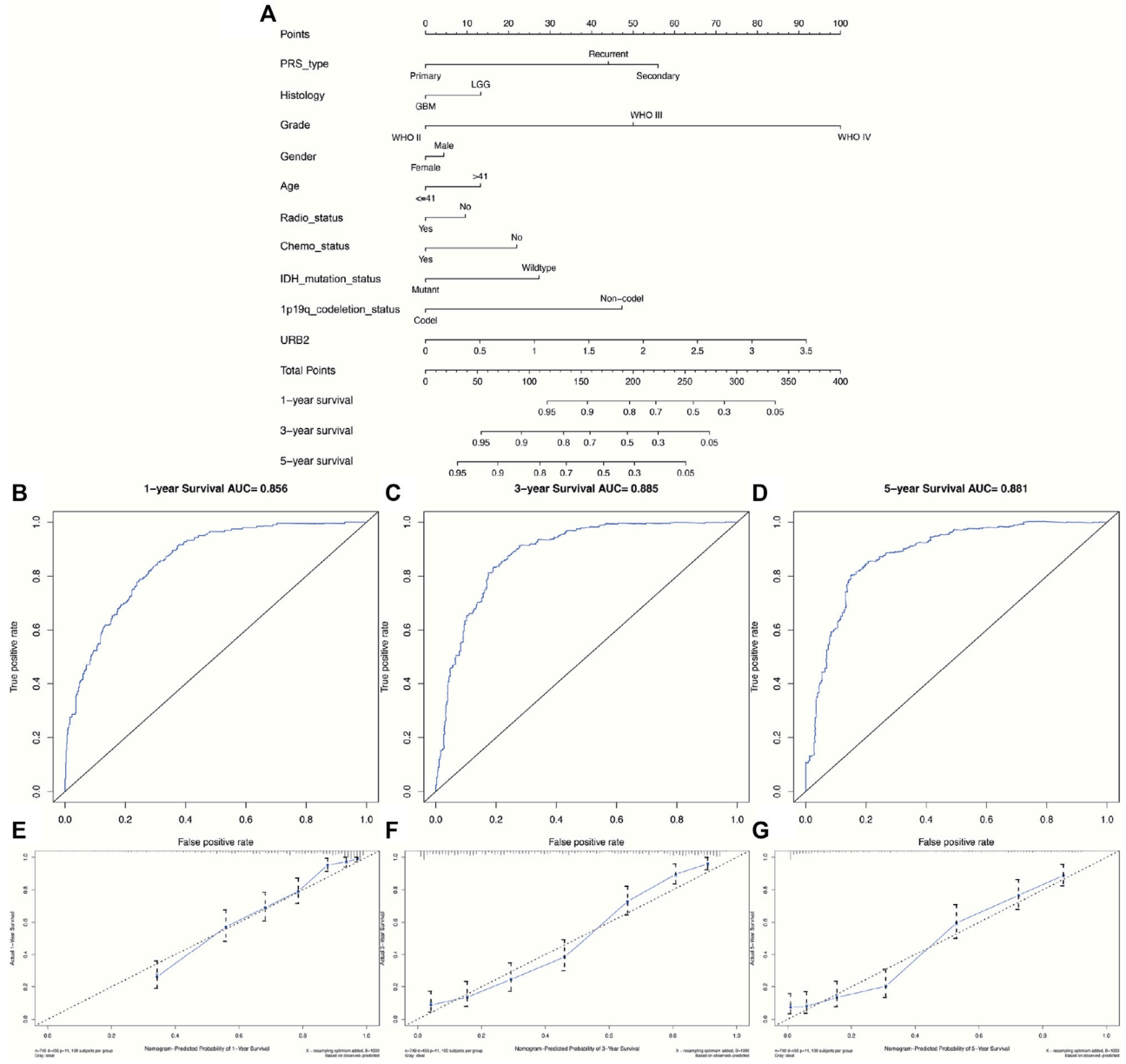

FIGURE 5
Evaluation of URB2 expression as a prognostic indicator for glioma. The nomogram uses clinical parameters and expression of URB2 to predict overall survival for glioma patients **(A)**. Analyses of the ROC curves for the OS of URB2 expression in the CGGA cohort over a 1-year, 3-year, and 5-year period **(B–D)**. An analysis of the nomogram for the prediction of survival over time **(E–G)**.

roles of URB2 in tumorigenesis and progression in glioma have not been reported. Therefore, URB2 was evaluated in glioma in terms of prognostic and immunological values in the present study.

In our research, we demonstrated that the expression of URB2 is higher in glioma than adjacent normal tissue, an indication that OS may be poor. This performance has also been verified in the GEO dataset, CGGA dataset, and Western blot (WB) analysis. The protein expression of URB2 in GBM also showed the same result in the CPTAP database. In the CGGA database, low expression of URB2 has a strong correlation with better pathological stage, histological grade, and longer OS in glioma patients. Cox regression analysis revealed that URB2 may be a predictor for prognosis in glioma patients. URB2 expression in patients with gliomas was incorporated with nine clinicopathological variables to generate a risk score, including IDH mutation status, grade, sex, histology, age, radio status, Chemo status, PRS type, and 1p/19q codeletion status. The nomogram also performed well in predicting one-, three-, and 5-year mortality, with AUCs of 0.856, 0.885, and 0.881, respectively. We further performed GSEA between tissues with different URB2 expression levels to explore the role of URB2 in glioma pathogenesis. We found that several key signaling pathways, including the KEGG cell cycle, ERBB signaling

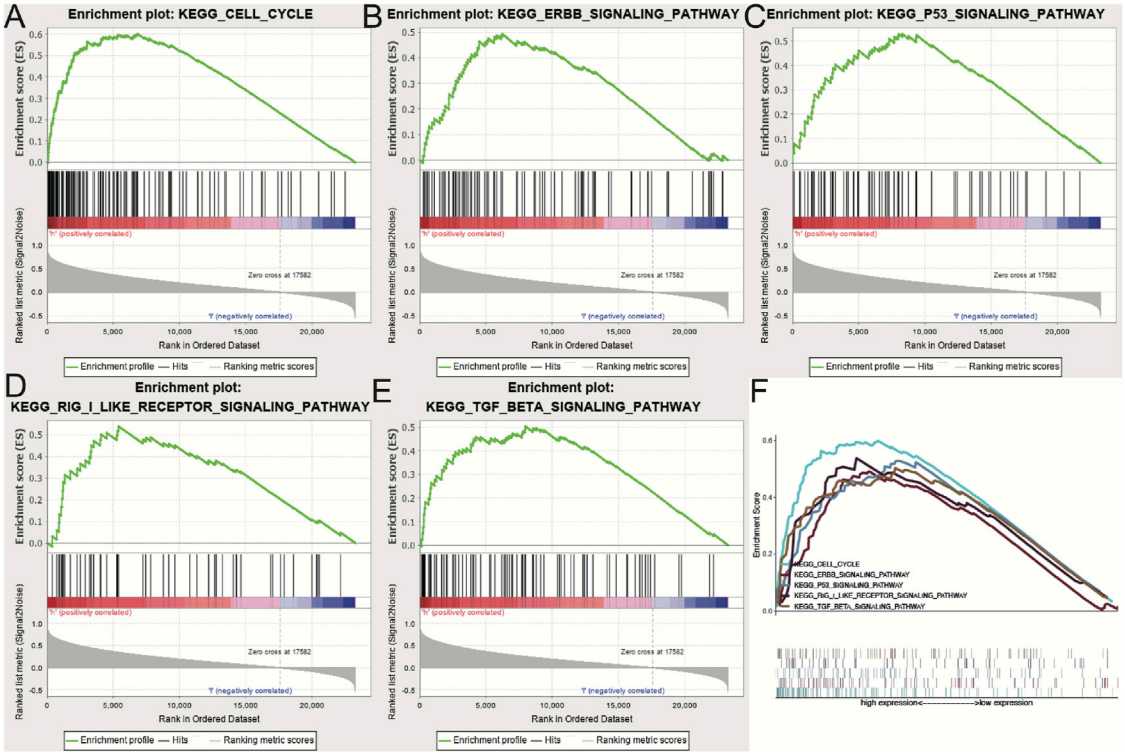

FIGURE 6
Enrichment of pathways and genes identified by GSEA **(A–E)**. The CELL cycle **(A)**, ERBB signaling pathway **(B)**, P53 signaling pathway **(C)**, RIG I like receptor signaling pathway **(D)** and TGF beta signaling pathway **(E)** are differentially enriched in URB2-related glioma. **(F)** On the basis of their normalized enrichment score (NES), the five signaling pathways most highly enriched are displayed.

pathway, TGF beta signaling pathway, RIG I-like receptor signaling pathway, and p53 signaling pathway, were correlated with URB2 expression. Moreover, we revealed that URB2 expression was strongly associated with the tumor immune microenvironment, immune cell infiltration, immune checkpoint molecules, and immune cells. Using CellMiner, we further found two drugs (fludarabine and XL-147) correlated with URB2, which means that inhibitors of these two drugs can be potential treatment drugs for immune therapy in glioma.

Nomograms are often used in various cancer types to intuitively predict prognosis (Xu et al., 2021a; He et al., 2022). Previous literature has reported that age, chemotherapy status, histopathology, radiotherapy status, IDH, tumor recurrence, and 1p/19q were common prognostic markers in gliomas (Qu et al., 2021; Huang et al., 2022). Our study constructed a nomogram for predicting the OS of glioma patients according to the CGGA dataset based on ten independent prognostic factors, including 1p/19q codeletion status, PRS type, Radio status, Histology, Chemo status, Gender, Age, IDH mutation status, Grade, and URB2. The established nomogram performed moderately with respect to the C-index, ROC curves, and calibration plots with regard to predicting OS for gliomas. Similarly, previous studies have been conducted to predict patient survival by constructing prognostic models for glioma with satisfactory results. By constructing a prognostic model such as a nomogram can more accurately predict the prognostic value of patients with glioma (Qu et al., 2020). Overall, we were successful in building an accurate nomogram plot of glioma patient prognosis.

Then, we determined five URB2-related signaling pathways by means of GSEA, including the CELL cycle, RIG I-like receptor signaling pathway, ERBB signaling pathway, P53 signaling pathway, and TGF beta signaling pathway. As reported, ERBB receptor tyrosine kinases play a key role in both normal physiology and cancer. Many epithelial tumors contain mutations of ERBB2, and clinical studies indicate that they are correlated with tumor progression (Hynes and MacDonald, 2009; Xu et al., 2022). When cells are exposed to different stress signals, their p53 signaling pathway is activated, activating several transcriptional programs, including cell cycle arrest, senescence, DNA repair, and apoptosis, leading to tumor growth inhibition (Marei et al., 2021). There are a large number of previous studies on TGF beta signaling pathway. Studies have shown that the TGF-beta signaling pathway has different roles in the different stages of human cancer progression (Manni and Min, 2020; Baba et al., 2022). TGF-beta acts as a cancer suppressor in the initial stage of tumorigenesis (de Caestecker et al., 2000; Zhang et al., 2017; Chandra Jena et al., 2021). Nevertheless, TGF-β acts as a proto-oncogene in the later stage of tumor to promote tumor development (Katz et al., 2013; Huynh et al., 2019). Currently, dysregulation of the TGF-β signaling pathway can be detected in many cancers, such as colon cancer and breast cancer (Sheen et al., 2013; Villalba

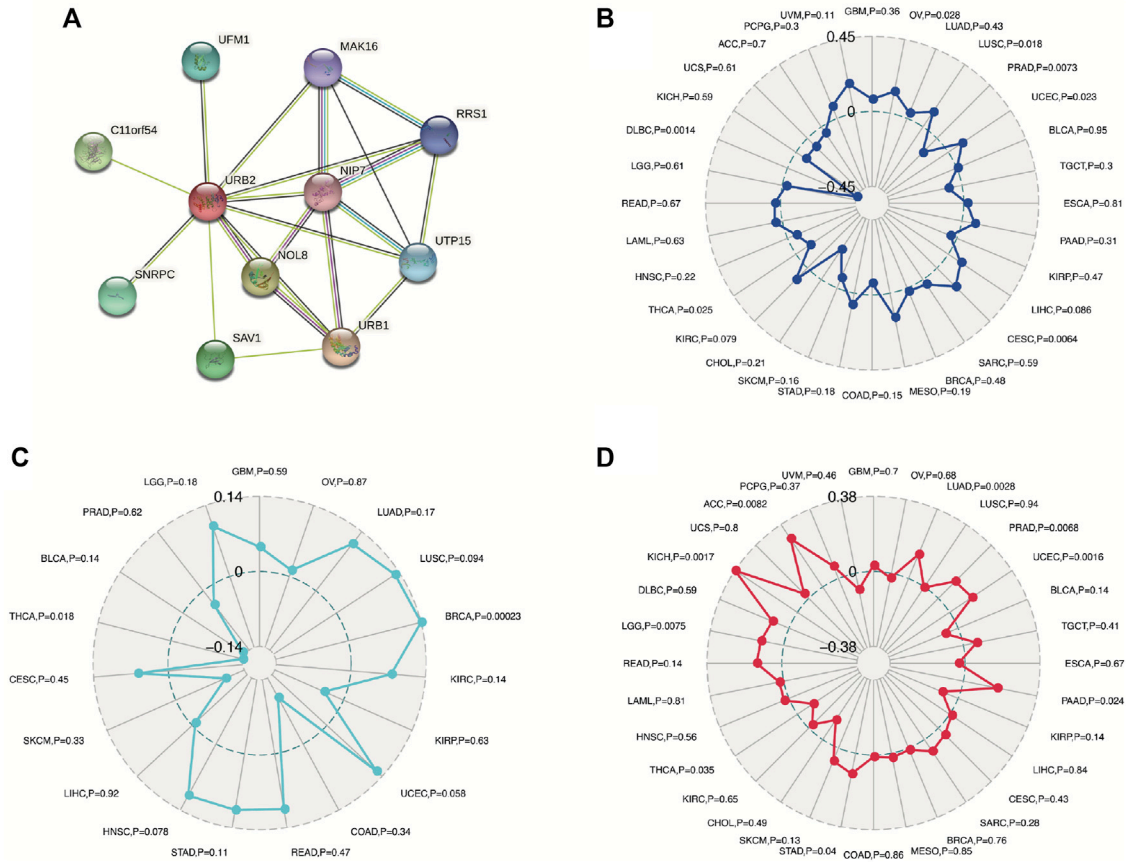

FIGURE 7
Associations between URB2 and PPI **(A)**, MSI **(B)**, TNB **(C)**, and TMB **(D)** in TCGA dataset.

et al., 2017). In summary, our results reveal potential signaling pathways and biological functions correlated with URB2, which are instructive for further functional studies of URB2.

With regard to the relationship between immunity and URB2, we demonstrate that the expression of URB2 is significantly associated with immune cells, tumor immune microenvironments (TIMs), and immune checkpoint molecules (ICMs). The activation of immune checkpoint blockade appears to be one of the most promising ways to activate therapeutic antitumor immunity (Pardoll, 2012). Additionally, the characterization of the tumor microenvironment (TME) within a patient's tumor enables us to predict and guide immunotherapeutic responses (Binnewies et al., 2018). Tumor cells can influence the surrounding cells through the TME, which not only facilitates the development of tumor cells, but also evades the surveillance of the immune system and thus affects the therapeutic effect (Quail and Joyce, 2013). In addition to tumor cells, TME also includes non-malignant cells, extracellular matrix, surrounding vascular system, and signaling molecules (Hanahan and Coussens, 2012). TME is characterized by nutrient deprivation, high acidity, hypoxia, and an immunosuppressive microenvironment, through which tumor cells are able to consolidate their advantage and gain a competitive position (Shi et al., 2020). Immunotherapy for tumors, which is the activation of the body's anti-tumor immunity, including ICIs, T-cell transfer therapy, monoclonal antibodies, cancer vaccines and immune system modulators, has become one of the most promising and advanced anti-cancer strategies (Topalian et al., 2020). Immunotherapy is dependent on the interaction between tumor cells and immune cells in TME. In addition, the development of nanotechnology and nanomaterials also provides powerful tools for immunotherapy of tumors. Some of these biomaterials (e.g., dendrimers) can be used as carriers for immunologically active drug delivery in cancer through implantation, injection, and transdermal delivery, providing a more advanced approach to immunotherapy (Cai et al., 2020; Gao et al., 2021). Local delivery of immunotherapy through these materials can activate the immune response, reduce the drug dose and achieve high efficacy and safety of the treatment. In some latest studies, nano adjuvants have been used to enhance immunotherapy response and boost anti-tumor immunity through synergistic light-mediated immunotherapy (Zhu et al., 2023). Because of its high specificity and long-lasting antitumor effects, light-mediated immunotherapy has been regarded as a promising therapy for cancer treatment (Monaco et al., 2022). As a result, tumor immunotherapy has been seen as a method for controlling and eliminating cancer. It has been shown that cancer immunotherapy, in particular ICI, has yielded very promising

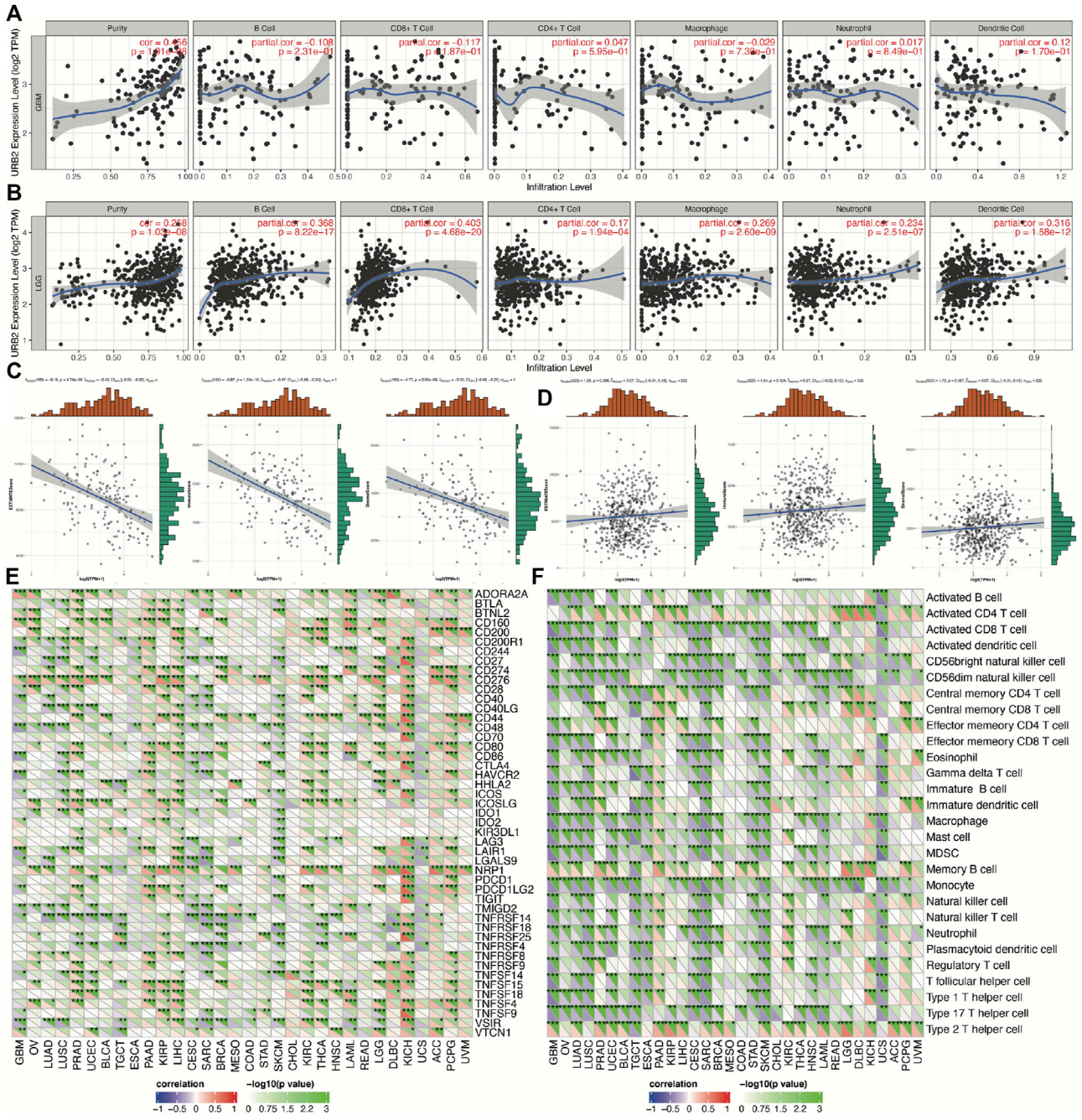

FIGURE 8
Immune relevance of URB2 in glioma patients. Associations between URB2 and immune infiltrations in GBM **(A)** and LGG **(B)**, tumor microenvironment in GBM **(C)** and LGG **(D)**. Expression of URB2-related immune checkpoint genes in different tumors **(E)**. Expression of URB2-related immune cell pathway marker genes in different tumors **(F)**.

clinical results for a wide range of cancer types, which has triggered considerable interest as a new therapeutic approach for glioma (Assi et al., 2018). Rather than directly killing tumors, immunotherapeutic drugs enhance the human immune system, which results in more effective tumor death and longer-lasting cancer remission while causing fewer side effects.

Furthermore, a correlation was also found between the expression of URB2 in six immune-infiltrating cells taken from the TIMER database. Previous studies have revealed that tumor-infiltrating immune cells (TIICs) play a key role in glioma patients (Liu et al., 2017). TIIC is part of the complex microenvironment. More specifically, it plays a critical role in promoting or inhibiting tumor growth (Domingues et al., 2016). In this research, we evaluated immune infiltration based on URB2 expression and demonstrated that URB2 expression positively correlated with B cells, $CD8^+$ T-cells, and Dendritic cells in LGG; however, no correlation was found in GBM. Then, we evaluated the StromalScore, ImmuneScore, and

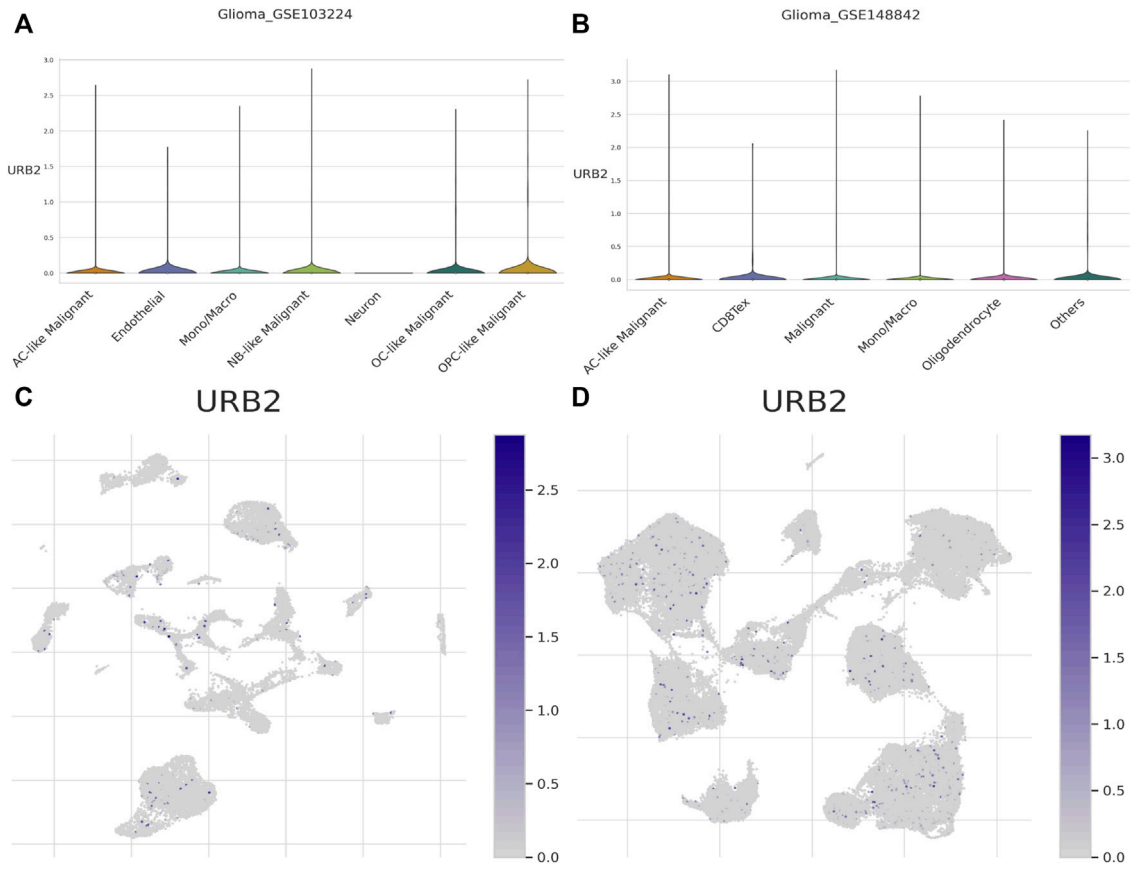

FIGURE 9
UMAP plots and violin plots. Violin plots of URB2 expression in various types of annotated cells in the GSE103224 and GSE148842 datasets are shown in **(A, B)**, respectively. UMAP plots of URB2 expression in various types of annotated cells in the GSE103224 and GSE148842 datasets are shown in **(C, D)** respectively.

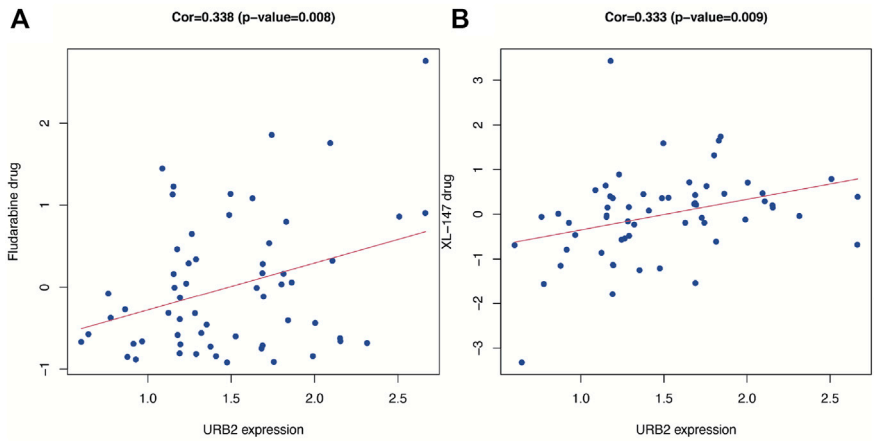

FIGURE 10
Drug response analysis. The correlation between drug sensitivity (Fludarabine and XL-147) and URB2 in Cellminer database. The scatter plots are ranked by *p*-value.

ESTIMATEScore to determine whether URB2 expression correlates with the microenvironment around gliomas. The URB2 phenotype may be associated with immune suppression in GBM but not in LGG, as we found immune involvement in GBM but not in LGG. Furthermore, several immune checkpoints that have been implicated in gliomas were evaluated and

associated with URB2 using immune checkpoint analysis. Multiple immune checkpoints correlated significantly with URB2 in LGG as well as GBM, suggesting that immune therapy could be targeted at some of these immune checkpoints. Several immune cells associated with URB2 in gliomas were expressed. These findings showed that gliomas are associated with a dysfunctional immune system, given that the microenvironment in which gliomas develop is immunosuppressive. We further found two drugs (fludarabine and XL-147) with a correlation with URB2, which means that inhibitors of these two drugs can be potential treatment drugs for immune therapy in glioma.

In recent years, research on single-cell sequencing and single-cell data analysis has become very popular and has been used in various tumor studies, especially in brain tissue (Wouters et al., 2020; Zhang et al., 2021). In the study of tumors, it can identify the tumor and immune microenvironment, the heterogeneity of the tumor, and the mechanisms associated with the development and evolution of the tumor (van Galen et al., 2019; Zilionis et al., 2019). In breast cancer, for example, scRNA-seq can examine the multi-omic features of individual cells, thus mapping tumor microenvironment (TME) in breast cancer, which also supports precise treatment. In glioma, the spatial, molecular, and functional heterogeneity of tumor-associated immune cells can be investigated to identify immunotherapeutic targets (Abdelfattah et al., 2022). In conclusion, we can better understand the molecular characteristics of glioma by scRNA-seq, which is important for the development of new therapeutic strategies.

In addition, microsatellite instability (MSI) is defined as MMR-impaired DNA mismatch repair (MMI) causing genetic hypermutability. Genetic hypermutability results from impaired DNA mismatch repair (MMR). The presence of MSI indicates that the function of MMR is not normal (Boland and Goel, 2010). MSI is associated with all types of cancers, including brain cancer (Eckert et al., 2007; Latham et al., 2019), even if MSI phenotyping appears to be closely linked with specific clinicopathological features, primarily in colorectal cancer (Boland and Goel, 2010). Screening for gene mutations in MSI and MMR has been seen as important in the treatment of patients with glioma (Leung et al., 1998; Xu et al., 2021b). Thus, we analyzed the correlation between MSI and the expression of URB2 in glioma. Our results showed no association between MSI and URB2 expression in either GBM or LGG, with p values of 0.36 and 0.61, respectively. In many cancer types, tumor mutational burden (TMB) can be used as a biomarker (Johnson et al., 2017). Our results indicated that URB2 expression had no correlation with TMB in GBM, with p values of 0.7, but had a significant association with TMB in LGG ($p = 0.0075$).

Last, this study has several highlights. In addition to being discovered in the CGGA dataset, URB2 expression has also been verified in the TCGA dataset, GEO database, and Western blot analysis, which makes our results more reliable. Furthermore, we not only identified the correlation between URB2 and immunity through multiple perspectives but also identified immunotherapeutic agents targeting URB2 in glioma. Most importantly, this is the first study of the prognostic role of URB2 and the immunological role of URB2 in tumorigenesis and progression in glioma. This study also has some limitations, such as the lack of clinical information. Aside from tumor biology, several other factors can also affect the prognosis of glioma patients, including the clinical medical data related to their treatment center. Thus, the role of the URB2 gene has not been fully investigated, and few previous articles have discussed this. The specific role of URB2 in glioma has not been fully investigated experimentally. Therefore, there is a strong need for further experimental work to verify the prediction.

5 Conclusion

Together, our research indicated that URB2 plays an oncogenic role in gliomas. According to Cox regression analyses, URB2 was considered an independent factor for glioma. GSEA was applied to search for URB2-associated pathways, including the ERBB and P53 signaling pathways. Additionally, the nomogram we performed demonstrated that URB2 may be a valid predictor, whether alone or in combination with other clinical factors. More importantly, a close relationship between immunity and URB2 was found, which is preliminary and underling evidence that the immune response contributes to glioma progression, suggesting novel approaches to immune therapy for glioma. Finally, further *in vitro* and *in vivo* experiments are necessary to verify our results.

Data availability statement

The original contributions presented in the study are included in the article/Supplementary Materials, further inquiries can be directed to the corresponding authors.

Ethics statement

The studies involving human participants were reviewed and approved by Ethical Committee for Human Investigation of the Shanghai General Hospital and the Second Hospital affiliated to Zhejiang University. The patients/participants provided their written informed consent to participate in this study.

Author contributions

CF, ZZ, PH, and HX performed bioinformatic analysis. CF, ZZ, and YH performed and analyzed experiments. ZZ, YH, YD, and LY were involved in data analysis and interpretation. AZ, AS, and ML designed the experiment, interpreted the data, and wrote the manuscript. All authors reviewed and approved the manuscript.

Funding

This work was supported by the Natural science foundation of Shanghai (18ZR1430400) and the Zhejiang Provincial Natural Science Foundation of China (LY22H090020).

Conflict of interest

The authors declare that the research was conducted in the absence of any commercial or financial relationships that could be construed as a potential conflict of interest.

Publisher's note

All claims expressed in this article are solely those of the authors and do not necessarily represent those of their affiliated organizations, or those of the publisher, the editors and the reviewers. Any product that may be evaluated in this article, or claim that may be made by its manufacturer, is not guaranteed or endorsed by the publisher.

Supplementary material

The Supplementary Material for this article can be found online at: https://www.frontiersin.org/articles/10.3389/fphar.2023.1113182/full#supplementary-material

References

Abdelfattah, N., Kumar, P., Wang, C., Leu, J. S., Flynn, W. F., Gao, R., et al. (2022). Single-cell analysis of human glioma and immune cells identifies S100A4 as an immunotherapy target. *Nat. Commun.* 13 (1), 767. doi:10.1038/s41467-022-28372-y

Assi, R., Kantarjian, H., Ravandi, F., and Daver, N. (2018). Immune therapies in acute myeloid leukemia: A focus on monoclonal antibodies and immune checkpoint inhibitors. *Curr. Opin. Hematol.* 25 (2), 136–145. doi:10.1097/MOH.0000000000000401

Baba, A. B., Rah, B., Bhat, G. R., Mushtaq, I., Parveen, S., Hassan, R., et al. (2022). Transforming growth factor-beta (TGF-β) signaling in cancer-A betrayal within. *Front. Pharmacol.* 13, 791272. doi:10.3389/fphar.2022.791272

Binnewies, M., Roberts, E. W., Kersten, K., Chan, V., Fearon, D. F., Merad, M., et al. (2018). Understanding the tumor immune microenvironment (TIME) for effective therapy. *Nat. Med.* 24 (5), 541–550. doi:10.1038/s41591-018-0014-x

Blakeley, J. (2008). Drug delivery to brain tumors. *Curr. Neurol. Neurosci. Rep.* 8 (3), 235–241. doi:10.1007/s11910-008-0036-8

Boland, C. R., and Goel, A. (2010). Microsatellite instability in colorectal cancer. *Gastroenterology* 138 (6), 2073–2087.e3. doi:10.1053/j.gastro.2009.12.064

Bush, N. A., Chang, S. M., and Berger, M. S. (2017). Current and future strategies for treatment of glioma. *Neurosurg. Rev.* 40 (1), 1–14. doi:10.1007/s10143-016-0709-8

Cai, L., Xu, J., Yang, Z., Tong, R., Dong, Z., Wang, C., et al. (2020). Engineered biomaterials for cancer immunotherapy. *MedComm* 1 (1), 35–46. doi:10.1002/mco2.8

Chandra Jena, B., Sarkar, S., Rout, L., and Mandal, M. (2021). The transformation of cancer-associated fibroblasts: Current perspectives on the role of TGF-β in CAF mediated tumor progression and therapeutic resistance. *Cancer Lett.* 520, 222–232. doi:10.1016/j.canlet.2021.08.002

de Caestecker, M. P., Piek, E., and Roberts, A. B. (2000). Role of transforming growth factor-beta signaling in cancer. *J. Natl. Cancer Inst.* 92 (17), 1388–1402. doi:10.1093/jnci/92.17.1388

Domingues, P., González-Tablas, M., Otero, Á., Pascual, D., Miranda, D., Ruiz, L., et al. (2016). Tumor infiltrating immune cells in gliomas and meningiomas. *Brain Behav. Immun.* 53, 1–15. doi:10.1016/j.bbi.2015.07.019

Eckert, A., Kloor, M., Giersch, A., Ahmadi, R., Herold-Mende, C., Hampl, J. A., et al. (2007). Microsatellite instability in pediatric and adult high-grade gliomas. *Brain Pathol.* 17 (2), 146–150. doi:10.1111/j.1750-3639.2007.00049.x

Gao, Y., Shen, M., and Shi, X. (2021). Interaction of dendrimers with the immune system: An insight into cancer nanotheranostics. *VIEW* 2 (3), 20200120. doi:10.1002/viw.20200120

GBD 2016 Brain and Other CNS Cancer Collaborators (2019). Global, regional, and national burden of brain and other CNS cancer, 1990-2016: A systematic analysis for the global burden of disease study 2016. *Lancet Neurol.* 18 (4), 376–393. doi:10.1016/S1474-4422(18)30468-X

Ghouzlani, A., Kandoussi, S., Tall, M., Reddy, K. P., Rafii, S., and Badou, A. (2021). Immune checkpoint inhibitors in human glioma microenvironment. *Front. Immunol.* 12, 679425. doi:10.3389/fimmu.2021.679425

Hanahan, D., and Coussens, L. M. (2012). Accessories to the crime: Functions of cells recruited to the tumor microenvironment. *Cancer Cell* 21 (3), 309–322. doi:10.1016/j.ccr.2012.02.022

He, L., Wang, X., Jin, Y., Xu, W., Lyu, J., Guan, Y., et al. (2022). A prognostic nomogram for predicting overall survival in pediatric wilms tumor based on an autophagy-related gene signature. *Comb. Chem. High. Throughput Screen* 25 (8), 1385–1397. doi:10.2174/1386207324666210826143727

Huang, C., Qiu, O., Mao, C., Hu, Z., and Qu, S. (2022). An integrated analysis of C5AR2 related to malignant properties and immune infiltration of gliomas. *Cancer Innov.* 1 (3), 240–251. doi:10.1002/cai2.29

Huynh, L. K., Hipolito, C. J., and Ten Dijke, P. (2019). A perspective on the development of TGF-β inhibitors for cancer treatment. *Biomolecules* 9 (11), 743. doi:10.3390/biom9110743

Hynes, N. E., and MacDonald, G. (2009). ErbB receptors and signaling pathways in cancer. *Curr. Opin. Cell Biol.* 21 (2), 177–184. doi:10.1016/j.ceb.2008.12.010

Iacob, G., and Dinca, E. B. (2009). Current data and strategy in glioblastoma multiforme. *J. Med. Life* 2 (4), 386–393.

Johnson, A., Severson, E., Gay, L., Vergilio, J. A., Elvin, J., Suh, J., et al. (2017). Comprehensive genomic profiling of 282 pediatric low- and high-grade gliomas reveals genomic drivers, tumor mutational burden, and hypermutation signatures. *Oncologist* 22 (12), 1478–1490. doi:10.1634/theoncologist.2017-0242

Katz, L. H., Li, Y., Chen, J. S., Muñoz, N. M., Majumdar, A., Chen, J., et al. (2013). Targeting TGF-β signaling in cancer. *Expert Opin. Ther. Targets* 17 (7), 743–760. doi:10.1517/14728222.2013.782287

Korman, A. J., Peggs, K. S., and Allison, J. P. (2006). Checkpoint blockade in cancer immunotherapy. *Adv. Immunol.* 90, 297–339. doi:10.1016/S0065-2776(06)90008-X

Latham, A., Srinivasan, P., Kemel, Y., Shia, J., Bandlamudi, C., Mandelker, D., et al. (2019). Microsatellite instability is associated with the presence of lynch syndrome pan-cancer. *J. Clin. Oncol.* 37 (4), 286–295. doi:10.1200/JCO.18.00283

Leung, S. Y., Chan, T. L., Chung, L. P., Chan, A. S., Fan, Y. W., Hung, K. N., et al. (1998). Microsatellite instability and mutation of DNA mismatch repair genes in gliomas. *Am. J. Pathol.* 153 (4), 1181–1188. doi:10.1016/S0002-9440(10)65662-3

Liu, Z., Meng, Q., Bartek, J., Jr., Poiret, T., Persson, O., Rane, L., et al. (2017). Tumor-infiltrating lymphocytes (TILs) from patients with glioma. *Oncoimmunology* 6 (2), e1252894. doi:10.1080/2162402X.2016.1252894

Manni, W., and Min, W. (2020). Signaling pathways in the regulation of cancer stem cells and associated targeted therapy. *MedComm* 3 (4), e176. doi:10.1002/mco2.176

Marei, H. E., Althani, A., Afifi, N., Hasan, A., Caceci, T., Pozzoli, G., et al. (2021). p53 signaling in cancer progression and therapy. *Cancer Cell Int.* 21 (1), 703. doi:10.1186/s12935-021-02396-8

Monaco, H., Yokomizo, S., Choi, H. S., and Kashiwagi, S. (2022). Quickly evolving near-infrared photoimmunotherapy provides multifaceted approach to modern cancer treatment. *VIEW* 3 (3), 20200110. doi:10.1002/viw.20200110

Omuro, A., and DeAngelis, L. M. (2013). Glioblastoma and other malignant gliomas: A clinical review. *Jama* 310 (17), 1842–1850. doi:10.1001/jama.2013.280319

Ostrom, Q. T., Gittleman, H., Liao, P., Vecchione-Koval, T., Wolinsky, Y., Kruchko, C., et al. (2017). CBTRUS Statistical Report: Primary brain and other central nervous system tumors diagnosed in the United States in 2010-2014. *Neuro Oncol.* 19 (5), v1–v88. doi:10.1093/neuonc/nox158

Ostrom, Q. T., Gittleman, H., Stetson, L., Virk, S. M., and Barnholtz-Sloan, J. S. (2015). Epidemiology of gliomas. *Cancer Treat. Res.* 163, 1–14. doi:10.1007/978-3-319-12048-5_1

Pardoll, D. M. (2012). The blockade of immune checkpoints in cancer immunotherapy. *Nat. Rev. Cancer* 12 (4), 252–264. doi:10.1038/nrc3239

Qu, S., Liu, S., Qiu, W., Liu, J., and Wang, H. (2020). Screening of autophagy genes as prognostic indicators for glioma patients. *Am. J. Transl. Res.* 12 (9), 5320–5331.

Qu, S., Qiu, O., and Hu, Z. (2021). The prognostic factors and nomogram for patients with high-grade gliomas. *Fundam. Res.* 1 (6), 824–828. doi:10.1016/j.fmre.2021.07.005

Quail, D. F., and Joyce, J. A. (2013). Microenvironmental regulation of tumor progression and metastasis. *Nat. Med.* 19 (11), 1423–1437. doi:10.1038/nm.3394

Reinhold, W. C., Sunshine, M., Liu, H., Varma, S., Kohn, K. W., Morris, J., et al. (2012). CellMiner: A web-based suite of genomic and pharmacologic tools to explore

transcript and drug patterns in the NCI-60 cell line set. *Cancer Res.* 72 (14), 3499–3511. doi:10.1158/0008-5472.CAN-12-1370

Rosado, I. V., Dez, C., Lebaron, S., Caizergues-Ferrer, M., Henry, Y., and de la Cruz, J. (2007). Characterization of *Saccharomyces cerevisiae* Npa2p (Urb2p) reveals a low-molecular-mass complex containing Dbp6p, Npa1p (Urb1p), Nop8p, and Rsa3p involved in early steps of 60S ribosomal subunit biogenesis. *Mol. Cell Biol.* 27 (4), 1207–1221. doi:10.1128/MCB.01523-06

Sheen, Y. Y., Kim, M. J., Park, S. A., Park, S. Y., and Nam, J. S. (2013). Targeting the transforming growth factor-β signaling in cancer therapy. *Biomol. Ther. Seoul.* 21 (5), 323–331. doi:10.4062/biomolther.2013.072

Shi, R., Tang, Y-Q., and Miao, H. (2020). Metabolism in tumor microenvironment: Implications for cancer immunotherapy. *MedComm* 1 (1), 47–68. doi:10.1002/mco2.6

Sriraman, S. K., Aryasomayajula, B., and Torchilin, V. P. (2014). Barriers to drug delivery in solid tumors. *Tissue Barriers* 2, e29528. doi:10.4161/tisb.29528

Stewart, L. A. (2002). Chemotherapy in adult high-grade glioma: A systematic review and meta-analysis of individual patient data from 12 randomised trials. *Lancet* 359 (9311), 1011–1018. doi:10.1016/s0140-6736(02)08091-1

Topalian, S. L., Taube, J. M., and Pardoll, D. M. (2020). Neoadjuvant checkpoint blockade for cancer immunotherapy. *Science* 367 (6477), eaax0182. doi:10.1126/science.aax0182

van Galen, P., Hovestadt, V., Wadsworth Ii, M. H., Hughes, T. K., Griffin, G. K., Battaglia, S., et al. (2019). Single-cell RNA-seq reveals AML hierarchies relevant to disease progression and immunity. *Cell* 176 (6), 1265–1281.e24. doi:10.1016/j.cell.2019.01.031

Villalba, M., Evans, S. R., Vidal-Vanaclocha, F., and Calvo, A. (2017). Role of TGF-β in metastatic colon cancer: It is finally time for targeted therapy. *Cell Tissue Res.* 370 (1), 29–39. doi:10.1007/s00441-017-2633-9

Wesseling, P., and Capper, D. (2018). WHO 2016 Classification of gliomas. *Neuropathol. Appl. Neurobiol.* 44 (2), 139–150. doi:10.1111/nan.12432

Wouters, J., Kalender-Atak, Z., Minnoye, L., Spanier, K. I., De Waegeneer, M., Bravo González-Blas, C., et al. (2020). Robust gene expression programs underlie recurrent cell states and phenotype switching in melanoma. *Nat. Cell Biol.* 22 (8), 986–998. doi:10.1038/s41556-020-0547-3

Xu, S., Qi, J., Bie, Z. X., Li, Y. M., Li, B., Guo, R. Q., et al. (2021). Local progression after computed tomography-guided microwave ablation in non-small cell lung cancer patients: Prediction using a nomogram model. *Int. J. Hyperth.* 38 (1), 1366–1374. doi:10.1080/02656736.2021.1976852

Xu, Y., Mohyeldin, A., Nunez, M. A., Doniz-Gonzalez, A., Vigo, V., Cohen-Gadol, A. A., et al. (2021). Microvascular anatomy of the medial temporal region. *J. Neurosurg.* 137, 747–759. doi:10.3171/2021.9.JNS21390

Xu, Y., Nunez, M. A., Mohyeldin, A., Vigo, V., Mao, Y., Cohen-Gadol, A. A., et al. (2022). Microsurgical anatomy of the dorsal clinoidal space: Implications for endoscopic endonasal parasellar surgery. *J. Neurosurg.* 137, 1418–1430. doi:10.3171/2021.12.JNS211974

Yuan, J., Levitin, H. M., Frattini, V., Bush, E. C., Boyett, D. M., Samanamud, J., et al. (2018). Single-cell transcriptome analysis of lineage diversity in high-grade glioma. *Genome Med.* 10 (1), 57. doi:10.1186/s13073-018-0567-9

Zhang, C., Xiong, B., Chen, L., Ge, W., Yin, S., Feng, Y., et al. (2021). Rescue of male fertility following faecal microbiota transplantation from alginate oligosaccharide-dosed mice. *Gut* 70 (11), 2213–2215. doi:10.1136/gutjnl-2020-323593

Zhang, H., Liu, T., Zhang, Z., Payne, S. H., Zhang, B., McDermott, J. E., et al. (2016). Integrated proteogenomic characterization of human high-grade serous ovarian cancer. *Cell* 166 (3), 755–765. doi:10.1016/j.cell.2016.05.069

Zhang, Y., Alexander, P. B., and Wang, X. F. (2017). TGF-B family signaling in the control of cell proliferation and survival. *Cold Spring Harb. Perspect. Biol.* 9 (4), a022145. doi:10.1101/cshperspect.a022145

Zhao, W., Dovas, A., Spinazzi, E. F., Levitin, H. M., Banu, M. A., Upadhyayula, P., et al. (2021). Deconvolution of cell type-specific drug responses in human tumor tissue with single-cell RNA-seq. *Genome Med.* 13 (1), 82. doi:10.1186/s13073-021-00894-y

Zhu, H., Yang, C., Yan, A., Qiang, W., Ruan, R., Ma, K., et al. (2023). Tumor-targeted nano-adjuvants to synergize photomediated immunotherapy enhanced antitumor immunity. *VIEW*, 20220067. doi:10.1002/viw.20220067

Zilionis, R., Engblom, C., Pfirschke, C., Savova, V., Zemmour, D., Saatcioglu, H. D., et al. (2019). Single-cell transcriptomics of human and mouse lung cancers reveals conserved myeloid populations across individuals and species. *Immunity* 50 (5), 1317–1334.e10. doi:10.1016/j.immuni.2019.03.009

Frontiers in Pharmacology

Explores the interactions between chemicals and living beings

The most cited journal in its field, which advances access to pharmacological discoveries to prevent and treat human disease.

Discover the latest Research Topics

See more →

Frontiers

Avenue du Tribunal-Fédéral 34
1005 Lausanne, Switzerland
frontiersin.org

Contact us

+41 (0)21 510 17 00
frontiersin.org/about/contact